IAEA-TECDOC-483

NUCLEAR THEORY FOR FAST NEUTRON NUCLEAR DATA EVALUATION

PROCEEDINGS OF AN ADVISORY GROUP MEETING
ORGANIZED BY THE
INTERNATIONAL ATOMIC ENERGY AGENCY
AND HELD IN BEIJING, 12–16 OCTOBER 1987

A TECHNICAL DOCUMENT ISSUED BY THE
INTERNATIONAL ATOMIC ENERGY AGENCY, VIENNA, 1988

NUCLEAR THEORY FOR FAST NEUTRON NUCLEAR DATA EVALUATION
IAEA, VIENNA, 1988
IAEA-TECDOC-483
ISSN 1011–4289

Printed by the IAEA in Austria
November 1988

PLEASE BE AWARE THAT
ALL OF THE MISSING PAGES IN THIS DOCUMENT
WERE ORIGINALLY BLANK

The IAEA does not normally maintain stocks of reports in this series. However, microfiche copies of these reports can be obtained from

INIS Clearinghouse
International Atomic Energy Agency
Wagramerstrasse 5
P.O. Box 100
A-1400 Vienna, Austria

Orders should be accompanied by prepayment of Austrian Schillings 100,– in the form of a cheque or in the form of IAEA microfiche service coupons which may be ordered separately from the INIS Clearinghouse.

FOREWORD

Fusion reactor research and nuclear fission technology application programmes are being actively pursued in a number of IAEA Member States. For design, operation and safety calculations performed in the framework of these programmes, complete sets of evaluated fast neutron nuclear data are required. Applied nuclear reaction theory and nuclear model calculations are needed to complement the available experimental data and to check their mutual consistancy.

In order to meet this requirement and to review the current situation, the IAEA Nuclear Data Section, with endorsement by the International Nuclear Data Committee (INDC) at its 15th Meeting in June 1986, and in co-operation with the Institute of Atomic Energy (IAE), Beijing as host, held this Advisory Group Meeting on Nuclear Theory for Fast Neutron Nuclear Data Evaluation during the week 12-16 October 1987 at Beijing, China. The meeting was attended by 39 scientists from twelve Member States and two international organizations. Twenty-six invited and twelve contributed papers were presented at the meeting.

The meeting dealt primarily with the requirements of theoretically calculated fast neutron nuclear data, optical potential, compound theory, pre-compound theories, isomeric state cross sections and comparison of nuclear model codes.

The objectives of the meetings were:

- to review the recent developments and current status of nuclear theories used in evaluation and calculation of fast neutron nuclear data;

- to review nuclear structure theories needed in neutron nuclear data calculations, particularly the nuclear level density;

- to discuss and specify open problems in neutron reaction theories and models;

- to make specific recommendations concerning the information exchange, research co-operation programmes and intercomparison of computer codes.

The proceedings contain all invited and contributed papers presented at the meeting as well as the conclusions and recommendations and the Chairman's summary of the meeting.

The Agency wishes to acknowledge the support of the Ministry of Nuclear Industry, China, and to express its appreciation to the Institute of Atomic Energy for hosting the meeting. It is particularly indepted to Dr. Zhou Enchen, the local organizer of the meeting and the staff of the Division of Nuclear Physics of the Institute of Atomic Energy for their assistance before and during the meeting. Finally it would like to thank Professor P.E. Hodgson for his excellent assistance in the scientific preparation and conduct of the meeting, and to the members of the Organizing Committee of the meeting and the chairmen of the meeting sessions and working groups for their outstanding work.

EDITORIAL NOTE

In preparing this material for the press, staff of the International Atomic Energy Agency have mounted and paginated the original manuscripts as submitted by the authors and given some attention to the presentation.

The views expressed in the papers, the statements made and the general style adopted are the responsibility of the named authors. The views do not necessarily reflect those of the governments of the Member States or organizations under whose auspices the manuscripts were produced.

The use in this book of particular designations of countries or territories does not imply any judgement by the publisher, the IAEA, as to the legal status of such countries or territories, of their authorities and institutions or of the delimitation of their boundaries.

The mention of specific companies or of their products or brand names does not imply any endorsement or recommendation on the part of the IAEA.

Authors are themselves responsible for obtaining the necessary permission to reproduce copyright material from other sources.

CONTENTS

PRE-COMPOUND NUCLEAR THEORY (Session IV)

ISOMERIC CROSS-SECTION (Session V)

INTERCOMPARISON OF NUCLEAR MODEL COMPUTER CODES (Session VI)

SUMMARY OF THE ADVISORY GROUP MEETING

P.E. Hodgson

1. Introduction

It is not practicable, nor would it be desirable, for me to attempt to summarise all the ideas and results already presented at this meeting. Many of the papers are themselves summaries of whole areas of our subject, both experimental and theoretical. The papers themselves are available as a permanent record of this work.

My task, as I see it, is to reflect on the meeting as a whole, to assess to what extent the stated objections of the meeting have been achieved, to select and discuss some of the most important new developments, and to present some suggestions for the future. This must be done in the context of this meeting, which is concerned primarily with nuclear data evaluation, which must take priority over the drive for deeper physical understanding which is the main concern of more academic conferences in nuclear physics.

I propose to begin by discussing the whole process of establishing reliable cross-sections for nuclear processes, and then to consider some particular problems in more detail. This will be illustrated by examples taken from the papers presented to this meeting. Finally the extent to which the objectives of the meeting have been realised will be assessed.

2. Data

All our work is based on the results of measurements. If then we are interested in establishing a data base for a particular reaction the first stage is to collect together the results of all the measurements of that reaction, and to subject them to critical evaluation as described by Prof. Vonach. It is sometimes found that the data are discrepant, and it is then essential to remove this discrepancy before proceeding further. This requires critical evaluation and possibly the rejection of some results, a process requiring experience, insight and judgement. If this is not sufficient to produce consistency the measurement must be repeated. It is useless to compare theories with discrepant data to a level of accuracy greater than that permitted by the data discrepancies. It is also useless to try to retrieve the situation by applying statistics.

The importance of judgement is illustrated by stories about Fermi, who kept a small notebook in which he recorded the factors by which he multiplied the uncertainties in their results as reported by experimental physicists. During the early days of the Manhatten Project, the reactor designers required many cross-sections that had not yet been measured. So they asked Fermi, who said he did not know. But then they mentioned one cross-section after another, until they hit on a number that did not make Fermi frown, and used that in their design calculations. I am not of course recommending such a procedure, unless you know someone with the judgement of Fermi.

This meeting has provided many examples of the vital importance of achieving high precision. This requires long, hard and often tedious work, but is the only way we can test our theories properly. An outstanding example of such work is provided by the measurements of the neutron spectrum from the fission of californium shown by Dr Frohner. With such data it is possible to draw serious conclusions, and this is assisted by statistical evaluation. Another example is provided by the accurate 7 and 22 MeV neutron cross-sections obtained by the Ohio group that gave definite evidence of the inadequacy of the usual parametrisation of the optical potential. This in turn, combined with other, accurate data, has enabled the neutron optical model to be developed in a more physical way through the use of dispersion relations. The importance of accurate

data cannot be stressed too strongly. Again and again in the history of physics it has opened the door to new physical understanding. As Prof. Vonach emphasised, just one accurate point, combined with some theoretical understanding, often enables a whole range of cross-sections to be accurately specified. I would like also to mention the desirability of establishing complete sets of data, that is the cross-sections in all the channels of a particular reaction. This provides a much more stringent test of nuclear theories.

3. Theoretical Interpretation

When a good data base has been established, some regularities may be apparent, and they can be represented by some analytical expression. These can range from the semi-empirical formulae (such as the Kalbach-Mann systematics) to physical models (such as the optical model). These expressions contain many parameters that are adjusted to fit selected data. They may be used to predict more data over a wider range, often to a precision that is very useful for practical purposes. Some of these models have over the years been developed to quite a high degree of sophistication. Prof. Konshin has shown us in great detail the success of the optical model in representing neutron cross-sections.

If a phenomenological theory fits the data, then further progress is achieved only by extending the range and accuracy of the data. Sooner or later definite discrepancies will appear, and then we are faced by a choice. The easy way out is to increase the number of parameters, and thus to restore the fit. This can always be done, but soon becomes meaningless. Furthermore it actually reduces the predictive power, since the **more** accurately we fit data over a limited range the **less** accurate the extrapolation beyond that range.

Ultimately the only satisfactory solution is to attain a deeper physical understanding, as has recently happened with the optical model. It is then possible to fit the data more accurately with fewer parameters, and furthermore the theory may be extrapolated with greater confidence.

Discrepancies between theory and data should be taken very seriously. They mean either that the data is wrong or the theory is inadequate or both. It is not good enough just to publish a discrepant comparison and leave it at that. There have been several examples in this meeting of new physics that has resulted from taking discrepancies seriously. Another example is provided by Dr Mackintosh's work on the inversion procedures that resulted from taking seriously the discrepancies between the best available optical model calculations and experiment.

When one has a new theory it is tested against experiment; if good agreement is found, further progress can come only from more data. Disagreement can be met once again by additional parameters or by further deepening the theory and so on.

Frequent reference has been made to microscopic theories of nuclear reactions, in particular by Prof. Zhuo Yizhong. These are not able to fit the data so well as the macroscopic theories, but are exceedingly valuable through the additional physical insight that they provide. In this way they guide the parametrisation of the phenomenological theories in a more physical direction and thus ensure that they fit a wider range of data.

4. The Status of Theories

(a) The optical model

For many years the optical model has provided a reliable way of calculating unknown elastic scattering cross-sections to high accuracy, as shown by the review of Prof. Konshin. It is notable, however, that different parametrisations have to be used in different ranges of neutron energy. Dr Arthur showed how it is being successfully extended to higher energies. A deeper understanding has recently been attained by the application of dispersion relations, as described by Dr Hodgson,and it is now of prime

importance to test this against as large a database as possible. This should lead to the establishment of a reliable neutron potential over the whole energy range.

The dispersion relation analysis of neutron data requires the results of measurements over the whole energy range, from bound states at negative energies to scattering states at positive energies. Since the contributions to the real potential from the dispersion integral are mainly within about 30 MeV of the Fermi surface, it is necessary to have data from outside this region to define the Hartree-Fock potential with confidence. This is provided by analyses like that presented by Dr Young.

Also required are the energies of the bound single-particle states, and these have not yet been systematically tabulated. It may well prove desirable to establish a database of nuclear bound state energies. Since the single-particle states are usually fragmented, this would also have to be included in the database. These are important because they define the imaginary part of the optical potential at negative energies and also give the energy range over which the single-particle strength must be distributed in the multistep direct calculations, as described by Dr Marcinkowski.

(b) The compound nucleus theories

The detailed review of Dr Frohner and the report of Working Group 1 show that the compound nucleus theory is now well understood. More precise comparisons with experimental data should enhance our confidence on its predictive power.

In the context of data evaluation, the Weisskopf-Ewing theory provides a simple yet accurate way of calculating the cross-sections of many reactions. At lower energies where resolved levels contribute, the Hauser-Feshbach theory must be used, and at higher energies pre-equilibrium effects become important. There is however an intermediate region where the cross-sections are quite large and can be evaluated by the Weisskopf-Ewing theory and its use for this purpose deserves further consideration.

The correlation of nuclear parameters in Hauser-Feshbach calculations was analysed by Dr Kanda, using the experimental data for neutron-induced reactions on Co and Ni. The results of Hauser-Feshbach calculations were also presented by Dr Yu Zi-qiang and Dr Zuo Yi-Xin and supplemented by DWBA calculations of the direct contribution before comparison with some (n,p) data.

A comprehensive analysis of the more important reaction channels from 3 to 20 MeV in a range of nuclei has been contributed by Dr Wang Shu-Nuan. The optical model, the Hauser-Feshbach theory, the exciton model and the statistical model are combined to give cross-sections for a range of structural and fissile nuclei.

(c) Pre-equilibrium theories

The historical development of pre-equilibrium theories was summarised by Prof. Seeliger, who has also provided much valuable data in regions where pre-equilibrium reactions are important. Dr Gruppelaar, Prof. Seeliger and Dr Blann reviewed the exciton and unified models, and Dr Hodgson and Dr Marcinkowski the quantum mechanical theory. Some aspects of these theories are now being treated in considerable detail.

In spite of a vast amount of work over many years, these theories are still in a relatively unsatisfactory state. We have not yet found out how to do these calculations in a simple transparent, physically-based and reliable way. However I have the impression that steady progress is being made and that this is not an unattainable goal. Certainly much of the basic physics is now clear, and that is a great step forward.

One of the difficulties in testing these theories is that they involve a series of distinct sections, in each of which the physical processes are modelled in different ways with different parameter choices. It is not possible to test each section independently; it is only the whole calculation that can be compared with experiment. Furthermore, the many adjustable parameters give the theories considerable flexibility. It is thus relatively easy to fit any particular known set of data but much more difficult to predict an unknown cross-section with any confidence.

The quantum mechanical theories are in principle preferable, particularly where angular distributions are required. However they still suffer in practice from too much flexibility and more work certainly needs to be done on them.

In the context of neutron data evaluation the exciton model codes are extremely useful, and are likely to provide the best way of calculating unknown cross-sections rapidly and relatively accurately.

One important result of this meeting is a growing realisation of the importance of including collective excitations in calculations of neutron emission spectra. It is a familiar experience to find that the calculated cross-section falls below the measured one at the highest neutron energies. This is attributable to the excitation of low-lying collective states, and we know very well how to include these using the coupled-channels formalism. However there are also collective states at higher energies, in particular the grant multipole resonances, and these may well contribute to the neutron emission spectrum at lower emission energies. If this possibility is omitted, the calculated cross-section will be too low, as was found in the calculations reported by Prof. Vonach. The cross-sections due to these collective excitations can be calculated by the coupled-channels formalism or by the DWBA if the coupling is small. These methods are now well understood. The contributed papers by Liu Dun-Huan, Zhon Hong-Mo and Zhang Xiao-Chen gave some results of calculations of direct inelastic scattering using the DWBA.

(d) Nuclear Level Densities

The cross-sections of all reactions to continuum states are directly proportional to the final state level density, and so an accurate knowledge of this is essential. In many cases this sets a limit to the accuracy attainable in nuclear reaction calculations. A partial exception is provided by reactions when one channel is dominant; the total cross-section is then limited by the reaction cross-section, which is quite accurately known from the optical model, and so is relatively insensitive to the nuclear level density.

Dr Pronyaev presented a comparison between combinational and thermodynamic methods of calculating nuclear level densities, and analysed the inaccuracies of the microscopic level density calculation methods using various quasi-particle and collective excitation spectrum approximations. A nuclear level density formula with low-energy correction was described in a contributed paper by Dr Lu Haitao.

The pre-equilibrium theories also require exciton state densities at the various stages of nuclear excitation. The simple expressions of Williams and Ericson have been widely used, but are based on rather simple assumptions. Efforts are being made to develop more realistic methods of evaluating exciton state densities, and at this meeting we have heard about the work of Dr Zhang Jingshan and Dr Reffo. This is certainly one of the ways in which the accuracy of pre-equilibrium calculations can be improved.

It would be useful to make a critical evaluation of level density formulae and parameters, and to tabulate the results.

(e) Fission Cross-sections

The recent developments in theory of fission neutron spectra have been discussed by Dr Maerten and in the report of Working Group 1. The statistical model has been used successfully to calculate the neutron spectrum, and the results are in impressive agreement with the very accurate experimental data, as shown for ^{252}Cf by Dr Froehner. The theoretical methods for the calculation of fast neutron fission cross-sections were reviewed by Dr Ohsawa.

(f) Isomer ratios

The account by Dr Gruppelaar showed that some progress is being made in the difficult task of establishing some systematic behaviour of isomer ratios, an exceedingly important problem for reactor design. He showed how model calculations can provide a

useful guide to the best way to systematise the data. This provides a further illustration of the importance of nuclear theory for data evaluation.

(g) The (p,n) and (n,p) charge exchange reactions

The theories of the (p,n) reaction were reviewed by Prof. Conde, who also showed how this reaction may be analysed together with the corresponding neutron and proton elastic scattering data. This is an important area that deserves further consideration.

(h) Neutron Radiative Capture

A detailed review of the theory of neutron radiative capture was presented by Prof. Yukun Ho. He described the various contributions to the measured cross-sections, and the methods used to calculate them. The results of several calculations were compared with the experimental data, and showed how well these reactions are now understood. The effects of nuclear structure on neutron radiative capture cross-sections were described by Prof. Menapace.

There was little subsequent discussion of this important area, and this could perhaps be made the subject of a future meeting.

(i) Computer Code Intercomparisons

A series of international computer code intercomparisons has been organised under the auspices of the NEA Data Bank in Paris, with the support of the IAEA. In the present series, the results of the intercomparison of optical model codes is now published, and an intercomparison of Weisskopf-Ewing and Hauser-Feshbach codes is in progress. A detailed intercomparison of exciton model pre-equilibrium codes and theories has also been completed by Gruppelaar and Nagel. When sufficient codes are in operation, it is to be hoped that an intercomparison of the quantum-mechanical pre-equilibrium codes will also be made.

(j) Accuracy

We were asked in the statement of the objectives of this meeting 'to specify and evaluate the accuracy attainable in present calculations of neutron reaction data'. This is extremely important, for unless we know the accuracy of a predicted cross-section, we cannot use it. And yet rather few papers have made any attempt to specify the accuracy of their theories for data evaluation. Part of the reason for this is its complexity. It is not possible to say, for example, that the optical model will predict cross-sections to an accuracy of say 10%. It is more complicated than that. Some cross-sections, for example the total cross-section for neutron interactions, can probably be predicted to better than 5%. Others, such as differential cross-sections, are predictable to less accuracy, say 10%. More accurate estimates of the accuracy of predictions can be obtained by theory intercomparisons such as that described by Prof. Vonach.

Some thought should perhaps be given to the problem of the best way to present these estimates of accuracy in a convenient yet comprehensive way. Dr Kanda has shown us the usefulness of error matrices, and these may be adaptable to a wider context.

5. Assessment of Attainment of Objectives

The emphasis of this meeting was placed on applied nuclear theory and the nuclear models used for fast neutron nuclear data computations.

It is appropriate to recall the objectives of the meeting and to assess the extent to which they have been achieved. The objectives were as follows:

1. "To review the recent developments and current status of nuclear theories used in evaluation and calculation of fast neutron nuclear reaction data, especially the Weisskopf-Ewing, Hauser-Feshbach, exciton model, Feshbach-Kerman-Koonin theories, and the optical model".

On the whole this was discussed very thoroughly, and a clear picture of the current status of all these theories resulted. A possible exception is the Weisskopf-Ewing theory which has potentialities for fast and reliable calculation of nuclear data that do not seem yet to have been sufficiently realised.

2. "To review nuclear structure data needed in neutron nuclear data calculations, particularly nuclear level densities, transition probabilities, and branching ratios".

Considerable attention was paid during the meeting to nuclear level densities, but relatively little to transition probabilities and branching ratios. There were no systematic evaluations or recommendations concerning the nuclear structure data needed.

3. "To specify and evaluate the accuracy attainable in present calculations of neutron nuclear reaction data, with particular attention to the degree of parameter adjustment that is needed to fit the experimental data, together with an assessment of the accuracy attainable in the calculation of unmeasured cross-sections".

This was implicitly covered in many papers, but apart from the paper of Prof. Vonach there was little attempt to specify the accuracies obtainable in a systematic and useable way. A good estimate of the accuracy attainable in the calculation of unmeasured cross-sections will be obtained for a particular case from the blind intercomparison described by Prof. Vonach.

4. "To consider the unification of the various models in order to provide an accurate account of the experimental data for a range of nuclei over the whole neutron energy range up to 100 MeV of interest to nuclear applications, (fission, fusion, biomedical, geological and industrial applications)".

   This was well done, as described in the report of Working Group 2.

5. "To discuss and specify open problems in neutron nuclear reaction theory and models, especially to identify the areas where further work needs to be done to improve existing theories and the accuracy of the calculations made with them".

This was considered in detail, as described in the report of Working Group 2, and in many of the contributed papers, particularly those of Prof. Seeliger, Dr Blann, Dr Gruppelaar, Dr Hodgson and Dr Marcinkowski. Several specific recommendations for further work were made by the two Working Groups.

There are some other possible projects for further consideration:

(a) The use of proton data. This subject was included among the main topics to be covered in this meeting, but it was not considered explicitly. The method follows from the fact that the cross-sections of proton reactions can often be measured more accurately than those of the corresponding neutron reactions. They can then be accurately analysed to give an understanding of the reactions and the theory used to calculate the neutron cross-sections. This remains a potentially useful method, and further work remains to be done to analyse its range of applicability and the attainable accuracy.

(b) It would be useful to establish a complete and consistent set of experimental data for a selected reaction at a particular incident energy, for example that relating to the interaction of 14 MeV neutrons with ^{59}Co or ^{93}Nb. By this is meant the total cross-sections of all contributing reactions, as well as the energy and angular distributions of the emitted neutrons, protons and alpha-particles. This would provide a most useful basis for testing nuclear theories.

6. "To summarize the recent progress in theoretical computation of fast neutron nuclear data and associated nuclear model computer codes, especially the progress made in the intercomparison of nuclear theory computer codes (optical model,

coupled-channels, Weisskopf-Ewing, Hauser-Feshbach, exciton model and Feshbach-Kerman-Koonin theories) and to recommend further intercomparisons".

The report of Working Group 2 and several of the contributed papers provide assessments of the present situation in this area.

There are now very many computer codes in general use that are designed to carry out standard calculations with the same formalism. It is however often found that the same input parameters give discrepant results when inserted in different codes. Before using a code it is therefore essential to check it against a standard calculation. Benchmarks for this purpose are being established by an international programme of code comparisons organised under the auspices of the NEA Data Bank in Paris, with the support of the Director Mr J.Rosen and Dr N.Tubbs. This programme was described in an invited paper.

7. "To make specific recommendations concerning the development of international co-operation in theoretical neutron physics, in particular concerning the organisation of information exchange, research co-operation programmes and international meetings".

This was not formally discussed at any stage of the meeting, but informal discussions yielded the following suggestions.

(a) Information Exchange

(i) It would be useful to prepare bibliographies of papers relating to certain very limited problems, such as isomer ratios. These could be prepared and continually updated by a specialist working in the area, and distributed by the IAEA to all interested.

(ii) It is not always easy to obtain information about meetings on subjects relating to neutron data. It would be useful to compile a list of such meetings during say the last five years, also giving information about how to obtain the proceedings of the meetings.

(iii) Advance information on future meetings would also be most valuable. Firm invitations should be sent to invited speakers and others as soon as possible. This is essential to enable participants to obtain reservations on economy flights and in some cases to obtain the necessary visas.

(b) Research Co-operation programmes

The support of the IAEA in this area is most valuable. It would be useful to circulate information on the currently available means of supporting both long (1 or more years) and short research visits.

(c) International Meetings

It is recommended that these should continue, and that a list of the most appropriate subjects for such meetings should be made.

6. Conclusion

This has undoubtedly been a useful meeting, and we now see more clearly than before how neutron theories should be developed and applied to fast neutron data evaluation.

It remains for me to express our thanks to the International Atomic Energy Agency for sponsoring this meeting, and to our Chinese hosts for their organisational work and for making us all so welcome in Beijing.

Summary of Working Group 1

COMPOUND NUCLEAR THEORY AND LEVEL DENSITIES

Chairman:	**F. Fröhner**	(Federal Republic of Germany)
Participants:	**E. Menapace**	(Italy)
	H. Condé	(Sweden)
	A.J. Deryutter	(Belgium)
	H. Märten	(German Democratic Republic)
	P.G. Young	(United States of America)
	Y. Kanda	(Japan)
	T. Ohsawa	(Japan)
	B.D. Kuzminov	(Union of Soviet Socialist Republics)
	C.A. Philis	(France)
	Yizhong Zhuo	(China)
	Xiangwan Du	(China)
	Benai Zhang	(China)
	Zhenpeng Chen	(China)
	Ziqiang Yu	(China)
	Tingjin Liu	(China)
	Xiaocheng Zhang	(China)
	Wang Da Hai	(IAEA)

Conclusions and Recommendations

The present status was reviewed and discussed for the following areas:

(1) the theory of compound nuclear reactions
(2) model calculations of fission cross sections
(3) models for fission neutron spectra
(4) the theory of level densities .

A number of recommendations and conclusions emerged.

1. Resolved Resonances

The formalism describing resolved resonances, R-matrix theory, is well established. The Reich-Moore (RM) approximation, with weak channels such as photon channels taken into account by complex level energies of the form $E_0 - i\Gamma_\gamma/2$, has provided excellent descriptions of fissile-actinide cross sections

(see recent analyses of Pu-239 and Pu-241 cross sections by Derrien and the ORELA group and Pu-239 work of Yankov, Janeva et al.) as well as lighter nuclei (Fe, Ni, etc.) where the windows in the total cross section are not well described by simpler approximations. These are needed if information required for RM calculations are missing, for instance level spins or partial widths for individual fission or inelastic-scattering channels.

Fast Doppler broadening techniques are available for tabulated cross sections (kernel broadening, e. g. SIGMA1 code) or for calculations directly from resonance parameters (Turing method, DOBRO code).

The formats are satisfactory on the whole. An inconvenience of ENDF is the unavailability of the Reich-Moore formalism for inelastic-scattering channels as they are needed for instance for Fe-57 or Ni-61. Another shortcoming of ENDF is the impossibility to calculate the distant-level term of the R-matrix from level-statistical parameters (strength functions, average partial widths). The use of fictitious distant levels is cumbersome, that of energy-dependent effective nuclear radii theoretically ill-defined. It is recommended to remove these shortcomings.

2. Unresolved Resonances

2.1 Calculation of average cross sections from transmission coefficients

The theory appropriate for the calculation of resonance-averaged cross sections is Hauser-Feshbach theory with width fluctuation corrections. For three decades it was hampered by the fact that it was easy to calculate the average total cross section from average parameters exactly but not the partial cross sections. The various prescriptions for the width fluctuation corrections derived from Monte Carlo studies (Moldauer; Hofmann, Tepel, Richert and Weidenmueller) are approximations of questionable generality and accuracy. This long-standing problem has recently been solved in two ways.

- The maximum-entropy approach has yielded the statistical distributions (ensembles) for the S- and R-matrix elements (Mexico City, Karlsruhe).

Average cross sections can be calculated as averages over these distributions, but this becomes complicated if many channels are open.

- Methods from the many-body theory of disordered systems were employed to average the partial cross section expressions over the Gaussian Orthogonal Ensemble (GOE) of Hamilton matrices for compound systems (the usual statistical model of compound-nuclear reactions). The resulting GOE triple integral (Verbaarschot, Weidenmueller, Zirnbauer; Heidelberg) is at present the most convenient tool for the computation of resonance-averaged cross sections , easily applied to many open channels, photon channels in particular.

Both approaches give practically the same numerical results. The second one is implemented in the FITACS code (Karlsruhe) and has been used for simultaneous fits to U-238 total, capture and inelastic-scattering cross sections from 4 to 500 keV.

Direct interactions can be included after diagonalisation of the transmission matrix (Engelbrecht-Weidenmueller transformation), but programs for this and for the calculation of angular distributions must be developped. More comparisons should be made between the GOE triple integral results and calculations with the conventional approximations for a broader range of nuclides and reaction type configurations, including fission channels. In any case it is recommended to use the exact triple integral, since it treats width fluctuations and elastic enhancement rigorously.

The GOE averaging method has been generalised to multi-step compound reactions by the Heidelberg group, work on multistep direct reactions is in progress. It looks promising to apply also the maximum-entropy method to the multistep reaction problem.

2.2 Optical model

Optical-model calculations provide the basic input for the particle channels in average cross section calculations. In recent years the theory has matured to a stage where microscopic and semi-microscopic calculations based on measured or adjusted (effective) nucleon-nucleon interactions and Hartree-Fock results are becoming competitive with adjusted phenomenological optical potentials. The time appears ripe for wide-scale intercomparison between microscopic/semi-microscopic calculations and phenomenological optical potentials. Moreover, it is interesting that the

BUU-(Boltzmann-Uhlenbeck-Uehling) theory of heavy-ion reactions appears to be applicable also to nucleon-induced reactions. Studies of this possibility are encouraged.

The usefulness of dispersion relations between the real and imaginary part of the optical potential for dealing with the Fermi-surface anomaly affecting low-energy cross sections and with the energy dependence of optical-model parameters has been demonstrated. They should be applied in future optical-model work. Work is recommended to implement this new tool in computer codes.

Although global optical-model potentials for incident neutrons and protons have reached a high degree of dependability, optical-model potentials for d, t, alpha and other light particles need to be improved. It is noted that these reaction channels have increased in importance in recent years because of their relevance in fusion technology.

Coupled-channels calculations provide off-diagonal S-matrix elements (direct-reaction components). They are needed for inclusion of direct processes in GOE average cross section calculations and generally for good descriptions of (n,n'), (n,f), ... reactions, 2nd and 3rd chance fission, photon emission etc. It is still difficult to couple a large number of channels. It is therefore recommended to couple only the most important channels, such as low-lying collective states, and deal with the others by spherical or spherical/deformed calculations ("asymmetric" approach).

2.3 Photon channels

The interacting-boson approximation (IBA) is being used for instance at Bologna to calculate photon transition probabilities between discrete levels, and between giant-dipole resonance states and low-lying collective states. The importance of gamma-spectrum calculations for fusion blanket studies is noted: 50 % of the energy deposition in the first walls of fusion reactors are due to gamma heating. Gamma spectrum calculations, in turn, are dependent on realistic, i. e. coupled-channels, calculations.

It is therefore recommended to study the potential of the IBA in greater depth.

2.4 Fission channels

The most serious problems in a coherent description of the region of unresolved resonances are encountered in fission cross section calculations. They require not only detailed fission barrier shapes but also detailed transition state information: The detailed energy dependence of average fission cross sections can be reproduced with carefully adjusted residual (n,n') levels and collective (n,f) transition states, as shown e. g. by White (LANL) for U-235, but this is laborious and ambiguous. Available crude transition state density estimates (e. g. Lynn's recipes) are not sufficient for a detailed description. Recent work by Ignatyuk and coworkers (Obninsk) appears to improve the situation. Japanese work with careful account of angular momentum and parity was reported by Ohsawa at the present meeting. In view of this recent progress it is recommended to convene a Specialist Meeting on "Fission Cross Section Calculation Using Fission Barrier Transition States" in about two years' time (1989).

3. Fission Neutron Spectra

The theory of fission neutron spectra is developping rapidly. The Statistical Model Approach uses a large body of input information (A, Z, kinetic energy, excitation, temperature, spin, etc.), compound nuclear theory for the calculation of compound formation cross sections, level density formulae and so on, and thus provides a testing ground for a large variety of nuclear data. A large data base exists already for this purpose. The spontaneous fission of Cf-252 is therefore recommended as a standard not only for the fission neutron spectrum (as in the past) but for all experimentally accessible aspects of spontaneous fission. U-235 can play a similar role as a standard for neutron-induced fission which permits study of energy-dependent aspects of fission.

The specialist meeting on the Cf-252 fission neutron spectrum to be held just before the Tokyo conference in 1988 which was recommended at Leningrad in 1986 is strongly endorsed.

On the other hand it was noted that the maximum-entropy approach leading to a Watt spectrum as the simplest physically meaningful analytical form for the fission neutron spectrum gives a very good fit to existing recent data over 4 decades of intensity up to about 20 MeV. There is no significant deviation of the data from a Watt spectrum; the chi-square per degree of freedom is close to 1. The Watt spectrum is therefore a sufficiently good description for all applied purposes.

4. Level Densities

Level density problems are encountered in practically all Hauser-Feshbach and exciton model calculations. One source of input for the theory are level schemes. Considerable delays were noted in many mass chain evaluations. A deficiency of levels not detected in measurements because of the nature of the incident particle or because of large spin transfer was noticed in many compilations. As isomeric ratios are sensitive to level density input, and as they are important for activation and fusion conceptual studies, it is recommended to devote increased effort to include isomeric-level information in mass chain evaluations.

Available level density formulae and their parameters should be checked systematically against microscopic theories such as combinatorial shell model calculations or exciton model and BCS studies. Collective enhancement factors (vibrational and rotational) of various forms are being used, but there are many ambiguities, and the question of a compensating depletion at higher energies is not answered satisfactorily yet. More work is therefore needed on level densities and on simplified analytical recipes, with adequate account of angular momenta and parities. Exciton calculations should, as a rule, be done in two-component form.

The CRP on (p,n) and (alpha,n) reactionscross sections for level density determination is strongly endorsed.

Summary of Working Group 2

PRECOMPOUND MODELS AND CODES

Chairman:	**H. Gruppelaar**	(Netherlands)
Participants:	**M. Blann**	(United States of America)
	P.E. Hodgson	(United Kingdom)
	Dunhuan Liu	(China)
	A. Marcinkowski	(Poland)
	V.Pronyaev	(Union of Soviet Socialist Republics)
	G. Reffo	(Italy)
	D. Seeliger	(German Democratic Republic)
	H. Vonach	(Austria)
	Jingshang Zhang	(China)
Observers:	**Feizong Huang**	(China)
	Shunuan Wang	(China)
	Siwen Wang	(China)
	Lishan Yao	(China)

1. CONCLUSIONS ON THEORETICAL DEVELOPMENTS

1.1. Quantum-mechanical codes

Quantum-mechanical multistep-direct and multistep-compound models have been reviewed in the papers of Hodgson, Seeliger and Marcinkowski. After lengthy discussions in the working group on the applicability of the FKK theory and the approach followed by Tamura the following conclusions were formulated:

a. In addition to multistep-direct (MSD) and multistep-compound (MSC) components a third, continuum collective term should be added. This is important to describe the high-energy part of the emission spectrum, in particular for scattering reactions and at relatively low incident energy. The 1-phonon component is probably the most important term (inclusion of higher-order collective terms may introduce a "double counting" problem). This conclusion also applies to the semi-classical models (cf. 1.2d). Further information on this topic is given in the papers of Seeliger and of Kalka et al. It is noted that for direct discrete-level excitation the standard coupled-channels methods should be applied.

b. Present MSD calculations predict the shape of the angular distributions rather well, but may fail to predict the absolute cross-sections. Work is needed to improve the predictive power of these models, see also the paper of Marcinkowski.

c. The fraction of MSC is determined by subtracting the MSD component from the reaction cross-section (derived from an optical-model calculation). Since the absolute calculation of the MSD component is not always reliable (see point b) more work is needed to determine the MSC/MSD ratio by alternative methods.

d. Like in MSD theory, the MSD model predicts the angular distributions very well, although these are usually quite flat, except for light nuclides and at very low incident energies.

1.2. Semi-classical models

For practical calculations related to nuclear-data evaluations the quantum-mechanical models and notably the MSD models are quite complex. Therefore, so-called semi-classical models such as the exciton model and the (geometry-dependent) hybrid model are very important in actual applications. For low incident energies these models have to be combined with modern Hauser-Feshbach theory (see WG-1) and for the excitation of discrete levels the coupled-channels (or DWBA) method should be applied. The introduction of spin- and parity- into exciton-type of models is discussed in Section 1.3. Review papers on the semi-classical models were presented by Blann, Gruppelaar et al. and Seeliger. The working group formulated the following conclusions and recommendations:

a. The questions raised by Bisplinghoff (quoted in the review of Blann) on the foundation of the exciton model should be answered. One of these questions concerns a discrepancy between the (3p,2h) state density and the population of (3p,2h) states by the nuclear cascade. Another related point concerns the equal a-priori probability assumption employed and its interpretation in terms of complete configuration mixing.

b. The adopted (energy-dependent) parametrization of the average matrix element $\langle M^2 \rangle$ should be clearly stated in papers. In addition it is suggested to give the value of $\lambda^+(n=3)$ at one energy (E = 14.5 MeV). A simple, but still physically founded parametrization, can be derived from the nucleon-nucleon intranuclear scattering cross-section according to early work of Gadioli et al. For applications over a high-energy range second-order effects in energy should be accounted for.

c. Surface effects should be included in the exciton model, in particular for the description of the high-energy part of the emission spectrum at energies above about 20 MeV. The methods are available: geometry-dependent hybrid model of Blann et al. and recent work of Kalbach.

d. Inclusion of a direct, collective continuum emission term in the exciton model is necessary to obtain agreement with experimental data at the high-energy part of the spectrum (see also 1.1a). In the review paper of Seeliger there are suggestions on how to obtain this goal.

e. The 2-component model contains more physics and is in particular important if realistic state densities from combinatorial calculations are used in the calculations (cf. Section 1.4e). A recent formulation of this model is given by Kalbach.

f. The use of a model that distinguishes between open and closed configurations deserves further study, in particular if simplified MSC and MSD models are considered. There is a paper of Kalbach on this subject, related to the angular-distribution systematics.

1.3. Unified-model development and microscopic foundation

The final aim of the development of a "unified pre-equilibrium and equilibrium exciton model" is to obtain a microscopically well-founded model with full angular-momentum conservation, that is sufficiently simple to be used in nuclear data evaluation to replace the current generation of Hauser-Feshbach codes with a correction for pre-equilibrium effects. The working group noted that progress has been made in this direction (see e.g. the review of Gruppelaar) and formulated the following conclusions and recommendations:

a. An important conclusion is that the internal transition rate λ^+ and the emission rate W are not much dependent on the compound spin J, implying that the spinless exciton model actually is quite good in this respect (as holds for the Weiskopf-Ewing formula compared to Hauser-Feshbach theory at high energies). This information can be used to simplify unified-model formulations (since the unified model is close to the MSC model of FKK, a similar remark applies to MSC theory). There is one reservation: the above-mentioned conclusion holds for not too small values of the spin cut-off parameter $\sigma^2(n)$ at low values of the exciton number.

b. Reasons for further development are: consistent model formulation both for continuum emission and for excitation of discrete states (also in secondary emission), study of the foundation of more simple models

(benchmark code) and its potential to calculate angular distributions, at least in the sense of MSC of FKK (random-phase approximation).

c. Further development of the model to calculate the asymmetric component of the angular distribution in the framework of the unified model should be encouraged, e.g. on the lines indicated by Plyuiko and more recently by Fu.

d. One should also explore links with direct models (MSD of FKK, model of Tamura).

e. The microscopic foundation of the unified model should be investigated. The main question is: what are the steps and approximations to derive a unified exciton model (master equation approach) from the (time-dependent) Schrödinger equation?, c.f. the review of Gruppelaar et al.

1.4. Specific topics

In addition to the above broad categories a number of specific topics was discussed in some detail. Some observations and conclusions are given below.

a. Complex-particle emission

The situation with respect to complex-particle emission in pre-equilibrium models is not satisfactory; the predictive power of the models is low. One of the reasons is that the preformation of an complex particle is not easy to model. During the working group discussion Zhang Jingshang presented a paper in which a simplificaton of the cluster pick-up model of Iwamoto and Harada is proposed, for use in the exciton model.

b. Pre-equilibrium γ-ray emission

In addition to more complex theories the model by Akkermans and Gruppelaar also applied in the MSC spin-dependent model by Oblozinsky should be considered for wider application, at least as an alternative for the complete neglect of direct and semi-direct γ-ray emission in the current generation of statistical pre-equilibrium/equilibrium codes, cf. review paper of Gruppelaar et al.

c. High-energy requirement

The extension of the models towards higher energies may provide a test of the physics employed in the models. For such an extension surface effects should be included and the expressions for the level densities should be

adjusted (e.g. to the one of Ignatyuk). Furthermore, precompound effects in secondary emission should be accounted for (standard techniques are available). It is probably not necessary to adopt spin-dependent models, but this statement may require further foundation. The descriptions for the calculation of angular distributions should be extended. Work is in progress to extend the systematics of Kalbach and Mann. See further the reviews by Blann and Young.

d. Particle-hole state densities

Only a short discussion was devoted to this subject, but it was realized that (p,h) state and level densities play a crucial role in all statistical models. We refer to review papers of Reffo and Blann and to the contributed paper of Zhang Jingshang and also to the conclusions of WG-1. The following observations were made in the discussion of WG-2:

- An exact calculation of the Pauli-correction term A(p,h) and an accurate approximate expression for this quantity was provided by Zhang Jingshang at this meeting.
- Results of combinatorial calculations can be inserted directly into the (2-component) exciton model by adopting a fast routine such as the one used by Blann. Reffo has shown that in particular for light nuclides and for magic or near-magic nuclei (but also for other nuclei at low energies) there are large fluctuations in the state densities (as a function of energy).
- Reffo has made comparisons between results of combinatorial calculations and the frequently used Williams formula. Parametrizations turn out to be difficult because of shell-model fluctuations (these should disappear at very high energies, which is still to be investigated). Also the energy shift is difficult to parametrize. Only for the spin cut-off parameter $\sigma^2(n)$ a fairly good parametrization can be obtained, except near shell closure.

2. RECOMMENDATIONS

2.1. General recommendations

Although already many suggestions and recommendations were given, a special session of the working group was devoted to formulate recommendations on the following topics:

a. High-priority requirements for models and codes

From the recommendations given in Section 1, the following three were emphasized by the working group:

- addition of a continuum collective term [cf. Sections 1.1(a) and 1.2(d)];
- addition of a proper α-emission description [cf. Section 1.4(a)];
- addition of precompound γ-ray emission [cf. Section 1.4(b)].

b. Experimental-data requirements to test theoretical models

The working group did not discuss in detail the experimental-data requirements for nuclear data evaluation, with the exception that measurements of non-elastic cross-sections at 2 to 20 MeV with the sphere transmission method should be reconsidered. Such data can be measured with high precision and may help to determine the reaction cross-sections much more accurately than can be achieved at present (according to a suggestion by Vonach). For the test of theory and models the following two categories of data are wanted:

- More double-differential neutron emission cross-sections in the energy range between 7 and 26 MeV are required (data at 14.5 and to a lesser extend data at 26 MeV are already available). It is suggested to perform these measurements for Fe, Nb and perhaps also for W. For Pb the experimental data are satisfactory; for Nb there are already reliable data at 14.6 and 25.7 MeV.
- More measurements of isomeric activation cross-sections, in particular for reactions leading to high-spin isomers. These measurements are requested at various energies, with priority at 14 to 15 MeV. They are needed to test the models and preliminary systematics of isomer ratios (cf. paper of Gruppelaar and Kopecky).

c. Codes for mass production of reaction cross-sections

In particular for the production of large data files with activation cross-sections for application in fusion-reactor technology, codes are necessary for fast and yet reliable predictions of nuclear data. So far for this purpose the code THRESH is frequently adopted. However, this code has serious limitations and should be replaced by better codes which contain more physics and are yet fast and simple to run. There are two ways to achieve this goal; in both cases the use of modern (super) computers is

advantageous:

- The preferred method is to use well-tested existing statistical equilibrium/pre-equilibrium codes and to simplify the input of these codes by means of default options and built-in systematics.
- To a certain extent simple models e.g. those without angular momentum conservation could be used, again with simplified input. As examples of such codes we mention the geometry-dependent hybrid code ALICE (no γ-ray competition, thus restricted to energies above a few MeV) and the exciton model code GRAPE (further reduction of input necessary). Both codes may be able to yield better predictions than THRESH, but for energies below a few MeV the predictions become unreliable.

d. Uncertainty estimates of calculated cross-sections

A general recommendation for evaluators is to supply the data together with covariance matrices. This is of particular importance for standard cross-sections and dosimetry cross-sections and cross-sections for a few very important reactor materials. Although it is aimed to supply all cross-sections with covariance information, this is at present not always done. Instead it is recommended to give at least some minimum information about uncertainties, e.g. broad uncertainty bands. For evaluations primarily based upon model calculations, there are two sources of errors, one due to uncertainties in the model parameters and one due to inherent "model uncertainties". The last-mentioned errors are difficult to estimate; nevertheless this should be attempted, cf. the paper of Vonach on this subject.

2.2. Recommendations to the NDS of IAEA

The working group made the following suggestions and recommendations to the Nuclear Data Section of the IAEA:

a. Intercomparison of evaluations

Since a number of new evaluations are forthcoming, such as BROND, ENDF/B-VI, JEF-2, JENDL-3 there is within the coming years a good possibility to compare these evaluations, with the aim to identify problem areas and to assess the spread in the evaluated data. The IAEA could play a role in the coordination of such intercomparisons, c.f. the paper of Vonach on this subject.

b. Code and model intercomparisons

As a continuation of a series of code and model intercomparisons performed by the NEA Data Bank (see paper of Hodgson on this subject), the following topics are suggested for the near future (recommendaation for a joint NDB-IAEA action):

- model and code intercomparison on the calculation of photon-production spectra and isomer ratios;
- model and code intercomparison of multistep-direct reaction codes.

Both subjects are highly relevant for the production of nuclear data for fusion reactors. The second topic may be premature (too few participants).

c. Existing coordinated research programmes (CRP)

The working group has reviewed the following three existing CRP's of the Agency:

- Methods for the evaluation of cross-sections of structural materials.
  This CRP is mainly directed to the further development of nuclear reaction models to describe cross-sections of structural materials. It covers a great deal of the subject of the present AGM. Its programme is endorsed. It is recommended that the NDS informs the CRP participants at an early stage on the conclusions of this meeting, in particular on the inclusion of continuum direct-collective excitation effects in the models and on the isomer-ratio calculation problem. If possible, the programme should be changed towards solving these problems. The papers of this AGM should be forwarded to the CRP participants.
- Double-differential cross-section and activation measurements.
  The DDX measurement programme is well-defined and in accordance with recommendation 2.1(b). The linked activation measurement programme is as yet not defined. In fact, a very large number of activation data is needed for fusion technology, but it seems difficult to include all requirements in this CRP. Therefore it is recommended to measure with the same facility and targets as used for the DDX experiments, simultaneously the activation cross-sections for all channels. Measurements with other targets should satisfy the following conditions:
  . concentrate on a few isotopes and perform measurements and analyses of high quality (see also AGM, Gaussig);
  . do not repeat experiments for which there are reliable existing data;
  . ask forthcoming Specialists Meeting on the "International Nuclear Data

Library for Fusion Reactor Technology" advice, e.g. on the measurement of activation of high-spin isomers (see also recommendation 2.1(b)); perform some cross-section calculations (if possible) for the isotopes measured.

- Determination of level densities from (p,n) and (α,n) cross-section data.
  This programme was not discussed in much detail, but in view of the need for reliable level-density information as a function of energy, the programme is endorsed.

d. Suggestions for future CRP's

The working group recommended to consider the following topics for future Coordinated Research Programmes:

- Evaluation of activation and transmutation cross-sections for fusion reactor technology, including excitation functions and isomer ratios. In addition the systematics of 14.5 MeV data and isomer ratios should be refined. Further advice on the need for such programme could be asked from the Specialists' Meeting on the "International Nuclear Data Library for Fusion Reactor Technology". It is noted that probably only worldwide participation could guarantee the creation of an extended activation file based upon evaluation rather than on mass-produced numbers from (too) simple codes.
- Double-differential cross-sections for higher energies (up to several hundreds of MeV), cf. 1.4(c).

e. Message to the forthcoming Specialists' Meeting on Nuclear Data Library for Fusion

Independent of the possibility of defining a CRP on the evaluation of activation cross-sections (see point d above) the working group felt that the participants of the forthcoming Specialists Meeting on the "International Nuclear Data Library for Fusion Reactor Technology" should consider the possibility to arrange a world-wide evaluation activity, coordinated by the Agency, on activation and transmutation cross-sections for fusion reactor technology.

f. Suggested topic for a future Specialists' meeting

A topic with growing importance, e.g. for fusion technology, is that of the measurement, calculation and evaluation of photon-production cross-

sections and related quantities such as γ-ray strength functions, direct, semi-direct and precompound γ-ray emission and isomer ratios. The working-group recommends to organise a specialists' meeting on this topic.

Recommendation to be included in WG 1

It is recommended to perform measurements of inelastic neutron scattering cross-sections at low incident energies on vibrational nuclides (such as Pd and Ru isotopes) as support to theoretical developments of Hauser-Fesbach theory in the presence of direct reactions.

3. RECENT COMPUTER CODES

The following table was obtained following a request of Seeliger to the participants of the plenary session.

Table 1. Information sheet on computer codes (recent developments only)

Name (code)	Name (author/institute)	Underlying theories (models)	Quantities to be calculated c.s., ang. distr., multipart. etc.
ANNE	H. Märten, TU Dresden.	Complex Cascade, Evaporation Model (statistical-model approach to fission U, Em).	energy and angular distribution of prompt fission neutrons, n-multiplicition (differential in regard of fragment data).
GMNM	H. Märten, A. Ruben, TU Dresden.	Generalized Madland-Nix Model.	energy and angular distribution of prompt fission neutrons for any fission reaction TKE (total kinetic energies), excitation energies of fragements.
EMPIRE	K. Stankiewiz, M. Herman, Warsaw, Poland.	FKK, SMCR.	c.s., multipart., emmission spectra, isomeric c.s.
FITACS	F. Fröhner, KfK.	Hauser-Feshbach + width fluctuations (GOE).	simultaneous fit to $\bar{\sigma}$, $\bar{\sigma}_n$, $\bar{\sigma}_\gamma$, $\bar{\sigma}_f$ in unresolvent region ($<^n 0.5^\gamma$ MeV^f for for actinides).
HFTT	Huang Feizong et al., Dept. Tech. Phys. Beijing Univ., PR China.	EM + EW.	for about 20 nuclei.
AMAPRE	H. Kalka, TU Dresden.	Exciton Model with Master Eqs.	nucleon emission, angular distribution by KM systematics up to 30 MeV.
EXCIFON	H. Kalka, TU Dresden.	SMC and SMD including phonon excitation	nucleon emission, angular distribution by KM systematics up to 30 MeV.
GRUKON	V. Sinitza, FEI, Obninsk, USSR.	B-W, MLBW, R-M, A-A appracohes in the resolved resonances region, B-W in unresolved region.	all cross-sections in the resolved and unresolved resonance region, many options for evaluated file preparation.
EVPAR	G. Manturov, FEI, Obninsk, USSR.	statistical theory in the unresolved resonance region, with input data as neutron and γ-strength functions.	all cross-sections in the unresolved resonance regions, the output of the code in the ENDF-5 format for file 2.
MIDESC	V. Pronyaev, FEI, Obninsk, USSR.	nuclear structure approach to nuclear reactions, second-order DWBA code (keywords: phonons, Green-function, doorway states).	total, elastic, inelastic scattering cross-sections, strength functions in the semi-microscopic approach.
GRAPE	H. Gruppelaar, ECN Petten, Netherlands.	exciton model with full master-equation solution, leading particle method with KK ang. distr.	c.s., ang. distr., multiparticle emission, γ-ray emission.
GNASH'	E. Arthur, LANL.	modified H.F. version to use "s-wave approximation".	σ, $d\sigma/d\Omega$ (via Kalbach), $d\sigma/d\varepsilon$, level σ's.
GNASH"	E. Arthur, LANL.	modified H.F. version to use Weisskopf/ Ewing theory.	σ, $d\sigma/d\Omega$ (via Kalbach), $d\sigma/d\varepsilon$, level σ's.

INTRODUCTORY TALK

(Session I)

REQUIREMENTS OF THEORETICAL EVALUATIONS

H. VONACH
Institut für Radiumforschung und Kernphysik,
University of Vienna,
Vienna, Austria

Abstract

The paper discusses the need for the use of nuclear theory in evaluation work, the way in which nuclear theory should be used in conjunction with the existing experimental data in order to achieve the most accurate results and the problem of uncertainty estimates of theoretically calculated cross-sections. It is shown that the comparison of different evaluations provides a very simple and general method to derive such uncertainty estimates. Finally it is pointed out that the almost simultaneous completion of new evaluated data files in U.S., Japan and Western Europe expected for next year together with the continuing evaluation work in China and Russia will provide a unique chance for such comparisons in near future.

---

1) Introduction

Why do we need at all nuclear theory for the evaluation of neutron cross-sections?
Which are the most important problems and issues which determine the quality of such evaluations?
How accurate are our present theoretically calculated cross-sections?
Which methods are available to estimate this accuracy quantitatively?

It appears to me that these are some of the most important questions to be addressed at this meeting and thus I will devote this introductory lecture to these topics. Of course it will not be possible to fully cover these subjects in a single lecture but I hope I will at least succeed to stimulate your interest in these problems so that they will also be discussed in a number of the more specialized lectures from different points of view.

2) Need for theoretical evaluations

At present we have a somewhat strange situation:
We are not able to calculate cross-sections from first principles. We do not know the nucleon-nucleon interaction exactly and - even more importantly - we cannot solve the Schrödinger equation for the nuclear many-body problem exactly. Instead we have to use very simplified nuclear reaction models, which are partly even semi-classical. We do not have reliable theoretical methods to estimate the accuracy of these reaction models and to predict the model parameters. Thus at present the quality of our reaction models can only be judged by their agreement with experimentally determined cross-sections.

In spite of these difficulties, however, all files like ENDF/B, JENDL, or SOKRATOR have been derived from theoretical calculations using the mentioned nuclear reaction models instead of using the experimental data directly.

There are several reasons for this:
a) The main reason is the enormous amount of data neeeded in our evaluated data files (for example for neutron transport calculations). These data cannot be measured within reasonable time and cost.

b) There is a need for nuclear data like cross-sections for short-lived fission products, which cannot be measured at all.

c) Using cross-sections from nuclear model calculations it is easy to assure the internal consistency of the evaluated data like energy conservation or consistency between all, differential, partial and total cross-sections.

This situation will not change in future. Considering the rather declining world-wide efforts in nuclear data measurements, there will be a rather slow growth of experimental cross-section data and most of

the cross-sections needed for the large general-purpose files will have to come from theoretical calculations certainly in the next decades.

This situation is somewhat different for smaller evaluations of accurate cross-section data for special purposes, e.g. the standard and dosimetry files. If cross-section uncertainties of the order of a few percent are needed this can at present only be achieved by precision measurements. For such evaluations theoretical calculations will probably remain less important.

3) Basic requirements for the derivation of neutron cross-sections by means of nuclear theory

3.1) General Remarks

As already pointed out, it is impossible to do reliable cross-section calculations without a sound experimental data base; if we want to do a cross-section evaluation for some nucleus like ^{56}Fe we have to go through the following steps:

a) Collect and evaluate all experimental cross-section data about the selected nucleus.

b) Select the best models for the theoretical description of the reactions of neutrons with the nucleus in question.

c) Determine the various free parameters of the nuclear models (e.g. optical potentials, level densities, transition matrix elements) by comparison of the calculated cross-sections with the experimental data base established in step a.

d) Perform a complete cross-section calculation with the parameter set derived in step c.

In fact what the calculations do is to interpolate and extrapolate from the region of experimentally known cross-sections into the regions of neutron energy and reaction type where no data exist, in order to get the needed complete description of all neutron cross-sections over the energy range of the evaluations (typically 0-20 MeV).

The result of such calculations therefore depends as much on the experimental data chosen for the parameter determination as on the theoretical models used. This means: step a and step b are equally important for the quality of evaluated cross-sections derived from nuclear model calculations. Thus I will in the following concentrate on these two questions.

3.2) Selection of experimental data used as input for theoretical cross-section calculations

Existing experimental cross-section data are in many cases discrepant or not directly suited for comparison with calculations. For example double-differential neutron emission cross-sections have frequently been reported in the lab- instead of the c.m.-system. In addition, the meaning of the quoted experimental errors is quite different in different papers. Thus it is certainly not sufficient to just use a collection of raw experimental data such as the EXFOR file as data base; but each theoretical evaluation should be preceded by a thorough critical review of the existing data base resulting in one set of recommended experimental cross-section values with reliable effective 1σ uncertainties.

In order to achieve this goal essentially three steps are needed /1/.

A. Preprocessing and/or renormalization of the experimental data.
B. Judgement of the relative weights to be given to the different data sets.
C. Combining all experimental data to one data set of properly weighted averages which summarizes the existing information in a simple way.

Step A involves procedures like renormalization of cross-sections to improved standard cross-section and radioactive decay data, calculation of angle-integrated neutron-emission spectra from double-differential data etc. As this meeting is devoted to the use of nuclear theory I will refer to the literature for further details /1-4/.

Step B is the most important one; it determines to a large extent the accuracy of any evaluation.

If we combine different experimental data in the conventional way by using the inverse squares of the uncertainties as relative weights, we must be sure that all uncertainties are comparable effective 1σ errors including all systematic error components. For this purpose the uncertainty analysis of each experiment has to be checked for the proper inclusion of systematic errors and for the confidence level associated and according to their checks all reported uncertainties have to be converted into comparable effective 1σ errors. Only after this renormalization of the uncertainties has been done it is possible to judge the consistency of the experimental data base and to make the important decision about disregarding obviously wrong data. It is this step where the experience of the evaluator is needed most.

The combination of the data (step C) can subsequently be done by means of standard statistical methods. If ultimate accuracy is needed least square methods including all correlations between different cross-sections are needed. This has been done for example in the forthcoming ENDF/B-VI standards evaluations /5/. In other cases simpler procedures have been used quite successfully /1-4/.

Figs. 1 and 2 show two examples for such "experimental evaluations". Fig. 1 shows the excitation functions for the $^{63}Cu(n,2n)$ reaction from the evaluation of Tagesen et al. /2/ and Fig. 2 shows the angle-integrated energy-differential neutron emission spectrum for natural lead for 14.1 MeV incident neutrons from the recent evaluation of Pavlik and myself /4/.

Both figures demonstrate that many cross-sections are known much better than one would guess if one just looks at the raw data. They show clearly that the full use of the existing experimental information is much superior to the procedure of using only some rather small arbitrary subset of the existing measurements, which has been followed in many - even recent - evaluations.

It appears to me that this point - the optimum use of the existing experimental information - should get much more attention than in the past because wrong decisions made in this first step cannot be corrected anymore in the subsequent evaluation process.

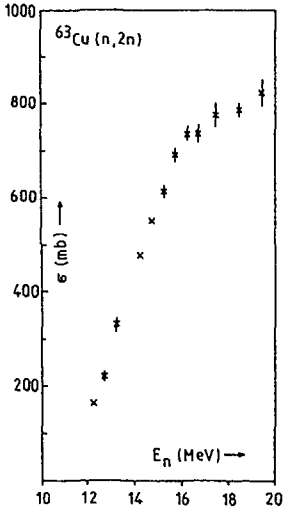

Fig. 1: Cross-section for the reaction $^{63}Cu(n,2n)$ derived as weighted average from all existing experimental data before 1979 (from Ref. 2).

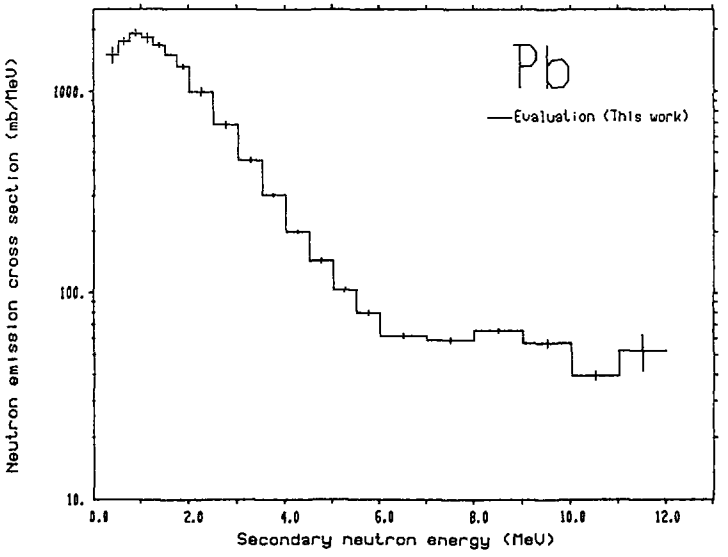

Fig. 2: Angle-integrated neutron emission cross-section $d\sigma/dE_n$, of lead for 14.1 MeV incident neutrons derived as weighted average of all existing experimental data (data from Ref. 4).

Thus important evaluations should perhaps be performed jointly by an experiment-oriented and a theory-oriented evaluator. The former should evaluate the experimental data in a similar way as described before /1-4/ and give his result to the latter as the basis for testing his theoretical models and the determination of the model parameters.

3.3) Choice of the best models for the theoretical description of neutron induced nuclear reactions

This topic will be addressed in many of the following talks; thus I will restrict myself to very few remarks.

There is now general agreement that we need three types of processes, direct, preequilibrium and compound nucleus (equilibrium) reactions for a complete description of fast-neutron induced reactions and it is also generally accepted that the compound nucleus decay is adequately described by the Hauser-Feshbach formalism.

Concerning the proper description of direct and precompound processes there are still many open questions, which will also be discussed here in the next days. I just want to point out that all existing models (including the so-called quantum-mechanical ones) are based on a number of approximations of unknown quality. Thus the judgement of the relative merits of the various approaches has to remain their success in reproducing the experimental data with a minimum number of free parameters.

Finally I would like to mention that it is important to find parametrizations of the various model parameters (preequilibrium transition probabilities, level densities etc.) which are smooth functions of A, Z and energy. This is very important for cross-section evaluations for nuclides for which no or very few experimental data are available and parameters have to be taken from systematics. It would be very interesting to compare the various preequilibrium models in this respect.

4) Accuracy of calculated cross-sections

4.1) General remarks

There is an increasing demand that evaluated nuclear data files should provide at least approximate uncertainty information. In evaluation work based predominantly on experimental data there have been successful efforts to provide such information. For example the new ENDF/B-VI standards file will have complete covariance information derived from a very careful statistical analysis of all data.

There have been, however, very few uncertainty estimates for theoretically calculated cross-section and many evaluators feel that quantitative statements about the accuracy of their calculated cross-sections are not possible. As the large general purpose nuclear data files will have to come from calculation also in forseeable future this is one of the most serious problems in the field of nuclear data evaluation. If we generally want to have uncertainty estimates for evaluated cross-sections we must solve the problem of deriving such estimates for the theoretically calculated ones. The remainder of this lecture will thus be devoted to this problem.

As a starting point I will briefly summarize the procedures we follow in the case of purely experimental data: In the case of a measured quantity we may derive the uncertainty from an estimate of all identified sources of error and the laws of error propagation (internal error). Alternatively one can estimate the uncertainty from the scatter of the different measurements (external error) and a comparison of both types of estimates allows a judgement of the quality of the error estimates.

In principle we may use these procedures also to calculated cross section. On the one hand we may try to estimate the error of some calculated cross-section from a detailed error estimate (including both the parameter uncertainties and the basic deficiencies of the theoretical models, on the other hand we may simply compare different evaluations of comparable quality and estimate the uncertainties of the various cross-sections from the deviations between the different evaluations. In the following I will briefly discuss these two methods and give some examples for their application.

4.2) Error estimates of calculated cross-sections derived from detailed error analysis

If we calculate some cross-sections by means of our present nuclear reaction models we have to consider two kinds of uncertainties:

i) Uncertainties in the various input parameters like optical potentials or level densities.

ii) Basic deficiencies of the used reaction models.

The former are much easier to estimate than the latter, therefore we have to discuss the two cases of predominance of either error source i or ii separately.

If we have little or no experimental data for some nucleus we will have to estimate the model parameters from systematics and admit rather large uncertainties for these parameters. In this case the cross-section uncertainty will be dominated by the parameter uncertainties (error source i) and it can be calculated rather straight-forward /3/.

If we assume that the calculated cross-sections $\sigma(E_n)$ are functions of n input parameters $p_1 \ldots p_n$ which are known with uncertainties $\Delta p_1 \ldots \Delta p_n$ the uncertainty of the cross-sections is given by

$$\Delta\sigma(E_n) = \left[\sum_{i=1}^{n} \left(\frac{\partial\sigma(E_n)}{\partial p_i}\right)^2 \Delta p_i^2\right]^{1/2}$$

where the quantities $\frac{\partial\sigma}{\partial p_i}(E_n) \cdot \Delta p_i$

have to be derived from model calculations with all parameters fixed at their most probable values except p_i which is changed by the estimated amount Δp_i from its normal value

$$\left(\frac{\partial\sigma}{\partial p_i}\right)\Delta p_i = \sigma(p_1, \ldots p_i + \Delta p_i, \ldots p_n) - \sigma(p_1, \ldots p_i, \ldots p_n)$$

This approach has been followed by Strohmaier et al. in their evaluation of the ^{93}Nb(n,n')^{93m}Nb cross-section /3/. In this case the uncertainties of the following parameters were included: Optical model parameters, level density parameters, γ-strength function, spin cut-off factor, transition matrix element in precompound calculation and spin and parity assignments in the decay scheme.

Fig. 3 shows the result of this calculation and a number of experimental measurements which all were performed after the completion of the described calculation. The data confirm the calculation within its stated uncertainty limits.

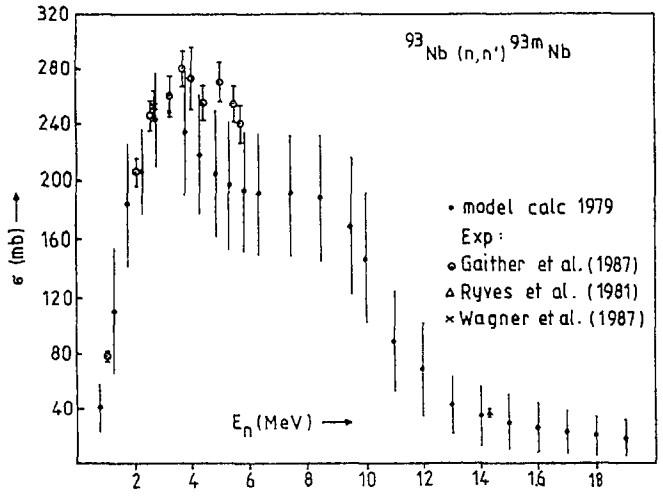

Fig. 3: o ... ^{93}Nb(n,n')^{93m}Nb cross-section and cross-section uncertainties derived from model calculations according to method described in Ref. 3.
o △ x ... measurements performed after completion of the calculations.
(After publication of Ref. 3 an input error was detected the calculated ^{93}Nb(n,n')^{93m}Nb. This figure contains the corrected cross-sections which are about 15 % smaller and correspond to the model parameters listed in V.3 and V.4 of Ref. 3.)

A somewhat more complicated situation arises if we have an accurate cross-section measurement $\sigma(E_1)$ at one energy E_1 and want to calculate the whole excitation function and estimate the uncertainty of that calculation. In that case we have to restrict the allowed volume $\Delta p_1 . \Delta p_2 \ldots \Delta p_n$ in the parameter space by the condition that any allowed combination of parameters has to reproduce $\sigma(E_1)$ within its experimental error $\pm \Delta\sigma_{exp}(E_1)$.

An approximate procedure to derive cross-section uncertainties in this case has also been developed by Strohmaier et al. /3/. It works in the following way:

a) An excitation function is calculated using our best a priori choice of the parameters $p_1 \ldots p_n$.

b) The parameters are slightly modified in order to fit the theoretical excitation function to the known value $\sigma_{exp}(E_1)$ at the neutron energy E_1.

c) A large number of excitation functions with modified parameters are calculated in the following way. In each calculation one of the parameters p_i is varied by its maximum estimated uncertainty Δp_i and simultaneously some other parameter p_j is varied by some amount $f.\Delta p_j$ ($|f| \leq 1$, Δp_j = uncertainty of parameter p_j) whereby f is chosen in such a way that $\sigma_{calc}(E_1)$ remains within the limits $\sigma_{exp}(E_1) \pm \Delta\sigma_{exp}(E_1)$.

As the result of this procedure we get a band of excitation functions all constrained to the value $\sigma_{exp} \pm \Delta\sigma_{exp}$ at E_1 and we may take as calculated cross-section the center of the band and half of the width as its uncertainty. Fig. 4 shows the $^{31}P(n,p)^{31}Si$ excitation function derived in this way in Ref. 3.

A quite different situation arises if an evaluation is performed for all cross-sections of some nucleus like ^{56}Fe where cross-sections are known experimentally for many reactions and neutron energies. Then the parameters $p_1 \ldots p_n$ are determined to a large extent by the condition that the best overall fit between the measured and calculated cross-sections is achieved. In this case we may no longer neglect

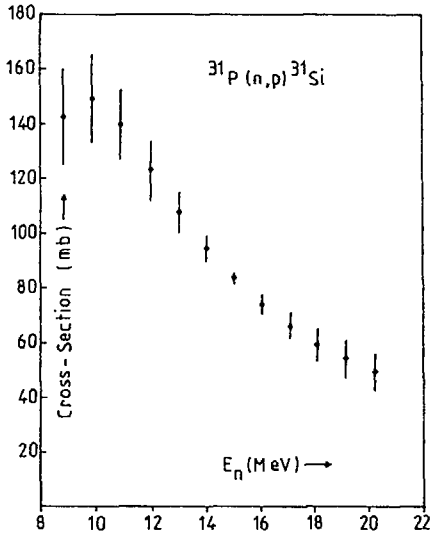

Fig. 4: $^{31}P(n,p)^{31}Si$ excitation function including uncertainties derived from calculations fitted to one accurate measurement at 14.8 MeV (from Ref. 3).

the second source of uncertainty, the basic deficiencies of the theoretical models and it is necessary to get an estimate for this uncertainty also.

This is the most difficult problem as the influence of the various approximations used in the derivation of the models on the cross-section values cannot be estimated quantitatively by theoretical methods. The only information we can use is the quality of the overall fit of the theory to the experimental data. If the experimental data are sufficiently accurate it will show up that the theory is not able to accurately reproduce the shape of experimental excitation functions and particle spectra even after optimum parameter adjustment. As an example Fig. 5 shows the fit to the $^{56}Fe(n,p)^{56}Mn$ cross-section obtained by Uhl and Strohmaier /6/ in their evaluation of all fast neutron cross-sections for some structural materials. As the figure shows it is not possible to reproduce the experimental cross-sections to better than about 10 % over the full energy range. Similar results

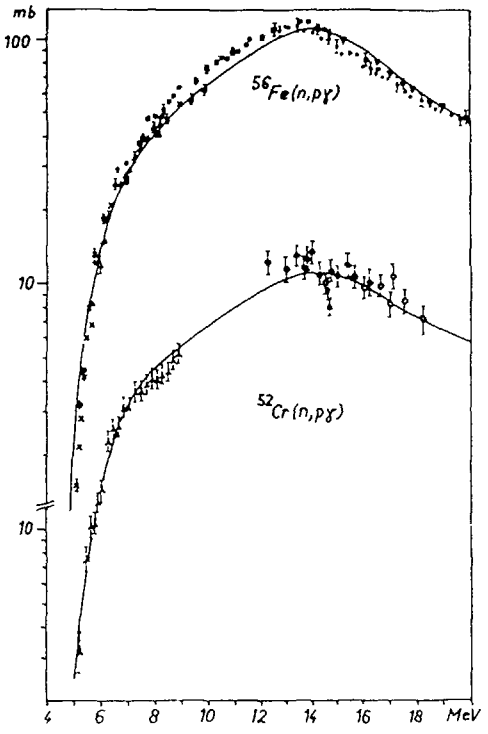

Fig. 5: Comparison of calculated excitation functions for the $^{56}Fe(n,p)^{56}Mn$ and $^{52}Cr(n,p)$ reactions with experimental data (Fig. 3 of Ref. 6).

of residual deviations in the 10 - 20 % range have been found in many other cases and it appears reasonable to assume an uncertainty of about this size for all calculated cross-sections as consequence of the basic deficiencies of the nuclear reaction models.

Thus, in the important case of theoretical evaluations with parameters adjusted to fit a wide variety of experimental data, the two types of error, basic deficiencies of the models and effects of parameter uncertainties, will be of comparable magnitude and thus will have to be estimated separately as described before and then added in quadrature. The relative magnitude of these two uncertainties will vary considerably within such evaluation. For cross-sections, where good experimental data exist, the effect of the parameter uncertainties will be small and the total uncertainty will be the mentioned 10-20 % inherent to present model calculations, for cross-sections where no data exist or only data at very different neutron energies, the effect of parameter uncertainties will also become important and has to be included.

Thus a detailed uncertainty analysis of complete isotopic evaluations derived by nuclear model calculations are possible in principle, but it is a formidable task and about as time-consuming as the evaluation itself. Therefore to my knowledge no such work has been reported.

4.3) Uncertainty estimates derived from intercomparison of different evaluations

Because of the described difficulties in the direct error analysis of calculated cross-sections it would be very desirable to have some simpler and faster methods for such estimates. It appears to me that the method of detailed comparison of different evaluations - although it has to my knowledge as yet not been used - may provide such a possibility.

If we have two or better 3 really independent evaluations of comparable quality all uncertainties in the described evaluation process (step a-d section 3.1) should manifest themselves in the deviations of the different calculated cross-sections from each other and one can estimate the accuracy of the calculated cross sections from these deviations in the same way one estimates the uncertainty of some experiment from the scatter of different measurements of about equal quality.

In the following I show some examples for such comparisons.

Figs. 6-9 show a detailed comparison of fast neutron cross-sections from recent evaluations of Strohmaier and Uhl /6/ and Arthur and Young /7/ for ^{56}Fe for 10-30 MeV incident neutron energy. Both evaluations were done at the same time (appr. 1980) by experienced evaluators according to the state of the art; thus the deviations between these two evaluations give you some crude measure for the accuracy achievable in such model calculations.

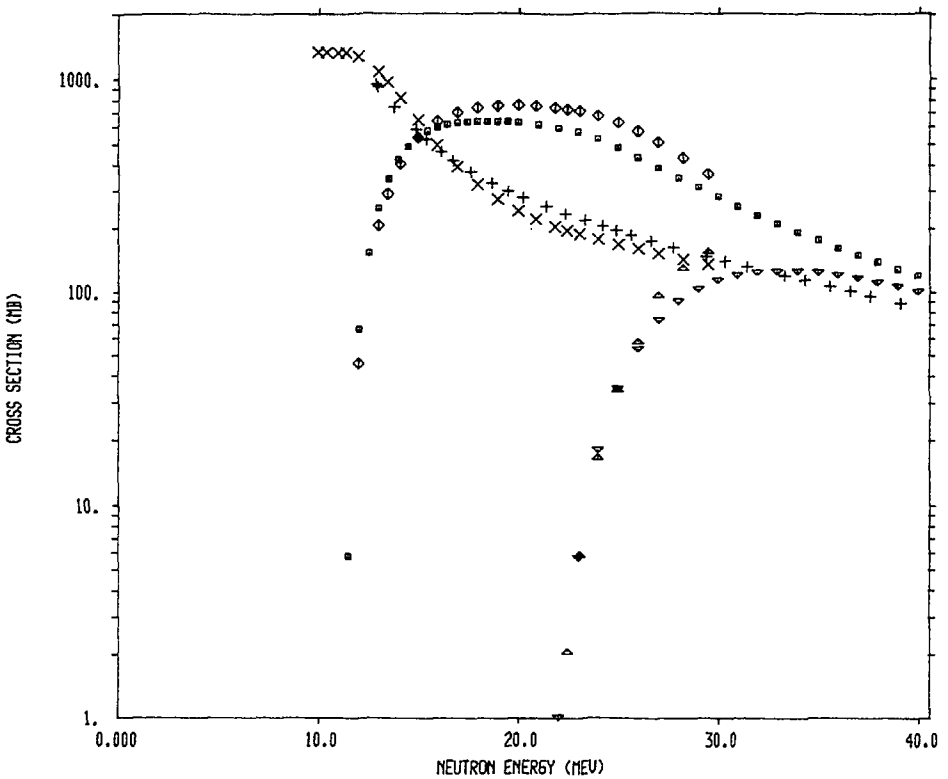

Fig. 6: Comparison of evaluations for ^{56}Fe
x ... (n,n'), ◇ ... (n,2n), Δ ... (n,3n) Strohmaier-Uhl /6/
+ ... (n,n'), □ ... (n,2n), ▽ ... (n,3n) Arthur-Young /7/

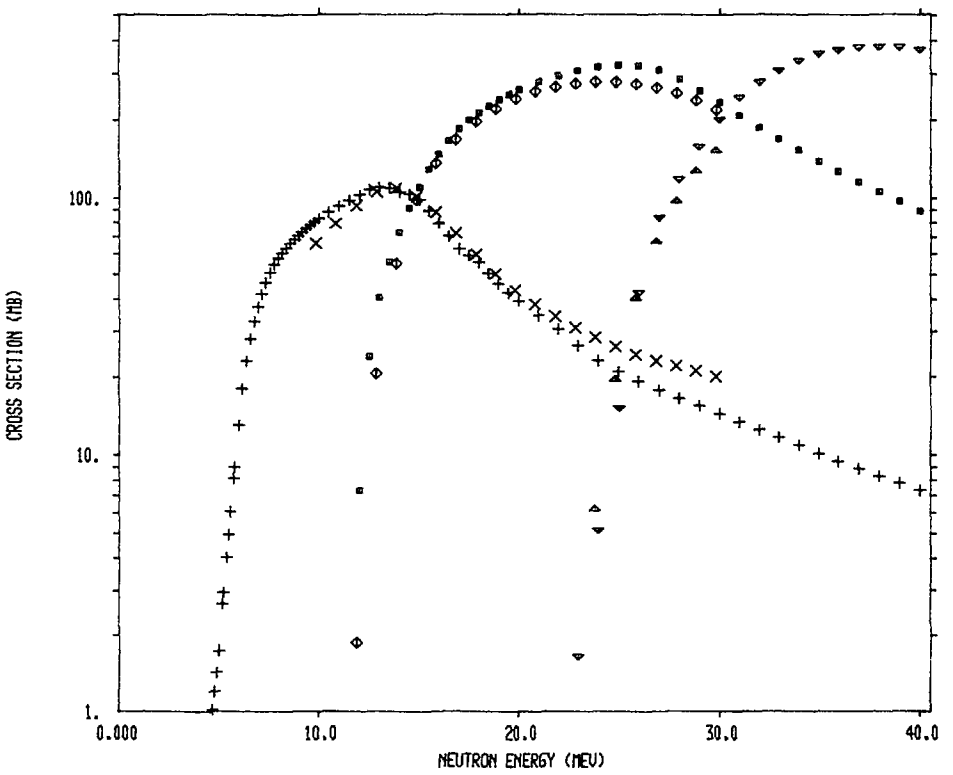

Fig. 7: Comparison of evaluations for ^{56}Fe
x ... (n,p), ◇ ... (n,np), Δ ... (n,2np) Strohmaier-Uhl /6/
+ ... (n,p), □ ... (n,np), ▽ ... (n,2np) Arthur-Young /7/

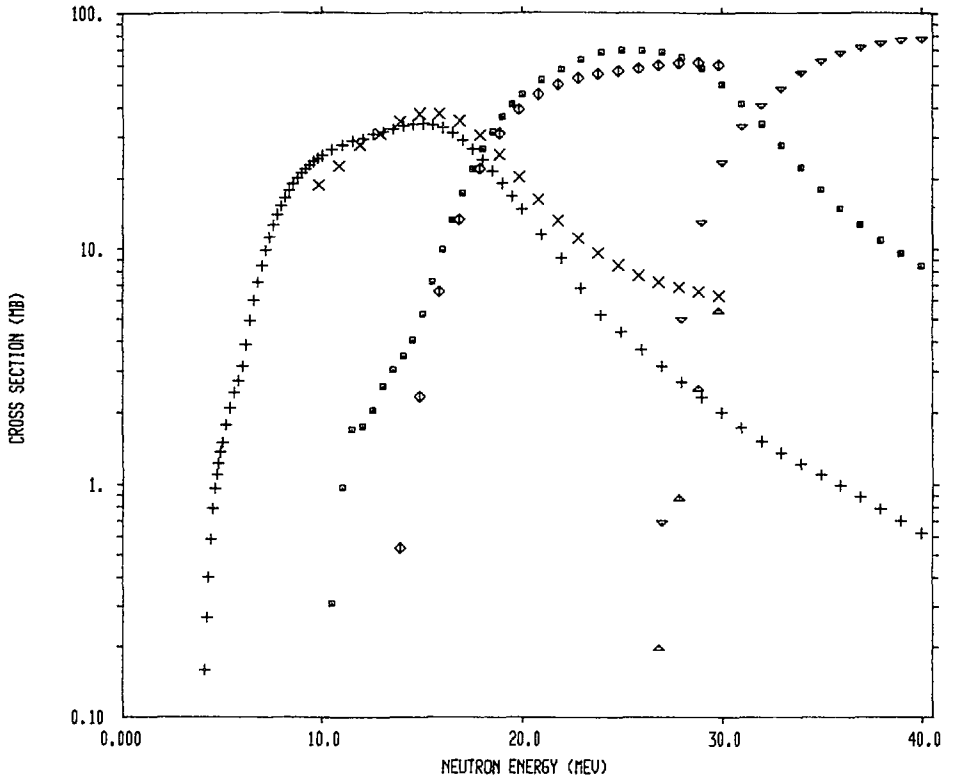

Fig. 8: Comparison of evaluations for ^{56}Fe
× ... (n,α), ◇ ... (n,nα), △ ... (n,2nα) Strohmaier-Uhl /6/
+ ... (n,α), □ ... (n,nα), ▽ ... (n,2nα) Arthur-Young /7/

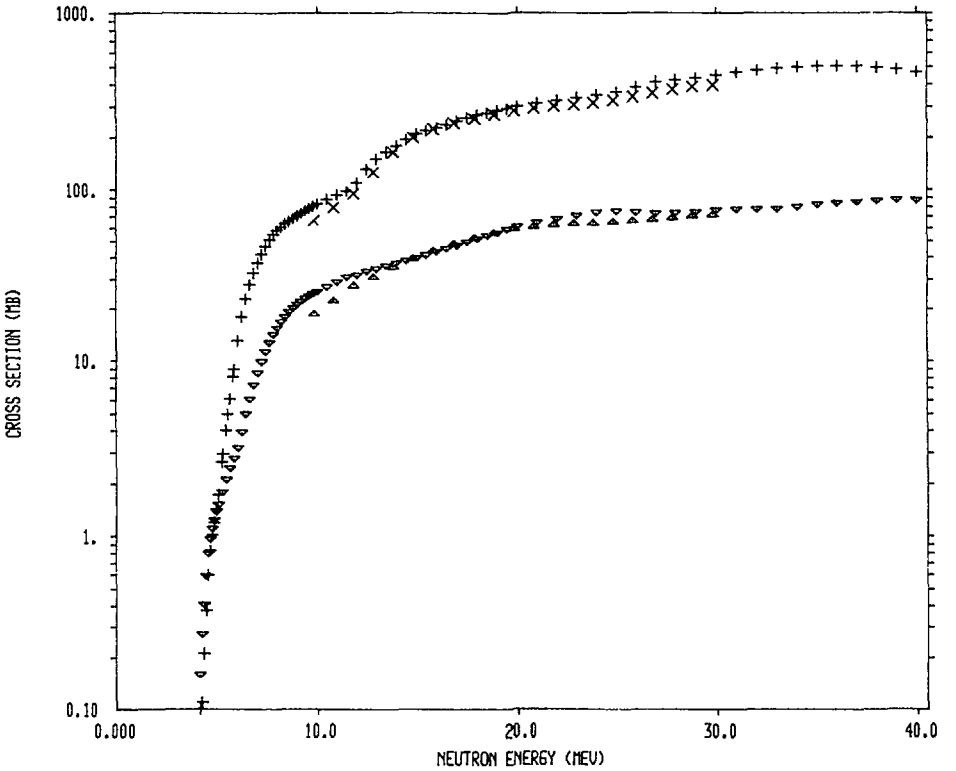

Fig. 9: Comparison of evaluations for ^{56}Fe
× ... p-production, △ ... α-production Strohmaier-Uhl /6/
+ ... p-production, ▽ ... α-production Arthur-Young /7/

As the figure shows it seems now to be possible to predict activation and gas production cross-sections with an accuracy of about 20% up to at least 20 MeV. For higher energies, uncertainties for specific activation cross-sections may quickly become larger as can be expected if we go from a region where the theory is fitted to existing measurements into a region where no measurements exist. There is a remarkable agreement between the gas-production cross-sections of both evaluations up to the highest energies.

As second example Fig. 10 shows the predictions for the angle-integrated secondary neutron cross-sections from the interaction of 14 MeV neutrons with natural lead for four different recent evaluations: ENDL-84 /8/, ENDF/B-V /9/, EFF-1 /10/ and BROND /11/.

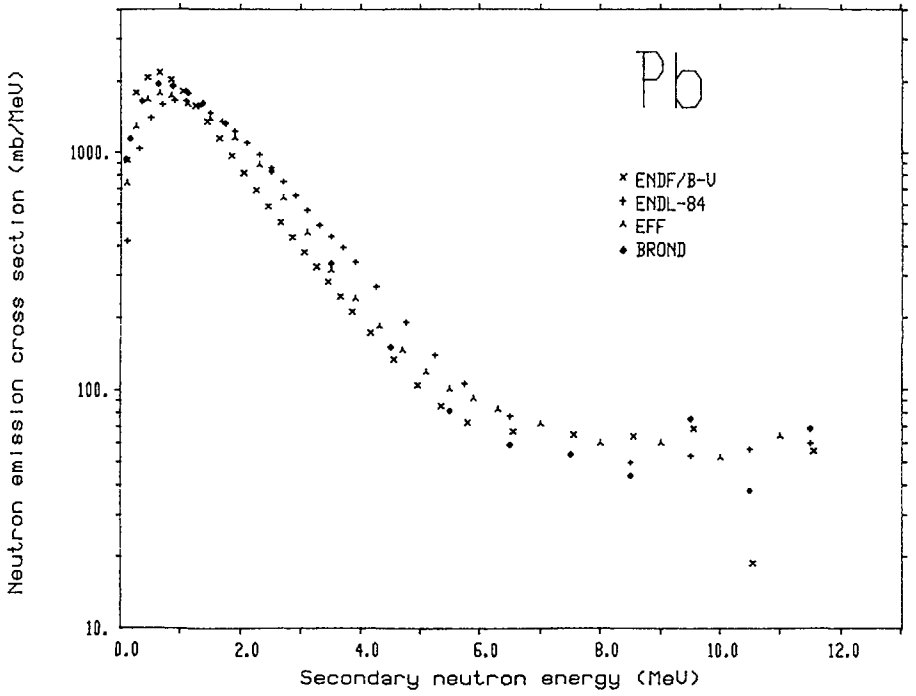

Fig. 10: Comparison of evaluations for the angle-integrated secondary neutron emission cross-section of lead for 14.1. MeV incident neutrons

ENDL-84	(1984)	EFF-1	(1986)
ENDF/B-V	(Mod.2)	BROND	(1986)

This figure shows our present capability to calculate energy spectra of neutrons because we can compare it with the "true values" displayed in Fig. 2. From this comparison one can see:

a) All evaluations deviate from the experimental "best values" by not more than about 20 %.

b) The deviations between the different evaluations are of about the size of the deviation of the evaluations from the "true values", thus comparison of Figs. 10 and 2 confirms the conjecture that realistic uncertainty estimates can be derived from comparison of different evaluations.

c) Comparison of Figs. 2 and 10 further shows that an average of the shown evaluations gives a better description of the true cross-sections than the individual evaluations.

d) One can clearly see the progress achieved in the most recent evaluation work. The two 1986 evaluations (EFF-1 and BROND) are definitely in better agreement with each other and with experiment than the two older ones. It appears that a 10 % accuracy in evaluated secondary neutron emission cross-sections may be achievable.

Of course one has to use some caution if one really wants to extract quantitative uncertainty information from such comparisons. Excellent agreement between just two evaluations (as in Figs. 6-9) may occur by chance and even if more than two evaluations exist there may be common uncertainties.

Just now, however, we have the fortunate situation that several new evaluations of the most important nuclei are to appear in near future due to the release of ENDF/B-VI, JEF-2, JENDL-3 and the Chinese and Russian evaluation work. Therefore it appears to me that a detailed comparison of these evaluations will be the fastest and easiest way to derive meaningful error estimates for all the new evaluations. One could obviously create an even better evaluation by forming an average between the different evaluations which all have the same ENDF/B format.

It appears to me that the IAEA should try to initiate and coordinate such a truly world-wide effort.

ACKNOWLEDGEMENTS

The author gratefully acknowledges the support from Dr. A. Pavlik, Dr. B. Strohmaier, Dr. S. Tagesen and Dr. M. Uhl in preparing this lecture.

REFERENCES

/1/ H. Vonach and S. Tagesen, Proc. Int. Conf. on Nuclear Data Evaluation Methods and Procedures, Brookhaven, Sept. 1980, Rpt. BNL-NCA 51363 Vol. II, p. 621

/2/ S. Tagesen, H. Vonach and B. Strohmaier, Physics Data 13-1 (1979) Fachinformationszentrum Karlsruhe, Germany

/3/ B. Strohmaier, S. Tagesen and H. Vonach, Physics Data 13-2 (1980) Fachinformationszentrum Karlsruhe, Germany

/4/ A. Pavlik and H. Vonach, Physics Data, Fachinformationszentrum Karlsruhe (to be published)

/5/ A.D. Carlson et al., Proc. Int. Conf. on Nuclear Data for Basic and Applied Science, Santa Fe, May 1985, Vol. 2, p. 1429, Gordon and Breach, New York 1986

/6/ B. Strohmaier and M. Uhl, Proc. Int. Conf. on Nuclear Data for Science and Technology, Antwerp, Sept. 1982, p. 552, Reidel Pub. Comp. Dordrecht 1983

/7/ E.D. Arthur and P.G. Young, Rpt. LA-8626-MS (ENDF-304) (1980)

/8/ ENDL-84, The Lawrence Livermore National Laboratory Evaluated Nuclear Data Library; data received from IAEA Nuclear Data Section

/9/ P.G. Young, priv. comm.

/10/ H. Gruppelaar, priv. comm.

/11/ D. Hermsdorf, Rpt. INDC (GDR)-039/L (1986)

OPTICAL POTENTIAL

(Session II)

THE NEUTRON OPTICAL MODEL POTENTIAL

P.E. HODGSON
Nuclear Physics Laboratory,
Oxford University,
Oxford, United Kingdom

Abstract

The present status of optical model calculations of neutron scattering and interactions is reviewed, with special emphasis on more recent developments and the more promising lines of research. The use of dispersion relations to provide an extra constraint on the potential is discussed, together with their application to studies of the Fermi surface anomaly. The application of potential inversion techniques to determine the form of the potential is also considered.

1. Introduction

The neutron optical potential remains an essential tool for analyses of neutron scattering and reaction data, and continuing efforts are devoted to determining it with higher precision over a wide range of energies and nuclei. Many precise optical model analyses have been made with potentials adjusted to optimse the fits either to individual nuclei or to ranges of nuclei across the periodic table. The parameters of these potentials have been tabulated (Perey and Perey, 1974, 1976) and the results of many analyses discussed in review articles (Hodgson, 1971, 1984ab).

This work will certainly continue, and enough new analyses have been made since the last review to provide material for a new review. However it is more interesting to concentrate on work that embodies new ideas, and to try to assess their usefulness for the practical problems of understanding and describing neutron interactions.

In recent years neutron analyses have greatly increased in accuracy, and it has become clear that a simple optical model parametrisation is no longer able to give acceptable fits to the experimental data. In particular, the depth of the real potential shows a non-linear behaviour around the Fermi surface; this is often referred to as the Fermi surface anomaly. Precision analyses have also shown that it is no longer adequate to assume that the radius of the real potential is independent of neutron energy.

It is of course possible to accommodate these and other departures from the simple optical model by more complicated parametrisations, but in the absence of theoretical guidance concerning the form of the parametrisation these are inevitably arbitrary and are unlikely to be applicable outside the domain where they are fitted to experimental data. What is required is a theoretical understanding of these anomalies that gives the most appropriate form of the potential, so that when it is fitted to a restricted range of data it can be extrapolated over a wider energy range with some confidence because it has a sound physical basis.

This theoretical understanding is provided by the dispersion relations that connect the real and imaginary parts of the optical potential. These have indeed been known for some time, but it is only in recent years that the neutron data has achieved the precision that enables them to be fully exploited. Several detailed analyses have now shown that they are able to account in some detail for the apparently anomalous behaviour of some optical model parameters, and thus make possible a consistent and accurate analysis of neutron data that has a sound physical basis.

In this review we are concerned with energies up to about 50 MeV. At the higher energies in this range the analysis is straightforward since only shape elastic processes contribute. At lower energies the analysis is complicated by the presence of compound elastic processes: the cross-sections fluctuate with energy and the energy average can be calculated from statistical theory. Inevitably this reduces the accuracy attainable. At low energies rather few partial waves contribute to the scattering, and this raises the question of the adequacy of the optical model description.

A broader view of the problem of determining the low-energy neutron optical potential may be obtained by setting it within the context of the concept of the nuclear mean field that extends from negative to positive energies. This potential behaves in a continuous way over the whole energy region: the overall nearly-linear variation of the real part of the potential is the Hartree-Fock field, and its energy dependence is attributable to the use of local instead of a non-local form for the potential. At negative energies the potential is defined by the bound single-particle states. The imaginary part of the potential also varies continuously, and at negative energies is defined in terms of the energy spread of the fragmentation of the single-particle states due to the residual interactions.

The energy variation of the imaginary part of the potential is centred on the Fermi energy, and close examination of the real part shows that it departs from linearity around the Fermi energy. This is the so-called Fermi surface anomaly, which perhaps should be called the Fermi surface effect, since it is now well understood. This effect significantly alters the optical potential in the energy region about 20 MeV either side of the Fermi surface, and so is important in the energy region covered by this review.

From this broader point of view of the optical potential we can use a much wider range of data to determine the low energy neutron optical potential: not only the elastic scattering and total cross-section data in this energy region but also the data on bound single-particle states. Furthermore, the real and imaginary parts of the potential are connected by the dispersion relations, and this not only explains the Fermi surface effect but also determines the parameters of the potential with higher precision.

In Section 2 the nuclear mean field is discussed in more detail, and in the following section its detailed parametrisation is given, with particular attention to the aspects that are inconsistent with the standard parametrisation. In Section 4 the dispersion relations are described and expressed in a form suitable for the analysis of experimental data. Some results obtained by applying the dispersion relations are summarised in Section 5, and conclusions drawn concerning the form of the optical potential. In Section 6 we return to the problem of the 'fine structure' of the optical potential, and summarise the present situation. Finally in Section 7 some results obtained by applying potential inversion techniques to determine the radial form of the potential are described.

2. The Nuclear Mean Field

The one-body potential between a nucleon and a nucleus is a concept that has been extensively used to unify a wide range of phenomena in nuclear structure and nuclear reaction physics. At negative energies, the eigenvalues of the potential may be identified with the centroid energies of the bound single-particle states and at positive energies the potential gives the differential cross-sections and polarisations of nucleons scattered by nuclei.

Many studies of both bound and scattering states have enabled the parameters of the potential for a wide range of nuclei to be established with some precision. The centroid energies of the bound single-particle states can be obtained from distorted wave analyses of the cross-sections of nucleon transfer reactions, together with the widths of the fragment distributions. These energies and widths can be described quite accurately for a range of nuclei by a real potential with parameters that depend only on the mass number and the nuclear asymmetry parameter (Millener and Hodgson, 1973; Malaguti and Hodgson, 1973). Furthermore, this potential can be used, in conjunction with single-particle occupation numbers also derived from analyses of nucleon transfer reactions, to calculate nuclear charge and matter distributions that are in gocd accord with the experimental data (Malaguti *et al*, 1978, 1979ab, 1982, Brown *et al* 1979, 1984; Ray and Hodgson, 1979.

This potential varies with energy in a continuous way from the negative energies appropriate to the bound states to the positive energies of the scattering states. This energy variation has been described for the real central term by Bauer *et al* (1982), and for the spin-orbit term by Cooper and Hodgson (1980). The imaginary term is included in the optical potential for scattering states in order to account for the flux removed from the elastic channel by non-elastic processes. It can also be defined for negative energies by relating it to the width of the single-particle fragment distribution.

In all these analyses the real and imaginary parts of the optical potential are adjusted independently to fit the experimental data. There is however an important connection between them provided by the dispersion relations (Hodgson, 1984; Mahaux *et al* 1985), and these give an additional constraint that can be used to define the potential more precisely. It is the principal aim of this paper to describe how this can be done, and to evaluate the advantages of this method of analysis.

3. Phenomenological Characteristics of the Nucleon Optical Potential

We begin this section by summarising the overall characteristics of the nucleon optical potential, as determined by phenomenological analyses of elastic scattering and polarisations. For convenience of calculation the optical potential is written in the form

$$V(r) = V_c(r) + U f_u(r) + iW g(r) + \left(\frac{\hbar^2}{m_\pi c}\right)^2 \frac{1}{r} U_S \frac{df_s}{dr} \mathbf{L}.\boldsymbol{\sigma} \qquad (3.1)$$

where $V_c(r)$ is the electrostatic potential of the nucleus (included only in the proton optical potential), U, W and U_S are the real, imaginary and spin-orbit potential depths and the form factors $f_i(r) = [1 + \exp\{(r - R_i)/a_i\}]^{-1}$, $g(r) = f_W(r)$ (Saxon-Woods or volume form) or $g_s(r) = -4a_W df_W(r)/dr$ (derivative Saxon-Woods or surface form).

These form factors are no more than approximate representations of the radial variations of the potentials, and it will be shown below that there are important differences between them and the more precise forms revealed by the dispersion relations and by the potential inversion techniques.

Many analyses of experimental data have shown that the real potential depth U decreases almost linearly with nucleon energy, and in addition shows some non-linear behaviour in the region of the Fermi energy, as shown in Fig.3.1. The overall dependence can be expressed as a function of energy (Bauer *et al* 1982)

$$U = 52.4 - (0.37 \pm 0.02)E + (0.0007 \pm 0.0001)E^2 + 24\frac{N-Z}{A} + 0.4\frac{Z}{A^{1/3}}. \qquad (3.2)$$

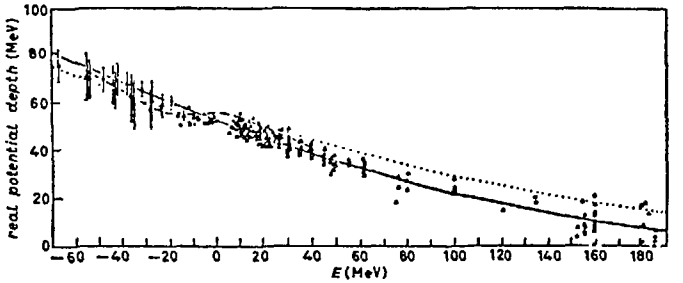

FIG.3.1.

Depth of real central optical potential for protons as a function of proton energy, corrected for the isospin and Coulomb terms. The curves refer to the quadratic fit (full curve) and to the calculations of Brown *et al* (1979) (dotted curve) and of Mahaux and Ngô (1981) (dashed curve) (Bauer *et al*, 1982).

This smoothly-varying part of the potential is identified as the Hartree-Fock field, and its energy dependence is attributed to the non-locality of the potential. The anomalous behaviour in the vicinity of the Fermi surface, called the Fermi Surface Anomaly, is attributed to the effect of coupling to non-elastic channels.

The spin-orbit potential has a small energy dependence that can be represented for the whole energy range from negative to positive energies by (Cooper and Hodgson, 1980)

$$U_s = 6.5 - 0.023E \qquad (3.3)$$

The energy variations of the real potential shown in Fig.3.1 can be conveniently described by an effective mass m^* defined by (Hodgson, 1983)

$$\frac{m^*}{m} = 1 + \frac{dV}{dE} \qquad (3.4)$$

Since the overall energy variation (3.2) and the Fermi surface anomaly have distinct physical origins it is useful to describe them by separate effective masses $\tilde{m}$ and $\bar{m}$ defined respectively by

$$\frac{\tilde{m}}{m} = \left(1 - \frac{m}{k}\frac{\partial V}{\partial k}\right)^{-1} \quad \text{and} \quad \frac{\bar{m}}{m} = 1 + \frac{\partial V}{\partial E} \qquad (3.5)$$

The overall energy variation then gives

$$\frac{\tilde{m}}{m} = 0.73 + 0.0007E \qquad (3.6)$$

The Fermi surface anomaly is described by an effective mass that peaks at the Fermi energy and Brown, Dehesa and Speth (1979) have proposed for the total effective mass the expression

$$\frac{m^*}{m} = 0.64 + \frac{0.36}{[1 + |E - E_F|/2\hbar\omega_0]^2} \qquad (3.7)$$

where $\hbar\omega_0 = 41A^{1/3}$. The energy variation corresponding to this expression is included in Fig.3.1.

The energy dependence of the imaginary potential is more difficult to determine because the form factor has predominantly the surface form at low energies, changing continuously to the volume form at higher energies. Furthermore, the experimental data do not fix the strength of the imaginary potential as accurately as that of the real part. At low energies the energy variation of the imaginary potential determined from analyses assuming only a volume form is approximately (see Fig.5.2)

$$W = W_0(E - E_F)^2 \tag{3.8}$$

More precise optical model analyses have provided evidence that the parametrisation (3.1) is inadequate. In particular, there is evidence that the radial dependence is not adequately represented by the Saxon-Woods form (Hodgson 1984) and that if nevertheless it is constrained to have the Saxon-Woods form then the radius and diffuseness parameters vary with energy.

As an example of such work, analyses of experimental data on the elastic scattering of 30, 40 and 61.4 MeV protons by ^{208}Pb and several other nuclei by Sinha and Edwards (1970, 1971) showed that an improved fit to the differential cross-section is obtained by adding a surface-peaked potential of the Saxon-Woods derivative form to the usual Saxon-Woods potential. Initially they interpreted this additional potential as an isospin term, but this possibility was later excluded when it was found that the improvement persists in nuclei like ^{40}Ca, for which the isospin term must be zero.

Another example is provided by the work of Finlay *et al* (1985) on the scattering of 7 and 22 MeV neutrons by ^{208}Pb. Optical model analyses of the differential cross-sections gave significantly different values of the geometrical parameters at the two energies: $r_R = 1.254$. $r_I = 1.31$ fm at 7 MeV and $r_R = 1.18$, $r_I = 1.26$ fm at 22 MeV. It was found possible to fit these and other data from 0 to 24 MeV with potentials having energy-dependent geometrical parameters $r_R = 1.302 - 0.0055E$, $r_I = 1.363 - 0.0042E$, $a_I = 0.7$ and $a_R = 0.162 + 0.019$ fm. If the data are analysed with energy-independent form factor parameters the overall fits are significantly poorer, and the optimum real potential depth departs from the linear dependence at low energies. The volume integral of the real potential shows an anomalous departure from linearity with energy in the region of the Fermi Surface.

Subsequently, detailed optical model analyses of the elastic scattering of neutrons by yttrium and bismuth have also provided evidence for energy-dependent form factor parameters (Lawson, Guenther and Smith 1986, 1987).

4. The Dispersion Relations

Theoretical studies of the optical potential show that it is complex and also non-local both in space and in time. The spatial non-locality is equivalent to a momentum dependence and the temporal non-locality to an energy dependence and so we write it as $V(k, E)$. It is an analytic function of the energy and therefore satisfies the dispersion relation

$$V(k,E) = \frac{1}{2\pi i}\int_c \frac{V(k,E')}{E' - E}dE' \tag{4.1}$$

Since the potential is complex it may be separated into real and imaginary parts

$$V(k,E) = V(k,E) + iW(k,E) \tag{4.2}$$

Substituting into (4.1) and separating into real and imaginary parts gives

$$V(k,E) = \frac{1}{2\pi}\int_{-\infty}^{\infty} \frac{W(k,E')}{E' - E}dE' \tag{4.3}$$

$$W(k,E) = \frac{1}{2\pi}\int_{-\infty}^{\infty} \frac{V(k,E')}{E' - E}dE' \tag{4.4}$$

These dispersion relations connect the real and imaginary parts of the optical potential, and thus impose additional constraints on the phenomenological analyses.

To apply them to the analysis of experimental data, we separate the real potential into the Hartree-Fock field $V_{HF}(k)$ that depends only on the momentum and an energy-dependent part $V(E)$, giving

$$V(k,E) = V_{HF}(k) + \frac{1}{2\pi}\int_{-\infty}^{\infty} \frac{W(E')}{E' - E}dE' \tag{4.5}$$

This provides the required connection between the real and imaginary parts of the phenomenological potential, and also enables us to understand the empirical energy dependence shown in Fig.3.1. The overall linear energy dependence is attributed to the Hartree-Fock field, and the 'anomalous' behaviour centred on the Fermi energy is attributed to the effect of the imaginary potential.

The practical application of the dispersion-relation (4.5) encounters the difficulty that the integral of the imaginary part of the potential extends over an infinite energy range. This may be overcome in two ways, firstly by separating the imaginary potential into two parts and secondly by using subtracted dispersion relations. These will now be discussed.

The first method depends on a separation of the imaginary potential into surface-peaked and volume components

$$W(r) = W_s(r) + W_v(r) \tag{4.6}$$

Phenomenological optical model analyses with both surface-peaked and volume imaginary potentials show that the former dominates at low energies while the latter becomes important only for energies of some tens of MeV. Each gives a contribution to the real potential of its own radial form. Since the major part of the real optical potential $V_{HF}(r)$ has the volume form $W_v(r)$ has the effect of altering its depth by a rather small amount at energies far from the Fermi energy and thus has the effect of altering the curvature of $V_{HF}(E)$.

The surface-peaked potential $W_S(r)$ however gives a small surface-peaked addition to the real potential centred at the Fermi energy, and this has the effect of increasing its radius. Since most of the phenomenological analyses are made with fixed radius R this implies a phenomenological potential of increased depth.

The second method uses subtracted dispersion relations. From (4.5) we obtain

$$V(K,E) - V(K,E_F) = \frac{(E-E_F)}{2\pi i}\int_{-\infty}^{\infty} \frac{W(E')}{(E'-E)(E'-E_F)}dE' \qquad (4.7)$$

This integral converges sufficiently rapidly for it to be evaluated unambiguously. It is therefore possible to use phenomenological values of $W(E)$ obtained from analyses with the volume form only. Mahaux and Ngô have divided this integral into two parts corresponding to the polarisation contributions from energies above the Fermi surface and correlation contributions from energies below the Fermi surface.

All the potentials in these dispersion relations are r-dependent, with the parametrisation described in Section 3. The phenomenological analyses however determine certain moments of the potential with greater accuracy than the individual parameters of the potential. It is thus often useful to work with dispersion relations integrated over the radial variable. Particularly useful is the volume integral per nucleon defined by

$$J_V = \frac{4\pi}{A}\int_0^{\infty} V(r)r^2 dr \qquad (4.8)$$

The corresponding dispersion relation is

$$J_V(E) = J_V^{HF}(k) + \frac{1}{2\pi}\int_{-\infty}^{\infty} \frac{J_W(E')}{E'-E}dE' \qquad (4.9)$$

In general one can define the q^{th} moment of the potential

$$J_V^{(q)} = \frac{4\pi}{A}\int_0^{\infty} V(r)r^q dr \qquad (4.10)$$

which satisfies the dispersion relation

$$J_V^{(q)}(E) = J_V^{(q)HF}(k) + \frac{1}{2\pi}\int_{-\infty}^{\infty} \frac{J_W^{(q)}(E')}{E'-E}dE' \qquad (4.11)$$

Subtracted dispersion relations for the integrated potentials can be defined as before.

The physical reason for the Fermi potential anomaly is the coupling between the elastic and inelastic channels, which is greatest when the incident energy is comparable with the energies of the excited states. The effect of the inelastic scattering given either by the complete set of coupled equations connecting the wavefunctions in all open channels or by the imaginary potential in the simple phenomenological optical model. It is thus possible to calculate the effect on the real potential in the simple optical model of the coupling to inelastic channels by using the coupled-channels formalism to generate a differential cross-section and then fitting it with an optical potential. Several analyses made in this way have confirmed that the coupling to inelastic channels does produce changes in the real potential similar to the observed Fermi potential anomaly (Gyarmati *et al*, 1981).

5. Applications of the Dispersion Relations

In this section we describe several applications of dispersion relations to elastic scattering data that account for the Fermi surface anomaly and also show how the optical potentials can be extrapolated from positive to negative energies.

Ahmad and Haider (1976) used the dispersion relation (4.5) to calculate the surface-peaked component of the real potential from the surface-peaked component of the imaginary potential. For this analysis, they used the potentials found by Van Oers (1971) for 10-60 MeV protons elastically scattered by ^{40}Ca. The depths of the surface-peaked potentials, together with the resulting surface-peaked real potential, is shown in Fig.5.1.

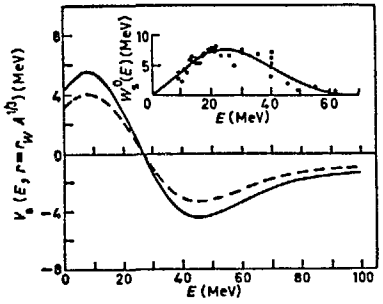

FIG.5.1.

The real surface-peaked component V_S of the optical potential as a function of energy for $a_w = 0.549$ (full curve) and $a_w = 0.732$ (dashed curve). The inset shows the imaginary surface-peaked potential as a function of energy obtained by Van Oers (1971) from an optical model analysis of the elastic scattering of protons by ^{40}Ca (Ahmad and Haider, 1976).

This calculation was possible because the surface-peaked imaginary potential falls to zero around 60 MeV, so that the dispersion integral converges. The analysis is however subject to the difficulty that it is not possible to separate the volume and surface-peaked components very accurately by a purely phenomenological analysis. If the imaginary potential is taken to have only the volume form, the depth may be determined more accurately, and convergence can still be obtained by using the subtracted dispersion relation (4.7). This was done by Mahaux and Ngô (1979), using the energy variation of the imaginary potential shown in Fig.5.2. The values of the strength of the imaginary potential were obtained from single-particle spreading widths for negative energies, from neutron strength functions at small positive energies and from elastic scattering data at higher energies. These data show some scatter, but at small values of $(E - E_F)$ they are consistent with the quadratic form

$$W \propto (E - E_F)^2 \qquad (5.1)$$

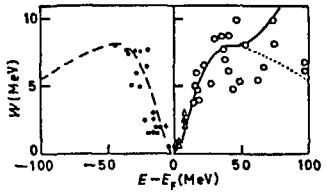

FIG.5.2.

Energy dependence of the imaginary part of the optical potential for medium-light nuclei (Mahaux and Ngô, 1979).

At energies more than 40 MeV above or below the Fermi surface the value of the imaginary potential is very uncertain, but use of the subtracted dispersion relation ensures that this has little effect on the calculation of the real part of the potential.

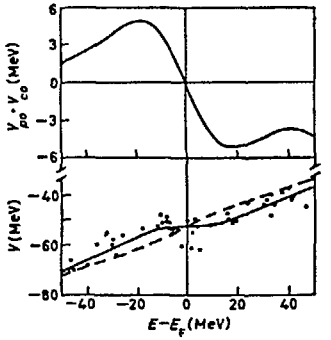

FIG.5.3.

The sum of the polarisation and correlation contributions to the real part of the optical potential, together with the total real potential as a function of energy (Mahaux and Ngô, 1979).

The results of this calculation are shown in Fig.5.3. In the analysis, they split the dispersion integral into two parts corresponding to the polarisation contributions from energies above the Fermi surface and the correlation contributions from energies below the Fermi surface. When these are added together it is found that the result is quite similar for energies less than 40 MeV to that obtained by Ahmad and Haider (noting the difference in sign between the definitions of the real potential). The energy variation of the effective mass corresponding to the polarisation and correlation contributions were obtained using (4.7) and are shown in Fig.5.4. Combining this with the value

of $\tilde{m}$ obtained from the overall energy variation gives the results for m^* also included in this figure. Similar results for the energy variation of the effective mass have also been obtained from nuclear structure calculations (Bortignon *et al*, 1982).

This peaking of the effective mass in the region of the Fermi surface describes the Fermi surface anomaly and enables the energy variation of the real part of the potential to be calculated. The results are shown in Figs.3.1 and 5.3.

The dispersion relations can also be used to extrapolate the optical potential from positive to negative energies. Smith, Guenther and Lawson (1985) has done this for the potential describing the elastic scattering of neutrons by ^{93}Nb using the dispersion relation (4.9) for the volume integrals of the potential. Phenomenological optical model analyses of the differential cross-sections for the elastic-scattering of 2–14 MeV neutrons by ^{93}Nb gave potentials with volume integrals with the energy variations

$$\left.\begin{aligned} J_V^{(E)} &= 445 - 2.4E \\ J_W^{(E)} &= 52 + 3E \end{aligned}\right\} 0 \le E \le 14 \text{ MeV} \qquad (5.2)$$

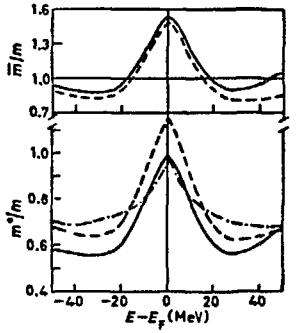

FIG.5.4.

The energy variation of the effective masses $\tilde{m}/m$ and m^*/m around the Fermi energy obtained using the dispersion relation (3.7) from the energy-dependent imaginary potential shown in Fig.5.2 (full curve). The dashed curve corresponds to the parametrisation (2.8) (Mahaux and Ngô, 1979).

To apply the dispersion relation the energy variation of J_W outside this range was described by the expressions

$$\begin{aligned} & J_W^{(E)} = 102 - 0.6E \quad \text{for } E > 14 \text{ MeV} \\ \text{and} \quad & J_W^{(E)} = 0.52(E+10)^2 \quad \text{for } -20 \le E \le 0 \text{ MeV} \end{aligned} \qquad (5.3)$$

This enabled the energy variation of $J_V(E)$ to be calculated for negative energies, and the result is shown in Fig.5.5. At negative energies it can be compared with the integrals of the potentials corresponding to discrete bound states. Subsequently similar analyses have been made for the potential describing the scattering of neutrons by yttrium and bismuth (Lawson *et al* 1986, 1987).

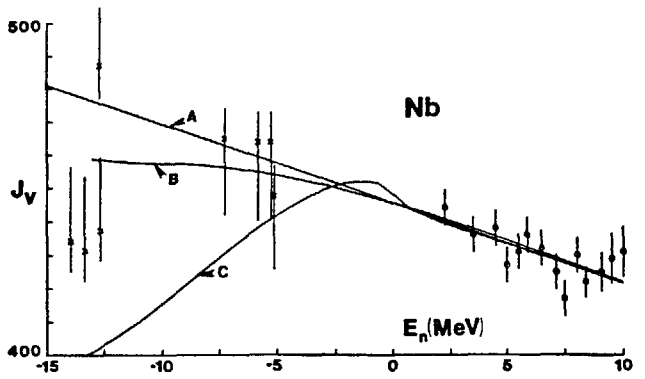

FIG.5.5.

Volume integral per nucleon of the real neutron potential for ^{93}Nb for bound and unbound energies. The points at positive energies are obtained from optical model analyses of elastic scattering data and those at negative energies from the binding energies of particle and hole state. The curves show: A, a linear fit to the scattering data; B, the energy variation calculated from the expression of Brown *et al* and C, calculated from a dispersion relation formula (Smith, Guenther and Lawson 1985).

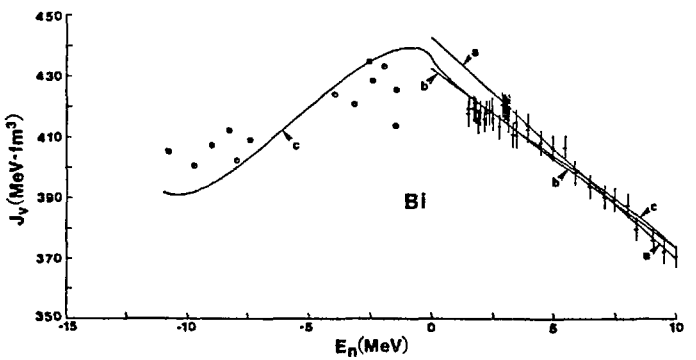

FIG.5.6.

Volume integral per nucleon of the real neutron potential for ^{209}Bi for bound and unbound energies. The points at positive energies are obtained from optical model analyses of elastic scattering data and those at negative energies from the binding energies of particle and hole states. The curves show: a, a linear fit to the scattering data from 4.5 to 10 MeV; b, a linear fit to all scattering data; c, calculated from a dispersion relation formula (Lawson, Guenther and Smith, 1987).

The results for bismuth are of particular interest because of the relatively large number of single-particle states that can be used to determine the potential at negative energies. As shown in Fig.5.6, the curve obtained using the dispersion relations fits the overall trend of this data quite well.

The dispersion relations (4.11) for the moments of the potential have been used by Mahaux and Sartor to extrapolate to negative energies the potential for neutrons scattered by ^{208}Pb. They calculated the moments corresponding to q = 0.8, 2 and 4 and noted that these moments suffice to define the three parameters U, R and a of the real part of the optical potential. To apply the dispersion relations, they represent the energy variation of the moments of the imaginary potential by the expression due to Brown and Rho (1981)

$$J_W^{(q)}(E) = -W_q \frac{(E-E_F)^2}{(E-E_F)^2+\sigma_q^2} \tag{5.4}$$

This is compared with the experimental data for q = 2 in Fig.5.7. They also assumed that the moments of the Hartree-Fock field have a linear energy dependence given by

$$J_V^{HF(q)}(E) = B_q + C_q E \tag{5.5}$$

These two expressions were then inserted in the dispersion relation (4.11) and the parameters B_q and C_q adjusted to optimise the fit to the data, with the result for q = 2 shown in Fig.5.7b. This clearly shows the anomaly in the region of the Fermi surface. The extrapolation to negative energies can be compared with the potentials

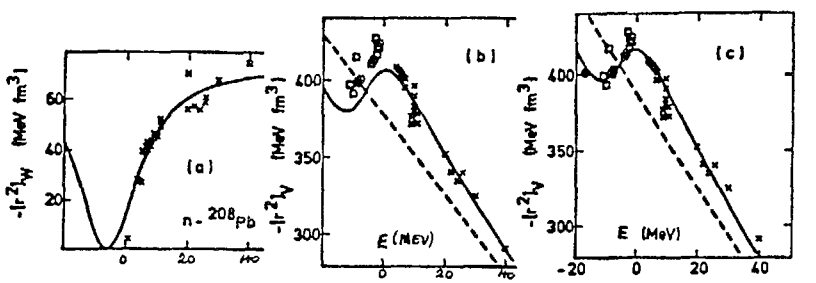

FIG.5 7.

The energy dependence of the volume integrals of (a) the imaginary and (b) and (c) the real parts of the optical potential for neutrons on ^{208}Pb. The crosses are empirical values from phenomenological optical potentials. The curve in (a) is a least squares fit using the parametrisation (5.4). The curves in (b) are the calculated values of $J_V^{(2)HF} = B_2 + C_2 E$ (dashed line) and of $J_V^{(2)}$ (solid curve) obtained by determining B_2 and C_2 by a least squares fit to the scattering data (crosses). The open squares show the experimental values of $J_V^{(2)}(E_j)$ for the bound single-particle states obtained by adjusting the Saxon-Woods potential depths $U_V(E_j)$ using the shape parameters $R_V(E_j)$ and $a_V(E_j)$ obtained from the extrapolated values of $J_V^{(q)}(E_j)$ for q = 0.8, 2 and 4. The curves in (c) are similar except that the open squares are included in the data set used to determine B_q and C_q. The full dot gives the result for the $h_{11/2}$ state (Mahaux and Sartor, 1986).

corresponding to the neutron bound states, and shows qualitative agreement. The fit to these states was improved by adding a spin-orbit term to the potential to allow the energies of these bound states to be calculated and then repeating the fitting procedure including both the scattering and the bound state data. This gives the result shown in Fig.5.7c, which is in excellent agreement with the data. The curve was further extrapolated to the deeply bound $1h_{11/2}$ state at -15.9 MeV and good agreement found.

The resulting energy variations of the three moments of the potential enable the parameters of the potential to be determined as a function of energy, and these are shown in Fig.5.8. The dashed lines correspond to the Hartree-Fock potential alone and the full lines show the effect of adding the dispersive correction. This figure shows the limitations of the Saxon-Woods parametrisation of the optical potential.

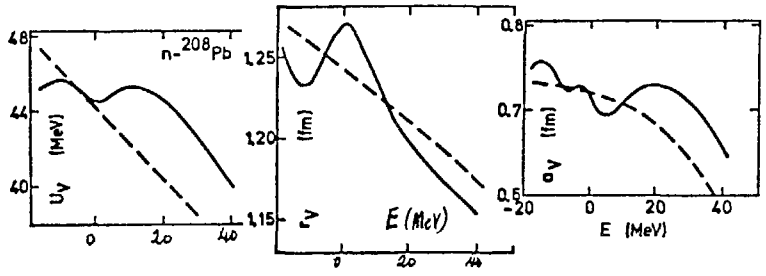

FIG.5.8.

The energy dependence of the parameters of the real part of the Saxon-Woods optical potential. The dashed curves were obtained from the moments $J_{HF}^{(q)HF}(E)$ of the Hartree-Fock field for $q = 0.8$, 2 and 4. The solid curves were obtained from the moments $J_V^{(q)}(E)$ of the real part of the complete potential (Mahaux and Sartor, 1986).

A particularly detailed analysis of the interaction of neutrons with ^{208}Pb from -20 to $+165$ MeV has been carried out by Johnson, Horen and Mahaux (1987) making full use of the dispersion relations to constrain the values of the parameters of the potential. The Hartree-Fock field was described by a Saxon-Woods potential with parameters $V_H = 46.4$ MeV, $r_0 = 1.24$ fm and $a = 0.68$ fm at the Fermi energy (-6 MeV) with an energy dependence $\exp(-\alpha E)$, where $\alpha = (m/2\hbar^2)\beta^2$ and $\beta = 0.74$ fm; this gives

$$V_H(E) = 46.4 - 0.31(E - E_F) \qquad (5.6)$$

in the vicinity of the Fermi surface.

The imaginary part of the optical potential was assumed to be symmetric about the Fermi energy and to consist of surface-peaked and volume components with depths represented by the linear segments shown in Fig.5.9. The parameters defining these segments and the associated energy-independent radius and diffuseness parameters were determined by analysis of the experimental data. The dispersive corrections to the real part of the potential obtained by inserting these surface-peaked and volume imaginary potentials in the dispersion relation (4.3) are also shown in Fig.5.9. The optimum

values of the real and imaginary potential depths obtained from this parametrisation are compared with the best fit values at each energy in Figs.5.10 and 5.11. Throughout this analysis the spin-orbit potential was fixed to the values $U_s = 5.75$ MeV, $r_s = 1.105$ fm, $a_s = 0.50$ fm.

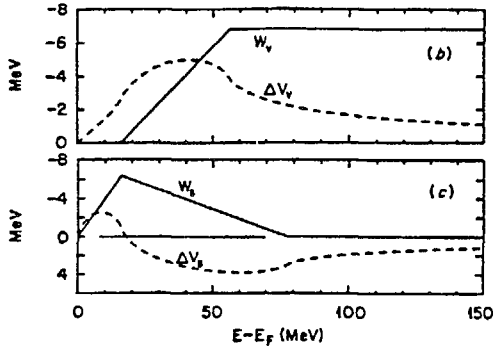

FIG.5.9.

The energy dependence of the depths of the volume and surface peaked components of the imaginary optical potential (full lines) together with the corresponding corrections to the real optical potential obtained using the dispersion relations (dashed curves) (Johnson *et al* 1987).

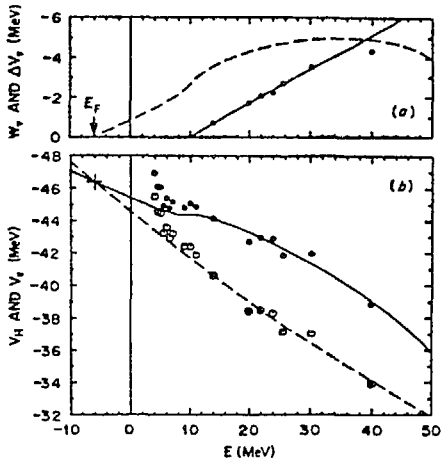

FIG.5.10.

(a) The depth of the volume imaginary potential (full line) compared with optical model analyses, together with the corresponding correction to the real potential obtained from the dispersion relation (dashed curve)
(b) The depth of the Hartree-Fock potential (dashed curve) and the total depth obtained by adding the dispersion correction (full curve) (Johnson *et al*, 1987).

This potential gives an excellent fit to the differential and total cross-sections and analysing powers for neutron scattering by ^{208}Pb, and also to the eigenvalues of the bound single-particle states and the values of the single-particle wavefunctions at large distances as determined from sub-Coulomb pick-up experiments. Furthermore, it automatically explains the special features of the potential that were found in previous optical model analyses, in particular the near-independence of the real potential depth on energy from 4 to about 20 MeV and the decrease with energy of the radius of the potential in the same energy region. Additional calculations showed that the fit to the data may be still further improved by allowing the potentials to depend on orbital angular momentum.

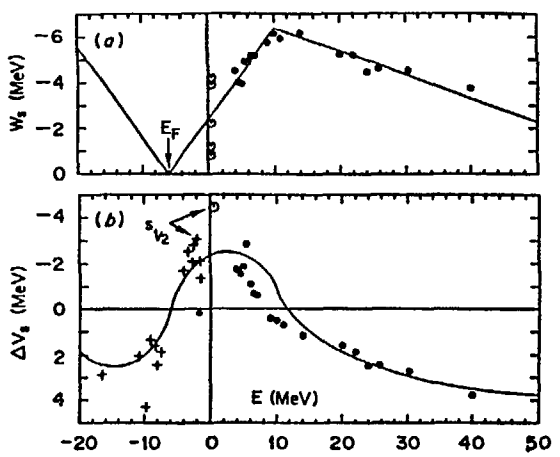

FIG.5.11.

(a) The depth of the surface imaginary potential (full line) compared with the results of optical model analyses.
(b) The depth of the dispersive correction to the real potential compared with the results of optical model analyses (solid points) and values obtained by the energies of bound single-particle states (crosses) (Johnson *et al*, 1987).

Another indication of the usefulness of the dispersion relations is provided by the analysis of the inelastic scattering of 5–11 MeV neutrons with excitation of the 3^- state in ^{208}Pb recently made by Cheema and Finlay (1987). Previous analyses gave a sharp increase of the deformation length for energies less than 11 MeV. Cheema and Finlay repeated the analysis using potentials and form factors that include the dispersion correction and found that the deformation lengths at low energies were reduced to values consistent with those obtained from data at higher energies.

Further support for the usefulness of the dispersion relations is provided by the analysis of the analysing power for the elastic scattering of 9.9 to 16.9 MeV neutrons by ^{40}Ca recently carried out by Delaroche and Tornow (1987). Previous analyses of the differential cross-sections and analysing powers required a small imaginary spin-orbit potential and even then the fits to the analysing powers were not satisfactory (Honoré *et al*, 1986). However when the analysis was repeated using potentials satisfying the dispersion relations a much improved fit to the analysing powers was obtained without an imaginary spin-orbit term, as shown in Fig.5.12.

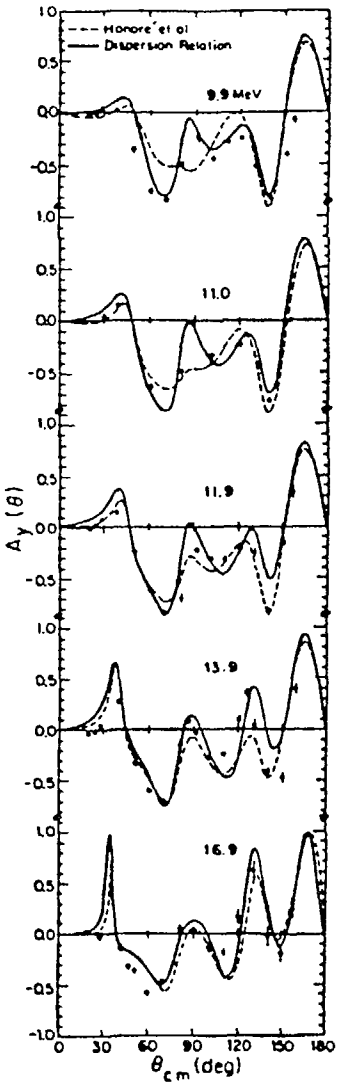

FIG.5.12.

Analysing powers for the elastic scattering of 9.9 to 16.9 MeV neutrons by ^{46}Ca compared with optical model calculations with an imaginary spin-orbit term (dashed curves) and without an imaginary spin-orbit term but using dispersion-relation potentials (full curves) (Delaroche and Tornow 1987).

6. The Fine Structure of the Optical Potential

Accurate optical model analyses of the differential cross-sections for the elastic scattering of protons by a series of medium weight nuclei have shown that the potential depth depends not only on the nuclear asymmetry parameter $\alpha = (N - Z)/A$ but also on the isospin $T_Z = \frac{1}{2}(N - Z)$ (Perey and Perey, 1968; Novo *et al*, 1981).

The available neutron data are not yet sufficiently accurate to show this effect but as it is very likely to be present it is appropriate to consider it here.

The fine structure in proton optical potentials shown by the 11 MeV data of Perey and Pery can be fitted by a variety of phenomenological expressions (Hodgson, 1970, 1985) of the form

$$V_p = V_0 - \gamma E + \beta A^{\alpha} + \epsilon V_1 + \gamma V_c \tag{6.1}$$

where $\epsilon = (N \sim Z)/A$ is the nuclear asymmetry parameter, V_1 is the isovector potential and γV_c the Coulomb correction term. Equally good fits to the data can be obtained with the exponent $\alpha = -\frac{1}{3}$, $\frac{1}{3}$ or 1, with corresponding optimised values of β. The dependence of the potential on the mass number is indeed suggested by the folding model.

A more fundamental explanation of the fine structure was provided by Yang and Rapaport (1986), who showed that it essentially disppears if the energy is measured from the Fermi surface. This gives

$$V_p = V_0 - \gamma(E - E_F) + \epsilon V_1 + \gamma V_c \tag{6.2}$$

It is notable that in their analysis they used values of $\gamma = 0.78$ at 11 MeV and $\gamma = 0.60$ at 14 MeV obtained from the analysis of Perey (1963). These are much higher than the value $\gamma = 0.3$ corresponding to the Hartree-Fock field and are a consequence of the additional term introduced by the coupling to higher states and given by the dispersion relation.

More recently, a very extensive global optical model analysis of proton and neutron elastic scattering data has been made by Varner *et al* (1987). They used a potential with a radius parameter

$$R = r_{00} + r_0 A^{1/3} \tag{6.3}$$

instead of the usual $R = r_0 A^{1/3}$. Their global potential fits the data very well, and thus accounts for the fine structure. The reason for this is probably that the more flexible parametrisation (6.3) of the radius parameter is essentially equivalent to the addition of the A-dependent term in (6.1), through the well-known VR^2 ambiguity. It may however be suggested that an equally good, and perhaps even better fit to the data would be obtained by measuring the energies from the Fermi surface and using the simpler parametrisation of the radius.

At higher energies, the 65 MeV data of Noro *et al* has been fitted by Haider *et al* (1984) using potentials obtained from Brueckner theory nuclear matter calculations. It remains to be shown that it can also be understood using the model of Yang and Rapaport, using the lower value of γ appropriate to the Hartree-Fock field.

7. Potential Inversion

The application of the dispersion relations as described in the previous sections shows how the Fermi potential anomaly can be understood as the addition of a surface-peaked imaginary term to the underlying volume term in the real part of the potential. All this work is carried out in the framework of the Saxon-Woods and derivative Saxon-Woods parametrisation of the real and imaginary parts of the potential. Since we are now looking at relatively fine details of the potential it may be asked whether this parametrisation is sufficiently accurate for the purposes. This question is given added weight by the analysies at higher energies that certainly show that the Saxon-Woods parametrisation of the real potential is inadequate.

It thus becomes important to see whether the Saxon-Woods potential is really satisfactory at low energies, and if not whether it can be improved. This can be done if the potential could be determined from the experimental data, without the use of standard analytical form factors. This is the classical potential inversion problem, to which much attention has been devoted over the years.

Potential inversion proceeds through the intermediate stage of the phase shifts or their equivalent scattering matrix elements S_L. The differential scattering cross-sections and polarisations can be expressed by simple analytical formulae in terms of the scattering matrix elements. It is thus relatively easy to obtain the matrix elements corresponding to a particular set of experimental data, providing it is sufficiently accurate. If it is not sufficiently accurate, there may be distinct sets of matrix elements that give equally good fits to the same set of data. The meaning of 'sufficiently accurate' can only be found in each case by detailed numerical analysis. Iterative methods have been devised to obtain the matrix elements from the data, using as starting values those obtained from a phenomenological optical model analysis.

The problem is then to determine the potential from the scattering matrix elements. There are very general theorems that enable the potential to be reconstructed from a knowledge of the matrix elements at all energies. What is needed, however, is a practical method of obtaining the potential from data at a limited set of energies, subject to some restrictions concerning the form of the potential. In general, the potential is highly non-local and dependent on the orbital angular momentum, and a set of data restricted to one or a few energies is certainly insufficient to determine all these features. It is thus necessary to restrict the potential to a form that is sufficiently flexible to explore the inadequacies of the Saxon-Woods parametrisation and yet not so general that it cannot be determined with sufficient accuracy. This may be achieved by allowing a genral radial dependence, but no non-locality, and in some cases by also allowing a parametrised angular momentum dependence.

A practical technique for potential inversion has been developed in recent years by Mackintosh and colleagues (Mackintosh 1979; Mackintosh and Kobos 1976, 1979; Ioannides and Mackintosh 1985, 1986, Mackintosh and Ioannides 1985). Their iterative perturbative procedure is based on the observation that the response of the scattering matrix elements S_L to perturbations in the optical potential are generally quite linear. The method begins with a reference potential $V_0(r)$ that can be the best phenomenological potential that determines a set of $S_L^{(0)}$ that are good approximations to the known accurate S_L obtained from the data. Next one selects a set of linearly independent potential perturbations $U_i(r)$ that enable the potential to be adjusted in a systematic and comprehensive way. For each of these the response $\Delta S_L^{i_v}$ of the S_L can be determined

$$S_L^{(1)} = S_L^{(0)} + \Delta S_L^{(i)} \tag{7.1}$$

Then we require that

$$S_L = S_L^{(0)} + \sum_i a_i \Delta S_L^{(i)} \tag{7.2}$$

Solution of this set of equations for the a_i gives the required potential

$$V(r) = V_0(r) + \sum_i a_i U_i(r) \tag{7.3}$$

Since the relation (7.2) is only approximately linear, the calculation must be iterated to convergence.

The practical details of this calculation, in particular the choice of basis functions, can only be studied numerically, and this gives information on the speed of convergence and the reliability of the potential obtained. Many such calculations have now been made by Mackintosh and colleagues, and as a result the iterative-perturbative procedure has been developed so that it can give reliable information on the potential for a variety of interactions.

In the present context we are primarily interested in whether the potential inversion method has produced any results relevant to the dispersion relations analysis of elastic scattering. In a recent survey Mackintosh and Ioannides (1985) remark that one limitation of their method is that it is unreliable at low energies, that is about 25 MeV for protons. Essentially this is because the small number of partial waves at these energies implies that the system is not sufficiently determined. The choice of basis functions is then critical and makes it difficult to establish a unique potential. This is a severe limitation in the present context, as we are mainly interested in lower energies. Nevertheless, there may still be relevant results that have been obtained by the potential inversion method.

When applied to accurate nucleon elastic scattering data, phenomenological analyses give very good overall fits but there remain significant deviations that correspond to quite high values of χ^2. These deviations certainly indicate inadequacies in the form of the potential used. Studies using the potential inversion method have now shown that precise fits to the data can be obtained by using either a L-dependent potential or one that oscillates radially (Kobos and Mackintosh, 1979). This has been done by inverting the S_L obtained from L-dependent potentials. Inversion of the S_L obtained from a L-dependent potential of the Majorana form $V(r)(1 + C(-)^L)$ gave potentials with the same volume integral as $V(r)$. Thus knowledge of the volume integral gives no information about possible L-dependence of the potential.

More relevant to the dispersion relations are the results of applying potential inversion to elastic and inelastic scattering simultaneously. As has been remarked already the physical origin of the Fermi surface anomaly is the coupling to inelastic channels; this coupling increases the imaginary part of the potential and thus affects the real part in a way that can be calculated using the dispersion relations. The coupled-channels formalism enables this to be studied explicitly. These coupled equations contain the so-called 'bare' potential and the equations themselves contain the coupling terms. If this is replaced by the single equation for the elastic channel alone, the optical potential now has to include implicitly the effects of the coupling. The relation between the 'bare' and 'dressed' potentials can be studied by finding the potentials in the two cases that give the same scattering matrix elements, and this can be done by the potential inversion method.

These calculations have been done both for inelastic scattering and for transfer reaction channels. As an example, Ioannides and Mackintosh have analysed the elastic and inelastic scattering of 104 MeV alpha-particles by ^{20}Ne, taking into account the coupling to the 2^+ and 4^+ excited states. They found that the volume integral of the real potential is $J_R = 367.5$ MeV fm^3 for the bare potential and 346.2 MeV fm^3 when the coupling to the excited states is included. This is just the enhancement of the potential that has been found phenomenologically and accounted for by the dispersion relation analysis. Subsequent calculations showed similar effects on proton potentials due to the coupling to pickup channels.

Acknowledgments

This review was finalised following discussions with Professors R.L. Walter and W. Tornow (Duke University), W.J. Thompson (University of North Carolina), B.A. Brown (Michigan State University) and R.W. Finlay (Ohio University) and I am grateful to them all for providing me with the opportunity to visit their universities, for their detailed comments and for kindly permitting me to quote the results of their unpublished work. I also acknowledge gratefully the receipt of unpublished work by C.H. Johnson, D.J. Horen and C. Mahaux, and by R.D. Lawson, P.T. Guenther and A.B. Smith.

References

Ahmad I and Haider W, 1976 *J. Phys.* **G2** L157

Bauer M, Hernandez-Saldana E, Hodgson P E and Quintanilla J, 1982 *J. Phys.* **G3** 525

Bortignon P F, Broglia R A, Dasso C H and Fu D-J, 1982 *Phys. Lett.* **B108** 247

Brown B A, Bronk C R and Hodgson P E, 1984 *J. Phys.* **G10** 1683

Brown B A, Massen S E and Hodgson P E, 1979 *Phys. Lett.* **85B** 167

Brown G E, Dehesa J S and Speth J, 1979 *Nucl. Phys.* **A330** 290

Brown G E and Rho M, 1981 *Nucl. Phys.* **A372** 397

Cheema T S and Finlay R W, 1987 Proceedings of the Kiev Conference

Cooper S G and Hodgson P E, 1980 *J. Phys.* **G6** L21

Delaroche J P and Tornow W, 1987 *Phys. Lett.* (In press)

Finlay R W, Annand J R M, Petler J R and Dietrich F S, 1985 *Phys. Lett.* **155B** 313; 1987 Private communication

Finlay R W, 1987 Proceedings of the Kiev Conference

Gyarmati B, Lovas R G, Vertse T and Hodgson P E, 1981 *J. Phys.* **G7** L209

Haider W, Kobos A M, Rook J R and Pal K F, 1984 *Nucl. Phys.* **A419** 521

Hodgson P E, 1970 *Nucl. Phys.* **A150** 1; 1983 *Contemp. Phys.* **24** 491; 1984a *Nuovo Cim.* **81A** 250; 1984b *Rep. Prog. Phys.* **47** 613; 1985 Neutron-nucleus Collisions. Ed. J.Rapaport, R.W.Finlay, S.M.Grimes and F.S.Dietrich. *AIP Conf. Proc.* **No.124** (New York) 1

Honoré G M, Tornow W, Howell C R, Pedroni R S, Byrd R C, Walter R L and Delaroche J P, 1986 *Phys. Rev.* **C33** 1129

Ioannides A A and Mackintosh R S, 1985 *Phys. Lett.* **161B** 43; 1985 *Nucl. Phys.* **A438** 354; 1986 *Phys. Lett.* **169B** 113

Johnson C H, Horen D J and Mahaux C, 1987 *Phys. Rev.* **C36** 2252

Kobos A M and Mackintosh R S, 1979 *Ann. Phys. (NY)* **123** 359

Lawson R D, Guenther P T and Smith A B, 1986 *Phys. Rev.* **C34** 1599; 1987 *Phys. Rev.* (In Press)

Mackintosh R S, 1979 *J. Phys.* **G5** 1587

Mackintosh R S and Ioannides A A, 1985 International Workshop on Advanced Methods in the Analysis of Nuclear Scattering Data, Berlin June 18–20

Mackintosh R S, Ioannides A A and Thompson I J, 1986 *Phys. Lett.* **B178** 1

Mackintosh R S and Kobos A M, 1976 *Phys. Lett.* **B62** 127; 1979 *J. Phys.* **G5** 359

Mahaux C, Bortignon P F, Broglia R A and Dasso C H, 1985 *Phys. Rep.* **120** 1

Mahaux C and Ngô H, 1979 *Phys. Lett.* **B100** 285

Mahaux C, Ngô H and Satchler G R, 1987 *Nucl. Phys.* **A**

Mahaux C and Sartor R, 1986 *Phys. Rev. Lett.* **57** 3013

Malaguti F and Hodgson P E, 1973 *Nucl. Phys.* **A215** 243

Malaguti F, Uguzzoni A, Verondini E and Hodgson P E, 1978 *Nucl. Phys.* **A297** 287; 1979a *Nuovo Cim.* **49A** 412; 1979b *Nuovo Cim.* **53A** 1; 1982 *Revista Nuovo Cim.* **5** 1

Millener J and Hodgson P E, 1973 *Nucl. Phys.* **A209** 59

Noro T, Sakaguchi H, Nakamura M, Hatamaka K, Ohtani F, Sakamoto H and Kobayashi S, 1981 *Nucl. Phys.* **A366** 189

Perey C M and Perey F G, 1986 *Phys. Lett.* **26B** 123; 1974 *Atom. Data Nucl. Data Tables* **13** 293; 1976 *Ibid* **17** 1

Ray L and Hodgson P E, 1979 *Phys. Rev.* **C20** 2403

Sinha B C and Edwards V R W, 1970 *Phys. Lett.* **B31** 273; 1971 *Ibid* **B5** 391

Smith A B, Guenther P T and Lawson R D 1985, *ANL/NOM-91*

Van Oers W T H, 1971 *Phys. Rev.* **C3** 1550

Varner R L, Clegg T B, McAbee T L and Thompson W J, 1987 *Phys. Lett* **185** 6

Yang Y and Rapaport J, 1986 *Nucl. Phys.* **A454** 359

SEMI-MICROSCOPIC THEORY OF THE NUCLEON OPTICAL POTENTIAL BASED ON EFFECTIVE INTERACTIONS — FROM NON-RELATIVISTIC TO RELATIVISTIC

Yingqi GU, Yinlu HAN, Zhongyu MA, Qingbiao SHEN,
Ye TIAN, Jingshang ZHANG, Ping ZHU, Yizhong ZHUO
Institute of Atomic Energy,
Beijing, China

Abstract

Both non-relativistic and relativistic optical potentials are studied by utilizing effective Skyrme interactions and effective Lagrangian based on Walecka model, respectively. The first and second order mass operators of one-particle Green function in nuclear matter are derived and applied within the local density approximation (LDA) to finite nuclei. From a rather extensive comparison with experimental data of various quantities of interests, it is concluded that the obtained microscopic optical potentials have good predictive capability to be applied to nuclear data evaluations when experimental data are lacking.

1. INTRODUCTION

The optical potential is one of the most fundamental theoretical tools in the analysis of nuclear reaction data and hence in the data evaluation. The phenomenological optical model with many adjustable parameters can reproduce the experimental data quite well, but cannot however, predict the unknown data with certainty. Thus, the derivation of the optical potential from the more basic theory is one of the important problems in nuclear theory which is of both theoretical and practical interest.

As early as 1959 Bell and Squires[1] showed that from the point of view of the many-body theory the optical potential can be identified with the mass operator of the one-particle Green function. This identication has made it possible to utilize the many-body theory technique to obtain a microscopic optical potential (MOP) without any

free parameter. In practical application, however, the mass operator cannot be calculated exactly since it would mean to solve the many-body problem itself,therefore this theory remained a formal one for a long time in the past. Only in recent years with some appropriate approximations developed,have the actual calculations of the MOP become possible. Basically two different approaches have been formulated. One is the "nuclear matter approach"[2-5] in which one starts from the realistic nuclear force to calculate the mass operator by Bruechner-Hartree-Fock (BHF) approximation in nuclear matter, then the MOP for finite nuclei is obtained within LDA. Thus, the MOP for all target nuclei can be obtained in principle. Another approach is the "nuclear structure approach"[6,7],in which one only applies the effective nuclear force by means of random phase approximation (RPA) to calculate the MOP for some specific nuclei. Thus, this approach takes into account of features of the nuclear structure of the target nucleus, while the "nuclear matter approach" considers the effects of the nuclear structure only in an average way (via the LDA).

Both approaches have their merits and limitations. Since we are more interested in the global properties of the optical potential, encouraged by the success of the nuclear matter approach and that of the effective Skyrme interactions in non-relativistic case and Walecka model in relativistic case, we adopt a simpler and more economical way for MOP calculation. We calculate the mass operator of one-particle Green function only up to the second order in nuclear matter by using the Skyrme interactions and effective Lagrangian based on Walecke model for non-relativistic and relativistic cases, respectively. The optical potential for finite nuclei is then obtained as usual by LDA. Since above-mentioned effective interactions can be viewed as effective G matrices in the Hartree-Fock (HF) calculation[8-10], we let only the first-order mass operator $M^{(1)}$ represent the real part of the optical potential and consider the imaginary part of the second-order mass operator $M^{(2)}$ as the imaginary part of the optical potential. Of course, this approach is not as basic as the MOP based on the realistic nuclear force in certain sense, but by using the above-mentioned effective interactions we can get very simple, in most cases analytical, expressions for the optical potential, which is physically more transparent and easier to apply. We are certainly aware that the various effective interactions, including above-mentioned ones, which are primarily designed to reproduce the nuclear ground-state properties, may not be adequate for deriving the optical potential. It has indeed been shown[11] that different Skyrme interactions give almost the same good agreement for the HF ground state but yield quite different results for excited states. Thus, for the non-relativistic optical potential we have performed the calculations and comparisons with nearly all kinds of Skyrme interactions available. The calculated results show that there indeed exist some Skyrme interactions which yield optical potentials comparable to the phenomenological ones in fitting the empirical data[12,13]. Considering both the real and imaginary parts of the optical potential as a whole it has been found[13] that among all versions of the Skyrme interactions GS2[11] and SKa[14] are the best. In the same manner, for the relativistic optical potential we start from an effective Lagrangian with two adjustable isoscalar meson coupling constants (g_σ, g_ω) chosen to reproduce the nuclear matter saturation properties. This is just the Walecka model. Studies have been performed with various modifications to this model by including the effects of the isovector mesons π and ρ and the effects of the non-linear σ terms. It is surprizing to find that the most simple Walacka model yields the best results.

In this talk we present the main results so far obtained with the effective interactions for both non-relativistic and relativitic optical potentials which are called semi-microscopic optical potentials in contrast with the microscopic optical potentials based on realistic nuclear force.

In Sec. 2, we present the basic theory of the optical potential and the calculated results for the non-relativistic case. In Sec. 3, the relativistic optical potential is formulated and the obtained results are discussed. Finally, a short summary is given in Sec.4.

2. NON-RELATIVISTIC OPTICAL POTENTIAL BASED ON SKYRME INTERACTIONS

2.1. Formalism

The propagation of a nucleon in nuclear matter with momentum $\vec{K}$ and energy E is described by the one-particl Green function, which is given by

$$G(\vec{K},E)=1/(E-(\hbar^2\vec{K}^2/(2m))-M(\vec{K},E)), \qquad (1)$$

where $M(\vec{K},E)$ is the mass operator of the one-particle Green function, which has been proved within nuclear many-body theory to be equivalent

to the optical potential[1]. As we have already mentioned for the effective interactions that we only need to keep the lowest orders in the perturbation expansion of M(K,E) in terms of the interactions,

$$M(\vec{K},E)= M^{(1)}(\vec{K})+ M^{(2)}(\vec{K},E) \ . \qquad (2)$$

The first-order term $M^{(1)}$ is just the HF mean field which represents the real part of the optical potential. The second-order term $M^{(2)}$ determines the lowest-order contribution to the imaginary of the optical potential. The real part of $M^{(2)}$ which is considered elsewhere[12], is not discussed in this talk although it improves the energy-dependent behaviour of the real part of the optical potential around Fermi energy. Thus the real part of the optical potential is just given by the HF mean field V^{HF}.

The HF mean field $V^{HF}_{\alpha\alpha}$ is written as

$$V^{HF}_{\alpha\alpha}= M^{(1)}_{\alpha\alpha}= \sum_{\lambda} V_{\alpha\lambda,\alpha\lambda}\ n_{\lambda} \ , \qquad (3)$$

where

$$n_{\lambda}=\begin{cases}1 & \text{below the Fermi surface.}\\ 0 & \text{above the Fermi surface.}\end{cases} \qquad (4)$$

The matrix elements $V_{\alpha\lambda,\alpha\lambda}$ are given by

$$V_{\alpha\lambda,\alpha\lambda} =\langle\alpha\lambda|V|\alpha\lambda\rangle_A \qquad (5)$$

with A denoting antisymmetrization.

The imaginary part of the second-order mass operator (retarded part) is written as

$$\mathrm{Im}M^{(2)}_{\alpha\alpha}= -\frac{1}{2}\pi\sum_{\mu\lambda\nu} V_{\alpha\lambda,\mu\nu}V_{\mu\nu,\alpha\lambda}\, n_{\lambda}(1-n_{\mu})(1-n_{\nu}) \\ (E+\varepsilon_{\lambda}-\varepsilon_{\mu}-\varepsilon_{\nu}), \qquad (6)$$

where ε_{λ}, ε_{μ} etc. are the HF single-particale energies.

It is noted that for the conventional Skyrme interactions which contain three-body interaction as well, additional terms would appear in both $M^{(1)}$ and $M^{(2)}$ [12]. However the SKa and GS2 shown in this talk are density-dependent two-body interactions which are two special cases of the so-called extended Skyrme force which is expressed in an unified form as[13]

$$V_{12}(\vec{R},\vec{r})=t_0(1+x_0p_\sigma)\delta(\vec{r}) +\tfrac{1}{6}t_3(1+x_3p_\sigma)\,\rho^{\alpha}(\vec{R})\delta(\vec{r}) \\ +\tfrac{1}{2}t_1(1+x_1p_\sigma)(\vec{K}'^2\delta(\vec{r}) +\delta(\vec{r})\vec{K}^2) \\ +\tfrac{1}{2}t_4(1+x_4p_\sigma)(\vec{K}'^2\rho(\vec{R})\delta(\vec{r}) +\delta(\vec{r})\rho(\vec{R})\vec{K}^2) \\ +t_2(1+x_2p_\sigma)\vec{K}'\cdot\delta(\vec{r})\vec{K} +t_5(1+x_5p_\sigma)\vec{K}'\cdot\rho(\vec{R})\delta(\vec{r})\vec{K} \\ +iW_0(\vec{\sigma}_1+\vec{\sigma}_2)\cdot\vec{K}'\times\delta(\vec{r})\vec{K}. \qquad (7)$$

with

$$\vec{r}=\vec{r}_1-\vec{r}_2 \qquad \vec{R}=\tfrac{1}{2}(\vec{r}_1+\vec{r}_2) \qquad (8)$$

and the relative momentum operators

$$\vec{K} =(\tfrac{1}{2i})(\vec{\nabla}_1-\vec{\nabla}_2) \qquad (9a)$$

acting on the wave function on the right,

$$\vec{K}'=-(\tfrac{1}{2i})(\vec{\nabla}_1-\vec{\nabla}_2) \qquad (9b)$$

acting on the wave function on the left. The quantities p_σ and σ_i denotes the spin exchange operator and the Pauli spin matrices, respectively. The various sets of the extended Skyrme force parameters are listed in table 1.

TABLE 1. PARAMETERS OF THE EXTENDED SKYRME FORCE

	t_0 MeV.fm^3	t_1 MeV.fm^5	t_2 MeV.fm^5	t_3	t_4 MeV.fm^8	x_0	x_1	x_2	x_3	x_4	W_0 MeV.fm^5	α	Ref
GS1	-1268	887	-77.3	14485	-1853	0.150	0	0	1	1	105	1	
GS2	-1177	670	-49.7	11054	-775	0.124	0	0	1	1	105	1	
GS3	-1037	336	-7.3	5774	883	0.074	0	0	1	1	105	1	
GS4	-1242	760	-146.2	19362	-2157	0.206	0	0	1	1	105	1	
GS5	-1152	543	-118.6	15989	-1079	0.182	0	0	1	1	105	1	
GS6	-1012	209	-76.3	10619	579	0.139	0	0	1	1	105	1	
SG0I	-1089	558.8	-83.7	8272	0	0.412	0	0	0	0	130	1	
SG0II	-2248	558.8	-83.7	11224	0	0.715	0	0	0	0	130	1/6	
SKa	-1602.78	570.88	-67.70	8000	0	-0.02	0	0	-0.286	0	125	1/3	
SKb	-1602.78	570.88	-67.70	8000	0	-0.165	0	0	-0.286	0	125	1/3	
SKM	-2645	385	-120	15595	0	0.09	0	0	0	0	130	1/6	
SGI	-1603	515.9	84.5	8000	0	-0.02	-0.5	-1.731	0.1381	0	115	1/3	
SGII	-2645	340	-41.9	15595	0	0.09	-0.0588	1.425	0.06044	0	105	1/6	

t_5(MeV.fm^8)=0 x_5=0

In nuclear matter the single-particle wave function is given by the plane wave

$$\psi_\alpha = \Omega^{-1/2} e^{i\vec{K}_\alpha \cdot \vec{r}} \chi_{\sigma_\alpha} \chi_{\tau_\alpha} \qquad (10)$$

where χ_{σ_α} and χ_{τ_α} are the spin and isospin wave function, respectively, and Ω is the volume. Substituting the wave function and the Skyrme force into the expression of $V_{\alpha\mu,\lambda\nu}$ we can easily obtain the nucleon optical potential for the general asymmetric nuclear matter. The analytical expressions for both real and imaginary parts of the optical potential have been given elsewhere[12-13], since they are too lengthy to be written down here.

2.2. Local Density Approximation (LDA)

The simplest way to obtain the optical potential for a finite nucleus from that for nuclear is to apply the LDA[3,15], i.e. to assume that the optical potential at location r in a finite nucleus is the same as in a uniform infinite nuclear matter whose density would be the local value $\rho(r)$. we also assume that the densities of neutrons and protons in a spherical nucleus have the same spacial distribution and are expressed by the empirical formula given by Negele[13],

$$\rho_K(r) = \rho_{0K}/(1+\exp((r-c)/a)),$$

$$K=N \text{ or } Z \qquad (11)$$

where

$$\rho_{0K} = 3K/(4\pi c^3(1+\pi^2 a^2/c^2)), \qquad (12)$$

$$c=(0.978+0.0206A^{1/3})A^{1/3},$$

$$a=0.54. \qquad (13)$$

This local density approximation implies a local momentum according to

$$\rho = 2/(3\pi^2)K_F^3 . \qquad (14)$$

2.3. Numerical Results and Discussions

We have performed rather extensive calculations with different versions of Skyrme interactions ranging from the conventional Skyrme forces SI-SVI to their various modified forms. In the following we just show the calculated results with GS2 and SKa as the representatives, since among all versions of the Skyrme interactions GS2 and SKa are best in fitting the empirical data.

Fig.1 shows the shape of both the real and imaginarg parts of the neutron optical potential for ^{208}Pb at E_n=20 MeV calculated with GS2 and SKa. They are quite close to the phenomenological optical potential (POP).

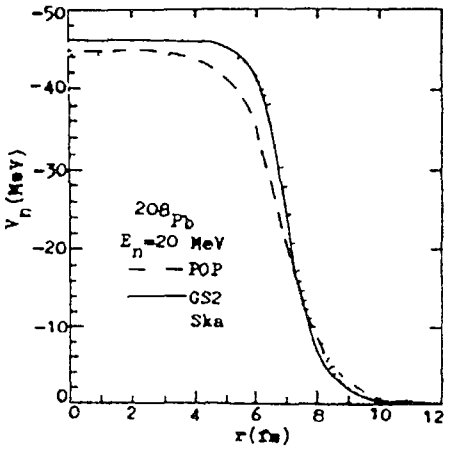

FIG 1(a)

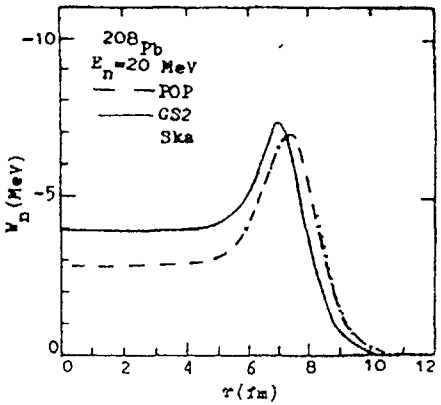

FIG 1(b)

Radial dependence of the neutron optical potential for ^{208}Pb at energy E_n = 20 MeV.
(a) The real parts. (b) The imaginary parts.

From the point of view of fitting the experimental data the optical potential is not unique. However, the calculated results are mainly sensitive to the volume integrals per nucleon namely

$$J_V = -\frac{1}{A}\int V(\vec{r})d\vec{r} \ , \ J_W = -\frac{1}{A}\int W(\vec{r})d\vec{r} \ . \qquad (15)$$

The dependence on the mass number of the volume integrals per nucleon of the real and imaginary parts of the computed optical potential and the comparison with the empirical values[16-18] are shown in Fig.2(a) and (b), in which a number of even-even nuclei ranging from A=12 to 238 near β-stability line are chosen. It

is shown that the results with GS2 and SKa are very close to the empirical values and the theoretical values obtained by POP and BHF approximation[16].

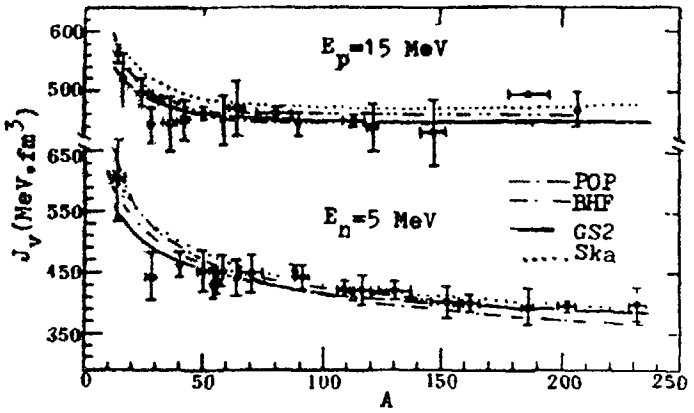

FIG.2(a)

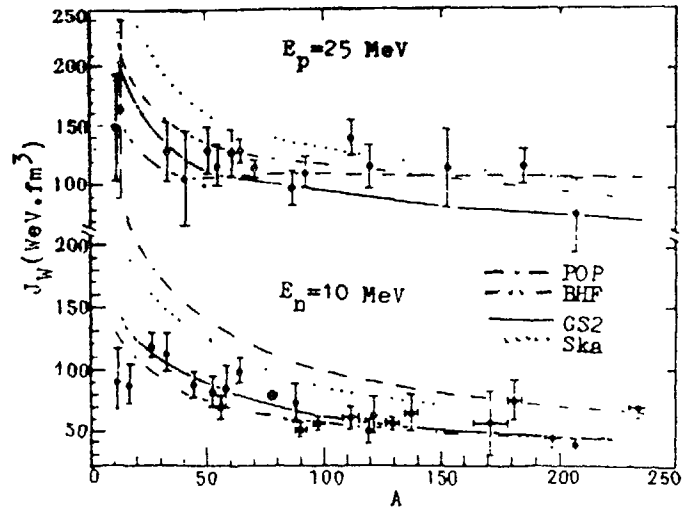

FIG.2(b)

The volume integral per nucleon of the optical potential against the mass number A, for neutrons at the bottom, for protons on the top. The dots and crosses represent the empirical values[16]. (a) The real parts. (b) The imaginary parts.

We have calculated the neutron total cross sections, elastic scattering cross sections, nonelastic cross sections and neutron and proton angular distributions of the elastic scattering for a large numbers of nuclei by using the obtained optical potential with GS2, SKa and the POP. The global analysis shows that the calculated results without adjusting any parameter can fit the experiments pretty well in a rather wide energy region from light nuclei to heavy ones.

Fig.3(a),(b) and (c) show the calculated neutron total cross sections for ^{12}C, ^{40}Ca, ^{44}Ca and ^{208}Pb, respectively. It seems that they can reproduce the experimental data quite well. Both the neutron and proton elastic scattering angular distributions for a number of target nuclei at various incident energies are shown in Fig.4(a) and (b). It is seen that all the tendency of the angular distribution, positions and absolute values of the peaks and valleies are in good agreement with the experimental data.

As the code MUP-2 of CNDC has the function to produce a complete set of nuclear data either with POP or with semi-microscopic optical potential based on Skyrme interactions. As an example the calculated results of the angular distributions with GS2 for ^{98}Mo at different bombarding energies of neutron are illustrated in Fig.5. It is amazing to see that the agreement between theory and experiment is so perfect without any free parameters in this optical potential like POP. It is particularly interesting to note that by including the compound elastic scattering contribution in such a way the theory can still agree with the experimente data so well even for neutron incident energy as low as 0.5 MeV.

3. RELATIVISTIC OPTICAL POTENTIALS BASED ON WALECKA MODEL

3.1 Motivation and Basic Consideration

As it is shown in the previous section that the semi-microscopic approach in the non-relativistic optical potential calculations is quite successful. However, due to the zero range of the Skyrme interactions the results are limited to nucleon energy around 50Mev above the Fermi energy. In order to extend the energy domain of validity it might be interesting and useful to go beyond the non-relativistic approach. Furthermore the sucesses of Dirac

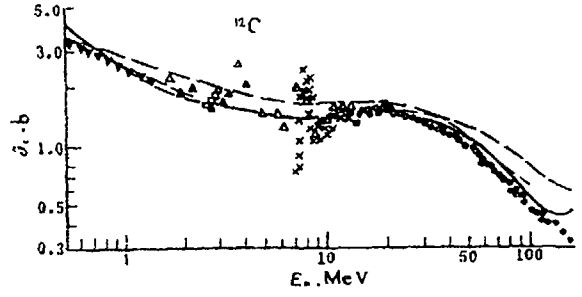

FIG.3(a)

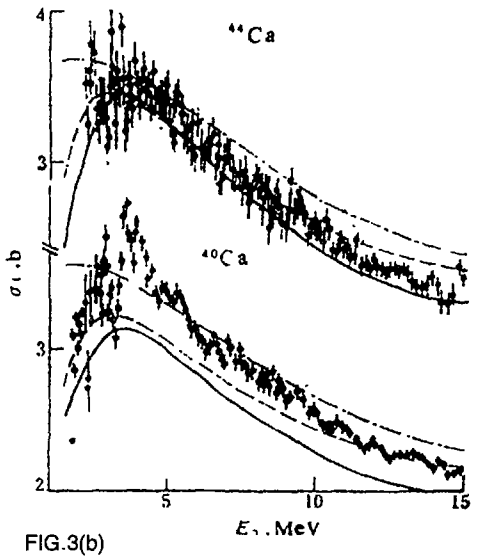

FIG.3(b)

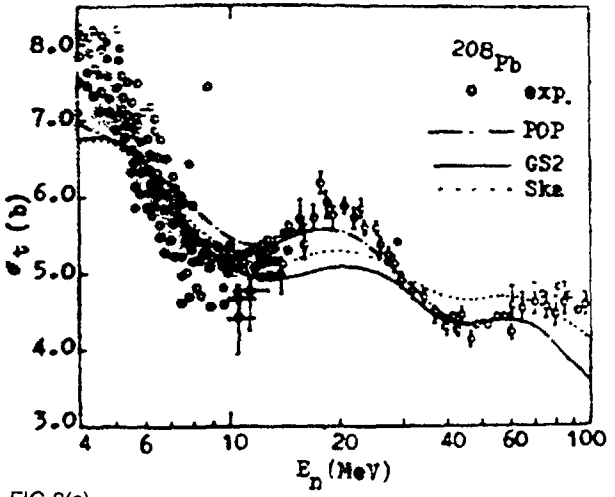

FIG.3(c)

Comparison of the theoretical values of the neutron total cross sections.
(a) For ^{12}C. (b) For ^{40}Ca and ^{44}Ca. (c) For ^{208}Pb.

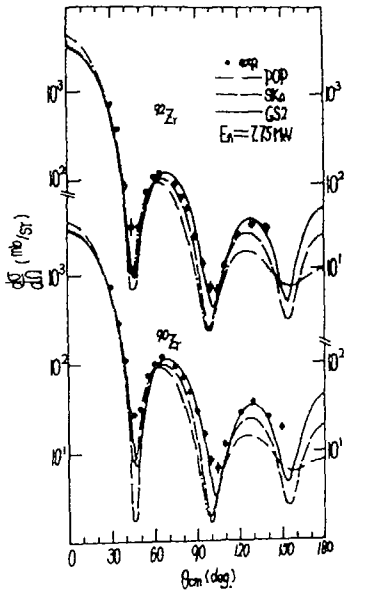

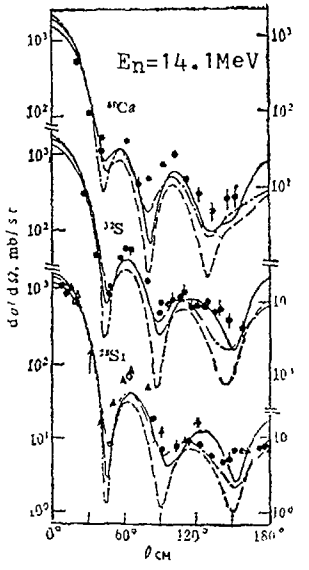

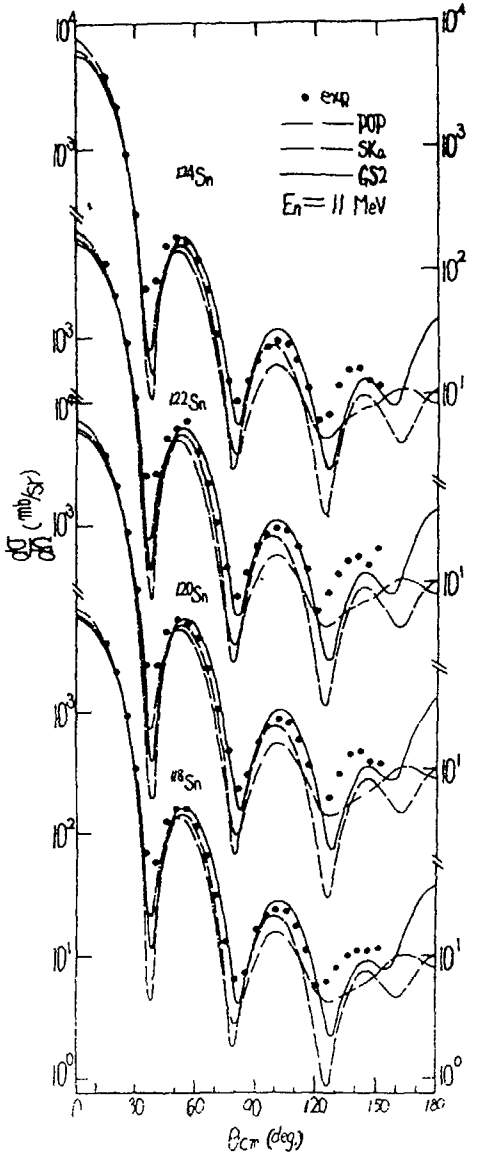

FIG.4(a)

(a) The angular distributions of the neutron elastic scattering on various nuclei at E_n = 7.75 MeV, 11 MeV and 14.1 MeV respectively.

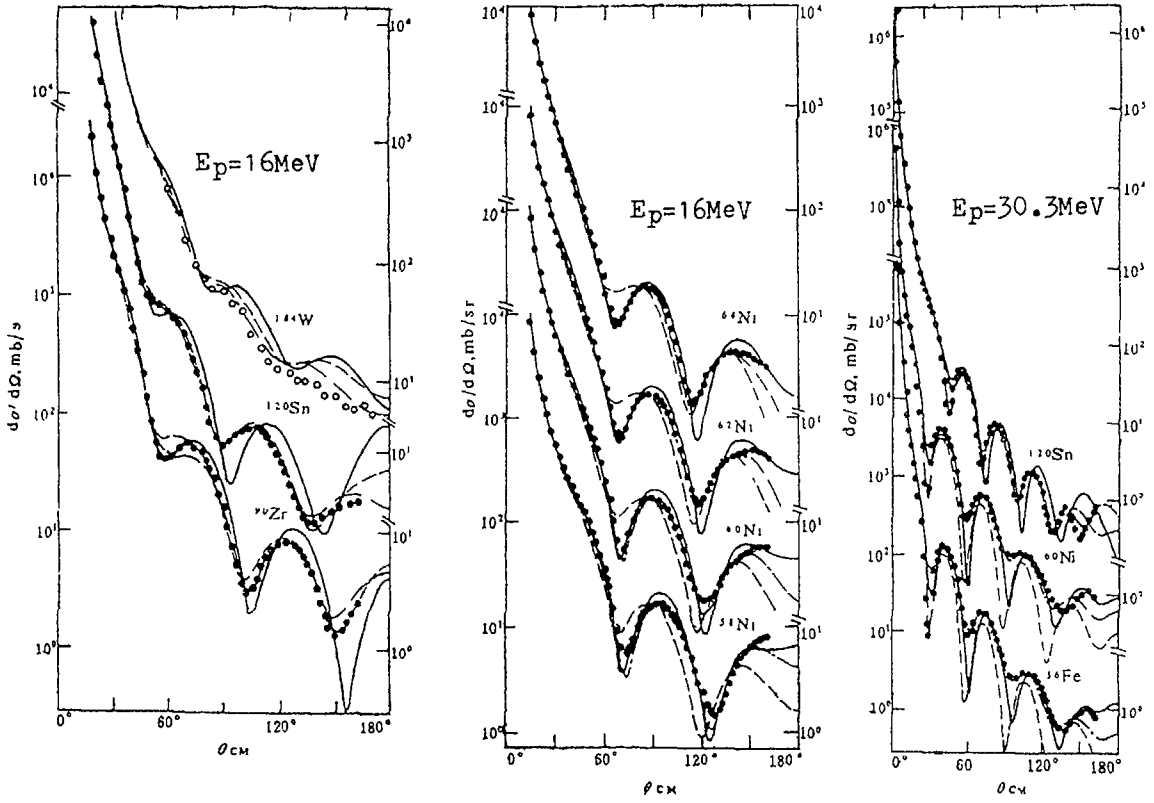

FIG.4(b)

(b) Same for proton projectile on various nuclei at E_p = 16 MeV and E_p = 30.3 MeV.

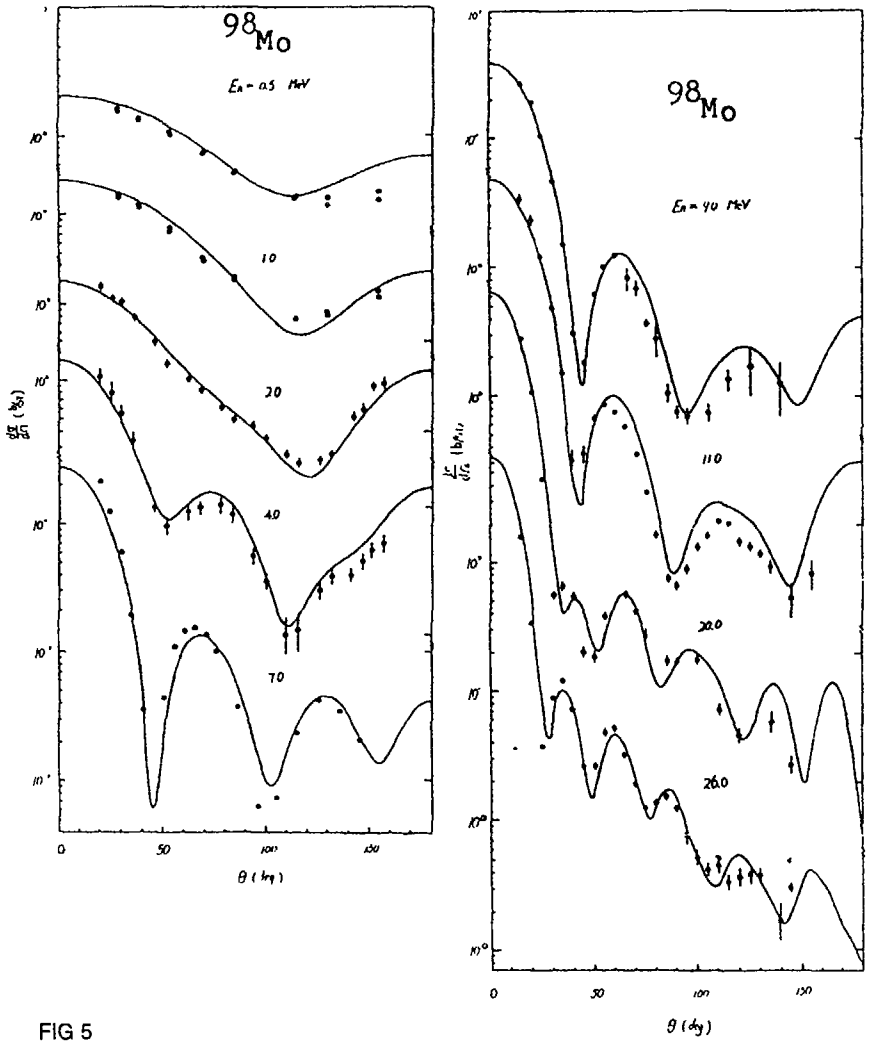

FIG 5

The angular distributions of the neutron elastic scattering on ^{98}Mo with GS2 by including the compound elastic scattering contributions with MUP-2 code.

phenomenology suggest that a relativistic treatment is required in an analysis of the spin observables in nucleon-nucleus scattering.

At present most of works on microscopic level with the relativistic description of nucleon-nucleus scattering are based on the relativistic impulse approximation[20], which are highly successful for the description of the elastic scattering at energy around 50Mev and above. Extending the relativistic formalism to the energy region below 300Mev, the relativistic Brueckner-Hartree-Fock (RBHF) approach is adopted by Shakin and coworkers[21]. This approach, however, is still far from complete by now as the numerical calculations are concerned. Encouraged by the success of the semi-microscopic optical potential based on Skyrme interactions for non-relativistic case, we follow the same idea and procedure to go over to the relativistic case by starting from an effective Lagrangian with two adjustable isoscalar meson coupling constants (g_σ , g_ω) fitting the nuclear matter saturation properties, i.e. Walecka model. We let only the Hartree-Fock term represent the real part of the optical potential and calculate the imaginary part to the lowest order. LDA is also applied in order to obtain the optical potential for finite nuclei. In order to compare with the non-relativistic optical potentials the Schrodinger equivalent potential are obtained.

3.2 Formalism

We consider an effective Lagrangian density with two adjustable isoscalar meson exchange coupling constants g_σ and g_ω ,

$$\mathcal{L} = \bar{\psi}(i\gamma^\mu\partial_\mu - M)\psi + \frac{1}{2}(\partial^\mu\sigma\partial_\mu\sigma - m_\sigma^2\sigma^2) + \frac{1}{2}m_\omega^2\omega^\mu\omega_\mu - \frac{1}{4}F^{\mu\nu}F_{\mu\nu} - g_\sigma\bar{\psi}\sigma\psi - g_\omega\bar{\psi}\gamma^\mu\omega_\mu\psi \qquad (16)$$

with

$$F_{\mu\nu} = \partial_\mu\omega_\nu - \partial_\nu\omega_\mu$$

where ψ, σ , ω_μ are the nucleon, σ and ω meson field operators, respectively. The values of nucleon and meson masses are taken from the experiments, M = 938.9 Mev, while m_ω = 783 Mev. The mass of hypothetical σ meson is fixed to m_σ = 550 Mev, which is commonly used in the nucleon-nucleon interaction. The two effective coupling constants g_σ and g_ω are adjusted to reproduce the nuclear matter saturation properties in the Dirac-Hartree-Fock approximation.

Because of the translational and rotational invariance of infinite nuclear matter the mass operator of the one-particle Green function may, in general, be written as

$$\Sigma(k,E) = \Sigma^S(k,E) + \gamma^0\Sigma^0(k,E) + \vec{\gamma}\cdot\vec{k}\,\Sigma^V(k,E) \qquad (17)$$

which corresponding to scalar, vector and three-vector potentials, respectively.

The calculations of the mass operator of the one-particle Green function are first carried out in the nuclear matter up to second orders as mentioned above. For finite nuclei it is obtained within the LDA. Thus, the Dirac equation for a nucleon in a nucleus reads

$$\left[\vec{\alpha}\cdot\vec{p}\,(1+\Sigma^V(r)) + \gamma_0(M + \Sigma^S(r)) + \Sigma^0(r)\right]\psi = E\psi \qquad (18)$$

In comparison with the phenomenology scalar-vector model, as usually employed in Dirac phenomenology, equation (18) can be more conveniently rewritten in terms of the effective scalar $\tilde{U}_S$ and vector $\tilde{U}_0$ potentials (S-V potential)

$$\left[\vec{\alpha}\cdot\vec{p} + \gamma_0(M + \tilde{U}_S) + \tilde{U}_0\right]\psi = E\psi \qquad (19)$$

where

$$\tilde{U}_S = \frac{\Sigma^S - \Sigma^V M}{1 + \Sigma^V} = \tilde{V}_S + i\,\tilde{W}_S \qquad (20a)$$

$$\tilde{U}_0 = \frac{\Sigma^0 + E\Sigma^V}{1 + \Sigma^V} = \tilde{V}_0 + i\,\tilde{W}_0 \qquad (20b)$$

It is clear from eq. (20) that the three-vector potentials perhaps are important and can not be neglected for the S-V potential. The negative real and positive imaginary three-vector potentials will change the energy-dependent behavior of the S-V potential[22]. The real part of the three-vector potential MV_V is relatively small, while the imaginary part of that MW_V increases rapidly with the energy and become comparable in magnitude with the scalar and vector potentials. Thus the strong energy dependence of the imaginary parts will be somewhat suppressed. These features are disirable to improve the high energy behavior of the optical potentials.

For comparison with the non-relativistic case the Schrodinger equivalent potential is obtained by eliminating the small compo-

nents of the Dirac spinor in eq.(19),

$$\left[\frac{p^2}{2m} + U_{eff} + \vec{\sigma}\cdot\vec{L}\ U_{so} \right] \psi = \frac{k^2}{2M}\psi$$

with

$$U_{eff} = \tilde{U}_s + \frac{E}{M}\tilde{U}_o + \frac{1}{2M}(\tilde{U}_s^2 - \tilde{U}_o^2) \qquad (21a)$$

and

$$U_{so} = -\frac{1}{2Mr}\frac{d}{dr}\ln(M + E + \tilde{U}_s - \tilde{U}_o) \qquad (21b)$$

where

$$E^2 = k^2 + M^2.$$

3.3 Numerical Results and Discussions

The calculated results of the Schrodinger equivalent potentials at vsrious energies for ^{40}Ca are shown in Fig.6. The wine-bottle bottom shape of the real central potential appears at energies around 200Mev (see Fig.6a). The shape of the imaginary central potential changes from surface dominant to volume dominant with the increase of the energy (see Fig.6b). The scalar and vector potentials have the opposite signs in the spin-orbit potential of eq.(21b). It automatically yields a large spin-orbit potential (see Fig.6c). All these characteristic features are in coincidence with those found in the empirical potentials of the Dirac phenomenology. At high energy (larger than 300MeV) the strength of both the real and imaginary parts of potentials rise too fast with the energy, which is unsatisfactory. The comparison of the volume integrals with the empirical values also show a good agreement only up to 300MeV[22].

We have calculated the angular distributions,analyzing powers and spin rotation functions of proton elastic scattering on ^{40}Ca at various incident energies, and for a number of target nuclei at 65MeV of proton projectiles by using the obtained Schrodinger equivalent potential, which are compared with the experimental data[23-27] and shown in Fig.7 and 8. It is seen that the theory can reproduce nicely all the experimental values except in the backward angle region.

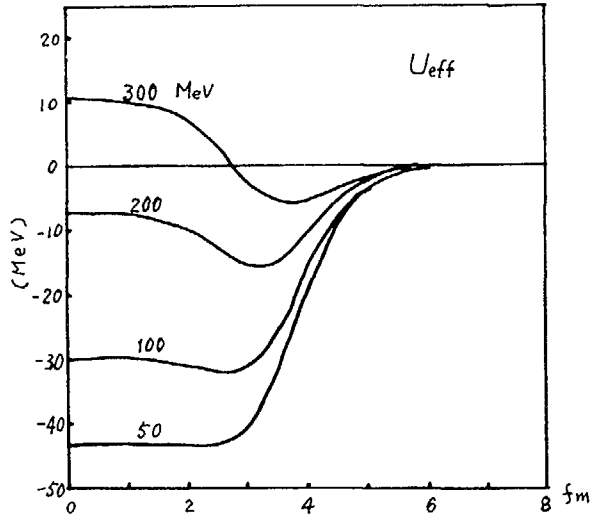

FIG.6(a)

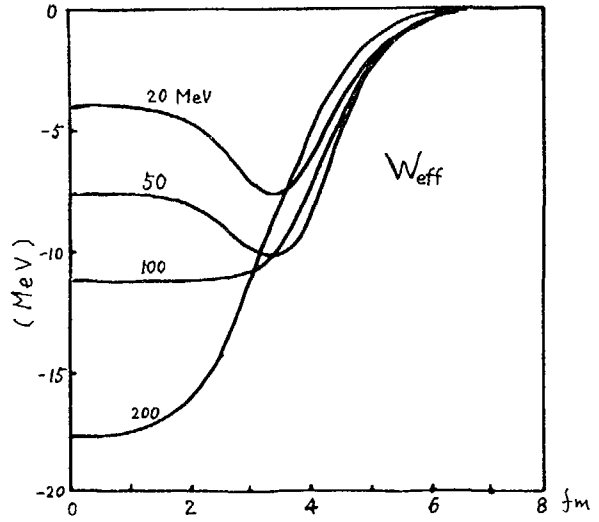

FIG.6(b)

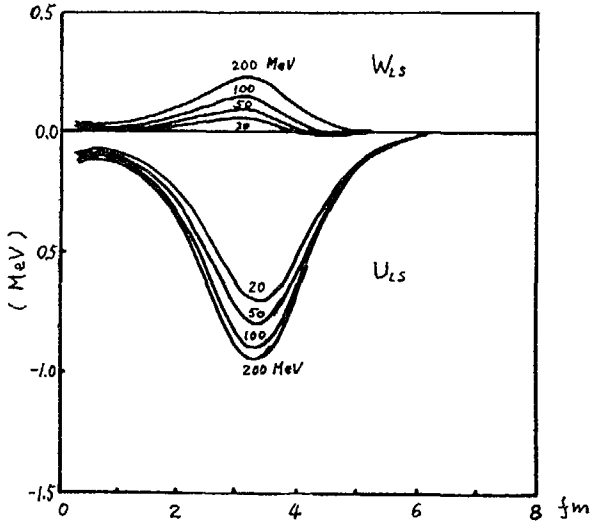

FIG.6(c)

Schrodinger equivalent potentials for ^{40}Ca at various energies E_n =30, 80, 200, 400 and 500 MeV. (a), (b), (c) are for real central, imaginary central and spin-orbit potentials, respectively.

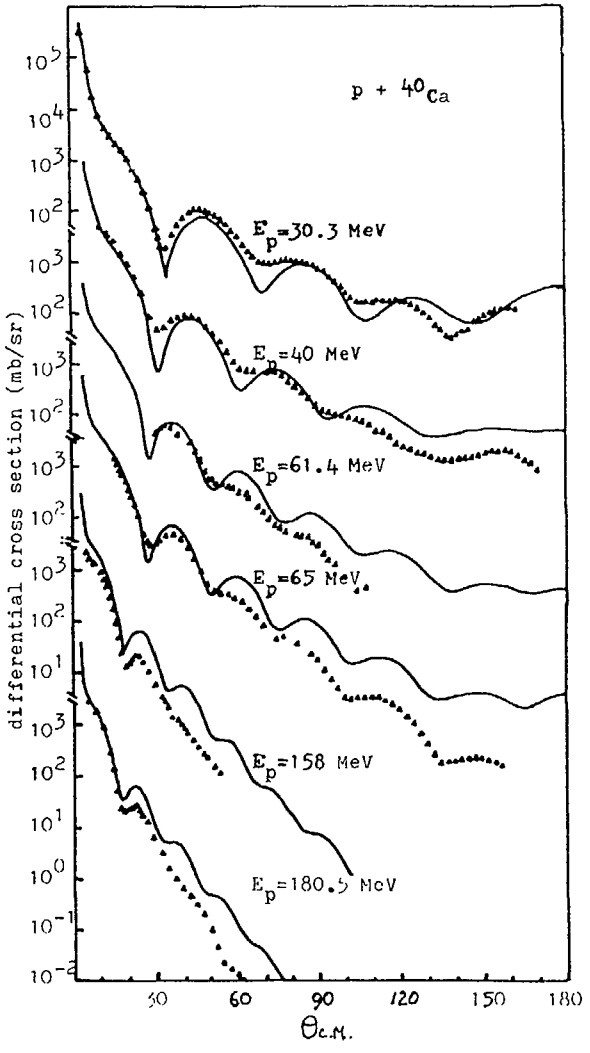

FIG.7(a)

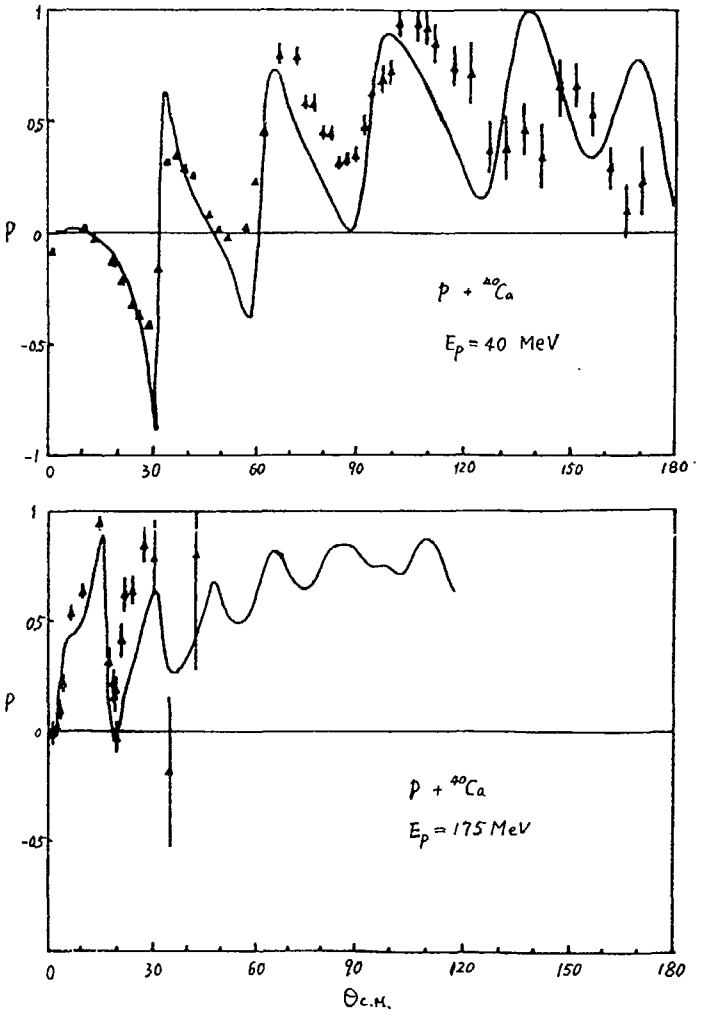

FIG.7(b)

The proton elastic scattering on ^{40}Ca at various energies.
(a) The angular distributions. (b) Analyzing powers.

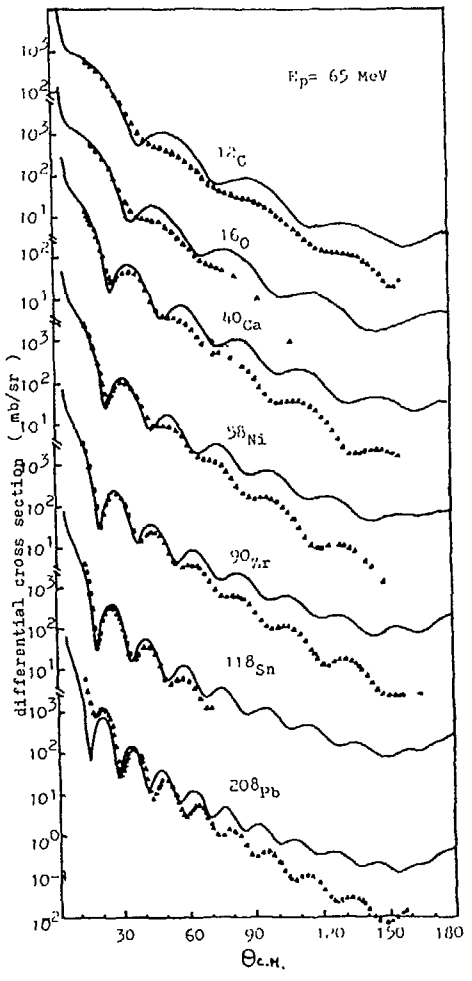

FIG.8(a)

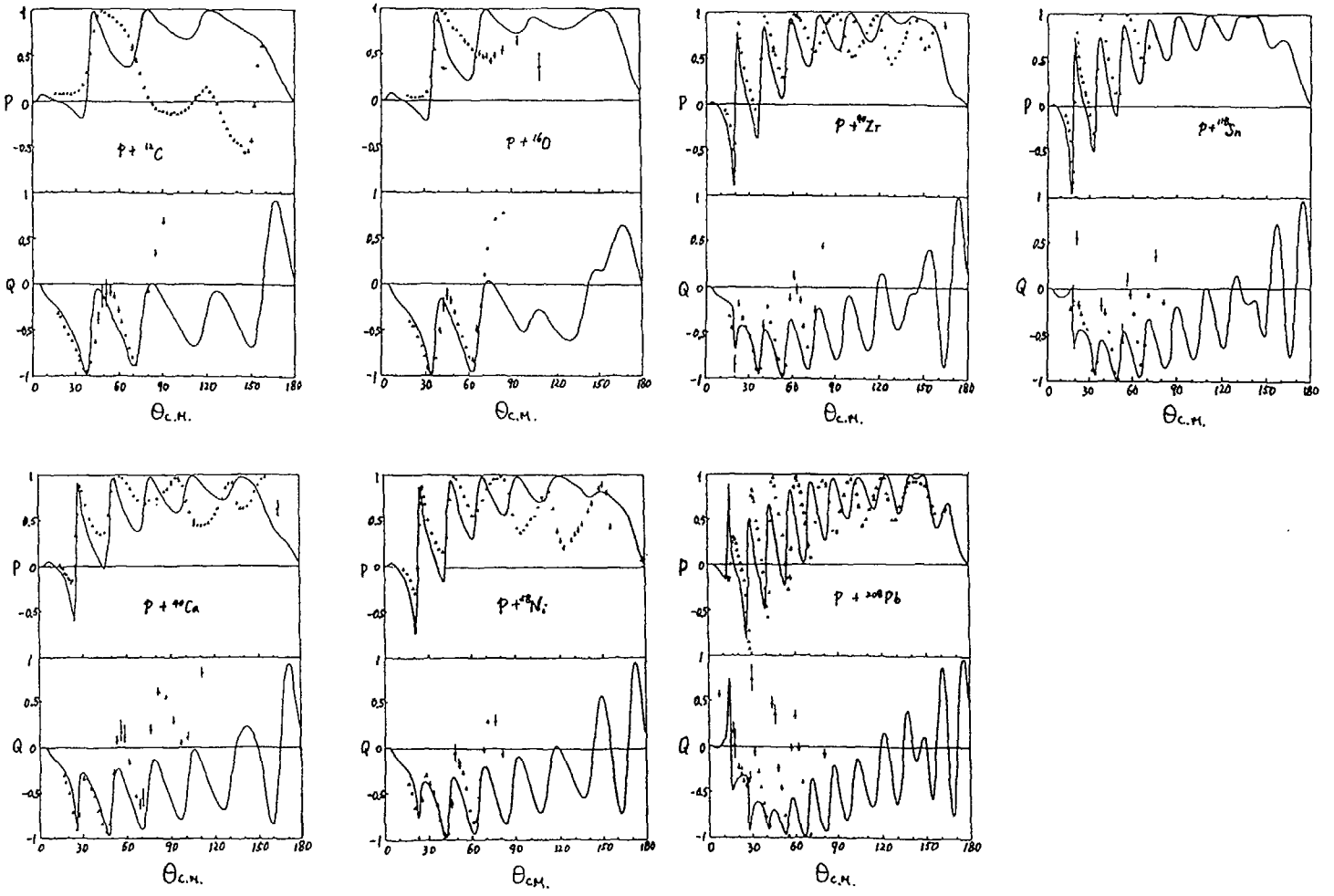

FIG.8(b)

The proton elastic scattering on various target nuclei at E_p = 65MeV. (a) Angular distributions. (b) Analyzing powers and spin rotation functions.

4. SUMMARY

In this talk we have presented the progress of our efforts on the semi-microscopic theory of the nucleon optical potential based on effective interactions both for non-relativistic and relativistic cases. The first and second order mass operators of one-particle Green function in nuclear matter are first calculated and then applied within the local density approximation to finite nuclei. It is shown that for certain energy regions (up to 60MeV for non-relativistic and 300MeV for relativistic cases) the potential depth, shape, as well as the energy dependence are in reasonable agreement with those of the phenomenological optical potential and those based on realistic nuclear force. The calculated results, such as the volume integrals, total cross sections, angular distribution and spin observables of the elastic scattering reproduce the empirical and experimental data quite nicely.

The comparison among the different versions of Skyrme interactions for non-relativistic case shows that the GS2 and SKa are best. While in the relativistic approach we start with the Walecka model and also try various modifications to this model by including the effects in presence of the π and ρ mesons, as well as the non-linear σ terms. It turns out that the simplest Walecka model gives the best results.

I would like to conclude this talk by saying that the proposed semi-microscopic optical potentials have the good enough predictive power to be applied to the nuclear data evaluation when experimental data are lacking. In order to check the real reliability in practice more systematic studies should be done in the future.

REFERENCES

1). J.S. Bell and E.J. Squires, Phys. Rev. Lett. 3(1959)96.

2). J.P. Jeukenne, A. Lejeune and C. Mahaux, Phys. Rep. 25C(1976) 83.

3). J.P. Jeukenne, A. Lejeunne and C. Mahaux,Phys. Rev. C16(1977) 80.

4). F.A. Brieva and J.R. Rook, Nucl. Phys. A291(1977) 317.

5). L.S. Celenza and C.M. Shakin, Relativistic Nuclear Physics: Theories of Structure and Scattering, World Scientific Publishers, Singapore(1985).

6). N. Vinh Mau and A. Bouyssy, Nucl. Phys. A257(1976) 189.

7). V. Bernard and Nguyen Van Giai, Nucl. Phys. A327(1979) 397; A348(1980) 75.

8). D. Vautherin and D.M. Brink, Phys. Rev. C5(1972) 626.

9). J.W. Negele and D. Vautherin, Phys. Rev. C5(1972) 1472.

10).B.D. Serot and J.D. Walecka, Adv. in Nucl. Phys. 16(1985).

11).S. Krewald, V. Klemt, J. Speth and A. Faessler, Nucl. Phys. A281(1977) 166.

12).Shen Qingbiao, Zhang Jingshang, Tian Ye, Ma Zhongyu and Zhuo Yizhong, Z. Phys. A303(1981) 69.

13).Zhuo Yizhong, Shen Qingbiao and Tian Ye, Advances of Chinese Sciences, Physics, 1(1986) 231.

14).H.S. Köhler, Nucl. Phys. A258(1976) 301.

15).J.W. Negele, Phys. Rev. C1(1970) 1260.

16).C. Mahaux, Microscopic Optical Potentials, Lecture Notes in Physics, Vol. 89, Berlin, Heidelberg, New York, Springer, 1979,P1 .

17).S. Kailas and S.K. Gwpta, Phys. Rev. C17(1978) 2236.

18).S. Kailas and S.K. Gwpta, Phys. Lett. 71B(1977) 271.

19).B.C. Clark, S.H. Hama and R.L. Mercer, in The Interactin Between Medium Energy Nucleons in Nuclei-1982(H.O. Meyer, ed.) AIP Conference Proceedings No.97, P.260, AIP, New York 1983, B.C. Clark, Devlopment of the Dirac Scattering Approach, Invited talk presented at the Los Alamos Workshop on Relativistic Dynamics and Quark-Nuclear Physics, June 2–June 14, 1985.

20).J.A. McNeil, J. Shepard and S.J. Walace, Phys. Rev. Lett., 50 (1983) 1439.
J. Shepard, J.A. McNeil and S.J. Walace, Phys. Rev. Lett., 50 (1983) 1443.

21).L.S. Celenza and C.M. Shakin, Relativistic Nuclear Physics: Theories of Structure and Scattering, World Scientific, 1986.

22).Ma Zhongyu, Zhu Ping, Gu Yingqi and Zhuo Yizhong, Proc. of Beijing Intern. Symp. on " Physics at Tandem ", Beijing, China, May 26-30, 1986.

23). B.W. Ridly and J.F. Turner, Nucl. Phys. 58 (1964) 497.
24). L.N. Blumberg, E.E. Gross, A. Van der Wonde, A. Zucker and R.H. Bassel, Phys. Rev. 147 (1966) 812.
25). C.B. Folmer, J.B. Bail, A. Scott and M.L. Whiten, Phys. Rev. 181 (1969) 1565.
26). A.Johansson, U. Svanberg and P.E. Hodgson, Ark. Fys. 19 (1961) 541.
E. Hagberg, A. Ingermarsson and B. Sundguist, Phys. Sci. 3 (1971) 245.
27). H. Sakaguchi, private communication.

USE OF THE MULTI-CHANNEL COUPLING METHOD FOR THE NEUTRON STRENGTH FUNCTION DESCRIPTION

A.V. IGNATYUK, V.P. LUNEV,
V.G. PRONYAEV, E.L. TRYKOV
Institute of Physics and Power Engineering,
Obninsk, Union of Soviet Socialist Republics

Abstract

Neutron cross sections in the iron region were calculated in the framework of the multi-channel coupling method. Channels dominating in the formation of the optical potential imaginary part were taken into account. This approach allows the consistent description of s-, p- and d- neutron strength functions to be reached as well the total cross sections for low energy neutrons.

Consideration of coupling between an elastic channel and strongly excited ones in the direct reactions inelastic scattering channels improves the description of the average cross sections for neutrons with the egergy up to 4÷5 Mev [1]. However, for the majority of the nuclei with a mass number A = 40 - 60, lying in the region of the $3S_{1/2}$ giant resonance of the s-neutron strength function, the simultaneous selfconsistent description of the strength functions and total neutron cross sections in the few channel variants of the channel coupling method is complicated. In particular, it is impossible to describe the observed ^{56}Fe total cross section for neutrons with the energy 0,5 - 4,0 MeV at any physically grounded parameters of optical potential (in case of their weak energy dependence). The values of the p-neutron strength functions typical for this region of nuclei are too high in comparison with experimental data [1]. As early as in previ-

ous publications [2] it was proposed, that these difficulties are due to the existence of intermediate structures in the cross sections which cannot be described by a spherical optical model or few-channel variants of the channel coupling method with a high value of the optical potential imaginary part. Microscopic calculations in the framework of the second order Born approximation method have shown [3], that channels, related to collective phonon excitations of the nuclei, make the main contribution to the imaginary part of the optical potential. In this paper we are going to make a more complete analysis of the role of these excitations in the approach which is more strict than the Born approximation. We shall emlpoy the multi-channel coupling method (MCCM) based on the same physical ideas as microscopic calculations [3], but which is free from the drawbacks of the low order perturbation theory. Furthermore, the contribution from the channel coupling to the real part of the optical potential is taken into account in the MCCM in the consistent way; this is rather difficult to do in the Born approximation of the nuclear structure approach.

All channels strongly coupled with an elastic one have been included into consideration. For low energy neutrons and even-even spherical nuclei they are first of all the inelastic scattering channels with excitation of the low lying collective one- and two- phonon states. It is natural to assume, that the role of other channels, which are not related with collective excitations is insignificant and can be taken into account on an average through the small imaginary addition (on the order of a few hundreds keV) to the real part of optical potential. This small imaginary part provides a necessary averaging on the narrow resonances and allows the definition of the average neutron strength functions and transmission cofficients [4] to be introduced.

The computer time needed for the solution of the system of coupled equations is sharply increased as the number of equations [5] grows. From this point of view it is more convenient to use the ECIS - code [6] based on the iteration method of solution, which has an approximately linear dependence of the time expenditure from the number of the equations. Form-factors of the transition potentials betwen elastic and inelastic scattering channels with excitation of the one-phonon states were taken in the form

$$F_\lambda(r) = \frac{\beta_\lambda}{\sqrt{2\lambda+1}} R_0 \frac{dV_0(r)}{dr} \qquad (1)$$

where λ is multipolarity of the phonon excitations, Ro - the nuclear radius, $V_0(r)$ - the depth of the real part of the optical potential and β_λ - the parameter of the dynamical deformation taken from the compilation of experimental data [7]. For the channels of the two - phonon excitations of the target - nucleus, the form-factor (1) was used for coupling between these channels and channels with excitation of the corresponding one - phonon components.

The calculations were performed for two values of the imaginary part of the optical potential: W_s = 0.2 MeV and W_s= 0.4 MeV. All geometrical parameters of the potential as well as parameters of the spin-orbital interaction were taken the same for all the considered nuclei (see Table 1). A number of one - and two-phonon states taken into account in the MCCM calculations are given in the last column.

TABLE 1. PARAMETERS OF THE POTENTIAL AND NUMBER OF THE PHONONS TAKEN INTO ACCOUNT IN THE MCCM CALCULATIONS

Nucleus	V_0, MeV	W_s, MeV	$r_0 = r_s = r_{so}$ fm	$a_0 = a_s = a_{so}$ fm	N_{ph}
^{52}Cr	49.1	0.2; 0.4	1.24	0.40	22
^{54}Fe	51.2	0.2; 0.4	1.24	0.40	17
^{56}Fe	48.2	0.2; 0.4	1.24	0.40	18
^{58}Fe	47.5	0.2; 0.4	1.24	0.40	16
^{58}Ni	49.8	0.2; 0.4	1.24	0.40	23
^{60}Ni	48.7	0.2; 0.4	1.24	0.40	19

The calculations have demonstrated noticeable sensitivity to the choice of the real part of the optical potential and averaging interval. One of the reason of this is incompleteness of the configuration space of the states (channels) to be taken into account and leading to the exclusion of the pole pecularities from the configurations of the complex nature making contribution at the energies under consideration.

Results of the MCCM calculations of the reduced neutron strength functions averaged on the 1 MeV interval in comparison with the available experimental data are shown in Fig.1. The disagreements for p- neutron strength functions at some nuclei

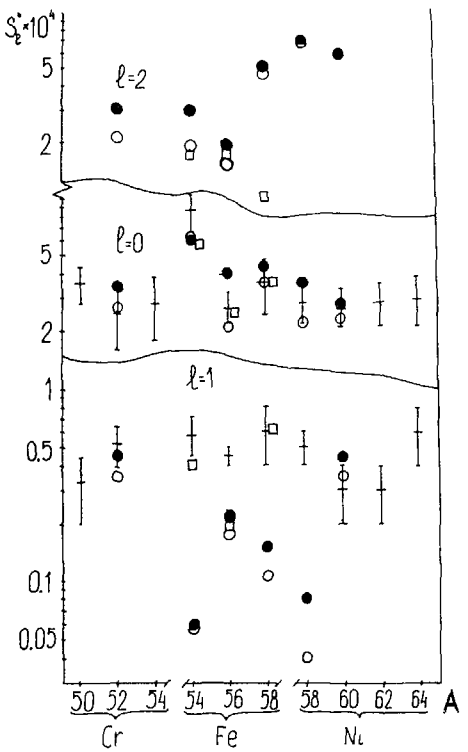

Fig. 1. Reduced strength functions for s- (l=0), p- (l=1) and d- (l=2) neutron at nuclei of iron region. Crosses with error bars present data [8], squares-evaluated data [9], closed and open circles-results of the MCCM calculations with W_s=0.4 and 0.2 MeV, respectively. The SOM results [10] are shown by a dotted curve.

draw attention. The main reason for this in our opinion, is due to the fact that a great deal of resonances, whose spins were not identified [8] but their widthes contribute to the p- neutron strength function definition actually belong to the system of d- resonances. Thus the new measurements on ^{56}Fe with rather complete identification of the spins of resonances in the energy range up to 350 keV (squares in Fig.1) resulted in a twofold decrease of the p- neutron strength function value and led to a good agreement with those obtained in the MCCM not only for p- but also for d- neutron strength function.

The MCCM calculations have shown the correctness of the well known semi-empirical evaluation of the reduced d- neutron strength function as that equal to the value for s- wave. Strength functions for p- neutrons of the iron region nuclei obtained in a spherical optical model (SOM) with potential of the standard geometry determined on the description of the s- neutron strength function are noticeably higher than the values given in [8,9]. This is a clear indication that the absorption in the elastic scattering channels with different orbital momenta can be different.

Consideration of coupling with the inelastic scattering channels is known to lead to the changes of the effective optical potential for the elastic scattering channel [11]. To demonstrate this we may compare the volume integrals from real parts of the optical potentials found in the MCCM (Table 1) with those in the SOM [12] and values of the volume integrals from average nuclear field determined in the condition of the description of the single particle states positions near the Fermi surface in the shell model [13].

Results of this comparison are shown in Fig.2. The MCCM volume integrals are 50 - 60 MeV. fm^3 less than those determined in spherical optical or shell models, but have the similar isotopical dependence.

Let us itroduce a supplementary assumption that the addition to the real part of the optical potential appearing as a result of the channels coupling has a surface form; this seems true for the tran-

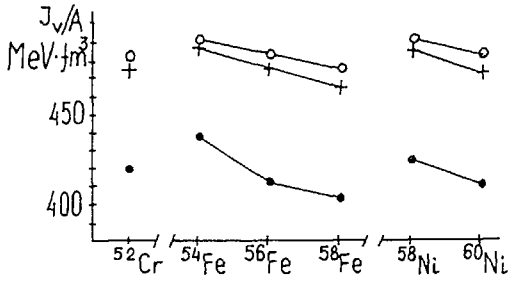

Fig.2. Volume integrals from real part of the optical potential (average field of the shell model) of the nucleus. Designations are: open cirles - for SOM potential [12], crosses - for potential of the shell model average field [13], closed circles present the values obtained in the MCCM.

sitional potentials with form-factor (1). Then a question can be raised about the calculation of its value through the determinati - on for each orbital wave of the locally equivalent potential of the SOM from the description of the corresponding diagonal elements of the MCCM scattering matrix. For this purpose the locally equivilent optical potential for each orbital wave and neutron energy may be determined as a sum of the potentials given in table 1 and a momentum dependent complex surface addition. The results of calculation for ^{58}Ni nucleus have shown that the value of the addition to the real part of the potential due to the channel coupling for small averagings ($W_s \sim$ hundreds of the keV) has a strong energy depen - dence caused by the existence of the door-way states with the 1 particle $\otimes$ 1 phonon structure. Its average value for ^{58}Ni nucleus (in the energy range 0 - 1 MeV) is small for p-wave and results in the increase of the total volume potential of the real part at 20 - 40 MeV. fm^3 for s- and d- neutrons.

Taking into account the coupling of numerous channels allows a consistent description of the averaged strength functions and low enegry neutron cross sections to be obtained.

REFERENCES

1. Bychkov V.M. at al - Fiz.Elem. Chast. i at. Yadra, 1983, v.14, N° 2, p.373 (in Russian).
2. Shakin C. - Ann.Phys., 1963, v.22, p.373.
3. Lovas I. - Nucl.Phys., 1966, v.81, p.353;
   Lev A., Beres W.P., Divadeenam M. - Phys.Rev., 1974,v.C9,p.2416;
   Pronyaev V.G. - In: Nucl.Data for Sci. and Technol.: Procee - dings of the Intern.Conf. (Antwerp, 1982),Holland,1983, p.532.
4. Tamura T. - Rev.Mod.Phys., 1965, v.37, p.679.
5. Moldauer P.A., Phys.Rev., 1964, v.135B, p.642.
6. Raynal J. - Material of Workshop on Nuclear Model Computer Codes, 16 Jan - 3 Feb. 1984, Trieste.
7. Nuclear Data Sheets, 1970, v.B3-3,4;
   1978, v.A23, n.4.
8. Mughabghab S.F., Divadeenam M., Holden N.E. - In: Neutron Cross Sections, N.Y. - L., Academic Press, 1981, v.1.
9. Pronyaev V.G., Ignatyuk A.V. - In: Voprosy at. nauki i tekhniki, ser. Yadernye Konstanty, 1986, N° 3, p.13,(in Russian).
10. Moldauer P.A., - Nucl.Phys., 1963, v.47, p.65.
11. Knyazkov O.M., Sorokin A.I. - Ann. der Physik, 1974, b.31, n.3, p.227.
12. Beechetti F.D., Jr., Greenlees G.W., - Phys.Rev., 1969, v.182, p. 1190.
13. Chepurnov V.A. - Yad.fizika, 1967, v.6, p.955 (in Russian).

DIRECT INELASTIC SCATTERING AND NUCLEAR COLLECTIVE EXCITATION

Dunhuan LIU
Wuhan University,
Wuhan

Hongmo ZHOU, Xiaochen ZHANG
Nankai University,
Tianjing

China

Abstract

Using the DWBA theory the differential cross section for inelastic scattering of neutron has been calculated. In order to calculate neutron nuclear data the computer program has been made.

The statistical theory including pre-equilibrium in the program MUP-2[4] of calculating the fast neutron data for medium- heavy nucleus has considered actually direct reaction mechanism in certain extend. Therefore, theoretical calculation of cross-section and energy spectrum have been much improved than one calculated by just using optical model and H-F statistical theory. It however can't calculate the cross-section of neutron inelastic scattering for discrete state, which becomes quite important at higher incident energy. This paper considers neutron inelasting scattering for collective excitation. The calculation of which is becoming one important part of the improved program.

The direct inelastic scattering for collective excitation induced by neutron can be calculated by using DWBA and coupled-channel method[1]. However, the coupled-channel calculations are generally lengthy and the adjustment of optical parameter is very difficult. Owing to the cross-section of inelastic scattering is usually one decimal smaller than elastic scattering for many nuclei and coupling between reactions is not strong, we can still calculate it with DWBA. We think elastic scattering and total cross-section is very important, which should be described as exactly as possible, and other reaction channels may be treated as perturbation. Because of adjusting optical potential parameter and the expansing of potential of deformed nuclei in sphercal-harmonic function (not in Taylor series) the present DWBA has retained higher order effect which is not the normal first order approximation.

The important contribution in direct inelastic scattering, except for few filled shell nuclei, comes from collective excitation of target nuclei, especially from the much lower collective excitation levels. In order to further improve MUP-2 program, it should be done to enlarge spherical optical potential to deformed one, the potential should be non-spherical symmetry (R is the function of θ, φ).

For spherical nuclei, whose equilibrium shape is spherical, the potential is expended in taylor series.

For non-spherical nuclei there is apparent rotational spectrum. We consider axial symmetry deformation in intrinsic coordinate space and expand the potential into spherical harmonic, The Hamiltonian of the whole system is

$$H=-\frac{\hbar^2}{2\mu}\nabla^2+H_t+V(r,\theta,\varphi)$$
$$=-\frac{\hbar^2}{2\mu}\nabla^2+H_t+V_{diag}(r)+V_{coupl}(r,\theta,\varphi) \quad (1)$$

where H_t is collective motion Hamiltonian of target nuclei. H_t takes harmonic oscillator model for spherical nuclei and RVM[2] for deformed nuclei and nuclei intransitional region. Owing to the presence of V_{coupl}, the redial equations is a group of coupled equation.

$$\left[\frac{\hbar^2}{2\mu}\frac{d^2}{dr^2}-\frac{\hbar^2}{2\mu}\frac{l(l+1)}{r^2}-V_{diag}(r)+E_n\right]R^{JM}_{nlj}(r)$$

$$=\sum_{n'l'j'}V^{JM}_{nlj;n'l'j'}(r)\;R^{JM}_{n'l'j'}(r) \qquad (2)$$

$$V^{JM}_{nlj,n'l'j'}=\left\langle(Y_{ljm_j}\otimes\phi_{I_nm_n})_{JM}\middle|V_{coupl}(r,\theta,\varphi)\middle|(Y_{l'j'm_j'}\otimes\phi_{I'_nm'_n})_{JM}\right\rangle$$

Solving the following equation

$$\left\{\frac{d^2}{dr^2}-\frac{l(l+1)}{r^2}-\frac{2\mu}{\hbar^2}V_{diag}(r)+K_n^2\right\}R^{JM}_{nlj}(r)=0 \qquad k_n^2=2\mu E_n/\hbar^2 \quad (3)$$

gets the total cross section $\sigma_t(OM)$, the differential and integral cross sections for shape elastic scattering $\frac{d\sigma_{se}}{d\Omega}$, $\sigma_{se(OM)}$, the absorption cross section $\sigma_A(OM)$ and the wave functions $R^{JM}_{nlj}(r)$. Solving eq. (2) with DWBA, gets the differential and integral cross sections $\frac{d\sigma^{DW}_{nn'}}{d\Omega}$, $\sigma^{DW}_{nn'}$ for inelastic scattering.

For spherical nuclei, the zeroth order approximation just is the solution of former spherical optical potential. For deformed nuclei, the parameter of optical potential should be changed.

The relation between theoretical and experimental cross section can be shown as following table:

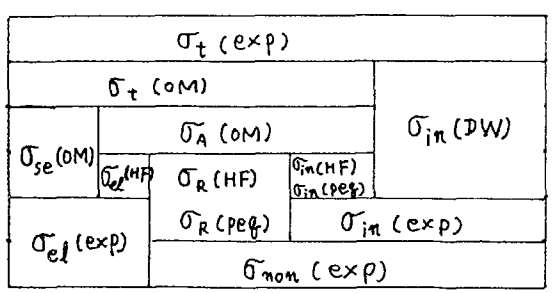

The optical potential parameter can be adjusted according to the relation as mentioned in table.

We have calculated $W^{182,184}$ with DINS[6] which is a program of calculating neutron inelastic scattering. The analysis of calculation for W^{182} can be expressed as following.

Figure 1 is the comparson between theoretical and experimental results of elastic scattering differential cross section. The experimental data takes from J.R.M. ANNAND and R. W. FINLAY. The theoretical parameters are:
AR=0.63, ASO=0.5, AS=AVV=0.47, XR=1.26, XSO=1.11, XS=XV=1.28, VO=45.11, V1=0, V2=0, V3=0, V4=0, Wo=5.72, W1=0, W2=0, UO=0. U1=0, VSO=5.75, β_2=0.223, β_4=-0.056, β_6=-0.01.
The symbols above are the same as that used in MUP-2. Figure 1 indecates that the coincidence with the elastic scattering is better at small angles then at large angles. Figure 2 indicates the comparision of theoretical and experimental results for inelastic scattering and the deviation appears at large angle as mentioned above. If the parameters are adjusted more carefully, the results should be improved. Figure 3 shows excitation function of (n,n')2+ state. The experimental spots and HF+peq calculation are supplied by Ma Gong-Gui [5], and we can see that even though we have considered pre-equilibrium emission, the theoritecal values are much lower than the experimental ones. After adding the direct inelastic scattering cross section, the theoretical values will get fair improving. But the theoretical values are in excess of normal value at higher energy tail.

The cross section of (n,n')2+, (n,n')4+ and (n,n')6+ have been calculated and compared each other. For the general nuclei, the cross section of 4+ state is one decimal smaller than that of 2+ states, 6+ states is two decimal smaller than 2+ states. The differential and integral inelastic cross section for W^{184} have been calculated. The optimum optical potential paraters were searched to fit to the data of total cross section and differential elastic and integral inelastic scattering with program AJDFOM[7] that searches automatically optimum parameters of the deformed optical potential in order to fit to the experimental data. The optical potential parameters searched

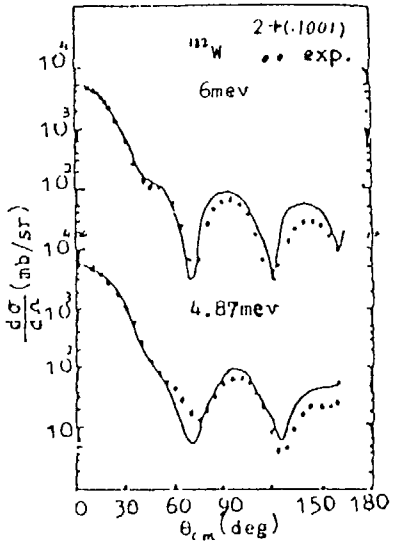

FIG.1. Comparison between theoretical and experimental results of elastic scattering differential cross-section.

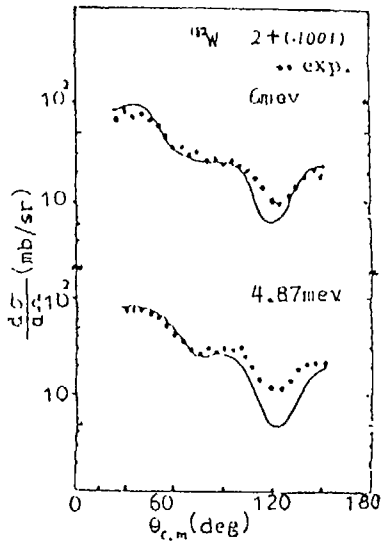

FIG.2. Comparison between theoretical and experimental results of (n,n')2+.

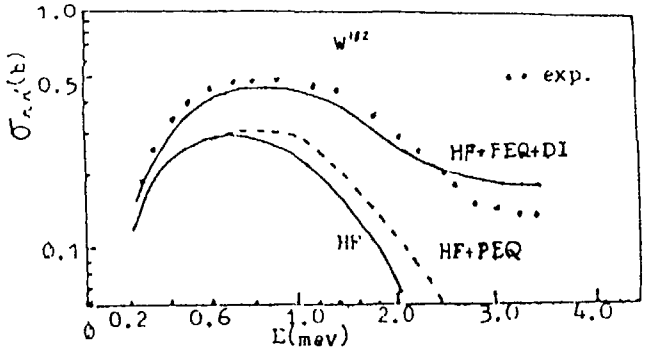

FIG.3. Comparison of excitation function of (n,n')2+ between theoretical and experimental.

are AR=0.614, AS=0.364, AVV=0.364, ASO=0.614, XR=1.182, XS=1.253, XV=1.253, XSO=1.182, UO=-1.853, U1=1.015, VO=48.032, V1=-0.56, V2=0.082, VSO=3.1, WO=9.206, W1=0.337, β_2=0.24, The results shown in Fig. 4, 5 show that the calculation results are well in accord with experimental data[9] after adding inelastic scattering cross section to compound one.[8]

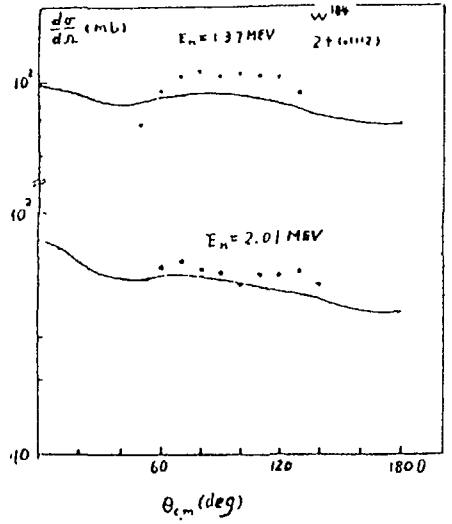

FIG.4. Comparison between theoretical and experimental results of (n,n')2+.

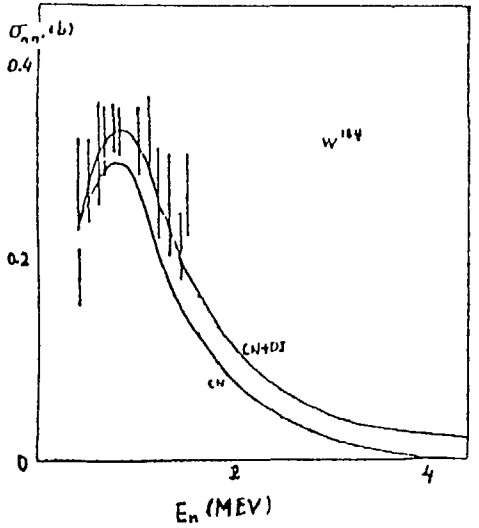

FIG.5. Comparison of excitation function of (n,n')2+ between theoretical and experimental.

REFERENCES

1. G.R. Satchler, Derect Nuclear reaction (OXFORD UNIVERSITY, OXFORD, 1983)
   T. Tamura, Rev, mad. Phys. 7, (1965) 679
   P.H. Bassel etal, Phys. Rew. 128(1962)2693
2. Liu Dun-Huan ACTA Physica Sinice 21 (1965)952
3. J.R.M. ANNAND and R.W. Finlay, Nucl. Phys. A441 (1985)234
4. Yu Zi-Qiang etsl. CNDC-8501, 129 (1986)
5. Ma Gong-Gui, unpublished (1985)
6. Zhang Xiao Chen, etal. unpublished (1985)
7. Zhou Hong-Mo, etal. unpublished (1986)
8. Zhou Zi-Lin, HSJ-78223 (1978)
9. Kinco-Tsukade, etal, Nucl. Phys. A125(1969)641

A PRELIMINARY MEDIUM ENERGY NUCLEON-NUCLEUS PHENOMENOLOGICAL OPTICAL MODEL POTENTIAL

D.G. MADLAND
Los Alamos National Laboratory,
Los Alamos, New Mexico,
United States of America

Abstract

Initial results are presented for the determination of a medium-energy nucleon-nucleus phenomenological optical-model potential. The starting point for this work is the phenomenological optical-model potential of Schwandt et al., which is based on measured elastic scattering cross sections and analyzing powers for polarized protons ranging from 80 to 180 MeV. This potential is modified optimally to reproduce experimental proton reaction cross sections for ^{27}Al, ^{56}Fe, and ^{208}Pb, as a function of energy, while allowing only minimal deterioration in the fits to the elastic cross sections and analyzing powers. Further modifications in the absorptive potential were found necessary to extrapolate the modified potential to higher energies. The final potential is converted to a neutron-nucleus potential by use of standard Lane model assumptions and by accounting approximately for the Coulomb correction. Comparisons of measured and calculated proton reaction and neutron total cross sections are presented for ^{56}Fe.

INTRODUCTION

In order to carry out realistic calculations of specific medium-energy neutron- or proton-induced reactions, a minimal requirement is that the optical-model potential used satisfactorily reproduce the scattering observables upon which it is based at these energies. In particular, the integrated observables should be well reproduced, namely, the proton total reaction cross section σ_R and the neutron total cross section σ_T, in order that the calculated specific reactions all sum to the correct physical value. In this work, we have used our preliminary results[1] in obtaining a phenomenological nucleon-nucleus optical-model potential for medium-energy scattering that optimally reproduces the integrated observables. We describe here how this potential is obtained and how its predictions compare to the measured observables.

Our starting point is the phenomenological proton optical-model potential of Schwandt et al.[2] This potential is based upon experimental elastic scattering and analyzing power angular distributions for target masses A and incident proton energies E_p in the ranges

$$24 \le A \le 208 \quad \text{and}$$
$$80\ \text{MeV} \le E_p \le 180\ \text{MeV}, \tag{1}$$

respectively. The data were analyzed in the framework of a relativistic Schrödinger-type wave equation generated by appropriate reduction of the Dirac equation, as described in Ref.3. A local, energy-dependent, complex potential of Woods-Saxon form was assumed and best-fit parameters were obtained for each individual experimental data set by performing least-squares adjustments. The resulting sets of parameters were then examined for simple dependencies with respect to the incident proton energy, the target mass number, and the target asymmetry parameter (N-Z)/A. In this way, Schwandt et al.[2] obtained the global phenomenological proton optical-model potential that we take as our starting point.

METHOD

We define our goal as a global phenomenological nucleon-nucleus optical-model potential valid for target masses and incident nucleon energies in the ranges

$$24 \le A \le 208 \quad \text{and}$$
$$50\ \text{MeV} \le E_n, E_p \le 400\ \text{MeV}, \tag{2}$$

respectively. Comparing Eqs. (1) and (2), we see that there are two tasks. The first is to extend the energy range of the proton potential downwards to 50 MeV and upwards to 400 MeV. The second is to attempt to transform the extended proton potential to a neutron potential valid for the same energy range.

The method that we use consists of the following: We adjust *only* the parameters of the proton central absorptive potential to optimally reproduce the experimental proton total reaction cross section in the extended energy range. All other parameters remain at their original values. In particular, the spin-dependent absorptive potential remains unchanged due to the fact that, at this early stage, we have not included experimental spin-dependent observables from the extended energy range in our analysis. We perform the adjustments to the parameters of the absorptive potential allowing only *small* changes in the calculated elastic scattering and analyzing power angular distributions. Assuming a satisfactory proton potential is obtained with this method, the transformation to the corresponding neutron potential is made by using a simple Lane model, namely,

$$(N - Z)/A \rightarrow -(N - Z)/A, \tag{3}$$

wherever this factor appears in the modified potential, and by using a simple Coulomb correction[4] in the real central potential, namely,

$$V_{corr} = 0.4\ Z/A^{1/3}. \tag{4}$$

We note here that no Coulomb correction was explicitly included in the real central part of the original proton potential of Schwandt et al.[2] Thus, to obtain the neutron potential, we assume that this correction is present implicitly in the real central part of the proton potential so that we then simply *subtract* Eq. (4) to complete the transformation.

Our preliminary results have been obtained by considering the target nuclei ^{27}Al, ^{56}Fe, and ^{208}Pb together with corresponding experimental proton total reaction cross sections and neutron total cross sections for the energy range given by Eq. (2). It was observed that the original proton potential of Schwandt et al.[2] predicts a total reaction cross section σ_R that increases strongly with increasing incident energy as one approaches the upper end of the range of validity for the model, 180 MeV, and in fact diverges as the energy is increased further (beyond the range of the potential). The source of this divergence is the strong energy dependence chosen for the strength W_v of the central absorptive potential, namely, a third-order polynomial in the incident energy.

We solve this problem by dividing the modified potential into two regions: a lower energy region in which no divergence occurs in σ_R and an upper energy region where the divergence in σ_R begins and grows with increasing energy. We then change the form of W_v in the upper region so as to remove the divergence. An energy grid of 31 points was chosen to span the range given by Eq. (2), and a number of survey calculations were performed to determine the dividing point between the two regions. In this way, the value 140 MeV was determined. Thus, we define the two regions of the potential as follows:

$$\text{Region I:} \quad 50\ \text{MeV} \le E_n, E_p \le 140\ \text{MeV}, \quad \text{and}$$
$$\text{Region II:} \quad 140\ \text{MeV} \le E_n, E_p \le 400\ \text{MeV}. \tag{5}$$

82 Similarly, a number of survey calculations were performed on the same energy grid, in which various forms of the absorptive potential were tested. These calculations, for protons incident on ^{27}Al, ^{56}Fe, and ^{208}Pb, lead to the following adjustments in the central absorptive part of the original potential of Schwandt et al.[2]

Region I: W_v is unchanged, r_I is unchanged, and $a_I = a_0 + a_1 E$ has the change $a_0 \rightarrow a_0 - 0.05$ fm $= 0.27$ fm. (6)

Region II: $W_v = W_0 + W_1 E - W_2 E^2 + W_3 E^3$ has the change $W_v \rightarrow W_0' + W_1' E$, $r_I = r_0 - r_1 E$ has the change $r_I \rightarrow r_0'$, and $a_I = a_0 + a_1 E$ has the change $a_I \rightarrow a_0'$. (7)

In Eqs. (6) and (7), W_v, r_I, and a_I are the strength, radius, and diffuseness of the modified central absorptive potential while E is either the incident proton energy E_p or the incident neutron energy E_n (discussed later). We refer to the original potential of Schwandt et al.[2] together with the adjustments given by Eqs. (6) and (7) as the modified potential for the range given by Eq. (2). Additional calculations were performed, for protons incident on the same target nuclei, to determine more precise values of the parameter a_0 appearing in Eq. (6) and the parameters W_0', W_1', r_0', and a_0' appearing in Eq. (7). The value of a_0 remained the same while the values obtained for the remaining parameters are

$$W_0' = 7.314 \text{ MeV} \quad (8)$$

$$W_1' = 0.0462, \quad (9)$$

$$r_0' = 1.17 \text{ fm, and} \quad (10)$$

$$a_0' = 0.59 \text{ fm for } ^{27}\text{Al}, \quad = 0.66 \text{ fm for } ^{56}\text{Fe}, \quad = 0.79 \text{ fm for } ^{208}\text{Pb}. \quad (11)$$

RESULTS

We now discuss the results obtained using this modified potential. We consider first our results for protons and use ^{56}Fe as an illustrative example. In Fig. 1, we compare experimental total reaction cross sections for ^{56}Fe with values calculated from the original potential of Schwandt et al.[2], for its energy range given by Eq. (1), and with values calculated from the modified potential, for its energy range given by Eq. (2). Although the experimental data are sparse, they clearly constrain the central absorptive potential to an energy-dependence that is well approximated by a linear assumption. On the other hand, the third-order assumption of the original potential clearly leads to unphysical values of σ_R in the upper half of its energy range. Almost identical conclusions are obtained for the two potentials for ^{27}Al and ^{208}Pb. We note here that the modified potential is discontinuous at the boundary point of Regions I and II. However, the magnitude of the discontinuity is small. Next, we examine the changes in the elastic scattering and analyzing power angular distributions that are caused by the modifications to the original potential, as summarized by Eqs. (6)-(11). For comparison purposes, we assume that the original potential well represents these observables and therefore that a comparison of the predictions of the modified potential to those of the original potential is equivalent to comparisions with the measured observables. We choose energies that are 10 MeV below and above the

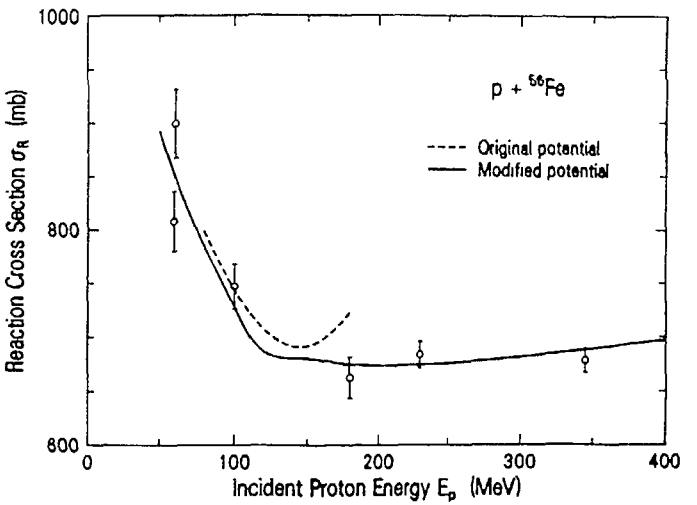

Fig. 1. Comparisons of measured and calculated proton reaction cross sections for ^{56}Fe.

boundary point of 140 MeV and show the elastic scattering angular distributions in Figs 2 and 3 (as ratios to Rutherford scattering to enhance the sensitivity), and show the analyzing powers in Figs. 4 and 5. The elastic scattering hardly changes at all in Region I, for the entire angular range, and changes significantly, in Region II, only at angles above about 70° where the elastic scattering is approximately six orders of magnitude down from the forward scattering. Thus, the changes in the elastic scattering due to the modifications of the potential are small. The same conclusion is reached for the analyzing powers, shown for the same two energies in the two regions in Figs 4 and 5 Again, the analyzing power hardly changes at all in Region I, and changes significantly, in Region II, only at angles above about 120°. Very similar results to those just described are obtained in comparing the elastic scattering and analyzing power angular distributions calculated for ^{27}Al and ^{208}Pb. Our conclusion is that the modification of the original potential of Schwandt et al.[2], to extend the range of the potential and to improve the calculated values of the total reaction cross section, has not overly deteriorated the predictive ability for elastic scattering and analyzing power angular distributions.

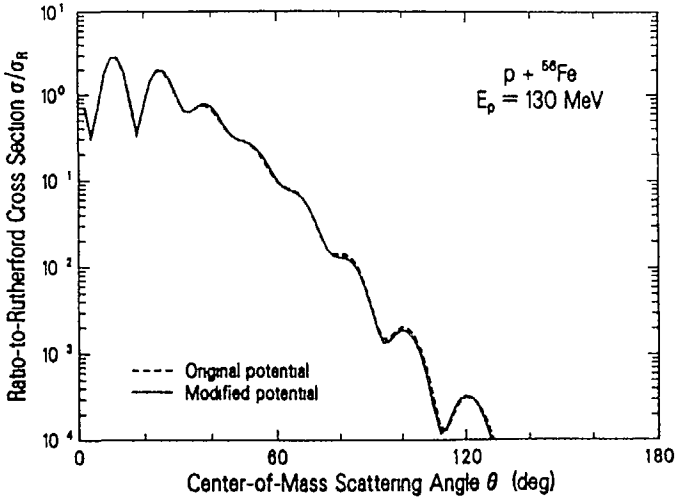

Fig 2 Comparison of calculated elastic angular distributions for the p+^{56}Fe reaction using the original potential and using the modified potential (Region I)

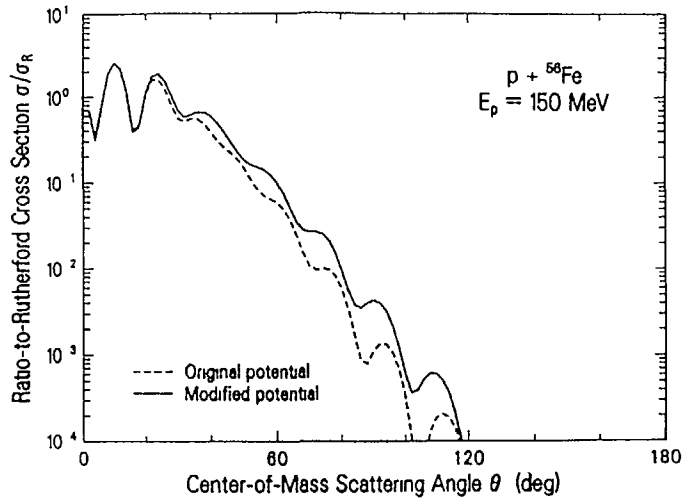

Fig 3 Comparison of calculated elastic angular distributions for the p+^{56}Fe reaction using the original potential and using the modified potential (Region II)

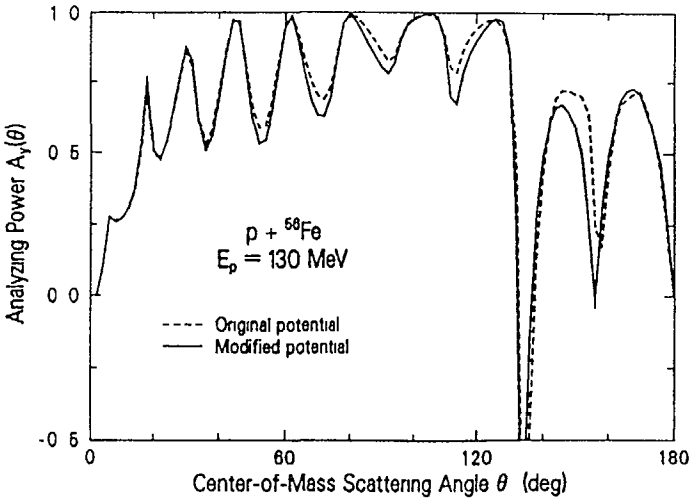

Fig 4 Identical to Fig 2 except for the analyzing power

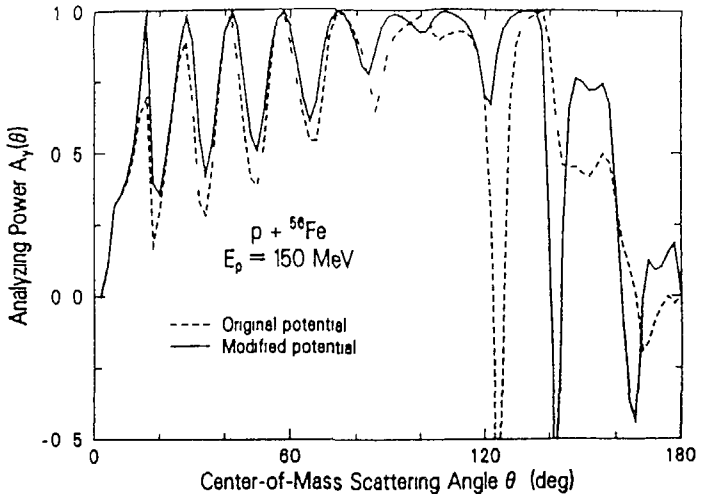

Fig 5 Identical to Fig 3 except for the analyzing power

Using the same modified potential, together with the transformation to neutron projectiles given by Eqs (3) and (4), we consider our results for neutron scattering and again use ^{56}Fe as an illustrative example In Fig 6, we compare experimental total cross sections for ^{56}Fe with values calculated from the original potential of Schwandt et al [2], for its energy range given by Eq 1, and with values calculated from the modified potential, for its energy range given by Eq (2), but in both cases for *only* the contribution due to the Lane model in transforming the proton potential to a neutron potential. Fig. 7 is identical to Fig 6 except that the contributions due to *both* the Lane model and the Coulomb correction in transforming the proton potential to a neutron potential are included Inspection of Fig 6 shows that both potentials overpredict the experimental neutron total cross sections, by approximately 15%, when including only the Lane model contribution, and that the values calculated from the original potential are beginning to diverge at the upper end of its range Inclusion of the contribution from the Coulomb correction, however, reduces the overprediction to approximately 5% for both potentials, as shown in Fig 7 Again, the values calculated from the original potential begin to diverge at the upper end of its range Similar results are obtained for ^{27}Al and ^{208}Pb Our conclusion is that the transformation given by Eqs (3) and (4) allows the calculation of neutron total cross sections to an accuracy of about 5% At this time, we have not yet examined in detail the elastic scattering and analyzing power angular distributions for neutrons as very little experimental data are available

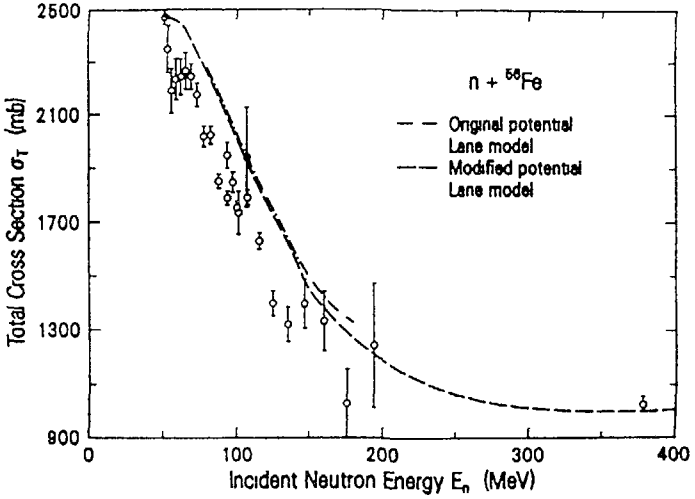

Fig 6 Comparisons of measured and calculated neutron total cross sections for ^{56}Fe Only the simple Lane model, Eq (3), has been employed.

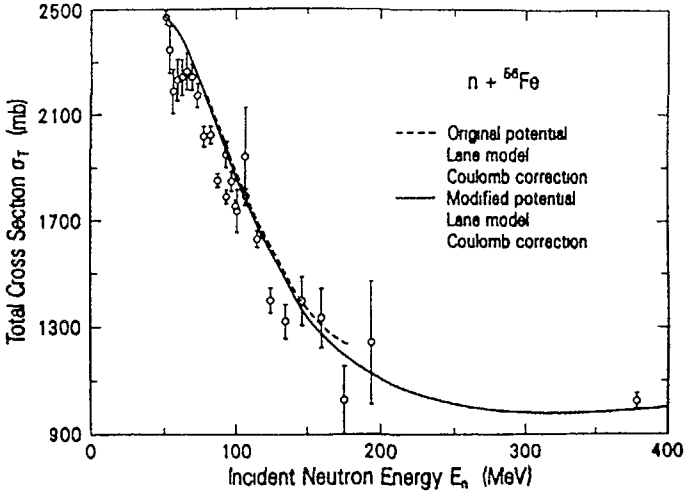

Fig 7 Comparisons of measured and calculated neutron total cross sections for ^{56}Fe The simple Lane model, Eq (3), and the approximate Coulomb correction, Eq (4), have been employed

CONCLUSIONS

The overall conclusions from this preliminary work on obtaining a medium-energy global phenomenological nucleon-nucleus optical-model potential are that (1) the present potential is of sufficient accuracy that *specific* neutron- and proton-induced reactions can be calculated with expectations that they sum to the correct physical value, and that simultaneously (2) the angular-dependent proton elastic scattering observables are *reasonably* well reproduced, while the angular-dependent neutron elastic scattering observables *may* be reasonably well reproduced.

REFERENCES

1. D. G. Madland, Bull. Am. Phys. Soc. 31, 1230 (1986).
2. P. Schwandt et al., Phys. Rev. C 26, 55 (1982).
3. A. Nadasen et al., Phys. Rev. C 23, 1023 (1981).
4. F. G. Perey, Phys. Rev. 131, 745 (1963).

NEW PARAMETRIZATION OF THE OPTICAL MODEL POTENTIAL FOR NEUTRON REACTIONS

O.V. KONSHIN
Byelorussian State University,
Minsk, Union of Soviet Socialist Republics

Abstract

Analysis of experimental data available within the framework of the optical model showed that a deep minimum in the total cross-sections at energies below 3 MeV as well as level excitation functions for nuclei with A = 40 ÷ 60 cannot be reproduced by existing parametrizations. The information on single-particle state energies as the extrapolation of the optical potential to the negative energy region was included into the analysis made. As a result, a new optical model parametrization is proposed.

One of the long-standing tasks in the development of the optical model is the search for parametrizations which can describe all experimental data available in the wide range of neutron energies and nuclear masses. The use of a purely pheonomenological approach often leads to non-physical potential parameters, application of only a microscopic approach does not provide the accuracy required for nuclear data evaluation.

Different spherical optical parametrizations available in the literature [1 - 13] were analysed in the present work. Nuclei ^{51}V, ^{52}Cr, ^{56}Fe, $^{58,60,62,64}Ni$, ^{89}Y, ^{93}Nb, ^{96}Mo, ^{100}Ho, $^{206,207,208}Pb$ and ^{209}Bi were included into the analysis.

Comparison of experimental and calculated results for σ_t, $d\sigma_n/d\Omega$, $\sigma_{nn'}$ allows to select three typical groups of nuclei.

Nuclei from the region of the maximum of the strength function (^{51}V, ^{52}Cr, ^{56}Fe, $^{58,60,62,64}Ni$) belong to the first group. For this group parametrizations [4, 2] and similar to them, like [6], give a poor agreement

with the experimental data on the level excitation functions practically in the whole neutron energy region considered (Fig. 1). More successful are parametrizations of [9] and [8], although they do not solve the problem of reproducing $\sigma_{nn'}$ at energies below 3 MeV. The parametrization which gave a good agreement with experimental data on $\sigma_{nn'}$ at low energies should be used with great care at higher energies. Fig. 2 illustrates the calculations of neutron elastic angular distributions for ^{56}Fe at E_n = 13,92 MeV using the parametrization of Moldauer [1].

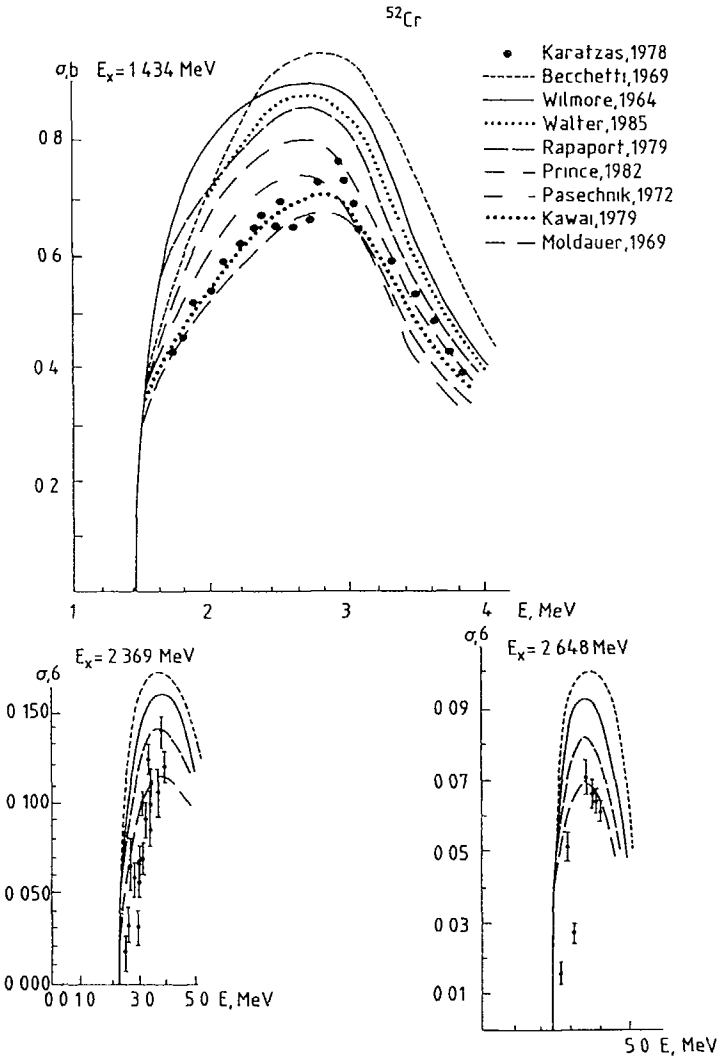

Fig. 1 Comparison of experimental and calculator data for level excitation functions of ^{52}Cr for different optical parametrizations.

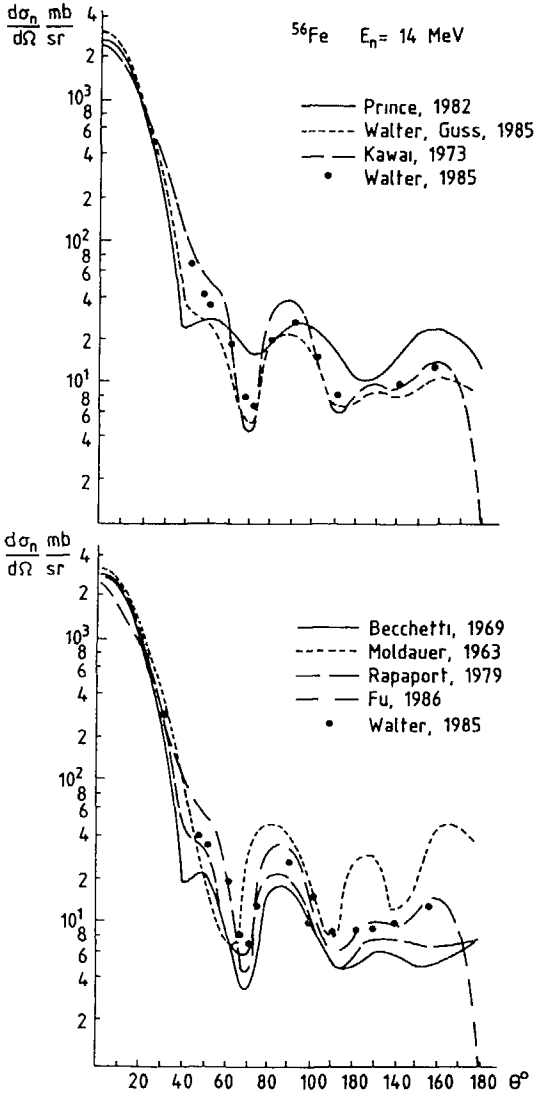

Fig. 2 Comparison of calculated and experimental data for neutron elastic angular distributions for ^{56}Fe at 14 MeV.

No existing global and regional parametrizations of the optical potential are able to reproduce a deep minimum in σ_t in the energy region below 2 ÷ 3 MeV for the nuclei considered. A part of the problem, as Smith [14] assumes, is experimental, e.g. taking into account the self-shielding effect can lead to increasing σ_t on 10 %. However, the difficulties at low energies should not be explained only by shortcomings in experimental techniques and the problem of a cross section averaging in the highly fluctuating region.

Hence, for this group of nuclei some difficulties arise. Optical parameters based on data at high energies cannot be reliably extrapolated to the low energy region. There is also a large difference in the reaction cross-sections σ_r due to different optical model parametrizations. Uncertainties in neutron transmission coefficients at low energies lead to less accurate and reliable not only level excitation cross sections but the threshold reaction cross sections (n, 2n), (n, p) etc. as it is shown by Young [15].

To the second group of nuclei belong the nuclei from the region of the strength function minimum: ^{89}Y, ^{93}Nb, ^{96}Mo, ^{100}Mo (see Fig. 3). For these nuclei the data on total and reaction cross sections, differential elastic and inelastic neutron scattering can be satisfactorily described in a wide range of neutron energies. In this case one can obtain a satisfactory agreement between experimental and calculated data in the whole energy region, taking as a basis, for example, parametrization [9], as it was done in [16].

In case of the third group of nuclei - Pb and Bi - the problem of description of elastic neutron differential cross sections is added to the problem of level excitation function calculations which takes place for light nuclei.

As a method of resolving such additional difficulty, Finlay et al. [17] proposed to introduce the energy dependent geometry parameters.

Traditionally, for the optical parameters the energy dependence is taken to be only in the well depth. For reproducing energies of low lying single-level states (lower than the Fermi energy ε_F) it is necessary to

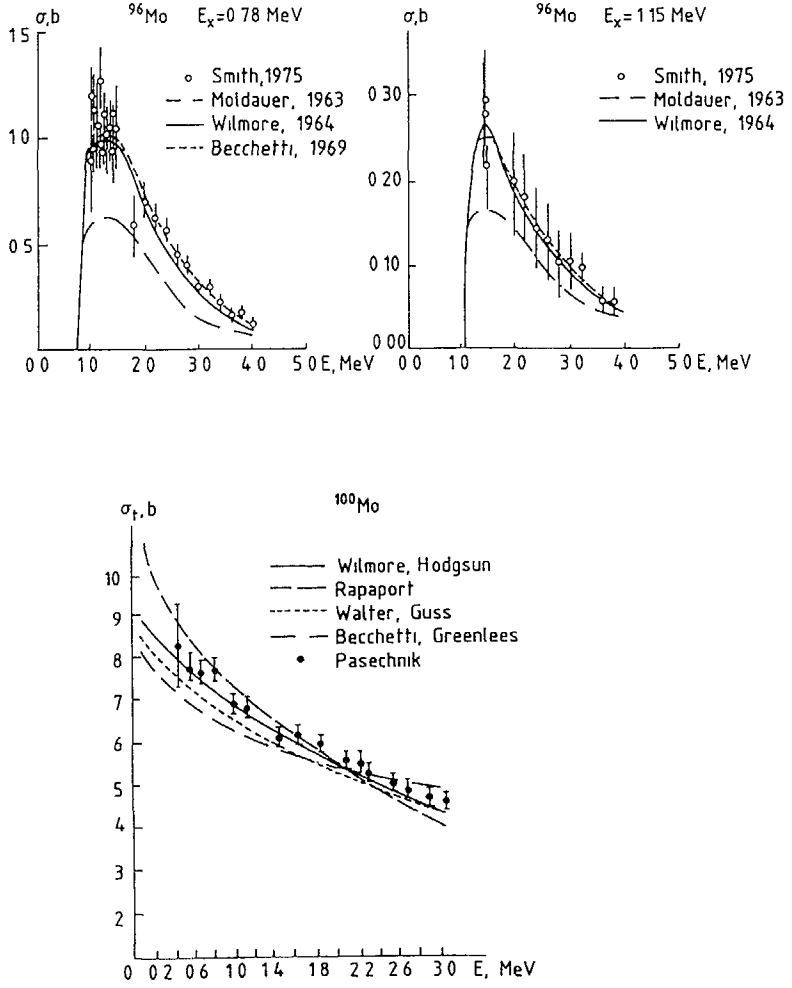

Fig. 3 Comparison of experimental and calculated data for level exciation functions and the total cross section for Mo.

use the energy dependence of the type: $V(E) = V_o - 0,4\ E$ $(E < 0)$, which corresponds to the effective mass value $m^*/m \simeq 0,6$. Although it is a more strong energy dependence compared to the one of the optical potential: $V(E) = V_o - 0,3\ E$, $m^*/m \simeq 0,7$, on the whole, the average field of the nucleus can be described as a continuous function of energy.

There exists a problem of single-particle spectra of weakly bound states (higher and in the region of the Fermi energy ε_F, $\varepsilon_F = -12$ MeV for ^{40}Ca and $\varepsilon_F = -5,6$ MeV for ^{208}Pb), so called anomaly in the Fermi energy region [18 - 21]. The calculations made for ^{208}Pb showed that experimental values of single-state energies near and higher the Fermi energy ε_F can be reproduced in the calculations using the static potential (the potential of a constant depth, effective mass $m^*/m = 1$) [22].

It is necessary to take into account that empirical information on single-particle potential of the shell model is very scarce and limited to experimental values of single-particle state energies for magic nuclei ^{208}Pb and ^{40}Ca, which is not sufficient for definite conclusions on $V(r, E)$ as it was shown in [23]. Additional information on neutron cross sections should be involved when considering optical potential parameters.

Calculations made by Mahaux and Ngo [24], [21], based on application of the dispersion relation, predict for ^{208}Pb a growth of the volume integral J_v up to 20 MeV and the equality to zero of the derivative dJ_v/dE at $\sim 3,5$ MeV. Note that the present analysis of experimental data for ^{208}Pb does not confirm these conclusions.

All the calculations were done only for ^{208}Pb (as well as the parametrization of Finlay [17]). The natural question arises about light nuclei for which principal problems of the extrapolation of optical potential parameters to the low energy region exist.

In Fig. 4 the values of $\langle r^2\rangle_v = 4\pi/A \int V(r)\, r^2\, dr$ are shown for different parametrizations used for ^{208}Pb and ^{59}Ni. The respective $\langle r^2\rangle_v$ corresponding to single-particle bound state energies [18] are also shown. As one can see, the values of $\langle r^2\rangle_v$ which are necessary for the accurate reproduction of the states near the Fermi energy ($2\ p_{1/2}$, $1\ f_{5/2}$, $2\ p_{3/2}$ for ^{59}Ni) and for the weakly bound states near the edge of the potential well ($3\ s_{1/2}$, $2\ d_{5/2}$, $1\ g_{9/2}$ for ^{59}Ni) are different, although in principle they can be described by the same set of parameters (with a poor agreement with the experimental values of the single-particle energies).

A great variety of parameter sets for single-particle states for ^{208}Pb (Fig. 4) can be explained by the attempts to reproduce either the states immediately near the Fermi energy or the weakly bound states near the well edge. For example, parameters [22] give the following energies for the states near the Fermi energy $\varepsilon_F = -5,6$ MeV : $2\ g_{9/2}$ ($-3,683$ MeV), $3\ p_{1/2}$ ($-7,232$ MeV), which are near to the experimental values $-3,74$ and $-7,38$ MeV, but for the last state $3\ d_{3/2}$ the calculated value $\varepsilon = -0,604$ MeV, experimental $-1,42$ MeV. Parameters [25] give respectively $-4,052$, $-7,547$ and $-1,358$ MeV and they describe better the weakly coupled states rather than the states near ε_F. Both sets of parameters [22] and [25] are energy independent and correspond to $m^*/m = 1$, but their volume integrals equal 407,07 MeV . fm^3 and 443,95 MeV . fm^3.

Taking into account a unique description of both bound states energies at $E < 0$ and scattering at $E > 0$, one can consider as asymptotic values of $\langle r^2\rangle_v$ at $E \to 0$ equal to 443,95 MeV . fm^3 for ^{208}Pb and 551,1 MeV . fm^3 for Ni. No one existing optical parametrization gives such large values.

In Fig. 5 comparison is made of energy dependence of V_R and r_R for the real part of the optical potential for ^{58}Ni. The potential parameters which give the correct values of the bound $3\ s_{1/2}$ and $2\ d_{5/2}$ states are denoted by crosses. As one can see, Moldauer's parametrization gives a large value of $\langle r^2\rangle_v$ due to a larger r_R rather than V_R which is the smallest.

One can formulate the following task: to find such modification of parametrization [8] which would give an increase of J_v up to 444 MeV . fm^3 for ^{208}Pb (~ 15 % increase) and 551 MeV . fm^3 for Ni (~ 20 % increase). For the nuclei from the region of the strength function minimum (for example, ^{89}Y) the parametrization [9] gives $[r^2]_v = 444$ MeV . fm^3

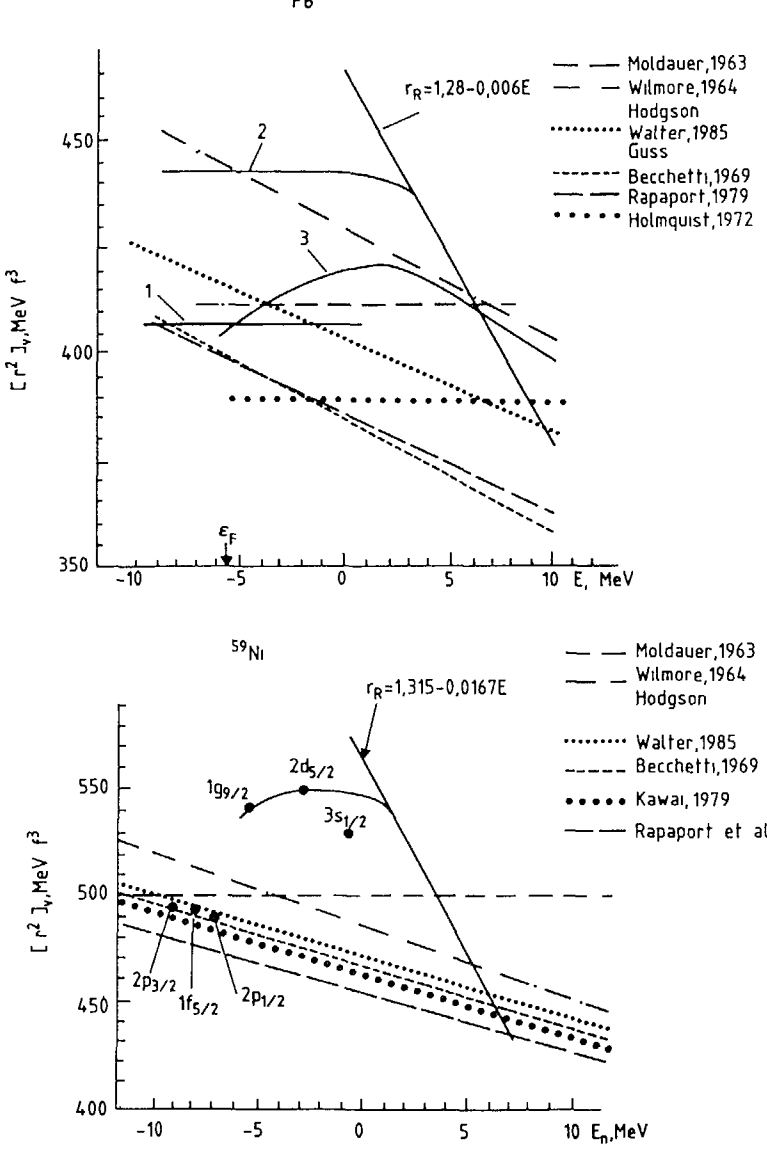

Fig. 4 Comparison of $\langle r^2 \rangle_v$ for different parametrizations. Curves: 1 - calculations using parameters from [22], 2 - parameters from [25], 3 - predictions by Mahaux et al. [24].

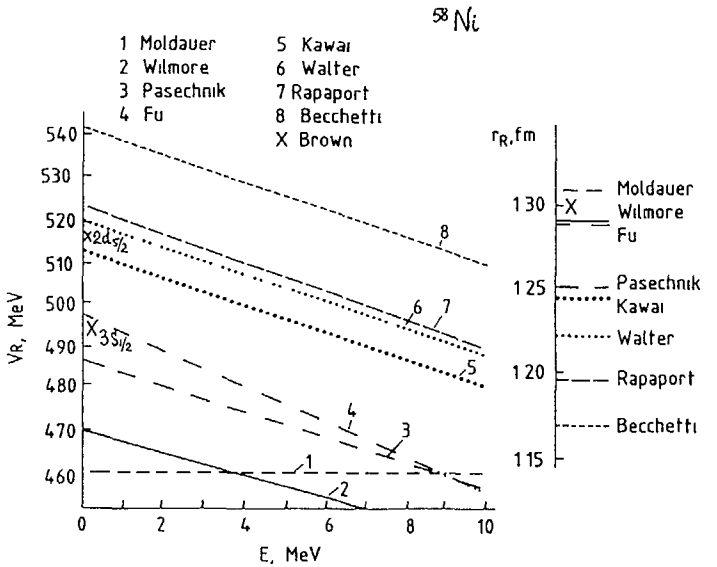

Fig. 5 Energy dependence of V_r for the real part of the optical potential for different parametrizations.

which is only 4 % lower than the value necessary for obtaining the correct energies for weakly bound states (this is the reason why the parametrization [9] can satisfactorily describe experimental data for these nuclei.)

The parametrization of Wilmore and Hodgson [2] seems to satisfy the request to describe weakly bound states (see Fig. 4 for ^{208}Pb), but leads to too high reaction cross sections at low energies. The answer to this question is in Fig. 6 and 7.

In Fig. 6 and 7 momenta $\langle r^2 \rangle_w$ of the imaginary part of the optical potential are presented for ^{208}Pb and ^{52}Cr. As one can see from Fig. 5, $\langle r^2 \rangle_w$ rapidly increases with energy in the region E < 15 MeV in the parametrization by Rapaport et al. [8], and then comes to the saturation value which possibly can be due to the opening of non elastic channels connected with low-lying collective excitations. And only the potential parameters [8] correspond to values $\langle r^2 \rangle_w$ obtained by Mahaux [26]. The parameters by

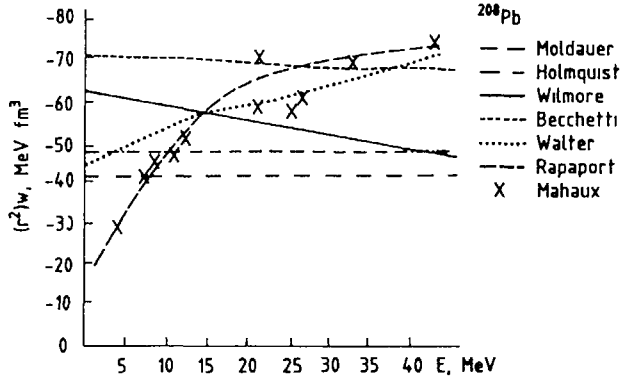

Fig. 6 The values of $\langle r^2 \rangle_w$ for ^{208}Pb.

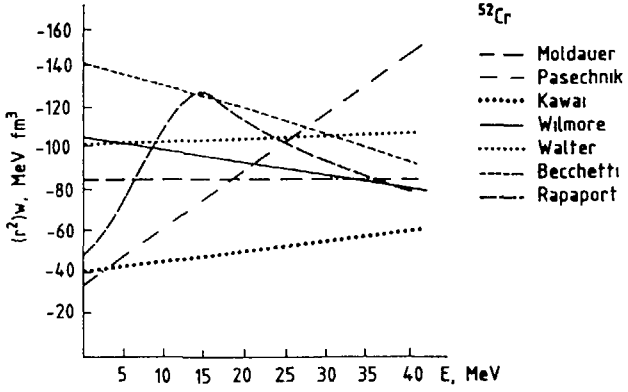

Fig. 7 The values of $\langle r^2 \rangle_w$ for ^{52}Cr.

Walter et al. [19] also show some growth with energy increasing. All the rest show either a constant $\langle r^2 \rangle_w$ in the whole energy region ([1], [5]) or even increasing $\langle r^2 \rangle_w$ in the low energy region ([4], [2]). At the same time a prominent feature of regional potentials for ^{52}Cr [11] is a practically linear increase of $\langle r^2 \rangle_w$ with energy.

Nonlinearity in the imaginary part of the potential must lead to changing the real part at low energies according to the dispersion relation method [24].

The introduction of the following expression for the radius of the real part of the potential [8]:

$$r_R = 1{,}315 - 0{,}0167\ E, \qquad a_R = 0{,}663 \tag{1}$$

gives the possibility to eliminate problems at low energies discussed above.

All the other parameters are taken to be as in [8]:

$$V_R = 54{,}19 - 0{,}33\ E - (22{,}7 - 0{,}19\ E)\eta, \quad \eta = N-Z/A,$$
$$W_D = 4{,}28 + 0{,}4\ E - 12{,}8\ \eta, \quad r_I = 1{,}295, \quad a_I = 0{,}59.$$

Such modification allows to use the parametrization [8] also in the energy region below 7 MeV.

The results of the calculations made with such parameters for Cr, Ni, Fe are given in Fig. 8 - 11. As one can see the modified potential parameters allow to describe not only a minimum in σ_t at $E_n < 3$ MeV, but also the data on excitation functions for ^{58}Ni, ^{52}Cr.

Note that the r_R-values (1) lead to too high J_v when extrapolating to the region of bound states ($E < 0$). Indeed, at $E = 0$ for ^{58}Ni $r_R = 1{,}315$ fm amd $V_R = 53{,}41$ MeV and for the correct description of the 2 $d_{5/2}$ - state $r_R = 1{,}3$ fm and $V_R = 51{,}5$ MeV [18] are required. It demonstrates the possibility of the J_v-curve coming to the saturation region and having a maximum.

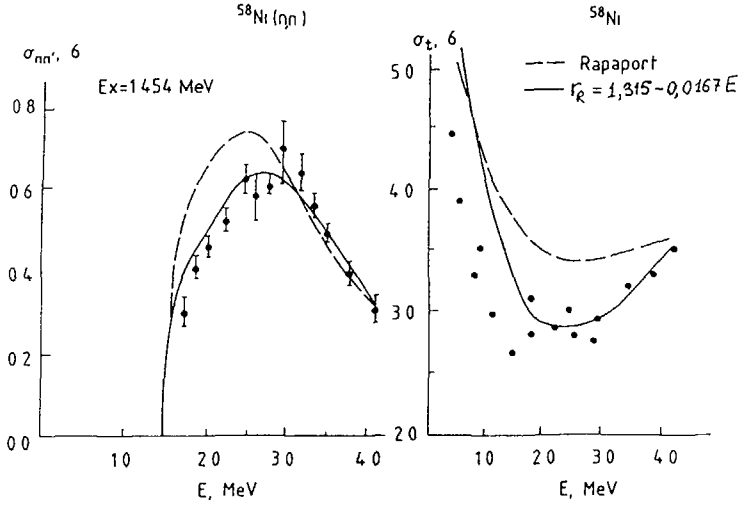

Fig. 8 Comparison of experimental and calculated data for σ_t and the level excitation function for ^{58}Ni (-- parametrization [8], - use r_R in form (1)).

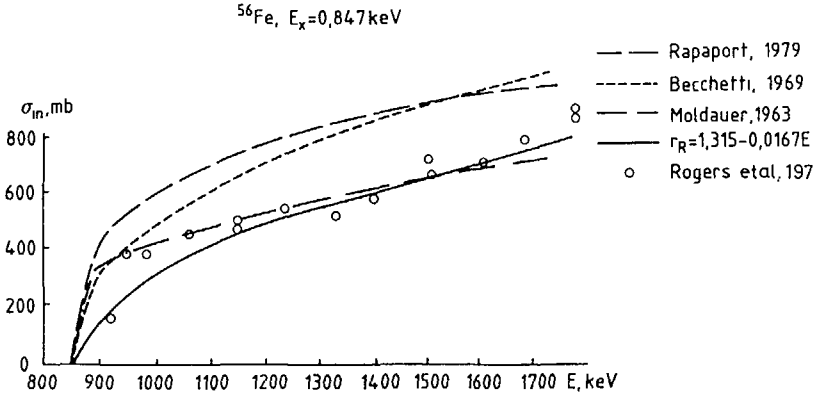

Fig. 9 Comparison of experimental and calculated data for the level excitation function of ^{56}Fe.

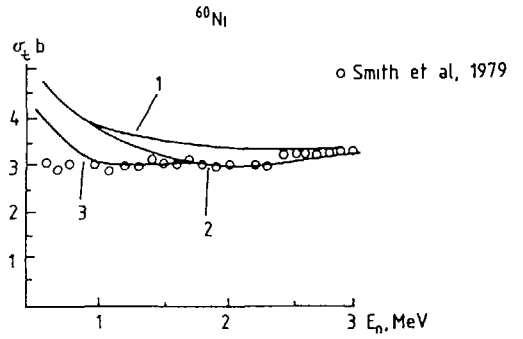

Fig. 10 Comparison of experimental and calculated data for σ_t ^{60}Ni (1 - traditional OM parametrization; 2 - use r_R in form (1); 3 - calculations with the parameter set (3)).

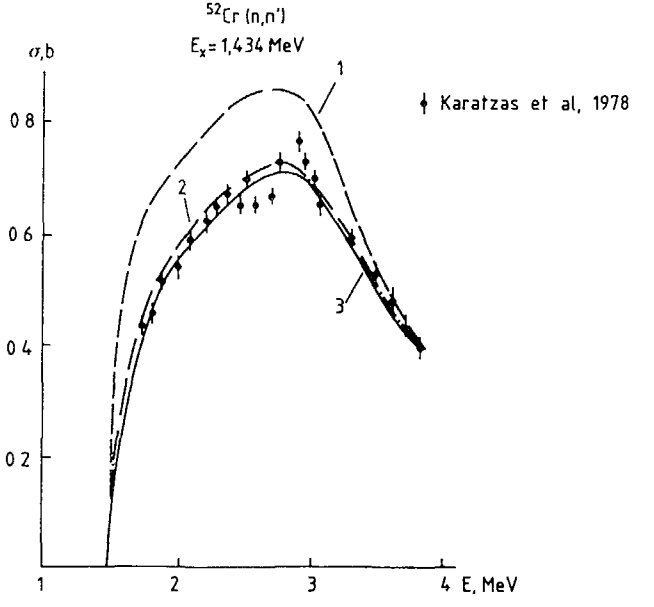

Fig. 11 Comparison of experimental and calculated data for the level excitation function of ^{52}Cr (1 - parametrization [8]; 2 - calculations with r_R, a_R, w_D, a_I from (1), but V_R on 2 Mev less to describe weakly bound states; 3 - calculations with the parameter set (1)).

From the physical point of view such discontinuity in parameters is not desirable and, besides, the use of the geometry parameters in form (1) in the energy region below 1 MeV does not lead to some improvements in comparison to the traditional approach. Therefore, the assumption about the J_v-saturation region at $E_n \sim 1$ MeV looks reasonable and the maximum in the J_v-curve might be at low negative energies (see the solid curve in Fig. 4).

In the region below 1 MeV the parameters obtained by the direct extrapolation from the weakly bound state region should be used, e.g. r_R = 1,3 fm and V_R on 2 MeV less than parametrization [8]. At energies higher than 1 MeV the use of such extrapolated V_R does not lead to remarkable differences in cross sections compared to the usually used V_R (see curve 3 in Fig. 11).

The introduction of the energy dependent radius is equivalent, in a mathematical sense, to the addition of a surface term to the real part of the optical potential. For example, for Ni, instead of using V_R in the form (1), one can add to the real part a surface term: $V_D = 9{,}925-1{,}45E$ with the geometry parameters as for the imaginary part: $r_D = 1{,}295$ fm, $a_D = 0{,}665$ fm, keeping all the other parameters as in [8]. As a result, we obtain the same J_v-value as in case of the energy dependent r_R, and both versions are equivalent from the point of view of describing experimental data.

For nuclei ^{208}Pb, ^{209}Bi principal difficulties at reproducing differential cross sections $\frac{d\sigma_n(\theta)}{d\Omega}$ up to energy 10 MeV are arising [17]. Unlike of Cr, Ni, Fe, for Pb, Bi it is essential to introduce the energy dependent geometry in a wide energy region from 0 to 10 MeV.

Based on the analysis of experimental data on differential cross sections for Pb and Bi [17], [27-31] in the energy region from 0,5 to 11 MeV, we came to the conclusion of the necessity of introducing the following energy dependent geometry parameters for Pb, Bi:

$$\begin{aligned} r_R &= 1{,}28-0{,}006E, & a_R &= 0{,}663 \\ r_I &= 1{,}295, & a_I &= 0{,}07+0{,}0314E \end{aligned} \qquad (2)$$

In case of Pb the growth of the J_v-curve takes place in a wide energy region $E_n \leq 10$ MeV than for Ni (see Fig. 4). Mahaux et al [24] using the dispersion relation method predicted the increase of J_v in the very wide energy region up to 15 MeV and a maximum at 3,5 MeV. As we can see, the difference in the J_v-curves obtained in [24] and in the present work is the following: the growth of the J_v-curve takes place up to ~ 10 MeV, but not up to 15 MeV; (b) there is no distinct maximum in the region of 4 MeV, although there is a saturation of the J_v-growth in the region 0÷3 MeV. The maximum in the J_v-curve might lie at low negative energies and correspond to the energies of weakly bound single-particle states.

In the energy region En ≤ 1 MeV for Ni and En ≤ 3 MeV for Pb the best description of experimental data can be reached under the assumption of the "static" potential, e.g. the potential with the constant depth and the radius of the real part. The parameters of the optical potential can be taken as follows:

$$\begin{aligned} V_R &= 52{,}2-22{,}7\,\eta, \quad \eta = \frac{N-Z}{A}, \quad a_R = 0{,}663 \text{ fm}, & r_R &= 1{,}30 \text{ fm (Ni)} \\ & & r_R &= 1{,}27 \text{ fm (Pb)} \end{aligned} \qquad (3)$$

$$W_D = 4{,}28+0{,}4E-12{,}8\,\eta, \quad a_I = 0{,}07+0314E, \quad r_I = 1{,}295 \text{ fm}.$$

Taking the parameter set (3) one can reproduce weakly bound state energies as well as the data on neutron scattering using one and the same parameters.

Experimental data on neutron differential cross sections for Pb and Bi [27] at 0,5; 1,0; 2,5 MeV can be well reproduced using the parameter set (3). The problem of describing the level excitation function for ^{209}Bi can also be solved (Fig. 12). A better description of the total cross-sections for Ni at energies below 1 MeV can be obtained using the parameter set (3) (Fig. 13).

The introduction of the energy dependent a_I leads to a smaller value of J_w at E=0 and to a faster decrease of J_w when approaching the point E=0. And at the same time, decrease of a_I with energy decreasing leads to the decrease of the strength functions and gives their values more close to the

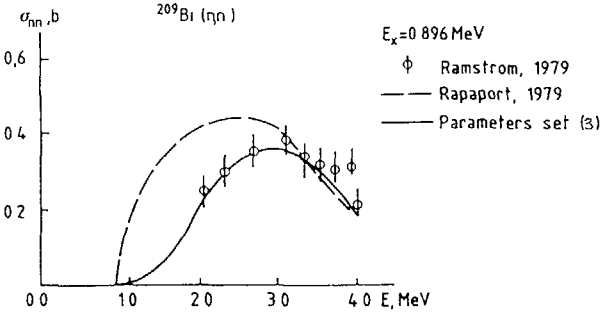

Fig. 12 Comparison of experimental and calculated data for the level excitation function of ^{209}Bi (--- calculations with the parametrization [8], ___ parameters (3)).

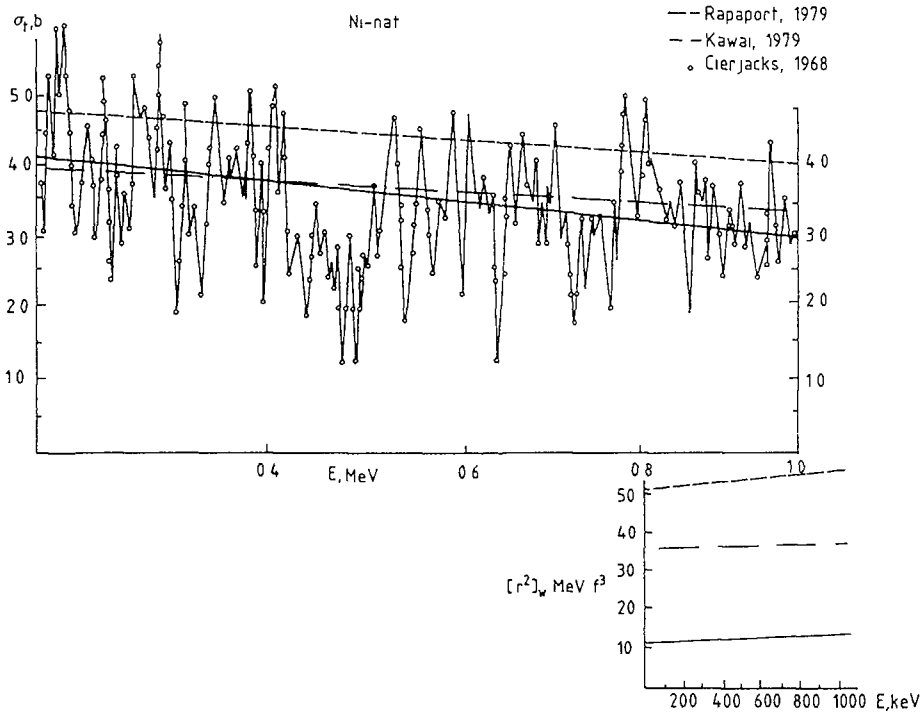

Fig. 13 Comparison of experimental and calculated data for the total cross section of Ni (--- calculation with parametrization [8], - • - parametrization [13], ___ parameter set (3)).

experimental data (comparable with the predictions using the parametrization of Moldauer [1]).

Hence, analysis of additional information at low energies as well as the information on single-particle bound states (as the extrapolation of the optical potential to the negative energy region) cause some doubts on the usual assumption on non-energy dependent geometry parameters near the Fermi energy region. Therefore, the introduction of energy dependent radius as the extrapolation from low positive energies may look natural.

REFERENCES

[1] MOLDAUER, P.A., Nucl. Phys. 1963, V.47, p.65.

[2] WILMORE, D., HODGSON, P.E., Nucl. Phys., 1964, V.55, p. 673.

[3] ENGELBRECHT, C.A., FIEDELDAY, H., Ann. Phys., 1967, V.42, p. 262.

[4] BECCHETTI, F.D., GREENLEES, C.W., Phys. Rev., 1969, V.182, p. 1190.

[5] HOLMQUIST, B., WIEDLING, T., J. of Nucl. En., 1972, V.27, p. 543.

[6] PATTERSON, D.M., DOBRING, R.R., GALONSKY, A., Nucl. Phys., 1976, V.A263, p. 261.

[7] MADLAND, D.G., YOUNG, P.V., Proc. of the Intern. Conf. on Neutron Physics and Nuclear Data for Reactors and Other Applications, Harwell, OECD, 1978, p. 349.

[8] RAPAPORT, J., KULKARNI, V., FINLAY, R.W., Nucl. Phys., 1979, V.A330, p. 15.

[9] WALTER, R.K., GUSS, P., Proc. of the Intern. Conf. in Nuclear Data for Basic and Applied Science, Santa Fé; 1985, in: Radiation Effects, 1986, V.95, p. 73.

[10] FU, C.Y., HETRICK, D.M., Update of ENDF/B-V Mod.-3 Iron, Neutron Producing Cross Sections and Energy Angle Correlation, ORNL/TM-9964, 1964.

[11] PASECHNICK, M.V., KORZH, I.A., KASHUBA, I.E., Proc. of the Conf. on Neutron Physics, Kiev, 1972, part 1, p. 253.

[12] BERSILLON, O., CAPELT, B., PHILLIS, C.A., Proc. of the Intern. Conf. on Nuclear Data for Science and Techn., Antwerp, 1982, p. 665.

[13] KIKUCHI, I., SEKINE, N., Evaluation of Neutron Nuclear Data of Natural Nickel and its Isotopes for JENDL-2, JAERI-M85-101, 1985, p. 195.

[14] SMITH, A., Nucl. Sci. Eng., 1979, V.72, p. 293.

[15] YOUNG, P.G., Proc. of the Specialists' Meeting on the Use of the Optical Model for the Calculation of Neutron Cross Sections below 20 MeV, Paris, 1985, p. 127.

[16] LAWSON, R.D., GUENTHER, P.T., SMITH, A.B., Phys. Rev., 1986, V.34, p. 1599.

[17] FINLAY, R.W., ANNAND, J.R.M., PETLEV, J.S., Phys. Let., 1985, V.155B, p. 313.

[18] BROWN, G.E. et al, Nucl. Phys., 1963, V.46, p.589.

[19] BERTSCH, G.F., KUO, T.T.S., Nucl. Phys., 1968, V.A112, P.204.

[20] BROWN, G.E. et al, Nucl. Phys., 1979, V.A330, p. 290.

[21] MAHAUX, C. et al, Phys. Rep., 1985, V.120, p. 1.

[22] BLOMQUIST, J., WAHLBORN, S., Arkiv Fysik, 1960, V.16, p. 545.

[23] MAHAUX, C., SARTOR, R., Nucl. Phys., 1987, V.A468, p. 193.

[24] MAHAUX, C., NGO, U., Nucl. Phys., 1982, V.A378, p. 205;
Nucl. Phys., 1983, V.A410, p. 271.

[25] BHATTACHARYA, R., Zeit. Phys., 1985, V.A322, p. 665.

[26] MAHAUX, C., SARTOR, R., Phys. Rev., 1986, V.C34, p. 2119.

[27] MOORE, S.O., Optical Model Analysis of the Elastic Scattering by the Lead Isotopes and Bismuth. Report BNL-50151 (T-520), 1968, p. 42.

[28] GUNTHER, P., SMITH, A., WHALEN, J., Nucl. Sci. Eng., 1980, V.75, p. 69.

[29] OLSSON, N., HOLMQUIST, B., RAMSTROM, E., Nucl. Phys., 1983, V.A385, p. 285.

[30] ANNAND, J., FINLAY, R., DIETRICH, F., Nucl. Phys., 1985, V.A443, p. 249.

[31] BAINUM, D.E., FINLAY, R.W., RAPAPORT, J. et al., Phys. Rev., 1977, V.C16, p. 1377.

THE (p,n) REACTION AND THE OPTICAL MODEL

H. CONDÉ
Department of Neutron Research,
Uppsala University,
Uppsala, Sweden

Abstract

Optical model calculations for neutron and proton scattering and (p,n)-reactions are compared with recent experimental results. In particular, the influence of the nuclear structure on the calculation of the (p,n)-reaction cross section is high-lighted. Use of the (p,n)- and (n,p)-reactions for studies of isovector excitations is discussed and recent results are given. Plans are presented of (n,p) cross section measurements at the The Svedberg Laboratory, Uppsala University.

Introduction

The phenomenological (macroscopic) optical model potential (POMP) has been used with great success to reproduce neutron and proton scattering data. More recently, improvements of optical model potentials obtained from microscopic calculations (MOMPs) based on first principles - i e nucleon-nucleon effective potentials - have also resulted in a fair agreement with experiments. Several MOMPs have been developed based on different nucleon-nucleon interactions and treatments of the nuclear density dependence. The present paper compares recent experimental nucleon-nucleus scattering results with POMP and MOMP calculations.

One of the main problems in optical model potential calculations is to make proper corrections for differences in the optical potential for incident protons and neutrons. The corrections to the isoscalar potential obtained for symmetric and uncharged nuclear matter are contained in the Lane symmetry term $[A^{-1}(t\cdot T)U_1]$ (1), correcting for the difference in neutron and proton numbers, the Coulomb correction and the difference in neutron and proton densities (n-skin) (2). The importance of these corrections are exemplified.

The (p,n)- and (n,p)-charge exchange reactions play important roles to determine the isovector part of the optical potential. This is contained in the Lane potential which in the macroscopic mode is written as $\pm\alpha U_1$ where α is the asymmetry parameter (α=(N-Z)/A, - for neutron and + for proton).

Recent measurements of (p,n) and (n,p) cross sections have resulted in discrepant data compared with model calculations based on both phenomenological and microscopic optical potentials. There are indications that the influence of the nuclear structure plays an important role in describing these discrepancies (3,4,5).

Furthermore, the (p,n)- and (n,p)-reactions at higher incident nucleon energies ($E_{nucleon}$>50 MeV) are useful tools to study isovector excitations in nuclei. Results are presented of recent (p,n) and (n,p)-reaction studies of isovector excitations below 200 MeV. Plans are given of (n,p) cross section measurements between 50 and 200 MeV at the The Svedberg Laboratory (TSL), Uppsala University.

2 Phenomenological and microscopic model analysis of nucleon scattering data

The phenomenological optical potential (POMP) is made up of three parts, the real (U), the imaginary (W) and the spin-orbit (Us) potentials. Different terms enter these depending on whether the incoming nucleon is a proton or neutron. The real potential can be written

$$U_p = U_o - \varepsilon E + \alpha U_1 + U_c \qquad \text{(proton)}$$

$$U_n = U_o - \varepsilon E - \alpha U_1 \qquad \text{(neutron)}$$

where U_o is the scalar potential for uncharged and N = Z nuclei, εE the energy dependence correcting for the non-locality of the potential, αU_1 (α=(N-Z)/A) is the neutron-proton asymmetry term having a plus sign for proton and a minus sign for neutron and U_c the Coulomb correction term. Parameters are used to fix the forms and the depths of the potentials. In general, the form factors are fixed to average values and the fit to the experimental data are given by adjusting the potential depths. Good fits to experimental scattering data are observed in many cases (6) also with the use of global parameters which are obtained as average values in fitting experimental results over a wide mass and energy range.

Neutron elastic scattering data compared with POMP calculations were reported by Byrd et al (7) and Carlsson et al (8) for light and medium mass nuclei, respectively and were reviewed by Hansen (2). The neutron optical potential was estimated from proton phenomenological optical potentials corrected for the neutron-proton asymmetry according to the Lane formalism and the Coulomb effects. The symmetry potential had been obtained from measurements of quasi-elastic (p,n)-reactions to isobaric analogue states. The agreement between calculated and experimental neutron data was reasonable in most cases (fig 1) though the (p,n)-data were not well reproduced by the POMP calculations.

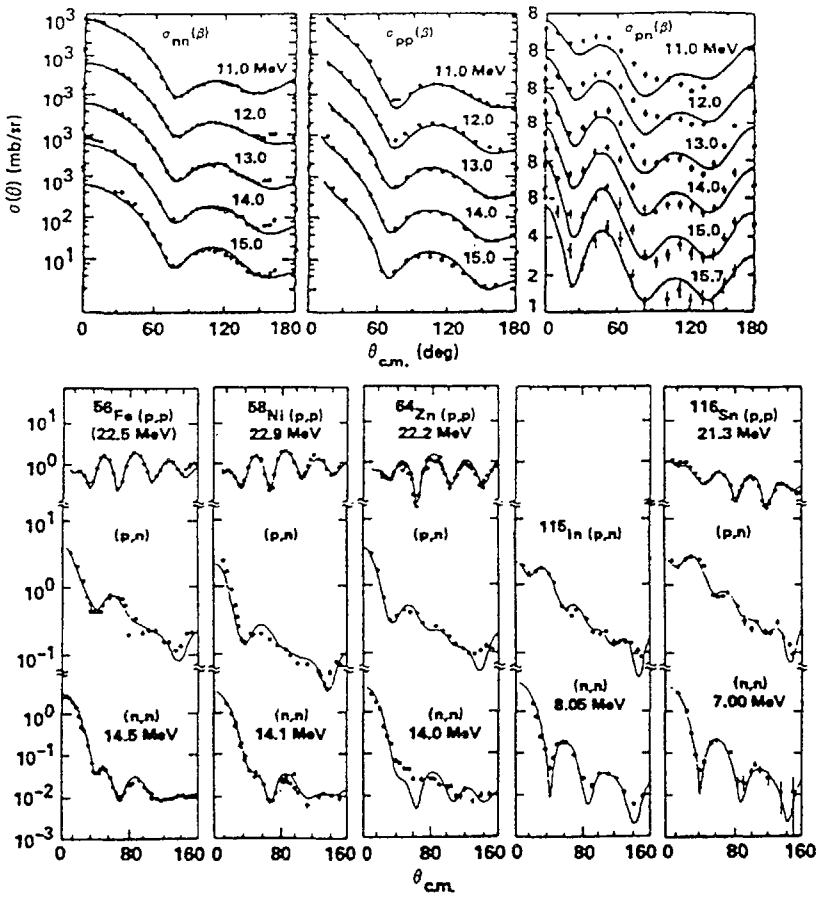

Fig 1. Calculations carried out with the Lane formalism and the data for ^{9}Be (upper, ref 7) and medium mass nuclei (lower, ref 8). From review by Hansen (2).

Several microscopic optical model potentials (MOMPs) exist. Two commonly used models, characterized as nuclear matter approaches, are the Jeukenne-Lejeune-Mahaux (JLM) model (9) and the Brieva-Rook-von Geramb (BRVG) model (10).

The JLM model uses the Reids hard core nucleon-nucleon interaction. The optical potential is calculated as a function of uniform medium density ρ and nucleon energy E. Subsequently, the optical potential in the nucleus is obtained by replacing ρ by the experimental observed nuclear density ρ_r.

The BRVG model, on the other hand, uses the Hamada-Johnstone nucleon-nucleon potential. A complex effective interaction (t-matrix) is computed as a function of the density and the nucleon energy E. The optical potential is obtained by folding the two-nucleon complex t-matrix with the nuclear density distribution of the nucleus.

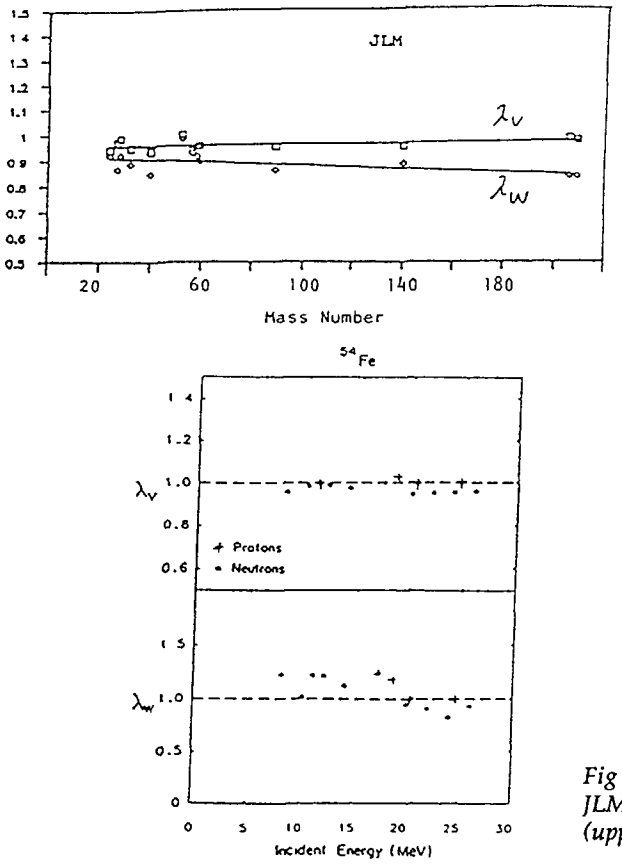

Fig 2a. Normalizing parameters for JLM optical potentials (upper ref 11, lower ref 12).

Recent neutron scattering measurements at E_n=21.6 MeV by Olsson et al (11) and proton and neutron scattering measurements between about 10 and 25 MeV by Mellema et al (12) give data in fair agreement with JLM model calculations (<10 %). In comparison with BRVG model calculations, the light element data by Olsson et al and the low energy data by Mellema et al, do both show a more pronounced deviation, in particular what concerns the imaginary part of the potential (fig 2a and 2b).

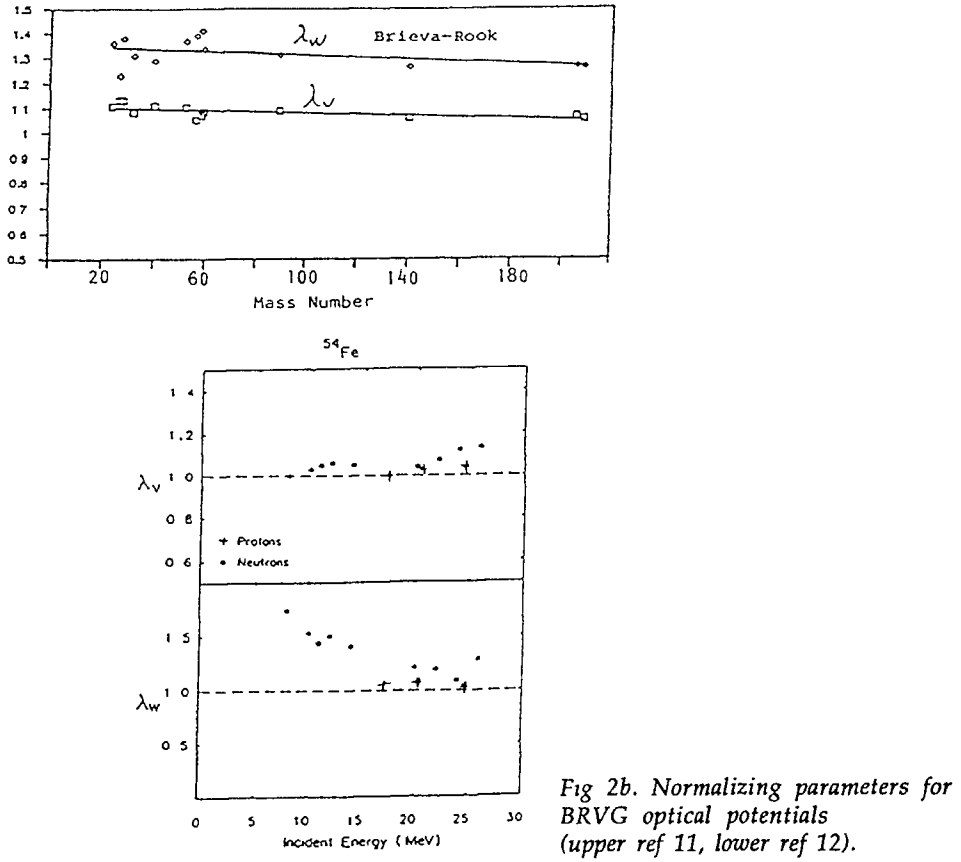

Fig 2b. Normalizing parameters for BRVG optical potentials (upper ref 11, lower ref 12).

The sensitivity of MOMP (JLM) calculations to the Coulomb correction was investigated by Dietrich and Petrovich (13) on ^{208}Pb (n,n) and (p,p). In particular, the real part of the potential for the protons is affected by the Coulomb correction (CC). A reasonable agreement was obtained betwen the proton and neutron data after the CC had been applied (fig 3a). Furthermore, the same data on ^{208}Pb were also used to demonstrate the sensitivity of the MOMP (BRVG) calculations to the neutron skin (13). The protons mostly feel the neutron distribution in the nucleus. Thus, the proton calculations improved noticeably, while the change in the (n,n) calculation is marginal (fig 3b).

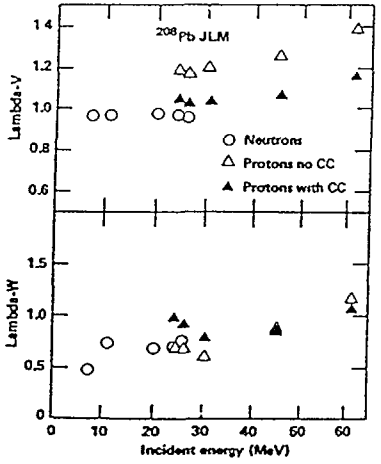

Fig 3a. Sensitivity of MOMP(JLM) calculations for ^{208}Pb(n,n) and (p,p) to the Coulomb correction (ref 13).

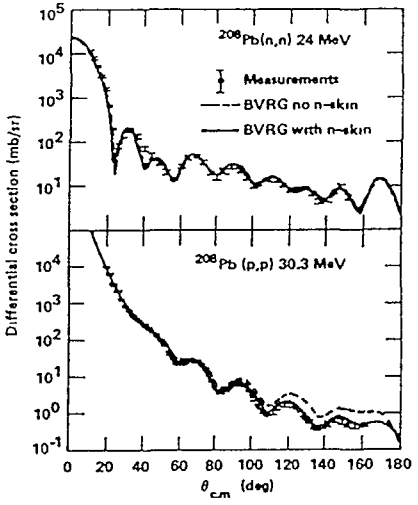

Fig 3b. Sensitivity of MOMP(BRVG) calculations for ^{208}Pb(n,n) and (p,p) to the neutron skin (ref 13).

3 Optical model estimates of (p,n) cross sections

In a comprehensive paper by Metha and Kailas (3) the proton-nucleus optical model potential at low energies (Ep < 10 MeV) and for nuclear masses A = 40-130 was reviewed. The phenomenological optical model parameters are mainly determined from proton absorption cross section measurements.

In general,

$$\sigma_{p,n} = \sigma_{abs} - \sigma_{CE}$$

$$\sigma_{el} = \sigma_{SE} + \sigma_{CE}$$

where σ_{CE} and σ_{SE} are the compound elastic and the shape elastic cross sections, respectively. Using the optical model one can calculate σ_{SE} and σ_{abs}. Experimentally $\sigma_{p,n}$ and σ_{el} are determined. At these low energies (E < 10 MeV) the elastic scattering is dominated by the Coulomb scattering and hence has a poor sensitivity to nuclear potential variations. However, σ_{CE} is negligible as compared to σ_{abs}, at low proton energies and above the neutron threshold, why $\sigma_{p,n} = \sigma_{abs}$ to a good approximation.

Mehta and Kailas compared the results of a large number of (p,n) cross section measurements with phenomenological optical model calculations. The shape parameters of the optical potential were taken from earlier works by Kailas et al (45 < A < 80) (14), Johnson et al (89 < A < 130) (15) and Viyogi (40 < A < 130) (16). In particular, it was observed that the imaginary potential depth varied with the target mass number in a manner, which could not be reproduced by different level density estimates. The dependence showed maxima and minima, the positions of which were reported to fall on straight lines when plotted as a function of $A^{1/3}$. They concluded that the behaviour was probably linked to nuclear structure properties (fig 4).

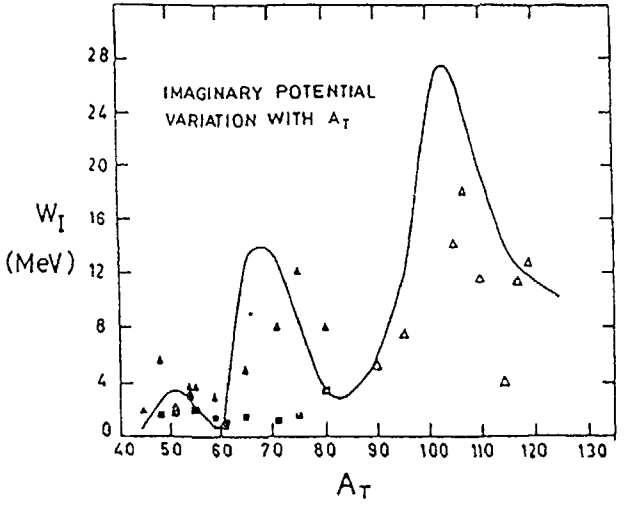

Fig 4a. The variation of the imaginary potential (W_I) with target mass number (A_T). The full line is the curve drawn through the phenomenological W_I-values. The points are estimated of W_I based on different level density assumptions (see ref 3).

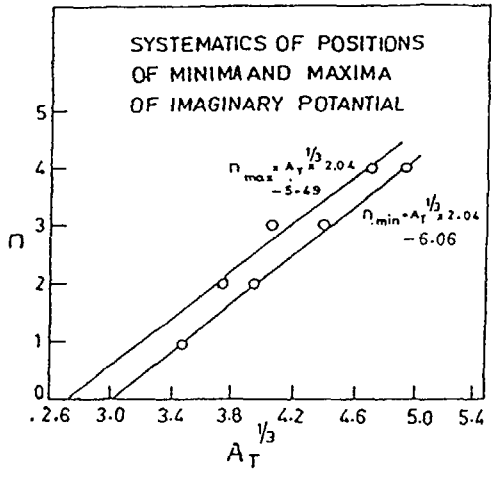

Fig 4b. The positions of the maxima (minima) of W_I as a function of $A^{1/3}$ (ref 3).

Experimental (p,n) cross section data are not very well described by the microscopic optical model. Calculations have been done for a few nuclei (^{48}Ca, ^{58}Ni, ^{90}Zr, ^{208}Pb). The shape of the angular distribution is reproduced rather well but the magnitude is underestimated with fairly large factors (factors 2 to 6).

Dietrich and Petrovich have compared BRVG and JLM nuclear matter optical model calculations of ^{208}Pb (p,n) IAS with experimental data between 25 and 45 MeV (13). The results (fig 5) indicate that the problems are connected with the magnitude of the isovector potential. Dietrich and Petrovich also focused attention on the fact that the ratio (R) between the real isovector (U_1) and isoscalar (U_0) terms in nuclear matter based microscopic optical potentials is significantly smaller than that found in phenomenological potentials and effective interactions. The ratio R calculated for neutron scattering on ^{208}Pb at 30 MeV using different microscopic optical models range from 0.2 to 0.3 while the same ratio calculated with a phenomenological optical potential (Becchetti-Greenlees) amounts to 0.5.

The imaginary part of the nucleon-nucleus optical potential has been calculated by Osterfeld and Madsen (5) using a nuclear structure approach. In this approach the optical potential is calculated to second order using random-phase approximation (RPA) transition densities to particle-hole intermediate states and an effective nucleon-nucleon interaction. The imaginary part of the isovector term of the nucleon-nucleus potential (W_1) is identical with the imaginary term of the charge-exchange transition

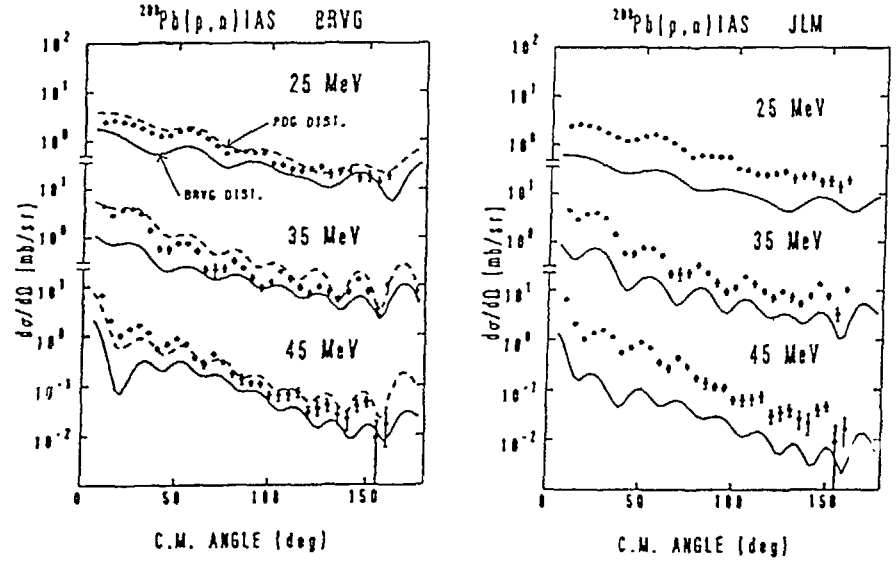

Fig 5. Microscopic BRVG and JLM model calculations of the differential cross sections for ^{208}Pb(p,n) IAS (full lines). Calculation using microscopic form factors and phenomenological distorting potentials (dashed line) (ref 13).

potential for the transition to the isobaric analogue state (IAS) of the ground state. A comparison of the calculated isovector potential W_1 with the phenomenological potential (W_1) of Becchetti-Greenlees shows a marked discrepancy both in magnitude and in radial position (fig 6). They concluded that the position of the peak is very sensitive to the details of the nuclear structure wave function. Especially, the transition densities to the collective intermediate states have to be in agreement with experiment in order to obtain the radial dependence surface peak of the imaginary potential at the right position.

4 Nuclear structure studies with (p,n)- and (n,p)-reactions

Perey and Perey (17) found that the real potential depth obtained from analysis with the same form factor lie on a family of lines of constant isospin (T) when plotted as a function of the nuclear asymmetry factor $\alpha = (N-Z)/A$. Noro et al (18) also found that the volume integrals of the real potentials lie on a family of curves of constant Z when plotted as a function of α. Referring to these observations, Hodgson (4) points out the importance to use a parameterization of the phenomenological potential that includes fine

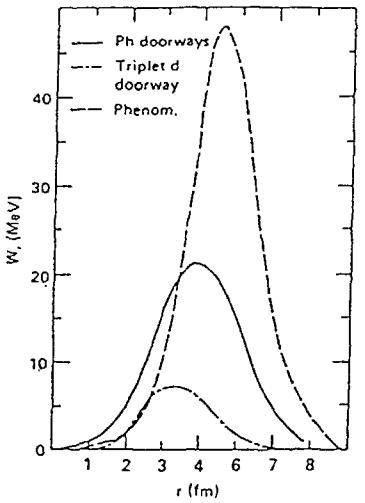

Fig 6. Comparison of the calculated imaginary isovector potential W_1 with the phenomenological potential (W_1) of Becchetti-Greenlees. Also the contribution of the intermediate deuteron channel to W_1 is shown (ref 5).

structure, which would strengthen the links between the optical potential and nuclear structure and puts them on a sounder physical basis.

The charge-exchange reactions (p,n) and (n,p) have played an important role in nuclear structure studies. The (p,n) reaction has been particularly valuable with the exploration of isobaric analogue resonances. Both (p,n) and (n,p)-reactions are powerful tools for studying isovector excitations without interference from isoscalar.

The (p,n)-reaction has been studied extensively at the Indiana University Cyclotron Facility (IUCF) (19-22) at energies above 100 MeV. In particular,Gamow-Teller transitions ($\Delta T = 1, \Delta S = 1, \Delta L = 0$) were studied. The strengths of these transitions for N≠Z nuclei should follow a model independent sum rule

$$S(GT) = B(GT^-) - B(GT^+) = 3(N-Z)$$

where $B(GT^-)$ denotes GT strength observed in β^- decay or (p,n) reactions and $B(GT^+)$ that in β^+ decay or (n,p). The GT strengths obtained from the (p,n) data of IUCF are about 40% smaller than predicted by the sum rule.

Different mechanisms have been proposed to explain the missing GT-strength, which involve the inclusion 2p2h - and/or 1Δ1h-excitations.

Other isovector states of great interest are the giant monopole and quadrupole excitations. The isovector monopole resonance (IVMR) has been observed in (π^-, π^0) reactions on ^{90}Zr and ^{120}Sn at $E_{\pi^-} = 165$ MeV by Bowman et al (23). Indications of the IVMR have also been resported by Brady (24) from (n,p)-reaction studies at 65 MeV on ^{90}Zr.

The (n,p)-reaction has been studied much less than the (p,n)-reaction mostly because of technical difficulties. At present, experiments are in progress or planned at TRIUMF, IUCF, LANL and TSL, Uppsala. The studies of multipole isovector excitations by the (n,p)-reaction is favourable because in nuclei having a neutron excess the reaction proceeds only through states of a definite isospin ($T_f = T_i + 1$), analogs of the T> states of the target nucleus with isospin T_i. In particular, investigations of the (n,p)-reaction are also of interest for testing the above mentioned problems connected with the missing GTR-strength in the (p,n)-reaction.

The neutron energy region from 50 to 185 MeV will be covered by the Uppsala (n,p)-facility. In this energy region, a large change in the relative strength of the central isospin-dependent terms in the nucleon-nucleus interaction is expected from theory. Assuming a local nucleon-nucleon effective interaction, Love et al (25) have shown that the ratio between the contributions from the central spin-dependent and spin-independent interactions to isovector excitations at zero momentum transfer increases from a value of about unity at 50 MeV to about ten at 200 MeV. Thus, the τ_+ component of the isovector monopole resonance should compete favourable with the Gamow-Teller resonance in the 0^o cross section in the lower part of the incident neutron region while the GTR will dominate in the high-energy region.

The experimental facility for (n,p)-reaction studies at TSL is shown in fig 7. The neutrons are produced in a thin ^7Li metal target (150 mg/cm^2) mounted in a water-cooled rig. After passage through the target the proton beam is deflected by means of two dipole magnets and focussed on a graphite block at the end of a well shielded beam dump. The nearly monoenergetic neutron beam ($E_n \approx$ 50-185 MeV) at 0^o is defined by a system of three collimators. The vacuum system for the neutron facility is terminated with a capton foil immediately after the first collimator. Charged particles produced by secondary neutron reactions in the capton foil and/or along the collimator channel will be deflected by a clearing magnet placed between the first and second collimator.

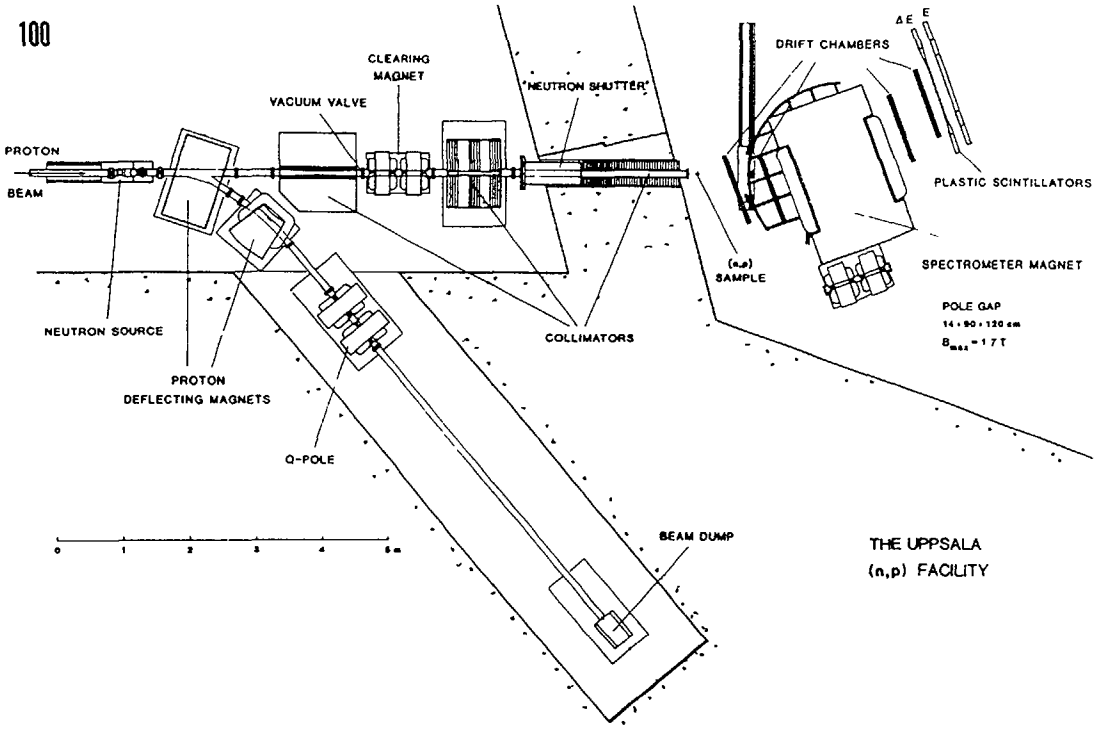

Fig 7. The Uppsala (n,p)-facility

The (n,p)-sample will be given a thickness which corresponds to an energy spread of the outgoing protons of about 0.7 MeV. A veto detector to register background protons in the neutron beam will be placed in front of the (n,p)-sample.

The (n,p)-spectrometer consists of a large uniform-field magnet with two drift chambers before the magnet and two after for ray-tracing. The trigger for the drift chambers is obtained from a telescope consisting of two plastic scintillators.

The emission angles and energies of the protons are determined off line for each event using a ray-tracing program based on magnetic field maps. The neutron beam will be monitored by a scintillator telescope and/or by recording protons from a plastic foil mounted in parallell with the (n,p)-sample. The over-all energy-resolution will be of the order of 1 MeV. Production runs with the facility is scheduled for late spring 1988.

I would like to thank Dr L Nilsson for valuable comments on the report.

References

1 A M Lane, Phys Rev Lett 8, 171 (1962), Nucl Phys 35, 676 (1962), Nucl Phys 37, 663 (1962), Rev Mod Phys 29, 191 (1957)

2 L F Hansen, Proc Specialist's Meeting on the Use of the Optical Model for the Calculation of Neutron Cross Sections below 20 MeV, Paris 13-15 Nov 1985, NEA Nuclear Data Committee Report, NEANDC-222/U (1986)

3 M K Mehta and S Kailas, Invited review paper for the Indian Academy of Sciences, Physics Journal PRAMANA, (1986)

4 P E Hodgson, AIP Conference Proceedings 124, 1 (1984)

5 F Osterfeld and V A Madsen, AIP Conference Proceedings 124, 26 (1984)

6 P E Hodgson, this procceding

7 R C Byrd, R L Walter and S R Cotanch, "Self Consistent Application of the Lane Model"

8 J D Carlsson, C D Zafiratos and D A Lind, Phys Rev Lett 30, 99 (1973) and Nucl Phys A249, 29 (1975)

9 J P Jeukenne, A Lejeune and C Mahaux, Phys Rev C15, 10 (1977) and Phys Rev C16, 80 (1977)

10 F A Brieva, J R Rook and H V von Geramb, Lectures Notes in Physics 89, 104 (1978)

11 N Olsson, B Trostell, E Ramström, B Holmqvist and F S Dietrich, The Studsvik Science Research Laboratory Report, NFL-48 (1986)

12 S Mellema, R W Finlay, F S Dietrich and F Petrovich, Phys Rev C28, 2267 (1983)

13 F S Dietrich and F Petrovich, AIP 124, 90 (1984)

14 S Kailas, M K Metha, S K Gupta, Y.P Viyogi and N K Ganguly, Phys Rev C20, 1272 (1979)

15 C Johnson, A Galonsky and R L Kernell, Phys Rev C20, 2052 (1979)

16 Y P Viyogi, PhD (Thesis), Calcutta University (1983)

17 C M Perey and F G Perey, Phys Lett B26, 123 (A68)

18 T Noro, H Sakaguchi, M Nakamura, K Hatamaka, F Ohtami, H Sakamoto and S Kobayashi, Nucl Phys A366, 189 (1981)

19 C D Goodman, C A Goulding, M B Greenfield, J Rapaport, D E Bainum, C C Foster, W G Love and F Petrovich, Phys Rev Lett 44, 1755 (1980)

20 D E Bainum, J Rapaport, C D Goodman, D J Horen, C C Foster, M B Greenfield and C A Goulding, Phys Rev Lett 44, 1751 (1980)

21 D H Horen, C D Goodman, C C Foster, C A Goulding, M B Greenfield, J Rapaport, D E Bainum, E Sugarbaker, T G Masterson, F Petrovich and W G Love, Phys Lett B95, 27 (1980)

22 J Rapaport, T Taddeucci, C Gaarde, C D Goodman, C C Foster, C A Goulding, D Horen, E Sugarbaker, T G Masterson and D Lind, Phys Rev C24, 335 (1981)

23 J D Bowman, H W Baer, R Bolton, M D Cooper, F H Cverna, N S P King, M Leitch, H S Matis, A Erell, J Alster, A Doron, M A Moinester, E Blackmore and E R Siciliana, Phys Rev Lett 50, 1195 (1983)

24 P Brady, Can Jour Phys 65, (1987)

25 W G Love, A Klein, K Nakayama and M A Franey, Can Jour Phys 65, (1987)

THE COMPLEX METHOD AND ITS APPLICATION TO THE AUTOMATIC ADJUSTMENT OF OPTICAL MODEL PARAMETERS

Hongmo ZHOU, Ziqiang YU,
Xiaocheng ZHANG, Yixin ZUO
Nankai University,
Tianjin, China

Abstract

An outline of the complex method and its application to the automatic adjustment of optical model parameters is given.

I. INTRODUCTION

The problem for adjusting automatically parameters in optical model is regarded as to carry out a least squares fit and minimizing the quantity χ^2 given by

$$\chi^2=\{\frac{W_t}{N_1}\sum_{j=1}^{N_1}[\frac{\sigma_e^{cal}(E_j)-\sigma_t^{exp}(E_j)}{\Delta\sigma_t^{exp}(E_j)}]^2+\frac{W_{non}}{N_2}\sum_{j=1}^{N_2}[\frac{\sigma_a^{cal}(E_j)-\sigma_{ce}^{cal}(E_j)-\sigma_{non}^{exp}(E_j)}{\Delta\sigma_{non}^{exp}(E_j)}]+$$

$$+\frac{W_{el}}{N_3}\sum_{j=1}^{N_3}\frac{1}{N_j}\sum_{i=1}^{n_j}[\frac{\sigma_{se}^{cal}(E_j,\theta_i)+\sigma_{ce}^{cal}(E_j,\theta_i)-\sigma_{el}^{exp}(E_j,\theta_i)}{\Delta\sigma_{el}^{exp}(E_j,\theta_i)}]^2\}/(W_t+W_{non}+W_{el}) \quad (1\text{-}1)$$

where $\sigma_e^{cal}(E_j)$, $\sigma_a^{cal}(E_j)$ and $\sigma_{se}^{cal}(E_j,\theta_i)$ are total, absorption cross section and shape elastic scattering angular distribution respectively and calculated by the optical model, and $\sigma_{ce}^{cal}(E_j,\theta_i)$ are compound nucleus scattering cross section and angular distribution and calculated within the framework of the width-fluctuation correction Hauser-Feshbach formula, E_j is the incident neutron energy in laboratory system, W_t, W_{non} and w_{el} are weight factors. It is obvious that $\chi^2\leq 1$ indicate optimum agreement. The χ^2 is a function of the n neutron

optical optential parameters which vary in a reasonable region

$$a_j \leq x_j \leq b_j \qquad j=1, \ldots, n \qquad (1\text{-}2)$$

where $x_1, \ldots, x_n$ are n neutron optical optential parameters.

II. THE COMPLEX METHOD

Consider constrained minimization problem

$$\text{Minimize: } f(x) \qquad x \in S \qquad (2\text{-}1)$$

$$S=\{x \mid g_j(x) \geq 0, \quad j=1,\ldots, m\} \qquad (2\text{-}2)$$

$$a_j \leq x_j \leq b_j, \quad j=1,\ldots, n \qquad (2\text{-}3)$$

where $x=(x_1,\ldots, x_n)^T$, $f(x)$ denote the objective function, $g_j(x) \geq 0$ $(j=1,\ldots,m)$ denote the implicit constraints, the inequalities (2.3) denote the explicit constraints.

In n-dimensional Euclidean space, a "polyhedron" with K-verties $x^{(1)},\ldots,x^{(k)}$ is termed a complex, where $K(>n+1)$ is generally taken $K=2n$,

Fundamental principle of the complex method is that the objective function values of the K-vertices of the complex are compared, the worst vertex, its objective function value is highest, is deleted and replaced by new vertex, thus a new complex is formed. In this way we can approach the minimum point step by step.

The execute process of the complex method is roughly divided into two stages: one of them is form of an initial complex, another is to find a minimum point by iteration.

The computing steps of the complex method:

1. Form an initial complex

(1) First, determine an initial feasible point $x^{(1)}$(a point which satisfies to constrained conditions (2-2) and (2-3) is termed a feasible point). Can use one of the following two methods.

a) Give it by man-made.

b) Produce it through the use of pseudo-random numbers. Through the following relation

$$\tilde{x}_j=a_j+r_j(b_j-a_j) \qquad (2\text{-}4)$$

can produce $\tilde{x}=(\tilde{x}_1,\ldots,\tilde{x}_n)^T$. r_j is a pseudo-random number uniformly distributed over the interval (0,1). If $\tilde{x}$ satisfies $g_i(\tilde{x})\geq 0$, $\tilde{x}$ is an initial feasible point $x^{(1)}$, if not, repeatedly use new $\{r_j\}_{j=1}^n$ and produce a new $\tilde{x}$ until $\tilde{x}$ satisfies $g_i(\tilde{x})\geq 0$.

(2) Determine (k-1) additional feasible points so that form the initial complex. Let we have found $t(t\geq 1)$ feasible points $x^{(1)},\ldots,x^{(t)}$ and $\tilde{x}^{(t+1)}$ by the relation (2-4):

a) If $\tilde{x}^{(t+1)}$ satisfies $g_i(\tilde{x}^{(t+1)})\geq 0$, take $\tilde{x}^{(t+1)}$ as $x^{(t+1)}$;

b) If not, let

$$\bar{x} = \frac{1}{t}\sum_{i=1}^{t} x^{(i)} \qquad (2\text{-}5)$$

and

$$\hat{x}^{(t+1)}=\bar{x}+0.5(\tilde{x}^{(t+1)}-\bar{x}) \qquad (2\text{-}6)$$

If $\hat{x}^{(t+1)}$ satisfies $g_i(\hat{x}^{(t+1)} \geq 0$, take $\hat{x}^{(t+1)}$ as $x^{(t+1)}$; otherwise replace $\tilde{x}^{(t+1)}$ of (2-6) by $\hat{x}^{(t+1)}$ and calculate a new $\hat{x}^{(t+1)}$, again and again to do it in this way until $\hat{x}^{(t+1)}$ satisfies $g_i(\hat{x}^{(t+1)} \geq 0$.

As soon as K feasible points have been found, the initial complex has been formed.

2. Find a minimum point by iteration.

(1) Calculate

$$f_j=f(x^{(j)}), \qquad j=1,\ldots,k$$

and

$$\bar{f}= \frac{1}{k}\sum_{i=1}^{k} f_i$$

If

$$\frac{1}{k}\sum_{i=1}^{k}(\bar{f}-f_i)^2 < \varepsilon \qquad (2\text{-}7)$$

means that the minimum point, $x^{(\ell)}$, has been found, it satisfies

$$f(x^{(\ell)})=\min_{1\le j\le k} f_j$$

In (2-7), $\varepsilon>0$ is a given convergence error. If (2-7) does not hold true, return to the following (2).

(2) Select the largest point $x^{(h)}$ and second-largest point $x^{(s)}$, that is

$$f(x^{(h)})=\max_{1\le j\le k} f_j$$

$$f(x^{(s)})=\max_{\substack{1\le j\le k\\ (j\neq k)}} f_j$$

and calculate

$$x^{(o)}=\frac{1}{k-1}\sum_{\substack{j=1\\ (j\neq h)}}^{k} x^{(j)}$$

(3) Take $\alpha>1$ (in general $\alpha=1.3$), by the following formula

$$x^{(\alpha)}=x^{(o)}+\alpha(x^{(o)}-x^{(h)}) \qquad (2\text{-}8)$$

calculate the reflect point $x^{(\alpha)}$. If $x^{(\alpha)}$ does not satisfies $g_i(x^{(\alpha)})\ge 0$, subtract one-half from α, again calculate a new $x^{(\alpha)}$ by (2-8). If the new $x^{(\alpha)}$ does not still satisfies $g_i(x^{(\alpha)})\ge 0$, again subtract one-half from α until $x^{(\alpha)}$ become a feasible point.

(4) Calculate

$$f_\alpha = f(x^{(\alpha)})$$

a) If $f_\alpha<f(x)^{(h)}$, replace $x^{(h)}$ by $x^{(\alpha)}$ so that to form a new complex, and return to (2).

b) If $f_\alpha\ge f(x^{(h)})$, subtract one-half from α and calculate a new $x^{(\alpha)}$ by (2-8) until $f(x^{(\alpha)})<f(x^{(h)})$. When α become a small, for example $\alpha<10^{-5}$, and still have no $f(x^{(\alpha)})<f(x^{(h)})$, replace $x^{(h)}$ by $x^{(s)}$ and return to (4) to continue the iteration.

III. A TYPICAL EXAMPLE

We have used the complex method to search automatically an optimum set of the neutron optical potential parameters for the natural sodium, magnesium and silicon elements. A typical example is for magnesium. There are three isotopes and $N_1=11$, $N_2=8$, $N_3=6$ and $n_j=10\sim20$. The number of the adjustable parameters, n, is equal to 9. The first vertex of the initial complex form is artificial selection which correspond to a better set of parameters. The other 17 verteis are selected by the program using stochastic method. The convergence error, ε, is taken to be 1.7. The weight factors $W_t=W_{non}=W_{el}=1$. Though 57 iterative stages and runing time being about two hours we have obtained $x^2=4.26$ where the contributions from total cross section and elastic scattering angular distribution are 0.58 and 8.7 respectively. These results are in good agreement with the experimental data as shown in Figures 1 and 2.

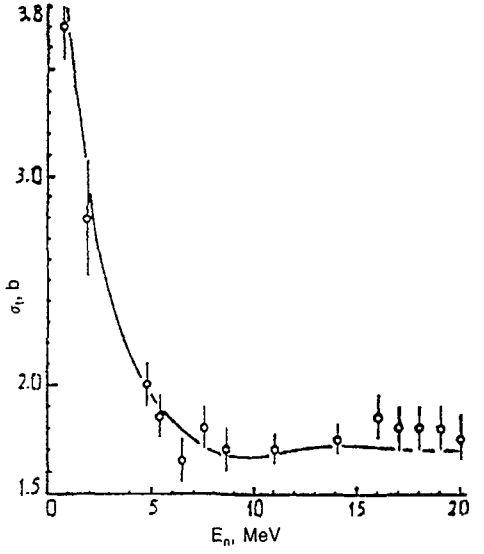

FIG.1. Natural magnesium cross-section.

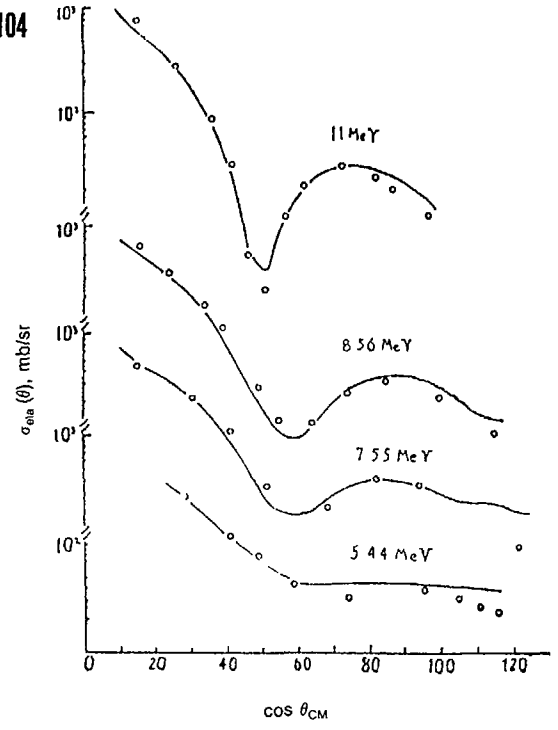

FIG 2 Elastic scattering angular distribution of natural magnesium

OPTICAL MODEL ANALYSIS OF FAST NEUTRON SCATTERING FROM ^{6}Li

Yaoyin ZHU, Yujun ZHANG,
Ruifa HUI, Manfen LIU
Jilin University,
Changchun, China

Abstract

A systematic optical model analysis of fast neutron scattering from ^{6}Li was given The optical model potential of Woods-Saxan form was used in analysis, considering the linear energy dependence of the real-well diffuseness Comparison between the calculated results and the experimental data was given

1.Introduction

Neutron scattering cross sections for light nuclei have been used in fusion reactor design studies. In n+^{6}Li reactions the elastic scattering cross sections are important ones,but the measurements of elastic scattering angular distributions are not complete. Thus an optical model analysis for neutron scattering from ^{6}Li is necessary.

At present, the difficulties in number of the particles and open channels are the obstructions for strict microscopic calculations of n+^{6}Li system.As it is known,the optical model for medium mass or heavy nuclei has been applied generally.In the last few years,the applications of optical model for light nuclei gradually increased. The optical model is more simple, it is easy to analyse experimental data over a wide energy range.In the present paper we engage in a systemic optical model analysis of fast neutron scattering from ^{6}Li.

2.Optical model potential

We choose the optical model potential of Woods-Saxan form

$$V(r) = -Uf(r, r_1, a_1) + i4Wa_2 \frac{d}{dr} f(r, r_2, a_2) +$$

$$+ U_s \left(\frac{\hbar}{m_\pi c}\right)^2 \frac{1}{r} \frac{d}{dr} f(r, r_3, a_3) \vec{\sigma} \cdot \vec{L}$$

$$f(r, r_j, a_j) = \left[1 + \exp\left(\frac{r - r_j A^{\frac{1}{3}}}{a_j}\right)\right]^{-1}, \quad j = (1, 2, 3)$$

Where U,W and U_s are the depth parameters of the real-well , imaginary-well and spin-orbit term respectively, r_j are the radius parameters,a_j are the surface diffuseness parameters.

The first consideration of optical model analysis is the choice of the parameters.For medium mass and heavy nuclei;there are generally accepted optical model parameters. The well depth parameters usually are dependent on energy. Because the individuality of light nuclei is very intense,thus there aren't common optical model parameters.We consider,when the incident neutron energy is not very high,for light nuclei, the elastic cross section and angular distribution are more sensitive to the surface action of optical potential real-well than its inside action.Thus they are sensitive to the real-well diffuseness.In this paper,we regard the real-well diffuseness a_1 as a linear function of incident energy.

P.W.Lisowski et al.have poinded out this idea,their paper has analysed the neutron scattering from ^{3}He.[3] But in the last few years, this idea has not been noticed. We think that it ought to be emphasized.

3.Calculated results

In the energy range 4.83-20MeV, the change of elastic and total cross section of n+^{6}Li reaction is slow. Near E_n=4.6 MeV (incident neutron energy in the laboratory system) the total cross section has a broad maximum (Fig.1.). According to the energy level scheme,E_n=3.5MeV and E_n=4.67 MeV correspond with two excited states of compound-system ^{7}Li, they are 10.25 MeV

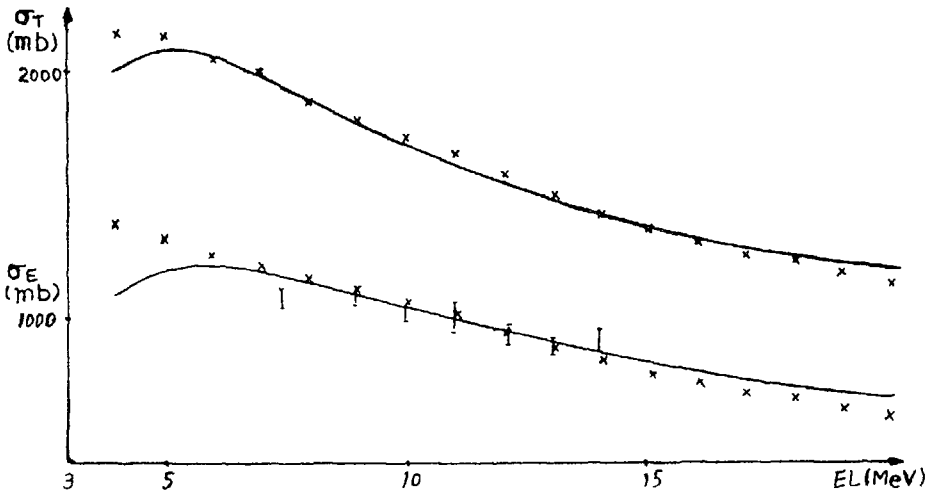

X: recommendation [2] I: experiment [3]

FIG.1. Excited curves of total and elastic scattering cross-section.

($J^\pi=\frac{3}{2}^-$,$T=\frac{1}{2}$) and11.25 MeV ($J^\pi=\frac{3}{2}^-$,$T=\frac{1}{2}$). Because the isospin is an approximate good quantum number for light nuclei,the ground -state isospin of ^{6}Li is zero,thus n+^{6}Li system is not corresponding with 11.25MeV excited state of compound-system ^{7}Li.The width of 11.25 MeV energy level is very small. This shows the broad maximum mainly is not the result of compound nuclear reaction. It is the result of optical potential scattering. A rational optical potential ought to indicata this broad maximum. In addition, 10.25 MeV energy level is wide. Moreover, it decays mainly through neutron.This shows that near E_n=3.56MeV the elastic scattering from compound-nuclear system can not be neglected.In order to avoid the influence of compound-elastic scattering,in the present paper,the optical model analysis of neutron scattering from ^{6}Li is confined to 4.83-20 MeV energy range.

Experimental data of total cross section are taken from Ref.2. For elastic scattering at 7-14MeV energy range,the data are taken from Ref.3. At 4-7 MeV energy range H.D.Knox at al. have given the figures of elastic scattering measurements.[4]

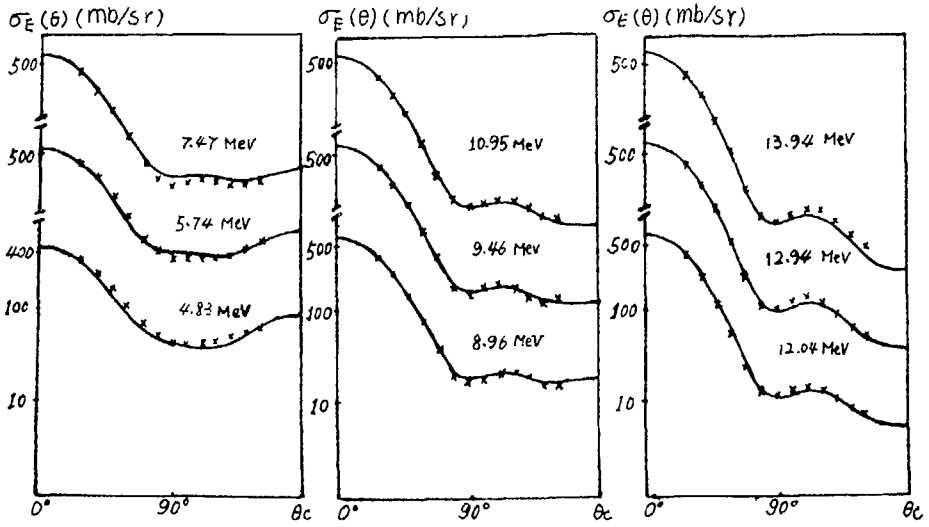

FIG.2. Elastic scattering differential cross-sections for ^{6}Li.

Their results nearly conform with Ref.2,thus at this and 14-20 MeV energy range the data of elastic scattering are taken from Ref.2. First,we have adjusted alone the parameters to aim at 4.83,7.47 and 13.94MeV. We have found that regarding the real-well diffuseness a_1 and imaginary-well depth W as a linear function of incident energy can obtain good agreement with the experiments.Then,we have adjusted jointly the parameters to aim at 4.83,5.74,7.47,9.96,12.04 and 13.94 MeV.Finally,we have obtained a set of optical model parameters:

$U=39.16$ MeV $\quad a_1=(0.9541-0.0257E_c)$ fm

$W=(2.85+0.41E_c)$ MeV $\quad a_2=0.49$fm

$U_s=8.91$ MeV $\quad a_3=0.58$ fm $\quad r_1=r_2=r_3=1.4$fm

The comparisons of the calculative results of total cross sections with the experiments have been given in the Fig.1. Fig.2 have given the results of elastic scattering angular distributions. Except 20MeV, the deviation of total cross sections is less than 4% . For elastic cross sections, when $E_n<13$ MeV Hogue's measurements are lower than Ref.2,when $E_n>13$ MeV Hogue's measurements are higher than Ref.2. The calculative results are between the two. The better fits to the elastic scattering angular distributions are obtained.

ACKNOWLEDGEMENTS

This work has been supported by the grants from The Ministry of Nuclear Industry of the Peoples Republic of China. The authors thank Mr.Li Zhi-wen and Piao Zhen-Lie for their help.

REFERENCES

1 P.W.Lisowski et al.,Proceedings of the International Conference on the Interaction of Neutron with Nuclei.2(1976), 1444.

2 CNDC,hsj-79250(hb),Vol.2,P.49(1978).

3 H.H.Hogue et al.,Nucl.Sci.Eng.,69,22(1979).

4 H.D.Knox et al.,Nucl.Sci.Eng.,69,223(1979).

COMPOUND NUCLEAR THEORY

(Session III)

RECENT PROGRESS IN COMPOUND NUCLEAR THEORY AND THE CALCULATION OF RESONANCE AVERAGED CROSS-SECTIONS

F.H. FRÖHNER
Institut für Neutronenphysik
und Reaktortechnik,
Kernforschungszentrum Karlsruhe,
Karlsruhe, Federal Republic of Germany

Abstract

- Recent years have seen a breakthrough in Hauser-Feshbach theory. Resonance-averaged partial cross sections including width fluctuation corrections and elastic enhancement can now be calculated exactly in the framework of the level-statistical theory of compound-nuclear reactions (i. e. for Hamilton matrices from the Gaussian Orthogonal Ensemble). A more general approach employing entropy maximisation has established the probability distributions for the R- and S-matrix, from which resonance-averaged cross sections can also be calculated. Both avenues lead to practically the same numerical results. Applications to coherent evaluation by simultaneous fitting of cross sections data for all open reaction channels in the unresolved-resonance region are presented. Problems with self-shielded resonance-averaged group cross sections are briefly addressed.

1. Introduction

Calculations of resonance-averaged cross sections, self-shielding factors and similar cross section functionals of interest in the unresolved resonance range are usually based on the statistical theory of compound nuclear reactions. This theory has evolved on two levels.

The "microscopic" level, involving compound resonances and their statistics, was explored first. One considers energy averages over intervals containing so many cross section resonances that a level-statistical treatment is possible. The simplest formal description is provided by R-matrix theory where each resonance of given spin and parity is characterised by a real level energy and a set of real width amplitudes for all open channels [1]. The probability distributions of the R-matrix parameters for pure compound-nuclear reactions were established by Wigner, Dyson, Porter, Rosenzweig and others more than 30 years ago (see [2]). The R-matrix expression for the total cross section is easily averaged over these distributions. One must simply average the S-matrix which, due to causality, has no poles above the real axis in the complex energy plane so that contour integration can be applied [3].

Averaging the R-matrix expression for partial cross sections, however, turned out to be extremely difficult, because absolute squares of S-matrix elements must be averaged. Pole expansion of the S-matrix yields seemingly more manageable formulae, but in spite of much effort the probability distributions of the pole parameters could never be derived from those of the R-matrix parameters. Although level-statistical Monte Carlo calculations indicated that the expression for average partial cross sections must resemble the Hauser-Feshbach formula with elastic enhancement and width fluctuation correction, involving only channel transmission coefficients (see Eq. 6 below), the exact form remained unknown [4, 5].

In this situation information theory seemed to offer the possibility to bypass the "microscopic" resonance details completely by treating them as a kind of noise superimposed on the "macroscopic" average cross sections obtained e. g. from optical-model calculations. This approach, first tried by Bloch [6], was pursued vigorously by Mello [7] who pointed out that the joint distribution of S-matrix elements can, in principle, be established by means of the information-theoretical method of entropy maximisation [8], for any given average (e. g. optical-model) S-matrix. Mello, Pereyra and Seligman [9] found that the Poisson kernel defined in the domain of unitary symmetric matrices [10] appears to be the required distribution, having all the properties that ergodicity and the analytic (causal) structure of S demand, while its form implies maximal information entropy for given transmission coefficients. Fröhner [11] arrived independently at the same result by direct entropy maximisation, utilising the R-matrix form of S, and techniques developped by Hua [10] for the assignment of a-priori probabilities (measures) of matrices. He derived first the maximum-entropy distribution for R which, in terms of S, becomes the Poisson kernel.

While the S- and R-matrix distributions were established on the macroscopic level, Verbaarschot, Weidenmüller and Zirnbauer achieved success on the microscopic level [12]. With new tools from many-body theory they finally succeeded in averaging the R-matrix expression for the partial cross sections over the resonance parameter distributions implied by the Gaussian Orthogonal Ensemble (GOE) of Hamilton matrices.

The following sections contain more explicit details of these newly developped techniques, some of them unpublished so far, in a notation (essentially that of [1]) which is customary in applied resonance theory.

2. Level Statistics and Heuristic Cross Section Averaging

For later reference and in order to establish the notation we begin with the basic formulae of the level-statistical theory of nuclear reactions. The partial cross section for a reaction leading from an entrance channel a to an exit channel b is determined by the collision matrix element S_{ab}:

$$\sigma_{ab} = \pi\lambda\!\!\!^{-2}_a g_a |\delta_{ab} - S_{ab}|^2 \,, \tag{1}$$

where $2\pi\lambda\!\!\!^{-}_a$ is the wave length of relative motion in the entrance channel, and g_a the spin factor. The S-matrix in turn can be expressed by the R-matrix [1],

$$(2) \qquad S_{ab} = \exp[-i(\phi_a+\phi_b)][(1-iR)^{-1}(1+iR)]_{ab} \ .$$

The exponential factor, containing hard-sphere phase shifts ϕ_a, is known once the (arbitrary) channel radii are fixed. The R-matrix elements

$$(3) \qquad R_{ab} = \sum_\lambda \frac{\gamma_{\lambda a}\gamma_{\lambda b}}{E_\lambda - E}$$

contain the real resonance parameters E_λ and $\gamma_{\lambda c}$. Note that we simplified by choosing the R-matrix boundary parameters so that $L_c^o = iP_c$ (in conventional notation, [1]), and by absorbing the barrier penetrabilities P_c in the $\gamma_{\lambda c}$. This is appropriate for the unresolved resonance region where one typically considers an averaging interval centred at E and so narrow that the energy dependence of the L_c^o and P_c as well as that of $\lambda\!\!\!^{-2}_a$ can be neglected. In terms of the level matrix A the collision matrix can be written [1] as

$$(4) \qquad S_{ab} = \exp[-i(\phi_a+\phi_b)] \ [\delta_{ab}+2i\sum_{\lambda,\mu}\gamma_{\lambda a}A_{\lambda\mu}\gamma_{\mu b}] \ ,$$

where

$$(5) \qquad (A^{-1})_{\lambda\mu} = (E_\lambda - E)\delta_{\lambda\mu} - i\sum_c \gamma_{\lambda c}\gamma_{\mu c} \ .$$

The E_λ and $\gamma_{\lambda c}$ may be identified with the eigenvalues and eigenvector components of the nuclear Hamiltonian which, to the extent that nuclear interactions are invariant under time reversal, can be represented as a real and symmetric N×N matrix, $H = H^* = H^T$. As suggested by Wigner [13] a simple statistical model of resonance reactions is obtained if H is considered as a member of the Gaussian Orthogonal Ensemble (GOE). It is derivable from the requirements that the $H_{\lambda\mu} = H_{\mu\lambda}$ be uncorrelated random variables, and that the form of their joint distribution must be invariant under rotations in the space of the eigenvectors, all orthogonal bases being equivalent [13]. The eigenvector components $\gamma_{\lambda c}$ have (in the limit of very many resonances, $N \to \infty$) the normal distribution around zero [14] suggested by Porter and Thomas [15]. In the absence of direct reactions there are no correlations between width amplitudes for different channels or different levels, or between width amplitudes and level energies, so that the average S-matrix $\bar{S}$ is diagonal. The eigenvalues, on the other hand, are highly correlated, forming a remarkably regular ("stiff") sequence exhibiting eigenvalue repulsion [16, 17]. The case with direct reactions can be formally reduced to the pure compound case by means of the Engelbrecht-Weidenmüller transformation [18].

The calculation of resonance-averaged partial cross sections by averaging Eq. 1 over the GOE, with S_{ab} given by Eq. 4, is easy only for well isolated resonances which overlap so little that eigenvalue correlations can be neglected. Assuming χ^2 distributions for the partial widths one obtains in this case [19]

$$(6) \qquad \bar{\sigma}_{ab} = \sigma_{pa}\delta_{ab} + \pi\lambda\!\!\!^{-2}_a g_a \frac{T_a T_b}{T}\left(1+\frac{2}{\nu_a}\delta_{ab}\right)\int_0^\infty dx \prod_c \left(1+\frac{2T_c}{\nu_c T}\right)^{-\delta_{ac}-\delta_{bc}-\nu_c/2} ,$$

where σ_{pa} is the potential-scattering cross section, $T_c \equiv 1 - |S_{cc}|^2$ the transmission coefficient for channel c, $T \equiv \sum T_c$, and ν_c the degree of freedom for the partial widths $\Gamma_{\lambda c} = 2\gamma_{\lambda c}^2$. The approximation $T_c \approx 2\pi\bar{\Gamma}_c/D$ (where D is the mean level spacing), valid for vanishing level overlap, was used to write the result in terms of the T_c. This is the Hauser-Feshbach formula with elastic enhancement (first pair of parantheses) and width fluctuation correction (integral) [4]. The transmission coefficients on which it depends are macroscopic quantities, obtainable without invoking the resonance description: the transmission coefficients for the particle channels can be obtained from the optical model, those for photon channels from the giant dipole resonance model and those for fission channels from the potential barriers of the channel theory of fission. It should be noted that $\nu_c = 1$ for single channels, but that in practical applications one often uses lumped channels with an effective ν_c differing from unity, for example to represent all fission or capture or particle channels that have the same total angular momentum and parity and thus involve the same resonances.

Generalisation of this expression to arbitrary level overlap proved extremely difficult. Of course one could always resort to Monte Carlo sampling of level energies and width amplitudes from the corresponding distributions, followed by point cross section calculation and averaging. The desired result is thus obtained, although with the statistical uncertainties and lack of transparency typical for the Monte Carlo method. Two main types of analytic functions have been demonstrated to reproduce the Monte Carlo results for pure compound reactions reasonably well.

Moldauer's prescription [20] consists in retaining Eq. 6 for arbitrary level overlap, with σ_{pa} interpreted as the direct cross section, $\sigma_a^{dir} \equiv \pi\lambda\!\!\!^{-2}_a \ |1 - \bar{S}_{aa}|^2$, and with the exact expression for the transmission coefficients

$$(7) \qquad T_c = \frac{4\pi s_c}{|1-i\bar{R}_{cc}|^2} \qquad \text{with} \qquad \bar{R}_{cc} = R_c^\infty + i\pi s_c \ ,$$

where $\bar{R}$ is related to $\bar{S}$ by Eq. 2, $s_c = \bar{\gamma}_c^2/D$ is the pole strength function and R_c^∞, the distant-level parameter, the Hilbert transform of s_c [1]. Furthermore, he considered the ν_c as functions of the T_c and chose these functions so as to describe the Monte Carlo results reasonably well while giving the correct limit for small level overlap (small transmission coefficients): ν_c in (6) is then to be replaced by

$$(8) \qquad \bar{\nu}_c = \nu_c\left[1.78 + (T_c^{1.218} - 0.78)e^{-0.228T}\right] .$$

The second practically important prescription is due to Hofmann, Richert, Tepel and Weidenmüller [21] who, in the spirit of Bohr's original compound-nuclear reaction model, take the partial cross sections as factorisable,

(9) $$\bar{\sigma}_{ab} = \sigma_{pa}\delta_{ab} + \pi\lambda\!\!\!^{-2}_{a} g_a \frac{V_a V_b}{V}\left[1 + (\omega_a - 1)\delta_{ab}\right]$$

with $V \equiv \sum V_c$. The elastic enhancement factors ω_c are expected to approach 3 for vanishing, 2 for very strong level overlap [22]. The authors found their Monte Carlo results adequately described by

(10) $$\omega_a = 1 + \frac{2}{1+T_a^{0.3+1.5T_a/T}} + 2\left(\frac{T_a}{T} - \frac{1}{n}\right)^2 ,$$

where n is the number of open channels. With these W_c the V_c can be found from

(11) $$V_a = \frac{T_a}{1+(\omega_a - 1)V_a/V} , \qquad a=1,2,\ldots n,$$

by iteration starting with $V_c = T_c$. The last equation follows directly from the unitarity of S.

Both prescriptions yield similar results for intermediate and strong absorption (level overlap). Moldauer's recipe is convenient for lumped channels and, by construction, yields the correct result in the limit of vanishing level overlap and few channels where the factorisation approximation fails. It is used for instance in the code FITACS written for automatic, simultaneous fitting of resonance averaged total, capture and fission cross section data [23]. The factorisation approximation is employed for instance in the widely used HAUSER code [24].

3. The Maximum-Entropy Principle

The fact that the average cross section expressions can depend only on "macroscopic" (optical model, giant dipole resonance, fission barrier, etc.) transmission coefficients [21], and that their exact form does not seem to depend critically on the level-statistical model chosen, suggests that "microscopic" resonance details, although needed for the derivation of average cross section expressions from resonance theory, drop out in the end result. A proven technique for sidestepping irrelevant microscopic complications in statistical problems is entropy maximisation [8]. Successfully used already by Gibbs [25] in thermodynamics and by Elsasser [26] in quantum statistics, it became definitely established as a general and powerful tool with the advent of information theory. It permits construction of a probability distribution which (a) is consistent with available macroscopic information while (b) being maximally noncommittal with respect to all other unknown circumstances. The key concept is that of information entropy, shown by Shannon [27] to be the unique, unambiguous measure of the indeterminacy implied by a given probability distribution. The information entropy is

(12) $$S_I \equiv -\sum_{\nu=1}^{n} p_\nu \ln p_\nu$$

if there are n distinct equivalent alternatives and the probabilities for their realisation are $p_1, p_2, \ldots p_n$. It is nonnegative , attaining its maximum if all alternatives are equally probable (maximal indeterminacy), and vanishing if one of them is realised with certainty (no indeterminacy). For a continuous probability distribution p(x) with a priori equivalent increments dx one has [28, 29]

(13) $$S_I = -\int dx\, p(x) \ln p(x) .$$

Let us now assume that information about p(x) is given in the form of expectation values (macroscopic data) for known real functions $f_k(x)$ (observables)

(14) $$\bar{f}_k = \int dx\, p(x)\, f_k(x) , \qquad k = 1, 2, \ldots K .$$

What is the probability density p(x) which satisfies these K equations but does not imply any other information? Since the last requirement in fact means maximal indeterminacy of p(x) apart from the conditions (14), we must solve the variational problem $S_I = \max$ with the K constraints (14) (and the additional constraints that p(x) is normalised to unity and $p(x) \geq 0$ for all x). The well-known solution, obtained by the method of Lagrange parameters, is

(15) $$p(x) = \frac{1}{Z}\exp\Big(-\sum_k \lambda_k f_k(x)\Big) .$$

This is manifestly positive, and properly normalised with

(16) $$Z = \int dx\, \exp\Big(-\sum_k \lambda_k f_k(x)\Big) .$$

The real Lagrange parameters λ_k are to be found from the K equations

(17) $$\bar{f}_k = -\frac{\partial}{\partial\lambda_k} \ln Z .$$

The λ_k are uniquely defined for linearly independent $f_k(x)$, but even if some of the $f_k(x)$ are redundant the resulting distribution p(x) is unique. Moreover, any other function satisfying the constraints has entropy less than that corresponding to p(x),

(18) $$\hat{S}_I = \ln Z + \sum_k \lambda_k \bar{f}_k ,$$

so our entropy is, in fact, maximal and p(x) is the unique solution of the variational problem (see e.g. Refs. 8, 29).

As a simple but important example let us assume that we know only the second moment, $\bar{x^2}$, of some distribution. The maximum-entropy algorithm (15)-(17) readily produces a Gaussian as our best (most objective)

guess, the Gaussian having the highest entropy among all distributions with the same second moment Other familiar examples are provided by thermodynamics, where Z is known as the partition function from which the macroscopic properties of a thermodynamic system are found by suitable differentiation, while the maximised information entropy (18) multiplied by Boltzmann's constant is identical with the physical entropy introduced by Clausius as an observable of a system with given macroscopic state variables Gibbs' canonical ensemble is obtained for given average energy, with the inverse temperature as Lagrange parameter The grand-canonical ensemble results, with the chemical potential as a second Lagrange parameter, if both the average energy and the average particle number are specified, etc Microscopic information about paths and collisions of the molecules constituting the system is not needed to describe its macroscopic behaviour

Application of the maximum entropy principle to matrix ensembles was discussed in particularly lucid fashion by Balian [30] The main complication is the need to generalise the equivalent increments dx in (13) and (14) suitably if the random variate is a matrix rather than a scalar We shall return to this problem in the next section At this point we just mention that in the case of real symmetric matrices, for instance, the GOE

$$(19)\qquad p(H)d[H] = \frac{2^{N(N-1)/4}}{(4\pi a)^{N(N+1)/4}} \exp\left[-\frac{\operatorname{tr} H^2}{4a^2}\right] \prod_{\lambda\le\mu} dH_{\lambda\mu} ,$$

$$a^2 = \frac{1}{N(N+1)} \overline{\operatorname{tr} H^2} = \frac{1}{N(N+1)} \overline{\sum_\lambda E_\lambda^2} , \qquad -\infty < H_{\lambda\mu} < \infty .$$

is obtained (see [11]) if nothing but the second moment of the eigenvalue spectrum ($\sum E_\lambda^2$ in our case) is given, as noted by Porter, ([2] p 46) In this sense the Gaussian Orthogonal Ensemble of real symmetric random matrices is a direct generalisation of the Gaussian distribution of real random numbers Of course, the GOE, constrained only by the second moment, cannot be expected to reproduce model-dependent secular features such as Fermi-gas or shell-model level densities or optical-model size resonances In fact, the semicircular GOE level density law found by Wigner [13] looks rather unphysical Moreover, the assumed independence of the Hamiltonian matrix elements is at variance with the predominantly two-body nature of internucleon forces [17] Nevertheless, the GOE gives an excellent description of the local level statistics (level spacing and width distributions) obtained experimentally in the resolved resonance region or theoretically with more general matrix ensembles [16] or in shell model calculations [17, 32]

4 Invariant Volume Elements for Matrices

Since the assignment of a-priori probabilities (measures) for matrix distributions (ensembles) is not treated in appropriate detail in the level-statistical literature, and since there has been already some confusion in the literature (about "Dyson's measure"), and finally since Beijing may be a good place for this, we give here a short account of the work of Hua Lo-Ken [10] as far as it is relevant to our topic In order to find suitable matrix generalisations for the equivalent, a priori equiprobable increments dx of Eqs 13 and 14 we must introduce a metric. For an arbitrary complex matrix Z we define the line element ds by

$$(20)\qquad ds^2 = \operatorname{tr}(dZ^+ dZ)$$

and interpret the independent real and imaginary parts of the matrix elements $Z_{ab} = X_{ab} + iY_{ab}$ as Cartesian coordinates, $X_{11} = x_1$, $Y_{11} = x_2$, $X_{12} = x_3$ etc in a space with as many dimensions as there are independent real parameters specifying the matrix Z Rewriting (20) in the form

$$(21)\qquad ds^2 = \sum_{a,b} [(dX_{ab})^2 + (dY_{ab})^2] = \sum_{\mu,\nu} dx_\mu g_{\mu\nu} dx_\nu$$

we can read off the metric tensor g The volume element in the space of the x_μ is then [10]

$$(22)\qquad d[Z] = \sqrt{\det g} \prod_\mu dx_\mu$$

It is obviously invariant under translations and rotations in this space, just as dx above was invariant under translations A real symmetric n×n matrix R has n^2 real elements, but because of $R_{ab} = R_{ba}$ only n(n+1)/2 of them are independent Therefore,

$$(23)\qquad ds^2 = \sum_a (dR_{aa})^2 + 2\sum_{a<b} (dR_{ab})^2 = \sum_{\mu,\nu} dx_\mu g_{\mu\nu} dx_\nu$$

and the n(n+1)/2-dimensional volume element in the parameter space is

$$(24)\qquad d[R] = 2^{n(n-1)/4} \prod_{a\le b} dR_{ab}$$

For unitary symmetric matrices S there are $2n^2$ real and imaginary parts of matrix elements, with n^2 unitarity and n(n-1)/2 symmetry relations existing between them Hence the number of independent parameters is the same as for real symmetric matrices, n(n+1)/2 This is consistent with the possibility to express each S-matrix unambiguously in terms of an R-matrix once the hard-sphere phases are fixed In fact, R is essentially what Hua [10] calls the parameter of S Differentiation of Eq 2 yields

$$(25)\qquad dS_{ab} = 2i \exp[-i(\phi_a+\phi_b)][(1-iR)^{-1} dR (1-iR)^{-1}]_{ab}$$

whence

$$(26)\qquad ds^2 = 4 \operatorname{tr}[(1+R^2)^{-1} dR (1+R^2)^{-1} dR] ,$$

the hard-sphere phases canceling due to the cyclic invariance of the trace, tr(AB) = tr(BA) In the space of the independent parameters of R (the x_μ introduced above) one finds the determinant of the metric tensor,

$$(27)\qquad \det g = 2^{n(3n+1)/2} \det(1+R^2)^{-(n+1)/2} ,$$

as is readily seen in a coordinate system in which $1+R^2$ is diagonal The invariant volume element is then

$$(28) \quad d[S] = 2^{n(n+1)/2} \det(1+R^2)^{-(n+1)/2} d[R]$$

with d[R] given by (24) This relationship between d[S] and d[R] is invariant under transformations of the form $S \to USU^T$ with a unitary matrix U, i e under transformations within the domain of unitary symmetric matrices (see [10])

Instead of Cartesian coordinates one can use "polar coordinates" (Hua [10]) These are obtained by explicit introduction of the eigenvalues of the matrix Denoting the diagonal form of a matrix by the subscript D we have $R = OR_DO^T$ with $O^TO = 1$ and $\det O = +1$, i e the real symmetric matrix R is diagonalised by a real orthogonal matrix O representing a pure rotation The real eigenvalues R_c can, without loss of generality, be considered as ordered, $R_1 < R_2 < \quad < R_n$, because the matrices O include those which produce reordering Differentiating OR_DO^T one gets, with $dO^TO = -O^TdO$,

$$(29) \quad dR = O(dR_D + \delta O\, R_D - R_D\, \delta O)O^T$$

where

$$(30) \quad \delta O \equiv O^TdO = -\delta O^T,$$

whence

$$(31) \quad ds^2 = \sum_c (dR_c)^2 + 2 \sum_{a<b} (R_a-R_b)^2\delta O$$

and, via the metric tensor for the polar-coordinate increments dR_c and δO_{ab},

$$(32) \quad d[R] = 2^{n(n-1)/2} \prod_c dR_c \prod_{a<b}|R_a-R_b|\delta O_{ab}$$

$$-\infty < R_1 < R_2 < \quad < R_n < \infty$$

The eigenvalues R_c of R imply eigenvalues $(1+iR_c)/(1-iR_c) = \exp(i\vartheta_c)$ for the random part of S, $(1-iR)^{-1}(1+iR)$ Substituting with $R_c = \tan(\vartheta_c/2)$ in Eq 28 one finds the polar coordinate form of d[S],

$$(33) \quad d[S] = 2^{n(n+1)/2} \prod_c d\vartheta_c \prod_{a<b}|\exp(i\vartheta_a)-\exp(i\vartheta_b)|\delta O_{ab} ,$$

$$-\pi < \vartheta_1 < \vartheta_2 < \quad < \vartheta_n < \pi$$

The absolute values of eigenvalue differences in Eqs 32 and 33 represent eigenvalue repulsion the smaller the difference, the smaller is its a-priori probability We note that eigenvalue repulsion is a universal feature of matrix ensembles It is encountered whenever "polar" coordinates are introduced Replacing R_{ab} by $H_{\lambda\mu}$ and R_c by E_λ one recognises that Eq 32 in fact describes the well known Wigner repulsion (see[2]) between the eigenvalues of the Hamiltonian H, i e between compound-nuclear levels

5 Maximum-Entropy Distributions for the S- and R-Matrix

We are now ready to employ entropy maximisation to find the joint distribution of S-matrix elements for the case that we know only the average S-matrix and, of course, the general features of the S-matrix,

- unitarity (from the conservation of overall probability),
- symmetry (from invariance under time reversal),
- no poles in the upper half of the complex energy plane (from causality)

The causality condition implies that with S one knows also $\overline{S^2} = \bar{S}^2$, $\overline{S^3} = \bar{S}^3$ etc , if the overbar is understood as an energy average with Lorentzian weight function, tractable by contour integration If we assume that the Lorentzian is so wide that the average involves many resonances (poles) we may safely equate energy averages and ensemble averages The importance of these "analyticity-ergodicity" conditions was emphasised by de los Reyes, Mello and Seligman [33] Although there is no question about the importance of causality, it should be understood that the maximum entropy technique, as a tool of inductive reasoning, does not really rely on established ergodicity [8]

We begin with the single-channel case For pure elastic scattering one has simply $S = \exp(i\vartheta)$ with real ϑ, and $d[S] = 2d\vartheta$, $-\pi < \vartheta \le \pi$ (see Eq 33) so that all phases ϑ are equiprobable a priori Since the averages of all positive powers of S are known one knows also the average of any function f(S) that can be expanded in powers of S Particularly convenient for the calculation of Z, Eq 16, is

$$(34) \quad f(S) = \ln(|S-\bar{S}|^2) = \ln(1-\bar{S}^*S) + \text{c.c.}$$

The power expansion of the last logarithm utilises all powers of S, hence the average

$$(35) \quad \overline{f(S)} = 2\ln(1-\bar{S}^*\bar{S}) = 2\ln T$$

utilises all the input data Maximising the information entropy for the distribution $p(\vartheta)$ with the last equation as constraint one gets

$$(36) \quad p(\vartheta)d\vartheta = Z^{-1}|1-\bar{S}^*e^{i\vartheta}|^{-2\lambda}\, d\vartheta ,$$

$$(37) \quad Z = \int_{-\pi}^{\pi} d\vartheta |1-\bar{S}^*e^{i\vartheta}|^{-2\lambda} .$$

In terms of the Legendre function for arbitrary subscript [34] $P_\lambda(x) = P_{-\lambda-1}(x)$, this can be written as

$$(38) \quad Z = 2\pi T^{-\lambda} \int_{-\pi}^{\pi} \frac{d\phi}{2\pi} \left(\frac{1-r^2}{1+r^2-2r\cos\phi}\right)^{\lambda} = 2\pi T^{-\lambda} P_{\lambda-1}\left(\frac{1+r^2}{1-r^2}\right) ,$$

where $r \equiv |S| = \sqrt{1-T}$, $\phi \equiv \arg \bar{S}^*S = \vartheta - \arg \bar{S}$ The derivative of $P_{\lambda-1}$ with respect to λ is

$$(39)\qquad \frac{\partial P_{\lambda-1}}{\partial\lambda} = \int_{-\pi}^{\pi}\frac{d\phi}{2\pi}\left(\frac{1+r^2-2r\cos\phi}{1-r^2}\right)^{\lambda-1}\ln\left(\frac{1+r^2-2r\cos\phi}{1-r^2}\right) .$$

For $\lambda = 1$ the integral is equal to $-\ln(1-r^2) = -\ln T$ and $P_{-1} = P_o = 1$, which shows that $\lambda = 1$ satisfies (17) with f given by (34). The maximum entropy distribution of ϑ, given $\bar{S}$, is thus

$$(40)\qquad p(\vartheta|\bar{S})d\vartheta = \frac{T}{|1-\bar{S}^* e^{i\vartheta}|^2}\frac{d\vartheta}{2\pi}, \qquad -\pi < \vartheta \le \pi .$$

This distribution, known as the Poisson kernel in potential theory, was first obtained by Lopez, Mello and Seligman [35] without entropy maximisation. They recognised that knowledge of all $\bar{S}^n$ and $\bar{S}^{*n}$ means knowledge of all Fourier coefficients of the probability density $p(\vartheta)$, whence $p(\vartheta)$ itself is readily obtained. As expected, microscopic information about the exact distribution of level energies does not appear in (40). It was actually verified in Ref. 33 via Monte Carlo sampling of resonance ladders that rather different level energy distributions lead to this ϑ-distribution, at least within the statistical accuracy of the Monte Carlo calculation.

Rewriting the Poisson kernel in terms of the R-function one gets a Cauchy distribution (Lorentzian), centred at the distant level parameter, and with a width proportional to the strength function [11],

$$(41)\qquad p(R|\bar{R})dR = \frac{1}{\pi}\frac{dx}{1+x^2}, \qquad -\infty < x \equiv \frac{R-R^{\infty}}{\pi s} < \infty .$$

If more than one channel is open the Fourier approach does not work. The reason is that the Fourier coefficients include averages over products involving both S and S^*, such as $S^*_{ab}S_{cd}$. As their poles occur both above and below the real axis, averaging by contour integration is not possible. Entropy maximisation, on the other hand, always works. In order to find the joint distribution of all S_{ab} we maximise the information entropy subject to the constraint

$$(42)\qquad \overline{\ln|\det(S-S)|^2} = \ln\det(1-\bar{S}^{+}\bar{S}) + \text{c.c.} = 2\ln\det T,$$

where $T = 1-\bar{S}^{+}\bar{S}$ is Satchler's transmission matrix [36]. This corresponds to replacement of the function $1-\bar{S}^*S$ in (34) by the scalar $\det(1-\bar{S}^{\dagger}S)$, where 1 is now the unit matrix. The determinant ensures utilisation of all possible averaged products of the S_{ab}, i. e. of all available macroscopic information. With the constraint (42) one gets

$$(43)\qquad p(S|S)d[S] \propto |\det(S-\bar{S})|^{2\lambda}d[S]$$

$$\propto |\det(R-\bar{R})|^{2\lambda}\det(1+R^2)^{-(n+1)/2-\lambda}d[R] ,$$

where the definition of $\bar{R}$ (given after Eq. 7) and eq. 28 were used to express everything in terms of the R-matrix (which, as usual, simplifies things considerably). The last expression suggests to try $\lambda = -(n+1)/2$. With this choice of λ one gets

$$(44)\qquad p(R|\bar{R})\,d[R] = C_n\frac{\prod_{a\le b}dX_{ab}}{\det(1+X^2)^{(n+1)/2}}, \qquad -\infty < X_{ab} \equiv \frac{R_{ab}-R^{\infty}_{a}\delta_{ab}}{\pi\sqrt{s_a s_b}} < \infty ,$$

$$C_n = \pi^{-n(n+1)/4}\,\frac{\Gamma((n+1)/2)}{\Gamma(1/2)}\prod_{c=1}^{n}\frac{\Gamma(n-c+1)}{\Gamma((n-c)/2+1)} .$$

This is a matrix generalisation of the scalar t-distribution of ordinary statistics. The normalisation is obtained by repeated application of the recursion relation (see [10])

$$(45)\qquad I_n(\lambda) \equiv \int_{-\infty}^{\infty}\frac{d[X]}{\det(1+X^2)^{\lambda}}$$

$$= 2^{(n-1)/2}\pi^{n/2}\,\frac{\Gamma\left(\lambda-\frac{1}{2}\right)\Gamma\left(2\lambda-\frac{n+1}{2}\right)}{\Gamma\left(\frac{1}{2}\right)\Gamma(2\lambda-1)}\,I_{n-1}\left(\lambda-\frac{1}{2}\right)$$

which permits reduction of the Integral I_n involving a real symmetric $n\times n$ matrix X to the analogous integral I_{n-1} involving the $(n-1)\times(n-1)$ matrix obtained from X by deletion of the n-th row and n-th column. The proof that the chosen λ is in fact correct can be based on the observation that the distribution of R in the single-channel case is also the marginal distribution of each diagonal element R_{cc} in the multi-level case: A given set of level energies E_λ and width amplitudes γ_λ defines the R-function completely. The distribution functions for level energies and width amplitudes (which need not necessarily be those of the GOE) being unchanged, the very same set could equally well occur in the multi-channel case for some channel, c say, if $\gamma_\lambda = \gamma_{\lambda c}$, $s = s_c$ and $R = R_{cc}$. At each energy E the diagonal element R_{cc} is then equal to R, hence the marginal distribution for R_{cc} must again be the Cauchy distribution (41). Actually one gets the Cauchy form as a by-product of the normalisation (in the second but last step) with our choice of λ, which confirms that (44) is the correct maximum-entropy distribution for the constraint (42). Rewriting it in terms of S one finds the Poisson kernel defined in the domain of unitary symmetric matrices [10]

$$(46)\qquad p(S|\bar{S})\,d[S] = C'_n\left(\frac{\det T}{\det|1-\bar{S}^{+}S|^2}\right)^{(n+1)/2}d[S]$$

$$C'_n = 2^{-n(3n+1)/4}C_n .$$

Introducing "polar" coordinates, i.e. writing $S = OS_DO^T$ (see Sect. 3) we get

$$(47)\qquad d[S] = \prod_c d\vartheta_c \prod_{a<b}\delta O_{ab}\left|e^{i\vartheta_a}-e^{i\vartheta_b}\right|$$

with the usual eigenvalue repulsion term. The Poisson kernel has all necessary properties. It is obviously positive, as required for a probability density, and satisfies

(48) $f(\bar{S}) = \int d[S] p(S|\bar{S}) f(S)$,

for any analytic matrix function f(S) [10]. Since analytic matrix functions are generally defined by power expansions this is just another statement of causality: With $\bar{S}$, $\overline{S^2}$, $\overline{S^3}$ etc. we know also the average of any analytic function of S. It is interesting to note that the Poisson kernel has the form $p(S|\bar{S}) = |\exp(f(S))|^2 = |\psi|^2$ which is typical for quantum-mechanical probability densities. There is undoubtedly a profound connection between information theory, causality and quantum mechanics and this might be one manifestation of it.

Let us now turn to applications of the maximum-entropy distributions of R and S. If only one channel is open, i. e. for pure elastic scattering, the cross section σ can be written in terms of ϑ as

(49) $\sigma = 4\pi\lambda^2 g \sin^2 \frac{\vartheta}{2}$.

This permits substitution of σ for ϑ in the Poisson kernel (40), with the result

(50) $p(\sigma|\bar{S})d\sigma = \frac{1}{\pi \sin\vartheta} \mathrm{Re}\left\{ \frac{e^{i\vartheta}+\bar{S}}{e^{i\vartheta}-\bar{S}} + \frac{e^{-i\vartheta}+\bar{S}}{e^{-i\vartheta}-\bar{S}} \right\} \frac{d\sigma}{4\pi\lambda^2 g}$, $\quad 0 \le \sigma \le 4\pi\lambda^2 g$.

The two terms on the right-hand side correspond to the two branches of the function ϑ(σ). Fig. 1 shows this distribution for two sets of input parameters which correspond roughly to the s-wave cross section of ^{56}Fe at 200 and 500 keV incident neutron energy. The peak position corresponds closely to the "natural" choice of the potential scattering cross section which is obtained if the potential-scattering phase is taken as $\phi = -(\arg \bar{S})/2$ so that $R^\infty = 0$. The Laplace transform of $p(\sigma|\bar{S})$,

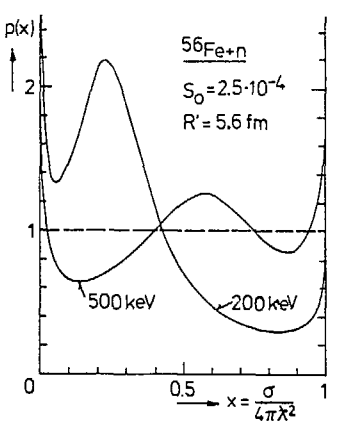

Fig. 1 - Distribution of the total s-wave cross section for ^{56}Fe+n for two average incident neutron energies, in 1-channel approximation (Eq. 50)

(51) $\overline{e^{-n\sigma}} = \int_0^\infty d\sigma\, p(\sigma|\bar{S}) e^{-n\sigma} = e^{-n\bar{\sigma}} \left(1 + \frac{n^2}{2} \mathrm{var}\,\sigma + \ldots\right)$

is the average transmission for sample thickness n (in nuclei/barn) if only one compound spin and parity contributes. If more than one partial wave contributes appreciably the cross section is a sum over partial waves, and the average transmission is a product over all of them,

(52) $\overline{e^{-n\sigma}} = \prod_c \overline{e^{-n\sigma_c}}$.

The average cross section is

(53) $\bar{\sigma} = \sum_c \bar{\sigma}_c = \sum_c \int_0^\infty d\sigma_c p(\sigma_c|\bar{S}) \sigma_c$

Obviously Eqs. 49-53 permit computation of the self-shielding correction to resonance-averaged transmission data by simple quadratures, as a convenient alternative to the usual Monte Carlo approach. It must be noted, however, that the method refers to the natural cross section and fails, unlike the Monte Carlo approach, if Doppler broadening is important. On the other hand it is well suited for average neutron transmission data of nuclides like Fe or Ni isotopes, for which elastic scattering predominates below the first inelastic threshold (e. g. below 846 keV for ^{56}Fe) while Doppler broadening is small.

Knowing the distributions of S- or R-matrix elements one can, in principle, calculate average cross sections rigorously and then check the heuristic prescriptions mentioned in Sect. 2. The dimensionality of the integrals to be computed for n open channels is n(n+1)/2. With polar coordinates and integration over angles (i. e. over the $\delta\Omega_{ab}$ in Eq. 25) one can reduce the dimensionality to n. In the simplest case of two equivalent channels ($T_1 = T_2 = 1-r^2$) one gets the following double integral for the nonelastic cross section,

(54) $\overline{|S_{12}|^2} = \frac{\pi}{4} \int_{-\pi}^{\pi} \frac{d\vartheta_1}{2\pi} \int_{-\pi}^{\pi} \frac{d\vartheta_2}{2\pi} \left\{ \sin^2 \frac{\vartheta_1 - \vartheta_2}{2} \prod_{c=1}^{2} \frac{1-r^2}{1+r^2-2r\cos\vartheta_c} \right\}^{3/2}$.

Fig. 2 shows a calculation of the elastic enhancement w, the essential parameter for this case, together with curves representing Moldauer's prescription and the factorisation approximation. Both approximations are seen to work well, with deviations from the maximum entropy result of less than 2 % . Friedman and Mello demonstrated that in the limit of very many channels (and strong level overlap) the Poisson kernel yields the Hauser-Feshbach formula without width fluctuation, as expected [37]. It is also possible to speed up cross section calculations in Monte Carlo work by sampling R-values from the known R-distribution instead resonance parameters, so that cross sections can be computed directly (via the S-matrix) from the R sample instead from a resonance ladder. This is much simpler but again works only if Doppler broadening can be neglected.

In general, however, first experience with the Poisson kernel or the R-distribution shows that their compact determinantal structure makes

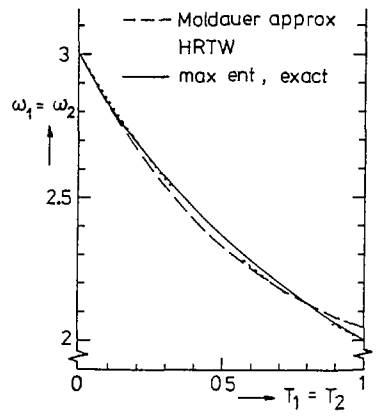

Fig 2 - Elastic enhancement factor for 2 equivalent reaction channels ($T_a = T_b$) Exact calculation with Poisson kernel (Eq 54), shown together with approximations (Eqs 6, 8 and 9, 10)

them quite intractable The next order of business should be to find practical ways to handle them, i e to find suitable expansions, to reduce the dimensionality of the integrals, to verify that the limit for vanishing level overlap is Eq 6, and to deal with the many weakly absorbing photon channels in a similar way as is usually done with Eq 6 (where one lumps them to get a χ^2-distribution with very large ν which in the limit leads to an exponential factor, see [38]) At this point, however, the microscopic approach has pushed ahead again

6 The GOE Triple Integral

Only a few months after the maximum-entropy distributions of the S- and R-matrix had been published (in Refs 9 and 11, resp) Verbaarschot, Weidenmuller and Zirnbauer presented an analytic solution to the problem of averaging partial cross sections over GOE resonance parameters [12] They started from the expression

$$(55) \qquad |S_{ab}|^2 = |\delta_{ab} + i \sum_{\lambda,\mu} \tilde{\gamma}_{\lambda a} A_{\lambda\mu} \tilde{\gamma}_{\mu b}|^2 ,$$

$$(56) \qquad (A^{-1})_{\lambda\mu} = H_{\lambda\mu} - E\delta_{\lambda\mu} - i \sum_{c} \tilde{\gamma}_{\lambda c} \tilde{\gamma}_{\mu c} ,$$

which is a generalisation of what Eqs 4 and 5 give for $|S_{ab}|^2$ the tilde indicates that the Hamiltonian H is left in its general nondiagonal form instead of being diagonalised, so that $\tilde{H}_{\lambda\mu}$ and $\tilde{\gamma}_{\lambda c}$ replace the more familiar $E_\lambda \delta_{\lambda\mu}$ and $\gamma_{\lambda c}$ of Eqs 4 and 5 Assuming a GOE Hamiltonian they managed, by a formidable display of analytic skill and with new tools from the many-body theory of disordered systems, to reduce the ensemble average of $|S_{ab}|^2$ over the GOE to a threefold integral Making full use of the symmetries of the GOE and using a generating function (analogous to the partition function Z of the maximum-entropy approach) involving both commuting and anticommuting (Grassmann) variables, the Hubbard-Stratonovitch transformation to simplify the resulting integrations, and going to the limit of infinitely many levels ($N \to \infty$ for the rank of H) by the method of steepest descent, they derived the expression

$$(57) \quad \overline{|S_{ab}|^2} = |\bar{S}_{ab}|^2 + \frac{T_a T_b}{\delta} \int_0^\infty d\lambda_1 \int_0^\infty d\lambda_2 \int_0^1 d\lambda \, \frac{\lambda(1-\lambda)|\lambda_1-\lambda_2|}{\sqrt{\lambda_1(1+\lambda_1)\lambda_2(1+\lambda_2)}(\lambda+\lambda_1)^2(\lambda+\lambda_2)^2}$$

$$\cdot \prod_c \frac{1-T_c\lambda}{\sqrt{1+T_c\lambda_1}\sqrt{1+T_c\lambda_2}} \left\{ \delta_{ab}(1-T_a) \left[\frac{\lambda_1}{1+T_a\lambda_1} + \frac{\lambda_2}{1+T_a\lambda_2} + \frac{2\lambda}{1-T_a\lambda} \right]^2 \right.$$

$$\left. + (1+\delta_{ab}) \left[\frac{\lambda_1(1+\lambda_1)}{(1+T_a\lambda_1)(1+T_b\lambda_1)} + \frac{\lambda_2(1+\lambda_2)}{(1+T_a\lambda_2)(1+T_b\lambda_2)} + \frac{2\lambda(1-\lambda)}{(1-T_a\lambda)(1-T_b\lambda)} \right] \right\}$$

Note that the analogous maximum-entropy expressions available so far involve at least n-dimensional integrals for n open reaction channels, whereas here we have a three-dimensional integral no matter how many open channels there are A particularly useful feature is the product over channels which permits a similar treatment of the lumped photon channels as does the channel product in Eq 6 Verbaarschot [39] confirmed correct behaviour of the triple integral in the limit of small level overlap He also checked averages computed with the triple integral against averages over the Poisson kernel In spite of the utterly different appearance of the multiple integrals in the two approaches he found the same numbers up to 3 or 4 digits, i e agreement within the numerical accuracy of the two computations This constitutes another, quite stringent verification of the irrelevance of resonance details The GOE triple integral, which fully accounts for width fluctuation corrections and elastic enhancement, can thus be used with confidence for the computation of average partial cross sections (instead of the heuristic analytical formulae derived from Monte Carlo calculations)

7 Cross Section Evaluation in the Unresolved Region

The role of nuclear theory in the evaluation of resonance-averaged cross section data is twofold First it provides average curves and smooth uncertainties where data show real fluctuations due to partially resolved resonance structure (at lower energies) or spurious fluctuations due to experimental effects (throughout the unresolved range) In the latter case experimental errors are reduced Furthermore, level-statistical theory permits simultaneous utilization of information from all open reaction channels, and also from other energy ranges, e g from the resolved-resonance range or from optical-model studies at higher energies Since it relates the average cross sections for all open channels in much the same way as R-matrix theory does for resonance cross sections, a coherent evaluation of all information provides powerful constraints

and reduces uncertainties drastically It is well known how simultaneous R-matrix fits to all data types available in the resolved region yield best estimates of R-matrix parameters (resonance energies and partial widths) In exactly the same way can resonance-(GOE-)averaged R-matrix theory, i e the GOE triple integral (and the well known total cross section expression $\bar{\sigma}_c \propto 1\text{-Re } \bar{S}_{cc}$), be employed in data fitting for all reaction types simultaneously in the unresolved region to find optimal estimates of Hauser-Feshbach parameters (strength functions and distant-level parameters or the equivalent transmission coefficients) The uncertainties and correlations obtained in the fits can then be used to establish confidence bands about the fitted curves

A recent example for such a coherent fit to resonance-averaged data is shown in Figs 3 - 5 Three types of neutron data for ^{238}U (total, capture and recent high-precision inelastic scattering cross sections) were fitted simultaneously in the energy range between 4 and 500 keV A-priori values for the s-wave were taken from the resolved region below 4 keV (strength function $S_0 = (1\ 15 \pm 12)\cdot 10^{-4}$, average level spacing $D_0 = 22\ 0 \pm 1\ 5$ eV, and average radiation width $\bar{\Gamma}_\gamma = 23\ 5 \pm 1\ 0$ meV) For the p-, d- and f-wave a-priori estimates were taken from optical-model and giant-dipole resonance systematics Higher partial waves and subthreshold fission were neglected The level-statistical theory employed is seen to describe the data well, and this is true for both Moldauer's heuristic prescription (Eqs 6, 7) originally used in the

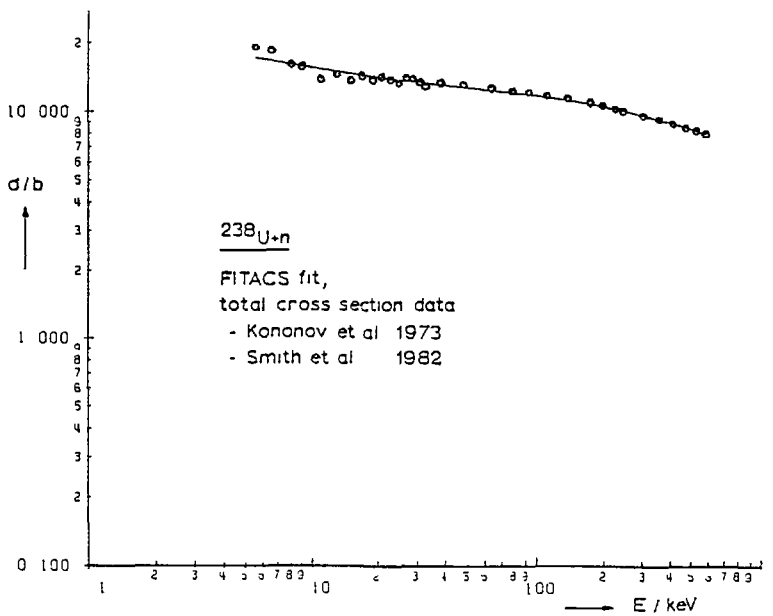

Fig 3 - Coherent fit to ^{238}U data in the unresolved-resonance region total cross section (for references see CINDA [53])

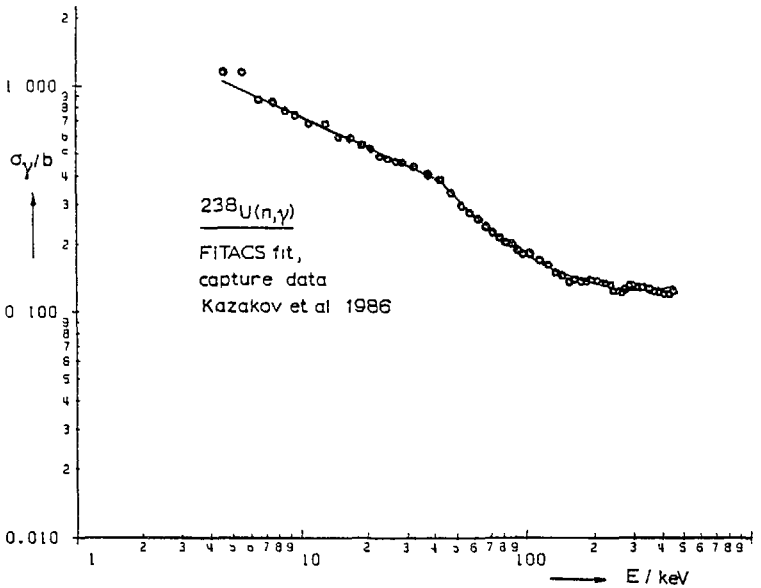

Fig 4 - Coherent fit to ^{238}U data in the unresolved-resonance region capture cross section (for references see CINDA [53]) Competition by inelastic scattering above about 45 keV causes the conspicuous discontinuity at that energy

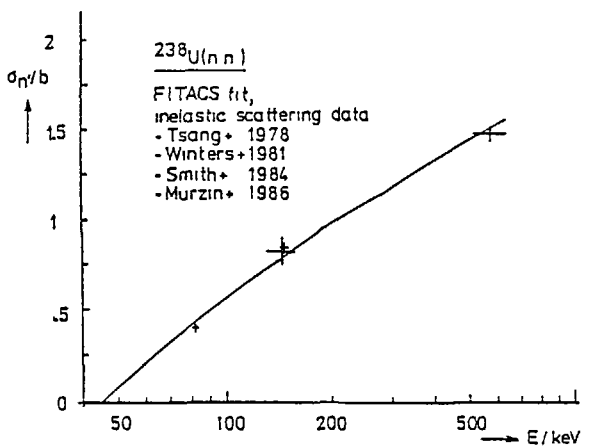

Fig 5 - Coherent fit to ^{238}U data in the unresolved-resonance region: inelastic-scattering cross section (for references see CINDA [53])

FITACS program [23], with which these fits were obtained, as well as for a new GOE version. Typical differences between the two versions amount to 1-3 % in partial cross section values for given average parameters, and even less if parameters are adjusted to fit given data. Therefore the modifications to evaluated cross sections necessitated by the more exact GOE treatment are quite small The main advantage offered by the GOE triple integral is the elimination of any doubts about the adequacy of the width fluctuation corrections In any case the fits obtained for the ^{238}U data shown in Figs 3 -5 are sensitive mainly to the neutron strength functions S_0 and S_1 and to the ratio $\overline{\Gamma}_\gamma/D_0$ (essentially the photon strength function), the neutron strength functions being quite well determined by the total and inelastic-scattering cross sections, the photon strength function by the capture data The results of fits to these (and many other) ^{238}U data sets point to a ratio $\overline{\Gamma}_\gamma/D_0$ which is several percent smaller than the ratio implied by the a-priori (resolved-resonance) values It looks as if the average s-wave radiation width for ^{238}U was less reliable than has been assumed for many years This problem is under study

8. Problems Self-Shielding

The presence of unresolved resonances in neutron cross sections manifests itself in self-shielding effects We encountered the simplest case, self-shielding in transmission measurements, already in Sect 5, Eq. 51, from which it is evident that for a given average total cross section the average transmission (over some finite interval containing many resonances) of a thick sample is larger if the cross section fluctuates than if it is smooth Because of the smoothing effect of Doppler broadening this means that the sample becomes more transparent as its temperature rises In a reactor region filled with a mixture of materials we can write the (n,x) reaction rate for a given nuclide, averaged over the region and over a finite (group) interval, as

$$(58) \qquad \langle\phi\sigma_x\rangle = f_x\langle\sigma_x\rangle\langle\phi\rangle \qquad \text{with} \quad \langle\ldots\rangle \equiv \int_{\Delta E}\frac{dE}{\Delta E}\ldots$$

The group boundaries are often taken as equidistant on a logarithmic energy (linear lethargy) scale, so that there is always the same number of groups per energy decade The most important reaction types x are fission, capture, elastic and inelastic scattering The cross section σ_x is to be understood as Doppler broadened Except at energies below a few meV Doppler broadening does not change the resonance areas, therfore the average (n,x) cross section $\langle\sigma_x\rangle$ does not depend on temperature (apart from edge effects at the group boundaries which become negligible if the group interval contains many resonances). Thus $\langle\sigma_x\rangle$ is essentially the usual energy-averaged cross section treated in Sects 1-6 We saw that it can be calculated accurately with the GOE triple integral

With $\langle\sigma_x\rangle$ out of the way we now focus our attention on f_x, the self-shielding or Bondarenko factor It depends both on temperature and on the cross sections of all other nuclides in the mixture (the "dilution") The data filed in Bondarenko-type group constant sets are

- self-shielded group cross sections $\quad \overline{\sigma}_x \equiv f_x\langle\sigma_x\rangle$ and
- self-shielding factors $\quad f_x = \dfrac{\langle\phi\sigma_x\rangle}{\langle\phi\rangle\langle\sigma_x\rangle}$

stored for each nuclide on a grid of temperatures T and dilution cross sections d The group cross section $\langle\sigma_x\rangle$ is defined so that by multiplying it with the average flux one gets the correct reaction rate With the definition of the covariance, $\mathrm{cov}(x,y) \equiv \langle xy\rangle - \langle x\rangle\langle y\rangle$, we can write

$$(59) \qquad f_x = 1 + \mathrm{cov}\left(\frac{\phi}{\langle\phi\rangle}, \frac{\sigma_x}{\langle\sigma_x\rangle}\right).$$

Now the flux is low where the cross section is high since neutrons do not live very long with energies coinciding with resonances: they are either absorbed or scattered Because of this flux depression across resonances the covariance is negative, and $f_x < 1$. On the other hand f_x must be positive since otherwise the average reaction rate would be negative Thus normally $0 < f_x < 1$.

We can be more explicit by invoking the narrow-resonance approximation (NRA), valid in the important case that resonances are narrow as compared to the mean energy loss of scattered neutrons (i e. in most fast-reactor work) In this approximation the flux is proportional to the reciprocal macroscopic total cross section, $\phi \propto 1/(\sigma+d)$, where $\sigma = \sum\sigma_x$ is the total cross section of the nuclide considered, while d represents the dilution by admixed materials We get now

$$(60) \qquad f_x = \left\langle\frac{1}{\sigma+d}\right\rangle^{-1}\left\langle\frac{\sigma_x}{\sigma+d}\right\rangle .$$

This shows that $f_x \to 1$ if either $T \to \infty$ or $d \to \infty$ (d being considered as constant in the Bondarenko scheme), whence $\langle\sigma_x\rangle$ is called the group cross section for infinite dilution (or the unshielded cross section)

The practically most important method for group constant calulation is the analytic method developped by Frolich [40] and Hwang [41] and improved recently by Sinitsa [42] The Bondarenko averages in (60) are calculated on the basis of the Statistical Model and with the NRA The simplest version includes the following approximations.

- Cross sections are written as sums over resonance sequences, one for each level spin and parity Within each sequence cross sections are approximated by sums of single-level Breit-Wigner (SLBW) terms
- Doppler broadening is described by the symmetric and asymmetric Voigt profiles ψ and χ (see e g [43])
- Interference between resonance and potential scattering (χ) is neglected.
- Bondarenko averages are calculated for each sequence, the other sequences being approximately represented by a smooth cross section added to the dilution d

The result can be written in the form

$$(61)\qquad \bar{\sigma}_x = f_x\langle\sigma_x\rangle = (\sigma_p+d)\left(1-\sum_s \frac{\langle\Gamma J\rangle_s}{D_s}\right)^{-1}\sum_s \frac{\langle\Gamma_x J\rangle_s}{D_s\cos\phi_s}$$

where σ_p is the potential scattering cross section of the nuclide considered, $\langle\ldots\rangle_s$ denotes an average over all partial widths for the s-th sequence (and summations are over sequences), J is the Dresner integral [43]

$$(62)\qquad J(\kappa,\beta) = \int_0^\infty dx\,\frac{\psi(x,\beta)}{\psi(x,\beta)+\kappa}$$

involving the symmetric Voigt profile

$$(63)\qquad \psi(x,\beta) = \frac{1}{\sqrt{\pi}}\int_{-\infty}^{\infty}\frac{dy}{\beta}\exp\left[-\left(\frac{x-y}{\beta}\right)^2\right]\frac{1}{1+y^2},$$

where $\beta = 2\Delta/\Gamma$ is the Doppler parameter, Δ the Doppler width, and

$$(64)\qquad \kappa = \frac{d+R_s}{\hat{\sigma}} \quad \text{with} \quad \hat{\sigma} = 4\pi\lambda^2 g_s\frac{\Gamma_n}{\Gamma}\cos\phi_s,$$

R_s describing GOE eigenvalue repulsion within the s-th sequence in approximate form. This is the fastest method available for group constant calculation. It is employed in many codes, e. g. ETOX (Batelle [44]), MIGROS (KfK, [45]), NJOY (LANL, [46]) and GRUCON (Obninsk, [42]).

The slowing-down method uses Monte Carlo sampled resonance ladders so that the calculation of the average reaction rates is reduced to the case of resolved resonances. The TIMS code written by Takano, Ishiguro and Mitsui [47] is an example.

Monte Carlo sampled resonance ladders are also used in the subgroup/multiband methods developped by Nikolaev et al. [48] and Cullen [49]. One stores, for each one of the (few) subgroups/bands, the quantities α_i, σ_i, σ_{xi} which are determined by matching Bondarenko averages obtained from the ladders as follows:

$$(65)\qquad \langle\sigma_x\rangle = \sum_i \alpha_i\sigma_{xi}, \qquad (66)\qquad \langle\sigma\rangle = \sum_i \alpha_i\sigma_i,$$

$$(67)\qquad \left\langle\frac{\sigma_x}{\sigma+d}\right\rangle = \sum_i \frac{\alpha_i\sigma_{xi}}{\sigma_i+d}, \qquad (68)\qquad \left\langle\frac{1}{\sigma+d}\right\rangle = \sum_i \frac{\alpha_i}{\sigma_i+d}.$$

Finally we mention the probability table method pioneered by Levitt [50], where from sampled resonance ladders the multivariate distribution

$$(69)\qquad p(\sigma,\sigma_n,\sigma_\gamma,\ldots) = p(\sigma)p(\sigma_n|\sigma)p(\sigma_\gamma|\sigma,\sigma_n)\ldots$$

is obtained. The distribution of the total cross section, $p(\sigma)$, is stored together with the conditional probabilities $p(\sigma_n|\sigma)$, $p(\sigma_\gamma|\sigma,\sigma_n)$,... in suitably discretised form, so that cross sections can be directly sampled in Monte Carlo calculations.

The problems with present self-shielding methods came into sharp focus when the first version of the Joint Evaluated File (JEF) of microscopic cross section data became ready for testing in reactor benchmark calculations and group constants had to be prepared. The following questions arose.

- How good is the purely statistical analytic method in comparison to Monte Carlo ladder methods?
- What are good techniques for the partially resolved region, i. e. the lower end of the "unresolved" region (4 to 10 keV for ^{238}U, for instance)?
- How serious are overlap effects, due to coincidence of strong resonances belonging to different materials, and how should they be handled?
- How should the known fluctuations of the cross sections σ around the secular average $\langle\sigma_x\rangle$ (as a function of E) be dealt with? (Simulating them on file by fluctuating p-wave strength functions is certainly not appropriate). In what detail should the fluctuations be represented in the files?
- Is the information allowed by ENDF rules sufficient for self-shielding calculations? Should evaluators in addition to unshielded average cross section $\langle\sigma_x\rangle$ and resonance-statistical parameters (strength functions, mean level spacings, degrees of freedom) also provide Bondarenko factors for zero dilution, $f_x(T,0) = \langle\sigma_x/\sigma\rangle/\langle 1/\sigma\rangle$, for instance for T=300 K (so that one would have the cross sections for infinite as well as zero dilution in the file)? Or should parameters for the biggest resonances in a partially resolved region be given together with a threshold value of Γ_n indicating that resonances with smaller neutron widths are missing and must be sampled from level statistics?
- What can be done to encourage experimenters to provide good data against which calculated self-shielding factors can be tested? There is an appalling lack of thick-sample transmission and self-indication data for different temperatures, similar to those produced by Block et al. [51].

A benchmark exercise undertaken by OECD/NEA (Saclay) aimed at answering some of these questions. Unshielded cross sections and self-shielding factors were to be calculated for the three nuclides ^{235}U, ^{238}U, and ^{239}Pu in three specified energy intervals, for T = 300 K and dilutions of 10 and 100 b. The energy intervals were chosen so that one could calculate from resolved resonance parameters or from level

statistics. The main candidates were analytic codes and the slowing-down code TIMS [47]. The calculations with resolved parameters do not concern us here; they mainly served to check whether the various codes gave the same answers with exactly specified resonances. In fact, differences at the 1 % level were encountered which, of course, exist also when sampled resonance ladders are used.

First a good reference solution had to be established. This was accomplished for ^{238}U by Ribon, Sauvinet and Moussalem [52] who, after studying and discarding a number of sampling methods, sampled width amplitudes by stratified sampling from Gaussians (i. e. according to the Porter-Thomas hypothesis [15]) and level energies from the GOE. The advantage in both cases is that the statistical scatter is smaller than with other methods without bias being introduced. Average results from several generated ladders reduced the uncertainty even further and provided estimates of the statistical (sampling) errors. These results are shown together with solutions from various codes in Table 1.

Table 1 - Selected Benchmark Results for ^{238}U+n
(s-wave only, T = 300 K, 2035 eV < E < 3355 eV)

$\langle\sigma_\gamma\rangle$ (b)	f_γ for d = 100 b	10 b	$\langle\sigma_n\rangle$ (b)	f_n for d = 100 b	10 b	Origin, Method
1.095 ±7	.705 ±2	.412 ±2	18.23 ±12	.797 ±3	.650 ±3	Ribon+/GOE ladders
1.082	.723	.444		.806	.670	UNRESW (THEMIS) (= Hwang code)
1.107	.713	.449	18.84	.821	.714	MIGROS, analytic, overlap
1.100	.700	.405				NJOY/UNRESR anal., no overlap
1.100	.704	.405				NJOY/UXSR analytic, overlap
1.09	.727	.430				TIMS, slowing down

Note: "overlap" in the last column means that a correction for resonance overlap (within resonance sequences, accounting for eigenvalue repulsion) was applied

From the performance of the Hwang code Ribon et al. concluded that the analytic method fails in this case for dilution cross sections of less than 100 b. In view of the numbers from the NJOY subroutines UNRESR and UXSR, however, this does not seem to be generally true. There is also evidence that the analytic GRUCON code works well for small dilution (see [42]). In any case we are far from the goal of 1 % accuracy for calculated self-shielding factors, and the results for ^{235}U and ^{239}Pu, where multilevel interference effects are stronger than for ^{238}U, are even more discrepant.

9. Summary

Summarising we can say that recent years brought a breakthrough in compound-nuclear theory. Analytic expressions for the distribution of S- and R-matrix elements were found by entropy maximisation independently in Mexico City and in Karlsruhe. Cross section distributions and average cross sections can be calculated from them in principle, but in practice this is not easy with present methods. The group at Heidelberg managed to derive a triple-integral expression for the average cross section by averaging over resonances (where so many attempts had failed in the past) and showed that it gives practically the same numbers as the multiple integral over the S-matrix distribution. This means that now, in addition to the "microscopic" distributions of the E_λ and $\gamma_{\lambda c}$ we know also the "macroscopic" distributions of the S_{ab} and R_{ab}, which offers new possibilities for simplified Monte Carlo sampling in the context of data reduction, multiple-scattering simulation etc. Most important, the GOE triple-integral formula permits rigorous calculation of average partial cross sections from transmission coefficients, with full account of width fluctuations and elastic enhancement.

Whereas the calculation of unshielded cross sections is no problem anymore, the desired accuracy of 1 % for self-shielding factors is not reached yet for small dilutions. The OECD/NEA benchmark exercise has furnished some results, however, which can now be applied to the improvement of existing codes for group constant generation. A number of other questions remains open, for instance about format extensions for ENDF-type files relevant to the unresolved region and, more principally, about the cross section detail to be given in the files (cross section fluctuations vs. smooth averages). New measurements of temperature-dependent thick-sample transmission and self-indication data are needed, against which evaluated data and calculational methods for self-shielding calculations can be checked.

ACKNOWLEDGEMENTS

It is a pleasure to thank P. Ribon (CEN Saclay) for communication of GOE resonance ladder sampling results, J.M. Verbaarschot, P. Pereyra and H.A. Weidenmüller (MPI, Heidelberg) for valuable discussions and J.M. Verbaarschot for a copy of his program for the calculation of the GOE triple integral. Steady support by the German Fast Breeder Project, G. Kessler and H. Küsters (KfK) is gratefully acknowledged.

REFERENCES

[1] A.M. Lane and R.G. Thomas, Rev. Mod. Phys. 30 (1958) 257;
J.E. Lynn, The Theory of Neutron Resonance Reactions, Oxford 1968;
F.H. Fröhner, Applied Neutron Resonance Theory, in Nuclear Theory for Applications, IAEA-SMR-43, Trieste 1980 (separately available as KfK-2669 (1978))

[2] C E Porter ed , Statistical Theory of Spectra Fluctuations, (Academic Press, New York and London, 1965)
[3] R G Thomas, Phys Rev 97 (1955) 224
[4] P A Moldauer, Phys Rev C11 (1975) 426, C12 (1975) 744
[5] C Mahaux and H A Weidenmuller, Ann Rev Nucl Part Sci 29 (1979) 1
[6] C Bloch, Nucl Phys A112 (1968) 257, 273
[7] P A Mello, Phys Lett B81 (1979) 103
P A Mello and T H Seligman, Nucl Phys A344 (1980) 489
[8] E T Jaynes Papers on Probability, Statistics and Statistical Physics, edited by R D Rosenkrantz (D Reidel Publishing Co , Dordrecht, 1983) ch 7 and 10
[9] P A Mello, P Pereyra, T H Seligman, Ann Phys 161 (1985) 254
The significance of the Poisson kernel seems first recognised in T H Seligman, Proc Escuela Latinoamericana de Fisica, Cali, Colombia 1982 (World Scient Publ , Singapore) p 674, see also P Mello, Varenna Conf on Nucl Reaction Mechanisms, Varenna, 1982, p 69
[10] L K Hua, Harmonic Analysis of Functions of Several Complex Variables in the Classical Domains, (Amer Math Soc , Providence, R I , 1963)
[11] F H Frohner, Proc Internat Conf on Nucl Data for Basic and Applied Sci , Santa Fe, N M , 1985 (Gordon and Breach, New York, 1986) p 1541, reprinted in Rad Effects 96 (1986) 199
[12] J M Verbaarschot, H A Weidenmuller and M R Zirnbauer, Phys Repts 129 (1985) 367,
[13] E P Wigner, Can Math Congr Proc (U of Toronto Press, Toronto, 1957) p 174, Ann Math 67 (1958) 325, both reprinted in [2] pp 188, 226
[14] C E Porter and N Rosenzweig, Suomal Tiedeakat Toimit (Ann Acad Sci Fennicae) AVI, No 44 (1960), reprinted in [2] p 235, see also C E Porter, in [2] p 2
[15] C E Porter and R G Thomas, Phys Rev 104 (1956) 483, reprinted in [2], p 167
[16] F J Dyson and M L Mehta, J Math Phys 4 (1963) 701, reprinted in [2] p 489
[17] T A Brody, J Flores, J B French, P A Mello, A Pandey, S S M Wong, Rev Mod Phys 53 (1981) 385
[18] C A Engelbrecht and H A Weidenmuller, Phys Rev C8 (1973) 859, H Nishioka and H A Weidenmuller, Phys Lett 157B (1985) 101
[19] L Dresner, Proc Int Conf on Neutron Interactions with the Nucleus, Columbia U , 1957, Report CU-175 (1957) 71, Lane & Lynn
[20] P A Moldauer, Nucl Phys A344 (1980) 185, cf also Ref [3]
[21] H M Hofmann, J Richert, J W Tepel and H A Weidenmuller, Ann Phys 90 (1975) 403
[22] G R Satchler, Phys Letters 7 (1963) 55
[23] F H Frohner, B Goel and U Fischer, Proc Meeting on Fast-Neutron Capture Cross Sections, Argonne, ANL-83-4 (1982) p 116
[24] F M Mann, Report HEDL-TME 76-80, Hanford (1976)
[25] J W Gibbs, "Elemertary Principles in Statistical Mechanics", Yale U Press (1902)
[26] W M Elsasser, Phys Rev 52 (1937) 987
[27] C E Shannon, Bell Syst Tech J 27 (1948) 379 and 623, reprinted in C E Shannon and W Weaver, "The Mathematical Theory of Communication" (Univ of Illinois Press, Urbana, 1949)
[28] E T Jaynes, "Information Theory and Statistical Mechanics", in Statistical Physics, vol 3, K W Ford ed (W A Benjamin, 1963), E T Jaynes, "Prior Probabilities", IEEE Trans Systems Sci and Cybern SSC-4 (1968) 227, both reprinted in [8] pp 39-76 and 114-130
[29] A Katz, "Principles of Statistical Mechanics", (Freeman, San Francisco - London, 1967)
[30] R Balian, Nuovo Cim 57B (1968) 183
[31] F J Dyson, J Math Phys 3 (1961) 140, reprinted in [2]
[32] J J M Verbaarschot and P J Brussaard, Phys Lett 87B (1979) 155
[33] J de los Reyes, P A Mello and T H Seligman, Z Physik A247 (1980) 247
[34] E T Whittaker and G N Watson, "Modern Analysis" (University Press, Cambridge, 1951)
[35] G Lopez, P A Mello, T H Seligman, Z Physik A302 (1981) 351
[36] G R Satchler, Phys Letters 7 (1963) 55
[37] W A Friedman and P A Mello, Ann Phys 161 (1985) 276
[38] L Dresner, Proc Conf on Neutron Interactions with the Nucleus, Columbia U , 1957, Report CU-175 (1957) 71
[39] J M Verbaarschot, Ann Phys 168 (1986) 368
[40] R Frolich, KfK 367 (1965)
[41] R N Hwang, Nucl Sci Eng 21 (1965) 523, 52 (1973) 157
[42] V V Sinitsa, Yad Konst 5(54) (1983) (= INDC(CCP)-225/G)
[43] L Dresner, Resonance Absorption in Nuclear Reactors (Pergamon Press, Oxford, 1960)
[44] R E Schenter, J L Baker and R B Kidman, Report BNWL-1002 (1969)
[45] I Broeders and B Krieg, Report KfK-2388 (1977)
[46] R E MacFarlane et al , Report LA-7584-M (1978)
[47] H Takano, Y Ishiguro and Y Matsui, Report JAERI-1267 (1980)
[48] M N Nikolaev et al , At Energiya 29 (1970) 11
[49] D E Cullen, Nucl Sci Eng 55 (1974) 387
[50] L B Levitt, Nucl Sci Eng 49 (1972) 450
[51] D R Harris, R C Block and R H Hwang, Proc Internat Conf on Nucl Data for Basic and Applied Sci , Santa Fe, N M , 1985 (Gordon and Breach, New York, 1986) p 505
[52] P Ribon, V Sauvinet and P Moussalem, Report CEA-N-2426 (1985), P Ribon, Ann Nucl Energy 13 (1986) 209
[53] CINDA, The Index to Literature and Computer Files on Microscopic Neutron Data, IAEA Vienna 1987

COMPARISON OF COMBINATORIAL AND THERMODYNAMIC METHODS OF CALCULATING NUCLEAR LEVEL DENSITIES

A.V. IGNATYUK, V.P. LUNEV, Yu.N. SHUBIN
Institute of Physics and Power Engineering,
Obninsk, Union of Soviet Socialist Republics

Abstract

The paper analyses the errors in microscopic methods of calculating nuclear level densities, errors due to various approximations of quasiparticle and collective excitation spectra.

A wide range of nuclear processes can be successfully described by applying statistical theory. In all practical applications of this theory, the level densities of excited nuclei play an important role. The Fermi-gas model [1] has been widely used analysing nuclear level densities on account of its simplicity. However, analysis of the statistical properties of nuclei based on microscopic methods developed in studies of the ground state and low-lying nuclear states has demonstrated that the Fermi-gas model has serious limitations and that a more rigorous description of level densities is required which allows in a self-consistent manner for the shell inhomogeneities of a single-particle spectrum, pair correlations of superconducting nucleons and coherent collective nuclear excitations [2]. Traditional analyses of all these effects have been based on thermodynamic calculations of the statistical characteristics of nuclei, which are equivalent to calculations of the corresponding thermodynamic functions in the superconductivity and Fermi liquid theories. In addition to these, direct calculations have also been carried out for spectra of highly excited levels in the superfluid nucleus model [3] and the quasiparticle- phonon model [4]. For light nuclei spectra methods have been intensively developed in recent years to analyse the characteristic values of the large-dimension matrices determining the highly excited levels [5]. Each of the above methods uses various approximations: these are essential to the calculations, but it is rather difficult to assess their influence on the final results. The errors introduced by them are, as a rule, not cleared up even when comparison is made with experimental data, as agreement is usually obtained at the expense of additional variations in the effective forces used or other equivalent model parameters. In this paper we would like to make a more detailed analysis of the basic approximations and errors of statistical and combinatorial level density calculations, based on a direct comparison of calculation results using the same initial model parameters.

ANALYSIS OF THE HOMOGENEOUS SPECTRUM MODEL

A very simple model which reflects the main patterns of change in the densities of excited nuclei states is a system of non-interacting fermions with an equidistant non-degenerate spectrum of single-particle levels. Using established statistical methods [1] an expression is easily obtained for the density of the excited states of such a system:

$$\rho(U) = \frac{1}{\sqrt{48}\,(U + t/2)} \exp\left\{2\sqrt{\frac{\pi^2}{6} g U}\right\} \qquad (1)$$

where g is the density of the single-particle states and t is the temperature related to the excitation energy U by the state equation $U = \frac{\pi^2}{6} g t^2 - t/2$.

For a uniform non-degenerate single-particle spectrum, the level density problem is equivalent to the combinatorial problem of the number of

ways of dividing a given positive integer into non-coincident integral positive terms. A solution to this last problem has been considered [6], and from a comparison of combatorial and statistical calculations it is clear that the errors in expression (1) are 23% for the lowest excited state with U = 1/g, falling to 5% at energy 5/g and to 1.2% at energy 10/g. The accuracy of statistical methods is thus already rather good for a homogeneous spectrum at energies higher than the first two or three excited levels of the system. It should be noted that Eq. (1) and similar relations for the two-component particle system are often used without the term t/2 in the denominator and the state equation. This term reflects the differences between the successive and simultaneous methods of calculating the integrals of the inverse Laplace transform which occur in the statistical calculations of level density. Without this term, the errors in Eq. (1) increase to 25% for U = 5/g and 15% for 10/g. Therefore, whereas for high excitation energies the differences between the two integral calculation methods are negligible, for low energies relations such as that in Eq. (1) - that is, expressions obtained by successive calculation of the integrals - are definitely to be preferred.

The uniform spectrum model is also widely used to calculate level densities for nuclei with a fixed number of excited particles and holes, a calculation required for describing precompound processes of nuclear decay [7]. For excitations of the type np - nh we have

$$\rho_{np-nh}(U) = \frac{g^{2n}(U-A_n)^{2n-1}}{(n!)^2(2n-1)!} \qquad (2)$$

where $A_n = n(n-1)/2g$ is a correction to take account of the influence of the Pauli principle [8]. The full density of the excited states in Eq. (1) can of course be obtained by a summation of all possible values of n.

A common practice in the analysis of nuclear excitations is to replace the particle-hole excitations by phonons. This approach is very effective in an examination of coherent collective excitations of nuclei, but it has also been used [4] for calculations of highly excited multi-phonon states of the nuclei. The homogeneous spectrum model makes it possible to trace the main errors in the phonon description of nuclear statistical features.

In the non-interacting particle model the phonon spectrum is identical to the spectrum of all possible particle-hole excitations, and for an equidistant scheme of levels the spectrum takes the form of a sequence $w_k = k/g$ with a phonon degeneracy equal to k, where k is a series of positive integers not exceeding the number of particles in the system. If we consider the phonons to be non-interacting, then, following the usual methods for calculating thermodynamic functions [2], we obtain the following relation for the excitation density with a given number of phonons:

$$\rho_{n\text{-phon}}(U) = \frac{1}{2\pi i}\int_{-i\infty}^{i\infty} d\beta\, e^{\beta U}\frac{1}{n!}\left\{\sum_k k\,\omega_k e^{-\beta\omega_k}\right\}^n = \frac{g^{2n}U^{2n-1}}{n!\,(2n-1)!} \qquad (3)$$

From comparison with Eq. (2) it is clear that the conversion to phonon language has led to the loss of the factorial n! in the description of level density. This factorial reflects the influence of the Pauli principle, which is not allowed for in Eq. (3) where the phonons are summed independently. The error of this method can easily be seen even from the lowest two-phonon excitation, corresponding to energy $\omega_1 + \omega_2 = 3$ g and degeneracy 2: for different phonons the particle appears in the same single-particle state, and the excitation accordingly violates the Pauli principle. Taking this exclusion into account, we obtain for the lowest 2p-2h excitation an energy 4/g and degeneracy 1. The influence of the exclusion similarly

manifests itself in the higher multi-phonon excitations, and the difference between the quantitites in expression (3) and (2) is in fact determined by the number of spurious states which arise in the independent phonon model. For the total density of excited states in this model we obtain the relation

$$\rho_{phon}(U) = \frac{1}{2\pi i}\int_{-i\infty}^{i\infty} d\beta\, e^{\beta U} \prod_{\kappa} (1 + e^{-\beta\omega_\kappa})^{K} = \\ = (6\pi)^{-1/2}\left[\frac{3\xi(3)g^2}{2U^4}\right] exp\left\{\frac{81}{16}\xi(3)g^2U^2\right\}^{1/3} \quad (4)$$

Where $\xi(3) = 1.21$ is the Riemann zeta function. The presence of a large number of spurious states leads to a significant difference between the energy dependence of $\rho_{phon}(U)$ and the Fermi-gas result in Eq. (1).

It should be noted that the factorials in expressions (2) and (3) are determined by the general laws of combinatorial analysis. For this reason the estimates obtained for the ratio of spurious to true excitations do not depend on the form of the single-particle spectrum - they should also apply to a realistic spectrum of shell model levels. However, when we go over to a two-component particle system, the restrictions on excitations constructed from proton and neutron particle-hole configurations are removed. In generalizing for a two-component system, we obtain for the ratio of the phonon excitation density to the particle-hole density values of 4/3 for n = 2 and 12/5 for n = 3. Thus, for the two-component system the relative number of spurious states is less than for the single-component, but as the structure of the excited configurations becomes more complex, the dominance of spurious states over true states grow steadily.

The need to eliminate spurious states makes the procedure for describing multi-phonon excitations rather complicated. To go beyond the limits of the quasiboson approximation is rather cumbersome even for two-phonon excitations [9], and extending the suggested methods to the more complex excitations requires extremely laborious calculations. However, it is precisely the excitations with $n \geq 3$ which are most interesting in analyses of the density of highly excited nuclear levels. For this reason, the success of the phonon model in describing level densities is largely determined by the accuracy of the methods used to eliminate spurious excitations. The homogeneous spectrum model examined above, which has a rigorous combinatorial solution, could serve as an effective test of such methods.

SHELL MODEL SINGLE-PARTICLE SPECTRUM CALCULATIONS

An important characteristic of realistic single-particle level schemes is their significant level degeneration and the non-uniform distances between levels. The shell inhomogeneities of the single-particle spectrum lead to a certain temperature dependence of single-particle state densities which is reflected in the energy dependence of the density of excited levels [2]. For the non-interacting particle model, it is a simple matter to calculate the spectrum and degeneracy of excited levels by considering all possible combinations of single-particle level populations. If levels below the Fermi energy are considered as hole states, the solution will be given by the relations

$$U = \sum_j |\varepsilon_j - \varepsilon_f| n_j \quad , \quad N(U) = \prod_j (2j+1)!/n_j!(2j+1-n_j)! \quad (5)$$

$$\sum_{\varepsilon_j < \varepsilon_f} n_j = \sum_{\varepsilon_j > \varepsilon_f} n_j$$

where n_j are integers varying from 0 to 2j + 1. The last relation in (5) defines the condition for conservation of the number of particles and holes which has to be observed in the analysis of level populations. Summing N for a given excitation energy level, we obtain the excited state density: $\rho(U) = \Sigma N/\Delta U$. If in this analysis we also consider how the projections of the angular momenta of excited states are distributed, then we can go beyond the state density to the density of the excited nuclear levels.

Figure 1 gives the results of state density calculations for the simplest excitations, 1p-1h and 2p-2h, for the doubly magic nucleus ^{56}Ni. For comparison, we also show calculations of 2p-2h excitations in the independent phonon approximation and calculations based on Eq. (2). When using the phonon approach i.e. when plotting 2p-2h excitations as the sum of all non-identical 1p-1h excitations, the state density is slightly over-

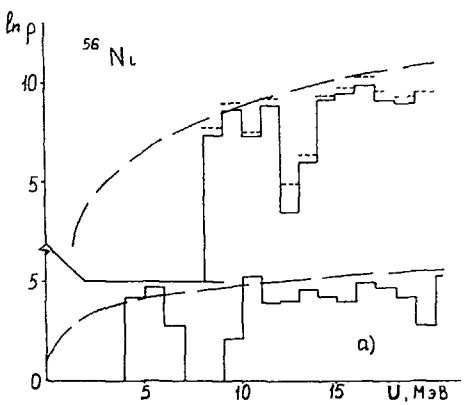

Fig. 1. Energy dependence of the density of (a) 1p-1h and (b) 2p-2h excitations of the ^{56}Ni nucleus. The solid histogram represents combinatorial calculations using the non-interacting particle model; the dotted line - calculations in the independent phonon model; and the dot-dash line - calculations in the continuous spectrum approximation (2).

estimated, and the excess obtained corresponds well on average with the above assessments of the contribution of spurious states associated with violation of the Pauli principle. At the same time, the simple uniform spectrum model relationship in (2) above entirely ignores shell inhomogeneities, which have a strong influence on the energy dependence of a state density with a small number of excitations. The shell gap in the single-particle spectrum also strongly increases the threshold of n-particle excitations. Both of these effects should play an important role in describing pre-equilibrium particle evaporation spectra, and the possible manifestations of such effects have been demonstrated in analyses of the ^{90}Zr(p,n) reaction [10].

Combinatorial calculation results for the total excited state density of the ^{56}Ni nucleus are shown in Fig. 2. For comparison, the results of thermodynamic calculations [2] are also given, carried out for the same

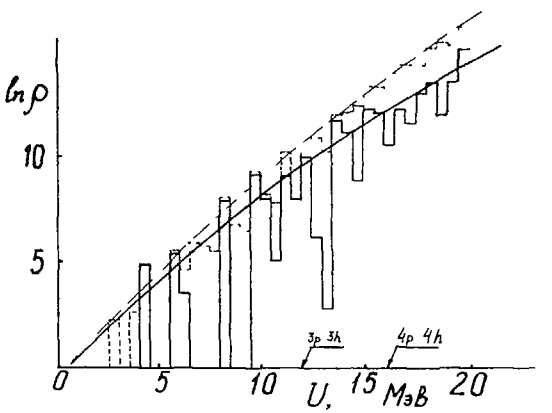

Fig. 2. Energy dependence of the total excited state density for the ^{56}Ni nucleus. The solid histogram represents combinatorial calculations using the non-interacting particle model; the dotted line - combinatorial calculations with adiabatic addition of 2^+ and 3^- vibrational excitations; and the dot-dash and double dot-dash lines - the equivalent thermodynamic calculations.

single particle level scheme. We see fairly good agreement between the combinatorial and thermodynamic calculations in their description of the main statistical trend - the exponential growth of excited state density. However, in the combinatorial calculations we find that significant fluctuations in the state density are characteristic, and that these are particularly pronounced at low excitation energies. The non-interacting particle model certainly overstates these fluctuations, as is particularly clear from a comparison of the model predictions with observed spectra of low-lying levels. Allowance for residual interactions eliminates the level degeneration and always leads to a more uniform distribution of energy levels. For this reason, combinatorial calculations using the simplified models make sense only when a sufficiently large energy interval ($\Delta U \gtrsim 1$ MeV) is used. Figure 3 compares combinatorial and thermodynamic calculations of the mean squares of the angular momentum projections for excited levels, which in fact determine the

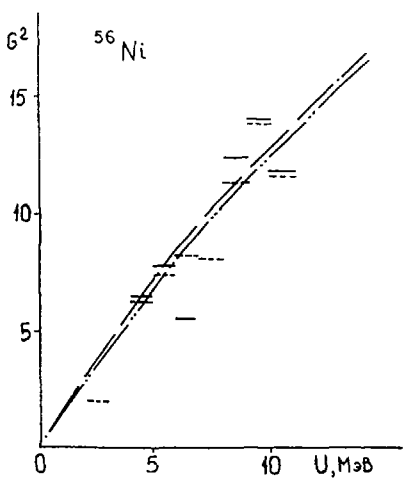

Fig. 3. Energy dependence of the level density spin dependence parameter. Notation as for Fig. 2.

level density spin dependence parameter. Figure 4 compares statistical and combinatorial distributions of density levels according to angular momentum. We find a close correspondence between the combinatorial and thermodynamic calculations in situations where the number of excited levels with different angular momentum values is greater than 10, and significant fluctuations in any or all statistical characteristics with a lower number of levels.

The non-interacting particle model does not reproduce quantitatively either the observed low-lying nuclear level spectra, nor the experimental data on the density of highly excited levels [2]. Thus, for realistic problems an analysis of nuclear level density variations due to effective interaction of particles is essential. The simplest model of such variations is an adiabatic addition to the particle-hole excitations of the nucleus by collective

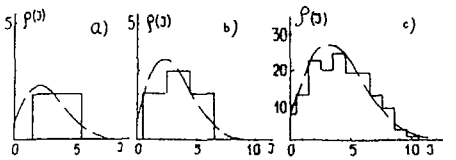

Fig. 4. ^{56}Ni level density distribution from angluar momentum in various excitation energy intervals: (a) 4-4.5 MeV, (b) 5.5-6.0 MeV, and (c) 8-8.5 MeV. Notation as for Fig. 2.

rotational and vibrational excitations [11]. If this approach is adopted, then for spherical nuclei the relations in the combinatorial problem have the following form:

$$U = \sum_j |\varepsilon_j - \varepsilon_f| n_j + \sum_\lambda \omega_\lambda n_\lambda$$

$$N(U) = \prod_j \frac{(2j+1)!}{n_j!(2j+1-n_j)!} \prod_\lambda \frac{(2\lambda+n_\lambda)!}{n_\lambda!(2\lambda)!} \qquad (6)$$

where λ is the multipolarity of the vibrational excitations and the populations (n_λ) of collective excitations are not limited. The particle-hole number conservation condition of course remains unaltered when the collective excitations are added. Figure 2 shows the excited state densities arising when we take into account a quadrupole mode with energy ω_{2+} = 2.7 MeV and an octupole mode with energy ω_{3-} = 4.9 MeV. In the thermodynamic description the corresponding increase in level density is defined by the coefficient

$$K_{vibr}(t) = \prod_\lambda (1 - e^{-\omega_\lambda / t})^{-(2\lambda+1)} \qquad (7)$$

From Eq. (7) it is not hard to see that, in the excitation energy interval considered here, the increase in level density is governed almost entirely by the quadrupole mode, and Fig. 2 shows the good agreement between the combinatorial and thermodynamic calculations in predicting this increase. It is also significant that allowance for collective excitations substantially reduces fluctuations in the combinatorial calculations of excited state density. Figure 3 shows values of the level density spin dependence parameter obtained when collective modes are taken into account. In the thermodynamic description, variations in the spin dependence parameter are defined by the expression

$$\delta\sigma^2 = \sum_\lambda \lambda(\lambda+1)(2\lambda+1)(1+\bar{n}_\lambda)/3 - \sum_\lambda (2\lambda+1)\omega_\lambda \bar{n}_\lambda \left(\frac{\partial \sigma^2}{\partial U}\right) \qquad (8)$$

where $\bar{n}_\lambda = [\exp(\omega_\lambda/t)-1]^{-1}$ represents boson populations in the collective excitations.

For non-magic nuclei, pair correlations of superconducting nucleons have to be taken into account, in addition to shell and collective effects. Methods for describing such correlations have been well developed, both for low-lying levels [12] and for the thermodynamic analysis of highly excited nuclear states [2].

However, the practical application of these methods to combinatorial calculations of excited state density is by no means simple. If we assume that the correlation functions Δ_0^τ and Fermi energies ε_f^τ of the proton and neutron subsystems do not depend on the excited configuration structure - that is, remain the same as for the ground state - then the excited state density can be found from Eq. (5), particle-hole energy being replaced in the first equation by the quasiparticle energy $E_j = \sqrt{(\varepsilon_j - \varepsilon_f)^2 + \Delta_0^2}$. The results of these calculations are presented in Fig. 5a. For the ^{56}Fe nucleus considered here, the correlation functions Δ_0^Z = 1.65 MeV and Δ_0^N = 1.21 MeV were obtained by solving the superconductivity theory equations using the

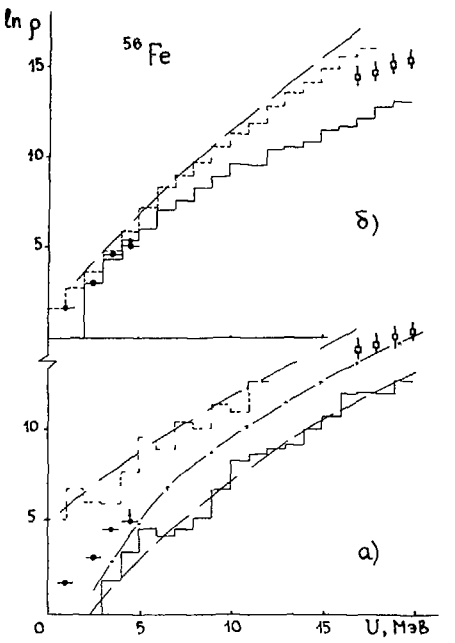

Fig. 5. (a) Calculation of excited state densities for ^{56}Fe using the superfluid nucleus model. The solid histogram represents combinatorial calculations with fixed values of Δ_Z and Δ_N; the dotted line - similar calculations with $\Delta_Z = \Delta_N = 0$; the dot-dash and double dot-dash lines - the equivalent thermodynamic calculations; ---x--- - thermodynamic calculations taking into account temperature variations in the correlation functions; ●- and □ - experimental data [14]. (b) Calculations with the addition of vibration excitations in the adiabatic approximation (dotted line, dot-dash line) and allowing for anharmonic and non-adiabatic conditions (solid histogram).

values of the pairing interaction constants recommended for mass numbers $A \leq 100$ [12]. To demonstrate the influence of correlation effects Fig. 5a also shows the results of calculations for zero values of the correlation functions - i.e. calculations performed in the non-interacting particle model. In addition to the combinatorial, Fig. 5 presents thermydynamic calculations in which the state density was determined by the saddle-pointed method and the thermodynamic functions were calculated from the equations of the superfluid nucleus model - at constant values of the correlation functions, and also with allowance for the temperature changes in these functions.

The combinatorial calculations may be criticized for relying on the condition of equal numbers of quasiparticles above and below the Fermi energy. This condition exists in the non-interacting particle model, but not in the superfluid nucleus model. If the calculations are performed without this condition, the number of excited states increases substantially, and the state denisty at high energies far exceeds the values obtained in the thermodynamic calculations. It can be shown that abandoning the final equation in (5) is equivalent to abandoning the condition of conservation of the number of protons and neutrons in the thermodynamic description of state density. An analysis of this kind overestimates the state density by a factor $2\pi(\delta z \cdot \delta N)^{1/2}$, where δz and δN are the particle number dispersions. Instead of placing limitations on the number of excited quasiparticles, the important thing would be to introduce a particle number conservation equation for each excited configuration. This approach entails replacing the Fermi energy by a chemical potential which depends on the particular configuration considered. As a result of the changes in chemical potential, the quasiparticle energy also changes and the total influence of the particle number conservation condition on the excited state density is approximately the same as the limitations on quasiparticle excitations.

In addition to the chemical potential fluctuations, a consistent theory also requires us to consider changes in the correlation functions for the excited states [12]. A rigorous analysis of these variations in the combinatorial calculations is rather complex and laborious [3]. However, the main ways in which an attenuation of the correlation effects influences our problem can be interpreted quite correctly on the basis of the thermodynamic calculations presented in Fig. 5a, which allow for temperature-related changes in the correlation functions of an excited nucleus.

Figure 5b shows the results of state density calculation with the addition of collective quadrupole and octupole excitations. Since, in the ^{56}Fe nucleus, the quadrupole mode energy is rather low ($\omega_{2+} = 0.85$ MeV), in the adiabatic approximation the collective increase in state density emerges as a high estimate for comparatively low excitation energies. This is clear not only from the experimental data in Fig. 5, but also from a direct comparison of the two-phonon excitation energy in the harmonic approximation with the observed position of the two-phonon triplet levels. In order to allow for the anharmony of collective excitations and the effective "destruction" of phonons for multi-quasiparticle excitations, we have introduced a phenomenological shift into the multiphonon excitation energies:

$$\omega_{n\,\mathrm{phon}} = n\,\omega_\lambda + n(n-1)\,\Delta_\lambda \qquad (9)$$

and have limited the "complexity" of the excited collective modes by the condition $n_{phon} + n_{qu/2} \leq 5$. This phenomenological treatment of anharmony and the non-adiabatic condition significantly reduces the state density for

high excitation energies and brings the calculations into line with the experimental data in the low energy region (Fig. 5b).

It is clear from a comparison of the state density calcultions in Fig. 5 with the available experimental data that the experiment can be described even by extremely simplified versions of the superfluid and collective models with only slight changes in their basic paramaters. Thus, in most cases the question whether a particular description of nuclear statistical properties is correct or not should be answered not from comparison with a rather limited set of direct experimental data on excited level densities, but from analysis of the applicability of the parameters used to describe the main spectroscopic characteristics of the low-lying levels. This being so, methods which describe neutron resonance densities without allowing for the collective effects caused by unwarranted reductions in the correlation functions of the nuclei cannot be considered satisfactory [3]. The same criticism can be made of methods based on spectral analysis of level densities [see expression (5)], in which all that has been achieved as yet is a description of the observed energy dependence of the level densities, whereas the link with the correlational and collective properties of low-energy nuclear excitations is lost.

If we want to analyse the methods of describing collective effects in highly excited nuclei, a very useful approach is to compare not the level density calculations themselves but the coefficients of collective increase in the state densities. Figure 6 shows calculations of these coefficients by various methods. As a complement to the above methods, Fig. 6 also shows the results of a phenomenological description of $K_{vibr}(U)$, obtained from a systemization of level density data for nuclei in the region of iron [13]. This systemization agrees fairly well with microscopic thermodynamic

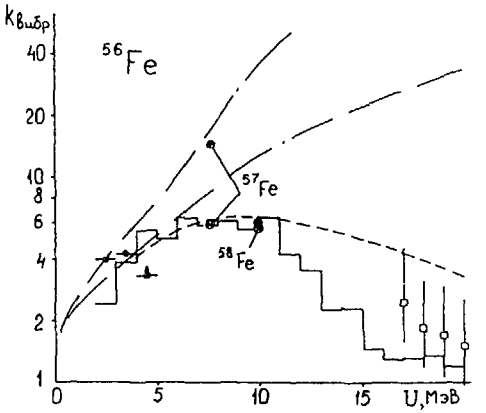

Fig. 6. Energy dependence of the coefficient of vibrational level density increase for ^{56}Fe. The double dot-dash line represents the adiabatic evaluation in (7); the dot-dash line - an evaluation taking anharmony into account; the dotted line - phenomenological systematization [13 the histogram - an evaluation based on combinatorial modelling of anharmonic and non-adiabatic nature; + - a calculation in the quasiparticle-phonon model [4]; x - thermodynamic calculations [2]; and ● and □ - the ratio of experimental level density data to superfluid nucleus model calculations.

calculations of the corresponding coefficients for neighbouring nuclei [2], and also with calculations in the quasiparticle-phonon model [4]. All these approaches point to the unsuitability of adiabatic methods of examining collective effects and to the need to allow for collective mode damping in highly excited nuclei. This is also indicated by the "experimental values" of K_{vibr}, defined as the ratio of the observed state density to the density calculated in the superfluid model.

CONCLUSIONS

Our analysis of various methods for calculating the densities of excited nuclear states has enabled us to evaluate the errors in combinatorial

calculations which arise when the Pauli principle is violated and the changes in correlation functions for highly excited nuclei are disregarded. We have shown that, if the same approximations are used in modelling the spectra of quasiparticle and collective excitations, the accuracy of a thermodynamic description of the statistical characteristics of nuclei is rather good over a wide range of excitation energies, excluding the near-threshold region of the first low-lying levels.

Deviations from an averaged thermodynamic description show up most clearly, it would seem, in the statistical characteristics of nuclei when the number of excited quasiparticles is small. The denisty of such excitations figures directly in the description of pre-equilibrium particle evaporation processes for various nuclear reactions, and special interest attaches to an analysis of effects emerging in these processes which are governed by shell non-uniformities of the single-particle spectrum and by the influence of pair correlations on the thresholds of multi-particle excitations.

At present there is no doubt that consideration of collective effects is indispensable in a description of nuclear statistical properties. However, a consistent theory of the damping of collective movements in highly excited nuclei has yet to be put forward and the validity of our present simplified phenomenological systematizations of such effects still requires testing on a wider range of experimental material. For this reason, a comprehensive analysis of the mixing of collective and multi-particle non-coherent nuclear excitations remains one of the pressing problems of nuclear statistical theory. This problem is not, of course, confined to calculations of nuclear level densities. It arises in the description of radiation force functions and optical potentials of highly excited nuclei, and also in the analysis of a wide range of dissipative phenomena in reactions involving nuclear fission or the fusion of heavy ions.

REFERENCES

[1] BETHE, H., Fizika yadra (Nuclear Physics), M. Gostekhizdat (1948) [translation into Russian].

[2] IGNATYUK, A.V., Statisticheskie svojstva vozbuzhdennykh atomnykh yader (Statistical properties of excited atomic nuclei), M. Ehnergoizdat (1983).

[3] HILLMAN, M., GROVER, J., Phys. Rev. 185 (1969) 1303.

[4] VDOVIN, A.I. et al., EhChAYa 7 (1976) 952.

[5] GRIMES, S.M. in: IAEA Advisory Group Meeting on Basic and Applied Problems of Nuclear Level Densities, BNL-NCS-51694 (1983) 57.

[6] HARDY, G.H., RAMANUJAN, S., Proc. London Math. Soc. 17 (1918) 75.

[7] GRIFFIN, J.J., Phys. Rev. Letters 17 (1966) 488.
BLANN, M. Phys. Rev. Letters 21 (1968) 1357.

[8] WILLIAMS, F.C., Nucl. Phys. A166 (1971) 231.

[9] DZHOLOS, R.V., MOLINA, Kh.L., SOLOV'EV, V.G., TMF 40 (1979) 245.
VORONOV, V.V., SOLOV'EV, V.G., TMF 57 (1983) 75.

[10] BLANN, M. et al., in: Methods for Calculation of Fast Neutron Nuclear Data for Structural Materials (Proc. Meet. in Bologna, October 1986) Vienna, IAEA (1987).

[11] BOR, O., MOTTEL'SON, B., Struktura atomnogo yadra (Structure of the atomic nucleus) M., Mir 2 (1977).

[12] SOLOV'EV, V.G., Teoriya sloznykh yader (Theory of complex nuclei), M., Nauka (1971).

[13] BLOKHIN, A.I., IGNATYUK, A.V., SHUBIN, Yu.N., Yad. Fiz. 47 3 (1987).

A NUCLEAR LEVEL DENSITY FORMULA WITH LOW ENERGY CORRECTION*

Haitao LU
Guizhou University,
Guizhou, China

Abstract

Based on the recommended level density formula of the Fermi gas model, considering the modification at low excitation energies, a level density formula is proposed. From the experimental data of mean neutron resonance spacing D-exp and cumulative numbers of levels No(E) for 264 nuclei, a set of suitable parameters is determined. With these parameters the calculated values agree very well with the experimental data.

1. Introduction

In 1936, an analytic expression for the nuclear level density in the framework of the Fermi gas model was first given by H.A.Bethe.[1] Later on this simple formula has been improved by various authors. A.Gilbert and A.G.W.Cameron[2] introduced a formula as composed four-parameter which is well known popular until now. At high excitation they adopted the conventional shifted Fermi gas formula. At low excitation energies they used a constant temperature formula. They developed a method for determining the parameters for the low-energy region in such a way that the formula best fits the low-energy levels and joins smoothly to the Fermi gas formula. However, due to its complicated structure the composed formula is rather inconvenient to use in statistical model calculations.

* This work is supported by the National Natural Science Foundation of China.

About ten years ago Wang Shunjin et al.[3] proposed a level density formula of the Fermi gas model. Their formula is quite universal and can fit the data for a wide mass region with only four free parameters. But this formula has a defect that at low excitation energies can not reproduce experimental data satisfectory. The present paper is concerned with the modification of this formula for improvement at low excitation energies and at the same time with all the merits retained.

2. Nuclear Level Density Formula

A nucleus which contains Z protons and N neutrons is a complex system of fermions. Each nuclear state is completely characterized by a set of quantum numbers (E,J,M,π). A nuclear level (E,J,π) is $(2J+1)$ fold-degeneracies. Consequently the nuclear level density $\rho(E)$ is given as

$$\rho(E)=\sum_J\sum_\pi\rho(E,J,\pi) \quad . \tag{1}$$

Under the assumption of random distribution of single particle state parities, the nuclear states are equally distributed among the two parities, as

$$\rho(E,J,\pi)=(1/2)\rho(E,J) \quad . \tag{2}$$

According to the argument of Bethe, the distribution law of nuclear levels in angular momentum J is a gaussian one

$$\rho(J)=((2J+1)/2\sigma^2)\exp(-(J+\tfrac{1}{2})^2/2\sigma^2) \quad , \tag{3}$$

where σ^2 is the so-called spin cut-off factor. It is energy-dependent.

Based on the Fermi gas model of nuclei, Bethe (1936,1937) got an analytic expression for nuclear level density

$$\rho(E)\sim\exp(2\sqrt{aE}) \quad . \tag{4}$$

In this paper we modify the level density formula given by Wang Shunjin et al. by introducing a factor (1+F) as follows

$$\rho(E)=(1+F)(t^{3/2}a^{\frac{1}{2}}/(12\sqrt{2\sigma^2}(U+t)^2))\exp(2\sqrt{aU}+1/8\sigma^2) \quad , \tag{5}$$

where the level density parameter "a" is taken as a function of energy E, mass number of the compound nucleus A, as follows:

$$a=(\alpha_1A+\alpha_2A^2)(1+\gamma_1\delta\exp(-\gamma_1E)+\gamma_2S\exp(-\gamma_2E)) \quad . \tag{6}$$

The excitation energy U is determined by

$$U=\frac{E+\delta(1-\exp(-\gamma_1 E))+S(1-\exp(-\gamma_2 E))}{1+\gamma_1\delta\exp(-\gamma_1 E)+\gamma_2 S\exp(-\gamma_2 E)} \quad . \qquad (7)$$

The nuclear temperature t is given by

$$t=(1+\sqrt{1+4aU})/2a \quad . \qquad (8)$$

The spin cut-off factor is

$$\sigma^2=\mu t A^{5/3} \quad , \qquad (9)$$

where the value of μ is taken as 0.0150 for even-even nuclei, 0.0075 for odd-odd nuclei and 0.0115 for odd-A nuclei.

The shell correction S is assumed to be determined by eq. (10) as below

$$S=Mexp-Mo \quad , \qquad (10)$$

where Mexp is the measured masses of nuclei and Mo is obtained from the semi-empirical mass formula given by Myers and Swiatecki.[4] According to them the pairing energy P is taken as

$$P=\begin{cases} 11/\sqrt{A} & \text{odd-odd} \\ 0 & \text{odd A} \\ -11/\sqrt{A} & \text{even-even} \end{cases} \quad . \qquad (11)$$

In order to avoid the trouble of the square root of a negative value, the pairing correction in our calculations, is assumed to be

$$\delta=\begin{cases} 11/\sqrt{A} & \text{odd-odd} \\ 5.5/\sqrt{A} & \text{odd A} \\ 0 & \text{even-even} \end{cases} \quad . \qquad (12)$$

3.The Correction Factor for Level Density at Low Energies

In case the correction factor (1+F) in equ.(5) becomes unity,the original form of the level density formula of Wang et al. is recovered. Therefore F should drop quickly as E increases, we take

$$F=(g-hE)\exp(qE-cE^2) \qquad c>0 \quad , \qquad (13)$$

where g and h are free parameters,and c equals 0.4, q equals 0 im our calculations.

According to Gilbert and Cameron the level density at low energies is given by

$$\rho_1(E)=(1/T)\exp((E-Eo)/T) \quad . \qquad (14)$$

This formula is known as "constant nuclear temperature" level density.This simple expression is based on the following fact: Gilbert and Cameron observed that in a general way the staircase plot of low lying level schemes in a semilog scale can be fitted by a straight line,i.e.

$$LnN(E)=(1/T)(E-Eo) \quad , \qquad (15)$$

where N(E) being the cumulative number of levels. In fact,eq. (15) is Taylor expansion of LnN(E) up to the first order in E, and is too much simplified. We expand LnN(E) in Taylor series up to second order of E

$$LnN(E)=bEo+gE-cE^2 \quad , \qquad (16)$$

where bEo,g and c are free parameters. Therefore, equ.(14) can be replaced by an improved formula,

$$\rho_1(E)=(g-2cE)\exp(bEo+gE-cE^2) \quad . \qquad (17)$$

For convenience we take as the low energy correction function

$$F=(g-hE)\exp(qE-cE^2) \quad . \quad c>0 \quad . \qquad (18)$$

Therefore, with the help of four additional constants g, h and q,c the properties of the constant temperature formula at the low energy region can be incorporated into the modified level density formula (5) in a natural way.

4.Results and Discussion

We have collected the following experimental data for 264 nuclei which are mostly taken from published literatures: the neutron separation energy Sn of the compound nucleus, ground state spin of the target nucleus,the neutron resonance spacing D-exp(s-wave average level spacing),the cumulative number (No) of levels (all spins) and the corresponding energy Eo. For a few nuclei among them the data of cumulative number No are not available.

The nuclei investigated in this work are in the mass region $33 \leqslant A \leqslant 235$. They are divided into three groups:odd mass, double even and double odd nuclei. The parameters determined for different groups differ slightly (see table 1.) from each other.

Table 1. The Level Density Parameters

nuclei	α_1	α_2	γ_1	γ_2
odd-A	0.1221	-0.0000386	0.50	0.0580
even-even	0.1211	-0.0000380	--	0.0500
odd-odd	0.1202	-0.0000390	0.85	0.0585

The results of our calculation can be summarized as below : 220 nuclei for which the calculated values of D are in good agreement with observed values; 38 nuclei for which the calculated values lie slightly outside the "error-bars" Of the experimental values; Only 6 nuclei for which the discrepancies between the calculated and observed values amount to an order of magnitude.

In principle, the parameters g and h should depend on the shell energy correction S and pairing energy correction. However, they are simply regarded as free parameters in this paper the values of g and h for each group of nuclei are determined from the cumulative number of levels. The agreement is not so well as in the case of neutron level spacing data. It could perhaps be further improved by taking into account of the shell and pairing effects.

ACKNOWLEDGEMENTS

The author wishes to express his sincere appreciation to Professor Zhou Yizhong for his help and suggestion. I am indebted to Professor Xu Gongou and Wang Shunjin for much valuable advice.

REFERENCES

1. H.A.Bethe,Phys.Rev.,50,(1936),332.
   Rev.Mod.Phys.,9,(1937),69.
2. A.Gilbert and A.G.W.Cameron,Can.J.Phys.,43,(1965),1446.
3. Wang Shunjin et al.,Physica Energiae Fortis et Physica Nuclearis,Vol.4,NO.2,(1980),236.
4. W.D.Myers et al.,Ark.Fys.,36,(1967),343.
   W.D.Myers and W.J.Swiatecki,Nucl.Phys.,81,(1966),1.

THEORETICAL METHODS FOR THE CALCULATION OF FAST NEUTRON FISSION CROSS-SECTIONS

T. OHSAWA
Department of Nuclear Engineering,
Kyushu University,
Fukuoka, Japan

Abstract

Methods of fission cross section calculation are reviewed and discussed. There are two methods.

The first is utilization of systematics and empirical data. This itself comprises two methods. One is application of systematics observed in fission cross section values in the MeV-region. Another is the use of fission probability data obtained from direct reactions such as (d,pf),(t,pf) in order to produce simulated neutron-induced fission cross sections.

The second method is theoretical model calculation based on the double-humped barrier concept of fission. In this report, the results of our analysis of fission cross sections for 24 actinide nuclides ranging from protactinium to californium are discussed. An attempt has been made to deduce the surface energy coefficient of liquid drop model from the fission barrier heights obtained in the present analysis.

1. Introduction: Incentives to the Present Study

One of the recent topics in reactor physics is the extended burnup of nuclear fuels in LWRs. This leads to production of many transuranium nuclei, such as neptunium, plutonium, americium, curium, berkelium and californium, in greater quantities. This brings about new needs of nuclear data for transuranium nuclides. Criticality safety at various phases of nuclear fuel cycle and actinide incineration by means of nuclear reactors and accelerators are examples of fields that require fission cross section data for these nuclides.

Another interest in the study of fission cross section is what is called "fission barrier anomaly" of actinides, i.e., the measured fission threshold enegies of actinides are only weakly dependent on fissility parameter, in disagreement with the LDM prediction [1]. It is interesting to try to account for this apparent anomaly and to find better relation between the fission barrier heights and surface energy coefficient of LDM.

2. Utilization of Systematics

2.1 Utilization of Systematics of Fission Cross Sections

Let us first discuss the utilization of systematics.

As is well known, Henkel [2] found that the fission cross sections at 3 MeV show linear correlation when plotted against the parameter $Z^{4/3}/A$. This systematics has been used to estimate fission cross sections in some old evaluations, but we do not think this is exact enough to be used for evaluation purposes nowadays.

In recent years, from the measurements of fission cross sections for more than 40 nuclides, Behrens et al. [3] found systematic relations in the cross section values for an initial excitation energy of 8 MeV. Figure 1 shows one of such systematics. For nuclei in the mass region $90<Z<94$ and $139<N<151$, fission cross sections increase linearly with Z at constant N, while they decrease linearly with N at constant Z. However, these rules are not applicable for heavier nuclides; in the region $Z>94$ and $N>144$, cross sections begin to depart from the

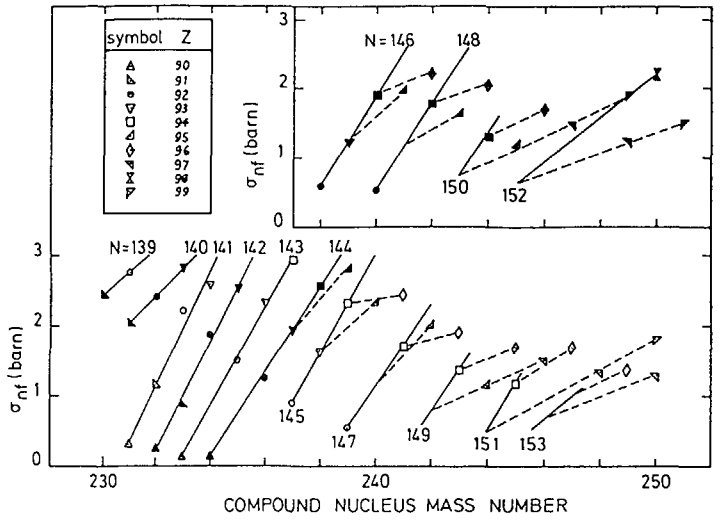

Fig. 1 Systematics observed in fission cross sections for an initial excitation energy of 8 MeV [Ref.3]

systematic trend. As will be mentioned later, this is caused by the change of relative heights of two fission barriers. Anyway, these systematics are useful for rapid estimation of unknown fission cross sections.

2.2 Utilization of Fission Probability Data from Direct Reactions

Another empirical method is using fission probability data obtained from direct reactions. Fission following stripping reactions such as (d,pf), (t,pf), (^{3}He,df), (^{3}He,tf) are the reactions often used for this purpose. This method has two strong points:

First, this method allows a broad survey of actinide nuclei starting from a limited number of available actinide targets. Thus, fission probability data for nuclei with short lifetime can also be measured using this technique.

Second, by appropriately choosing incident energy of the charged particles, it is possible to know the fission probability for nuclei whose fission barrier is lower than the neutron binding energy.

However, there are some conditions for this method to be applicable:

1- Experimental data on the fission probability are available for the required fissioning nucleus;

2- Angular momentum transfers for the neutron-induced and direct reactions do not differ greatly (This refers to entrance channels);

3- There areenough fission channels available, so that some angular momentum differences between the two reactions do not have an important influence on the competing decay reactions (This refers to exit channels, meaning that fission is the dominant decay process);

4- Reliable values of the compound nuclear (CN) formation cross section is obtained from independent source.
(In this respect, a remark should be made that the CN formation cross section calculated with SOM tends to be lower than that calculated with coupled-channel theory for actinides in the MeV region [4].)

If all of these conditions are fulfilled at least approximately, then neutron-induced fission cross sections can be calculated with the following formulas.

$$\sigma_f(En) = \sigma_R(En)\left[P_f^{(1)}(E^*) + \left\{1 - P_f^{(1)}(E^*)\right\} P_F^{(2)}(En) + \left\{1 - P_f^{(1)}(E^*)\right\} P_{F23}(En)\right]$$

$$P_F^{(2)}(En) = \frac{\int_0^{E^*-S_1} \varepsilon_1 \rho_A(E_1)\sigma_R(\varepsilon_1)P_f^{(2)}(E_1)d\varepsilon_1}{\int_0^{E^*-S1} \varepsilon_1 \rho_A(E_1)\sigma_R(\varepsilon_1)d\varepsilon_1}$$

$$P_{F23}(En) = \frac{\int_0^{E^*-S_1-S_2} \varepsilon_1 \rho_A(E_1)\sigma_R(\varepsilon_1)\left[1 - P_f^{(2)}(E_1)\right] P_F^{(3)}(E_1)d\varepsilon_1}{\int_0^{E^*-S_1-S_2} \varepsilon_1 \rho_A(E_1)\sigma_R(\varepsilon_1)d\varepsilon_1} \qquad (1)$$

$$P_F^{(3)}(E_1) = \frac{\int_0^{E_1-S_2} \varepsilon_2 \rho_{A-1}(E_2)\sigma_R(\varepsilon_2)P_f^{(3)}(E_2)d\varepsilon_2}{\int_0^{E_1-S_2} \varepsilon_2 \rho_{A-1}(E_2)\sigma_R(\varepsilon_2)d\varepsilon_2}$$

An example of such calculation is shown in Fig.2 for Pa-233 which is an important nuclei for thorium cycle development. Here we used fission probability data reported by Gavron et al.[5]. Drake [6] estimated the cross section value in the plateau region on the basis of an systematics reported by Henkel. Apparently his evaluation is an overestimate. In the new version of Japanese Eveluated Nuclear Data Library, JENDL-3, the newer evaluation by the present author based on the fission probability data been adopted.

3. Theoretical Method

3.1 History of Fission Theory

Now we proceed to theoretical model calculation based on the double humped barrier concept of nuclear fission. Let us first briefly review the historical development of fission theory.

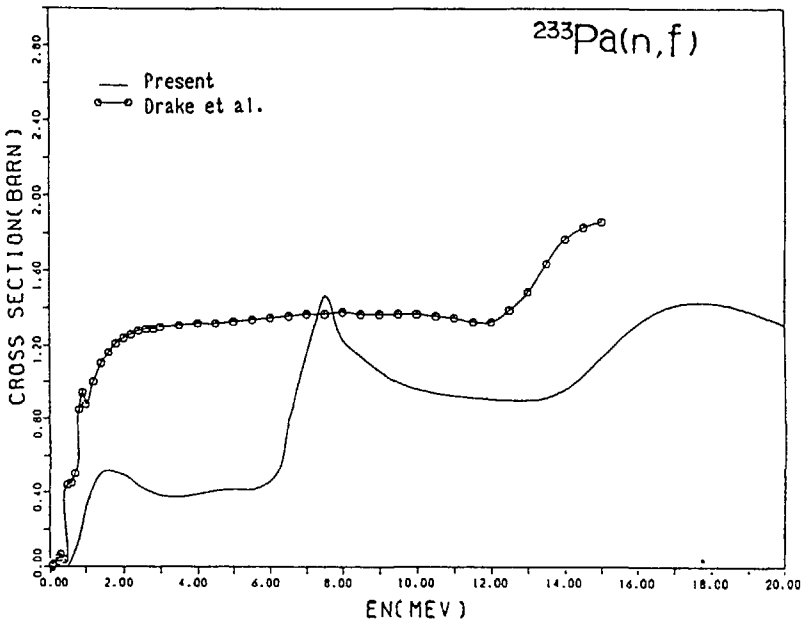

Fig. 2 Fission cross section of Pa-233 calculated using fission probability data. Drake's evaluation [6] is also shown.

As is well known, the fission theory began with the classical work of Bohr and Wheeler [7]. They presented a theoretical description of the fission phenomena within the framework of the LDM and this work plotted the course of research for many years to come.

At the 1-st Geneve Conference, Aage Bohr [8] presented a new model on the basis of the unified model of the nucleus. In this model, it is assumed that most of the excitation energy of the nucleus at the saddle-point is used up as deformation energy, so that the internal excitation energy of the nucleus is relatively low, that is, the nucleus

is "cold". Therefore we have several well-defined discrete collective transition states just above the barrier top, and these states are similar to those observed at the equilibrium-deformation state. These transition states act as excit channels to fission.

This model has been applied to the analysis of fission cross sections and other fission-related quantites such as fragment angular distributions. One of the successful application of this channel theory was the work of Kikuchi [9] of JAERI. He applied this model to the analysis of the spin- and energy-dependence of fission width of four fissile isotopes of U and Pu in the energy region less than 400 keV.

Later detailed analysis of the deformation energy surface led to the concept of double-humped barrier, first propoded by Strutinsky [10].

One of the possibilities to be examined is to extend the idea of the channel analysis to the case of double-humped barrier. However, simple extension of the channel-analysis technique to the double-humped barrrier model encounters a difficulty, since this introduces too many parameters in terms of spin, parity and energy for each of the many fission channels at the two barriers. The difficulty is more enhanced when we try to apply the method to the analysis of odd-mass compound nuclei or the fission cross sections at higher energies, where more and more fission channels come into play.

Fortunately, after the discovery of the double-humped nature of the fission barrier, the development of the fission theory has come into the phase of more sophisticated study of the deformation energy surface. These studies have revealed that, for most of the actinide nuclei, the 1-st barrier is axially asymmetric, i.e. gamma-deformed, while the second barrier is axially symmetric but mass-asymmetrically deformed.

Another important progress in relation to the theoretical analysis of the fission cross section is the development of the method of taking into account the collective enhancement of the level density. Bjørnholm, Bohr and Mottelson [11] have derived level density formulas that take into consideration of the increase of levels owing to the rotational motion of the nucleus, when the nucleus has lost some symmetric properties.

3.2 Basic Idea of the Present Study

The recent progress in understanding the detailed properties of the fission barriers and fission transition states has made it possible to calculate the fission cross sections without resorting to parameter search technique of many adjustable parameters. Our basic idea is to try to reduce the number of adjustble parameters by making the best use of the physical information available from the present knowledge on the fission barriers.

First, the barrier curvature parameters ($\hbar\omega_A$ and $\hbar\omega_B$) can be determined by fission isomer half-lives [12] and fission probability data [13,14].

Second, knowledge on the discrete transition states can be obtained from the channel analysis of the fission fragment angular distribution or from the theoretical estimation of quasi-particle levels at the saddle-point configulations.

Third, continuum transition states can be represented by the level density formula with appropriate collective enhancement factors corresponding to the nuclear shape at the saddle-point.

With all of these parameters fixed, the remaining adjustable parameters are only the heights of the two barriers.

3.3 Double-Humped Barrier Model

Now, going back to the basic physics of nuclear fission, let us briefly sketch the double-humped barrier model of fission.

The fission barrier is represented as a sum of macroscopic and microscopic components (Fig.3). The macroscopic part is described by the LDM, and the microscopic part is obtained by detailed calculation of the shell effects as a function of deformation. By superimposing the shell correction term on the LDM potential, we have a double-humped fission barrier. It should be noticed that there is a small sag at the g.s.-deformation. From theoretical calculations, it is known that the first barrier A is mass-symmetric and gamma-deformed, while the second barrier B is mass-asymmetric, as is shown schematically in Fig.3.

One of the evidences for the existence of the double-humped barrier is the observation of the intermediate structure in the subthreshold

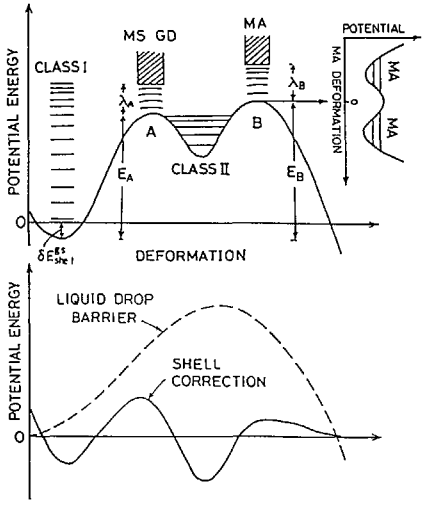

Fig. 3 Schematic diagram of fission barrier as a function of deformation in the fission mode.

fission cross section. The following example will serve as an illustration.

The total Hamiltonian of the fissioning system is composed of four parts:

$$H = H_\beta + \sum_i H_i + \sum_{i<j} H'_{ij} + \sum_i H''_{i\beta} \qquad (2)$$

The CN state wavefunction in the class-I states are described as linear combination of the product of wavefunctions of collective motion and intrinsic excitation. The same is true for the class-II states. The class-I and class-II states are coupled through the last term of the Hamiltonian, and we have the following equation for the coupling strength:

$$H''_{\lambda_I \lambda_{II}} = \sum_{\substack{\nu_I,\nu_{II} \\ \mu',\mu}} C^{\lambda}_{\nu_I \mu'} \langle \nu_I \mu' | H'' | \nu_{II} \mu'' \rangle \; C^{\lambda_{II}}_{\nu_{II} \mu''} \qquad (3)$$

An example of manifestation of this coupling is the grouping structure of fission resonances. This is caused by the enhancement of fission width due to:

1- Admixture of the class-II states into the resonance through the perturbing part H'' of the Hamiltonian;

2- Large fission width of class-II states (because the nucleus has to penetrate through only single barrier).

Figure 4(a) shows the fission cluster around 40 eV in neutron-induced fission of Np-237 [15]. In this case, many class-I states are weakly coupled with a single class-II state, thus only those resonances having the same spin 3- as the class-II states are enhanced. If you plot the fission widths, you have a distribution whose envelope

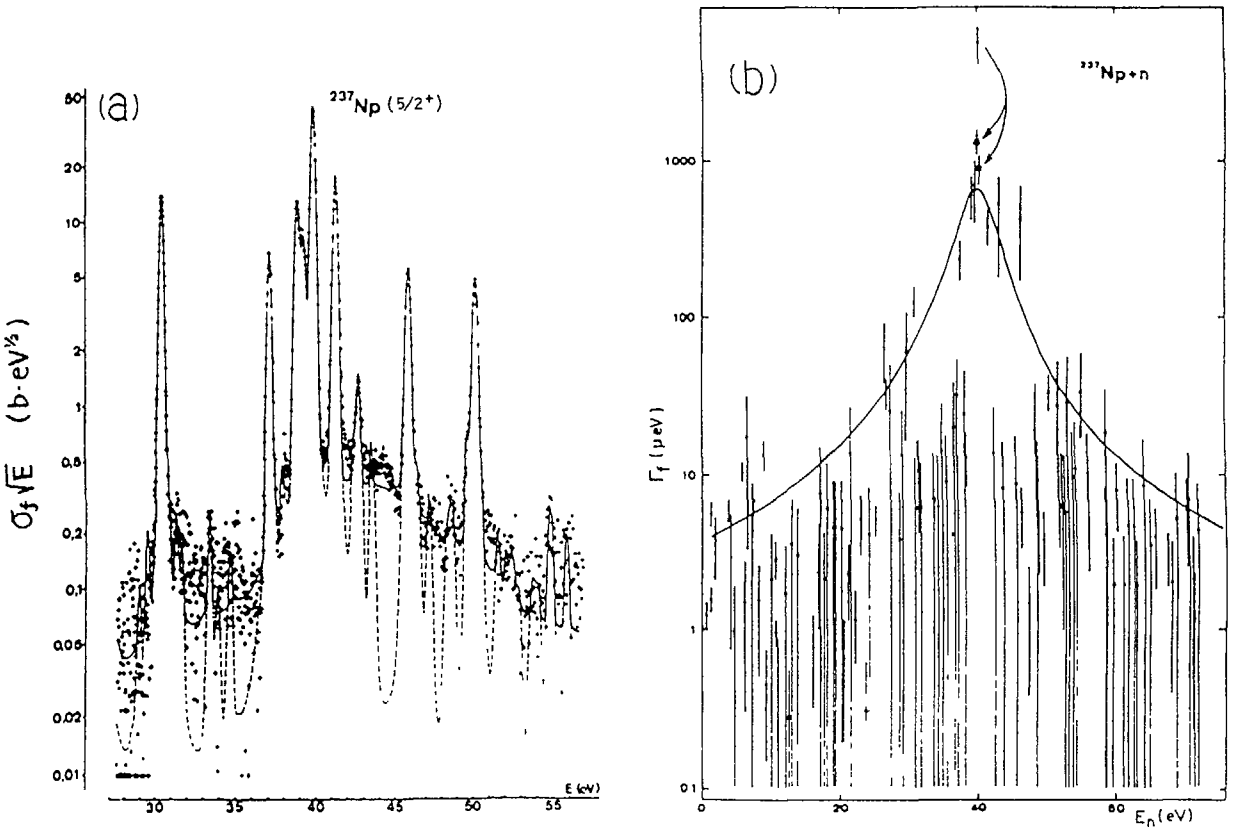

Fig. 4

Subthreshold fission resonances for Np-237 around 40 eV;
(a) Grouping structure of fission resonances (left)[15];
(b) Distribution of fission widths (right)[16].

is a Lorentzian (Fig.4(b) [16]). There is a point at the peak that is deviated from the general trend, but later it was found that the biggest resonance at 39.9 eV was in fact an overlap of two resonances [17]. Thus the corresponding fission widths come nearer to the Lorenzian curve, corroborating the theoretical estimate.

Similar resonance structure due to the coupling of class-I and class-II states can also be observed at energies near fission threshold for many of the actinides.

3.4 Analysis of Fission Cross Sections

a) Cross Section Formula and Transmission Coefficients

The formula used to calculate the fission cross section is the conventional Hauser-Feshbach type. The neutron transmission coefficients were calculated by meams of the optical model. The gamma-ray transmission coefficients were determined so as to reproduce the experimental gamma-ray strength functions.

The fission transmission coefficients were calculated on the basis of the Hill-Wheeler formula [18]:

$$T_A = \sum_{\mu} [\, 1 + \exp\{(2\pi/\hbar\omega_A)(E_A + E_\mu - E)\}]^{-1} + \int_0^{E-E_A-\lambda_A} \frac{\rho_A^{(A+1)}(E-E_A-\varepsilon_K, J)}{1 + \exp(-2\pi\varepsilon_K/\hbar\omega_A)} d\varepsilon_K \quad . \tag{4}$$

The first term describes the transmission through the discrete channels, and the second term describes the transmission through the continuum channels.

Assuming that the double-humped barrier is represented by two inverted parabolas connected in series, we have

$$T_f = T_A\, T_B/(T_A + T_B) \tag{5}$$

for the transmission of the two barriers.

In the subthreshold region we adopted the formula derived by Lynn and Back [19] for the fission probability averaged over the intermediate resonances distributed equidistantly.

b) Level Density Formulas

One of the essential quantities in the analysis of fission cross section is the level density, since the loss of rotational invarience of nuclear shape at barrier deformations leads to the occurence of some rotational degrees of freedom. This gives rise to what is called collective enhancement [11] of the level density.

For instance, for the beta-deformed nuclei, the level density is increased by a factor $\sigma^3/\sigma_{\shortparallel}$ compared to that for the spherical nuclei. For nuclei without axial and reflection symmetry, the level density is further increased by a factor $\sqrt{8\pi}\,\sigma_{\shortparallel}$. For nuclei only with reflection symmetry, or for nuclei with D2 symmetry, the level density is reduced by half or by one quarter, respectively. These factors come from the theorem that states that "if the nuclear shape is invariant with respect to a group of finite rotations, the number of states in the rotational bands are reduced by a factor representing the number of elements in the corresponding point group".

Here we adopted the equation

$$\rho(E,J) \simeq \frac{1}{4}(2J+1)\,\omega(E)\exp\{-\frac{J(J+1)}{2\bar{\sigma}^2(E)}\} \tag{6}$$

for the level density at barrier A, and

$$\rho(E,J) \simeq 2\,\frac{2J+1}{\sqrt{8\pi}\,\sigma_{\shortparallel}(E)}\,\omega(E)\exp\{-\frac{J(J+1)}{2\sigma_{\perp}^2(E)}\}\ , \tag{7}$$

for the level density at barrier B. The factor 2 in the last formula comes from the fact that the nucleus at barrier B is massasymmetrically deformed, so it does not have reflection symmetry.

The intrinsic state density $\omega(E)$ and spin-cutoff parameter $\sigma_{\shortparallel}^2$ have been calculated by Britt and Back [20] on the basis of the Strutinsky-type calculation of Larsson et al.[21] for three nuclides Ra-228, U-238 and Cm-248. We adopted these values for the three nuclides, and the values for other nuclei have been obtained by interpolation.

c) Discrete Transition States

As for the discrete transition states, only a little information is available, so we applied theoretical means to construct a sequence of levels.

For odd-mass nuclei, calculation of single-particle enegies in a deformed nucleus has been made by Larsson et al.[21]. We have to convert the single-particle energies e_i into quasi-particle energies E_i using the relation

$$E_i = [(e_i - \lambda)^2 + \Delta^2]^{1/2} - \Delta \qquad (8)$$

where λ is the Fermi energy. It should be noticed that this conversion results in remarkable "condensation" of states. Without this procedure, the states density would have been considerably underestimated. Some examples of the discrete transition states at barriers A and B as calculated with the above prescription are shown in Fig.5 .

For even-even nuclei, quasi-particle excitations are suppressed below the pairing gap, thus the only possible modes of excitation allowed in this region are the collective ones, that is, vibration with associated rotational bands. Possible one-phonon vibrational states are gamma-vibrational band with K =2+, mass-asymmetric vibrational states with K =0-, and bending mode of vibration with K =1-. The energies of the vibrational states have been mainly taken from the works of Back [12,13] and Lynn [22].

3.5 Results of Analysis

a) Doubly Even Targets

The results of calculations for doubly even target nuclei are shown in Fig.6. For Pu-244, the agreement between calculation and experiments is very good. On the other hand, for Cm-244 the calculation does not reproduce the near-threshold behavior of the cross section. This is because the present model does not explicitly take into account the intermediate structure caused by the coupling of class-I and class-II states.

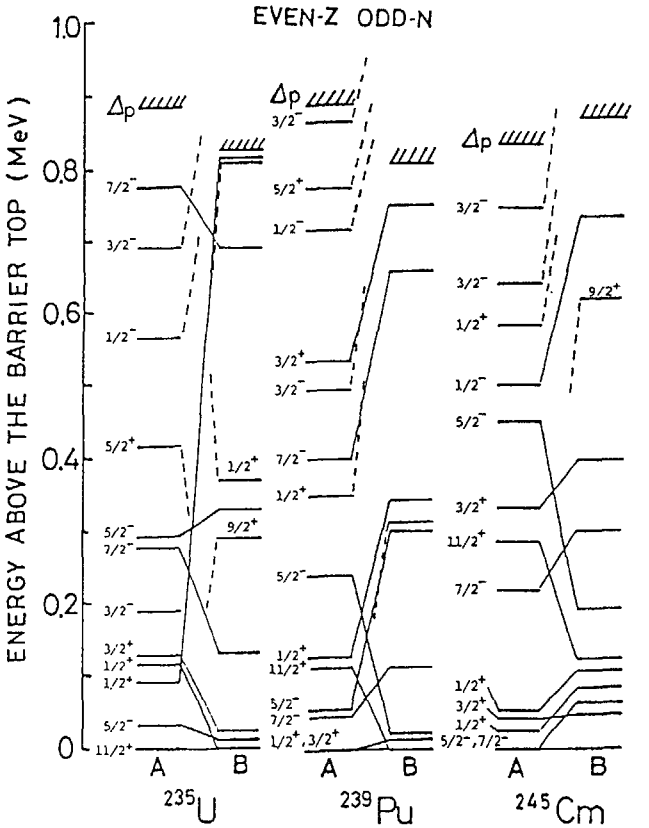

Fig. 5 Examples of quasi-particle states at barriers A and B for even-Z odd-N fissioning nuclei U235, Pu-239 and Cm-245.

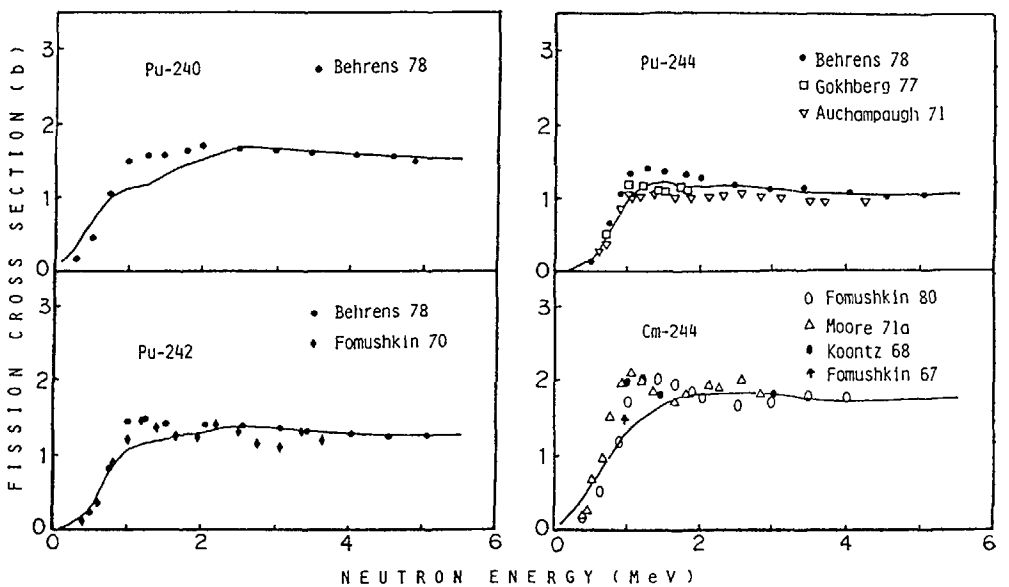

Fig. 6 Fission cross sections for even-even target nuclei.

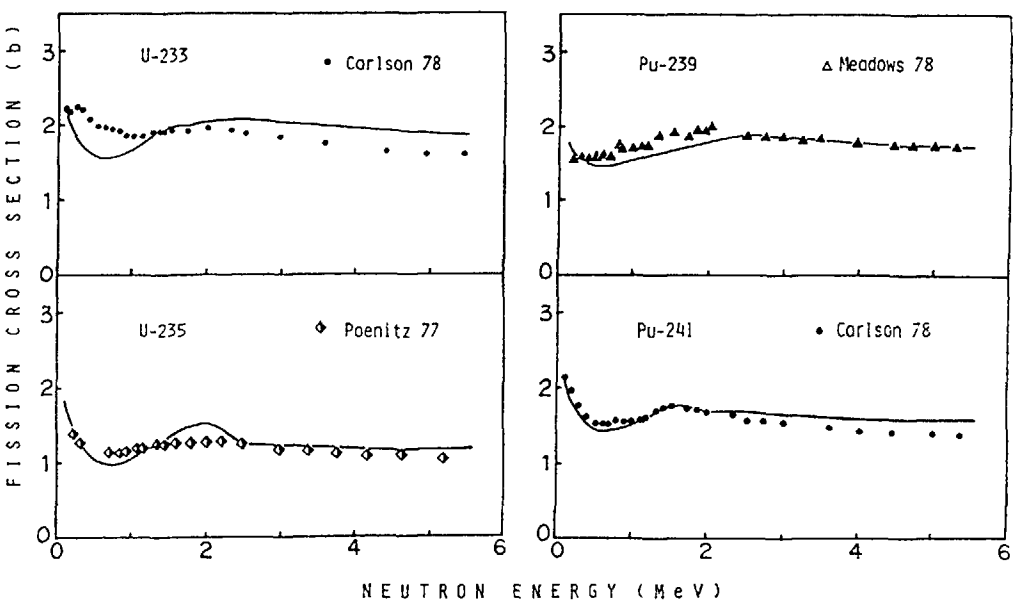

Fig. 7 Fission cross sections for odd-A target nuclei.

b) Odd-A Targets

The results for odd-A target nuclei are shown in Fig.7 For Pu-241, the agreement is excellent, while for U-233 there remain some discrepancies below 1 MeV. One of the reasons for this is that we used single set of collective transition states for all these cases. If we allow the transition states and pairing gaps vary their energies, it is possible to get better fits to the experimental data. But we did not do this, because trying to get the best fits to the measured data was not the primary aim of this work.

In the fitting procedure, we tried to reproduce the magnitude of the fission cross section in the plateau region, say around 3 MeV, since in this region the cross section is not affected by the coupling of class-I and class-II states.

c) Curium isotopes

For some of the Cm-isotopes, a broad hump is observed in the measured data, but the calculation did not reproduce the hump [Fig.8]. It seems that this is different from the intermediate structure caused by the coupling of class-I and class-II states, because the hump ocurrs at energies 2 to 4 MeV above the fission barrier, and its width is too broad. If this structure is actual, the nature of the bump-like behavior is hard to explain.

d) Comparison with Lynn's Barrier Heights

Table I summarizes the barrier heights obtained from the present analysis, and compares them with those reported by Lynn [22]. Evidently, the agreement is better for lighter actinides, while it is

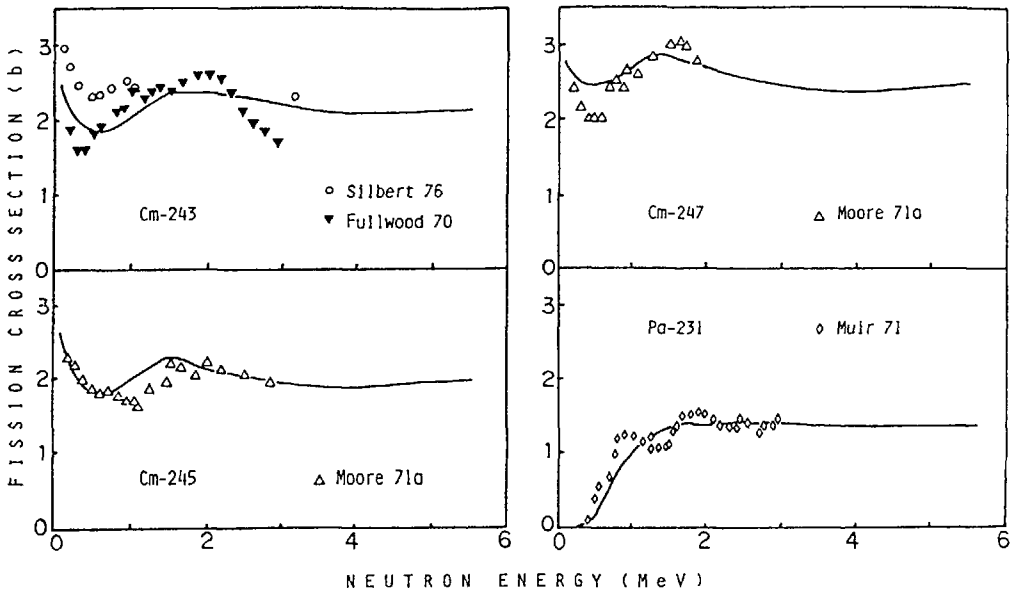

Fig. 8 Fission cross sections for Cm-isotopes.

worse for barrier B of heavier actinides. In Fig.9 , the abscissa is the present barrier height, and the ordinate is the Lynn's barrier height. Obviously there seems to be no considerable bias. Those data with greater deviations corresponds to barrier B of heavier actinides. The reason for the greater difference in the second barrier height in this region is that for heavier actinides, the second barrier is much lower than the first barrier, so that the calculated fission cross section is less sensitive to a change in E_B. Thus the uncertainty for these values are larger.

3.6 Systematics in Fission Barrier Heights

a) Systematic Relations for the Obtained Barrier Heights

We looked for the correlation between the barrier heights and other

Table I Fission barrier parameters obtained from fission cross-section analysis. Present results are compared with the results of Lynn (ref. 22)

Compound nucleus	Z-N[a]	B_n	Present results[b]				Lynn[22]		
			E_A	$E_A-\delta E^{\delta p}_{shell}$	E_B	$E_B-\delta E^{\delta s}_{shell}$	E_A	E_B	Reactions[c]
		MeV	MeV	MeV	MeV	MeV	MeV	MeV	
Pa-232	o-o	5.56	6.20	5.04	6.14	4.98	6.3	6.25	n
U-234	e-e	6.84	5.26	3.68	5.57	3.99	5.6	5.5	c + n
U-235	e-o	5.31	6.27	4.68	5.74	4.15	6.15	5.9	c + n
U-236	e-e	6.55	5.86	4.48	5.70	4.32	5.6	5.53	c + n
U-237	e-o	5.12	6.38	4.95	5.85	4.42	6.28	6.08	n
U-239	e-o	4.80	6.31	5.31	5.75	4.75	6.46	6.16	n
Np-238	o-o	5.48	6.31	4.33	5.79	3.81	6.19	5.9	c + n
Pu-239	e-o	5.66	5.86	3.36	5.68	3.18	6.26	5.66	n
Pu-240	e-e	6.53	5.99	3.84	5.22	3.07	5.57	5.07	c + n
Pu-241	e-o	5.24	5.63	3.46	5.67	3.50	6.14	5.54	c + n
Pu-242	e-e	6.30	5.60	3.79	5.23	3.42	5.55	5.05	c + n
Pu-243	e-o	5.04	5.72	3.88	5.65	3.81	6.04	5.44	n
Pu-245	e-o	4.72	5.42	4.05	5.48	4.11	5.86	5.26	n
Am-242	o-o	5.53	6.61	3.90	5.56	2.85	6.5	5.7	c + n
Am-243	o-e	6.38	6.17	3.84	4.75	2.42	6.25 6.08	5.65 5.38	c n
Am-244	o-o	5.36	6.42	4.00	5.49	3.07	6.37	5.57	c + n
Cm-244	e-e	6.80	6.20	3.33	5.14	2.27	5.8	4.5	c
Cm-245	e-o	5.52	6.15	3.12	5.80	2.77	6.32	5.02	n
Cm-246	e-e	6.45	6.00	3.31	4.98	2.29	5.65	4.35	n
Cm-247	e-o	5.16	6.15	3.45	5.33	2.63	6.16	4.86	n
Cm-248	e-e	6.21	5.61	3.26	4.25	1.90	5.7	4.6	c
Cm-249	e-o	4.71	5.61	3.48	5.03	2.90	5.66	4.36	n
Bk-250	o-o	4.97	6.20	3.48	5.31	2.59	6.12	4.12	n
Cf-253	e-o	4.79	5.52	2.97	4.44	1.89	5.43	3.6	n
			MeV		MeV		MeV	MeV	
curvature	o-o		0.6		0.42		0.65	0.45	
parameters	o-A		0.8		0.55		0.8	0.52	
($\hbar\omega$)	e-e		1.0		0.70		1.04	0.6	

a) Even-odd character of Z and N numbers.

b) δE_{shell} is the ground-state shell energy correction shown in Fig.1. The values were taken from ref. 23,

c) The reactions of the data used in the analysis. The symbol c stands for charged-particl induced reactions, such as (d,pf), (t,pf) etc., n stands for (n,f) reaction, and c+n their combination.

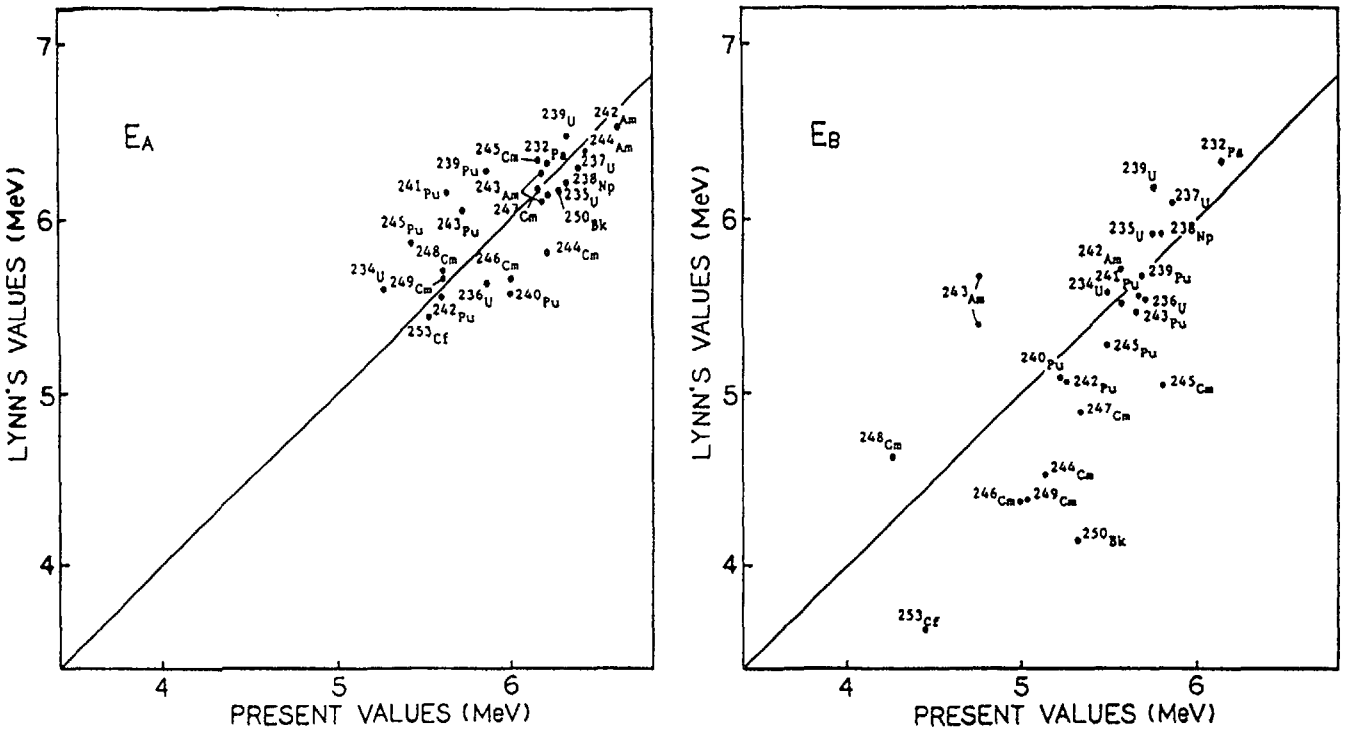

Fig. 9 Comparison of Lynn's barrier heights and those obtained from the present analysis.

parameters, such as neutron number, mass number, and fissility parameter. We found that the first barrier heights E_A tend to be peaked at the neutron number 147, althogh the data are rather scattered. In contrast to E_A, the second barrier heights E_B were found to increase linearly with $(1-x)^3$, where x is the fissility parameter defined as

$$x = \frac{3}{5}\frac{e^2}{r_0}\frac{Z^2/A}{2a_2[1-\kappa\{(N-Z)/A\}^2]} \qquad (9)$$

In both cases, it is apparent that the barrier heights for odd-odd compound nuclei are higher than those for even-even C.N., with those for odd-A C.N. tending to come in between.

b) Three-Component Analysis of Barrier Heights

In order to obtain a better systematic relation for fission barrier heights, an attempt was made to interpret the barrier heights in terms of a three-component approach. In this approach, it was assumed that

the barrier height was composed of a smooth macroscopic component E_{LDM} and an oscillating microscopic component:

$$E_A = E^A_{LDM} + \delta E^{gs}_{shell} + \delta E^{sp,A}_{shell} \quad , \tag{10a}$$

$$E_B = E^B_{LDM} + \delta E^{gs}_{shell} + \delta E^{sp,B}_{shell} \quad . \tag{10b}$$

The latter part was further subdivided into two components: the shell corrections at the ground state deformation and that at the saddle points. While shell correction at the saddle point is not easy to estimate, the shell correction at the g.s.-deformation can be obtained from a detailed analysis of nuclear masses.

As a step to isolate the liquid drop model (LDM) component, we subtracted g.s.-shell correction from the observed barrier heights, and plotted them as a function of $(1-x)^3A^{2/3}$(Fig. 10). This parameter is proportional to the LDM definition of fission barrier height:

$$E_f = (98/135)(1-x)^3 a^2 A^{2/3} \tag{11}$$

where a_2 is the surface energy coefficient of the LDM. It can be seen that good linear correlation exists between the quantities $E_B - \delta E^{gs}_{shell}$ and $(1-x)^3A^{2/3}$. This is in contrast with the case for barrier A, where, although similar linear correlation is observed, the data points are more scattered. Good linearity for barrier B means that LDM component of the barrier height is well isolated, in spite of the fact that the saddle-point shell correction has not yet been subtracted.

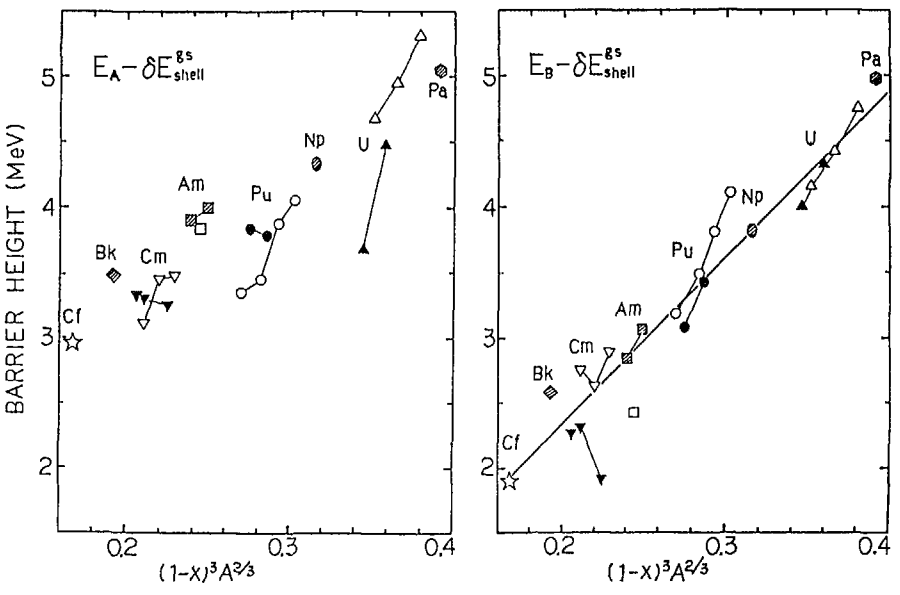

Fig.10 Systematics of corrected barrier heights

This, in turn, means that the shell effects at the saddlepoint has only small contribution to the height of the barrier B, while it has an appreciable contribution at barrier A. This result is consistent with theoretical prediction that the shell correction is damped at larger deformations.

Another fact that requires attention is that, in these figures, the even-odd effects on the barrier heights have disappeared. This means that the apparent even-odd difference of the barrier height is a reflection of even-odd difference in the g.s.-shell correction.

It is interesting also to ask: What is the implication of the slope of this correlation line? From the LDM definition of the barrier height, eq.(11), it can be seen that the slope is proportional to the

surface energy coefficient of the LDM. So we tried to deduce the surface energy coefficient from the slope. However, this is not straightforward, since the fissility parameter x itself includes a_2 in its definition. Thus we resorted to iterative calculation, assuming an initial guess for the coefficient a_2, deducing the value for a_2 from the slope of the line, comparing the obtained value with the initial guess, and repeating the procedure until good agreement was obtained between the two values. Thus we obtained the value 17.55 MeV.

This value is in good agreement with those adopted by different authors as can be seen from Table II. This implies that the LDM component of the barrier height is well separated, although the saddle-point shell correction has not yet been subtracted. This fact supports the above mentioned result that the shell correction is damped and small at larger deformations.

c) Fission Barrier Anomaly of Actinides

Another interesting point to be noted is that we can give an simple interpretation to the fission barrier anomaly of the actinides. As showed earier on, the barrier heights of the actinides are deviated from the LDM prediction with the surface energy coefficient equal to 17 MeV. This can be interpreted as follows: The LDM component decreases with mass number, while the g.s.-shell correction also decreases with increasing mass number. Therefore, the difference between the two quantites remains approximately constant.

4. Conclusions

To sum up the results of this report, we can conclude as follows:

1- Semi-empirical method of estimating unknown fission cross sections based on the fission probability data or the systematics among them is useful for providing required quantities in a rather simple manner.

2- Fission cross sections of 24 actinides were analyzed to deduce the fission barrier heights. It was found that:

Table II. Comparison of surface energy coefficients employed by differnt authors

Authors	a_2 (MeV)	r_0 (fm)	Remarks	Ref.
Present	17.55	1.2249	Fission barrier systematics	—
Vandenbosch	17.64 (17.28)[a]	1.1999	SFI[b] lifetime systematics	24
Myers	20.69 (19.93)	1.18	Droplet model of nuclear mass	23
Metag	17.8 (17.51)	1.2049	SFI lifetime systematics	25
Bohr-Mottelson	17.0 (17.2)	1.24	Fission barrier systematics	1
Myers-Swiatecki	17.9439	1.2249	Nuclear mass analysis	26
Green-Englen	17.23 (17.44)	1.24	Nuclear mass analysis	27

a) As can be seen from eq.(9), the fissility parameter depends on the product of nuclear radius parameter r_0 and surface energy coefficient a_2. In order to be sure that a_2's are compared on the same basis, the renormalized values based on r_0=1.2249 are shown in parentheses.

b) Spontaneously fissioning isomers.

a) Good systematic relation was extracted by correcting for the g.s.-shell effects;

b) Better correlation was observed for barrier heights E_B than for barrier heights E_A;

c) The surface energy coefficient a_2=17.55 MeV deduced from the systematics of barrier heights E_B was in agreement with the previous values obtained from nuclear mass analyses.

The above facts corroborate the theoretical estimate that the shell correction is damped at larger deformations corresponding to the second barrier.

3- Weak dependence of the fission barrier heights on fissility for actinides, or "fission barrier anomaly", was interpreted as due to offsetting of the lowering of the LDM barrier by the deepening of the g.s.-sag with increasing mass number.

REFERENCES

1) Bohr, A., and B. Mottelson: "Nuclear Structure", Vol.II, p.615(1975)

2) Henkel,R.L.: "Fast Neutron Physics" Part II, chapter V.R

3) Behrens, J. W.: Trans. Am. Nucl. Soc. 49, 196 (1985); Nucl. Sci. Eng. 65, 464 (1978); Phys. Rev. Lett. 39, 68 (1977)

4) Ohsawa, T., et al.: Research on Thorium Fuel, Reports of the Special Project Research on Energy, SPEY21 (1987) p.35

5) Gavron, A.,et al.: Phys. Rev. Let. 34, 827 (1975); Phys. Rev. C13, 2374 (1976)

6) Drake, M.K. : GA-7462 (1967)

7) Bohr, N., and J.A. Wheeler: Phys. Rev. 56, 426 (1939)

8) Bohr, A.: Proc. Int. Conf. on Peaceful Uses of Atomic Energy, Geneva 1955, Vol.2. p.220 (1956)

9) Kikuchi,Y., and An, S.: J. Nucl. Sci. Technol. 7, 157 (1974)

10) Strutinsky, V.A.: Nucl. Phys. 95, 420 (1967); ibid. A122, 1 (1968)

11) Bjørnholm, S., A. Bohr and A. Mottelson: Proc. Int. Symp. on Physics and Chemistry of Fission, Rochester (1974) p.367

12) Back, B.B., et al.: Nucl. Phys. A165, 449 (1971)

13) Back, B.B., et al.: Phys. Rev. C9, 1924 (1974)

14) Back, B.B., et al.: Phys. Rev. C10, 1948 (1974)

15) Paya, D.: Proc. Int. Symp. on Physics and Chemstry of Fission, Vienna (1969), p.307

16) Michaudon, A.: Proc. Int. Conf. on Statistical Properties of Nuclei, Albany (1971)

17) Plattard,S., et al. : Nucl. Sci. Eng. 61, 477 (1976)

18) Hill, D.L., and J.A. Wheeler: 89, 1102 (1953)

19) Lynn, J.E., and B.B. Back: J. Phys. A7, 395 (1974)

20) Britt, H.C., and B.B. Back: Private communication

21) Larsson, S.E., and G. Leander: Ref.(11), p.177

22) Lynn, J.E.: AERE-R7468 (1974)

23) Myers, W.D.: "Droplet Model of Atomic Nuclei", (1977), IFI/Plenum

24) Vandenbosch, R.: Ann. Rev. Nucl. Sci. 27, 1 (1977)

25) Metag, V., et al.: Nucl. Phys. A165, 289 (1971)

26) Myers, W.D., and W.J. Swiatecki: Ark. Fys. 36, 343 (1967)

27) Green, A.E.S., and N.A. Englen: Phys, Rev. 91, 40 (1953)

THEORETICAL MODELS AND COMPUTER PROGRAMS FOR THE CALCULATION OF PROMPT FISSION NEUTRON SPECTRA

H. MÄRTEN
Technische Universität Dresden,
Dresden, German Democratic Republic

Abstract

Prompt fission neutron emission has to be understood as a superposition of different mechanisms connected with the dynamics of fission directly (scission neutron emission) or indirectly (evaporation from a fragment diversity).

The general requirements to be met in calculating emission probabilities of prompt fission neutrons in the framework of a complex statistical-model approach (SMA) assuming evaporation from fully accelerated fragments (predominant mechanism of post-fission neutron emission) as well as recent approaches and computer codes are summarized.

It is shown that experimental multiple-differential emission probabilities of 252-Cf(sf) neutrons (specifically the energy spectrum as a nuclear standard) can be well reproduced by the use of a special SMA - the complex cascade evaporation model (CEM). Several global parametrizations of the optical potential for the calculation of the inverse cross sections of compound-nucleus formation have been tested.

The application of a complex SMA to any fission reaction has to be based on the theoretical or semi-empirical description of the fragment data needed (distribution in nucleon numbers, kinetic energy, excitation energy, angular momentum; fragment angular distribution). The present status is briefly discussed.

In the case of multiple-chance fission reactions, the SMA to post-fission neutron emission has to be connected with nuclear reaction theory including the calculation of the partial fission cross sections as well as of the spectra of pre-fission neutrons. The theoretical scheme for the adequate and consistent description of scattered-neutron cross sections, fission cross sections, fragment data, and post-fission neutron data is formulated and discussed. Several results of calculations based on the generalized Madland-Nix model (GMNM) in connection with a scission-point model (including semi-empirical, temperature-dependent shell corrections) for the description of fragment energies are presented for neutron-induced fission reactions.

---

1. Introduction

A large number of microscopic measurements have shown that the energy spectrum of prompt fission neutrons (PFN) is an evaporation-like distribution phenomenologically described by either a Maxwellian or a Watt spectrum.[1] Most of the observations are consistent with the theoretical concept of neutron emission from highly excited and rapidly moving fragments. However, PFN emission has to be understood as a superposition of different components corresponding to specific mechanisms[2]:

(i) scission neutron emission due to rapid nuclear-potential changes close to scission[3-7],

(ii) neutron emission (equilibrium, non-equilibrium?) during fragment acceleration (strongly correlated with the mechanisms of dissipation of deformation energy, ref. 8 and refs. therein),

(iii) neutron emission from neutron-unstable light charged particles (^{5}He, ^{6}He^{x}, ...) after ternary fission[2],

(iv) neutron evaporation from fully accelerated fragments (predominant mechanism),

(v) pre-fission neutron emission (equilibrium, pre-equilibrium) and, consequently, multiple-chance fission at rather high incidence energy.

Large-amplitude collective nuclear motion like fission as well as the single-particle excitation due to rapid changes of nuclear potential are still fundamental problems of nuclear physics. In spite of the developed qualitative understanding achieved the adequate quantitative description of these processes is mostly insufficient for practical considerations. As a consequence, secondary PFN mechanisms (items i-iii) corresponding to specific stages of nuclear fission (necking-in, scission, fragment acceleration and the simultaneous deformation energy dissipation, ternary fission resulting in

neutron-unstable light charged particles) are poorly understood. On principle, experimental PFN data (specifically multiple-differential emission probabilities) compared with calculations in the framework of a statistical-model approach (SMA) to the predominant mechanism should provide informations about the yield and detailed characteristics of secondary PFN. However, secondary-PFN data deduced by different authors in the last 25 years (see refs. cited in ref. 2) are quite uncertain and partly contrary. This is due to experimental and theoretical (SMA) uncertainties or errors. Too rough SMA approximations, i.e. the neglection of important aspects of PFN emission, can be the reason for wrong conclusions about secondary PFN from experiment-SMA comparisons.[2]

All PFN theories for practical applications have been based on a SMA to neutron emission from fully accelerated fragments. Is such a restriction justified? What are the requirements to be met in PFN spectrum calculations based on SMA? The present review is a continuation of previous papers[2,9-12].

2. SMA concept

As illustrated in synopsis 1, the SMA data basis, i.e. the fragment occurence probability P as a function of the "asymptotic" fragment variable set $\{p_f\}$, is mainly determined during the descent from saddle point to scission point. This fragment diversity $P(\{p_f\})$ depends on the initial-variable set $\{p_{FN}\}$ of the fissioning nucleus. However, fission theory fails to reproduce the bulk of experimental data with sufficient accuracy (despite of the developed qualitative understanding of nuclear fission) resulting in considerable restrictions in PFN theory. Therefore, the adequate account of the fragment distribution has to be based on empirical or semi-empirical methods. Note that the construction of the $P(\{p_f\})$ function is the most crucial problem in PFN theory.

Equilibrium emission (evaporation) of neutrons from a fragment specified by $\{p_f\}$ can be easily calculated in the framework of either Hauser-Feshbach (HF) theory[13] or Weisskopf model[14] (standard evaporation theory) considering competition to γ-ray de-excitation as well as cascade emission. If the fragment occurence distribution in p_f is known, it can be considered in an explicit manner inclusively or exclusively. However, the full distribution is often neglected, and calculations are carried out for the average $\overline{p_f}$ (exclusive/inclusive) only.

Neutron transition probabilities are commonly calculated in the framework of optical model based on a global potential covering at least the fragment mass number range 70 - 170. The typical course of the inverse cross-section σ_{inv} of compound-nucleus formation is represented in fig. 1 showing the differences for light ($A \lesssim 120$) and heavy fragments at low neutron energy ($\varepsilon \lesssim 100$ keV) specifically.[2,12]

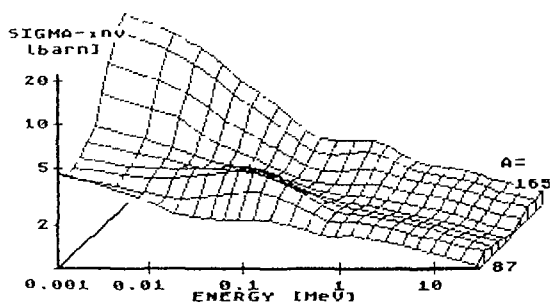

Fig. 1 Plot of the inverse cross section of compound-nucleus formation calculated in the framework of the optical model as a function of the neutron energy and mass number A

Concerning the level density $\varrho(U,I)$ description for fragments, either the Fermi-gas model formula with empirical parameters or semi-empirical methods including shell and pairing effects both depending on excitation energy are applied. Microscopic calculations are not common (see, however, ref. 15).

The SMA scheme for the almost exact calculation of PFN emission distributions in the centre-of-mass system (CMS) $\mathcal{C}(\varepsilon,\vartheta:\{p_f\})$ (ε,ϑ - CMS energy and angle with reference to fission axis), the transformation into the laboratory system (LS), and the weighted concentration taking into account the fragment occurence probability are outlined in synopsis 2. However, the full concept has not yet been realized due to the restrictions discussed above.

3. PFN models based on SMA

Recent SMA versions are characterized in synopsis' 3 - 7. They differ mainly concerning

- CMS spectrum shape description (synopsis 3),
- CMS anisotropy consideration (synopsis 3),
- complexity of $P(\{p_f\})$ (synopsis' 4 - 7).

All these PFN models were compared in the case of ^{252}Cf(sf) (nuclear standard) in refs. 10, 18, and 29 showing the applicability of all versions in the intermediate energy range 0.5 - 8 MeV. The correct description at very low and very high energy is only possible if taking into account the complex fragment distribution and the CMS anisotropy (CEM, GMNM). Both the MNM and the SCOFIN (HF) calculations underestimate PFN spectra at both ends.

In addition to PFN energy spectrum calculations, the CEM as well as the GMNM codes are suitable to describe double-differential energy and angular distributions of PFN (see below).

Note that the exact CMS-LS transformation is only possible in the case of the explicit consideration of the fragment distribution in A and TKE (cf. synopsis 2)[17] as done in CEM. The influence of several approximations as well as input data uncertainties has been studied in the framework of the CEM, see refs. 2, 9, and 17, indicating the uncertainty level of PFN data calculations.

4. Detailed CEM analysis of ^{252}Cf(sf) PFN emission

In order to investigate the yield and the influence of secondary mechanisms of PFN emission the CEM has been used to describe double-differential emission probabilities N(E,θ) measured in Dresden[30] on the basis of a new method recently. The experimental data cover the wide energy range 100 keV - 10 MeV (up to 18 MeV in polar direction) and the full angular range 0° - 180°. They are in rather good agreement with the recent CBNM Geel measurement[31].

The CEM calculations have been carried out on the basis of several optical models[32-35] which differ considerably regarding the $\sigma_{inv}(\varepsilon:A)$ description at rather low CMS energy ($\varepsilon \lesssim 100$ keV) for heavy fission fragments ($A \gtrsim 120$). Consequently, the N(E,θ) regions (LS) corresponding to low CMS energy are strongly dependent on the optical potential chosen. These are the crucial polar regions (θ = 0° and 180°) at E close to E_f (cf. synopsis 2, fig. 2).

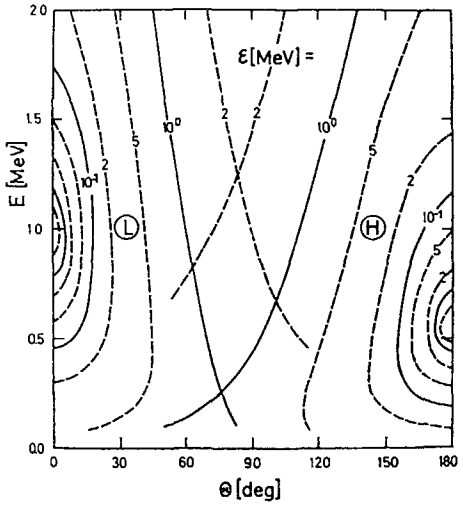

Fig. 2 Average CMS neutron energy as a function of the LS variables E and θ in the case of 252-Cf(sf)

Results of the calculations are shown in the figs. 3 - 6. The ^{252}Cf(sf) neutron energy spectrum calculated in the framework of the CEM is compared with the recent evaluation by Mannhart[36] in fig. 7.

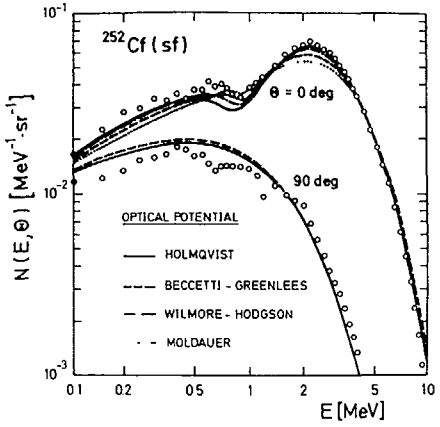

Fig. 3 Differential energy spectra of 252-Cf(sf) neutrons at 0 and 90 deg: circles - Dresden data[30], curves - CEM calculation for different optical potentials as indicated

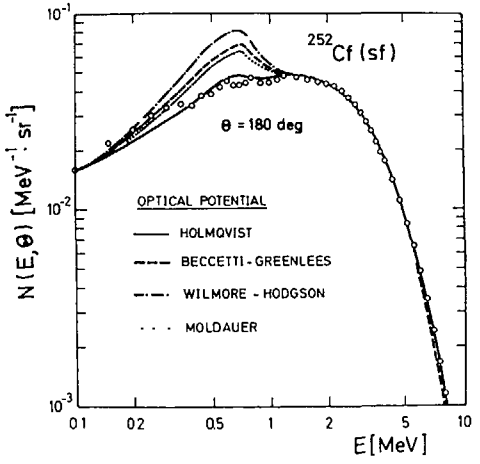

Fig. 4 As for fig. 3, but for θ = 180 deg

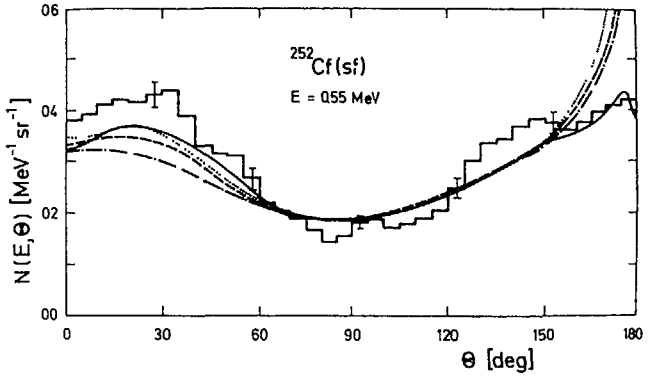

Fig. 5 252-Cf(sf) neutron angular distribution at 0.55 MeV lab. frame energy: histogram - Dresden data[30], curves - CEM calculation based on different optical potentials (cf. figs. above)

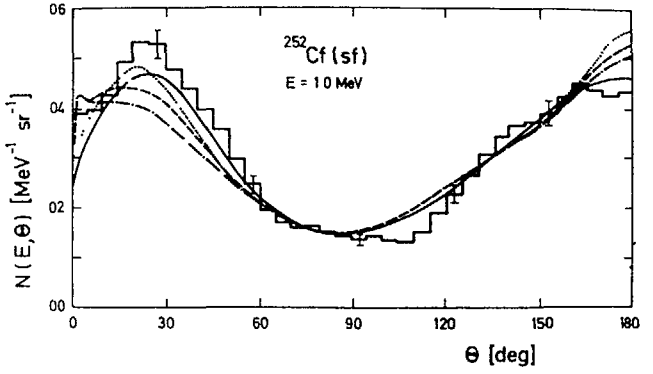

Fig. 6 The same as for the fig. 5, but for E = 1.0 MeV

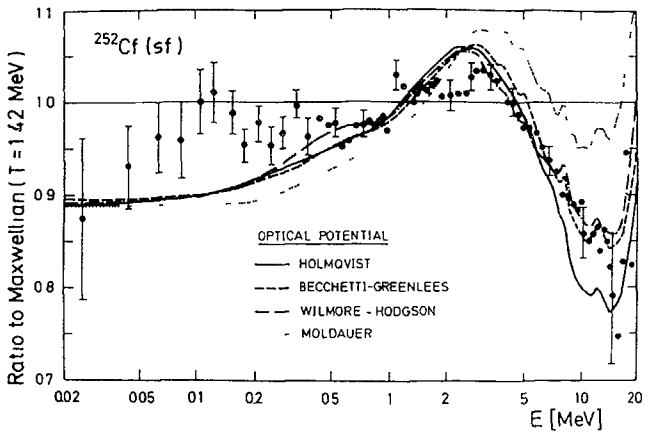

Fig. 7 The standard neutron spectrum from 252-Cf(sf) represented as ratio to a Maxwellian distribution with a 1.42-MeV temperature parameter: dots - Mannhart's evaluation[36], curves - CEM calculations based on different optical potentials as specified

The results obtained are the basis of the following conclusions:

(i) The complex CEM calculations are in rather good agreement with recent N(E,θ) data for ^{252}Cf(sf) covering a wide range in energy and angle. Consequently, neutron evaporation from fully accelerated fragments is confirmed to be the predominant emission mechanism.

(ii) Considering experimental as well as theoretical uncertainties, the upper limit of a central (i.e. isotropic in the lab frame of the fissioning nucleus) component of PFN has been estimated to be 5%. There is no significant indication of secondary mechanisms.

(iii) The best CEM description of ^{252}Cf(sf) N(E,θ) data has been obtained on the basis of Holmqvist's optical potential[35].

(iv) A complex SMA with the alone account of neutron evaporation from fully accelerated fragments is sufficiently accurate to describe PFN spectra for practical purposes.

5. GMNM applications

The GMNM (synopsis 5) is a simplified SMA. However, the most important characteristics of PFN emission are taken into account:

(i) approximative consideration of energy distribution and cascade emission (MNM concept),

(ii) inclusion of mass number dependence of PFN spectrum calculations,

(iii) simulation of neutron-γ competition by introducing the lower limit T_0 of integration over T (rest-nucleus temperature).

The free parameters of the GMNM, i.e. C or K and T_0 (synopsis 5), have been adjusted in the case of ^{252}Cf(sf).[12,20] Results are represented in the figs. 8 - 9.

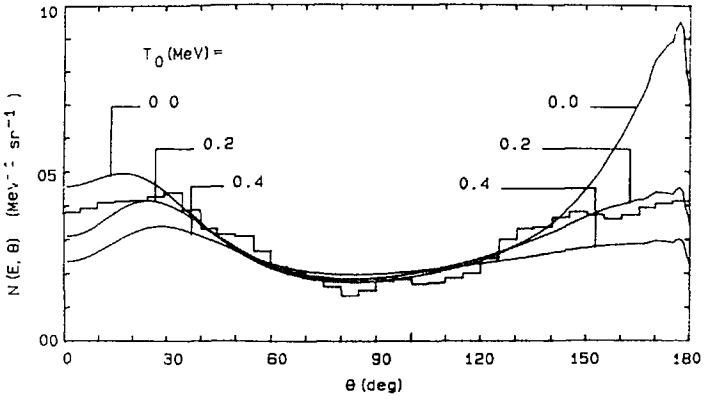

Fig. 8 252-Cf(sf) neutron angular distribution at E = 0.55 MeV: histogram - Dresden data[30], curves - GMNM calculations for different low-temperature limits T_0

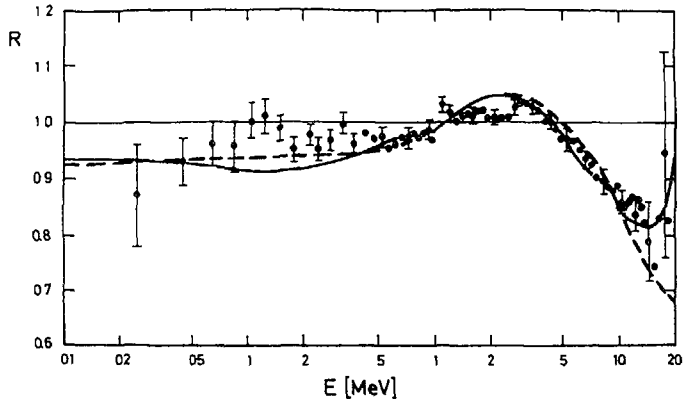

Fig. 9 Ratio R of the Cf neutron energy spectrum to a reference Maxwellian with T = 1.42 MeV: dots - Mannhart's evaluation[36], continuous curve - CEM, dashed line - GMNM

The GMNM including best-fit parameters enables an adequate description of the Cf neutron distribution in E and Θ. Its application to any fission reaction requires the rather accurate description of the energy partition on the fission fragments. The two-spheroid model (TSM) including semi-empirical, temperature-dependent shell correction energies for fragments at scission has been formulated[37] on the basis of Terrel s treatment[38]. Here, the classical concept of minimizing the potential energy at scission, assumed to be the sum of the Coulomb term and the deformation energies of the complementary fragments with spheroidal deformation, is the main supposition. The deviations of the deformability coefficients (deduced in the case of well-investigated fission reactions) from the liquid-drop model prediction can be interpreted as due to shell effects. Shell correction energies have been derived assuming the semi-empirical relation proposed in ref. 39. The shell correction data, which have to be diminished[40] as a function of nuclear temperature at scission, provide the basis for the calculation of fragment energies (kinetic energy, excitation energy) as a function of mass asymmetry in the case of any induced fission reaction in the Th-Cf region. Two examples of fission neutron spectra calculated in the framework of TSM-GMNM are represented in fig. 10. In these cases, the GMNM parameters have been used as in the Cf neutron spectrum calculation (fig. 9).

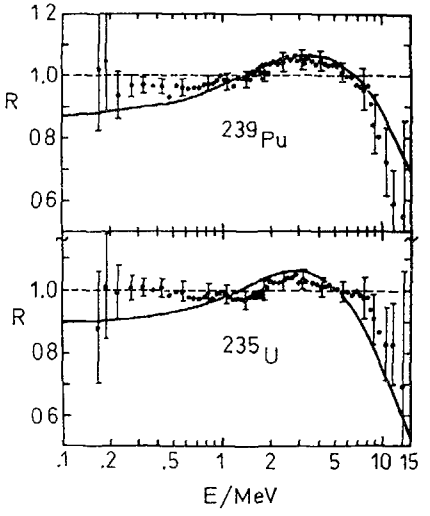

Fig. 10 The ratio of fission neutron spectra calculated in the framework of TSM-GMNM (continuous curves) to reference Maxwellians with T = 1.383 MeV and T= 1.318 MeV for the neutron-induced fission of 239-Pu and 235-U, respectively (experimental data - ref. 41)

The agreement between theory and experiment is remarkable. Thus, the GMNM combined with the TSM is suitable to describe fission neutron spectra of different reactions consistently on the basis of an unique parameter set.

6. PFN emission in multiple-chance fission reactions

In the case of rather high incidence energy, multiple-chance fission reactions, for instance (n,xnf), are considered separately for all possible x values in conjunction with the

statistical-model analysis of the partial fission cross sections $\sigma_{f,x}$ and scattered-neutron as well as γ-ray cross sections (code STAPRE[42], ref. 43). If $x \geqq 1$, the TSM calculations are carried out for average compound-nucleus excitation energies. Results for the ^{238}U fission induced by 14.5-MeV neutrons are represented in the figs. 11 - 14. The GMNM-TSM yields $\overline{TKE}(A)$ $\overline{E^x}(A)$, and prompt-neutron multiplicity curves $\bar{\nu}(A)$ which are in good agreement with experimental data[44]. Specifically, the dependence of the calculated $\overline{TKE}(A)$ curves on compound-nucleus excitation energy E^x_{FN} corresponds to experimentally determined trends. The higher E^x_{FN} the higher TKE in the symmetric as well as in the extremely asymmetric fission, the lower TKE in the case of the normally asymmetric mass fragmentation corresponding to the most probable mass split.

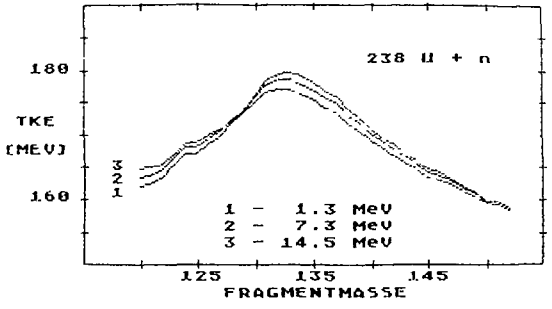

Fig. 11 Total kinetic energy $\overline{TKE}$ of fission fragments from 238-U(n,xnf) at 14.5 MeV incidence energy as a function of heavy-fragment mass number. The TSM calculation has been performed for all possible x assuming effective values of the incidence energy as indicated for $x \geqq 1$.

This is due to the diminution of shell effects with increasing scission point excitation energy and, hence, the change of the stiffness of both complementary fragments at scission.[37] Consequently, the $\overline{E^x}(A)$ and $\bar{\nu}(A)$ curves calculated exhibit a characteristic dependence on E^x_{FN} (fig. 12). A strong increase of $\bar{\nu}$ appears at A close to the double-magic mass number 132, whereas $\bar{\nu}(A)$ is little changed for the complementary light-fragment region.

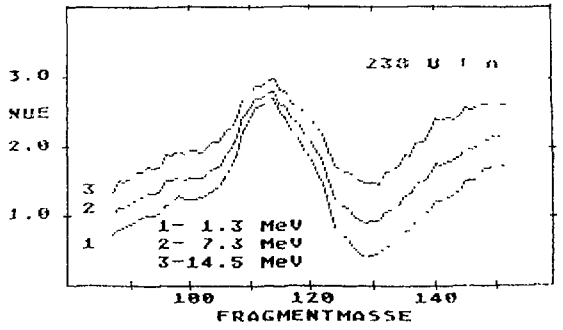

Fig. 12 Average prompt-neutron multiplicities $\bar{\nu}$ calculated in the framework of the TSM-GMNM as a function of the mass number of the fragments from 238-U(n,xnf) at 14.5-MeV incidence energy (cf. fig. 11).

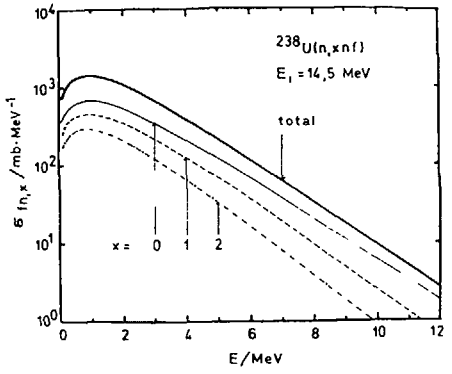

Fig. 13 Partial 238-U(n,xnf) prompt-fission neutron spectra calculated within the GMNM on the basis of TSM fragment energies (spectrum norm - $\bar{\nu}_x \cdot \sigma_{f,x}$, total - sum of the partial spectra).

Fig. 14 Partial anisotropies of prompt neutrons from 238-U(n,xnf) at 14.5-MeV incidence energy as well as the corresponding total post-fission neutron anisotropy (GMNM calculation in conjunction with STAPRE results).

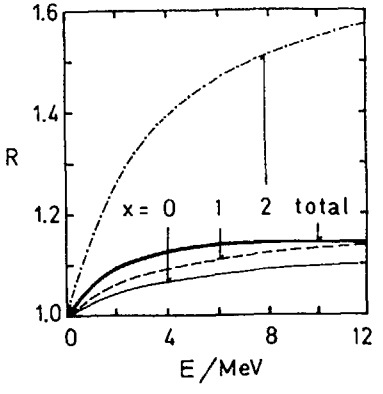

Fig. 13 represents the partial energy spectra of prompt post-fission neutrons. Their norm is defined by the total neutron multiplicity as well as by the partial fission cross-section (STAPRE). Taking into account the fragment angular distribution of the partial fission reactions the angular distribution of the post-fission neutrons can be calculated with reference to the incidence particle direction.

In the case of the multiple-chance fission, the partial fragment anisotropies are deduced from the total anisotropy curve by the use of statistical assumptions[45]. Fig. 14 shows the results of the calculation for U fission by 14.5-MeV neutrons (cf. synopsis 5).

7. Conclusions

Starting with a review on the basic principles of adequate calculations of fission neutron emission probabilities we compared recent theoretical treatments. Several statistical-model approaches are suitable to describe fission neutron spectra in the range corresponding to considerable emission probabilities. However, specific requirements have to be met to reproduce energy spectra in the full energy range as well as angular distributions in a consistent way.

Two complex statistical-model approaches (CEM and GMNM) have been used to analyse $^{252}Cf(sf)$ neutron emission.[12] The study indicates that the differential emission probabilities can be well reproduced (including the crucial polar regions). The GMNM has been adjusted on the basis of differential Cf data. In conjunction with the TSM (energy partition model), it is an adequate model to describe energy and angular distributions of prompt fission neutrons for applied purposes.

The TU Dresden concept for calculating PFN data in the Th-Cf region of fissioning nuclei with excitation energy less than about 25 MeV is a combination of a SMA to PFN emission with semi-empirical methods to describe fission fragment data (energy partition: $\overline{E^x}(A)$, $\overline{TKE}(A)$, fragment mass yield: P(A), fragment angular distribution - cf. synopsis 5). In the case of multiple-chance fission, the additional application of statistical reaction theory (STAPRE) is necessary to describe the partial fission cross sections as well as scattered-neutron cross sections in a consistent manner. Compared to previous treatments[19], the separate analysis of PFN emission for all possible chances as well as the consideration of the fragment mass number dependence are new steps in fission neutron theory.

REFERENCES

1 Proc. IAEA Consultants Meeting on Prompt Fission Neutron Spectra, Vienna, 1971 (IAEA, Vienna, 1972)

2 H. Märten et al., Proc. Int. Symp. Nucl. Phys. - Nuclear Fission -, Gaussig (GDR), 1985, ZfK-592(1986)1

3 R.W. Fuller, Phys. Rev. 126(1962)684

4 Y. Boneh, Z. Fraenkel, Phys. Rev. C 10(1976)893

5 V.A. Rubchenya, Leningrad report RI-28(1974)

6 P. Mädler, Z. Phys. A 321(1985)343

7 B. Milek, Thesis (1986), Technische Universität Dresden

8 H. Märten, D. Seeliger, J. Phys. G, in print

9 H. Märten et al., Proc. IAEA Consultants Meeting on the U-235 Fast-Neutron Fission Cross-Section and the Cf-252 Fission Neutron Spectrum, Smolenice (CSSR), 1983, INDC(NDS)-146/L(1983)199

10 H. Märten, D. Seeliger, Proc. IAEA Advisory Group Meeting on Nuclear Standard Reference Data, Geel, 1984 IAEA-TECDOC-335(1985)255

11 H. Märten, Proc. IAEA Advisory Group Meeting on Properties of Neutron Sources, Leningrad, 1986 IAEA-TECDOC-410(1987)144

12 H. Märten et al., Proc. Int. Conf. on Neutron Physics, Kiev, 1987, in press

13 W. Hauser, W. Feshbach, Phys. Rev. 87(1952)366

14 J. M. Blatt, V. F. Weisskopf, Theoretical Nuclear Physics, (New York, 1952)

15 E. Nardi et al., Phys. Lett. 43 B(1973)259

16 B. F. Gerassimenko, V. A. Rubchenya, Bulletin of Nuclear Data Centre, LIYaF, Vol. 12 (Leningrad, 1986)3

17 H. Märten, D. Seeliger, J. Phys. G 10(1984)349

18 H. Märten, D. Seeliger, Rad. Eff. 96(1986)99

19 D. G. Madland, J. R. Nix, Nucl. Sci. Eng. 81(1982)213

20 H. Märten, D. Seeliger, Nucl. Sci. Eng. 93(1986)370

21 A. Gavron, Phys. Rev. C 13(1976)2561

22 J. B. Wilhelmy et al., Phys. Rev. C 5(1972)2041

23 T. Ericson, V. Strutinski, Nucl. Phys. 8(1958)L 84

24 A. F. Grashin, M. V. Lepeschkin, At. En. 58(1985)59

25 R. L. Walsh, private communication (1986) and Proc. Int. Conf. on Neutron Physics, Kiev, 1987, in press

26 H. Märten et al., Proc. Int. Conf. Nucl. Phys., Gaussig, 1986, ZfK-610(1986)169

27 D. Lucas, H. Märten, to be published

28 H. Nifenecker et al., Proc. IAEA Symp. on Physics and Chemistry of Fission, Rochester, 1973 (IAEA, Vienna, 1974), vol. II, 117

29 H. Märten et al., INDC(NDS)-194(1987)

30 H. Märten et al., Nucl. Instr. Meth., in press, and Rad. Eff. 93(1986)41

31 C. Budtz-Jørgensen, H. H. Knitter, Rad. Eff. 93(1986)5

32 P. A. Moldauer, Nucl. Phys. 47(1963)65

33 D. Wilmore, P. E. Hodgson, Nucl. Phys. 55(1964)673

34 F. D. Becchetti, G. W. Greenlees, Phys. Rev. 182(1969)1190

35 B. Holmqvist, Arkiv Fysik 38(1968)403

36 W. Mannhart, Proc. IAEA Advisory Group Meeting on Properties of Neutron Sources, Leningrad, 1986, IAEA-TECDOC-410(1987)158

37 H. Märten et al., Proc. Int. Conf. Nucl. Phys., Gaussig, 1987

38 J. Terrell, Proc. IAEA Symp. on Physics and Chemistry of Fission, Salzburg, 1965 (IAEA, Vienna, 1965), vol. II, 3

39 M. Kildir, N. K. Aras, Phys. Rev. C 25(1982)365

40 A. Bohr, B. R. Mottelson, Nuclear Structure (Benjamin, New York), 1975

41 P. I. Johansson et al., Proc. Conf. on Nuclear Cross Sections and Technology, Washington, 1975, NBS SP 425 (1975)572

42 M. Uhl, Proc. Int. Conf. Nucl. Phys., Gaussig, 1982 ZfK-491 (1982) 155

43 A. V. Ignatyuk et al., Yad. Fiz. 42(1985)569

44 H. Yamamoto et al., J. Nucl. Sci. Techn. 16(1979)779

45 J. R. Huizenga, R. Vandenbosch, Nuclear Reactions II (1962)

Synopsis 1

GENERAL SCHEME OF NUCLEAR FISSION - SMA DATA BASIS

FN - fissioning nucleus characterized by an initial-variable set $\{p_{FN}\}$ =

$\{A_{FN}, Z_{FN}, E^x_{FN}, J_{FN}, K_{FN}\}$

- nucleon numbers
- excitation energy
- angular momentum
- projection quantum number

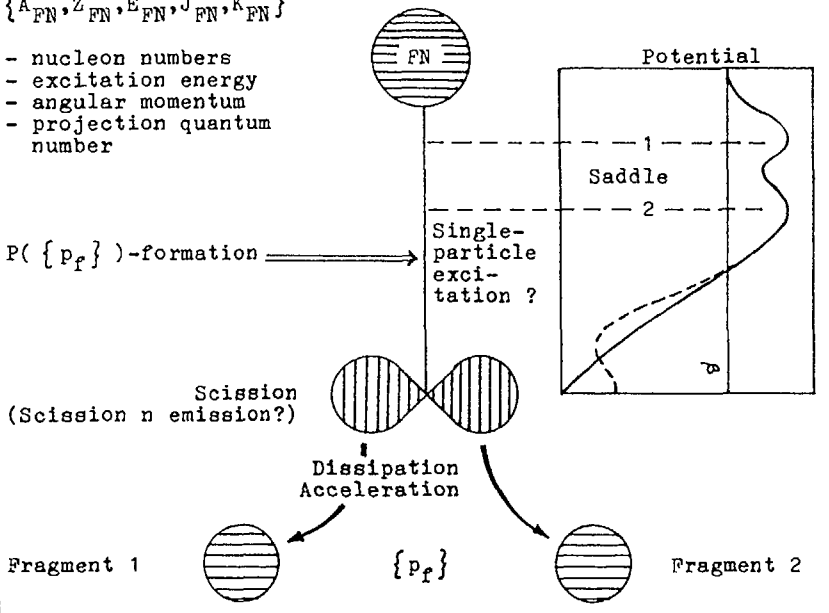

"Asymptotic" variables

$\{A_1, Z_1, E^x_1, E_{k1}, I_1, \delta_1, \ldots\}$ $\{A_2, Z_2, E^x_2, E_{k2}, I_2, \delta_2, \ldots\}$

Fragment occurrence probability P($\{p_f\}$) - asymptotic, i.e. assumed "after" acceleration and deformation energy dissipation, but before neutron emission (SMA assumption)

Total kinetic energy	:	$TKE = E_{k1} + E_{k2}$
Nucleon numbers	:	$A_{FN} = A_1 + A_2$; $Z_{FN} = Z_1 + Z_2$
Energy balance	:	$Q + E^x_{FN} = TKE + E^x_1 + E^x_2$
		Energy release $Q = f(A_{FN}, Z_{FN}, A_1, Z_1)$
Fragment angle	:	$\delta_1 = \pi - \delta_2$ for binary fission (CMS)

Synopsis 2

STATISTICAL-MODEL APPROACH TO PROMPT FISSION NEUTRON SPECTRA - SCHEME (one possible formulation)

CMS distribution $\mathcal{C}(\mathcal{E},\vartheta : A,Z,TKE) =$

$$\sum_i \left[\sum_I \int dE^x \cdot P_i\,(E^x,I : A,Z,TKE) \cdot \mathcal{C}_i(\mathcal{E},\vartheta : A-i,Z,E^x,I) \right]$$

i - cascade emission step

SCHEME OF CMS-LS TRANSFORMATION

SMA assumption: Neutron emission from fully accelerated fragments moving with the kinetic energy per nucleon

$$E_f = E_k/A = TKE \cdot (1/A - 1/A_{FN})$$

Transformation formula:

$$N(E,\theta : \{p_f\}) = \sqrt{\frac{E}{\mathcal{E}}} \cdot \mathcal{C}(\mathcal{E},\vartheta : \{p_f\})$$

LS-co-ordinates CMS-co-ordinates

$$\mathcal{E} = E + E_f - 2\cdot\sqrt{E\cdot E_f}\ \cos\theta$$

INTEGRATION, SUMMATION

$$N(E,\theta) = \sum_{A,Z} \int dTKE \cdot P(A,Z,TKE) \cdot N(E,\theta : A,Z,TKE)$$

$\downarrow$

$N(E)$

Synopsis 3

STATISTICAL-MODEL APPROACH (SMA) TO PROMPT FISSION NEUTRON EMISSION

Mechanism: Neutron evaporation from fully accelerated fragments

Basic requirements: Application of standard evaporation theory to neutron emission from highly excited fragments in competition to γ-ray emission

Consideration of cascade emission from a fragment diversity $\{p_f\}$

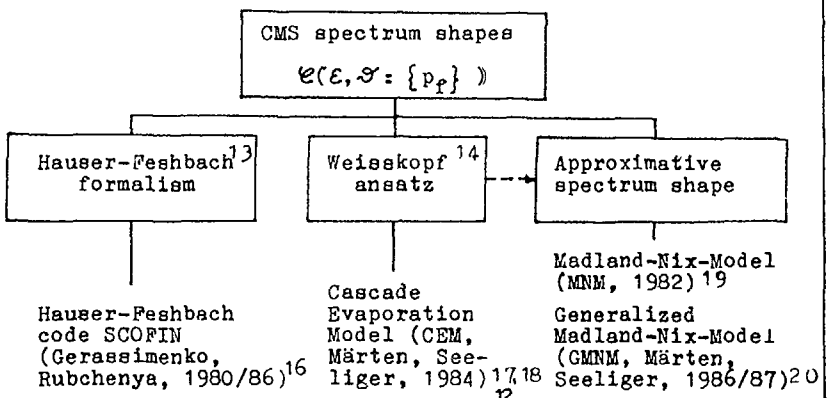

Computer codes for neutron nuclear data calculations

CMS anisotropy [21] due to fragment angular momentum (6 - 8 $\hbar$, aligned perpendicular to fission axis) [22]

Considerations:
- no (MNM, SCOFIN)
- semi-classical (CEM, GMNM) [23]
- microscopic (-)

Synopsis 4

APPROXIMATIVE SPECTRUM SHAPE - MNM SCHEME
(Madland, Nix, 1982)[19]

- $\{p_f\}$ reduced to averages for the fragment groups i = L,H
- Implicite consideration of the initial distribution in E^x as well as cascade emission by assuming a distribution in rest-nucleus temperature (idealized tri-angular shape)

$$- \varphi_i(\varepsilon) \sim \int_0^{T_m} dT \cdot \sigma_{inv,i}(\varepsilon) \cdot \varepsilon \cdot \exp(-\varepsilon/T) \cdot P(T)$$

- T_m - maximum rest-nucleus temperature to be deduced from the average fragment excitation energy

$$T_m = \sqrt{\overline{E^x} / a} \quad , \quad a = C / A$$

- Energy balance: $\overline{E^x} = \overline{E^x_{FN}} + \overline{Q} - \overline{TKE}$
- Analytic solution for $\sigma_{inv}(\varepsilon)$ = constant
- Free parameter: C
- Modifications : P(T) modified (more realistic ansatz) - Grashin et al., 1985[24]

  CMS anisotropy considered - Walsh, 1986[25]

Synopsis 5

APPROXIMATIVE SPECTRUM SHAPE - GMNM SCHEME
(Märten, Seeliger, 1986/87)[20]

- $\{p_f\} = \{A\}$, $\overline{Z}(A)$, $\overline{TKE}(A)$, $\overline{E^x}(A)$, cf. MNM scheme

$$- \varphi(\varepsilon : A) \sim \int_{T_0}^{T_m(A)} dT \cdot \sigma_{inv}(\varepsilon : A, \overline{Z}) \cdot \varepsilon \cdot \exp(-\varepsilon/T) \cdot P(T:A)$$

- T_0 - rough consideration of n/γ-competition
- $T_m(A) = \sqrt{\overline{E^x}(A) / a(A)}$, $a(A) = A / C$ or use of empirical data multiplied by a scaling factor K
- CMS anisotropy considered (approx.)
- Calculation of $\overline{TKE}(A)$ and $\overline{E^x}(A)$ in the framework of a

  SCISSION POINT MODEL (TWO-SPHEROID MODEL TSM)[26]

  with semi-empirical, temperature-dependent shell correction energies
- CMS-LS transformation using $\overline{E_f}(A) = f(A, \overline{TKE}(A))$
- $N(E,\Theta) = \sum_A P(A) \cdot N(E,\Theta:A) \longrightarrow N(E)$

  Semi-empirical description of the fragment mass yield curve P(A) (5-Gaussian approximation)[27]
- $G(E,\Psi)$, Ψ - angle with reference to incidence particle direction

  Transformation N → G based on the fragment angular distribution (experimental data or semi-empirical description - $K_0^2(E^x)$)
- Free parameter: T_0, C or K

Synopsis 6

CASCADE EVAPORATION MODEL - CEM SCHEME
(Märten, Seeliger, 1984/86/87)[17,18,12]

- $\{p_f\} = \{A, TKE, E^x\}$, $\bar{Z}(A)$, $\bar{I}(A)$

- Weisskopf ansatz

$$\varrho(\varepsilon : A, \bar{Z}, E^x) \sim \underbrace{\sigma_{inv}(\varepsilon : A, \bar{Z})}_{\text{Optical model}} \cdot \varepsilon \cdot \underbrace{\mathcal{S}(E^x - \overline{B_n}(A, \bar{Z}) - \varepsilon, I'=0, A-1)}_{\text{Semi-empirical description including shell and pairing correction both depending on } E^x}$$

- $$\varrho(\varepsilon : A, TKE) = \sum_i \int dE^x \cdot P_i(E^x : A, TKE) \cdot \varrho_i(\varepsilon : A-i, \bar{Z}, E^x) \cdot R(E^x)$$

with $$R(E^x) = \frac{\Gamma_n(E^x, \bar{I})}{\Gamma_n(E^x, \bar{I}) + \Gamma_\gamma(E^x, \bar{I})}$$, n/γ-branching ratio (total width')

- CMS anisotropy consideration according to the semi-classical description of Ericson, Strutinski (1958) on the basis of $\bar{I}(A)$

- Exact CMS-LS transformation resulting in $N(E, \Theta : A, TKE)$

- $P_0(E^x : A, TKE)$ deduced from experimental n-multiplicity distributions and $\bar{E}_\gamma$ data[28]
  + energy balance correction

- Complex CEM variant is only applicable to well-investigated fission reactions (availability of input data)

- Reduced CEM: $\{p_f\} = \{A, E^x\}$, $\overline{TKE}(A)$, $\bar{Z}(A)$, $\bar{I}(A)$
  for any fission reaction (combined with TSM)

- Note: CEM without any free parameters or arbitrary normalizations

Synopsis 7

HAUSER-FESHBACH CALCULATION - SCHEME
(Gerassimenko, Rubchenya, 1980/86 - code SCOFIN)[16]

- $\{p_f\} = \{A, E^x, I\}$, $\overline{TKE}(A)$, $\bar{Z}(A)$

  $\{p_f\} = \{A, Z, E^x, I\}$ possible, but infeasible in most cases

- $$\varrho(\varepsilon : E^x, A, Z) = \sum_I P(I : E^x, A, Z) \cdot \frac{\Gamma_n(\varepsilon : A, Z, E^x, I)}{\Gamma_n^t(A, Z, E^x, I) + \Gamma_\gamma^t(A, Z, E^x, I)}$$
  (n/γ-competition)

- $$\Gamma_n(\varepsilon : A, Z, E^x, I) = \sum_I \underbrace{\mathcal{S}(E^x - B_n(A, Z) - \varepsilon, I', A, Z)}_{\text{Semi-empirical description of level density}} \cdot \sum_{l,j} \underbrace{T_{lj}(\varepsilon)}_{\text{Optical model}}$$

- $\Gamma_n^t, \Gamma_\gamma^t$ - total width' of neutron and γ-ray emission, respectively

- CMS-LS transformation resulting in $N(E : A)$, $N(E)$

MULTIPLE-CHANCE FISSION IN NEUTRON-INDUCED REACTIONS (n,xnf)

Neutron-plus-actinide scattering system (incidence energy E_i)

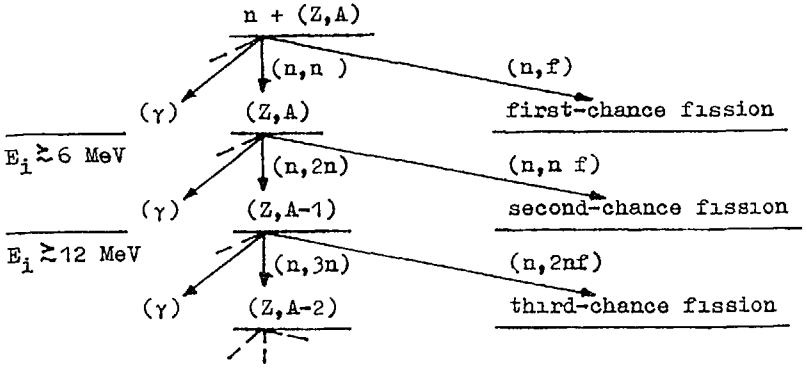

- Branching to the exit channels fission, neutron emission, γ-ray emission, ...
- Prompt post-fission neutron emission
- Pre-fission neutron emission
- SMA to be based on $P(\{p_f\}) = f(E^x_{FN})$
- Competition between the different possible multiple-chance fission reactions $\sigma_f = \sum_x \sigma_{f,x}$
- Analysis for each chance separately

WATT SPECTRUM FIT TO ^{252}Cf PROMPT FISSION NEUTRON DATA

F H FROHNER
Institut fur Neutronenphysik
und Reaktortechnik,
Kernforschungszentrum Karlsruhe,
Karlsruhe, Federal Republic of Germany

Abstract

- Recent measurements of the ^{252}Cf prompt fission neutron spectrum have been fitted with four types of theoretical models (1) a Maxwell spectrum, (2) a Watt spectrum, (3) a superposition of two Watt spectra representing a typical fission fragment pair, and (4) a relativistic generalisation of (3) Instrumental resolution has been accounted for by exploitation of the fact that the Watt spectrum and the free-gas Doppler broadening kernel are mathematically identical The Maxwell spectrum is inadequate, as expected, but a Watt spectrum with T_W = 1 18 MeV and E_W = 0 36 MeV fits all data well, except for those above 17 MeV from one set, with a chi-square that indicates no need for a more refined model The superposition of two Watt spectra and the relativistic generalisation do not improve the fit

1 Introduction

The spectrum of neutrons from spontaneous fission of ^{252}Cf is an international standard, because of its availability and metrological importance Quite early it was found to be fairly well described by a Maxwell or a Watt spectrum [1], with a maximum around 0 7 MeV Two things happened during the last decade Experimentalists produced a wealth of good data covering the range from a few keV to well above 20 MeV, establishing significant deviations from the Maxwellian shape At the same time theorists developed increasingly complex models based on the fragment distribution and on evaporation theory including the statistical model of compound nuclear reactions (cf e g [2, 3]) The state of the art was comprehensively reviewed at the Leningrad meeting in 1986 [4] This prompted the present study which tries to answer the question how well simple "macroscopic" models such as the Watt distribution can describe recent ^{252}Cf fission neutron data as compared to the more sophisticated "microscopic" theoretical models

2 The Watt spectrum and its relativistic generalisation

The observed fission neutron spectrum is the statistical outcome of a very large multitude of possible "microscopic" processes, all leading to

neutron emission, but differing in primary fragment pair formation, fragment excitation and spin, and decay paths leading to final fragments In such a situation it is meaningful to look for a "macroscopic" description which involves only a few average parameters What is the simplest set of average parameters for our problem? It is empirically well established that practically all fission neutrons are emitted from fully accelerated fragments, and that neutron emission is nearly isotropic in each fragment's rest system Each Cartesian momentum coordinate, for instance p', can therefore be taken as symmetrically distributed around zero in the fragment rest system, so that the lowest nonvanishing moment of the p'-distribution is $\langle p'^2 \rangle$ Neglecting all higher moments we can invoke the principle of maximum entropy [5] to find the p'_x-distribution with maximal information entropy (with a maximum of missing information, hence most conservative and objective) for the given $\langle p_x'^2 \rangle$ This is a Gaussian around zero with variance $\langle p_x'^2 \rangle$ With the same reasoning for the y and z coordinate, and with the notation $\langle p_x'^2 \rangle = \langle p'^2 \rangle /3 \equiv p_T^2/2$ one finds that the Maxwell-Boltzmann momentum distribution

$$\chi(\vec{p}')d^3p' = \frac{1}{\pi^{3/2}} \exp\left(-\frac{p'^2}{p_T^3}\right) \frac{d^3p'}{p_T^3}, \quad -\infty < p'_x,\ p'_y,\ p'_z < \infty \qquad (1)$$

has maximal entropy for given $\langle p'^2 \rangle$ After solid angle integration (with $d^3p' = p'^2 dp' d\Omega$), and rewriting everything in terms of energies (with $E \equiv p'^2/(2m)$ and $T \equiv p_T^2/(2m) = 3\langle E' \rangle /2$, m denoting the neutron mass) one gets the Maxwell spectrum

$$N_M(E'|T)dE' = \frac{2}{\sqrt{\pi}} \exp\left(-\frac{E'}{T}\right) \sqrt{\frac{E'}{T}} \frac{dE'}{T}, \quad 0 < E' < \infty, \qquad (2)$$

This emission spectrum, the simplest choice imaginable, works already quite well as comparison with Weisskopf's more physical evaporation formula [6],

$$N(E'|T)dE' \propto \exp\left(-\frac{E'}{T}\right) E' \sigma_C(E')dE', \qquad 0 < E < \infty, \qquad (3)$$

shows The Maxwell spectrum corresponds to a $1/\sqrt{E'}$ shape of the compound formation cross section σ_C, and this is in fact the shape of the relevant s-wave (inverse) cross sections up to several MeV Next we go from the fragment rest system to the lab system by means of the Galileo transformation $\vec{p}' = \vec{p} - m\vec{u} \equiv \vec{p} - \vec{q}$, where $\vec{u}$ is the fragment velocity and $\vec{q}$ the fragment momentum per nucleon Inserting this in (1) and integrating over all (equiprobable) directions of $\vec{u}$, for fixed $\vec{p}$, one obtains

$$\chi(p)dp = \frac{1}{\sqrt{\pi}} \left\{ \exp\left[-\left(\frac{p-q}{p_T}\right)^2\right] - \exp\left[-\left(\frac{p+q}{p_T}\right)^2\right] \right\} \frac{p}{q} \frac{dp}{p_T}, \quad 0 < p < \infty. \qquad (4)$$

In terms of energies, with the fragment kinetic energy per nucleon given by $E_W \equiv mu^2/2$, and $T_W \equiv p_T^2/(2m)$, this is the Watt distribution,

$$N_W(E|T_W)dE = \exp\left(-\frac{E_W}{T_W}\right) \frac{\sinh \sqrt{4EE_W/T_W^2}}{\sqrt{4EE_W/T_W^2}} N_M(E|T_W)dE, \quad 0 < E < \infty \qquad (5)$$

Note that the Watt distribution is nothing but a Maxwellian emission spectrum transformed from the fragment rest system to the lab system It reduces to the Maxwellian for $E_W \to 0$, and is proportional to it (but lower) for small E The two-parameter formula (4) or (5) is the simplest possible description of the fission neutron spectrum if u is interpreted as the average fragment speed A slight refinement results, without increase of the number of parameters, if one uses the empirical facts that the nuclear temperatures and the numbers of emitted neutrons are similar (on average) for the light and the heavy fragment mass peak One can then take $T_L = T_H$, $\bar{\nu}_L = \bar{\nu}_H$, $E_L = c_L E_W$, $E_H = c_H E_W$, and superpose two Watt spectra, one for a representative light and one for the complementary heavy fragment,

$$\bar{N}_W(E|T_W,E_W)dE = \frac{1}{2} \left[N_W(E|T_W, c_L E_W) + N_W(E|T_W, c_H E_W)\right] dE \qquad (6)$$

The constants $c_L = 2A_H^2/(A_L^2+A_H^2)$ and $c_H = 2-c$ are determined by momentum conservation, and the ratio $A_L/A_H = 108/144 = 3/4$ represents the most frequent mass split A final refinement concerns relativistic corrections, which amount to several percent at 20 MeV, the upper limit of the present study Going from the fragment rest system to the lab system by means of the relevant Lorentz transformation instead of the Galileo transformation, and replacing d^3p by the invariant measure on the energy shell, $mc^2 d^3p/H$ with $H = mc^2/\sqrt{1-\beta^2} = \sqrt{m^2c^4+p^2c^2}$, $\beta \equiv u/c$, one finds after angle integration

$$\chi(p)dp = \frac{1}{\sqrt{\pi}} \left\{ \exp\left[-\left(\frac{p-\beta H/c}{p_T\sqrt{1-\beta^2}}\right)^2\right] - \exp\left[-\left(\frac{p+\beta H/c}{p_T\sqrt{1-\beta^2}}\right)^2\right] \right\} \frac{p\sqrt{1-\beta^2}}{\beta H/c} \frac{dp}{p_T}. \qquad (7)$$

Obviously this reduces to (4) for $H \approx mc^2$, $\beta^2 \approx 1$ One can account again for emission from two complementary fission fragments with Eq 6

3 The data base

The following recent data sets were considered (below 20 MeV)

Authors	Year	Ref	Energies (MeV)	Neutron Detector	Fission Detector
Poenitz and Tamura	1983	7	0 2-10	black det	gas scint
Lajtai et al	1983	8	0 025-1 2	Li6 glass	ion ch
Bojcov et al	1983	9	0 01-3 0	U5 fiss ch	ion ch
Nefedov et al	1983	10	2 1-7 6	anthracene	ion ch
Marten et al	1984	11	8 8-20 0	NE-213	ion ch
Blinov et al	1984	12	0 04-11 5	U5 fiss ch	ion ch
Boldeman et al	1984	13	1 0-14 3	NE-102	ion ch
Bottger et al	1986	14	2 0-14 0	NE-213	ion ch
Chalupka et al	1986	15	14-30	NE-213	ion ch
Marten et al	1987	16	5-20	NE-213	ion ch

For more experimental details see the original references and also the very informative review papers [17, 18] All these data are of high quality and their consistency is impressive Only the ^{6}Li glass data of

Ref. 13 had to be rejected because they seem to be affected by multiple scattering across the ^{6}Li+n resonance at 240 keV. Following the authors' recommendation the "step two" values from Ref. 12 were used. Where only statistical errors were given systematic errors were estimated from the state of the art. As a first trial Boldeman's pre-evaluation [17] shown in Fig. 1 was fitted, and it was obvious that a Watt distribution fits well. Next all 10 data sets listed above were fitted, in order to find a reference Watt distribution for renormalisation of those data sets that were obtained from shape measurements normalised to Maxwellian fits with T_M = 1.42 MeV. Replacing the Maxwellian normalisations by Watt normalisations resulted in slight enhancements by factors between 1.001 and 1.011. Finally instrumental resolution was folded in, based on the documented flight path and timing uncertainties as well as on energy bin widths (unless the data were already corrected for this latter effect, as e. g. in Ref. 12). The convolution is easily carried out if one utilises the fact that the Watt distribution is formally identical with the free-gas Doppler kernel, for which it is well known that convolution of two kernels for temperatures T_1 and T_2 yields a kernel for $T_1 + T_2$ [19]. Therefore a Watt (or Maxwell) distribution can be broadened by simply raising the temperature slightly by an amount corresponding to the instrumental resolution width.

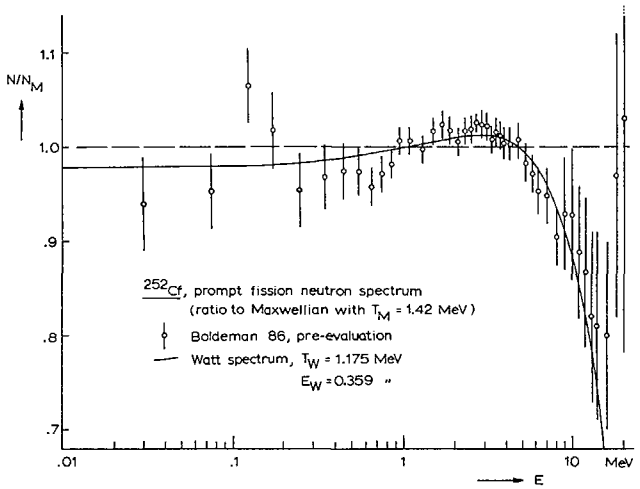

Fig. 1 - Point symbols: pre-evaluation of ^{252}Cf fission neutron data (Boldeman 1986 [17]); solid line: Watt distribution fitted to the data considered in the present paper. The Maxwell distribution (unit ordinate) is clearly inadequate, whereas the Watt distribution fits well except for the last three, relatively uncertain points.

4. Results and conclusions

A Maxwellian fit to the data gave T = 1.400 ± 0.001 MeV, and an unsatisfactory chi-square per degree of freedom, χ^2/ν = 893/471. On the other hand, a Watt fit (Figs. 2 and 3) gave

$$T = 1.175 \pm 0.005 \text{ MeV}, \quad E = 0.359 \pm 0.009 \text{ MeV}, \quad \rho(T, E) = -0.984,$$

with χ^2/ν = 489/470, where ρ is the correlation coefficient, showing almost complete anticorrelation between the two parameters. The confidence band around the fitted curve calculated from the correlated uncertainties has a width of about ±0.25 % at the lowest energies, ±0.12 % near the maximum at 0.7 MeV, and ±1.1 % at 20 MeV. Utilisation of two superposed Watt distributions (Eq. 6) did not improve this very satisfactory fit, the spectrum and chi-square changing only by fractions of a percent. The relativistic Watt distribution gave a slightly better fit near 20 MeV, but the overall result was worse, with χ^2/ν = 521/470. The contributions of the various data sets to chi-square indicate that the error estimates of Refs. 11, 13, 16 are somewhat optimistic, those of Refs. 8 , 9, 10 pessimistic, but not so much as to warrant a re-evaluation. The only real misfits are the lead-mine data of Ref. 15. They are significantly higher than the other data and the adjusted Watt spectrum above 17 MeV, see Fig. 3. In view of all other data, and keeping in mind the extremely small spectrum fraction and the experimental difficulties at these high energies, we can state that for practical purposes a Watt distribution with the parameters given above describes the ^{252}Cf fission neutron spectrum quite well up to 20 MeV (over roughly five decades of intensity), at least as well as available more elaborate "microscopic" models, but in a much simpler and thus more convenient way.

Note added in proof: A Watt spectrum fit to Mannhart's evaluated point data [4] yielded, in excellent agreement with the result given above,

$$T_W = 1.174 \pm 0.008 \text{ MeV}, \quad E_W = 0.361 \pm 0.014 \text{ MeV}.$$

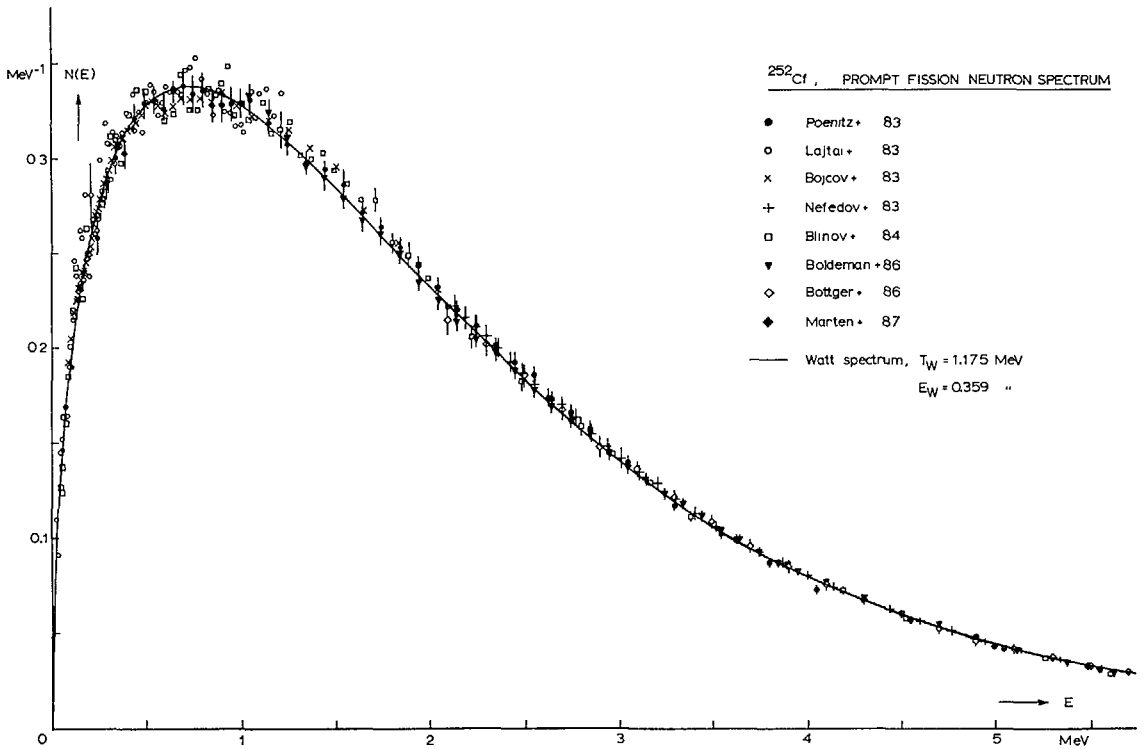

Fig. 2 - Utilised data below 5.7 MeV (error bars are mostly omitted for clarity's sake) and adjusted Watt distribution, showing the quality of the fit in the practically most important part of the fission neutron spectrum.

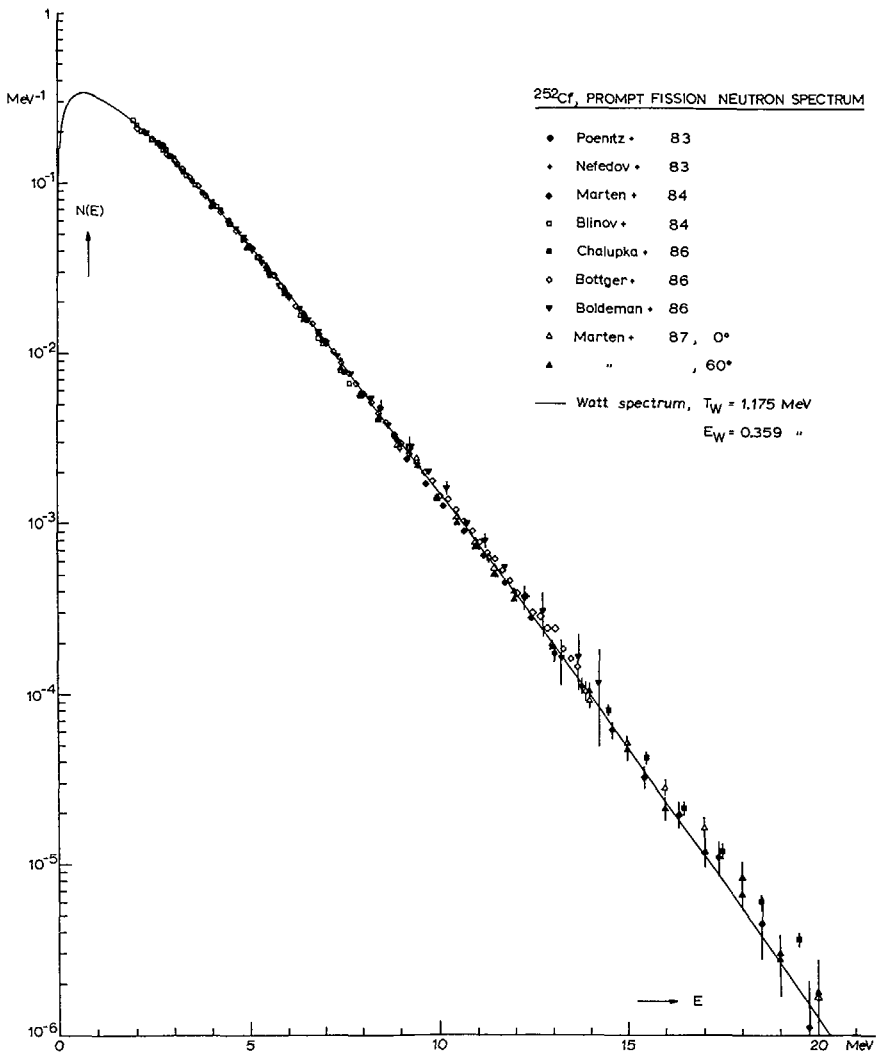

Fig. 3 - Utilised data above 3 MeV (error bars are mostly omitted for clarity's sake) and adjusted Watt distribution, showing the quality of the fit in the tail of the fission neutron spectrum.

ACKNOWLEDGEMENTS

It is a pleasure to thank K Okamoto, IAEA/NDS, for speedy transmittal of results presented at the Meeting on Properties of Neutron Sources, Leningrad 1986, the NEA Data Bank, Saclay, for data retrievals from their files, W P Poenitz and J W Boldeman for supplementary information about uncertainties, and W Mannhart for his pointwise evaluation [4] in numerical form

REFERENCES

[1] B E Watt, Phys Rev 87 (1952) 1952
[2] D G Madland and J R Nix, Nucl Sci Eng 81 (1982) 213,
[3] H Marten and D Seeliger, Nucl Sci Eng 93 (1986) 370
[4] Proc Meeting on Properties of Neutron Sources, Leningrad 1986, K Okamoto (ed), IAEA-TECDOC-410 (1987)
[5] E T Jaynes, Papers on Probability, Statistics and Statistical Physics, R D Rosencrantz (ed), Dordrecht 1983, ch 7 and 10
[6] V Weisskopf, Phys Rev 52 (1952), 295
[7] W P Poenitz and T Tamura, Proc Conf Nucl Data for Sci and Technol , Antwerp 1982, p 465,
W P Poenitz and T Tamura, Proc Smolenice Meeting 1983, INDC(NDS)-146 L, p 175
[8] A Lajtai, P P Djachenko, L S Kutzajeva, V N Kononov, P A Androsenko, A A Androsenko, Proc Smolenice Meeting 1983, p 177
[9] A A Bojcov and B I Starostov, Proc Kiev Conf on Neutron Physics 1983, Moscow 1984, vol 2, p 298
[10] V N Nefedov, B I Starostov, A A Bojcov, Proc Kiev Conf on Neutron Physics 1983, Moscow 1984, vol 2, p 285
[10] V N Nefedov, B I Starostov, A A Bojcov, Proc Kiev Conf on Neutron Physics 1983, Moscow 1984, vol 2, p 285
[11] H Marten, D Richter, D Seeliger, INDC(GDR)-28/L (1984)
[12] M V Blinov, G S Boykov, V A Vitenko, INDC(CCP)-238 (1984)
[13] J W Boldeman, B E Clancy and D Culley, Nucl Sci Eng 93 (1986) 181
[14] R Bottger, H Klein, A Chalupka, B Strohmaier, Ref [4] p 186
[15] A Chalupka, L Malek, S Tagesen, R Bottger, Ref [4] p 190
[16] H Marten, R Richter, D Seeliger, W D Fromm, R Bottger, H Klein, INDC(NDS)-194 (1987)
[17] J W Boldeman, Ref [4] p 125
[18] W Mannhart, Ref [4] p 158
[19] F H Frohner, Nucl Instr Meth 49 (1967) 89

CORRELATION OF NUCLEAR PARAMETERS IN HAUSER-FESHBACH MODEL FORMULA ESTIMATED FROM EXPERIMENTAL CROSS-SECTION DATA

Y KANDA, Y UENOHARA, H TSUJI
Department of Energy Conversion Engineering,
Kyushu University,
Fukuoka, Japan

Abstract

Correlation of nuclear parameters, level density parameters, pairing energies and optical model parameters, in Hauser-Feshbach model formula have been estimated from experimental data of neutron-induced reactions for Co and Ni. Correlation matrices for the level density parameter resulted from three cases of different combination of the nuclear parameters are compared to discuss effect of parameters in the formula. The correlation of reaction cross sections calculated from the estimated parameters is compared with the one obtained in the new evaluation from both differential and integral experiments.

1. INTRODUCTION

In nuclear data evaluation for neutrons, nuclear reaction model calculation is indispensable since available measurements are not always so many as to evaluate reaction cross sections from experimental data. Particularly, as a neutron energy region of nuclear application is extended into higher MeV, various kinds of nuclear reaction become physically possible but the reactions whose cross sections can be measured are technically limited to few reactions. In addition to the cross sections, evaluated covariance matrices for them are also demanded especially in application to neutron dosimetry.

Hauser-Feshbach model is one of the most fundamental model used to compute the reaction cross sections. The formula of the model has various nuclear parameters which must be empirically determined from observed quantities. Main parameters are level density parameters and pairing energies of residual nuclides and optical model parameters which are used to calculate transmission coefficients of emitted particles. They are concepts introduced into nuclear physics independent of the Hauser-Feshbach model formula and determined from experimental data unconnected directly with the Hauser-Feshbach model calculation. However, the results of the model calculation have not always agreed with the experimental reaction cross sections available for the comparison. Evaluators have perseveringly adjusted the parameters on the basis of their experience and insight until the agreement acceptable for themselves is reached. To improve such troublesome procedures, an evaluation method applying Baysian estimation was developed in the early works [1,2,3]: the parameters appearing in the Hauser-Feshbach model formula are automatically searched to reproduce available experimental data. We tried to estimate the parameters for neutron-induced reactions on Co and Ni, choosing only level density parameters, both those and pairing energies, and both those and optical model parameters used in computing transmission coefficients of emitted particles.

In the present study, correlations among the parameters estimated in the previous works [2,3] are compared with mutally and discussed. Then, they are applied to compute a covariance matrix representing the correlations of the reactions used in the estimation of the parameters. The covariance is discussed comparing with the one obtained in the cross section evaluations from differential and integral measurements [4].

II. PARAMETER ESTIMATION

The parameter estimation was described in the previous reports [1,2,5]. A brief description is presented here. The interesting parameters in our work are the level density parameters (a), the pairing energies (Δ), and the optical model parameters (OMP) of a neutron, proton and α-particle including a radius r_0 and a depth V_0 of real potential and a radius r_I and a depth W_I of imaginary potential, respectively. The works are summarized into three cases. The estimated parameters are only a (Case 1), a and Δ (Case 2) [3], and a and OMP (Case 3) [4]. In these works, a and Δ for seventeen residual nuclides in neutron-induced reactions of ^{59}Co, ^{58}Ni and ^{60}Ni were estimated and experiments for nine reaction cross sections and for four emitted charged-particle spectra were used.

III. RESULTS AND DISCUSSION

The correlation of the parameter a for three cases described above are shown in Fig. 1. It is a leading parameter in the model formula. The correlation is called strong for 100-75%, medium for 75-50%, weak for 50-25%, and none for 25-0%. In comparing correlation matrices, case 1 (a only) is different from case 2 (a and Δ) and similar to case 3 (a and OMP). In the cases 1 and 3, the correlation is strong between a for the target nuclide and a for the residual nuclide induced by the reaction whose measurements are adopted in the parameter estimation. In the case 2, it is medium or weak. It can be understood from the effects of each parameter in the model formula.

An application of the parameter correlation matrices is calculation of a covariance matrix for the reaction cross sections evaluated form the Hauser-Feshbach model calculation with the estimated parameters. In Fig.2, the result for ^{59}Co(n,α) and ^{58}Ni(n,p) is shown, as an example. It can be compared with the covariance shown in Fig.3 which was estimated by newly-developed evaluation method presented at Kiev conference [4]. It utilizes both differential and integral experiments. In the latter covariance, the cross correlation for both the reactions is none, and the correlation among energy regions in a reaction is localized in the regions where experimental data are available. In contrast to it, the correlation is strong in the former. The covariance matrix strongly depends on the evaluation method. It must be further studied which evaluation is preferable to utilization of covariance matrices, particularly in neutron dosimetry. This is conclusion to be pointed out with special emphasis in the present work.

(a) Case 1 (a only)

		^{55}Mn	^{56}Mn	^{54}Fe	^{55}Fe	^{56}Fe	^{57}Fe	^{58}Fe	^{59}Fe	^{57}Co	^{58}Co	^{59}Co	^{60}Co	^{57}Ni	^{58}Ni	^{59}Ni	^{60}Ni	^{61}Ni
		1	2	3	4	5	6	7	8	9	10	11	12	13	14	15	16	17
1	^{55}Mn	1000																
2	^{56}Mn	1	1000															
3	^{54}Fe	0	0	1000														
4	^{55}Fe	0	28	0	1000													
5	^{56}Fe	0	0	0	0	1000												
6	^{57}Fe	0	-4	0	4	0	1000											
7	^{58}Fe	-50	-239	0	236	0	-7	1000										
8	^{59}Fe	1	835	0	44	0	-6	347	1000									
9	^{57}Co	0	5	-1	-77	0	10	-43	-8	1000								
10	^{58}Co	0	29	0	976	0	4	241	46	-181	1000							
11	^{59}Co	0	930	0	25	0	-8	-222	865	-4	26	1000						
12	^{60}Co	0	-6	0	4	0	791	10	-8	9	4	-11	1000					
13	^{57}Ni	0	3	13	42	0	-8	-29	-5	914	-123	-3	-7	1000				
14	^{58}Ni	0	24	0	904	0	0	206	39	249	855	22	0	206	1000			
15	^{59}Ni	0	0	0	58	0	59	9	1	-168	41	0	51	-134	-29	1000		
16	^{60}Ni	0	-6	0	4	0	774	-9	-8	-7	3	-10	941	-6	0	45	1000	
17	^{61}Ni	0	0	0	0	0	-71	0	0	2	0	0	-47	2	0	15	194	1000

(b) Case 2 (a and Δ)

		^{55}Mn	^{56}Mn	^{54}Fe	^{55}Fe	^{56}Fe	^{57}Fe	^{58}Fe	^{59}Fe	^{57}Co	^{58}Co	^{59}Co	^{60}Co	^{57}Ni	^{58}Ni	^{59}Ni	^{60}Ni	^{61}Ni
		1	2	3	4	5	6	7	8	9	10	11	12	13	14	15	16	17
1	^{55}Mn	1000																
2	^{56}Mn	0	1000															
3	^{54}Fe	0	0	1000														
4	^{55}Fe	0	18	0	1000													
5	^{56}Fe	0	0	0	0	1000												
6	^{57}Fe	3	177	0	96	0	1000											
7	^{58}Fe	117	57	0	131	0	6	1000										
8	^{59}Fe	1	-140	0	36	0	-86	-236	1000									
9	^{57}Co	-2	-99	-1	-71	0	-89	15	64	1000								
10	^{58}Co	5	128	0	286	0	-13	112	-64	276	1000							
11	^{59}Co	1	494	0	35	0	123	182	117	-80	13	1000						
12	^{60}Co	0	99	0	-187	0	-151	-63	-32	-3	170	185	1000					
13	^{57}Ni	-2	-115	11	55	0	-49	-4	61	857	-314	-118	-2	1000				
14	^{58}Ni	0	-106	0	154	0	64	108	64	550	353	-108	137	292	1000			
15	^{59}Ni	0	-23	0	24	0	-10	23	22	-61	-18	-17	71	-66	68	1000		
16	^{60}Ni	-1	163	0	-53	0	623	100	-35	86	-226	193	193	159	134	62	1000	
17	^{61}Ni	0	-38	0	14	0	-125	-18	8	-13	37	47	-45	-28	-29	24	-242	1000

(c) Case 3 (a and OMP)

		^{55}Mn	^{56}Mn	^{54}Fe	^{55}Fe	^{56}Fe	^{57}Fe	^{58}Fe	^{59}Fe	^{57}Co	^{58}Co	^{59}Co	^{60}Co	^{57}Ni	^{58}Ni	^{59}Ni	^{60}Ni	^{61}Ni
		1	2	3	4	5	6	7	8	9	10	11	12	13	14	15	16	17
1	^{55}Mn	1000																
2	^{56}Mn	9	1000															
3	^{54}Fe	0	0	1000														
4	^{55}Fe	0	202	0	1000													
5	^{56}Fe	0	0	0	0	1000												
6	^{57}Fe	-4	66	0	-178	0	1000											
7	^{58}Fe	-108	-343	0	513	0	-87	1000										
8	^{59}Fe	4	846	0	-142	0	217	305	1000									
9	^{57}Co	0	-17	1	-11	0	-152	56	20	1000								
10	^{58}Co	0	-92	0	948	0	-257	485	9	29	1000							
11	^{59}Co	8	973	0	230	0	86	-334	881	-24	89	1000						
12	^{60}Co	-3	270	0	-176	0	784	-89	570	75	-134	342	1000					
13	^{57}Ni	0	6	30	-112	0	-62	-17	12	921	-79	1	-34	1000				
14	^{58}Ni	0	-77	0	933	0	-152	453	0	-1	969	-65	-78	86	1000			
15	^{59}Ni	1	29	0	-56	0	127	-24	73	9	115	57	179	71	205	1000		
16	^{60}Ni	-3	266	0	-244	0	855	-154	462	-151	-254	334	929	-62	-139	172	1000	
17	^{61}Ni	0	23	0	47	0	-234	46	120	60	101	36	125	18	68	59	39	1000

Fig.1 Correlation matrix of level density parameters a. The components representative to the residual nuclides of the reaction whose experiments were used in the parameter estimation are marked by squares; ▭ target nuclide, ▭ total cross section, ▭ (n,2n), ▭ (n,p), and ▭ (n,α).

^{59}Co(n,α) / ^{58}Ni(n,p)

		1	2	3	4	5	6	7	8	9	10	11	12	13	14	15	16	17	18
1	2.00E+01(MEV)	100																	
2	1.90E+01(MEV)	94	100																
3	1.70E+01(MEV)	53	76	100															
4	1.50E+01(MEV)	19	32	67	100														
5	1.30E+01(MEV)	38	52	64	65	100													
6	1.10E+01(MEV)	-27	-15	18	51	75	100												
7	9.00E+00(MEV)	-67	-57	-16	26	36	88	100											
8	7.00E+00(MEV)	38	-36	-22	8	38	80	85	100										
9	5.00E+00(MEV)	35	36	20	6	11	0	-8	36	100									
10	2.00E+01(MEV)	-12	-15	-12	2	12	-5	0	10	21	100								
11	1.90E+01(MEV)	-12	-14	9	6	-8	-2	1	-8	21	98	100							
12	1.70E+01(MEV)	-11	-13	-7	7	-7	0	2	5	16	94	94	100						
13	1.50E+01(MEV)	-4	2	18	25	21	23	18	14	3	17	24	45	100					
14	1.30E+01(MEV)	-2	5	21	23	24	24	18	13	1	20	-10	-16	44	100				
15	1.10E+01(MEV)	-7	-2	10	16	9	11	10	1	-10	18	30	9	16	70	100			
16	9.00E+00(MEV)	-9	-5	7	13	3	6	7	-2	-12	29	40	15	0	60	96	100		
17	7.00E+00(MEV)	-6	-1	10	8	2	4	5	-3	-8	13	19	-7	-22	56	77	88	100	
18	5.00E+00(MEV)	0	3	5	-1	0	-1	-1	-4	-4	-15	-12	-37	-49	33	48	62	88	100

Fig. 2 Correlation matrix of cross section for ^{59}Co(n,α) and ^{58}Ni(n,p) calculated from parameters estimated in case 3.

^{59}Co(n,α) / ^{58}Ni(n,p)

		1	2	3	4	5	6	7	8	9	10	11	12	13	14	15	16	17	18
1	2.00E+01(MEV)	100																	
2	1.90E+01(MEV)	33	100																
3	1.70E+01(MEV)	8	23	100															
4	1.50E+01(MEV)	10	17	30	100														
5	1.30E+01(MEV)	11	20	31	39	100													
6	1.10E+01(MEV)	1	3	4	5	11	99												
7	9.00E+00(MEV)	2	4	5	5	7	24	100											
8	7.00E+00(MEV)	2	4	6	6	8	24	22	99										
9	5.00E+00(MEV)	2	3	4	4	5	15	15	27	100									
10	2.00E+01(MEV)	0	0	0	0	0	0	0	0	0	100								
11	1.90E+01(MEV)	0	0	0	0	0	0	0	0	0	-26	100							
12	1.70E+01(MEV)	0	0	4	0	0	0	0	0	0	4	9	100						
13	1.50E+01(MEV)	0	0	0	1	0	0	0	0	0	4	7	14	100					
14	1.30E+01(MEV)	0	0	0	0	0	0	0	0	0	5	9	10	20	99				
15	1.10E+01(MEV)	0	0	0	0	0	0	0	0	0	3	2	2	1	4	100			
16	9.00E+00(MEV)	0	0	0	0	0	0	0	0	0	1	1	2	4	4	1	100		
17	7.00E+00(MEV)	0	0	0	0	0	0	0	0	0	1	1	2	4	5	1	27	100	
18	5.00E+00(MEV)	0	0	0	0	0	0	0	0	0	2	3	5	10	12	1	14	17	100

Fig. 3 Correlation matrix of cross section for ^{59}Co(n,α) and ^{58}Ni(n,p) evaluated from both differential and integral experiments[4].

REFERENCES

1) Y. Uenohara, M. Tsukamoto and Y. Kanda, Nucl. Sci. Technol. 20 787 (1983)

2) Y. Uenohara, Y. Kanda, T. Yugawa, Y. Yoshioka, Radiat. Eff. (GB), 95 195 (1986)

3) Y. Kanda and Y. Uenohara, "Covariances of Nuclear Model Parameters Generated from Experimental Information", IAEA Specialists' Meeting on Covariances Practices in the Field of Nuclear Data, Rome Italy, Nov. 17-19, 1986

4) Y. Kanda and Y. Uenohara, "Some Activation Cross Sections Evaluated Simultaneously by Differential and Integral Measurements", International Conference on Neutron Physics, Kiev USSR, Sept. 21-25, 1987

5) Y. Kanda and Y. Uenohara, "A Method to Evaluate Covariances for Correlated Nuclear Data", IAEA Specialists' Meeting on Covariances Practices in the Field of Nuclear Data, Rome Italy, Nov. 17-19, 1986

CALCULATION OF NEUTRON CROSS-SECTIONS OF ^{64,66,68}Zn FOR FUSION APPLICATIONS

P.G. YOUNG
Applied Nuclear Science Group,
Los Alamos National Laboratory,
Los Alamos, New Mexico

D.A. RUTHERFORD
Department of Chemical and
Nuclear Engineering,
University of New Mexico,
Albuquerque, New Mexico

United States of America

Abstract

Hauser-Feshbach statistical theory calculations are described for neutron reactions with ^{64}Zn, ^{66}Zn, and ^{68}Zn over the energy range 0.01 - 20 MeV. A neutron spherical optical potential is obtained by fitting neutron total cross sections and elastic angular distributions, together with low-energy resonance data. Preequilibrium effects are calculated with an exciton model, and direct reaction effects are included through DWBA calculations using deformation parameters from (p,p') scattering. The results are compared to experimental data, including new measurements of ^{64}Zn(n,p)^{64}Cu and ^{64}Zn(n,2n)^{63}Zn cross sections at 14.8 MeV.

INTRODUCTION

Zinc isotopes are of interest as activation and/or dosimetry detectors in fusion energy applications. In particular, the ^{64}Zn(n,p)^{64}Cu(12.7h) and ^{64}Zn(n,2n)^{63}Zn(38m) reactions are considered high priority dosimetry cross sections, and the ^{64}Zn(n,p)^{64}Cu, ^{64}Zn(n,γ)^{65}Zn(244d), and the ^{66}Zn(n,2n)^{65}Zn reactions are high priority activation cross sections.[1] Additionally, the ^{64}Zn(n,2p)^{63}Ni and ^{66}Zn(n,α)^{63}Ni reactions are of interest because they both lead to 100-year halflife ^{63}Ni.

Because of the varied interest in zinc isotopic cross sections, we have performed a Hauser-Feshbach statistical theory analysis of the ^{64,66,68}Zn isotopes. By fitting certain of the observed cross sections as well as possible with physically reasonable parameterizations, we hope to facilitate extrapolation of the experimental data to unmeasured energies and reactions. At present there are no natural or isotopic zinc evaluations in the ENDF/B-V data base; the present results will be available for Version VI of ENDF/B.

THEORETICAL ANALYSIS

The GNASH Hauser-Feshbach statistical theory code[2] was used to calculate all significant n+^{64,66,68}Zn reaction channels for the incident neutron energy range 0.1-20 MeV. Binary reaction cross sections and secondary energy spectra are calculated in GNASH by summing a width-fluctuation-corrected Hauser-Feshbach expression[3] over compound nucleus spin and parity $J\pi$,

$$\sigma_{cc'}^{J\pi} = \frac{<\Gamma_c^{J\pi}><\Gamma_{c'}^{J\pi}>}{<\Gamma^{J\pi}>} W_{cc'}^{J\pi} \qquad (1)$$

where c and c' represent entrance and exit channels, respectively. The quantities $<\Gamma_c^{J\pi}>$ are partial widths, which can be calculated from transmission coefficients, together with discrete and continuum level density information for the corresponding residual nuclei. The sum of all partial widths for given $J\pi$ appears as $<\Gamma^{J\pi}>$ in the denominator.

The factor $W_{cc'}^{J\pi}$ is a correction that accounts for fluctuations and correlations between the partial widths. Moldauer's integral method[4] and an approximation from Tepel et al.[5] for the number of degrees of freedom are used to calculate $W_{cc'}^{J\pi}$. The width fluctuation correction is most important at lower energies and is essentially unity above a few MeV.

Above about 6 MeV neutron energy, preequilibrium corrections using the exciton model of Kalbach[6] are applied to the populations and spectra calculated with Eq.(1). Parameters for the model were adjusted to give a preequilibrium fraction of 25% near 14 MeV. Above E_n = 4 MeV, tertiary and higher order reactions become energetically possible. The population and decay of states in these nuclei are also calculated by GNASH with full angular momentum conservation.

A maximum of experimental discrete level information (excitation energies, spins, parities, and gamma-ray branching ratios) is included in the calculations. At higher excitation energies, the level density formulation of Gilbert and Cameron[7] is used with nucleon pairing and shell corrections from the tables of Cook.[8] The continuum level densities are smoothly matched to the experimental discrete levels at lower energies and to the mean level spacing $<D_0>$ at an excitation energy corresponding to the neutron separation energy.

Direct reaction cross sections were calculated for low-lying states in ^{64,66,68}Zn. The distorted-wave Born approximation code DWUCK[9] was used, together with β_ℓ deformation parameters from proton inelastic scattering measurements on zinc isotopes.[10] The largest direct contribution occurred for the 2^+ first-excited state, reaching a maximum of 260 mb at E_n = 5 MeV in the case of ^{64}Zn.

Gamma-ray transmission coefficients were calculated from a gamma-ray strength function with a giant dipole resonance shape.[11] The normalization of the strength function was obtained by matching experimentally determined values of $2\pi<\Gamma_{\gamma 0}>/<D_0>$, where $<\Gamma_{\gamma 0}>$ is the mean γ-ray width for s-wave resonances.

A spherical optical model potential was used to calculate the neutron transmission coefficients. The potential was obtained by fitting measured neutron total cross sections between 2 and 20 MeV,[12] neutron elastic angular distributions between 3.2 and 14 MeV,[12] and low energy s- and p-wave neutron strength functions and the potential scattering radius inferred from experiments.[13] The SCATOPT code[14] was used for the analysis, with starting parameters from the n+Ni potential of Harper and Alford.[15]

Spherical optical potentials were also used to obtain transmission coefficients for protons and alpha particles. The global potential by Perey[16] was used for protons, while a potential obtained in an analysis of neutron reactions on Fe was adopted for alpha particles.[17]

RESULTS

The neutron potential that results from the spherical optical model analysis is given in Table I. The calculated s- and p-wave neutron strength functions and potential scattering radius are compared with experimentally inferred values[13] in Table II. The total cross section calculated with the neutron potential is compared with measurements[12] for elemental zinc in Fig. 1.

To test the proton optical potential, (p,n) cross sections were calculated for ^{63}Cu and ^{65}Cu and compared with measurements. These calculations employed the same neutron and proton transmission coefficients that were used in the zinc analysis. In addition, the same level density parameters (where appropriate), gamma-ray strength functions, etc., were used in all the calculations. The results for the ^{63}Cu(p,n)^{63}Zn and ^{65}Cu(p,n)^{65}Zn cross sections are compared with experimental data[18,19] in Fig. 2.

The calculated results for the ^{64}Zn(n,p)^{64}Cu cross section are compared with experimental values[12] in Fig. 3. Considering the large scatter in the experimental data, the agreement of the calculated and experimental results is reasonable. While experimental errors are relatively large for many of the measurements, recent precision results by Rutherford[20] have an uncertainty of only ± 3%, and the calculated cross section lies within 3% of that measurement.

The theoretical values of the ^{64}Zn(n,2n)^{63}Zn cross section are compared with the experimental data base[12] in Fig. 4. Again, good agreeement is found between the calculated and measured values. The precise value of Rutherford[20] at 14.8 MeV is again reproduced by the calculation to within ~ 3%.

TABLE I

NEUTRON SPHERICAL OPTICAL MODEL POTENTIAL USED IN ^{64}Zn CALCULATION

Potential (MeV)*	r_0 (fm)	a (fm)
$V_R = 49.11 - 16\eta - 0.376E$	1.295	0.58
$W_D = 8.545 - 8\eta$	1.295	0.48
$W_V = -0.094 + 0.197E$	1.295	0.58
$V_{SO} = 6.2$	1.12	0.48

*$\eta = (N-Z)/A$

TABLE II

LOW-ENERGY s- AND p-WAVE NEUTRON STRENGTH FUNCTIONS (S_0, S_1) AND POTENTIAL SCATTERING RADII (R') FOR Zn ISOTOPES

	S_0 (10^{-4})	S_1 (10^{-4})	R' (fm)	
^{64}Zn	1.70	0.60	~7.0	Exp.
	±0.16	±0.04	±0.7	
	2.08	1.03	7.2	Theory
^{66}Zn	1.97	0.70	~7.0	Exp.
	±0.2	±0.07	±0.07	
	1.93	1.05	7.3	Theory
^{68}Zn	2.2	0.39	~7.0	Exp.
	±0.3	±0.03	0.7	
	1.79	1.08	7.3	Theory

Experimental data are more limited for ^{66}Zn and, especially, ^{68}Zn reactions. Comparisons of the calculated (n,p) cross sections for ^{66}Zn and ^{68}Zn with experimental results are given in Fig. 5. Reasonable agreement with experiment is again found, although there is a very considerable spread in the measurements, especially for ^{68}Zn.

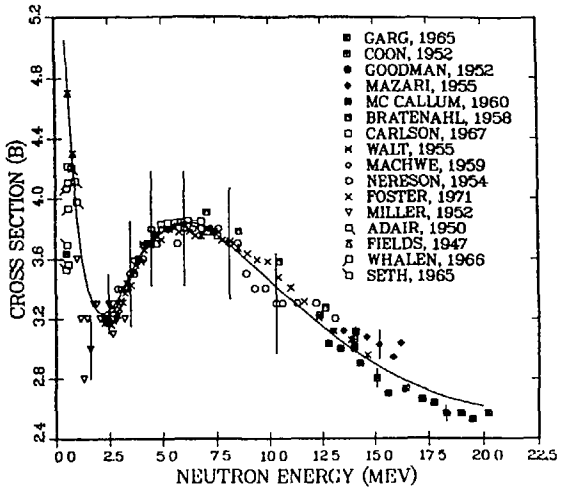

Fig. 1. Neutron total cross section of elemental zinc. The solid curve was calculated with the optical model potential described in the text.

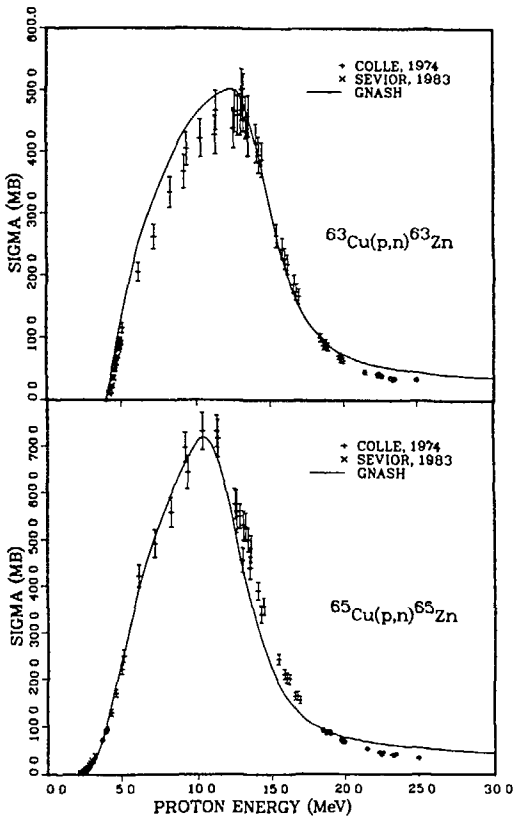

Fig. 2. Comparison of calculated and experimental ^{42,43}(p,n) cross sections for ^{63}Cu and ^{65}Cu.

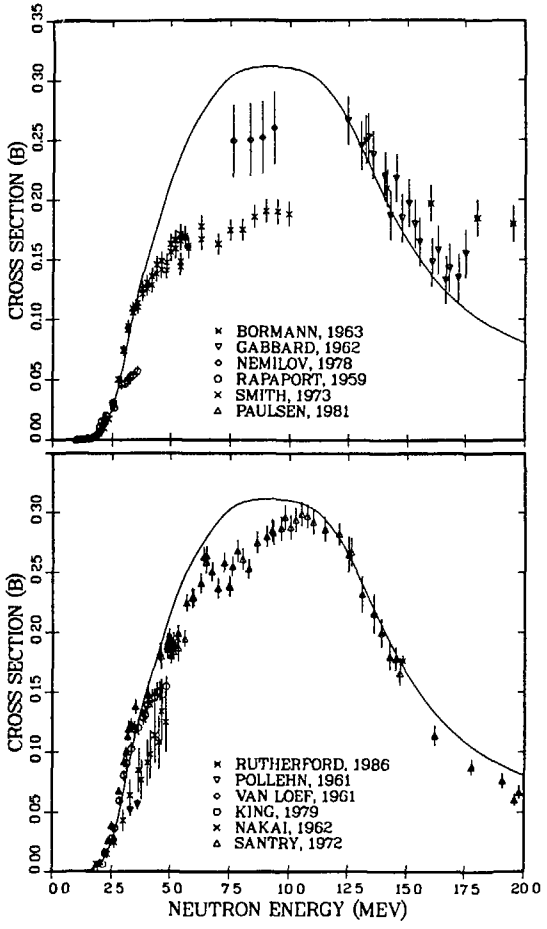

Fig. 3. Experimental and calculated values of the $^{64}Zn(n,p)^{64}Cu$ cross section to 20 MeV.

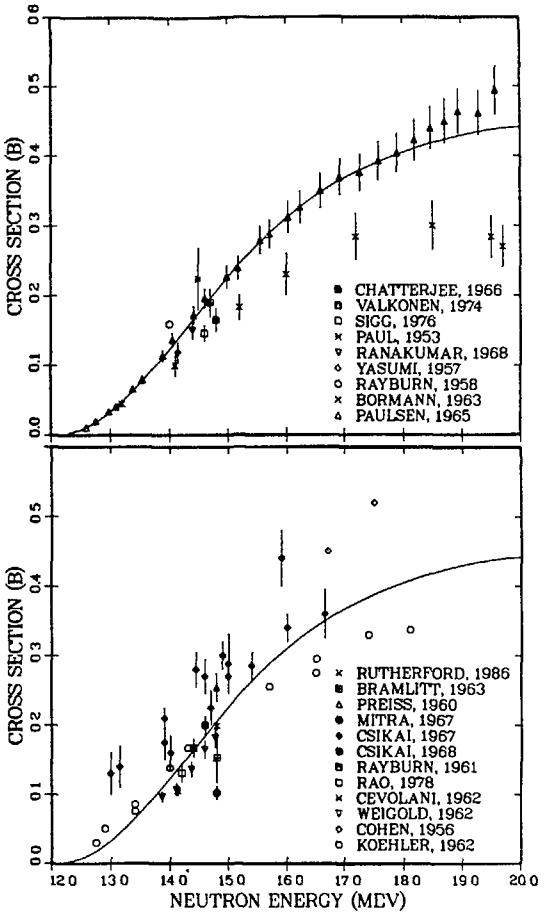

Fig. 4. Experimental and calculated values of the $^{64}Zn(n,2n)^{63}Zn$ cross section from threshold to 20 MeV.

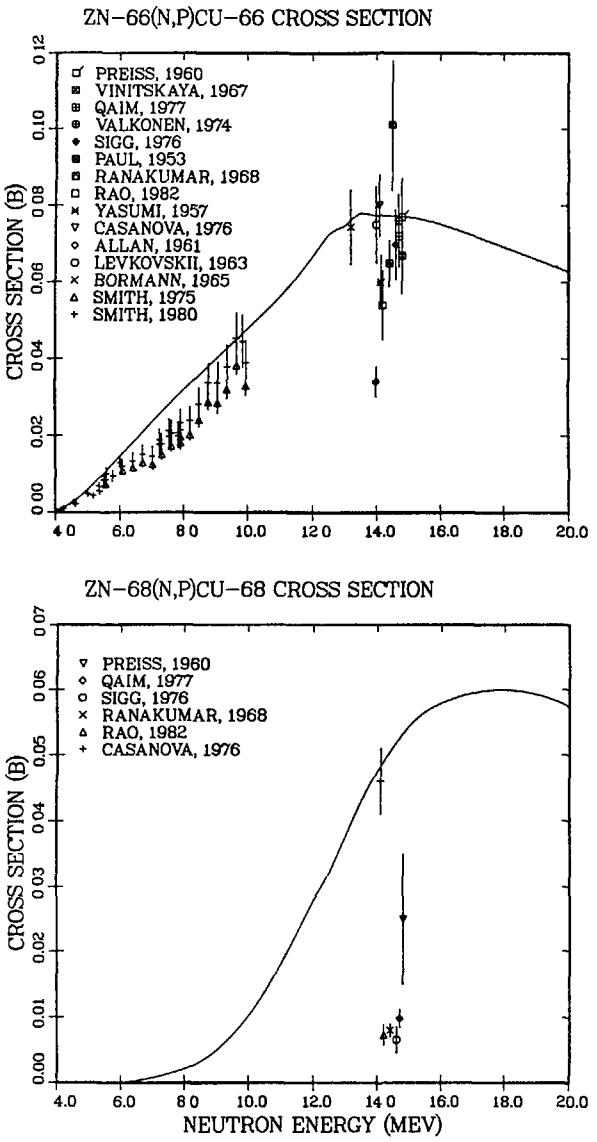

Fig. 5. Experimental and calculated (n,p) cross sections for ^{66}Zn and ^{68}Zn in the upper and lower halves of the figure, respectively.

SUMMARY REMARKS

To summarize, calculations of all neutron-induced reactions on $^{64,66,68}Zn$ were carried out for neutron energies between 0.1 and 20 MeV using a single set of nuclear models and parameters. The only parameters adjusted for the calculations were the neutron optical potential, which was fit to total and elastic scattering data and to low-energy resonance parameters, and the parameters of the preequilibrium model, which were arbitrarily adjusted to give a neutron preequilibrium fraction of ~ 25% near 14 MeV for ^{64}Zn.

Good agreement is found between calculated and experimental values, especially for neutron reactions on ^{64}Zn that have an abundance of experimental information available. The analysis results in predicted values for several other reactions of interest for fusion applications and for which there is little or no data. Finally, in addition to energy-dependent cross sections, the analysis produces complete energy spectra and angular distribution information. The combination of new theoretical and experimental results should lead to significantly improved $^{64,66,68}Zn$ data for ENDF/B-VI.

REFERENCES

1. E. T. Cheng, Fusion Tech. 8, 1423 (1985).
2. P. G. Young and E. D. Arthur, 'GNASH: A Preequilibrium Statistical Nuclear-Model Code for Calculation of Cross Sections and Emission Spectra," Los Alamos Scientific Laboratory report LA-6947 (Nov. 1977).
3. P. A. Moldauer, Phys. Rev. C11, 426 (1975).
4. P. A. Moldauer, Phys. Rev. C14, 764 (1976).
5. J. W. Tepel, H. M. Hoffmann, and H. A. Weidenmüller, Phys. Lett. 49B, 1 ·(1974).
6. C. Kalbach, "The Griffin Model, Complex Particles and Direct Nuclear Reactions," Z. Phys. A283, 401 (1977).
7. A. Gilbert and A. G. W. Cameron, "A Composite Nuclear-Level Density Formula with Shell Corrections," Can. J. Phys. 43,1446 (1965).
8. J. L. Cook, H. Ferguson, and A. R. de L. Musgrove, "Nuclear Level Densities in Intermediate and Heavy Nuclei," Aust. J. Phys. 20, 477 (1967).
9. P. D. Kunz, "DWUCK - A Distorted-Wave Beam Approximation Program," unpublished.
10. R. R. Johnson and G. D. Jones, Nucl. Phys. A122, 657 (1968).
11. P. Axel, Phys. Rev. 126, 671 (1962).
12. Experimental data available from the CSISRS compilation by the National Nuclear Data Center, Brookhaven National Laboratory, Upton, New York.
13. S. F. Mughabghab, M. Divadeenam, and N. E. Holden, Neutron Cross Sections, Vol. 1A, Academic Press, New York (1981).
14. O. Bersillon, Bruyeres-le-Chatel, France, personal communication to E. Arthur (1980).
15. R. C. Harper and W. L. Alford, J. Phys. G: Nucl. Phys. 8, 153 (1982).
16. F. G. Perey, Phys. Rev. 131, 745 (1963).
17. E. D. Arthur and P. G. Young, "Evaluated Neutron-Induced Cross Sections for $^{54,56}Fe$ to 40 MeV,": Los Alamos Scientific Laboratory report LA-8636-MS (1980).
18. R. Collé, R. Kishore, and J. B. Cumming, Phys. Rev. C9, 1819 (1974).
19. M. E. Sevior, L.W. Mitchell, M. R. Anderson, C. I. W. Tingwell, and D. G. Sargood, Aus. J. Phys. 36, 463 (1983).
20. D. A. Rutherford, "Theoretical and Experimental Cross Sections for Neutron Reactions on ^{64}Zn," Master of Science Thesis, University of New Mexico (1987).

RECENT ADVANCES IN NUCLEAR STRUCTURE STUDIES RELATED TO NEUTRON AND PHOTON PROCESSES

F. FABBRI, G. MAINO, E. MENAPACE, A. MENGONI
Comitato Nazionale per la Ricerca e per
lo Sviluppo dell'Energia Nucleare
e delle Energie Alternative,
Bologna, Italy

Abstract

Some recent results are discussed about nucleon cross section and photon production calculations in connection with nuclear structure studies.

---

1. INTRODUCTION

Nucleon capture reactions and related photon production cross sections and spectra have found important applications in addition to usual interest in basic nuclear physics research.

As far as applied sciences are concerned, neutronic design of nuclear reactors, shielding, energy deposition and radiation damage estimates, activation and isotope production data are of main interest.

Since nucleon radiative capture reaction covers about nine orders of magnitude of the incident nucleon energy, from thermal ($= 2.5 \times 10^{-2}$ eV) up to the MeV region, one is involved with many different reaction mechanisms and nuclear structure effects. It results a strong interplay between models of nuclear reactions and structure, the latter providing the basic information for cross sections and spectra calculations. In turn, nucleon and photon probes represent the classical tool in investigating some aspects related to the structure of nuclei.

In particular, photon induced processes are of main interest since electromagnetic interaction of radiation with matter is clearly understood within the framework of well-established QED theory, and therefore we can extract useful information on nuclear structure from these studies. Photon scattering experiments hold an important rôle, since this process has a direct character in the exit channel, on the contrary to the statistical decay by nucleon emission in photoabsorption reactions, and therefore provides detailed knowledge of properties of resolved levels, due to the high resolution of Ge(Li) detectors used in these measurements.

In any case, improved knowledge of nuclear structure allows more reliable investigation of nucleon-nucleus interactions, in order to elucidate the main aspects of nuclear reaction mechanisms.

In the following section, we briefly discuss the most important data in neutron capture and inelastic scattering cross-section calculations, which represent the main sources of photon production for $E_n \lesssim 20$MeV in structural materials (with mass number $A \simeq 50 - 60$). We review some recent, mainly theoretical, advances in nuclear structure studies applied to that purpose, and point out open problems of interest in current investigation.

2. NUCLEAR STRUCTURE STUDIES

In the energy range of interest in applied sciences, the mechanisms underlying neutron induced reactions involve many aspects of nuclear structure, starting from single-particle degrees of freedom up to complicated collective modes, both at low excitation energy and in the MeV region (giant resonances). Moreover, explanation of some aspects of nuclear reactions, even at low energies, requires the introduction of further degrees of freedom in nuclear matter (see sect.2.3).

In sect.2.1 we consider discrete nuclear spectra, where both single-particle and collective effects are present, and relevant electromagnetic transitions. These data are important in the treatment of compound-nucleus statistical decay and as final states in the valence and semidirect models of nucleon capture. Information on structure of low-lying collective states is needed in coupled-channel calculations of inelastic scattering cross sections.

Nuclear structure in the continuum, i.e. level density, is discussed in sect.2.2; it plays a crucial rôle, as well known, in the statistical model of nuclear reactions, but occurs in preequilibrium calculations too and in other topics as the spreading width of giant resonances.

Finally, we devote sect.2.3 to the investigation of some giant resonances whose excitation modes are concerned with photon decay following neutron capture.

2.1 Low-lying levels

Nuclei in the mass region around A $\simeq$ 50-60 are still feasible for shell model calculations with suitable nucleon-nucleon effective forces. However, according to the large dimensions of shell-model configuration space, some simplifications are often required in order to perform realistic calculations within the capabilities of present computers. To sum up, for nuclei in the fp shell a suitable scheme is needed to truncate the space of all possible states, by choosing the most important only. For instance, Vennínck and Glaudemans /1/, in their analysis of ^{54,55,56}Fe spectra, confine themselves to consider configurations with up to three $f_{7/2}$ holes (both for protons and neutrons), since they are predominant in the composition of low-energy state wave functions.

This truncation process is essential when one introduces the coupling between low-lying states and GR (giant resonances) degrees of freedom. For electric multipolarities $\lambda \geq 1$ and magnetic ones $\mu > 1$ the treatment of GR involves excitation of particle-hole states across a major shell closure ($1\hbar\omega$, $2\hbar\omega$, ... excitations). This fact increases prohibitively the dimension of relevant configuration space

For instance, McGrory and Wildenthal /2/ have performed shell model calculations of M1 excitation strength in ^{42,44,48}Ca assuming ^{40}Ca as inert core; thus they have considered a complete $f_{7/2}$ $f_{5/2}$ $p_{3/2}$

$p_{1/2}$ model space only, since M1 transitions can be built by neutron excitations in the 0 $\hbar\omega$ shell to a very good approximation. By increasing nuclear mass, the model fp-space grows rapidly of dimensionality with respect to ^{48}Ca, up to 10^4 times for ^{54}Fe, as an example.

As a consequence, one must deal with restricted configurations such as $1f_{7/2}^{n-1}\ (2p_{3/2}\ 1f_{5/2}\ 2p_{1/2})^1 \oplus {}^1f_{7/2}^n$ states /3/.

As shown in fig.1, in the fp shell collective features are already developed in low-energy spectrum, in heavier Fe isotopes a vibrational-like structure is observed from experimental levels /4/ and confirmed by shell model calculations /1/. The cluster of two-phonon states ($J^\pi = 0^+$, 2^+, and 4^+) has an average excitation energy roughly twice than the first 2^+ (one-phonon) state. ^{54}Fe, with 28 neutrons, shows the characteristics increase for (semi)magic nuclei of the energy gap between ground and first excited states. Collective Features in ^{56}Fe appear even more pronounced from the analysis of quadrupole moments and B(E2) transitions, whose enhanced values with respect to single-particle estimates strongly support the collective interpretation of low-lying structure.

Therefore, it seems worth while to apply also in this medium-mass region collective models of nuclei, like the interacting boson model (IBM) of Arima and Iachello /5/. Originally, the interacting boson approximation (IBA) was proposed by Feshbach and Iachello /6/, in order to deal with light weight nuclei /7/. It consists in assuming some basic building blocks to construct nuclear excited states, such as are simple predominant modes (defined normal modes), which are present in the correlated ground-state wave function to some extent. Therefore, excited states are obtained by introducing

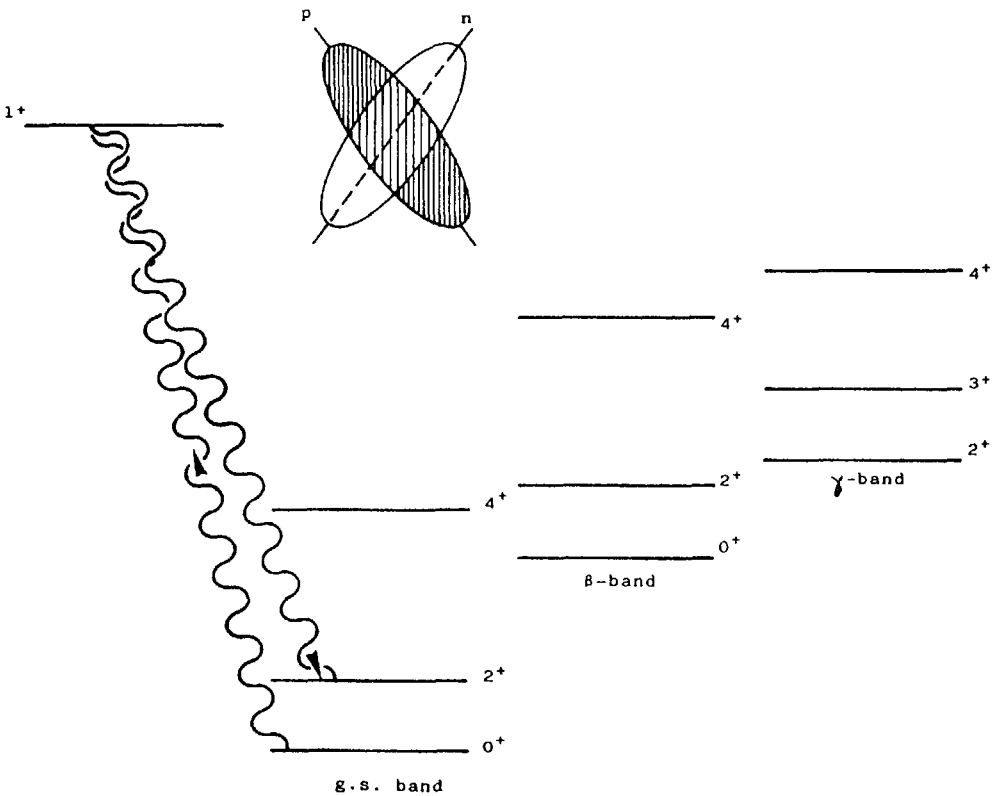

Fig. 1 - Photon scattering excitation of low-lying collective M1 state in a deformed nucleus /16/. A geometrical interpretation /17/ of the 1^+ state is also sketched.

on a phenomenological basis suitable interactions between the normal modes. The same philosophy underlies the usual formulation of IBM-1 /5/, which is commonly applied to (non-magic) *even-even* nuclei with *medium-heavy* mass. The normal modes are here represented by boson excitations made by neutron-neutron and proton-proton pairs in the active shell, coupled to L=0 and 2 angular momentum (s and d bosons, respectively).

To describe light nuclei, for instance in the sd shell where neutrons and protons occupy orbitals with identical quantum numbers, one must introduce neutron-proton s-d bosons in addition to the usual ones. The resultant model, in the two versions IBM-3 and IBM-4 of increasing complexity (see ref./8/ for a recent review), provides a satisfactory description of many features of sd shell nuclei /9/. In the mass region $A \simeq 50\text{-}60$, where protons occupy almost entirely the $1f_{7/2}$ shell, while neutrons lie in the beginning of subsequent major shell (fp), 1p-1h correlations are dominant in the ground-state. As *normal modes* it is more suitable to choose particle-hole-like bosons and then introduce the residual interactions among them.

The following Hamiltonian is thus considered:

$$\hat{H} = U_o + \hat{H}_o + \hat{H}_{int} \quad , \tag{1}$$

where U_o is a c-number, defined by the expectation value of $\hat{H}$

$$U_o = \langle \Phi_o | \hat{H} | \Phi_o \rangle \tag{2}$$

in the ground-state $|\Phi_o\rangle = \prod_{i \leq N} a_i^+ |0\rangle$, where the operator a_i^+ creates a state i below the Fermi energy ε_f, labeled by the quantum numbers $(n_i, l_i, j_i, m_i, t_i, m_i^t)$ and $|0\rangle$ is the particle vacuum.

Moreover,

$$\hat{H}_o = \sum_{\mu > E_F} \varepsilon_\mu a_\mu^+ a_\mu - \sum_{i \leq \varepsilon_F} \varepsilon_i b_i^+ b_i \quad , \tag{3}$$

where μ labels states above the Fermi energy, and

$$b_i^+ \equiv (-1)^{j_i + m_i + (1/2) + m_i^t} a_{-i} \quad . \tag{4}$$

Finally, the two-body interaction term, $\hat{H}_{int}$, is given by

$$\hat{H}_{int} = (1/2) \sum_{\alpha\beta\gamma\delta} V_{\alpha\beta\gamma\delta} : a_\alpha^+ a_\beta^+ a_\delta a_\gamma : \equiv \hat{H}_{p\text{-}h} + \hat{H}_{res} \quad . \tag{5}$$

A normal mode is then defined in the 1p-1h subspace as

$$B^+ \equiv \sum_{\mu,i} f_{\mu i} a_\mu^+ a_i \quad . \tag{6}$$

The one or two lowest states obtained by solving the relevant TDA (Tamm-Damcoff Approximation) equation of motion with inclusion of $\hat{H}_{p\text{-}h}$ are selected as IBA bosons. The nuclear excited states are then obtained by considering the residual interaction, $\hat{H}_{res}$, between the "normal" bosons.

According to the previous formalism, calculations have been carried out /10/ for ^{56}Ni , in quite good agreement with experimental data, thus providing a reliable model of nuclear structure (collective levels and electromagnetic transitions) for medium weight nuclei. In conclusion, the IBA framework provides an useful truncation scheme of the complete shell-model configuration space and assures feasible yet reliable calculations of properties of low-lying collective levels.

In particular, the IBA bosons suggest a close analogy with RPA "quasibosons": in fact, it is possible to show that IBA includes interaction terms between particle-hole modes, which are not considered in the commonly adopted RPA (random phase approximation). In this aspect, the microscopic formulation of IBA can be regarded as a generalization of RPA techniques.

Due to its calculation feasibility, the phenomenological IBM version is particularly suitable to the study of coupling between low- and high-energy (GR) collective modes, which implies, for instance, core renormalization effects of effective E2 charges /11/ and GR fragmentation /12,13,14/.

Finally, it is worth while to mention, within the framework of IBM-2/5/ which distinguishes between neutron and proton degrees of freedom, the prediction of existence of low-energy collective M1 transitions in deformed nuclei, observed for the first time by means of inelastic electron scattering reactions /15/ at excitation energies around 3 MeV. Subsequently, these states have been observed with nuclear resonance fluorescence (NRF) techniques which make use of bremsstrahlung photons and high-resolution Ge(Li) detectors /16/ (see fig.2). The better resolution so obtained allowed to identify several M1 components.

These "unnatural-parity" states ($J^{\pi} = 1^{+}$) with strong M1 transition rates to the 0^{+} ground-state, have been also predicted, even if at higher energies, by the geometrical model of Loludice and Palumbo /17/, where protons and neutrons in a deformed nucleus perform rotational oscillations against each other (see the picture in fig.2). Recently, Iachello has proposed /18/ that such 1^{+} states are not peculiar of deformed nuclei, but prototype of a whole class of collective states lying around 2-3 MeV of excitation energy, such as a possible 2^{+} state in spherical nuclei, with enhanced B (E2) value.

These modes are very interesting also as far as characteristics of gamma-ray decays and determination of branching ratios between resolved levels are concerned.

2.2 Nuclear level densities

By increasing excitation energies, nuclear levels are embedded in a continuum structure whose global description can be made only in a statistical way, by means of the level density formalism.

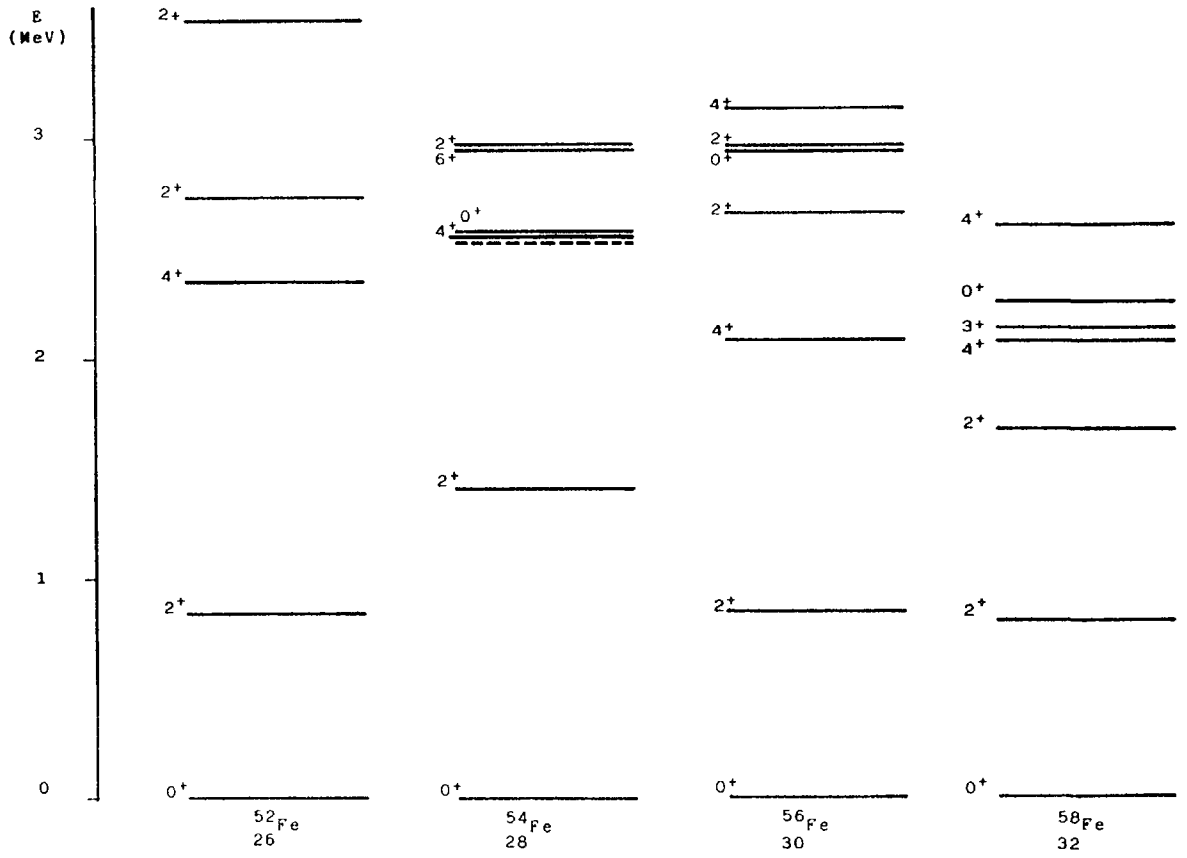

Fig. 2 - Experimental /4/ spectra of even-even iron isotopes.

Starting from seventies, many progresses have been accomplished in the derivation of microscopic models for nuclear level densities (for a recent review, see ref. /19/). Remarkable success in reproducing experimental data, mainly from average neutron resonance spacings, has been gained by shell-model statistical calculations, within the framework of the grand-partition function formalism, including both residual pairing interactions between like-nucleons in the Bardeen--Cooper-Schrieffer (BCS) approximation and blocking effect of single-particle configurations due to Pauli principle /20/. Moreover, this approach is particulary suitable to inclusion of parity distribution of nuclear level densities /21,22/, while the usual phenomeno-

logical formulae make the simple assumption of equiprobability for opposite parities. This hypothesis turns out to be true only for heavy nuclei ($A \gtrsim 90$) or excitation energies high enough (> 20-25 MeV). For structural materials (nuclei in the fp shell), at excitation energies around the neutron binding $B_n \approx 8$ MeV, level densities with apposite parities differ by a factor two or even more, as experimentally observed /23/ and confirmed by microscopic shell model plus BCS calculations. In fig. 3 the calculated

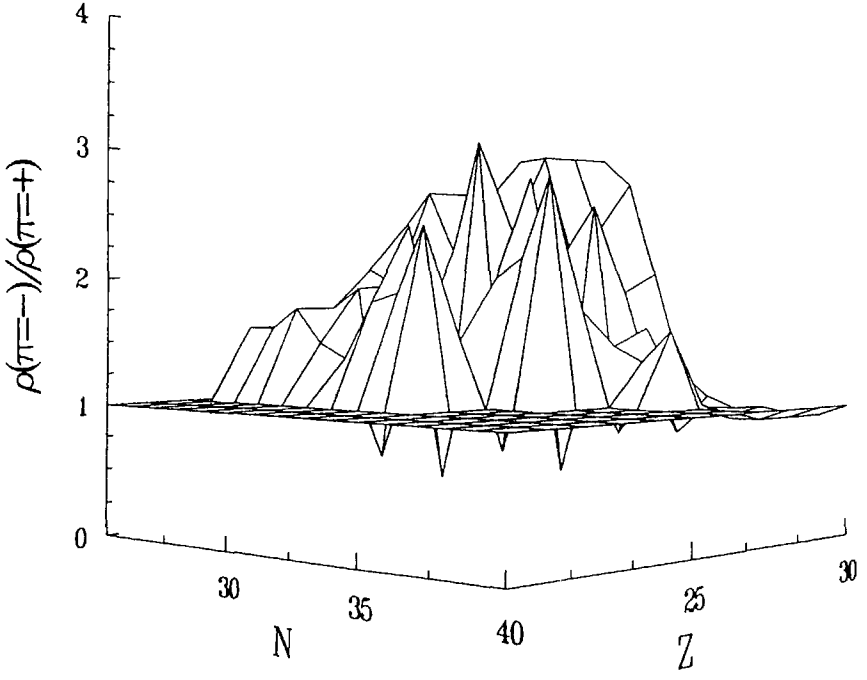

Fig. 3 - Ratios of negative-parity levels to positive-parity levels for selected nuclei in the f-p shell at excitation energies corresponding to the neutron binding energies, versus the number of neutrons (N) and protons (Z).

ratios of $\rho(\pi = -)$ to $\rho(\pi = +)$ for fp shell nuclei are show and the large discrepancies from the equiprobable hypothesis are evident. However, it has to be noted that the simple statistical estimates within the framework of usual BCS formalism /21,22/ must be taken with some caution, due to the fluctations in the quasiparticle number. This rough approximation could be avoided only by resorting to a projected formalism.

Therefore, this appraoch may fail in reproducing experimental results /24/; however, it represents an estimate of parity effects more reliable than the naive assumption of equiprobability.

Due to the great number of residual nuclei and excitation energies involved, microscopic calculations of level densities require too much computing time to be directly included in the usual codes for cross section evaluations. As a consequence, it is indispensable to assume semiempirical formulae, easily computable and so improved as to reproduce the main features of microscopic formalisms. Recently, many results have been obtained in this domain (see, for instance, ref. /25/ and papers quoted therein). We have found that a fair agreement with Nilsson-BCS calculations can be obtained by means of the following expressions, which admit an energy dependence of the "a" parameter.

$$\rho(E,M,\pi) = \frac{1}{12\sqrt{2}} \cdot \frac{\exp\left[2\sqrt{a(E)E}\right]}{\sigma a(E)^{1/4} E^{5/4}} e^{-M^2/(2\sigma^2)} F_{par}(E,\pi), \quad (7)$$

where E is the excitation energy, M the projection of angular momentum along a symmetry axis, π the parity and σ the spin cutoff factor, whose rigid-body value is assumed. The "a" parameter has the following energy dependence:

$$a(E) = \tilde{a}\,(1 + e^{-\gamma E}) , \qquad (8)$$

while the parity-dependence factor has the form of a logistic curve:

$$F_{par}(E,\pi) = (1/2)\,\mathrm{tgh}\,(\frac{\alpha E}{2}) , \qquad (9)$$

which, in the limit of high excitation energies, equals 1/2. The level density for a given angular momentum value, J, is thus obtained, as usual, by means of the relation:

$$\rho(E,J,\pi) = \rho(E,M=J,\pi) - \rho(E,M=J+1,\pi) . \qquad (10)$$

To sum up, we deal with three adjustable parameters, $\tilde{a}$, γ and α, to be determined for each nucleus on the basis of microscopic calculations and experimental data. As an example we show in figs. 4a and 4b the ^{56}Fe level density calculated by means of eqs. (7-10), in comparison with experimental information from both the cumulative number of discrete levels at low energy /26/, α-particle emission cross sections /27/ and Ericson fluctuations /28/. The relevant level density parameters are listed in Table I for iron isotope, together with

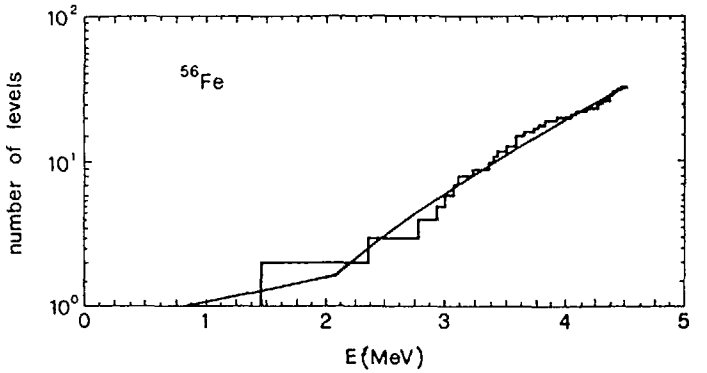

Fig. 4a- Comparison between the calculated level density of ^{56}Fe (solid line see eqs. (8-11) and Table I) and the observed levels /26/ up to E* = 4.5 MeV.

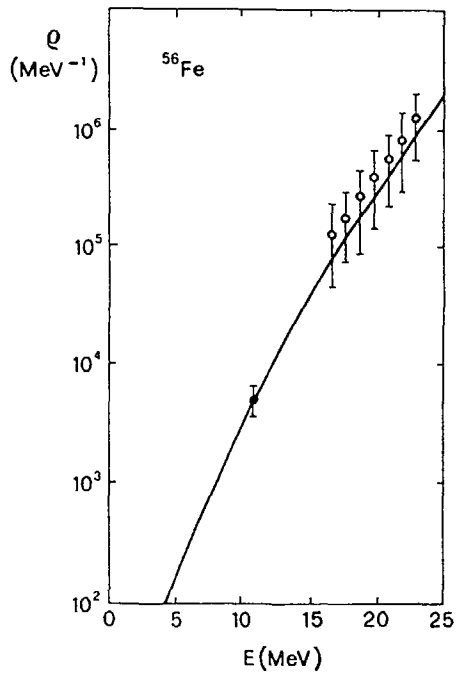

Fig. 4b- Level density of ^{56}Fe, solid line: calculated with parameters of Table I; experimental data from refs./27/ (•) and /28/ (o).

TABLE I. NUCLEAR LEVEL DENSITY PARAMETERS FOR IRON ISOTOPES

compound nucleus	B_n (MeV)	$\tilde{a}$ (MeV^{-1})	γ (MeV^{-1})	α (MeV^{-1})	<D>I=0 (keV) exp/29/	<D>I=0 (keV) calc.	<D>I=1 (keV) exp/29/	<D>I=1 (keV) calc.
53 Fe	10.684	6.57	0.45	0.20		4.6		1.05
54 Fe	13.379	4.70	0.31	0.14		3.9		1.2
55 Fe	9.299	6.06	0.25	0.16	13.+2.	15.0	4.4+0.2	2.5
56 Fe	11.197	5.64	0.64	0.16		4.7		1.4
57 Fe	7.646	7.04	0.32	0.17	17.+2.	17.4	4.0+0.4	2.5
58 Fe	10.044	6.27	0.81	0.19	6.0+1.	7.0	2.2+0.3	2.0
59 Fe	6.581	7.21	0.35	0.20	35.+15.	32.7	8.3+1.3	4.7

theoretical and experimental average level spacings for neutron s- and p-waves at the binding energies.

The parity dependence of nuclear level densities strongly affects nucleon cross section calculations. Fig.5 presents a comparison between $^{52}Cr(n, \gamma)$ cross sections calculated /30/ with and without inclusion of parity effects, all the other parameters in the statistical model being kept equal. Differences of 30-50% arise over the whole incident neutron energy range, even up to several MeV.

We conclude that parity effects in nuclear level densities must be taken into account, in order to perform reliable calculations of neutron cross sections, above all when measurements are not available as point of reference.

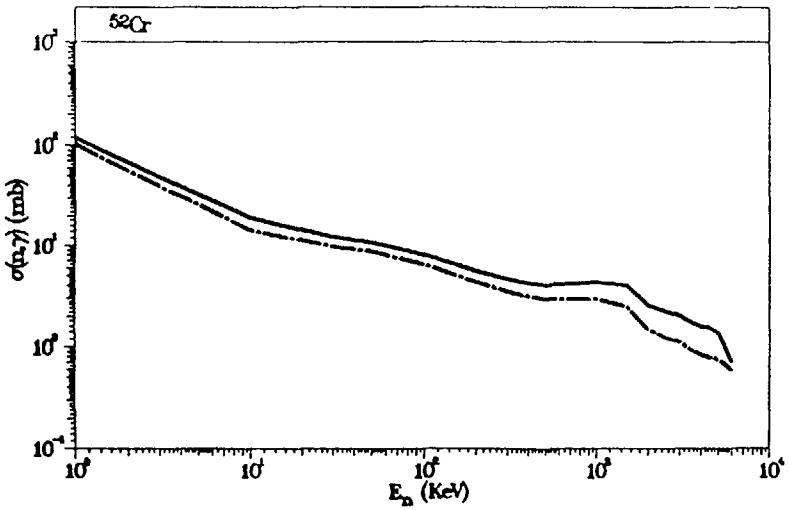

Fig. 5 - Neutron radiative capture cross section of ^{52}Cr calculated /30/ with the assumption of parity dependence in nuclear level densities (solid line) and with equiprobable parity distribution (dashed line).

A still open problem in nuclear level density has to be briefly discussed, i.e. the collective enhancement factors. All the previous quoted formalisms and calculations assume a spherical shape for the considered nuclei, without collective structure. The level density arises from single-particle configurations only. Really, we know that collective features in nuclear structure are important, even for light and medium mass nuclei in the neighbourhood of shell closures (see sect. 2.1). Therefore, one must include in level density expressions on enhancement factor to take into account collective patterns.

Bjørnholm, Bohr and Mottelson /31/ proposed simple formulae for deformed rotational nuclei (as in lanthanide and actinide regions) and spherical vibrational nuclei.

Their basic hypothesis implies that a collective, rotational or vibrational, band is built upon every single-particle nuclear configuration. This holds true for low energies but, with increasing excitation energies, the nucleus is getting to assume a spherical shape and collective contributions are vanishing. This behaviour is correctly reproduced in the approach by Hansen and Jensen /32/, who deal with the rotational enhancement for deformed nuclei, within the algebraic SU(3) model of Elliott /33/. In fact, a transition from axially deformed to spherical level density is found as a function of excitation energy.

An extension of this formalism to different kinds of collective motion (vibrational, γ-soft and triaxial nuclei, transitional shapes, etc.) would be highly desirable; the IBM could provide a natural and simple framework for such an extension, as proposed in ref./34/.

In conclusion, refined models of nuclear level density are essential tools in cross section calculations (see discussions in ref./30/ and papers quoted therein) and, furthermore, in the evaluation of photon production cross sections and, for instance, of contribution to the radiative cross section, σ_γ, arising from the (n, γn') reaction /35/:

$$\sigma_\gamma = \sigma_{n,\gamma} + \sigma_{n,m'} = \sigma_{n,\gamma} + \left(\frac{1-R}{R}\right)\sigma_{n,\gamma} = \frac{1}{R}\,\sigma_{n,\gamma} \,, \qquad (11)$$

where the fraction R of the primary gamma-ray distribution depends on the photon strength function and the relevant level density.

2.3 Giant resonances

Giant resonances are highly collective modes of nuclear excitation. Roughly speaking, they are based on strongly coherent particle-hole interactions in the shell-model language; in a liquid drop description they are made of shape vibrations or spin oscillations. The latter case, when nucleons with spin up and down,

respectively, move out of phase, corresponds to magnetic resonances. Moreover, when protons and neutrons oscillate in phase, the resonances have isoscalar character, otherwise isovector. In fig. 6, the lowest multipolarity resonances are pictorially shown (the monopole giant resonance E0, or "breathing mode", is not included). Giant resonances have been investigated by means of many probes, some of them are summarized in Table II.

For the first time, photoabsorption measurements allowed an identification of high-energy collective motion, the giant dipole resonance (GDR) (see ref./36/ for a review of GDR excitation in light nuclei). This

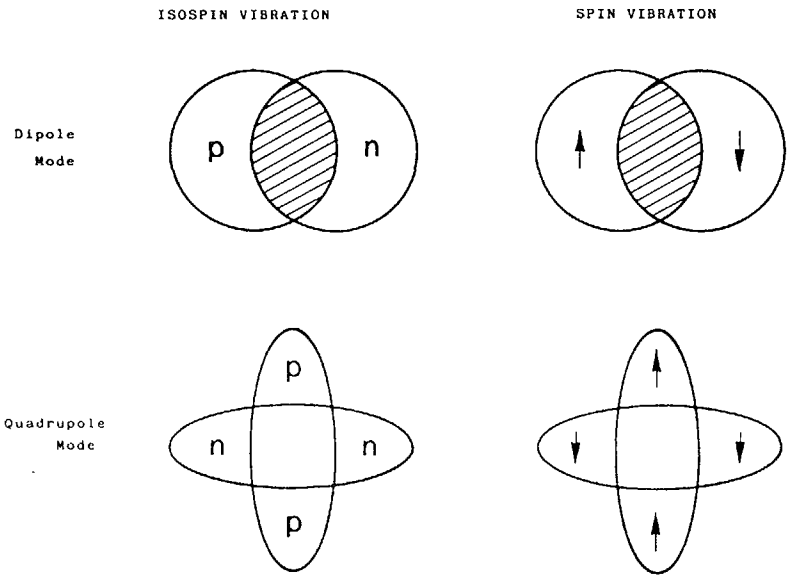

Fig. 6 - Pictorial representation of some collective modes in nuclei.

TABLE II. MAIN PROBES USED IN THE INVESTIGATION OF GIANT RESONANCES

GR	E0		E1	E2		>E2		M1		M2	
	(T=0)	(T=1)	(T=1)	(T=0)	(T=1)	(T=0)	(T=1)	(T=0)	(T=1)	(T=0)	(T=1)
(γ,γ')			×					×	×		
(γ,abs)			×	×	×						
(n,γ)			×	×	×	×	×	×	×		
(e,e')	×	×	×	×	×	×	×	×	×	×	×
(p,p')	×	×	×	×	×	×	×	×	×	×	×
(He, He')	×	×	×	×		×					
(α,α')	×				×		×				
heavy ion					×		×				
(p,n)								×	×	×	×
(π,π')								×	×	×	×

technique has been applied to the study of E2 giant resonances too. Moreover, investigation of subsequent GDR decay related to the coupling between GDR states and low-lying levels (collective, 2p-2h states, etc.) is useful to derive nuclear structure information; a typical well-known effect is the GDR fragmentation due to the coupling with the low-energy rotational motion. Another source of fragmentation lies in the different isospin components excited from the ground-state of nuclei with $T_o \neq 0$, whose nature is determined according to the isospin quantum numbers of final states populated by neutron and proton decays, respectively, of GDR states. A peculiar feature, that can be explained by a suitable fragmentation mechanism /13/, is the larger width of the second peak of GDR in deformed nuclei with respect to the first one at lower energy.

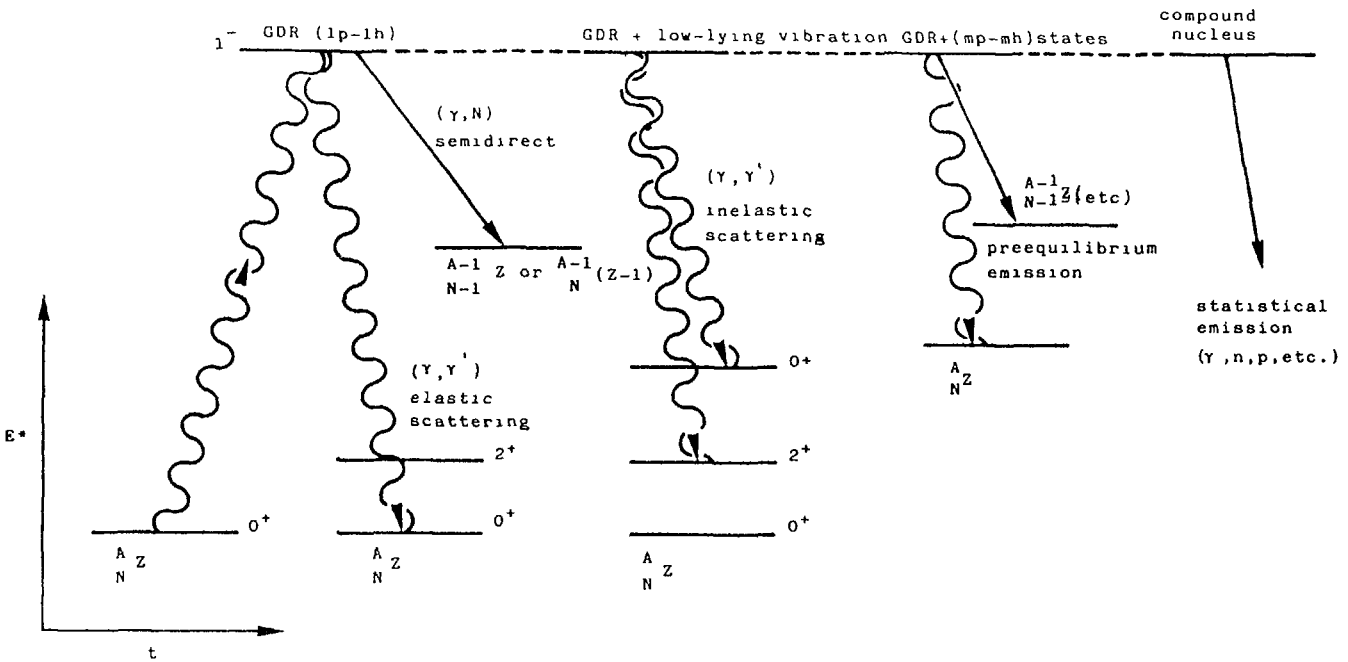

Fig. 7 - Sheme of possible decay processes following excitation of the giant dipole resonance (GDR) by photon absorption.

However, as outlined in sect.1, photon elastic and inelastic scattering reactions are particularly reliable in order to derive nuclear structure data from experiments and to check nuclear models. The nuclear structure information is contained in the Hamiltonian matrix elements between the initial, final and GDR excited states with angular momentum values I_i , I_f and I_n , respectively, by means of the definition of generalized polarizabilities, P_j , which are given by the following expression in the case of unpolarized photons and unoriented nuclei /37/:

$$P_j = \frac{4\pi}{3} \cdot \frac{E E'}{(\hbar c)^2} \sum_n \begin{Bmatrix} J & I_f & I_i \\ I_n & 1 & 1 \end{Bmatrix} \langle I_f \| \hat{D} \| I_n \rangle \langle I_n \| \hat{D} \| I_i \rangle$$

$$\times \left[\frac{1}{E_n + E' + \frac{\Gamma_n}{2}} + \frac{(-1)^j}{E_n - E - \frac{\Gamma_n}{2}} \right] + \delta_{if}\, \delta_{j0}\, (-1)^{2I_i} \sqrt{3(2I_i+1)}\, \frac{Z^2 e^2}{AMc^2} , \qquad (12)$$

where E (E') is the incident (emitted) photon energy, $\hat{D}$ the dipole operator, E_n and Γ_n , respectively, the energy and width associated to each fragmented GDR state and the summation runs over all GDR states. M is the nucleon mass, A and Z are, respectively, the

mass and charge numbers of target nucleus; the second term in the r.h.s. of eq.(12) accounts for the Thomson contribution in the elastic channel.

The photon scattering cross section is then given by:

$$\frac{d\sigma}{d\Omega} = \frac{1}{(2I_i+1)} \sum_{j=0}^{2} g_j \mid P_j \mid^2 , \qquad (13)$$

with

$$g_0(\theta) = (1/6)(1+ \cos^2\theta) ,$$
$$g_1(\theta) = (1/4)(1+ \sin^2\theta) , \qquad (14)$$
$$g_2(\theta) = (1/12)(13+ \cos^2\theta) .$$

Recent measurements of both elastic and inelastic photon scattering cross sections have been performed for medium weight nuclei /38,39/.

Analyses were carried out within the framework of the Dynamic Collective Model (DCM) /37/, that were able to reproduce many features. Recently, IBM has been extended to include GR degrees of freedom /12,14/ and proven to be an useful tool for investigating photon scattering experiments /13,42/. In particular, it seems to work better than DCM as for prediction of inelastic scattering cross sections are concerned /43,44/. Moreover, IBM, in its version IBM-3 /8/, provides a natural framework to discuss isospin effects on GDR fragmentation /45/.

A short digression is deserved to the determination of GR widths. The total GR width is substantially made by the addition of three contributions:

$$\Gamma = \Gamma_{coll} + \Gamma_{esc} + \Gamma_{damp} , \qquad (15)$$

where the first term, Γ_{coll} , takes into account the GR broadening due to the coupling with low-energy collective states and, therefore, is properly included in both DCM and IBM treatments. The escape width, Γ_{esc} , considers the GR decay to continuum states and is important for light and medium weight nuclei, above all.

The last contribution, Γ_{damp} , which is dominant in heavy nuclei, originates from the coupling between GR states (whose structure is essentially a coherent superposition of 1p-1h excitations) and 2p-2h or more complicated nuclear states.

A simple relation between the damping width and the level density of 2p-2h states, with right angular momentum and parity values at the GR excitation energy, is given by the Fermi golden rule:

$$\Gamma_{damp} = 2\pi\rho(2p\text{-}2h,\ J^{\pi}=1^{-},\ E_x) \overline{\langle 2p\text{-}2h \mid V \mid 1p\text{-}1h \rangle}_{(J^{\pi}=1^{-})} , \qquad (16)$$

where the matrix element represents an average interaction value. According to eq.(16), a comparison between experimental and calculated damping widths, by means of particle-hole level density formalisms, commonly used in preequilibrium reaction models, would be very interesting.

By matching experimental data and theoretical calculations, it is thus possible to derive detailed information on giant resonances, which in turn can be used for nucleon cross section estimates, for instance within the framework of direct-semidirect model of nucleon radiative capture. Conversely, analyses of measurements performed by means of the direct-semidirect model allow determination of GR shapes; in particular, the isovector quadrupole resonance may be observed from the experimental asymmetry in gamma-ray emission due to the interference with the high tail of GDR (see ref./46/ for a very recent work on this subject).

Detailed knowledge of giant resonance excitation functions is particularly useful for statistical model calculations of neutron cross section and photon production data, since the GR response of a nucleus to electromagnetic radiation and gamma-ray strength functions are related together by means of the Brink-Axel hypothesis. According to Brink's original idea, an identical resonance behaviour to that built on the nuclear ground-state is associated with each excited nuclear state. The gamma-ray strength function is then given by:

$$\frac{\langle \Gamma_\gamma(E) \rangle}{D_J} = \frac{1}{\pi^2 \lambda^2} \cdot \frac{1}{(2\Delta+1)} \langle \sigma_{\gamma\,abs}(E) \rangle \,, \qquad (17)$$

where D_J is the spacing of radiating states with spin J, λ is the absorbed photon wavelength and $\sigma_{\gamma\,abs}$ the absorption cross section for an incident photon with multipolarity Δ .

Many studies have been carried out to verify the validity of the Brink-Axel hypothesis, starting from the pioneering work by Axel, for E1/47,48/, E2/49/ and more recently M1/50/ transitions. Some discrepancies have been found that can be in part removed if one considers the energy dependence of the GR damping width, generally neglected in usual analyses based on eq.(17).

Investigation of the collective spin-flip M1 mode is a matter of current interest both from experimental and theoretical point of view. A favoured region for the existence of a M1 giant resonance comprises nuclei in the fp shell. In fact, in the scheme of simple shell model with independent particles, a collective M1 transition arises from a coherent $1f_{7/2}^{-1}\,1f_{5/2}$ particle-hole excitation. The M1 transition strength is then described by the following one-body operator (in units of $\sqrt{\frac{3}{4\pi}} \cdot \frac{e\hbar}{2Mc}$):

$$\hat{T}(M1) = \sum_{k=1}^{A} \left[g_l \hat{l}_k + g_s \hat{s}_k \right] = \sum_{\kappa=1}^{A} \left\{ \left[\frac{g_l}{2} \hat{l}_k + \frac{(g_p+g_n)}{2} s_k \right] - \left[\frac{g_l}{2} \hat{l}_k + \frac{(g_p-g_n)}{2} \hat{s}_k \right] t_{z_k} \right\} , \qquad (18)$$

where $\hat{l}_k$ and $\hat{s}_k$ are, respectively, the orbital angular momentum and spin operators associated with a single nucleon. $\hat{T}$ (M1) consists of an isoscalar and an isovector part, as evident from eq.(18), and is related to the Gamow-Teller strength function.

Really, in $^{48}Ca(e, e')$ experiments /51/ a M1 GR state, with quantum numbers $J^\pi = 1^+$, T = 4, has

been observed, However, as for other nuclei in the fp shell, like Cr, Ni and Fe isotopes, are concerned, the M1 GR appears to be largely fragmented and even suppressed from (p,n), (p,p') /52,53/, resonant photon scattering /54/ and (e,e') /3/ experiments.

This quenching of both M1 and Gamow-Teller resonances has been a challenge for theorists and various mechanisms have been invoked to explain it, as effects due to ground-state correlations, pion condensates, etc. One of most interesting possibilities lies in the removal of M1 strength to higher excitation energies by means of virtual Δ (1232)-hole excitations. In this respect, low-energy nuclear physics deserves a renewed interest as a source of information in elucidating structure and reaction mechanisms typical of intermediate-energy ranges and the rôle played by mesonic and baryonic degrees of freedom in nuclear matter.

3. Conclusions

Aim of this review is to outline the importance of reliable nuclear structure information in order to perform cross-section calculations. Particular emphasis has been paid to the strong interplay between structure features and reaction mechanisms. For instance, the usual neutron scattering coupled-channel calculations have been found very sensitive to the coupling to isoscalar giant resonances /55/ Other examples have been presented in section 2 Therefore, in the evaluation work, one is forced to take into account even most improved models of nuclear structure, also in order to check the reaction models and codes commonly adopted /56/. In figs (8-11), we show results of calculations for ^{56}Fe (n, γ) and (n, n'γ) reactions and related gamma-ray spectra, obtained by starting from nuclear structure data discussed in section 2. These are preliminary results of an evaluation for all stable Fe isotopes, presently undertaken at Nuclear Data and Codes Laboratory in Bologna. Similar results for Cr isotopes have been presented in refs. /30, 56, 57/. Finally, we must note that other degrees of freedom than nucleonic ones are also present in low-energy nuclear physics (sect 2 3) and cannot be neglected in a consistent treatment of reaction mechanisms.

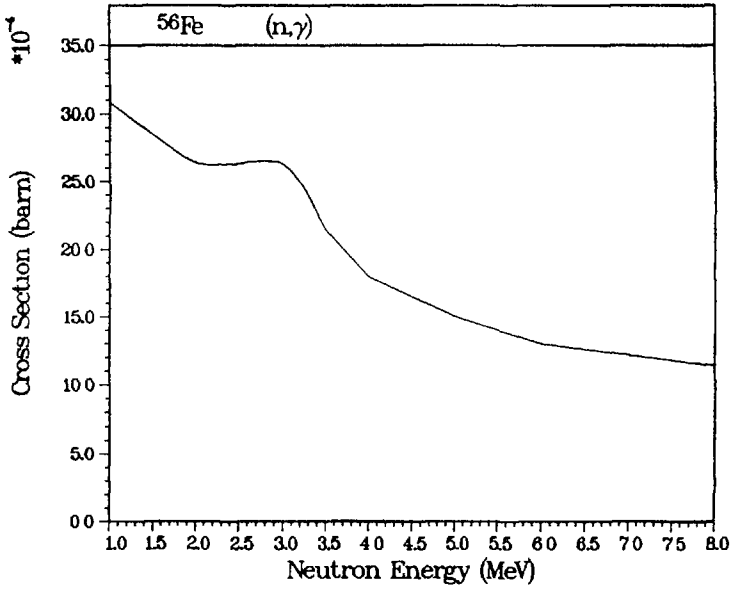

Fig. 8 - Calculated neutron capture cross section of ^{56}Fe.

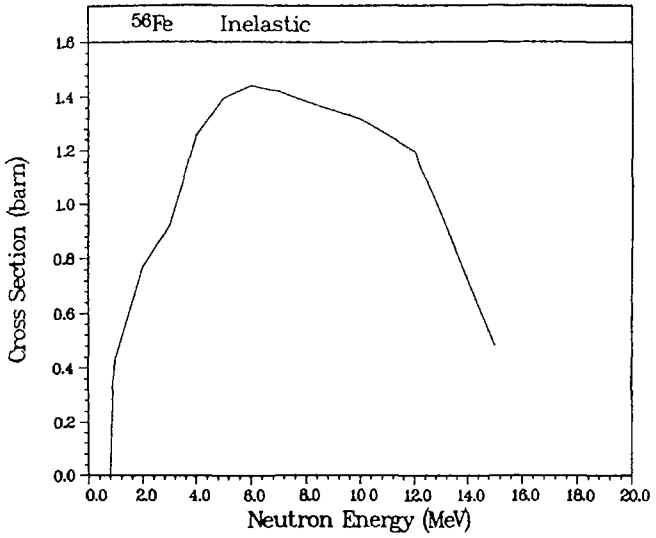

Fig. 9 - Calculated neutron inelastic scattering cross section of ^{56}Fe.

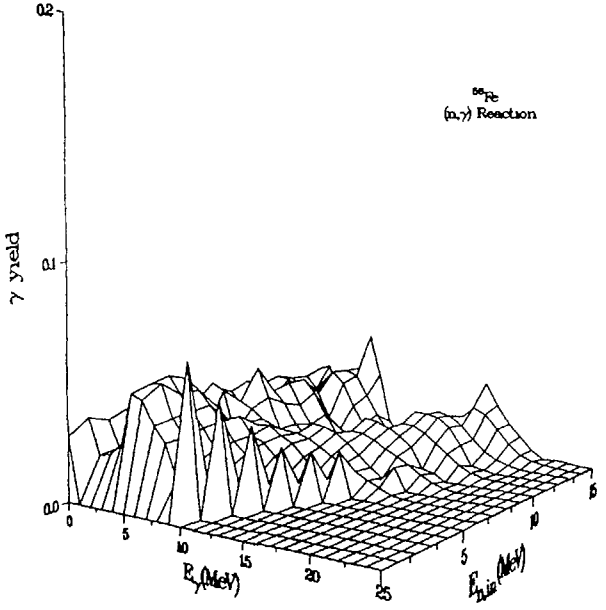

Fig.10 - Calculated spectrum of photons produced in ^{56}Fe (n, γ)reaction versus both incident neutron and emitted photon energies.

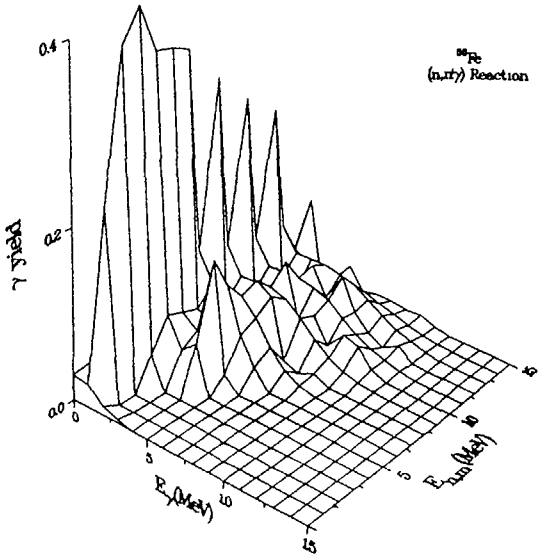

Fig. 11 - Calculated spectrum of photons produced in ^{56}Fe (n, n' γ) reaction versus both incident neutron and emitted photon energies.

REFERENCES

1. R. Vennink and P.W.M. Glaudemans, Z. für Phys. A. 294 241 (1980).

2. J.B. McGrory and B.H. Wildenthal, Phys. Lett. 103B, 173 (1981).

3. D.I. Sober, B.C. Metsch, W. Knüpfer, G. Eulenberg, W. Küchler, A. Richter, E. Spamer and W. Steffen, Phys. Rev. C31, 2054 (1985).

4. C.M. Lederer and V.S. Shirley (eds.), "Table of Isotopes", 7th ed., New York (1978).

5. A.Arima and F. Iachello, Ann. Rev. Nucl. Part. Sci. 31, 75 (1981).

6. H. Feshbach and F. Iachello, Ann. Phys. (N.Y.) 84, 211 (1974).

7. F. Iachello and S. Bastiani, Nucl. Phys. A228, 356 (1974).

8. J.P. Elliott, Rep. Progr. Phys. 48, 171 (1985).

9. P. Halse, J.P. Elliott and J.A. Evans, Nucl. Phys. A 417, 301 (1984).

10. T. Horibata and K. Taruishi, Phys. Rev. C33, 1496 (1986).

11. P. Park and J.P. Elliott, Nucl. Phys. A448, 381 (1986).

12. D.J. Rowe and F. Iachello, Phys. Lett. 130B, 231 (1983).

13. G. Maino, A. Ventura, L. Zuffi and F. Iachello, Phys. Rev. C30, 2101 (1984) and Phys. Lett. 152B, 17 (1985).

14. G. Maino, A. Ventura, P. Van Isacker and L. Zuffi, Europhys. Lett. 2, 345 (1986).

15. D. Bohle, A. Richter, W. Steffen, A.E.L. Dieperink, N. LoIudice, F. Palumbo and O. Scholten, Phys. Lett. 137B, 27 (1984).

16. U.E.P. Berg, C. Bläsing, J. Drexler, R.D. Heil, U. Kneissel, W. Naatz, R. Ratzek, S. Schennach, R.Stock, T. Weber, H. Wickert, B. Fischer, H. Hollick and D. Kollewe, Phys. Lett.149B, 59 (1984).

17. N. LoIudice and F. Palumbo, Phys. Rev. Lett.41, 1532 (1978) and Nucl. Phys. A326, 193 (1979).

18. F. Iachello, Phys. Rev. Lett.53, 1427 (1984).

19. A.V. Ignatyuk, "Statistical Properties of Excited Atomic Nuclei", chapt. 1-3, engl. transl. in report I.N.D.C. (CCP) - 223/L (I.A.E.A., Vienna, 1985).

20. G. Maino, E. Menapace and A. Ventura, Nuovo Cim. A57, 427 (1980).

21. A. I. Blokhin and A. V. Ignatyuk, Sov. J. Nucl. Phys. 23, 31 (1976).

22. G. Maino and A. Ventura, Lett. Nuovo Cim. 37, 561 (1983) and Comp. Phys. Comm. 43, 303 (1987).

23. H. M. Agrawal, J.B. Garg and J.A. Harvey, Phys. Rev. C30,1880 (1984).

24. G. Maino, Phys. Rev. C35, 1598 (1987).

25. G. Maino and E. Menapace, Radiat. Effects 95, 1135 (1986).

26. Huo Junde, Hu Dailing, Zhou Chunmei, Han Xiaoling, Hu Baohua and Wu Yaodong, Nucl. Data Sheets 51, 1 (1987).

27. R. Fischer, G. Traxler, M. Uhl and H. Vonach, Phys. Rev. C30, 72 (1984).

28. J.R. Huizenga, H.K. Vonach, A.A. Katsanos, A. J. Gorski and C. J. Stephan, Phys. Rev.182, 1149 (1969).

29. S.F. Mughabghab, M. Divadeenam and N.E. Holden, "Neutron Cross Sections", vol.1, part. A, New York (1981).

30. A. Mengoni, F. Fabbri and G. Maino, Nuovo Cim. 94A, 297 (1986).

31. S. Bjørnholm, A. Bohr and B.R. Mottelson, in Proceed. of the 3rd Int. Symp. on the Physics and Chemistry of Fission, Rochester (1973), vol. I, p.367.

32. G. Hansen and A.S. Jensen, Nucl. Phys. A406, 236 (1983).

33. J.P. Elliott, Proc. Roy. Soc. A245, 128 (1958).

34. G. Maino and A. Ventura, in Proceed. of the Int. Conf. on Nuclear Physics, Florence (1983), vol.1, p.83.

35. S. Joly, Nucl. Sci. Eng.94, 94 (1986).

36. R.A. Eramzhyan , B.S. Ishkhanov, I.M. Kapitonov and V.G. Neudatchin, Phys. Rep. C136, 229 (1986).

37. W. Greiner and J. Eisenberg, "Nuclear theory", vol.1, Amsterdam (1975).

38. T.J. Bowles, R. J. Holt, H.E. Jackson, R.M. Laszewski, R.D. McKeown, A.M. Nathan and J.R. Specht, Phys. Rev. C24, 1940 (1981).

39. A.S. Alimov and I.M. Piskarev, Sov. J. Nucl. Phys.39, 676 (1984).

40. H. Arenhövel and H.J. Weber, Nucl. Phys. A91, 145 (1967).

41. H. Arenhöve and J.M. Maison. Nucl. Phys. A147, 305 (1970).

42. G. Maino, A. Ventura, P. Van Isacker and L. Zuffi, Phys. Rev. C33, 1089 (1986).

43. F.G. Scholtz and F.J.W. Hahne, Phys. Lett. 123B, 147 (1983).

44. A.M. Nathan, in Proceed. of Int. Conf. on Nuclear Structure, Reactions and Symmetries, Dubrovnik (1986), R.A. Meyer and V. Paar, eds., vol.1, p.385.

45. G. Maino, to be published.

46. R. Zorro, I. Bergqvist, S. Crona, A. Håkansson, A. Likar, A. Lindholm, L. Nilsson and N. Olsson, to be published in Nucl. Phys.

47. C.M. McCullagh, M.L. Stelts and R.E. Chrien, Phys. Rev. C23, 1394 (1981).

48. S. Raman, O. Shahal and G.G. Slaughter, Phys. Rev. C23, 2794 (1981).

49. W.V. Prestwich, M.A. Islam, and T.J. Kennett, Z. für Phys. A315, 103 (1984).

50. J. Kopecky and R.E. Chrien, to be published in Nucl. Phys.

51. A. Richter, Nucl. Phys. A374, 177c (1982).

52. C. Gaarde, Nucl. Phys. A396, 127c (1983).

53. J. Rapaport, T. Taddeucci, T.P. Welch, C. Gaarde, J. Larsen, D.J. Horen, E. Sugarbaker, P. Koncz, C.C. Foster, C.D. Goodman, C.A. Goulding and T. Masterson, Nucl. Phys. A410, 371 (1983).

54. T. Chapuran, R. Starr, R. Vodhanel and M.K. Brussel, Phys. Rev. C30, 54 (1984).

55. J.P. Delaroche, P.P. Guss, C.E. Floyd, R.L. Walter and W. Tornow, Phys. Rev. C27, 2385 (1983).

56. A. Mengoni, F. Fabbri and G. Maino, in Proceed. 6th Int. Symp. on Gamma-Ray Spectroscopy and Related Topics, Leuven (1987).

57. A. Mengoni, F. Fabbri and G. Maino, ENEA report RT/TIB/85/38, Rome (1985).

UNIFIED MODEL OF (n,γ) REACTION AND CALCULATIONS OF NEUTRON INDUCED PHOTON PRODUCTION DATA

Yukun HO
Nuclear Science Department,
Fudan University,
Shanghai

Jingfeng LIU
Physics Department,
Zhengzhou University,
Henan Province

China

Abstract

The mechanism of radiative neutron capture reaction is classified and reviewed accordingly to the hierarchy of quasi-particle number in the excited configurations. An unified model to calculate (n,γ) cross sections is studied. Underlain by the model, a computer code to calculate neutron induced photon production data has been developed. Some results by using this program are illustrated and compared with measured data.

The mechanism of radiative neutron capture reaction is classified and reviewed according to the hierarchy of quasiparticle number in the excited configurations (figure 1, A: potential capture; B: valence capture; C: interference between potential and valence capture; D: radiative capture in compound elastic scattering channels; E: semidirect capture; F: annihilation of 3Q(2p1h) configurations; G: inelastic valence capture; H: radiative capture in compound inelastic channels; I: compound nucleus process (statistical model)). For each process, the following questions are discussed: physical significance, schematic representation, calculational formula, test of characteristics that distinguish the mechanism, comparison of theory with data, and remaining problems. Basing on these analyses, an unified model to calculate (n,γ) cross sections is being studied. Underlain by the model, a computer code to calculate neutron induced photon production data has been developed, including also contributions from cascade decay of residual nucleus via other reactions by statistical model. Some results by using this program are illustrated and compared with measured data. Due to limitation in space this paper can only contain headlines of the analyses, model and code.

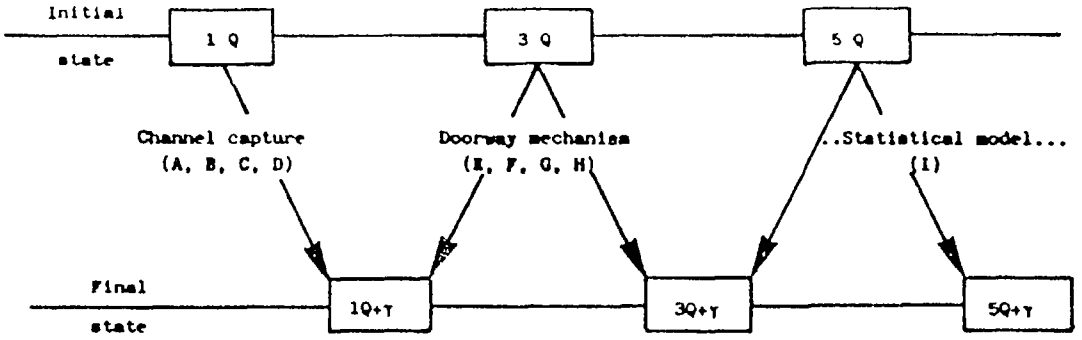

FIG.1.

1. TRANSITIONS FROM ONE-QUASIPARTICLE CONFIGURATIONS - CHANNEL CAPTURE

1.1 Channel wave function and channel capture cross section

$$U^{+J}_{\ell j}(r) = \mathrm{Re}\langle U^{+J}_{\ell j}\rangle + \frac{1}{2}\sum_{\lambda(J)} \frac{\Gamma^{\ell j}_{n\lambda}}{E_\lambda - E - \frac{1}{2}\Gamma_\lambda} \frac{\mathrm{Im}\langle U^{+J}_{\ell j}(r)\rangle}{\mathrm{Im}\langle K^{J}_{\ell j}\rangle} , \qquad (1)$$

$$\sigma^{ch}_{\ell j, f} = \frac{4}{3}\frac{k_\gamma^3}{\hbar v}\frac{\pi}{k^2}\sum_J \frac{(2J+1)}{2(2I+1)} \langle \ell j J \| D_1 \| \ell_f j_f J_f\rangle^2 \qquad (2)$$

$$(2J_f+1)S_f \frac{4}{|1-\mathrm{i}\,K^J_{\ell j}|^2}\left|\int_R r\, U^{+J}_{\ell j}(r)\, U_{\ell_f j_f}(r)\,dr\right|^2$$

1.2 Potential capture

A. The schematic representation is as plotted in fig. 2-a.

B. Calculational formula.

C. Tests to identify the characteristics of the mechanism.

- Check the final state correlation outside the resonances $\sigma^{po}_{\ell j,f} \propto S_f$).
- Check the linear dependence of $\sigma^{po}_{\ell j,f} \propto E_\gamma$.
- compare the magnitudes of measured and predicted partial capture cross sections.
- Observe the interference effect between potential and valence capture in (γ,n) and (n,γ) reactions.

D. Points to be cleared up.

- Look for a global optical model potential.
- The controversyon testing the relation $\sigma^{po}_{\ell j,f} \propto E_\gamma$.
- The controversyon using a square well.

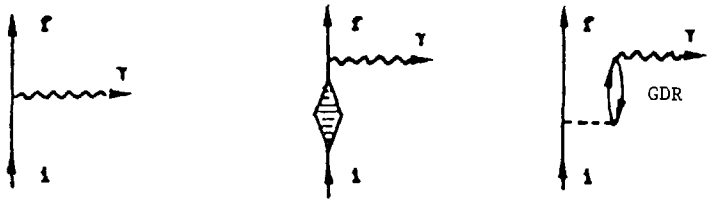

FIG.2. Schematic representations of the potential capture (a), the radiative capture in the compound nucleus elastic scattering channel (b) (the vertex designates the formation of compound nucleus) and the semi-direct capture (c) (the dash line refers to the nucleon–nucleon coupling).

1.3 Valence capture

A. Physical significance: contribution to the resonance capture from the entrance channel configuration.

B. Calculational formula:

$$\Gamma^{v}_{\lambda\gamma f} = \frac{4}{3}\frac{k_\gamma^3}{\hbar v}\,\langle \ell_J J|D_1|\ell_f j_f J_f\rangle\,(2J_f+1)\,S_f\,\bar{e}^2 \qquad (3)$$
$$\frac{1}{|1-i\langle K^J_{\ell j}\rangle|^2}\left[\frac{\int_R^\infty r\,\mathrm{Im}\langle U^{+J}_{\ell j}(r)\rangle\,U_{\ell_f J_f}(r)\,dr}{\mathrm{Im}\langle K^J_{\ell j}\rangle}\right]^2 \Gamma^{\ell J}_{\lambda n}$$

C. Tests to identify the characteristics of the mechanism.
- Check the initial and final state correlation
- Compare the magnitudes of the measured and predicted partial radiative widths.
- Check the gamma-ray energy dependence $(\Gamma^{v}_{\lambda\gamma f} \sim E_\gamma^2)$.
- Observe the interference effect between valence and potential capture.

D. Remaining problems.
- Some examples for which the model fails to reproduce the data.
- Systematic discrepancy between model-predicted and data in the 3p and 4s region.
- controversy on the existence of non-statistical effect in the 4S region.
- "Maverick transition" of EI effective charge and "silent majority".
- Explain the observed alternative correlations.

1.4 Interference effect between potential and valence capture

A. Calculational formula

$$\sigma^{ch}_{0^+,f} = \sigma^{po}_{0^+,f}\left[1-\frac{(a^J-R')k\int_R^\infty r\,N_{0^+}(r)\,U_{\ell_f J_f}(r)\,dr}{\int_R^\infty r\,\mathrm{Re}\langle U^{+J}_{0^+}(r)\rangle U_{\ell_f j_f}(r)\,dr}\right]^2. \qquad (4)$$

B. Constructive and destructive interference and examples.

1-5 Resonance-averaged channel capture cross sections

A. Calculational formula

$$\langle\sigma_f^{ch}\rangle = \frac{4}{3}\frac{k_\gamma^3}{\hbar v}\frac{\pi}{k^2}\sum_{\ell J}\frac{(2J+1)}{2(2I+1)}\,\langle \ell J\|D_1\|\ell_f J_f J_f\rangle\cdot \qquad (5)$$
$$(2J_f+1)\,S_f\,\bar{e}^2\,(R^{J(B)}_{\ell J\ell_f J_f}+R^{J(V)}_{\ell J\ell_f J_f}+R^{J(C)}_{\ell J\ell_f J_f}).$$

B. Physical significance: the sum of the first two terms is a direct capture of the shape elastic scattering wave, the third is a radiative capture in the compound elastic channel (fig. 2-b).

C. Some preliminary results.
- The fluctuation term (the third one) is the dominant one at $E_n < 1$MeV.
- The fraction of $\langle\sigma_f^{ch}\rangle$ in the total capture cross section.

2. TRANSITIONS FROM THREE QUASIPARTICLE CONFIGURATIONS - DOORWAY MECHANISM

2.1 Formalism

A. The general formalism by Lane.

B. The quasiparticle-phonon model by Soloviev.

2.2 Semidirect capture

A. The schematic representation is as plotted in fig. 2-c.

B. Calculational formula

$$\sigma^{DSD}_{1J,f} = \frac{4}{3}\frac{k_\gamma^3}{\hbar v}\frac{\pi}{k^2}\sum_J\frac{2J+1}{2(2I+1)}\,\langle 1J\|D_1\|1_f J_f J_f\rangle \qquad (6)$$
$$(2J_f+1)\,S_f\,\bar{e}^2\,|T_D+T_{SD}|^2\ ,$$

where T_D and T_{SD} are the direct and semidirect capture amplitudes, respectively.

C. Tests to identify the characteristics of the mechanism.
- The giant resonance structure in gamma-ray yield curves.
- The structure $(\sigma^{DSD} \sim S_f)$ in gamma-ray spectrum.
- Systematic comparison in wide ranges of energy for various projectiles.

D. Remaining problems.
- give reasonable explanations of the complex particle-phonon coupling function and the magnitude of its imaginary part.
- Some examples for which the model fails to reproduce the data.
- Giant E2 and MI resonances and their contributions.

2.3 Annihilation of 3Q(2p1h) configurations

A. Possible candidates.
- Resonance capture exhibiting modest S_f but a low fraction of $\Gamma^{v}_{\lambda\gamma f}$.
- common doorways for p-wave neutron strength and MI radiative strength in Pb isotopes.
- The correlation between MI and EI partial radiative strengths in some nuclei such as Cl and Fe isotopes.
- The 5.5 MeV pigmy resonance.

B. Open problems.
- The distribution of 3Q configuration fragments.
- The characteristics to identify contributions from 3q configurations.

2.4 Inelastic valence capture.

2.5 Resonance-averaged inelastic channel capture

A. Physical significance: radiative capture in the compound inelastic scattering channels.

B. calculational formula

$$\langle \sigma_f^{ich} \rangle = \frac{\pi}{k^2} \sum_{\ell j J \ell' j'} \frac{(2J+1)}{2(2I+1)} \frac{T_{\alpha \ell j} T^J_{f,\beta \ell' j'}}{T^{J\pi}} W^{J\pi}_{\alpha \ell j \beta \ell' j'} \quad (7)$$

where $T^J_{f,\beta\ell'j'}$ is the radiative transmission coefficient in the compound inelastic scattering channel.

C. Open problems: the way to calculate $T^J_{f,\beta\ell'j'}$ and S_f' - the spectroscopic factor in the inelastic channel.

D. Preliminary results.

3 TRANSITIONS FROM 5Q AND ABOVE 5Q CONFIGURATIONS, STATISTICAL MODEL

3.1 Basic assumptions and calculational formula of the statistical model.

3.2 Distribution of EI and MI strength function.

3.3 Distribution of EI and MI partial radiative widths - verification of Porter-Thomas rule

3.4 Brink-Axel postulate and its verification.

3.5 Resonance-averaged spectroscopy.

4 CALCULATIONS OF NEUTRON INDUCED PHOTON PRODUCTION DATA

Based on the analyses above, a model code to calculate neutron induced gamma-ray production data, including gamma-ray production cross section, photon multiplicities, photon energy spectra as well as reaction and level cross sections, has been developed in China. These data are needed in many applications such as gamma-ray heating calculations for reactors, weapon effect predictions, material damage estimates and shielding design calculations. In addition to multi-step Hauser-Feshbach model, the principle feature of this program is that a special attention has been paid to the calculations of non-statistical processes in radiative capture reaction, which mainly produce higher energy gamma ray. As we know the higher energy component of photon is crucially important for photon transportation, shielding calculations and damage estimates.

In this code, the full energy range is divided into two regions. At higher energy region, specifically MeV region of neutron incident energy and dense discrete resonance region where average over incident energy is meaningful, the code provides resonance-averaged reaction cross sections and photon production data. Four processes are expected to contribute to the radiative neutron capture cross section in this energy region, namely compound nucleus cascade de-excitation, radiative capture in compound elastic and inelastic channel, and direct-semidirect capture. Multistep Hauser-Feshbach model and statistical cascade de-excitation model are used to calculate the initial populations of compound nucleus at each step and de-excitation of residual nucleus other than radiative capture reactions. At lower neutron incident energy, e.g. the region below the first resolved resonance or where an effective resonance average can not be performed, three processes are taken into account in the code to calculate radiative capture cross sections, i.e. cascade de-excitation of compound nucleus, potential and valence capture. The interference effect between the last two terms are explicitely included.

The Troubetzkoy's formalism are used to calculate cascade de-excitation of compound nucleus by emission of gamma-ray, where angular momentum and parity effect are taken into account. This code accepts the Becchetti-Greenless global optical model to provide particle transmission coefficients and Brink-Axel giant dipole resonance model to calculate gamma-ray transmission coefficients. The level density expressions are those of Gilbert-Cameron with the pairing and shell parameters of Cook.

This code has been used to provide systematic data set, and the following are a number of examples.

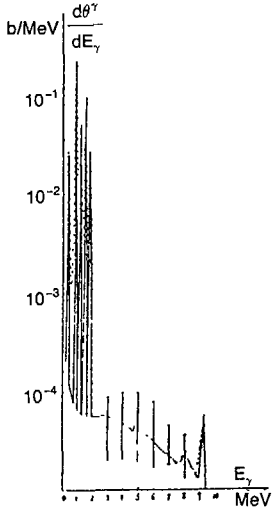

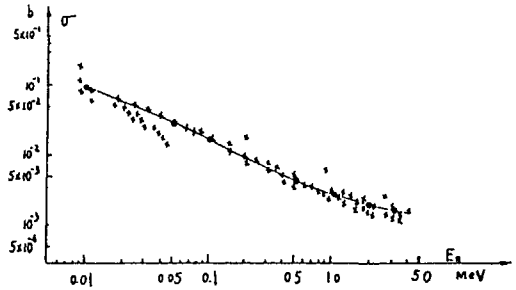

FIG.3. Cross-sections and gamma ray energy spectrum (θ = 125), ^{55}Mn (n,r).

——— Calculated ,

---- ϕ × Measured .

PRE-COMPOUND NUCLEAR THEORY

(Session IV)

RECENT DEVELOPMENTS AND APPLICATIONS FOR PRECOMPOUND NUCLEAR THEORY

M. BLANN
Physics Department,
Lawrence Livermore National Laboratory,
Livermore, California,
United States of America

Abstract

New considerations on consistent effective level densities for precompound decay are reviewed and tested for the hybrid model formulation. The importance of using realistic single particle levels for few quasi-particle densities is illustrated via (p,n) reactions on four Zr isotope targets. Some review is given of combinations of precompound plus Hauser-Feshbach approaches. The status of semi-classical and quantal approaches to calculating angular distributions is also discussed. We present comparisons of experimental and calculated angular distributions, particle spectra and excitation functions for reactions with nucleons and heavy ions up to and beyond 100 MeV, as examples of data being requested by modern technology.

1. INTRODUCTION

The goal of this presentation is to enumerate active areas of development in precompound decay theory as they apply to nuclear data evaluation, and new areas of application of both new and presently used precompound decay theory. The latter represent extrapolations to higher energy data and for a broader range of projectiles.

We are all familiar with reactor applications of nuclear data, and that is the main reason we are here. But medicine and industrial technology have started to request nuclear data covering a broader range of incident energies and projectile mass. Medical applications require knowledge of reactions of energetic charged particles which will optimize production of a given radioisotope while keeping production of undesireable isotopes at an acceptable minimum. Knowledge is also sought of reactions of very energetic heavy ions for direct therapeutic purposes.

There is a rapidly growing interest in medium energy proton induced reactions. Much of this comes from the microelectronics industry. A single cosmic ray may cause a memory bit to change polarity (a 'single event upset'). Components become inoperable due to prolonged radiation. Satellites and space shuttles may become activated; knowledge of relevant nuclear reactions permits choice of materials to minimize activation.

Our colleagues in basic research are becoming increasingly interested in medium energy hadron reaction data; design of calorimeters for research with relativistic heavy ion beams requires knowledge of interaction cross sections for the resulting hadron showers. The IAEA is already active in providing information in some of these areas. IAEA and many of us present here are likely to become more active in these broader areas in the near and medium term future.

I would first like to discuss recent developments in the very important area of partial state densities used in preequilibrium decay models.[1,2] Recent work suggests that Ericson type expressions[3,4] are inconsistent to use beyond the first term in the exciton summation. Next on this topic I would discuss the importance of replacing equidistant single particle levels with shell model levels when working with nuclei near shell closures. I shall discuss $\rho_n(E)$ based on shell model single particle levels; Reffo will discuss the more general case of $\rho_n(E,J)$.

Secondly, I would like to introduce the topic of angular distributions and mention semi-classical and quantal approaches. This is an area which I think is under active development, from which fruitful results as a reliable predictive tool may still be off in the future. We will hear more about this from experts in talks 4.3 and 4.4 later in this session; I shall give my less knowledgeable impressions.

A topic which has received and is receiving much attention is the 'unified precompound-compound' decay model. We have several present among our hosts who are working on this interesting problem, and Dr. Gruppelaar will summarize the status of this approach; I shall defer to the next talk (4.2) on this subject.

Finally, I would like to mention the challenge of extending our horizons and our modelling codes to reactions induced at projectile energies in excess of the 20 MeV reactor neutron energy limit. I shall present examples of some code intercomparisons and code vs. experimental data comparisons in this regime. Then I shall summarize some of those areas which I believe to be fertile ground for future developments.

2. PARTIAL STATE DENSITIES

2.1 Consistent equidistant spacing results

Precompound decay models assume populations of sequentially excited configurations denoted by exciton numbers from some initial value n_o to some final value, e.g., n. A second assumption is that transitions between (and within) exciton configurations proceed via 2-body (nucleon-nucleon) collisions.[1,2] It was shown by Blann et al that the 3 quasiparticle state density of Ericson could be derived (to within 20%) as the consequence of the cascade initiated by the projectile on the Fermi gas distribution of target nucleons.[5] Given that the transition to the next hierarchy results from a two-body process from

$$N_n(E) = \frac{(gE)^2}{2!1!2!} \qquad (1)$$

equally likely partitions of energy, the question Bisplinghoff[6] (and in a more formal context, Weidenmuller[7]) raised is whether or not the Ericson 5-exciton density represents the population of the next hierarchy of configurations, as has been assumed in nearly all hybrid/exciton model formulations to date.

We may use the three exciton populations to estimate the number of excitons at each energy ϵ above the Fermi energy,

$$N(\epsilon)d\epsilon = \frac{N_{n-1}(E-\epsilon)}{N_n(E)} = \frac{\rho_{n-1}(E-\epsilon)}{\rho_n(E)} \quad . \qquad (2)$$

We can use this number of 'projectiles' to weight the three exciton configuration resulting from this mini-cascade, since it has been shown that the three exciton result is valid for the two body process. Then we can sum (integrate) over all the mini-cascades which will populate a particular final nucleon excitation.

The above describes the process followed by Bisplinghoff, for both the hybrid and exciton model approaches. Results may be found in his article and are not repeated here.[6] Bisplinghoff found that in neither case did the Ericson 5 exciton density result. The consistent formulation of Bisplinghoff has been applied within the framework of the hybrid model. One result is shown in Fig. 1 for the ^{93}Nb(n, n') spectrum.[8] No significant change in the angle integrated spectrum results, but note that the contribution of the n=5 term changes by a factor of 2. This would affect e.g. the calculated angular distribution at back angles. This effect may well be greater in the exciton formulation, and it should be tested. Here we definitely have a new development deserving further work!

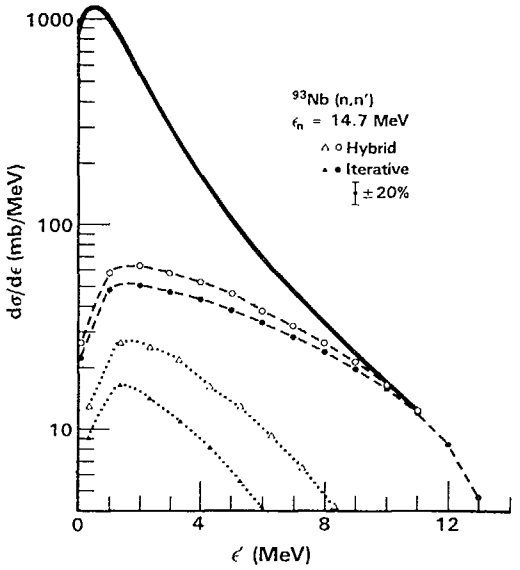

Figure 1. Calculated ^{93}Nb(n,n') spectra for 14 MeV incident neutron energy. The dashed curves connecting open circles represent the sum of the first two exciton hierarchy contributions in the hybrid model formulation. The dotted curve connecting open triangles represents the contribution of the second exciton hierarchy. The solid line shows the result when the equilibrium contribution is added; it is only shown where the sum of evaporation plus precompound significantly exceeds the precompound only contribution. An error bar of ±20% is shown to gauge the significance of the difference between the two sets of calculated results. Curves connecting closed circles and triangles represent the use of Bisplinghoff's approach.

2.2 Realistic Partial State Densities

For highly deformed nuclei and for mid-shell nuclei, the average spacing of single particle levels, and the fluctuation about this average supports the use of partial state densities of the type given by Ericson[3] and Williams.[4]

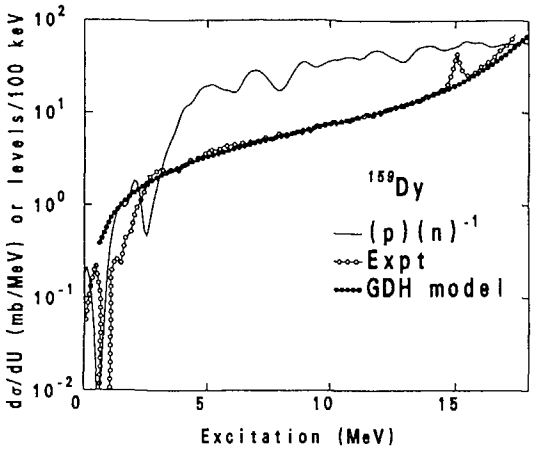

Figure 2. Calculated and experimental spectra for the reaction ^{159}Tb(p,n) with 25 MeV incident protons. The solid curve is the (1p,) (1n)$^{-1}$ two quasi particle density for ^{159}Dy with δ = 0.31 plotted as levels per 100 keV. Open points joined by line segments are the experimental angle integrated spectrum. The dashed curve is the result of the geometry dependent hybrid model (GDH). The GDH and experimental results are plotted as mb/MeV vs residual excitation.

An example of an experimental and calculated (p, n) spectrum on a deformed rare earth target is shown in Fig. 2, and it may be seen that, as expected, the precompound decay calculation using equidistant model level densities gives an excellent result.[9]

In Fig. 3 we show a shell model level spacing scheme for four Zr target isotopes.[9,10] If we consider (p,n) reactions, it is clear that there is a high probability of making a ground state transition with the ^{90}Zr target, and a very much smaller one for the ^{91}Zr target-due to the lone neutron leading to the ground state in the latter case. We further would expect a 3-4 MeV gap between ground and excited states for the ^{91}Zr target; in short, we expect shell structure effects to strongly influence the precompound spectra in this sequence of target isotopes. That this is the case may be seen in Fig. 4, where we compare experimental spectra on four Zr targets with precompound calculations using Ericson-Williams partial state densities. The discrepancies for the highest neutron energies are qualitatively in agreement with considerations based on the shell model scheme in Fig. 3.

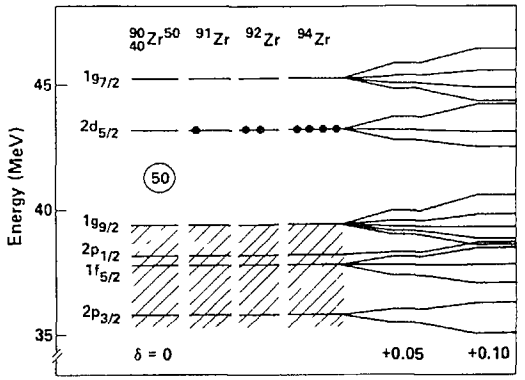

Figure 3. Schematic diagram showing single particle levels for Zr isotopes using the Seeger-Howard single particle spacings. Deformation parameters of δ = 0, +0.05, and +0.1 are shown. Occupation of the $2d_{5/2}$ levels by neutrons is indicated by solid circles. This figure is from Ref. 9.

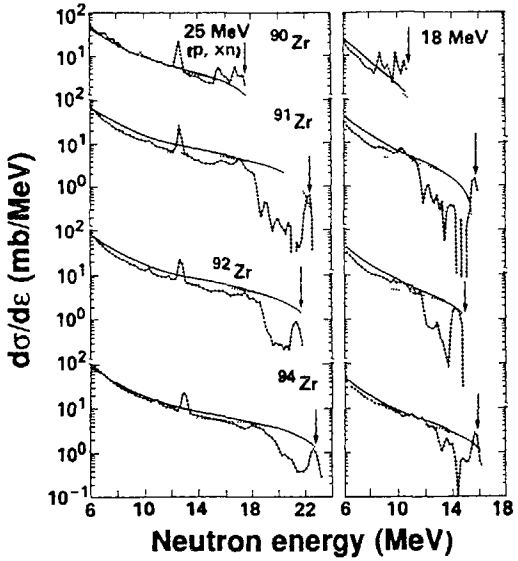

Figure 4. Calculated and experimental (p,xn) spectra for proton energies of 18 and 25 MeV on targets of ^{90,91,92,94}Zr. Solid points represent the experimental angle integrated data corrected for background and for isotopic impurities. The solid curves are results of the geometry dependent hybrid model plus evaporation model calculations. The dotted curves are the contribution of the first (n_0=3) exciton number to the total calculated neutron spectra. Arrows represent end point energies. (From Ref. 9).

We have made a first attempt to improve this situation by generating two and three exciton densities from single particle levels due to Seeger-Howard[10] or Seeger-Perisho[11] using the method of Williams et al.[12,13] These have been incorporated into the ALICE[14] hybrid precompound code subroutine; results[15] are shown in Fig. 5. In this first attempt we have improved the agreement between experimental and calculated spectra with respect to shape at low residual excitations. Transition rates must still be modified to remain consistent with the reduced state densities. We hope that this will result in an improvement in the magnitude of the calculated spectra. Use of spin dependent densities with shell model levels should permit improved modelling of e.g. isomer ratios, and of course knowledge of pairing shifts and shell shifts from calculations of this type will be valuable to the development of 'unified models'. This topic is relevant to the presentations of Gruppelaar and Reffo. We are however at a point of development in precompound decay theory of going beyond equidistant spacing models for level densities, at least on an exploratory basis.

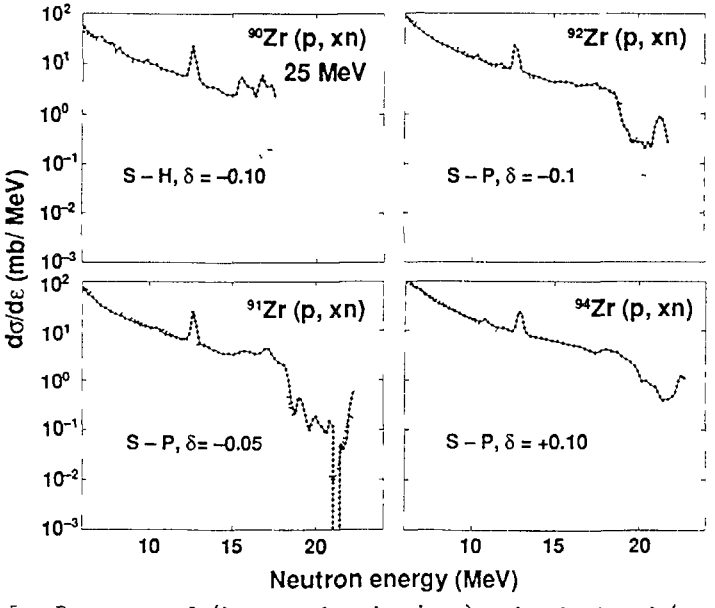

Figure 5. Experimental (heavy, closed points) and calculated (p,n) spectra on Zr isotopes for 25 MeV incident proton energy. The ALICE calculations used few quasi-particle densities for 2 and 3 excitons which were generated with shell model single particle levels as described in Refs. 12,13.

Several works have combined pre-equilibrium models with Hauser-Feshbach equilibrium theory in a two-step approach rather than via a master equation. Scobel and co-workers have done this with good success in reproducing isomer ratio measurements at excitations up to 55 MeV.[16,17] Avrigeanu et al. have also combined the geometry dependent hybrid model with a Hauser-Feshbach code, paying very close attention to level density treatments.[18] They have incorporated the level density work of Ignatyuk et al.[19] with a backshifted Fermi gas, and achieved most impressive results in reproducing both particle spectra and excitation functions for neutron induced reactions of Ti isotopes. More recently Avrigeanu et al. have added a spin dependence to the GDH partial state densities as a further improvement, giving a two-step approach to the unified model.[20] An example of the ^{46}Ti(n,p) spectrum calculated with this approach is shown in Fig. 6. It will be interesting to

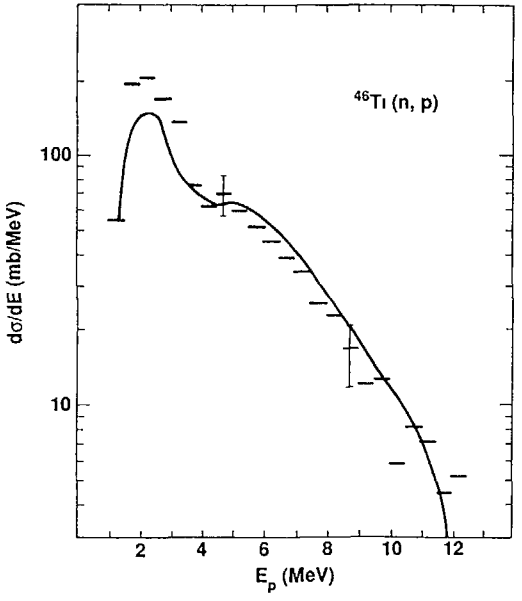

Figure 6. Calculated and experimental proton spectrum of ^{46}Ti(n,p) with 14.6 MeV neutrons from combined spin dependent precompound plus Hauser-Feshbach model. This figure provided from recent work of Avrigeanu et al[20]. Bars are experimental results, solid line is the total calculated result.

follow the progress of all of these approaches in the near term future. I should point out the existence of many other precompound plus Hauser-Feshbach codes including Marcinkowski's EMPIRE code, the LANL-GNASH I code, the ENEA code, and others.

3. ANGULAR DISTRIBUTIONS

The most convenient approach to the problem of the angular distribution is the semi-classical approach of Goldberger[21] and of Hayakawa et al.[22] This model, which is the scattering of a nucleon with a Fermi gas was first applied to the precompound problem by Mantzouranis et al.[23] The more rigorous type of formulation generally used in precompound decay was due to Sun-Ziyang et al,[24] and was further developed by others.[25,26,27] These models clearly reproduce the angular distributions forward of 90° quite well. The back angles require attempts at quantal corrections involving refractive and diffractive processes. In Fig. 7 we show an example of such an approach for the ^{90}Zr(p,n) angular distribution with 25MeV incident protons.[27]

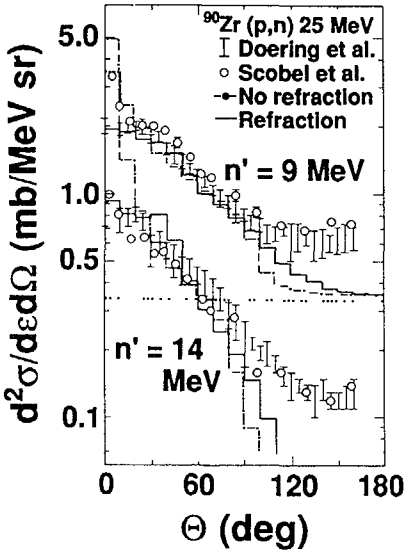

Figure 7. Calculated and measured angular distribution for the ^{90}Zr(p,n) reaction at 25 MeV incident proton energy. Data are due to Galonsky et al and Scobel et al. Calculated angular distributions are based on a Goldberger type of N-N scattering kernel with (solid histogram) or without (dot-dash) Snell's law refraction.

There is some difficulty in reproducing the back angle yields. Some exciton model calculations of the angular distributions have given better results than those shown in Fig 7. An important test to be applied will be an extension to a broad range of incident particle energies. As more data become available we will be in a better position to test these models.

In Fig. 8 we see an estimate of diffractive perturbations on the angular distribution, which emphasizes the importance of quantal phenomena in the lower energy regime. This suggests that we will need to use formal quantal theories for dependable predictive calculations. There are two main quantal approaches available. One is the theory of Feshbach et al,[28] which involves a quantal calculation of a single scattering kernel for a nucleon incident on a target nucleus, and the scattered nucleon leaving the residual nucleus after an inelastic scattering process. Contributions from higher order scattering processes are obtained by an incoherent folding of the single scattering kernel. This involves a $1/S^2$ term which the authors don't know how to

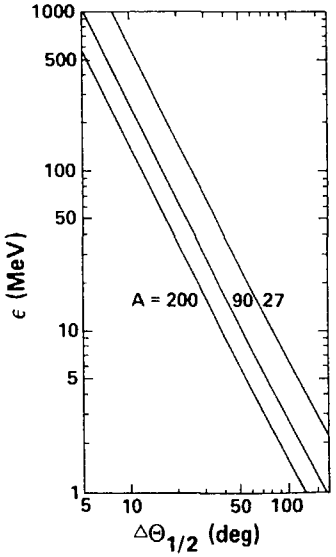

Figure 8. Half-angle versus nucleon energy due to the diffractive relationship of $R\Delta\theta \geq \bar{n}/k$ for targets of A = 27, 90, and 200. The radius used is the half-density radius of the Myer's droplet model. Half-angle refers to one-half the angular opening symmetric about 0°. (From Ref. 27).

calculate.[29] Additionally, Tamura has indicated that there may be some large errors in the FKK formulation, with errors of factors of up to 200 which are tending in some cases to cancel.[30] Clearly there are some questions needing to be answered on this topic; we may hear more in talks to be presented.

The above comments notwithstanding, the FKK approach has given impressive results in many applications to date. In Fig. 9 we show comparisons with the ^{65}Cu(p,n) angular distribution for 26 MeV incident protons.[31] This is but one of many very successful applications of FKK theory to data.[32] However I would also point out that a preliminary calculation for ^{208}Pb (p,n) at 26MeV proton energy gave results which were an order of magnitude in disagreement with experimental yields[33] (we emphasize that this was a preliminary result). Clearly more needs to be done before the theory of FKK becomes a dependable predictive tool for evaluators. The approach of Tamura[34] is a more rigorous one for treating the multistep direct component. Additionally Tamura has made some of his codes available. It is difficult to understand why more work has not been done with Tamura's theory; this approach deserves more attention and trial in the future. An example of Tamura's theory compared with experimental data is shown in Fig. 10.[34]

I do not feel that there is as yet a proven predictive model or theory for precompound angular distributions. This is a fruitful area for further study, about which we will hear more in this conference. Perhaps the problem is no greater than coming to understand how to prepare the necessary input for existing theories.

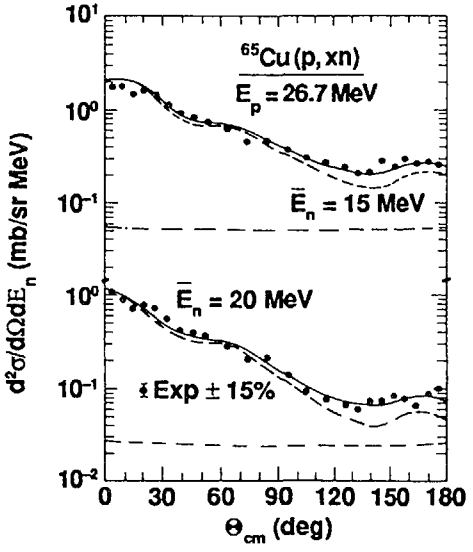

Figure 9. Experimental (dots) and calculated (solid and dashed curves) angular distributions for ^{65}Cu(p,xn) at 26.7 MeV incident proton energy. The solid curve is the result of the quantal theory of Ref. 28 giving the sum of multistep compound plus multistep direct contributions. The dashed line gives only the multistep direct contribution. (From Ref. 31).

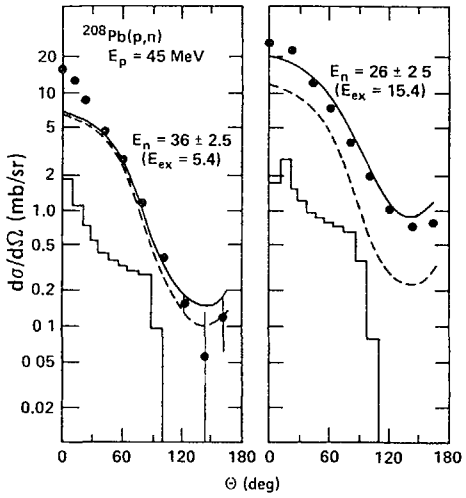

Figure 10. Angular distributions for ^{208}Pb(p,n) at 45 MeV incident energy. The data (circles) are due to Galonsky et al; the dashed curve is the single scattering result of Ref. 34, and the solid curve the result of single plus double scattering according to the theoretical result of Ref. 34. The solid histogram is the semiclassical single scattering result based on the work of Refs. 21-27.

4. HIGHER ENERGIES/NON REACTOR APPLICATIONS

Many requests are being made for nuclear data in areas beyond the reactor energy range. Medical physics and astrophysics require the abilities to calculate excitation functions to quite high energies. Medical physics also has an interest in reaction properties of highly energetic heavy ions; the electronics industry is interested in reactions of nucleons in the cosmic ray energy region. For many of these applications it is essential that precompound decay codes treat multiple precompound decay processes. It is important to be developing and testing our codes in this domain so that they are ready to address the higher energy regime. A few examples will be presented.

Many excitation functions have been measured and analyzed by precompound models. A few results for proton induced reactions at energies up to 200 MeV are shown in Fig. 11. Measurements and analyses were done by Michel and his collaborators.[35] The codes may be seen to work quite satisfactorily throughout this energy range, which includes the range relevant to medical isotope production[36]. In Fig. 12 we see experimental and calculated spectra from the 90 MeV (p,n) reaction on ^{27}Al. The HETC (Bertini intranuclear cascade), LANL GNASH II and ALICE code results are shown. These results are due to Pearlstein at BNL, who is in process of preparing a medium energy evaluated data file.[37] A comparison of model and experimental results at 318 MeV incident proton energy is shown in Fig. 13, and a (p,n) excitation function extending to 1 GeV is shown in Fig. 14. These figures are from Pearlstein based on experimental data of Meier et al., at LANL.[37] The model calculation does quite well for the excitation function (Fig. 14) but not as well for the more detailed angular distributions in Fig. 13. Clearly improvement is needed in our modeling of angular distributions at higher energies.

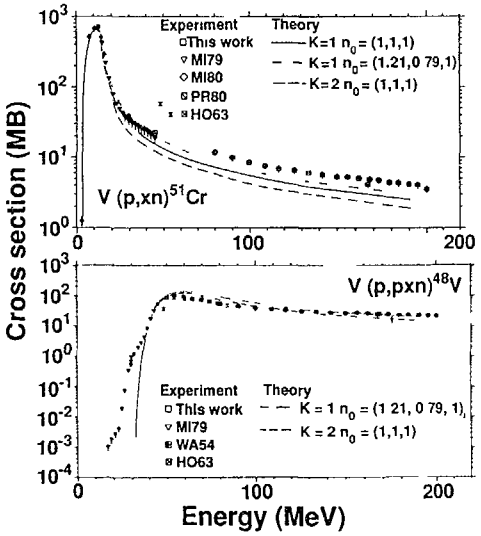

Figure 11. Calculated (ALICE) and experimental excitation functions for proton induced reactions on natural vanadium. These results are from Ref. 35. The code default parameter values are k=2 and n_0 = 3 (1.21, 0.79, 1) (n,p,h).

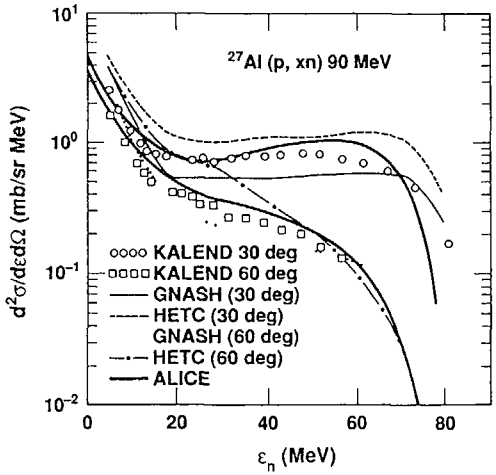

Figure 12. Experimental and calculated ^{27}Al(p,n) spectra for 90 MeV incident protons. Data are from Kalend et al. Calculated results are from the ALICE, HETC, and GNASH codes. Spectra are for angles of 30° and 60°. Figure is from S. Pearlstein (37).

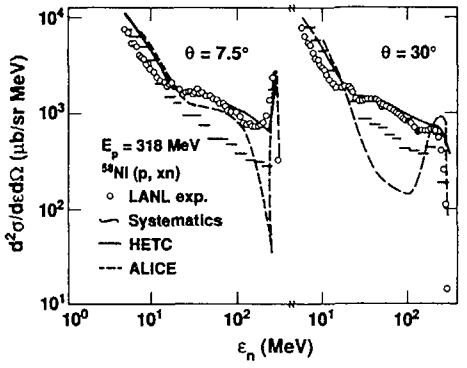

Figure 13. Experimental and calculated spectra for the reaction $^{58}Ni(p,xn)$ at 7.5° and 30° angles. Incident proton energy was 318 MeV; data are from the group of M. Meier, LANL. Calculated results are based on the ALICE code, the Bertini intranuclear cascade (HETC) and on systematics due to S. Pearlstein. This figure is due to S. Pearlstein, (Ref. 37).

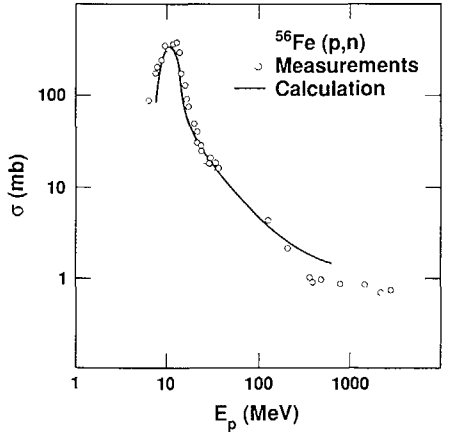

Figure 14. $^{56}Fe(p,n)$ excitation functions versus ALICE calculations. Data deduced by Pearlstein extend to ≈3 GeV. ALICE calculations were performed by Pearlstein to 800 MeV (Ref. 37).

Finally, in Fig. 15 we show some neutron spectra from heavy ion reactions which were gated on central collision processes.[39,40] Here the precompound decay models work quite well, reproducing the spectra to within the experimental uncertainties. In this area we need a broader range of gated experimental measurements, and we need to test codes to still higher energies. We note that the precompound parameters used in these calculations were those which had been proposed 10 years before the experiments were performed,[41,42] verifying the predictive power of the model in this reaction regime.

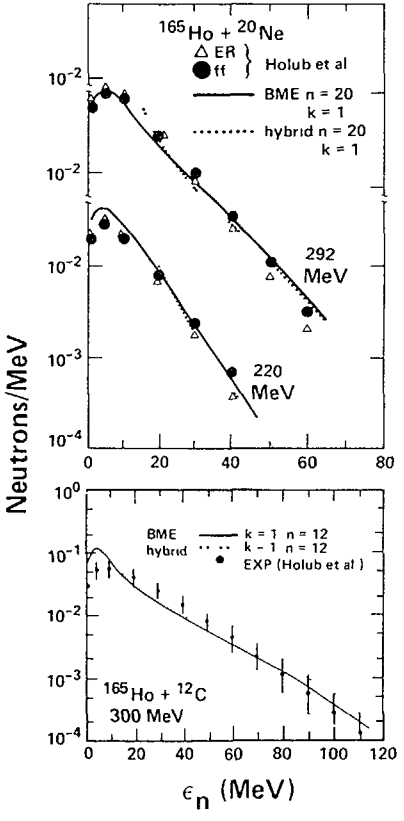

Figure 15. Neutron spectra from the reaction $^{20}Ne + ^{165}Ho$ at 220 and 292 MeV beam energy and $^{12}C + ^{165}Ho$ at 300 MeV beam energy. The open triangles and closed circles represent evaporation residue and fission fragment gated spectra from Refs. 39 and 40. The dotted curve is the result of the hybrid and evaporation model result form code ALICE, and the solid curve is the result of the Boltzmann master equation.[43].

5. CONCLUSIONS

Our codes work well for many applications in the reactor energy region. We should explore Bisplinghoff's contribution on modifying exciton densities for terms beyond the first exciton configuration. This may affect angular distribution calculations, and possibly spectral shapes. We have seen that shell structure effects may have a very pronounced influence on precompound spectra, and we should start code modifications to accommodate few quasiparticle densities (at least for the leading term in the series) calculated with realistic single particle levels. More work needs to be done in seeking the best means of generating these single particle levels, and in testing the limits of simple incoherent permutations of these levels without residual interactions in calculating realistic exciton densities.

While I have not discussed it here, work also needs to be done on supplementing our semi-classical incoherent precompound calculations with coherent direct reaction theories for population of low lying collective states. Similarly quantal theories for calculation of angular distributions need further development, so that they may become dependable, readily available predictive tools for the evaluator.

Finally, there is not so much a new development as a new need for the ability to calculate data at higher energies for various needs of modern technology. The experimental data base is sparse, but increasing. Requests for information are also increasing. This new regime will challenge us, and at the same time present a stringent test of the physics in our codes at lower energies. Preequilibrium models have come a long way in 2 decades; much further development and exploration remains to be done.

REFERENCES

1. J. J. Griffin, Phys. Rev. Lett. 17, 478 (1966).
2. M. Blann, Ann. Rev. Nucl. Sci. 25, 123 (1975).
3. T. E. O. Ericson, Adv. Phys. 9, 423 (1960).
4. F. C. Williams, Jr., Phys. Lett. B31, 184 (1970).
5. M. Blann, A. Mignerey and W. Scobel, Nukleonika 21, 335 (1976). M. Blann and H. K. Vonach, Phys. Rev. C28, 1475 (1983).
6. J. Bisplinghoff, Phys. Rev. C.33, 1569 (1986).
7. H. Nishioka, J. J. M. Verbaarschot and H. A. Weidenmuller, Annals Physics 172, 67 (1986).
8. M. Blann and J. Bisplinghoff, Z. Phys. 326, 429 (1987).
9. W. Scobel et al., Phys. Rev. C30, 1480 (1984).
10. P. A. Seeger and W. M. Howard, Nucl. Phys. A238, 491 (1975).
11. P. A. Seeger and R. C. Perisho, Los Alamos National Laboratory Report No. LA 3751, 1967 (unpublished).
12. F. C. Williams, Jr., A. C. Mignerey and M. Blann, Nucl. Phys. A207, 619 (1973).
13. K. Albrecht and M. Blann, Phys. Rev. C8, 1481 (1973).
14. M. Blann, Lawrence Livermore National Laboratory Report UCID 20169, 1984 (unpublished) and references therein.
15. M. Blann, T. Komoto, G. Reffo, F. Fabbri and S. M. Grimes, Lawrence Livermore National Laboratory Report UCRL 95397 (1986) unpublished.
16. M. Marten, A. Schuring, W. Scobel and H. G. Probst, Z. Phys. A322, 93 (1985).
17. H. H. Bissem et al., Phys. Rev. C22, 1468 (1980).
18. M. Avrigeanu, M. Ivascu and V. Avrigeanu, Atomkernenergie . Kerntechnik 49, 133 (1987).
19. A. V. Ignatyuk, G. N. Smirenkin, A. S. Tishin, Yad. Fiz. 21, 255 (1975).
20. V. Avrigeanu, private communication (1986).
21. M. L. Goldberger, Phys. Rev. 74, 1268 (1948).
22. S. Hayakawa, M. Kawai and K. Kikuchi, Prog. Theor. Phys. 13, 415 (1955).
23. G. Mantzouranis, H. A. Weidenmuller and D. Agassi, Z. Phys. A276, 145 (1976).
24. Sun Ziyang, Wang Shunuan, Zhang Jingshang and Zhuo Yizhong, Z. Phys. A305, 61 (1982).
25. J. M. Akkermans, H. Gruppelaar and G. Reffo, Phys. Rev. C22, 73 (1980). J. M. Akkermans, Phys. Lett. 82B, 20 (1979).
26. C. Costa, H. Gruppelaar and J. M. Akkermans, Phys. Rev. C28, 587 (1983).
27. M. Blann, W. Scobel and E. Plechaty, Phys. Rev. C30, 1493 (1984).
28. H. Feshbach, A. Kerman and S. E. Koonin, Ann. Phys. (N.Y.) 125, 429 (1980).
29. A. Kerman, private communication (1984).
30. T. Udagawa, K. S. Low and T. Tamura, Phys. Rev. C28, 1033 (1983).
31. Y. Holler et al., Nucl. Phys. A442, 79 (1985).
32. R. Bonetti and L. Colli-Milazzo, Workshop on Coincident Particle Emission from Continuum States, Bad Honnef, Federal Republic of Germany (1984).
33. W. Scobel, private communication (1986).
34. T. Tamura, T. Udagawa and H. Lenske, Phys. Rev. C26, 379 (1982).
35. R. Michel, G. Brinkmann, H. Weigel and W. Herr, Nucl. Phys. A322, 40 (1979).
36. R. Michel, F. Peiffer, and R. Stuck, Nucl. Phys. A441, 617 (1985). R. Michel and M. Gallas, Nucl. Phys. A404, 77 (1983). R. Michel and M. Galas, Int. J. Appl. Radiat. Isot. 34, 1325 (1983). R. Michel and G. Brinkmann, Nucl. Phys. A338, 167 (1980).
37. S. Pearlstein, private communication (1987).
38. E. Holub et al., Phys. Rev. C28, 252 (1983).
39. E. Holub et al., Phys. Rev. C33, 143 (1986).
40. M. Blann, Phys. Rev. 35, 1581 (1987).
41. M. Blann, Proceedings of the International School on Nuclear Physics 1974, ed. A. Ciocanel (Editura Academic Republicii Socialiste Romania, Bucharest 1976) p. 249; Nucl. Phys. A235, 211 (1974).
43. M. Blann, Phys Rev. C31, 1245 (1985).

204 RECENT DEVELOPMENTS IN EXCITON AND UNIFIED MODELS

H. GRUPPELAAR, J.M. AKKERMANS
Netherlands Energy Research Foundation,
Petten, Netherlands

Abstract

A review is given of the recent developments of the exciton model in its master-equation formulation. Progress has been made in the modelling and the calculation of angular distributions, gamma-ray emission, particle-hole level densities, preformation factors for complex particle emission and two-fermion models. The most interesting development, however, is the integration of precompound and compound models by including angular-momentum conservation. At present this unified model is successful in predicting angle-integrated quantities. It is essentially equivalent to the quantal multi-step compound models, but it has some computational advantages. We discuss possibilities for further integration of precompound and compound models on a quantum-mechanical basis and suggest some directions for future work.

1. INTRODUCTION

This paper summarizes some of the conclusions of recent review papers [1-3] and gives some additional comments on recent developments of the exciton model and the unified model, so far as relevant to neutron-induced reactions for technological applications; we refer also to the results of an international nuclear model and code intercomparison [4]. An early review paper was written by Blann [5]. We restrict ourselves in this paper to the exciton model in its master-equation formulation and do not discuss developments of hybrid models, since these are covered in another review paper presented at this meeting. For the same reason we do not discuss in detail the multi-step compound and multi-step direct theories, such as the one of Feshbach, Kerman and Koonin (FKK) [6].

Recent developments of the exciton model (EM) are described in Sect. 2.1. For the description of angular distributions (see also the review in [7]), the projectile (or rather the "fast" particle) is followed on its way through nuclear matter. In this approach, on which recent viewpoints are presented in Sect. 2.2, the number of collisions k is a leading quantity. The approach is quite successful, in spite of the neglect of quantum-mechanical refraction and diffraction effects.

The exciton model in its full master-equation representation predicts both the precompound and the compound parts of the cross sections and contains the Weisskopf-Ewing model as a limiting case. Extension of the exciton model by including angular momentum and parity conservation leads to a "unified" model that contains the Hauser-Feshbach model as a limiting case. This is the subject of Sect. 3.1. The extension is not a trivial one, since there are many conservation and consistency rules that have to be obeyed. The unified exciton model [2] strongly resembles the multi-step compound part of the FKK model [3], but it has some advantages among which we mention the fact that no separation is made between multistep compound and multi-step direct components nor that the "never-come-back assumption" is required.

Obviously, the next step towards unification is to introduce angular distributions into the unified exciton model. This is discussed in Sect. 3.2. Recalling that the Hauser-Feshbach model already contains angular distributions, the main difficulty is the introduction of a (forward-peaked) angular-distribution computation capability into the precompound part of the model in a consistent way.

In Sect. 3.3. some comments are made with respect to the microscopic foundation of the exciton model and possible further theoretical developments. Some concluding remarks are presented in Sect. 4.

2. PROGRESS IN EXCITON-MODEL DEVELOPMENT

2.1. Angle-integrated cross-sections

It is assumed that the main parameter besides the excitation energy E that characterizes the nucleus during the initial phase of a reaction is the exciton number n(p,h), which is the sum of the number of particles p above the Fermi level and holes h below the Fermi level. In this picture the ground state of the nucleus has n = 0. The system of target and projectile (nucleon) has n = 1 and the first internal collision leads to a state with n = 3. A subsequent collision usually leads to a state n = 5 and next to n = 7,9 etc. (never-come-back approximation). However, it is also possible that a state returns to a state with lower exciton number or remains in the same exciton state. This extremely simple picture (Fig. 1) actually means that if we speak about an exciton "state" n we mean a class of states with many different (p,h)-configurations that have in common that their exciton number is equal to n. The number of such states is determined by the state density $\omega(p,h)$. If we use no other (quantum) numbers to specify the different configurations all transition and emission rates (λ and W, respectively) only depend upon the exciton numbers involved. In that case the well-known master equation for the exciton distribution q(n,t) reads:

$$\frac{dq(n,t)}{dt} = \sum_m \lambda(m \to n)\, q(m,t) - [W_t(n) + \sum_m \lambda\,(n \to m)]\, q(n,t). \qquad (1)$$

Integration over time immediately gives the time-integrated master equation:

$$-q(n,t=0) = \sum_m \lambda(m \to n)\, \tau(m) - [W_t(n) + \sum_m \lambda\,(n \to m)]\, \tau(n), \qquad (2)$$

where q(n,t=0) is the initial exciton distribution, taken as δ_{n3}, and $\tau(n)$ is the mean lifetime of exciton state n.

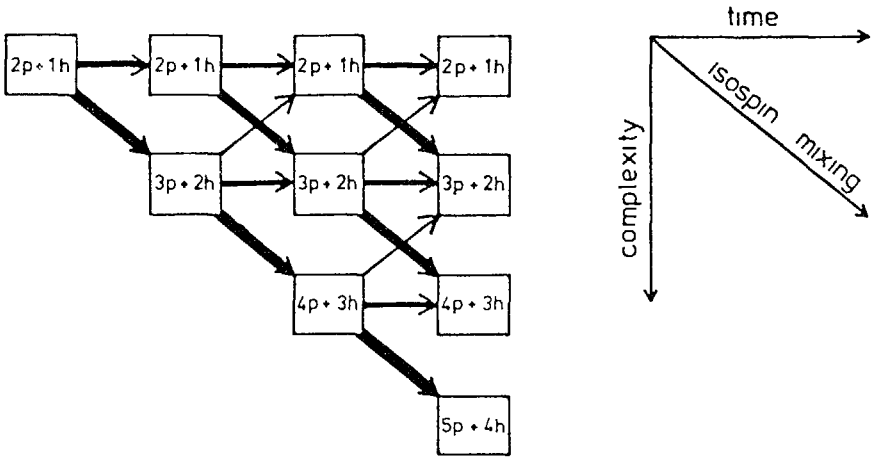

Fig. 1 Scheme of multi-step reactions induced by a nucleon in the exciton model The initial state is assumed to be the 2p1h state For certain applications (e g. γ-ray emission) it might be better to assume 1p0h as the initial state. (Figure taken from [1])

Solution of the (time-integrated) master equation gives the values of the mean lifetimes that can be used to calculate the differential cross-section:

$$\frac{d\sigma(a,b)}{d\varepsilon} = \sigma_a \sum_n W_b(n,\varepsilon)\ \tau(n). \qquad (3)$$

The foundation of the above-mentioned exciton model (EM) is further discussed in Sect. 3.3. The most typical assumption is that the system is only characterized by the exciton number n. In quantum-mechanical terms n is a good quantum number of the unperturbed Hamiltonian H_o, but not of the total Hamiltonian H_o+V. The classes of states with different n values are mixed through the subsequent collisions as described by the master equation (cf. Fig. 1). Bisplinghoff [8] also claims that complete configuration mixing is assumed between all states with the same value of n (such an assumption is not necessary, see Sect. 3.3). We note here that the spin and parity are good quantum numbers of the total Hamiltonian. Introduction of these quantum numbers leads to a set of master equations, one for each combination of J and Π, cf. Sect. 3.1. It is also possible to distinguish between protons and neutrons by extending the master equation (two-component exciton model [9-11]). Furthermore, it is possible to distinguish between "open" and "closed" configurations [12]. In fact, it is always possible to extend the master equation by adding additional configuration specifiers. However, in order to be practical one likes to limit the number of these additional specifiers to a minimum. Therefore it is always necessary to lump a large number of configurations and to use "average" transition and emission rates.

The introduction of the two-component model [9,10] certainly is an improvement, because it is more physical. Recently an extensive paper on this subject was presented by Kalbach [11]. The master equation becomes much more complicated, and so does the parametrization of state densities and transition rates, although the expressions for the emission rates are simplified (no need for "isospin mixing" factors to account for the proton-neutron distinguishability) There are some problems with regard to the values of the mean square residual matrix element M^2 occurring in the internal transition rates which depend on the interaction between two protons, two neutrons or a proton and a neutron [11]. An advantage is that the two-component (p,h)-state densities are basically consistent with the two-Fermion level density adopted in equilibrium models. Furthermore, it appears that the transition rates in the two-component model are more consistent with the values for the nucleon mean free path in nuclear matter than in the one-component case [9,10,21]. Rather than solving the full master equation, Kalbach proposes a closed-form expression for the pre-equilibrium part of the reaction, based on the neglect of pair annihilation rates. The results of calculations with the two-component model are not significantly different from those with the one-component model (this may depend on the assumptions made in Ref. [11]). Kalbach, however, expects that the two-component model "opens new avenues for studying pre-equilibrium pairing and shell effects, which should depend on the specific proton-neutron configuration".

The model that distinguishes between "open" and "closed" configurations [12] has the advantage that emissions from closed configurations are forbidden, which seems physically plausible and gives a connection with the FKK theory [6]. It was mainly introduced to distinguish between forward-peaked and isotropic angular distributions, see Sect. 2.2. In terms of this model emission from closed configurations is impossible (first a transition to an open configuration is required). However, there may be an inconsistency here, because the emission rate contains an inverse reaction cross-section deduced from the compound phase, where an average is taken over all configurations, although a large fraction of the configurations is closed and still emission is possible. The results of calculations with this model are only slightly different from those with the one-component model (this depends of course on the parametrization adopted [12]). An interesting conclusion is that there is no strong mixing between open and closed configurations, confirming an important FKK assumption.

It is of interest to note that the solution of the full master equation not only yields the precompound part of the cross-section, but also the compound part (Weisskopf-Ewing model). In this sense the EM is a "unified" model, see further Sect. 3. The unified treatment of pre-equilibrium and equilibrium parts slightly complicates the calculations. However, it is very advantageous for model developers, because the consistency requirements are quite helpful in defining the model and the parametrization (level density, emission rates, etc.). As an example, it is required that the sum over all (p,h) state densities should agree with the level density expression used in the Weisskopf-Ewing theory. This is not a trivial demand, which is a reason for many authors to split the description of the pre-equilibrium and equilibrium processes in two parts. However, it is a challenge to solve these problems.

A mathematically equivalent description is given by the "random-walk" model [13], that has also been applied in the STAPRE code [14]. In this model the fundamental parameter is the number of interactions k rather than the time. This representation is of interest, because it gives insight in the average number of collisions needed to reach a certain exciton state, its variance and other quantities related to the number of collisions rather than the exciton number (e.g. the forward peaking of the angular distribution, see further Sect. 2.2).

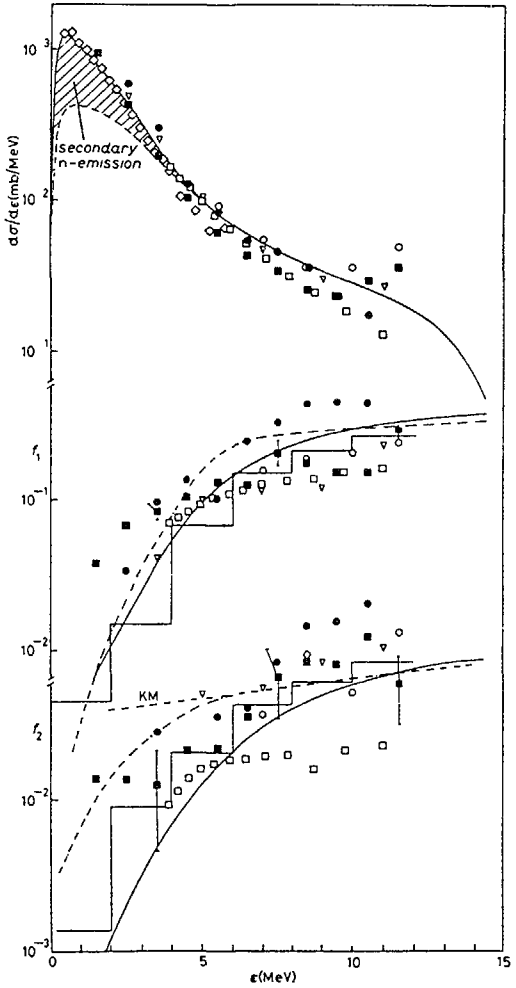

Fig. 2. Angle-integrated emission spectrum (upper part) and reduced Legendre coefficients f_1 for neutrons emitted from (n,xn) reactions on Nb at 14.6 MeV. The calculation data are from the code GRAPE [15] (without any adjustments; full curve), Kalbach-Mann systematics [28] (with a modification at low energies; dashed-dotted curves) and from the code TNG [32]. The experimental data references are quoted in [2]. (Figure taken from [2]).

The EM is basically an exclusive model. However, multi-particle emission can easily be included. The only difference to describe the secondary emission from a previously excited state is that the initial condition q(n,t=0) is no longer a Kronecker delta function, but a distribution function determined by the previous decay [13]. Therefore, the same routine that calculates primary emission can be used repeatedly. This method has been adopted in the GRAPE code [15]; see also the upper part of Figs. 2, 3.

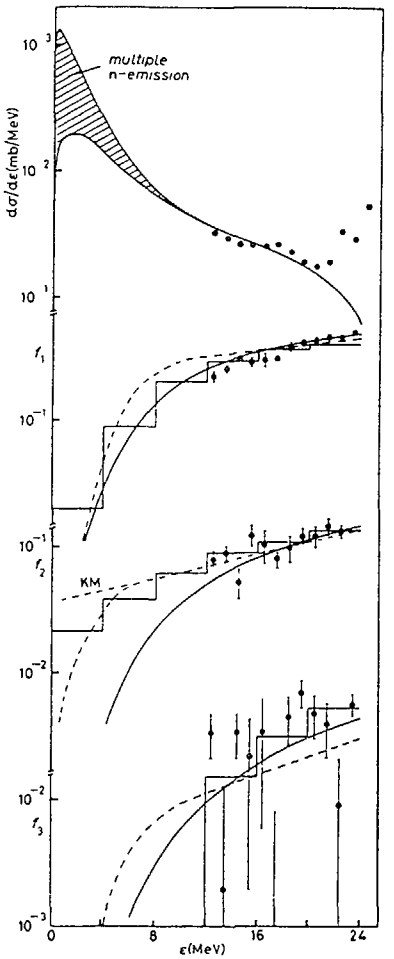

Fig. 3. Similar figure as Fig. 2, with incident energy equal to 25.7 MeV. (Figure taken from [2]).

A recent development of the EM is the introduction of γ-ray emission in the pre-equilibrium phase of the reaction by defining the γ-ray emission rates according to a generalization of the Brink-Axel hypothesis [16,17]. This generalization is not straightforward, since from photon absorption only (inverse) transitions with n = 0 → 2 are known, whereas in precompound decay a state with exciton number n can decay by γ-ray emission to a state with exciton number n-2 , but also to n (not to n+2 [16]). In particular, "direct" emission means a transition n = 1 → 1 and "semi-direct" emission means the sum of an n = 3 → 3 and an n = 3 → 1 transition. The relative magnitudes of the two transitions follow from the available (p,h)-configurations. The normalization can be deduced from the requirement that at equilibrium the emission rate should correspond with the usual Brink-Axel estimate [17]. This procedure was appplied to predict the primary γ-ray spectrum of the Nb(n,γ) reaction at 14 MeV, with remarkable success [17]. Although the method gives a very rough estimate of direct and semi-direct capture, it is probably useful as a first estimate. Moreover, it gives a prediction of γ-ray emission from states with n= 5,7, etc. that is not provided by existing theories. The above-mentioned method has been generalized to include spin and parity, see Sect. 3.1. and Fig. 7.

Another interesting development is the treatment of complex-particle emission according to the method of Iwamoto and Harada [18]. This cluster method has recently been simplified by Zhang et al. [19]. This model predicts normalized preformation factors F_m for the pick-up of m particles below the Fermi sea level. In the usual E.M. the value of m is restricted to 0, which means that e.g. α-emission is only possible after at least three interactions. This would imply that at low incident energies α-emission is virtually impossible, which is unphysical. The method of Refs. [18,19] is therefore an important improvement.

We do not discuss here in detail the developments in the description of state densities, but it is stressed that these quantities are the key parameters of all precompound models. The simple expression of Williams [20] are still frequently used. Modifications of this expression have been suggested for use in the two-component model [11] and for use in a unified model [21]. More fundamental changes (pairing corrections) have been suggested by Fu [22]. A very drastic method is to use directly (p,h)-levels from nuclear-model calculations [23].

2.2. Angular distributions

The most important contribution to the forward peaking of the angular distribution of particles emitted in the pre-equilibrium phase originates from the emission after the first collision, i.e. from the state with $n_0 = 3$ for nucleon projectiles. The shape of this angular distribution is connected to that of the intranuclear scattering kernel given by Kikuchi and Kawai (KK) [24], and denoted in normalized form by $G(\Omega\rightarrow\Omega',\varepsilon\rightarrow\varepsilon')$. This kernel should give a reasonably good description of the angular distribution of particles emitted from $n = n_0$, because emission from n_0 is dominated by emission after the first collision only. However, since we deal with a real nucleus rather than with infinite nuclear matter, finite-size effects and refraction effects lead to smoothing of the angular distribution. A simple way to include finite-size effects is by limiting the number of coefficients in the Legendre-polynomial expansion of G. This truncation results in an angular distribution over the full range of angles and energies, instead of a distribution with the severe kinematical restrictions implied by the use of the exact KK expression. Furthermore, at low incoming and outgoing energies refraction effects are important: they could be estimated by means of classical refraction theory [27]. Diffraction effects cannot be included in this picture.

Although the first collision is by far the most important one, the effect of other collisions cannot entirely be neglected, certainly not for low emission energies. Therefore the following "leading particle method" due to Mantzouranis et al. [25] could be adopted. After the first emission the coupled energy-angle distribution of the scattered nucleons is known. However, we can "follow" only one of the two scattered nucleons (in energy and direction). Assuming that the struck nucleon has very low energy and does not further interact we may choose to follow only the "fast" particle on its way through the nucleus. In Ref. [25] the free nucleon-nucleon scattering kernel G_f was adopted. Later, Sun Ziyang et al. [26] have used an energy-averaged KK kernel. Costa et al. [27] were the first to employ the full KK kernel and argued that for many purposes it would be sufficient to use this kernel for the first stage only. The most complete description is due to Iwamoto and Harada [18], who used the full KK kernel at all stages and furthermore made the following correction for the effect of interactions caused by the struck nucleons:

$$G_n(\Omega\rightarrow\Omega',\varepsilon\rightarrow\varepsilon',t=0) = a_n\, G(\Omega\rightarrow\Omega',\varepsilon\rightarrow\varepsilon') + (1-a_n)\,\delta(\Omega\rightarrow\Omega')\,\delta(\varepsilon-\varepsilon') \qquad (4)$$

with $a_n = 1$ for $n = 3$. The second term represents the fraction of interactions that do not change the direction of the leading particle. With these extensions the "generalized" master equation introduced by Mantzouranis [25] is further generalized. After integration over time the following equation is obtained:

$$-q(n,\Omega,\varepsilon,t=0) = \sum_m \lambda(m\rightarrow n) \iint d\Omega'd\varepsilon' G_m(\Omega'\rightarrow\Omega,\varepsilon'\rightarrow\varepsilon)\,\tau(m,\Omega',\varepsilon')$$

$$-[W_t(n) + \sum_m \lambda(n\rightarrow m) \iint d\Omega'd\varepsilon' G_n(\Omega\rightarrow\Omega',\varepsilon\rightarrow\varepsilon')]\,\tau(n,\Omega,\varepsilon), \qquad (5)$$

where ε and Ω refer to the leading particle and the initial condition is given by:

$$q(n,\Omega,\varepsilon,t=0) = \int d\Omega' R(E,\Omega_z\rightarrow\Omega')\, G(\Omega'\rightarrow\Omega,E\rightarrow\varepsilon')\,\delta(E-\varepsilon')\delta_{n3}\ , \qquad (6)$$

where $R(E,\Omega_z,\Omega')$ is the refraction kernel of the incoming beam [27].

Note that in the summations in Eq. (5) the n→n-2,n,n+2 transitions should be included. For $G_n(\Omega\rightarrow\Omega',\varepsilon\rightarrow\varepsilon') = G_f(\Omega\rightarrow\Omega')\delta(\varepsilon-\varepsilon')$ and neglecting refraction the generalized master equation of Mantzouranis is recovered; energy averaging over the KK kernel and assuming that $a_n = 1$ gives the equation of Sun Ziyang et al. [26], also used by Costa et al. [27], albeit that for $n_o = 3$ the full KK expression was adopted.

The solution of Eq. (5) can be simplified if a Legendre decomposition is made. Instead of Eq. (5) the following set of equations needs to be solved

for a relatively small number of ℓ-values:

$$n_\ell(n,\varepsilon,t=0) = \sum_m \lambda(m\to n) \int d\varepsilon' \mu_\ell(m\to n,\varepsilon'\to\varepsilon)\, \xi_\ell(m,\varepsilon') + -[W_t(n) + \sum_m \lambda(n\to m) \int d\varepsilon' \mu_\ell(n\to m,\varepsilon\to\varepsilon')]\, \xi_\ell(n,\varepsilon), \quad (7)$$

where $n_\ell, \mu_\ell, \xi_\ell$ are Legendre coefficients of the initial condition, the scattering kernel and the mean lifetime, respectively. The double-differential cross-section is calculated from:

$$\frac{d^2\sigma(a,b)}{d\varepsilon d\Omega} = \sigma_a \sum_n W_b(n,\varepsilon) \int d\Omega' R(\varepsilon,\Omega'\to\Omega)\, \tau(n,\Omega',\varepsilon) = \quad (8a)$$

$$= \sigma_a \sum_n W_b(n,\varepsilon) \sum_\ell \xi_\ell(n,\varepsilon)\, \rho_\ell(\varepsilon) P_\ell(\cos\theta), \quad (8b)$$

where the kernel $R(\varepsilon,\Omega'\to\Omega)$ and the coefficient $\rho_\ell(\varepsilon)$ refer to refraction of the outgoing beam.

Solution of these equations is simplified in the never-come-back approximation. In particular, for the important $n_0 = 3$ contribution it follows that

$$\xi_\ell(3,\varepsilon) = \frac{2\ell+1}{4\pi} \rho_\ell(E)\, \mu_\ell(3,E\to\varepsilon)\, \tau(3), \quad (9)$$

where $\rho_\ell(E)$ is the refraction coefficient of the incoming beam. Since for $n_0 = 3$ the never-come-back assumption is almost exact, this expression is quite accurate. For higher values of n the solution of Eq. (5) is more difficult. However, since the contribution of $n_0 = 3$ is the most important one, approximations are allowed. For instance it is possible to assume $a_n = 1$ and an energy-averaged KK kernel. This method was followed by Costa et al. [27], with results that are in very good agreement with the phenomenological systematics of Kalbach and Mann [28], see further Ref. [27] and Figs. 2, 3 (full and dashed-dotted curves, respectively).

A detailed comparison between experimental data and the above-mentioned theory reveals the following problems:
(i) at equilibrium an isotropic rather than a (symmetric) anisotropic angular distribution is obtained (note that for a meaningful comparison with experimental data the c.m. to lab. conversion is very important at low values of ε [49]); (ii) no interference patterns are predicted; (iii) the backward-angle cross sections are predicted somewhat too low. These problems are related to the semi-classical nature of the model and the fact that angular momentum is not explicitly taken into account in the model. For problem (i) a simple solution can be given by adding a term to the second-order coefficient based upon the work of Plyuiko [29] and introduced in the model by the present authors [15]. Problem (ii) cannot be solved by simple ad-hoc changes to the model; on the other hand the structure in the angular distribution is weak due to the large number of interfering channels. The last-mentioned problem is disturbing: it is difficult to find a convincing explanation for this deficiency within the framework of the model. Certainly, it is important to introduce finite-size effects and refraction effects, but this does not fully account for the underprediction of the experimental backward-angle cross section, that sometimes shows a small rise at angles near 180°. In practice one could make a slight upward adjustment of the f_2-coefficient to agree with the experimental data [2] (or completely follow a phenomenological description like that of Kalbach and Mann [28]). A possible explanation could perhaps be that the Fermi-distribution used in the KK expression should correspond to a non-zero nuclear temperature. This suggestion has recently been made by De et al. [33]. We note that in order to be effective, this non-zero temperature should be assumed already for the ground-state of the nucleus, which in the present theory is assumed to be cold.

Finally, we mention that since the n = 3 contribution is predominant the problem of the role of the struck nucleons is not a major one. Therefore, the modification of Iwamoto and Harada [18] is practically not very important. Furthermore, the introduction of a value of $a_n < 1$ leads to more forward peaking, because it is assumed that transitions in which struck nucleons are involved do not lead to emission. If one does so and assumes isotropic emission for the struck nucleons less forward peaking could result instead. This idea is taken up in the paper of Jun and Chenglie [34]. However, it is questionable whether such refinements apply for n = 3. Therefore, further progress can only be obtained if the description of the emission from n = 3 is improved.

In summary, the main features of the precompound angular distribution can be understood with the above-mentioned semi-classical theory. Quantitative predictions are possible and can be improved with the adjustment of one parameter (f_2) to experimental data. Alternatively the purely empirical Kalbach-Mann systematics [28] could be applied with some adjustments at low energies [2]. This systematic can easily be extended to very high energies [1], see also Fig. 4.

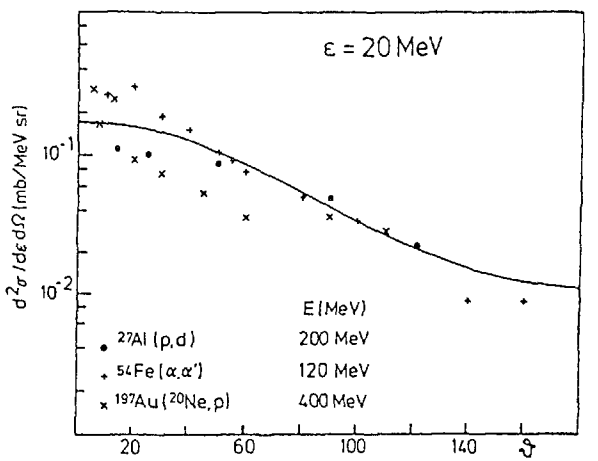

Fig. 4. Comparison of experimental and angular distributions at emission energy of ε = 20 MeV with the results of Kalbach-Mann systematics [28], extended by Machner [1]. It shows the insensitivity of these data to specific conditions of the reactions. (Figure taken from [1]).

3. PROGRESS IN UNIFIED MODEL DEVELOPMENT

Historically, the creation of a species of exciton models was motivated by the desire for a practical description of pre-equilibrium reactions, i.e., of reactions with characteristics in between those of direct and compound reactions. In this respect, it is highly successful. On the other hand, this development has actually given rise to quite different formalisms for these three reaction types. One would intuitively expect, however, that there exists a natural link between the pre-equilibrium exciton formalism and the compound reaction theory (notably the Hauser-Feshbach theory) and secondly also to direct reaction models (at least in the continuum). This is a deep problem, which has pragmatic aspects - using a single formalism and a single numerical code is very attractive for applicators, but the associated reduction of free parameters also creates its own problems - as well as fundamental aspects, since it touches upon the microscopic foundations of macroscopic nuclear-reaction theory. What we will call here the unified models, constitute an attempt to obtain a better integration of various reaction mechanisms within the framework of pre-equilibrium exciton theory. The present authors believe that the most fruitful starting point for this is the master-equation approach, due to its omnipresence in both classical and quantum statistical mechanics.

3.1. Angle-integrated cross-sections

A long-standing criticism regarding the exciton model is its neglect of angular-momentum information. This is undesirable for at least two reasons. First, angular-momentum effects may influence the calculated pre-equilibrium excitation functions, spectra and angular distributions. Second, from a unification point of view it renders impossible the merging of pre-equilibrium theory with Hauser-Feshbach theory, as the standard exciton model can only have as its equilibrium limit the Weisskopf-Ewing evaporation model. Very recently, two papers have appeared [35,36] that solve both these problems for the angle-integrated case. These papers build upon earlier investigations by Plyuiko [29], Reffo et al. [31], Fu [32] and Gruppelaar [33] and ideas taken from FKK theory [6].

A rather extensive exposition is given by Shi Xiangjun et al. [35]. They introduce a master equation that also includes the total angular momentum J and the parity Π of the composite nucleus (target plus projectile) as a characterization of the nuclear state under consideration, in addition to the excitation energy E and the exciton number n. The resulting master equation reads:

$$\frac{dq^{J\Pi}(n,t)}{dt} = \sum_m \lambda^{J\Pi}(m\to n)\, q^{J\Pi}(m,t) - [W_t^{J\Pi}(n) + \sum_m \lambda^{J\Pi}(n\to m)]\, q^{J\Pi}(n,t). \qquad (10)$$

We see that the master equation decomposes into a set of uncoupled equations, one for each value of J and Π. This is related to a general property that can be mathematically proved, stating that the master equation decouples in a manner as indicated above for each (macroscopically) conserved quantity. Incidentally, here we also find a physical explanation for the decoupling into various ℓ of the angular-distribution models discussed in Sect. 2.2: in these spinless models the orbital angular momentum of the system is conserved. Consequently, if we identify ℓ with the orbital angular momentum, the master equation is decomposable into a set of separate equations for each value of ℓ. Thus, we can give a natural physical interpretation to the purely mathematical proof, originally given in [37].

Returning to the spin-dependent master equation, we remark that its further treatment is as usual. Upon integration over time we obtain

$$-q^{J\Pi}(n,t=0) = \sum_m \lambda^{J\Pi}(m\to n)\, \tau^{J\Pi}(m) - [W_t^{J\Pi}(n) + \sum_m \lambda^{J\Pi}(n\to m)]\, \tau^{J\Pi}(n) \qquad (11)$$

with initial condition

$$q^{J\Pi}(n,t=0) = [\sigma_a^{J\Pi}/\sigma_a]\, \delta_{n3}, \qquad (12)$$

where

$$\sigma_a = \sum_{J\Pi} \sigma_a^{J\Pi} \qquad (13)$$

is the composite formation cross-section. The average emission spectra and cross-sections are given by

$$\frac{d\sigma(a,b)}{d\varepsilon} = \sigma_a \sum_{J\Pi} \sum_n W_b^{J\Pi}(n,\varepsilon)\, \tau^{J\Pi}(n). \qquad (14)$$

The transition and emission rates are calculated from time-dependent perturbation theory according to Fermi's golden rule, but now they include spins and parities. Here, one takes advantage from the fact that the densities of final states can be factorized into a spin part, a parity part (assumed to be equal to 0.5) and an energy-dependent part. The treatment of the angular-momentum couplings occurring in the expression for the transition rates [36] is similar to that in the FKK model [6]. The expressions for the emission rates are very similar to those used in Hauser-Feshbach theory, although the level density has become n-dependent.

The approach taken by Oblozinsky [36] is essentially the same, except for the fact that a never-come-back approximation has been introduced to the above equations (10,11). He extends the model by also considering the case that the emitted particle b is a photon. This is done by means of a direct generalization of the nonspin approach by Akkermans and Gruppelaar [17] to the case of angular-momentum conservation.

Furthermore, Shi Xiangjun et al. [35] discuss a number of methods in order to speed up the numerical model computations. Partly, these are based on the factorization properties of the level density formulae. Consequently, as demonstrated by Akkermans et al. [38], nested summations over spins can be replaced by very accurate analytical approximations. In addition, assuming a weak spin dependence of the transition and emission rates, one is able to find a very simple expression for the spin-dependent mean lifetimes in terms of the spinless ones. This effectively reduces the set of master equations (10) (totalling a number J_{max}) to a single one. Also this

approximation turns out to be very accurate [35]. The combined result of these computational optimizations is that the CPU time for a precompound/compound master-equation calculation reduces to that of a Hauser-Feshbach calculation or even less. The consistency requirements for the unified model have also a large impact on the (p,h) level densities and their spin distribution described by spin cut-off parameters $\sigma^2(n)$, cf. [35].

The observation that the transition and emission rates generally show a weak angular-momentum dependence is a basic one. A typical example is presented in Fig. 5. This finding is reported in both Refs. [35] and [36] as well as by various authors in the FKK line of work. Physically, this weak spin dependence can be explained by noting that even for simple exciton states a large number of angular-momentum couplings is possible. This washes out much of the selectivity in the angular-momentum structure. Accordingly, the calculated impact of spin effects on the angle-integrated emission spectra and cross-sections appears to be small. It is shown in [35] and [36] that this applies to both nucleon and γ-ray emission in nucleon-induced reactions, see Figs. 6 and 7. Thus, one is led to the conclusion that from a practical viewpoint the standard spinless models give quite reliable results.

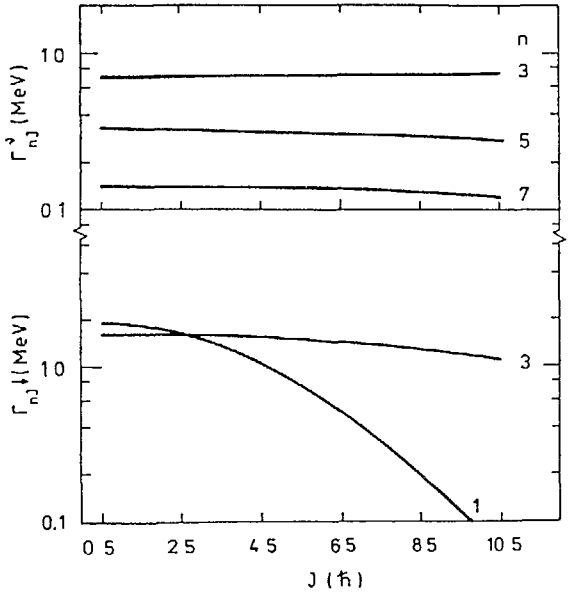

Fig. 5. Neutron emission and internal transition widths as a function of spin J upper and lower parts, respectively. This figure, taken from [35] shows that these rates are only weakly dependent on exciton number. Emission from the state with n=1 is only possibly by γ-rays.

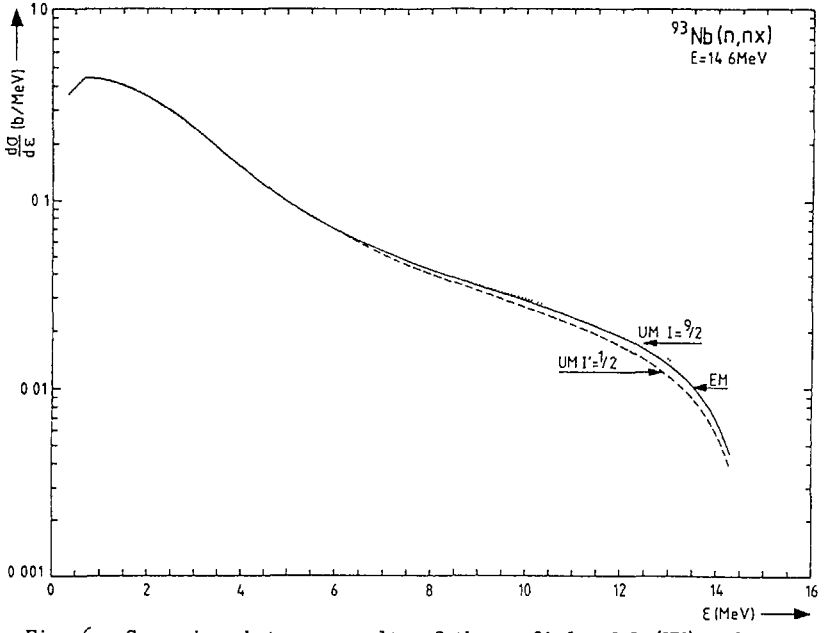

Fig. 6. Comparison between results of the unified model (UM) and the exciton model (EM) for the reaction ^{93}Nb(n,n'x) at 14.6 MeV. The dashed curve corresponds to a fictitious target spin I=1/2 (instead of I=9/2). This figure has been taken from Ref. [35].

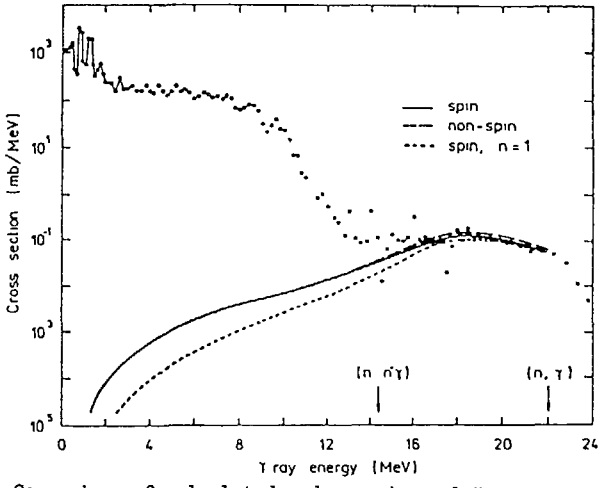

Fig. 7. Comparison of calculated and experimental γ-ray spectra for the reaction ^{56}Fe(n,γ) at 14.6 MeV. The calculation represents only the primary pre-equilibrium γ-rays. The full, dashed and dotted curves represent the unified model calculation, the exciton model calculation and the "direct" contribution from n=1, respectively. (Figure taken from Ref. [36]).

Nevertheless, the master-equation model with conservation of angular momentum has definite conceptual advantages over the usual exciton model. It can be rigorously demonstrated [35] that in the equilibrium limit it goes over into the continuum Hauser-Feshbach theory. This part is automatically included in the Eqs. (10)-(14). Hence, one can genuinely speak of an integrated precompound-compound theory. Also the standard exciton model and the Weisskopf-Ewing model can be derived from it. The relationships between these models are displayed in a transparant fashion in Fig. 8. Moreover, one can show that the angular-momentum conserving master equation integrated over time [i.e., Eq. (11)] is essentially equivalent to the AWM theory of Agassi et al. [39]. The somewhat evasive term "essentially" can be given a quite precise meaning here: it implies a further specification and implementation of the AWM theory in the following sense:

- the representation of nuclear state classes is in terms of quasiparticles (excitons);
- it is a first-order perturbation theory in the residual interaction;
- it is a leading-order theory of strongly overlapping resonances weakly coupled to the continuum;
- transition widths are estimated on the basis of equidistant Fermi-gas level density formulae (Ericson type).

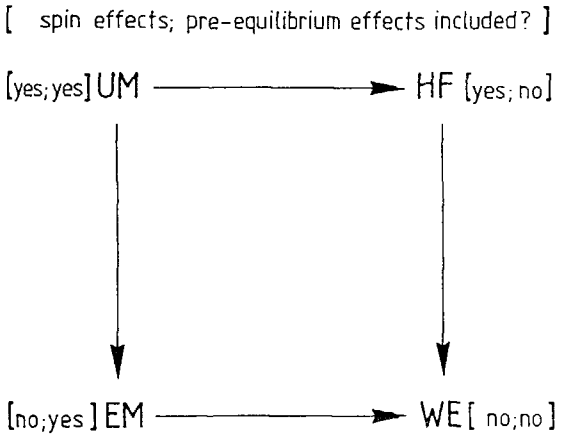

Fig. 8. Schematic of the relationships between the unified model (UM), Hauser-Feshbach model (HF), Weisskopf-Ewing model (WE) and the usual exciton model (EM). The arrows denote mathematical reduction by means of simplifying assumptions. (Figure taken from [35]). The horizontal arrows represent the assumption of equilibrium ($dq/dt = 0$), while the vertical arrows stand for the limit of a very large spin cut-off parameter ($\sigma^2 \to \infty$).

We point out, however, that all of these specifications can be relaxed without destroying the conceptually attractive and very powerful master-equation structure of the theory. For instance, it is not difficult to incorporate reasonably strong couplings to the continuum, which have recently been investigated by the Heidelberg group [40]. They suggest that this may also relieve difficulties in the model, discussed in Ref. [21], relating to level density and nucleon mean free path (mfp) parameters.

In summary, the angular-momentum conserving master-equation theory seems to us of interest for a number of reasons:

a. It is sufficiently specific and simple to be amenable for practical application (thereby showing that in many cases the results of spinless models are reliable).
b. At the same time, it is closely related to the AWM theory [39], so that a more fundamental quantum-statistical justification is possible and the exciton master equation no longer counts as purely phenomenological.
c. Many useful extensions can be envisioned which are straightforward and do not affect the basic structure of the theory.
d. It unifies in a single formalism several important nuclear-reaction mechanisms and theories, notably the Hauser-Feshbach, Weisskopf-Ewing and exciton models.
e. It enables extensions to describe cross-sections for the excitation of discrete levels if their structure is known.
f. A code based upon the unified model may serve as a benchmark for testing more simple approaches.
g. In order to describe angular distributions in a satisfactory way the starting point should be an angular-momentum conserving model.

3.2. Angular distributions

The statistical reaction model represented by Eqs. (10-14) can be extended in several directions in much the same way as has been done for the non-spin exciton model. This applies for example to multiple emission, complex particle absorption and emission, isospin (two-component) problems, more realistic level densities, etc. A very important generalization would be the inclusion of angular distributions. For the symmetric (multi-step compound) part of the angular distributions this is quite simple: since the model can be cast in a Hauser-Feshbach-like form, the symmetric angular distributions are obtained by an immediate generalization of Hauser-Feshbach theory, like performed by Plyuiko [29]. However, the main problem resides in the modeling of the observed forward-peaked angular distributions. Here, we also encounter the question of the relationship with direct reaction models. This problem appears not to be straightforward to solve.

Several different approaches presently in existence may be useful here, but they all seem to have their drawbacks, too. The most obvious procedure would be to in some way insert the "fast particle" approach [25] (see Sect. 2.2) in the spin-dependent master equation, cf. Ref. [31]. However, on several points this approach has a classical flavour and its microscopic justification is not entirely satisfactory.

Another possibility is to follow the methods used in the FKK theory [6]. However, in that case a separation should be made between multistep-direct and multistep-compound reactions. Although this is an improvement over the fast-particle assumption, it leads to two quite different formalisms. This is not very attractive from a unification point of view. The same applies to the never-come-back approximation embodied in FKK theory: the link with the Hauser-Feshbach model may be intuitively clear, but it is not really proved. In addition, the microscopic postulates are much more obscure in the FKK model [6] than in the AWM theory [39].

A third approach has been developed by Fu [48] who notes (following Plyuiko) that in two limiting cases the phases of the states connected by the residual matrix elements are known: at $n = 1$ (1p0h) there is a complete correlation, while at $n = n_{eq}$ (equilibrium) they are fully random. Introducing an extended Hauser-Feshbach equation, very similar to Eqs. (10)-(14), and using a phenomenological n-dependent weighting function, these two components can be linked. The disadvantage here is that this weighting function is purely empirical and is presently not calculated on a theoretical basis. We suggest to relate this weighting function to the number of collisions k rather than to n. It is also noted that progress is made if one could say something on the correlation of phases just after the first collision. In fact Plyuiko has already suggested to consider only $n=n_o$ (=3), albeit that he has followed the unrealistic assumption of fully correlated entrance and exit channels for n=3. At present the method of Fu seems to be the most practical one available in the spirit of the unified EM, albeit that there is one phenomenological parameter. Some results of this approach are given in Figs. 2 and 3 (histograms). Further work on this method is underway [48].

Finally, we want to mention the work of Tamura et al. [45] on multistep direct reactions. It is more general than that of FKK and its starting point resembles that of AWM (statistical properties of the nuclear Hamiltonian). On the other hand, the connection with multistep-compound reactions has not been studied. Also, the formalism is quite complicated in the higher steps. From the present point of view, the best solution would be to merge in some way the Tamura and AWM theories in a time-dependent (master equation) fashion. It is not clear, however, how this can be achieved, the more so if one aims at a theory amenable for routine applications.

3.3. Microscopic foundations of pre-equilibrium models

At first sight it may seem that this subject is rather esoteric and of no practical interest, since the phenomenological equations are convincing on the basis of physical intuition and their treatment is relatively straightforward. This seems to be the position taken by many researchers in the field. Nevertheless, we already saw in the previous section 3.2. that this subject enters the discussion of how to obtain a consistent description of pre-equilibrium angular distributions. Another domain where one actually encounters the microscopic aspects of precompound models, is the long-standing hybrid/exciton model controversy [41,42, and references therein]. Recently, this problem has been re-investigated by Akkermans [43] and above all by Bisplinghoff [8] from new angles. These authors both conclude that although the models are superficially similar, they embody two very different approaches. Not realizing this has caused a lot of confusion and a large part of the debate of Refs. [41] and [42] must be considered really off the point. The differences discussed in [8,43] are:

- The exciton model predicts exclusive spectra, whereas the hybrid model considers inclusive ones.
- The physical picture used in the two models is radically different: the exciton model is a systems approach (in that it considers the evolution of the eigenstates of the nuclear system as a whole), whereas the hybrid model is an individual-particle approach (it focusses on the development of single-particle states in a classical cascade-like manner).

The first remark is of a macroscopic nature only, but the second one relates to the microscopic point of view: the adoption of a nuclear shell model Hamiltonian versus a single particle one. This point alone does not yet suffice to explain the predicted differences in the observables. Bisplinghoff adds an interesting point, however, by arguing that the exciton model implicitly assumes a complete particle-hole configuration mixing within each exciton class, while the hybrid model presupposes the particle states to be pure, i.e., no configuration mixing at all. Thus, his conclusion is (albeit not cast in these terms) that not only the macroscopic basis of the models differs, but also their microscopic foundation. He suggests, then, that it should be possible to experimentally (i.e., macroscopically) discriminate between the microscopic postulates of the two models.

We see that on several accounts the microscopic aspects are also of applied interest and more work directed towards them would be useful. It appears that the AWM work, based on the randomness properties of the nuclear Hamiltonian, is the most general in this respect (also more general than FKK, according to McVoy and Tang [44]). Interestingly, the work of Tamura et al. [45] on multistep-direct reactions has a similar starting point. Further, we want to draw attention to the work by Bunakov [46] who discusses the conditions under which master equations can be derived for nuclear reactions (both direct and precompound) starting from the time-dependent Schrödinger equation. These conditions turn out to be very similar to those used by Agassi et al. [39] in stationary theory. This suggests that a common microscopic ground for a unified reaction theory can be found. Still, more work needs to be done in this area. For instance, the conditions under which the use of classes of states (exciton classes) is justified, are relatively unexplored. This has been called the "lumpability" problem in [43]. It is important, since one would like to deal with a small number of macroscopically significant variables instead of with the many millions of nuclear eigenstates. We have started to consider this problem and we give below some preliminary ideas [47]:

- It seems possible to derive an exciton master equation like Eq. (10) from the time-dependent Schrödinger equation. Due to the transition from consideration of individual eigenstates to that of state classes it is reasonable to assume certain randomness properties of the residual interaction, close to those of AWM. In addition, one has to introduce a coarse graining in time.
- If this is correct, the usual postulate of equal a priori probabilities of particle-hole configurations is a sufficient, but not really necessary condition in the derivation (as long as the number of states in a single exciton class is large).

- The same would apply to the statement by Bisplinghoff [8] on configuration mixing in the exciton model. His conclusion about complete configuration mixing is not compelling: it is again a sufficient but not necessary condition. In qualitative terms the resulting paradox can be resolved by pointing out that there may not be full intrinsic microscopic configuration mixing, but that in a coarse-grained, macroscopic description (and this is the only one that can be experimentally verified!) the system behaves as if there would be. This argument is also valid with regard to the equal a-priori probabilities.

Be this as it may, we believe to have indicated that there need not be an insuperable gap between well-founded microscopic theory and models such as the exciton model suited for routine calculations. Ideally, precompound and compound nuclear-reaction theory should be established as just another branch of nonequilibrium quantum statistical mechanics.

4. CONCLUSION

The exciton model is still being further developed. It is a model that certainly has increased our understanding of nuclear reactions. Moreover, the model is suitable for practical applications, in particular in the field of the evaluation of cross-sections for neutron-induced reactions. Recently, it has become possible to use the model not only for the prediction of cross-sections and energy spectra including γ-ray competition, but also for angular distributions. The model contains phenomenological parameters, but these are few and are reasonably constant over large mass and energy ranges. It seems viable to develop a reasonably satisfactory microscopic foundation for the exciton model. The most important recent development has been to generalize the model such that it includes explicit angularmomentum and parity conservation with the requirement that it should contain the Hauser-Feshbach model as a limiting case. Progress has been made in this unification effort, although the extended models are as yet not satisfactory with respect to the description of angular distributions.

REFERENCES

[1] H. Machner, Fast particle emission from nuclear reactions, Phys. Rep. 127 (1985) 309.
[2] H. Gruppelaar, P. Nagel and P.E. Hodgson, Pre-equilibrium processes in nuclear reaction theory: the state of the art and beyond, Riv. Nuovo Cim. 9 (1986) No. 7, p.1.
[3] P.E. Hodgson, H. Gruppelaar and P. Nagel, Radiat. Eff. 95 (1986) 27.
[4] H. Gruppelaar and P. Nagel, International model and code comparison on pre-equilibium effects, NEA Data Bank Newsletter 32 (1985) and NEANDC-204 "U", INDC (NEA) 6.
[5] M. Blann, Annu. Rev. Nucl. Sci. 25 (1975) 123.
[6] H. Feshbach, A. Kerman and S. Koonin, Ann. Phys. (N.Y.) 125 (1980) 429.
[7] H. Machner, Z. Phys. A327 (1987) 175.

[8] J. Bisplinghoff, Phys. Rev. C33 (1986) 1569.
[9] S.K. Gupta, Z. Phys. A303 (1981) 329.
[10] J. Dobeš and E. Běták, Z. Phys. A310 (1983) 231.
[11] C. Kalbach, Phys. Rev. C33 (1986) 818.
[12] C. Kalbach, Phys. Rev. C23 (1981) 124.
[13] J.M. Akkermans and H. Gruppelaar, Z. Phys. A300 (1981) 345
[14] B. Strohmaier and M. Uhl, Proc. IAEA Course on Nuclear Theory for Applications, Trieste, 1987, IAEA-SMR-43 (1980) 313.
[15] H. Gruppelaar and J.M. Akkermans, The GRAPE code system for the calculation of precompound and compound nuclear reactions, ECN-164 (1985) and Radiat. Eff. 95 (1986) 59.
[16] E. Běták and J. Dobeš, Phys. Lett. 84B (1979) 368.
[17] J.M. Akkermans and H. Gruppelaar, Phys. Lett. 157B (1985) 95.
[18] A. Iwamoto and K. Harada, Nucl. Phys. A419 (1984) 472.
[19] Zhang Jingshang, Wen Yuangi and Wang Shunuan, IAEA Coordinated Research Programme Mtg. on Methods for the Calculation of Fast Neutron Nuclear Data for Structural Materials, Bologna, October 1986.
[20] F.C. Williams, Phys. Lett. 31 (1970) 184.
[21] J.M. Akkermans and H. Gruppelaar, Z. Phys. A321 (1985) 605.
[22] C.Y. Fu, Nucl. Sci. Eng. 86 (1984) 344.
[23] G. Reffo, private communication (1986); see also the papers of G. Reffo and M. Blann, presented at this meeting.
[24] K. Kikuchi and M. Kawai, Nuclear matter and nuclear reactions (North Holland, Amsterdam, 1986), p.33.
[25] G. Mantzouranis, D. Agassi and H.A. Weidenmüller, Phys. Lett. 57B (1975) 220; G. Mantzouranis, H.A. Weidenmüller and D. Agassi, Z. Phys. A276 (1976) 145.
[26] Sun Ziyang, W. Shunuan , Z. Jingshang and Z. Yizhang, Z. Phys. A305 (1982) 61.
[27] C. Costa, H. Gruppelaar and J.M. Akkermans, Phys. Rev. C28 (1983) 587.
[28] C. Kalbach and F.M. Mann, Phys. Rev. C23 (1981) 112.
[29] V.A. Plyuiko, Sov. J. Nucl. Phys. 27 (1978) 623.
[30] A. De, S. Ray and S.K. Ghosh, J. Phys. G13 (1987) 1047.
[31] G. Reffo, F. Fabbri and C. Costa, Contr. Int. Conf. on Nuclear physics, Florence 1983, RT/FI(83) 10 (ENEA, Bologna,1983).
[32] C.Y. Fu, Proc. Int. Conf. on Nuclear cross-sections for technology, Rept. NBS-Sp-594 (1980), p. 757.
[33] H. Gruppelaar, Proc. IAEA Adv. Group Mtg. on Basic and applied problems of nuclear level densities, Rept. BNL-NCS-51694 (1983), p.143.
[34] Xu Jun and Jiang Chenglie, Z. Phys. A324 (1986) 153.
[35] Shi Xiangjun, H. Gruppelaar and J.M. Akkermans, Nucl. Phys. A466 (1987) 333.
[36] P. Oblozinsky, Phys. Rev. C35 (1987) 407.
[37] J.M. Akkermans, Phys. Lett. 82B (1979) 20.
[38] J.M. Akkermans, Shi Xiangjun and H. Gruppelaar, Comput. Phys. Commun. 43 (1987) 347.
[39] D. Agassi, H.A. Weidenmüller and G. Mantzouranis, Phys. Reports 22C (1975) 145.
[40] H. Nishioka, J.J.M. Verbaarschot, H.A. Weidenmüller and S. Yoshida, Ann. Phys. (N.Y.) 172 (1986) 67.
[41] E. Gadioli et al., Phys. Rev. C17 (1978) 2238.
[42] M. Blann, Phys. Rev. C17 (1978) 1871.

[43] J.M. Akkermans, Radiat. Eff 95 (1986) 103.
[44] K.W. McVoy and X T. Tang, Phys. Reports 94 (1983) 139.
[45] T. Tamura, T. Udagawa and H. Lenske, Phys Rev. C26 (1982) 379.
[46] V.E. Bunakov, Z. Phys. A297 (1980) 323.
[47] J.M. Akkermans, in preparation.
[48] C.Y. Fu, Symp. on Neutron cross-sections from 10 to 50 MeV, Brookhaven 1980, Vol.2 of BNL-NCS-51245 (1980) 675 and to be published
[49] H. Gruppelaar, D. Nierop and J M. Akkermans, Processing of double-differential cross-sections in the new ENDF-VI format - GROUPXS code description and users' manual -, ECN-182 (1986) and to be published

MULTISTEP COMPOUND PROCESSES IN NUCLEAR REACTIONS

P E HODGSON
Nuclear Physics Laboratory,
Oxford University,
Oxford, United Kingdom

Abstract

The quantum mechanical theory of multistep compound reactions due to Feshbach, Kerman and Koonin is reviewed and applied to the analysis of reactions of neutrons with ^{59}Co, ^{93}Nb and ^{209}Bi A detailed study is made of reactions at MeV, and in addition the total cross sections in several reaction channels are presented in the range 10–20 MeV Conclusions are drawn concerning the energy variations of the contributions of direct, pre equilibrium and compound nucleus reactions

1 INTRODUCTION

During the nineteen sixties, evidence accumulated indicating that is is possible for particles to be emitted after the first stage of a nuclear interaction but long before the attainment of statistical equilibrium, these are the pre equilibrium particles Many attempts have been made to understand such reactions in terms of a series of nucleon nucleon interactions within the target nucleus Starting with the pioneer work of Griffin[1], a series of semi classical or exciton models of varying complexity has been developed, and with appropriate choice of parameters these are often able to fit the observed energy and angular distributions of the emitted particles More recently, several quantum mechanical theories have been proposed, and these provide in principle a way of calculating the cross sections of pre equilibrium processes without the uncertainties of the semi classical approximations This makes it possible to analyse in a unified way the cross sections in all the contributing reaction channels at moderate energies

Pre equilibrium processes make substantial and in some cases dominant contributions to the cross sections of reactions initiated by neutrons from 10 to 20 MeV The multistep compound (MSC) theory of Feshbach, Kerman and Koonin[2] is described in section 2, and applied to some neution reactions on ^{59}Co and ^{93}Nb in section 3 The semi classical and quantum mechanical theories of multistep processes are discussed in section 4

This review includes some of the material already presented at the International Symposium on Physics at Tandem (Beijing, 1986) and then describes in more detail the work completed since then This new work includes a study of the energy variations of the cross sections in several reaction channels for the interactions of reactions with ^{93}Nb and ^{209}Bi This shows the contributions of the multistep processes to the cross sections as a function of neutron energy Particular attention has been given to the cross sections of alpha emitting reactions, and some new results are presented

2 THE QUANTUM-MECHANICAL THEORY OF FESHBACH, KERMAN AND KOONIN

The basic physical picture underlying the quantum mechanical multistep theory is the same as for the exciton model It is assumed that the interaction between the incident nucleon and the target nucleus takes place in a number of stages of increasing complexity To evaluate the probability of emission after the first stage but before the attainment of statistical equilibrium it is necessary to consider the mechanism of nuclear excitation in detail The nucleus is excited by a series of nucleon nucleon collisions between the projectile and the target nucleons These take place in stages, or doorway states of increasing complexity beginning with the projectile in the continuum The first interaction creates a particle hole pair, giving a 2 particle 1 hole (2p1h) state There are a large number of possible 2p1h states Subsequent interactions create additional particle hole pairs, giving 3p2h states and once again there are very many 3p 2h states for each 2p1h state This process continues until the excitation is spread through the nucleus to produce a fully equilibrated nucleus which then decays statistically

At each stage it is useful to consider separately the states with at least one particle in the continuum and the states with all particles bound, these states may be formally described by the projections P and Q acting on the total waveform Ψ, with $P+Q=1$ The set of states $P\Psi$ contribute to the multistep direct process and the complementary set of states $Q\Psi$ to the multistep compound process These states are shown in Figure 1, with the arrows indicating transitions from one configuration to another If only two body interactions are present these transitions can only take place between neighbouring stages, this is the chaining hypothesis

At each stage there are three possibilities excitation of an additional particle hole pair, de excitation of a particle hole pair and emission into the continuum The transition matrix for the de excitation of a particle hole pair is the same as the corresponding matrix for its excitation, but because the density of final states is so much greater for the states with more particle hole pairs the probability of excitation of an additional particle hole pair is much greater than that of de-excitation Thus transitions to states of greater complexity are much more probable than transitions to states of lesser complexity It is therefore good approximation to neglect the transitions going to states of lower exciton number, this is the never come-back assumption

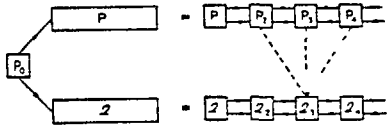

FIGURE 1 Multi step description of a nuclear reaction

The pre equilibrium emission can take place directly at each stage from the P chain, or indirectly from the Q chain In the latter case the emission process goes through states in the P chain, this can happen in three different ways as shown in Fig 1 The more energetic particles come from the early stages of the chain and the less energetic from the later stages

The time structure of the interactions is more complicated The multistep direct reactions take place down the P chain, and these direct processes take place rapidly

The transitions down the Q chain, on the other hand, take place much more slowly, and indeed a state of quasi equilibrium is attained at each stage so that the emission is compound in character with a symmetric angular distribution A large number of individual interactions take place at each stage, but nearly all of them leave the number of particles and holes unchanged It is only very occasionally that a collision results in a transition to a state of greater complexity or to the P chain and hence to the continuum To obtain the emission probabilities only these escape probabilities need be calculated, together with the probabilities for exciting a further particle-hole pair The vastly greater number of interactions taking place within each stage in the Q-chain without changing the exciton number are only important for their role in ensuring statistical equilibrium at each stage

The relative reaction fluxes passing down the P and Q chains depends strongly on the incident energy At low energies the Q chain interactions dominate, giving symmetric multistep compound angular distributions As the energy increases the P chain interactions become increasingly important until finally they are responsible for almost all the cross section giving forward-peaked multistep direct angular distributions The transitions between the P and Q chains are small and average out, so that the contributions of the P and Q chains can be evaluated separately, and their sum compared with experiment

To describe the multistep compound process mathematically, let $\Gamma_n^{\downarrow}$ be the damping width corresponding to the transition from the n^{th} to the $n+1^{\text{th}}$ state, and $\Gamma_n^{\uparrow}$ the escape width for the transition from the n^{th} state into the continuum The total width for the decay of the n^{th} state is therefore

$$\Gamma_n = \Gamma_n^{\downarrow} + \Gamma_n^{\uparrow} \tag{2 1}$$

The total probability for emission into the continuum from the n^{th} state is then the product of three factors for each value of the total angular momentum J

(a) the probability of formation of the compound system, which is given by the optical model expression

$$\sigma_C^{\ell J} = \pi\lambda^2 \frac{2\pi < \Gamma_{\ell J}^{in} >}{< D_{\ell J} >} \tag{2 2}$$

where the last factor is the strength function

(b) the probability of the system arriving to the N^{th} stage without particle emission This is given by the product of the probabilities of surviving the m^{th} stage,

$$\prod_{m=1}^{N-1} W_{m+1\ m} = \prod_{m=1}^{N-1} \frac{< \Gamma_{mJ}^{\downarrow} >}{< \Gamma_{mJ} >} \tag{2 3}$$

where $< \Gamma_{mJ}^{\downarrow} >$ is the damping width for the transition to a stage of higher exciton number and $< \Gamma_{mJ} >$ is the total width

(c) the probability that a particle will be emitted into the continuum from the N^{th} stage This is given by a sum over all possible emission processes divided by the sum over all processes Emission can take place in three ways, so the emission probability is given by the sum of products of emission widths $\Gamma_{NJ}^{\uparrow \ell s \nu}(U)$ and the

level densities $\rho_J^N(U)$ of the final states of the residual nucleus at excitation energy U. This gives the factor

$$\frac{\left\langle \Gamma_{NJ}^{\uparrow \ell s \nu}(U) \rho_J^N(U) \right\rangle}{< \Gamma_{NJ} >} \tag{2.4}$$

Collecting these factors together gives for the double differential cross-section for pre-equilibrium emission by the multistep compound process

$$\frac{d^2\sigma}{d\Omega d\epsilon} = \pi\lambda^2 \sum_J (2J+1) \left[\sum_{N=1}^{r} \sum_{ls\lambda\nu} C_{lsJ}^{\lambda} P_\lambda(\cos\theta) \sum_\nu \frac{< \Gamma_{NJ}^{\uparrow l e \nu}(U) \rho_J^N(U) >}{< \Gamma_{NJ} >} \right] \times$$
$$\times \left(\prod_{m=1}^{N-1} \frac{< \Gamma_{mJ}^{\downarrow} >}{< \Gamma_{mJ} >} \right) \frac{2\pi < \Gamma_{\ell J}^{in} >}{< D_{\ell J} >} \tag{2.5}$$

All the factors in the above expressions are calculated quantum-mechanically or, as in the case of the level density function, obtained from the known systematics of nuclear properties. The measured cross-section for the formation of the compound nucleus is used, and if it is not available it can be obtained from the optical model.

The particle-hole level densities are calculated using Ericson's expression based on the equidistant spacing model, with an additional factor giving the spin distribution

$$\rho_J^N(E) = \rho_N(E) S_J^N \equiv \rho_n(E) S_J^n \tag{2.6}$$

where $n = 2N + 1$ and

$$\rho_n(E) = \frac{g(gE)^{n-1}}{p!h!(n-1)!} \tag{2.7}$$

in which g is the total single-particle density and p, h the numbers of particles and holes ($n = p + h$).

The spin-dependent factor S_J^n is given by

$$S_J^n = \frac{2J+1}{\sqrt{\pi'} n^{3/2} j^3} \exp\left[-\frac{(J+\frac{1}{2})^2}{n\sigma^2} \right] \tag{2.8}$$

The spin cut-off parameter σ^2 is related to the nuclear temperature τ by the expression

$$\sigma^2 = 2C\tau \tag{2.9}$$

where $C \sim A^{2/3}/90$ (MeV^{-1}) and

$$E = a\tau^2 - \tau \tag{2.10}$$

and $a = \pi^2 g/6$.

Each of the widths corresponding to the three emission processes may be expressed as a product of three factors, the first depending on the level densities, the second on angular momentum coupling and the third on the wavefunctions of the interacting particles:

$$< \Gamma_{NJ}^{\uparrow \ell s \nu}(U) \rho_s^\nu(U) > = X_{NJ}^{\ell s \nu}(U) A_N^\nu(U) \theta_N^\nu(U). \tag{2.11}$$

The full expressions for the first two of these functions are given by FKK and the third is

$$\theta(U) = V_0 \left(\frac{4\pi}{3} r_0^3 \right) \frac{1}{4\pi} \int_0^\infty u_{j1}(r) u_{j2}(r) u_{j\ell}(r) u_{j3}(r) dr/r^2 \tag{2.12}$$

where V_0 is the strength of the residual two-body interaction and the radial wave functions $u_{j1}(r)$ and $u_{j2}(r)$ refer to the bound particles before the interaction, $u_{j3}(r)$ to the bound particle after the interaction and $u_{j\ell}(r)$ to the particle emitted into the continuum.

At lower energies where there are few contributing channels it is possible to fix the strength of the effective interaction V_0 directly and accurately by normalising the sum of the cross-sections in all the reaction channels to the total reaction cross-section σ_R obtained from the optical model potential or from experiment. Thus at a particular energy

$$\sum_i V_0^2 f_i(E) + \sum_j \sigma_j(E) = \sigma_R \tag{2.13}$$

where i, j label the reaction channels. $V_0^2 f_i(E)$ is the total reaction cross-section in the i$^{\text{th}}$ channel and $\sigma_j(E)$ that in the j$^{\text{th}}$ channel. In this expression the cross-sections in the first i channels are calculated using the multistep theory, and those in the remaining j channels are either calculated by the Weisskopf-Ewing theory or taken from experimental data.

In the calculations reported here we evaluate the matrix elements using constant wavefunctions inside the nucleus and a two-body interaction of zero range as originally suggested by FKK. This of course overestimates the cross-sections and so thus requires small values of the effective interaction V_0. In a subsequent calculation Bonetti and Colombo[3] repeated the calculation with realistic wavefunctions and a density-dependent Yukawa interaction and showed that the corresponding V_0 is consistent with that found in other analyses. The main effect of using these approximate wavefunctions is thus absorbed by the renormalisation of the effective interaction; the effect on the energy spectra is small. Making the calculations in this way substantially reduces the computation time.

Feshbach, Kerman and Koonin also derived an expression for the double differential cross-section for pre-equilibrium emission by the multistep direct process.

3. MULTISTEP ANALYSES OF NEUTRON-INDUCED REACTIONS

The Milan group has already made many calculations using the multistep compound and multistep direct theories[3]. More recently, the multistep compound theory has been used to calculate the inelastic spectrum of neutrons emitted when 14 MeV neutrons interact with ^{59}Co, ^{93}Nb and ^{209}Bi[4,5]. These reactions are particularly suitable to test the theory as much data are available, and they are also of practical importance.

At these energies, there are rather few open reaction channels and so it is possible to make a relatively complete analysis. In particular, the effective interaction strength can be fixed by the requirement that the sum of all the non-elastic cross-sections is the reaction cross-section.

Preliminary calculations of the total cross-sections in the various channels were made using the Weisskopf-Ewing[7] theory, and the results are shown in Fig.2. The optical potentials used are given in Ref.4. At energies less than 9 MeV only the (n,n'), (n,γ), (n,p) and (n,α) cross-sections are appreciable, and of these (n,n') accounts for about 97% of the total. The value of the effective interaction V_0 may therefore be

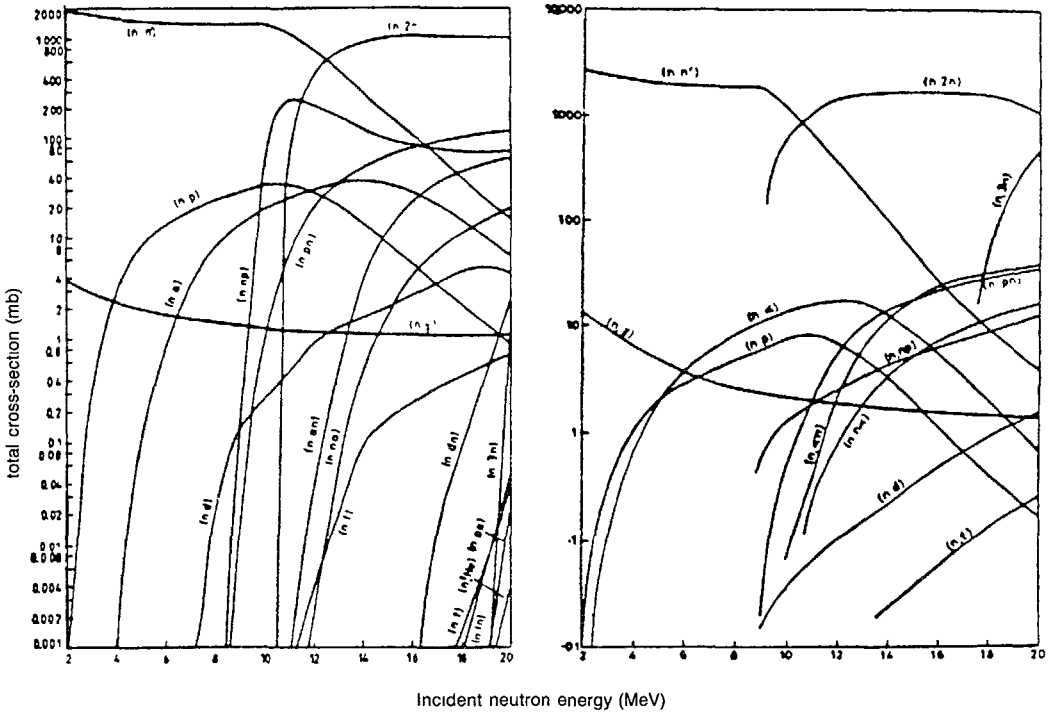

FIGURE 2 Total cross-sections of all reactions of neutrons on ^{59}Co and ^{93}Nb as a function of neutron energy calculated with the Weisskopf-Ewing theory.

determined accurately from equation(2.13) using the Weisskopf-Ewing values for the three smaller cross-sections. The main uncertainty comes from the calculated total reaction cross-section. At 14 MeV the situation is quite different; the $(n,2n)$ cross-section dominates, (n,n') is still large and (n,np) and (n,pn) are quite important. The measured neutron inelastic cross-section includes the neutrons from all these reactions, whereas the calculated neutron inelastic cross-section refers only to the neutrons emitted first, i.e. it gives the (n,n') cross-section together with half the (n,np) and $(n,2n)$ cross-sections but not those of the neutrons from (n,pn) or the second neutrons from $(n,2n)$.

Examination of the angular distributions of the emitted neutrons and protons show that they are almost symmetric, with a slight forward excess. This indicates that the reaction mechanism is predominantly compound, with a small direct contribution that for ^{59}Co can be estimated from the forward excess to be about 100mb for neutrons and about 20mb for protons. This direct contribution has now been calculated, and is included in the 30° distribution in Fig.3.

The total reaction cross-section for 14 MeV neutrons on ^{59}Co is 1370 ± 30mb (MacGregor *et al*[6]) and allowing 120 ± 40mb for direct processes leaves 1250 ± 50mb for compound nucleus processes. This is therefore the sum of the cross-sections of the

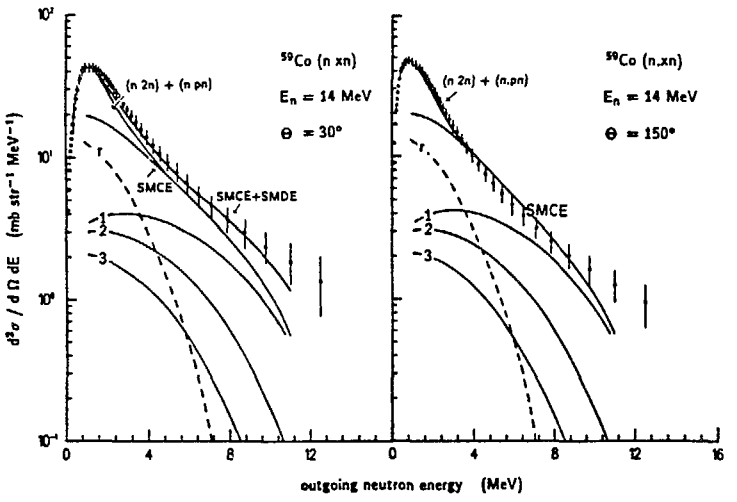

FIGURE 3 Energy spectra of neutrons emitted at 30° and 150° from ^{59}Co at an incident neutron energy of 14 MeV. The experimental data of Sal'nikov[9] are compared with statistical multistep compound (SMC) calculations. The curves labelled with the value of N show the contributions of N-step processes and the broken and dotted curves show those due to the residual r-stage processes for the (n,n') and the $(n,2n)+(n,pn)$ reactions respectively. The full curve gives the sum of these processes (Field[4]).

compound nucleus contributions to the contributing reactions, provided there are no direct contributions to the alpha emission reactions. This latter qualification can be tested when the corresponding angular distributions are available but since the total cross-sections in the alpha channels are small this will not significantly affect the analysis.

The multistep compound theory was used to evaluate the neutron and proton emission cross-sections, and the alpha-emission cross-sections were taken to have the value of 45mb given by the Weisskopf-Ewing[7] theory. Using the level-density parameters of Brancazio and Cameron[8], and taking the total compound nucleus cross-section to be 1250mb the value of V_0 was determined to be 0.90.

The emission of the first particle leaves the residual nucleus in a spectral distribution of excitation energies, and the theory may now be used to calculate the cross-section corresponding to the emission of a proton, neutron or alpha particle as second particle. This gives the $(n,2n)$, (n,np), (n,pn) and (n,α) cross-sections, and also the (n,n') and (n,p) in cases where there is no second particle emitted. The cross-sections of the two-particle emission reactions obtained in this way are appreciably smaller than the values obtained from the Weisskopf-Ewing theory alone because the possibility of pre-equilibrium emission of the first particle implies a lower excitation energy in the residual nucleus and hence reduced probability for the emission of a second particle.

These cross-sections are given in Table 1 and compared with the experimental values. This is only possible for the total $(n,2n)$, (n,p) and (n,α) cross-sections obtained from radiochemical analyses; in other cases cross-sections obtained must be combined before such comparisons are made. Thus only the total of the (n,np), (n,pn) and (n,d) reactions is obtainable radiochemically, and particle emission cross-sections, that can be measured as energy and angular distributions, refer to the sum of several separate reactions. Thus the total neutron emission cross-section is the sum of the cross-section for the emission of a neutron as first particle and that for the emission of a neutron as second particle (i.e. the sum of $(n,2n)$, (n,pn) and $(n,\alpha n)$). Using the values from Table 1 gives 1758mb as the total compound nucleus neutron emission cross-section. Adding the direct component of 100mb gives 1858mb, which may be compared with the value 1780 ± 100mb obtained from the experimental data of Sal'nikov *et al*[9].

Table 1

Total cross-sections of neutron reactions on ^{59}Co at 14 MeV

Reaction	Theory	Experiment	Reaction	Theory	Experiment
(n,n')	475	–	Neutron Emission	1858 ± 90	1780 ± 100[9]
$(n,2n)$	592	640 ± 90[15]	Proton Emission	149	97 ± 12[10]; 108 ± 22[11]
(n,pn)	72	$\gtrsim 35$[11]	Total Reaction	–	1370 ± 30[6]
(n,np)	25				
(n,p)	52	81 ± 10[12]; 75 ± 15[13]; 29 ± 4[14]			
(n,α)	43	30 ± 4[15]			
$(n,\alpha n)$	2	–			

The calculations also give the double differential cross-section for neutron emission, and this is compared with the experimental data of Sal'nikov *et al* in Fig.3.

In a similar way the proton emission cross-section may be obtained as the sum of the cross-section for the emission of a proton as first particle and that for the emission of a proton as second particle (i.e. (n,np)). This gives 149mb as the total compound nucleus proton emission cross-section, which may be compared with the value 97 ± 12mb obtained from the experimental data of Colli *et al*[10]. The double differential cross-section for proton emission is compared with the data in Fig.4.

A similar analysis was made of the reactions of 14 MeV neutrons on ^{93}Nb, and the calculated neutron emission spectrum is compared with the experimental data in Fig. 5 and the total cross-sections in Table 2. The calculated neutron emission spectrum for ^{209}Bi is compared with the data in Fig.6.

The calculations have now been made over a range of energies and compared with the experimental excitation functions for the $(n,2n)$, $(n,3n)$, (n,p) and (n,α) cross-sections.

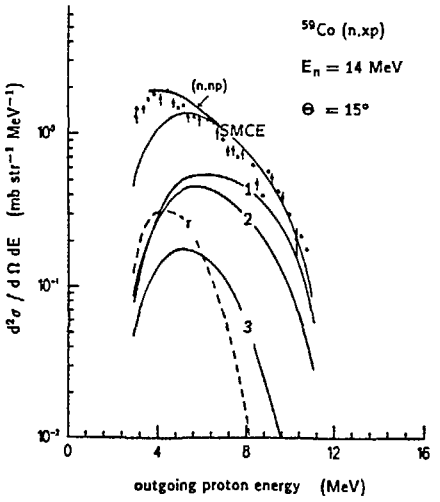

FIGURE 4 Energy spectrum of protons emitted at 15° from ^{59}Co at an incident energy of 14 MeV. The experimental data[10] are compared with the statistical multistep compound (SMC) calculations. The curves labelled with the values of N show the contributions of N-step processes and the broken and dotted curves those due to the residual r-stage processes for the (n,p) and the (n,np) reactions respectively. The full curve gives the sum of these processes (Field[4]).

Table 2

Total cross-sections of neutron reactions on ^{93}Nb at 14 MeV

Reaction	Theory	Experiment	Reaction	Theory	Experiment
(n,n')	347		Neutron Emission	2321	2500 ± 120[9]
$(n,2n)$	1283	1279 ± 88[16]	Proton Emission	76	44 ± 2[11]; 51 ± 8[22]
(n,pn)	35		Deuteron Emission	0.2*	8 ± 3[22]†
(n,np)	3		Alpha Emission	26*	14 ± 3[22]†
(n,p)	73		Total Reaction	–	1731 ± 30
(n,α)	–	11.1 ± 2.7[17]; 9 ± 2[18]; 9.5 ± 0.5[19], 9.3 ± 3[20]			
$(n,\alpha n)$	2	–			

* Weisskopf-Ewing Theory † At 15 MeV.

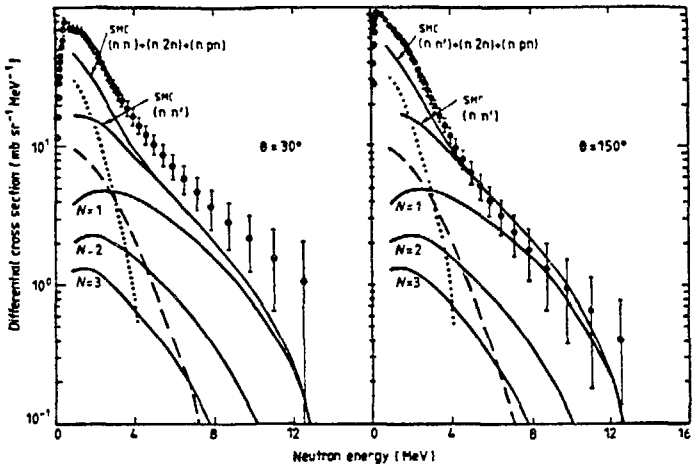

FIGURE 5 Energy spectra of neutrons emitted at 30° and 150° from ^{93}Nb at an incident neutron energy of 14 MeV. The experimental data of Sal'nikov[9] are compared with statistical multistep compound (SMC) calculations. The curves labelled with the value of N show the contributions of N-step processes and the broken and dotted curves show those due to the residual r-stage processes for the (n,n') and the $(n,2n)+(n,pn)$ reactions respectively. The full curve gives the sum of these processes.

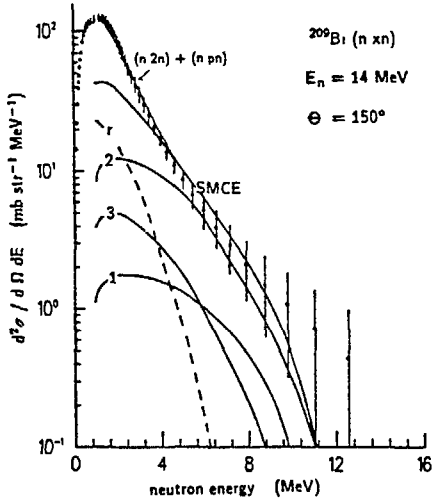

FIGURE 6 Energy spectrum of neutrons emitted at 150° from ^{209}Bi at an incident neutron energy of 14 MeV. The experimental data of Sal'nikov[9] are compared with statistical multistep compound (SMC) calculations The curves labelled with the values of N show the contributions of N-step processes and the broken curve that due to the residual r-stage process. The full curve gives the sum of these processes (Field[4])

The $(n,2n)$ and $(n,3n)$ cross-sections

The Weisskopf-Ewing calculation gives $(n,2n)$ cross-sections that are up to 30% greater than the measured values in the energy range from threshold to 20 MeV (Holub *et al*[23]). This difference is attributable to pre-equilibrium emission, which gives more neutrons of higher energy, which in turn reduces the energy of the residual nucleus and with it the probability of the emission of a second neutron, thus reducing the $(n,2n)$ cross-section. The magnitude of this reduction was calculated using the statistical multistep compound theory and the results are compared with experimental data in Fig.7.

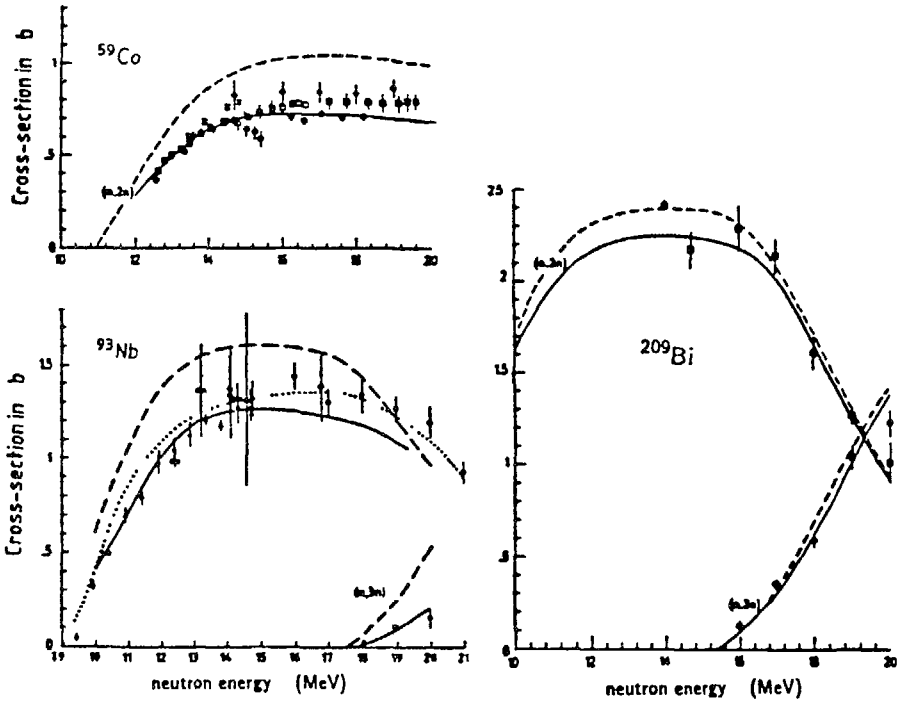

FIGURE 7 Excitation functions for the $(n,2n)$ and $(n,3n)$ reactions on ^{59}Co, ^{93}Nb and ^{209}Bi. The solid curves were calculated using the SMCE results as input for the second stage and the dashed curves using the Weisskopf-Ewing theory for both stages. References to the data on ^{59}Co may be found in Wilmore and Hodgson[15] and Hasan *et al*[26], those on ^{93}Nb in Strohmaier[24], and those on ^{209}Bi in Veeser *et al*[16]. The dotted curve for ^{93}Nb shows the result of exciton model calculations by Strohmaier[24] (Field[4]).

The (n,p) and (n,px) cross-sections

The measurements of proton emission by the activation method gives only the (n,p) cross-section whereas techniques detecting the emitted protons give the (n,px) cross-section, where x indicates the inclusion of all other proton-emitting reactions like (n,pn) and (n,np). The cross-sections of these reactions obtained by the Weisskopf-Ewing and statistical multistep compound theories are compared with some activation data in Fig.8.

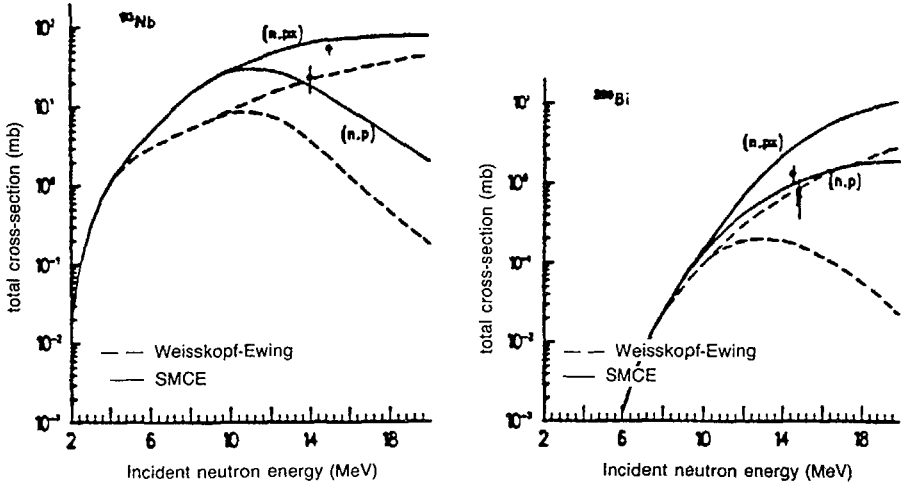

FIGURE 8 Excitation functions for the (n,p) reaction on ^{93}Nb and ^{209}Bi. The solid curves were calculated using the SMCE results as input for the second stage and the dotted curves using the Weisskopf-Ewing theory for both stages. References to the data on ^{93}Nb may be found in Strohmaier[24], and those on ^{209}Bi in Mukherjee *et al*[27]. (Field[4]).

The (n,α) and $(n,\alpha x)$ cross-sections

The same considerations as those mentioned in the previous section apply to (n,α) and $(n,\alpha x)$ reactions. Weisskopf-Ewing[7] calculations are compared with the experimental data for the excitation function in Figs.9 and 10 and for the energy spectrum of the emitted alpha-particles for an incident energy of 14 MeV in Fig.11. The excitation function for the (n,α) reaction calculated with the Weisskopf-Ewing theory was normalised to the data at low energies and falls substantially below the data for energies above 10 MeV. This is attributable to the pre-equilibrium component, and the exciton model calculations of Strohmaier[24] do indeed fit the data well. Measurements of the angular distribution of the emitted alpha-particles by Bormann *et al*[25] show a marked forward peaking, so the pre-equilibrium emission takes place by the multistep direct process. It is not surprising that the (n,α) pre-equilibrium cross-section is much greater

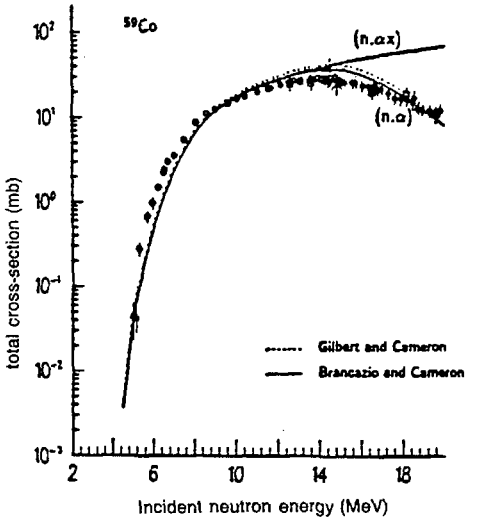

FIGURE 9 Excitation functions for the (n,α) reaction on ^{59}Co compared with the Weisskopf-Ewing calculations. The solid curves were calculated using the level density parameters of Brancazio and Cameron[8] and the dotted curves using those of Gilbert and Cameron[28]. References to the data may be found in Wilmore and Hodgson[15] (Field[4]).

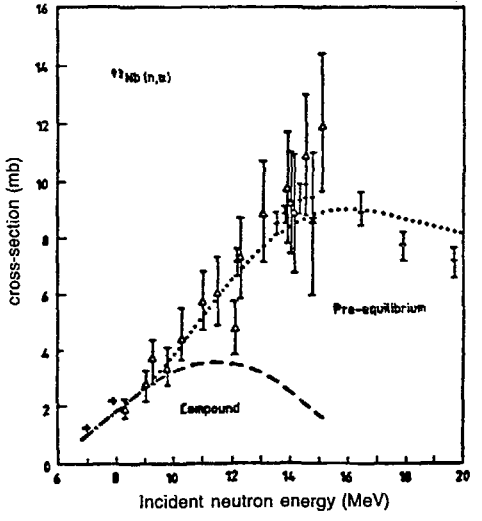

FIGURE 10 Total cross-section for the (n,α) reaction on ^{93}Nb compared with Weisskopf-Ewing calculations (dashed curves) and the exciton model calculations of Strohmaier[24] (dotted curve). The data are from Bramlitt and Fink[17] (x), Blosser *et al*[18] (⊙), Prestwood and Bayhurst[19] (+) and Tewes *et al*[29] (◇) (Strohmaier[24]).

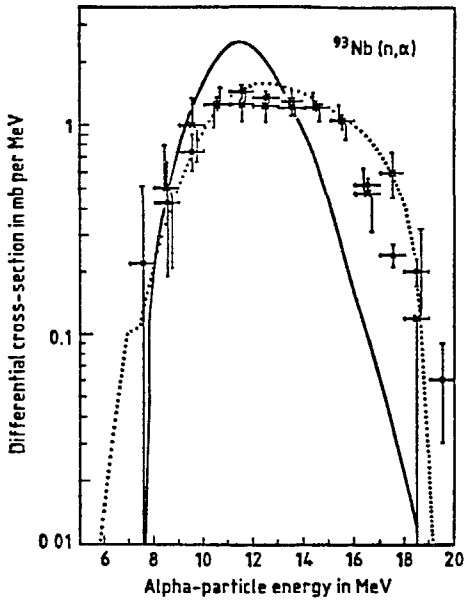

FIGURE 11 Energy spectrum of alpha-particles emitted from ^{93}Nb at an incident neutron energy of 14 MeV compared with normalised Weisskopf-Ewing calculations for the sum of the (n,α) and $(n,n\alpha)$ reactions (full curve) and exciton model calculations of Strohmaier[24] (dotted curve).

than the Weisskopf-Ewing[7] cross-section because if the alpha-particle is emitted with high energy the residual nucleus has not enough energy to evaporate a neutron. The alpha-particle emission spectrum in Fig.11 is the sum of the (n,α), $(n,\alpha n)$ and $(n,n\alpha)$ cross-sections and for comparison with the data the Weisskopf-Ewing calculations are normalised to the total alpha-emission cross-section of 10 mb. This comparison shows an excess of high-energy particles that is characteristic of pre-equilibrium emission, and this is confirmed by the exciton model calculations of Strohmaier[24]. Calculations of alpha-emission using the Feshbach-Kerman-Koonin theory are in progress.

These calculations of the pre-equilibrium cross-sections as a function of incident energy allow the changing contributions of the various reaction processes to be determined, and the results are shown in Fig.12. It will be noticed that the compound nucleus cross-section falls with increasing energy, while the direct cross-section rises. Within the compound nucleus cross-section, the contribution of the multistep compound process at first rises with energy, attains a maximum and then falls. The energy at which the multistep compound cross-section is maximal increases with target mass.

The present understanding of the cross-sections in the weaker channels such as (n,t) is unsatisfactory. There is very little experimental data and these cross-sections are generally much greater than those given by the statistical theories. It is likely that they are predominantly direct or multistep direct, but this will not be known until pre-equilibrium calculations are compared with accurate experimental data.

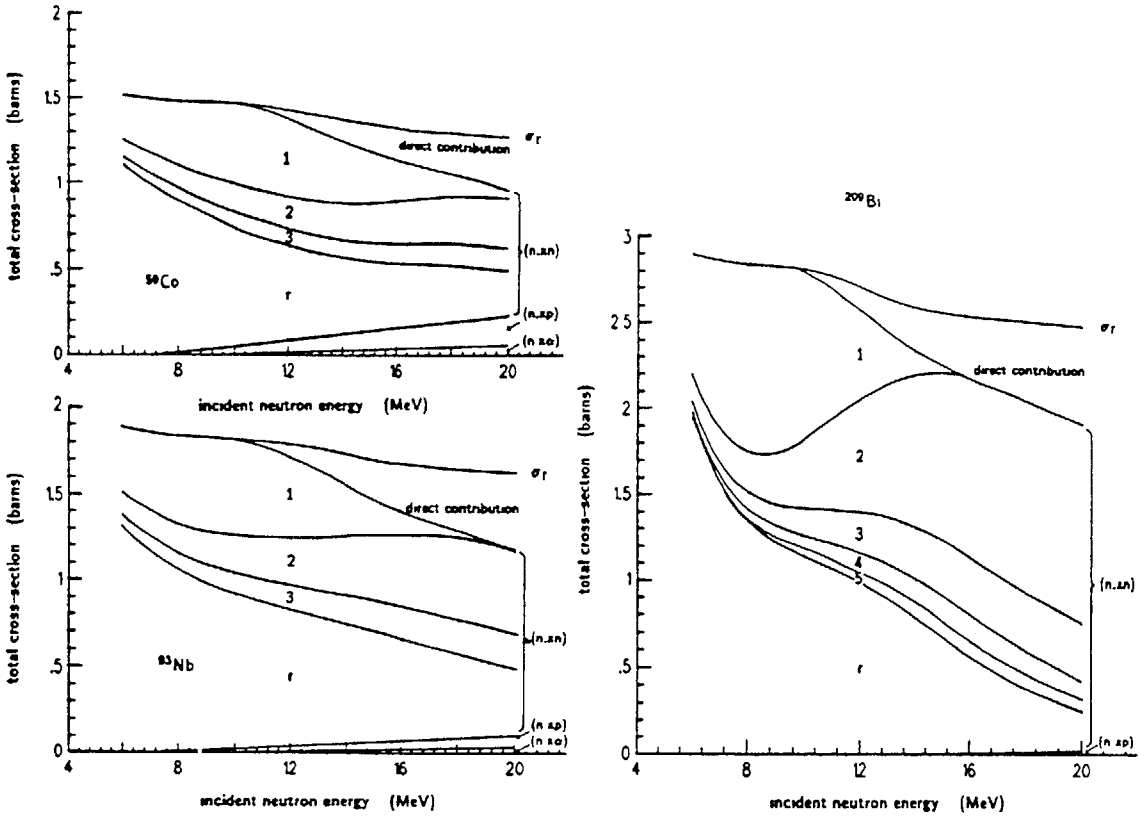

FIGURE 12 The total cross-sections as a function of incident neutron energy for ^{59}Co, ^{93}Nb and ^{209}Bi. The SMCE calculations are restricted to bound states and include the finite depth of the potential well.

4. DISCUSSION

The various pre-equilibrium theories differ appreciably in their flexibility, in several different respects. The semi-classical theories have been applied to a much wider range of reactions than the quantum-mechanical theories, in particular to those initiated by complex particles and those leading to the emission of many particles. By contrast, the quantum-mechanical theories have so far been confined to nucleon interactions with not more than two emergent particles. In the next few years the quantum-mechanical theories will certainly be applied to a wider range of reactions, but at present the semi-classical theories are the only ones that can be used for many of the more complicated reactions.

The semi-classical theories are also more flexible in that they have more model parameters than the quantum-mechanical theories. Here one must distinguish between internal parameters that are special to the particular theory and those that are fixed by some external constraint. As an example of the former we may mention the parametrisation of the residual matrix element in the exciton model which at present cannot be calculated from a more fundamental theory. In the latter category are the optical model and level density parameters. Here there is a further distinction that is important for the predictive power of these theories: reliable global optical potentials are now available for nucleons so that the cross-sections can be calculated from them for any nucleons with good accuracy. The particle-hole level density parameters, on the other hand, cannot be represented with sufficient accuracy by global formulae and only the total level density can be fitted to the experimental data for each nucleus. Therefore there is a strong need to obtain reliable expressions for these particle-hole level densities, in particular for the lowest stages. These considerations apply both to the semi-classical and to the quantum mechanical theories.

If all that is required is a fit to a particular data set, this can be achieved by both the semi-classical and the quantum-mechanical theories for the energy distributions of the emerging particles. The semi-classical calculation may require some adjustment of an 'internal' parameter, and both types are subject to the above remarks about 'external' parameters, particularly those relating to particle-hole level densities. In practice the range of applicability of the semi-classical models is often well known and it is not necessary to adjust "internal" model parameters in each computation. The differences between the results are therefore quite small and further calculations are needed to detect deviations in other energy and mass ranges.

With respect to angular distributions the quantum-mechanical effects may be more important. The most recent semi-classical models are based upon the scattering in infinite nuclear matter with quasi-classical descriptions of refraction and/or finite-size effects. Conceptually the quantum mechanical theories are of course superior. In particular, there are difficulties in the description of back-angle cross sections with the semi-classical theories that do not exist in quantum mechanical theories. This was illustrated recently by Holler *et al*[30] in a comparison of semi-classical and quantum-mechanical pre-equilibrium calculations for the ^{65}Cu$(p,\alpha n)$ reaction at 26.7 MeV. The hybrid model of Blann and Vonach[31] gives a good overall fit to the energy distribution of the emitted neutrons but is unable to fit the angular distribution in the very forward and backward directions. As shown in Figure 13(a) the back-angie discrepancy persists when refraction and finite-size effects are included in the calculations. Similar calculations have been made by Gruppelaar[32] using the PRANG code, giving the dotted curve in Figure 13(a). The differences are due to a truncation of the Legendre polynomial expansion to $\ell_{max} = 6$ and to an adjustment of f_2 by 20% just to avoid negative values of the scattering kernel. The resulting curve is still below the data at backward angles. Quantum-mechanical calculations with the FKK theory are however able to fit the data over the whole angular range, as shown in Figure 13(b). This shows that the quantum-mechanical theories are able to evaluate interference effects that are beyond the scope of the semi-classical theories. In addition, the description of finite-size effects leads to serious difficulties in the semi-classical models, which perhaps could be solved in a pragmatic way by utilizing the results for a systematic study of precompound angular distribution using quantum mechanical theories.

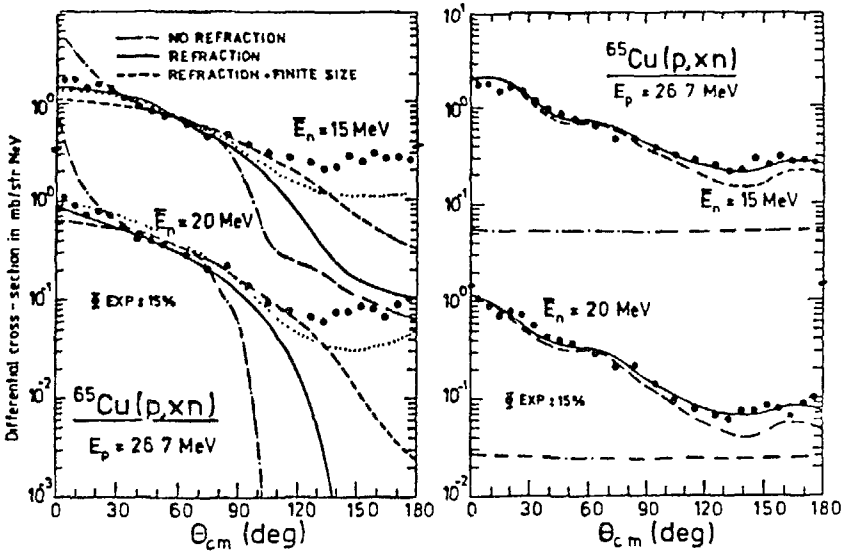

FIGURE 13

(a) Angular distributions for the ^{65}Cu(p,xn) reaction at 26.7 MeV compared with geometry-dependent hybrid model calculations. The data are plotted in ΔE_n = 1 MeV bins centred at energies E_n. The calculations are shown for pure NN-scattering (dot-dash), NN-scattering with entrance channel refraction (solid) and with refraction plus finite size correction (dashed)[30]. the dotted curve has been added and shows the results of using the same model (PRANG). If refraction effects are not included and a very large number of Legendre coefficients are used the dot-dash curve is reproduced. Introduction of entrance and exit refraction and truncation of $\ell_{max} = 6$ gives slightly better results as the dashed curve. Correcting for the negative values of the scattering kernel by increasing f_2 by 20% gives the dotted curve. A further increase of f_2 would fit the data.

(b) Angular distributions for the ^{65}Cu(p,xn) reaction at 26.7 MeV compared with FKK quantum-mechanical calculations. The statistical multistep direct contributions are shown by the dashed line, the statistical multistep compound by the dash-dot line and their sum by the solid line[30].

ACKNOWLEDGMENTS

This work is part of a programme of quantum-mechanical studies of pre-equilibrium reactions that is being carried out in collaboration with Prof. R. Bonetti (Milan), Dr D. Wilmore and Dr G.M. Field (Oxford) and I am grateful to them for permitting me to present their results. Some of these results have been presented, together with a survey of semi-classical theories by Dr H. Gruppelaar (Petten) and Dr P. Nagel (NEA Data Bank), to the International Conference on Nuclear Data for Basic and Applied Science held in Santa Fé, New Mexico in May 1985. A fuller account of this work was published in *Revista del Nuovo Cimento*[33].

REFERENCES

1. J.J.Griffin, *Phys. Rev. Lett.* **17**, 478 (1966).
2. H.Feshbach, *Proceeding of International Conference on Nuclear Reaction Mechanisms* Varenna (1977)
   H.Feshbach, A.Kerman and S.Koonin, *Ann. Phys.* (New York), **125**, 429 (1980)
   H.Feshbach, *Ann. Phys.* (New York), **159**, 150 (1985).
3. L.Avaldi, R.Bonetti and L.Colli-Milazzo, *Phys. Lett.* **94B**, 463 (1980).
   R.Bonetti, M.Camnasio, L.Colli-Milazzo and P.E.Hodgson, *Phys Rev.* **C24**, 71 (1981).
   R.Bonetti, L.Colli-Milazzo, I.Doda and P.E.Hodgson, *Phys. Rev.* **C26**, 2417 (1982).
   R.Bonetti and L.Colombo, *Phys. Rev.* **C28**, 980 (1983).
   R.Bonetti, L.Colli-Milazzo and M.Melanotte, *Phys. Rev.* **C27**, 1003 (1983).
   R.Bonetti, L.Colli-Milazzo, A.De Rosa, G.Inglima, E.Perillo, M.Sandoli and F.Shahin, *Phys. Rev.* **C21**, 816 (1980).
   R.Bonetti, L.Colli-Milazzo, M.Melanotte, A.De Rosa, G.Inglima, E.Perillo, M.Sandoli, V.Russo, N.Saurier and F.Shahin, *Phys. Rev.* **C25**, 717 (1982).
4. G.M.Field, R.Bonetti and P.E.Hodgson, *J. Phys. G***12**, 93 (1986)
   G.M.Field, Thesis Oxford (1987)
5. M.Herman, A.Marcinkowski and K.Stankiewicz, *Nucl. Phys.* **A430**, 69 (1984).
   K.Stankiewicz, A.Marcinkowski and M.Herman, *Nucl. Phys.* **A435**, 67 (1985).
6. M.H.MacGregor, W.P.Ball and R.Booth, *Phys. Rev.* **108**, 726 (1957).
7. V.F.Weisskopf and D.H.Ewing, *Phys. Rev.* **57**, 472 (1940).
8. P.J.Brancazio and A.G.W.Cameron, *Can. J. Phys.* **47**, 1029 (1969).
9. O.A.Sal'nikov, G.N.Lovchikova, G.V.Kotelnikova, A.M.Trufanov and N.I.Fetisov, *Yad. Fiz.* **12**, 1132 (1970); *Sov. J. Nuc. Phys.* **122**, 620 (1971).
10. L.Colli, S.Micheletti and M.Pignanelli, *Nuovo Cim.* **21**, 966 (1961).
11. K.R.Alvar, *Nucl. Phys.* **A195**, 289 (1972).
12. D.L.Allan, *Nucl. Phys.* **24**, 274 (1961).
13. R.S.Storey, W.Jack and A.Ward, *Proc. Phys. Soc.* **75**, 526 (1960).
14. F.L.Hassler and R.A.Peck, *Phys. Rev.* **125**, 1011 (1962).
15. D.Wilmore and P.E.Hodgson, *J. Phys.* **G11**, 1007 (1985).
16. L.R.Veeser, E.D.Arthur and P.G.Young, *Phys. Rev.* **C16**, 1792 (1977)
17. E.T.Bramlitt and R.W.Fink, *Phys. Rev.* **131**, 2649 (1963)
18. H.G.Blosser, G.D.Goodman and T.H.Handley, *Phys. Rev.* **110**, 531 (1958)
19. R.J.Prestwood and B.P.Bayhurst, Los Alamos Report La–2493, TID–4500 (1961)
20. P.Kulisic, V.Adjačić, N.Cindro, B.Lalovic and B.Strohal, *Nucl. Phys.* **54**, 17 (1964)
21. G.Traxler, R.Chalupka, R.Fischer, B.Strohmaier, M.Uhl and H.Vonach, *Nucl. Sci. Eng.* **90**, 174 (1985)
22. S.M.Grimes, R.C.Haight and J.D.Anderson, *Phys. Rev.* **C17**, 508 (1978)
23. E.Holub, N.Cindro, O.Bersillon and J.Jary, *Z. Phys.* **A289**, 421 (1979)
24. B.Strohmaier, *Ann. Nucl. Energy* **9**, 397 (1982)
25. M.Bormann, W.Schmidt, V.Schröder, W.Scobel and U.Seabeck, *Nucl. Phys.* **A186**, 65 (1972)
26. S.J.Hasan, A.Pavlik, G.Winkler, M.Uhl and M.Kaba, *J. Phys.* **G12**, 397 (1986)
27. S.K.Mukherjee, A.K.Ganguly and N.K.Majumder, *Proc. Phys. Soc. (Lond)* **77**, 508 (1961)
28. A.Gilbert and A.G.W.Cameron, *Can. J. Phys.* **43**, 1446 (1968)'
29. H.A.Tewes, A.A.Caretto, A.E.Miller and D.R.Nethaway, *University of California Radiation Laboratory Report* 6028–T (1960)
30. Y.Holler, A.Kaminsky, R.Langkau, W.Scobel, M.Trabandt and R.Bonetti, *Nucl. Phys.* **A442**, 79 (1985)
31. M.Blann and H.K.Vonach, *Phys. Rev.* **C28**, 1475 (1983).
32. P.E.Hodgson, G.M.Field, H.Gruppelaar and P.Nagel. *International Conference on Nuclear Data for Basic and Applied Science*, (Sante Fé) (1985); *Radiation Effects* **95**, 27 (1986)
33. H.Gruppelaar, P.Nagel and P.E.Hodgson, *Revista del Nuovo Cimento* **9** No.7.1 (1986)

Postscript

1. Prof. Seeliger has shown that there is an appreciable direct contribution to neutron inelastic scattering at lower energies due to the excitation of collective states. This should be included in Fig.12.
2. Prof. Vonach pointed out that measurements by Traxler *et al* (1985) of the angular distribution of the protons from the ^{93}Nb (n,p) reaction show a substantial forward excess. This indicates the presence of direct processes, which should be included in the analysis.
3. Prof. Blann mentioned some discussions of the validity of the Feshbach-Kerman-Koonin theory, in particular a resonance term and the comments of Udagawa *et al* (1983). It was already pointed out by Kawai (1980) that the FKK theory expresses the cross-sections of multistep direct reactions in terms of non-DWBA matrix elements whereas the calculations of Bonetti *et al* (1981) use DWBA matrix elements. Calculations with non-DWBA matrix elements do not fit the data at all well (Bonetti, 1983), show undesirable resonance phenomena (Kumabe *et al*, 1984) and are unsatisfactory in several other respects (Udagawa *et al* (1983)). This problem was solved by Feshbach (1985ab) who found that the energy-averaging process was carried out incorrectly by FKK, and that when this is rectified the non-DWBA matrix elements are converted to DWBA matrix elements. The original calculations of the Milan group are thus correct.

References

R. Bonetti, M. Camnasio, L. Colli-Milazzo and P.E. Hodgson, *Phys. Rev.* **C24**, 71, 1981.

R. Bonetti (Private communication) 1983.

H. Feshbach, *Ann. Phys. (New York)* **159**, 150, 1985a; Proc. Winter College on Fundamental Nuclear Physics, International Centre for Theoretical Physics (Trieste) (Ed. K.Dietrich, M.di Toro and H.J.Mang). 1605, 1985b.

M. Kawai (Private communication to H. Feshbach) 1980.

I. Kumabe, M. Haruta, M. Hyakutake and M. Matoba, *Phys. Lett.* **140B**, 272, 1984.

G. Traxler, R. Chalupka, R. Fischer, B. Strohmaier, M. Uhl and H. Vonach, *Nucl. Sci. Eng.* **90**, 174, 1985.

T. Udagawa, K.S. Low and T. Tamura, *Phys. Rev.* **C28**, 1033, 1983.

224 PROGRESS IN MULTI-STEP DIRECT REACTION THEORY

A. MARCINKOWSKI
Institute for Nuclear Studies,
Warsaw, Poland

Abstract

The current status of the multi-step direct theories and theirs application in evaluation of cross sections of nucleon induced reactions at energies between 11 and 62 MeV are reviewed. The interplay of the one-step process with respect to the multi-step processes are discussed.

1. Introduction

For a long time was the handy version of direct reactions theory, namely the DWBA applied to describe reactions resulting in discrete final states only. In such studies transitions that had large cross sections were naturally of prime interest. This however ment that the initial and final channels are strongly coupled and lead to coupled channels and coupled reaction channels calculations, which involve contributions of more complicated multi-step processes. Therefore we may consider all these methods as multi-step direct reaction method (MDR).

What we are however interested in is the application of the MDR theory to the precompound or preequilibrium reactions, i.e. inclusive nuclear reactions, in which one of the residual nuclei is unobserved and left in its continuum states. In such a case the analysis reduces again to the use of perturbative DWBA since among the large number of final continuum states involved the dominance of selected final states can normally be forgotten and the weak coupling picture assumed. This then means that we understand the MDR approach to be a DWBA theory, including higher order terms. Such a use of the MDR in the analysis of continuous spectra of reactions induced by light ions has been basically justified by Tamura et al. (TU) in ref.[1]) (see also refs. therein). These authors have derived expressions for the continuum cross sections by combining the DWBA cross sections with the spectroscopic density, which describes the statistical and the nuclear structure aspects involved in the reaction. Both microscopic and macroscopic models for calculation of the spectroscopic density have been also proposed and used in calculations.

In parallel Feshbach, et al.[2]) (FKK) formulated a formal basis for the MDR. Theirs statistical theory, completely quantum-mechanical retains many of the concepts already used in the semiclassical models of preequilibrium emission. The incident kinetic energy is spread through the composite system by a number of subsecuent two-body interactions and the nuclear states excited at each stage n of the interaction chain are characterized by theirs complexity, e.g. number of excited particles and holes . The theory assumes a chaining hypothesis, which restricts transitions to classes of states with n differing by unity. This theory distinguishes two types of processes the one that involves transitions between bound excited states of the composite nucleus, which contri-

bute to the statistical multi-step compound emission (SMCR) and the other that involves unbound excited states, which retain the memory of the direction of the projectile and contribute to the statistical multi-step direct yield (SMDR), characterized by the forward peaked angular distribution. The latter is obtained by assuming a random phase hypothesis, which however allows the matrix elements, with the same change of momentum as the particle in the continuum, to interfere constructively upon averaging. Eventually, in order to perform energy averaging of the cross section over the continuum states, the final state wave function is expanded in terms of exit modes. Each nuclear state excited in the chain of two-body interactions can reach an exit mode in a subsequent (last) transition.

As we are concerned more with results rather than methods and in the following sections the emphasis will be put on practical use of the cross section formulae derived in frames of the two theories, which have found most applications in cross section evaluations, and on calculations so far conducted, here seems to be a right place for a brief discussion of relations between the two theories and or other approaches. Again we are not interested in comparing both methods in every detail, which appears a difficult task because of the different presentations[1]), it seems however safe to say that both theories derive the one-step cross section in the same way. As for the two-step cross sections the situation resembles that of the FKK result for the SMCR. It was McVoy[3]) who has shown that the SMCR formula of FKK can be obtained as a special case of the more general fluctuation cross section derived by Agassi et al.[4]) within the random K-matrix formalism. The speciality of the FKK approach lies in inclusion of a never-come-back assumption, which prevents a unified description of the preequilibrium and equilibrium components.

In case of the SMDR it were Udagawa et al.[5]) who claim to have shown that the extreme simplicity of the FKK cross section has been obtained at the expense of three successive approximations, not present in the more exact DWBA two-step expression, which however have the tendency to cancel each others effest in certain calculations. In addition the cancelation is more so the case in the continuum cross sections, since these are obtained by summing the elementary model cross sections, corresponding to a variety of transferred angular momenta weighted with the spectroscopic density factors. The net result of the cancelation of the uncertainties in case of a (p,p') reaction on ^{208}Pb at 62 MeV leaves the FKK two-step cross sections overpredicted, by a factor of 2, with respect to the DWBA result, (see fig.1). This sounds rather insignificant if we take into account that the two-step component plays a role only for large energy losses at large angles. The higher order cross sections and or the heavy ion cross sections of FKK may deviate even more from the DWBA ones, e.g. this finds reflection in the works of the Milan-Naple group, who report the multi-step contributions systematically higher than those of TU[1]). The

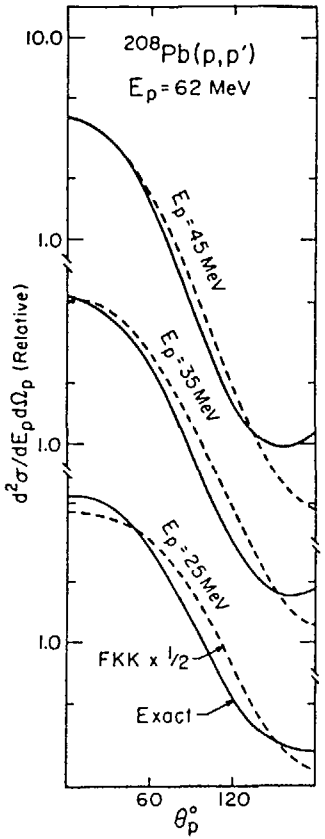

FIG.1. Comparison of the continuum cross sections obtained with and without the FKK approximations. Only two-step contributions were considered.

criticism, which the SMDR theory of FKK has suffered was debated by Hussein and Bonetti[6], Kumabe et al.[7] and has eased to some extend after Feshbach has shown, that at least one of the three approximations in question, namely the use of the DWBA matrix elements in the FKK cross section formula is justified when the energy averaging is conducted correctly[8]. The spectral decomposition of Greens function is discussed [30].

On the other hand it has to be said that the MDR method based on DWBA is also not free of problems, these however, like e.g the magnitude problem, pertain the application of the theory rather than its formulation and will be discussed in the following, though such a distingtion may sound arbitrary.

Quite recently Carlson and Merchant reported[9] on efforts aimed toward formulation of an improved preequilibrium model, which could be free of the criticism, suffered by the FKK theory. These authors have given statistical hypotheses on the two-body interaction matrix elements, which define the SMDR as well as the SMCR. The model specifies the average optical potentials, the Greens functions, wave functions and cross sections in terms of the average matrix elements. The resulting cross sections have the SMDR component of DWBA form and a SMCR component similar to that of ref.[4]. As it stands, the model is however too complex to be useful for practical calculations. Especially troublesome to conduct are also the calculations of the spectroscopic densities, which enter the cross section calculations. Nevertheless some numerical calculations have been completed for the ^{56}Fe(n,nem) at 14 and 26 MeV.

Let us mention for completeness also the earliest important steps on the way towards theoretical description of the forward-backward assymetry observed in the preequilibrium angular distributions. First was the intranuclear cascade model (INC) developed by the Oak Ridge and Brook-

haven groups[10,11]), followed later by the quantum-statistical master equation approach of Mantzouranis et al. (MWA)[12]). Both models succeeded in providing forward peaked angular distributions, which we now relate with the SMDR process. INC was applied to finite nuclei and proved well in fitting cross sections taken for protons with hundreds MeV incident energy. When used in analyses at tens of MeV the model underpredicted the reaction yields at backward angles. This was connected perhaps with assuming a clasical path between nucleon-nucleon collisions and with the neglect of diffraction effects. MWA calculates the cross sections also in a cascadelike way applied to an infinite nuclear matter. Probably because of this the series over the reaction steps converges rather slowly making the number of steps adopted in the calculation a sensitive parameter. Formally the MWA cross section expression is rather close to that of TU. It fits the angular distributions particularly well at lower spectral energies. At high spectral energies, where the surface region of the nucleus is known to play the dominant role in direct processes, the MWA calculations based on infinite nuclear matter give too little chance for particle emission[13]).

2. The Multi-Step Direct Reaction Continuum Cross Sections

2.1. DWBA continuum Cross Sections

The justification for the use of the DWBA method in continuum transitions is based on a statistical consideration. In continuum a large number of very complicated eigenstates are involved, even when a relatively narrow energy interval is assumed. The measured cross section per unit energy is an energy average of the sum of cross sections for excitation of these eigenstates. To calculate the cross sections to excite all these states is impracticable but statistical arguments can be invoked to replace this sum by another sum of cross sections for population a much smaller number of quite simple model states. The DWBA is very appropriate for calculation of such an energy average over model states, which for many applications appear to be the shell model particle-hole states or the RPA collective states. The energy averaged cross section as derived by TU[1]) reads

$$\frac{d^2\sigma^{(1)}(E_b)}{dE_b\,d\Omega_b} = \sum_B c_B(E_x)\,\frac{d\sigma_B^{(1)}(E_b)}{d\Omega_b} \qquad (1)$$

for one-step transitions, with $E_x = (E_a - Q^B) - E_b$, E_a and E_b being the incident and exit channel energies and Q^B being the Q - value for transition from the target A ground state to the ground state of B, and

$$\frac{d^2\sigma^{(2)}(E_b)}{dE_b\,d\Omega_b} = \sum_{BC}\int_{E_b-(Q^B-Q^C)}^{E_c-Q^C} c_B(E_x')\,c_C(E_x)\left\{\frac{d\sigma_{BC}^{(2)}(E_b,E_c)}{d\Omega_b}\right\}dE_c \qquad (2)$$

for two-step transitions, with $E_x' = (E_c + Q^B - Q^C) - E_b$. The elementary cross sections $d\sigma_B^{(1)}/d\Omega_b$ and $d\sigma_{BC}^{(2)}/d\Omega_b$ are the DWBA first and second order cross sections. The statistical assumption prohibits interference terms between

amplitudes creating different states B and C as well as between the one and two-step amplitudes. The $c_B(E_x)$ is a probability per unit energy that a state B is located at the excitation E_x. The continuum cross sections expressed by eq. (1) and (2) look simple but in numerical calculations they are still too much involved specially in case of the two-step calculations.

One way to make the calculations feasible is to remove in a justfiable manner the dependence on B and C of the elementary cross sections. One can see from DWBA consideration that this dependence arises from the dependence of the form factors f_J^{BA} . f_J^{BC} on B and C. In practice one uses theirs average $\bar{f}_J$ over large numbers of states or replaces them drastically by $\bar{f}$ an average over the transferred angular momentum J too (this is the LIFF approximation). This reduces (1) and (2) to

$$\frac{d^2\sigma^{(1)}(E_b,\Theta_b)}{dE_b\,d\Omega_b} = \sum_J \rho_J(E_x)\,\frac{d\sigma_J^{(1)}(E_b,\Theta_b)}{d\Omega_b}\,, \qquad (3)$$

$$\frac{d^2\sigma^{(2)}(E_b,\Theta_b)}{dE_b\,d\Omega_b} = \sum_{J_1,J_2}\int dE_c\,\rho_{J_1}(E_x)\rho_{J_2}(E_x')\sum_J \frac{d\sigma_{J_1J_2iJ}^{(2)}(E_b,E_c,\Theta_b)}{d\Omega_b} \qquad (4)$$

Here the definition $\rho_J(E_x)=\sum_B c_B(E_x)(d_J^{BA})^2$ for the spectroscopic density holds. By assuming LIFF the model state dependence of eqs. (3) and (4) occurs only through the square of the spectroscopic amplitude $(d_J{}^{BA})^2$. The early numerical calculations of TU have assumed LIFF and an appropriate model for ρ_J . In eqs. (3) and (4) $J \equiv \{lsj\}$ denotes a set of orbital, spin and total transferred angular momenta, respectively. For residual interaction of Wigner type there is no spin transfer s = 0 and J is replaced by l. In case of inelastic scattering or charge exchange reactions the averaging over the $|B\rangle = |(j_p j_n^{-1})\,lm\rangle$ one-ph states provides a form factor $\bar{f}_l(r)$, which is peaked at the surface of the nucleus, thus justifying introduction of a macroscopic, collective form factor (CFF)

$$\bar{f}_l(r) = \beta_l R_0 \frac{dU}{dr} \qquad (5)$$

The l - dependent deformation parameter may now be absorbed into the spectroscopic density ρ_l leaving the rest as LIFF. A choice of the spectroscopic density appropriate to the CFF (eq. (5)) means to obtain it as the distribution of β_l^2 in E_x. Allowing the probability distribution c(Ex) to take the Lorentzian form $c_B(E_x) = \frac{\Gamma}{\pi}\left[(E_x - E_B)^2 + {}^2\Gamma\right]^{-1}$ and remembering that d_J^{BA} is a purely geometrical factor $\langle j_p \| i^l Y_l \| j_h\rangle$ one can express ρ_l explicitly in terms of the single-particle response function X_1^{SP} [14])

$$\rho_l(E_x) = \beta_l^2\,\mathrm{Im}\,X^{SP}(E_x) \qquad (6)$$

with $$X_l^{SP}(E_x) = \frac{1}{\pi}\sum_B (d_J^{BA})^2 (E_x - E_B - i\Gamma)^{-1}, \qquad (7)$$

or after setting $d_J^{BA}=1$, $$\rho_l(E_x)=\beta_l^2\sum_B c_B(E_x) \qquad (8)$$

which has been used by Traxler et al.[15]). When RPA collective states B are choosen the spectroscopic density to be used is expressed by the RPA response function [16]). Assum-

ing (5) and (8) results in significant simplification of the calculations.

2.2. The Statistical MDR Cross Sections

The statistical assumptions made by FKK resulted in a double differential cross section for reaction from an unbound state having a particle of momentum k_i to a one of momentum k_f, which is a sum of terms corresponding to single-step and multi-step transitions. The multi-step cross section reads,

$$\left[\frac{d^2\sigma(\bar{k}_f,\bar{k}_i)}{dUd\Omega}\right]_{multi} = \sum_n \sum_{m=n-1}^{n+1} \int\frac{d\bar{k}_1}{(2\pi)^3}\cdots\int\frac{d\bar{k}_n}{(2\pi)^3}\frac{d^2W_{m,n}(\bar{k}_f,\bar{k}_n)}{dU_f d\Omega_f}\times$$

$$\times\frac{d^2W_{n,n-1}(\bar{k}_n,\bar{k}_{n-1})}{dU_n d\Omega_n}\times\cdots\frac{d^2W_{2,1}(\bar{k}_2,\bar{k}_1)}{dU_2 d\Omega_2}\left[\frac{d^2\sigma_{1i}(\bar{k}_1,k_i)}{dU_1 d\Omega_1}\right]_{single}, \quad (9)$$

with the double differential transition probability,

$$\frac{d^2W_{n,n-1}(\bar{k}_n,\bar{k}_{n-1})}{dU_n d\Omega_n} = 2\pi^2\rho(k_n)\rho_2(U)\langle|v_{n,n-1}|^2\rangle, \quad (10)$$

for a transition between the continuum states excited in the (n - 1) -th and n-th stage, leading to a change in the momentum of the continuum particle from k_{n-1} to k_n. The transition matrix element $v_{n,n-1}$ is of DWBA type

$$v_{n,n-1} = \int\chi_n^{(-)}(\bar{k}_n)^*\langle\psi_n|V(r)|\psi_{n-1}\rangle\chi_{n-1}^{(+)}(\bar{k}_{n-1})d\bar{r}, \quad (11)$$

whereas $\rho(k)$ and $\rho_2(U)$ in (11) are the space phase and the one-ph (2 excitons, repeatedly formed at each stage of reaction) state density.

The characteristic feature of the multi-step cross section given by eq. (9) is that it is written as a convolution of single-step direct cross sections, thus making the calculations rather simple to carry out. The angular distribution is forward peaked, as is the single-step cross section although the multiple folding will broaden it. In (10) one uses the squared matrix element averaged over many final continuum states. This averaging is straightforward since we expect the interference terms between different states as well as between different orbital angular momentum transfer to cancel out (no spin transfer is assumed for simplicity). One then obtains

$$\langle|v_{m,n-1}|^2\rangle = \sum_l(2l+1)\langle|v_{n,n-1}|^2\rangle_l R_2(l), \quad (12)$$

where $R_2(l)$ is the spin distribution function of the one-ph configurations $(\sum_l(2l+1)R_2(l)=1)$. In the same way the averaged single-step source term in (10) reads

$$\left[\frac{d^2\sigma(\bar{k}_f,k_i)}{dUd\Omega}\right]_{single} = \sum_l(2l+1)\rho_2(U)R_2(l)\left\langle\left(\frac{d\sigma}{d\Omega}\right)^{DWBA}\right\rangle_l \quad (13)$$

In practical calculations one assumes that the only contribution to the spins of final states is due to the transferred orbital angular momentum. For each transferred l-value the DWBA angular distributions are calculated microscopically for given values of ejectile energies and all possible ph-pairs, created by scattering of the particle in the continuum with a bound nucleon, in accordance with energy conservation. Spherical shell model orbitals are used to

define the states. An average of a reasonable number of these cross sections gives the last term in (13). For the interaction V(r) a Yukawa potential of 1.0 fm range is adopted. Its strength V_0 is a free parameter. The state density and its spin distribution are given by the Ericsson expression and Bethe's distribution , with spin cut-off parameter dependent on the number of excitons. The multi-step contribution is calculated in the same way because the differential transition probability (10) does depend on the stage n only via k_n. Substituting (12) into (10) and integrating over intermediate energies and angles provides the source term for the next stage. Still such calculation is a time consuming task because it requires $v_{n,n-1}$ for each incoming and outgoing energy, compatible with energy conservation, and for each angle and l-value. In the calculation both protons and neutrons should be considered where neccessary. In practice such distingtion does not make much change. In this way a lot of continuum cross sections have been calculated by the Milan - Naple group[17,18]) and more recently by the Milan - Hamburg group[19,20]). These results together with the results of TU[1,21]) and some others also will be discusses in what follows.

3. Numerical Calculations and Comparison with Experiment

3.1. The DWBA Continuum Cross Section Calculations

The DWBA MDR method has been proved by TU in a number of analyses of (p,p'), (p,α) data obtained at 62 MeV and some (n,n'),(p,n) data obtained at lower energy. The early analyses used LIFF and both single-particle and RPA response functions to construct the spectroscopic density. Despite of the overall good description of the angular distributions by using only the one-step and two-step cross sections this theory appeared not free of the magnitude problem. The excellent fit to the $^{27}Al(p,p')$ and $^{209}Bi(p,p')$ data[22]) was questioned[23]) and sebsequent analysis, which switched to use the RPA states instead of the shell-model ph-states did not improve enough[1]). It has been concluded that the simplifying use of LIFF, which in fact made the calculations commonly accessible, causes the difficulty in reproducing the absolute cross sections satisfactorily. The investigation of the use of microscopic form factors (MFF) together with (1) and (2) are underway[1]). In fig.2 the results are shown of preliminary calculations of a one-step cross section, obtained as a sum of 200 microscopic cross sections, corresponding to different ph-pairs and l's ranging up to 10. The calculation underestimates the experiment about 2.5 times. This gap has been filled using reasonable guesses for the two-step contribution and also for the proton singles emission that results from one-nucleon pick-up reactions. The same pertains the analysis of the $^{208}Pb(p,n)$ reaction. The (p,α) reaction has been studied first by TU[24]) and also by Dragun et al.[25]) at lower proton energies 44.3 and 34.6 MeV. A good agreement with experiment has been reached considering only the one-step direct cross sections

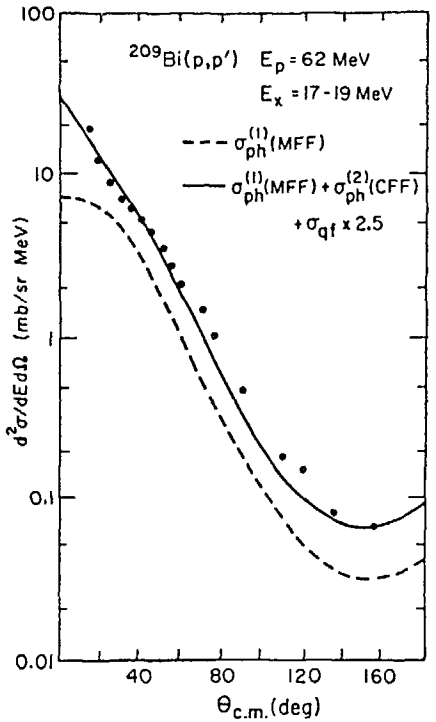

FIG.2. Comparison of the calculated (p,p') cross sections summed over the 2 MeV energy bin shown with the corresponding experimental data.

The dotted line represents the one-step cross section obtained by using the microscopic form factor, while the solid line was obtained by adding, to this one-step cross section, the two-step cross section estimated in the way explained in the text, and also the contribution from the (p,d^*) process.

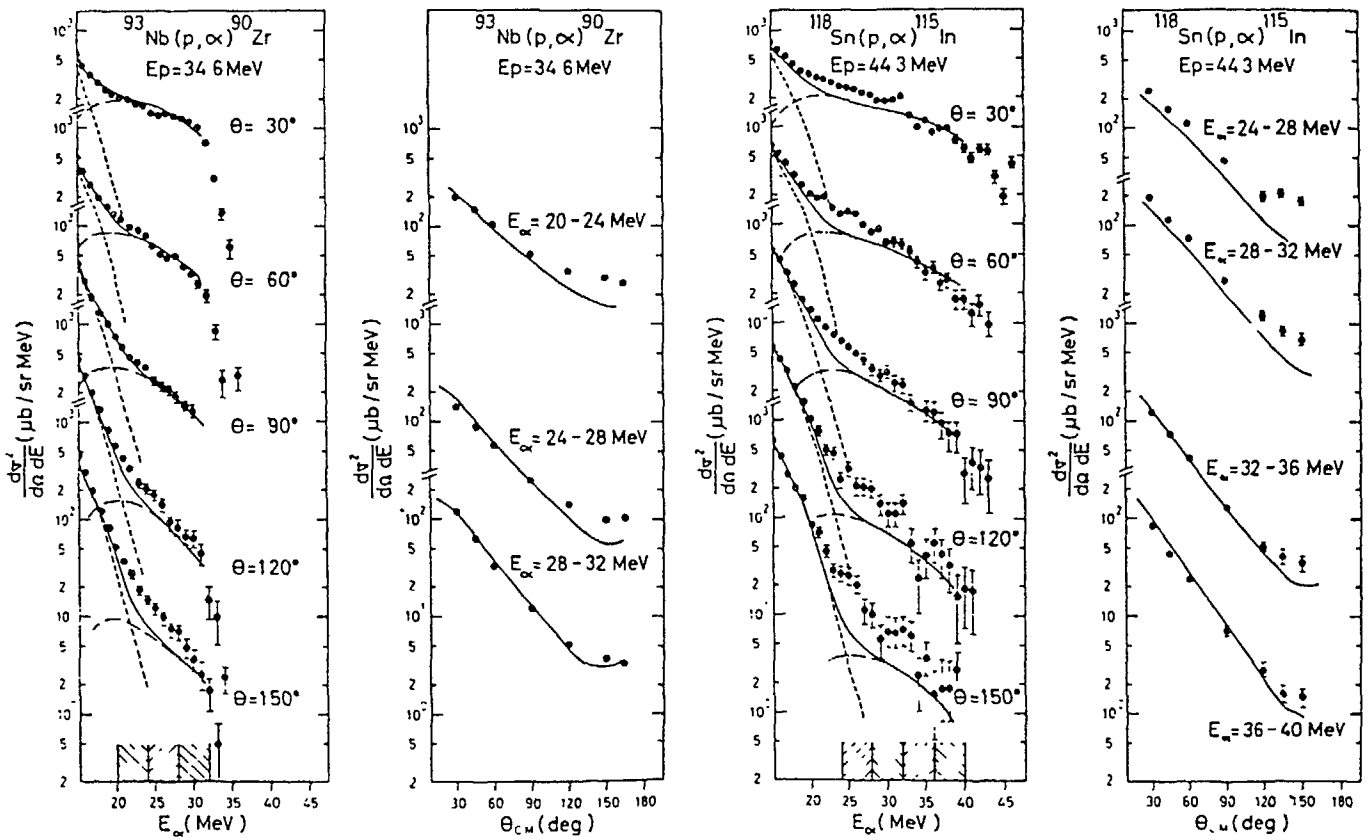

FIG.3.

in addition to the compound nucleus ones (see fig.3). Recently Tamura presented an analysis of some (n,n') data and the ^{65}Cu(n,p) data both taken at about 26 MeV, fig. 4. The low incident energy justifies the one-step calculations only. An interesting case was the application of the MDR theory at incident energies as low as 14 MeV, for inelastic neutron scattering on targets ranging from Fe to Au[26]. It was found that the two-step contribution amounted to only 10% of the one-step cross section. The predicted shapes of angular distributions were right but the absolute cross sections too low. Also Traxler et al.[15] report on the use of the ORION-TRISTAR code in theirs study of the ^{93}Nb(n,p)

reaction data measured at 14.1 MeV. These authors treated the γ_ℓ as adjustable parameter kept independent on l. The same conclusions have been drawn as in previous case. The cross sections fell down with decreasing spectral energy faster than experiment, fig. 4. Inconsistency has been also stated in parameterisation for different projectile energies.

The comparison presented in figs. 2-4 characterize the present state of art; good angular shapes and magnitude problems. The limited experience of these analyses indicates that up to 30-40 MeV of projectile energy the one-step process describes the experiment satisfactorily, though already at 62 MeV the two-step contribution dominates, in the excitation region 20-30 MeV, the backward angles.

3.2. The Statistical MDR Cross Sections

The SMDR theory of FKK has been used in studying (p,n) reactions at energies ranging from 25 to 45 MeV on a number of target nuclei Ca, Zr, Sn, Pb[17,18], as well as on Cu and Mo[19,20]. All these papers report a rather very good reproducibility of the experimental angular distributions and energy spectra, fig. 5. The shortfalls at high excitation energies, in fig. 5, are attributed to the omission of the MCR contribution. The strength V_o of the Yukawa interaction potential was the only free parameter. V_o-values extracted from comparison with experiment range from 25 to 27.5 MeV for the single-step calculat-

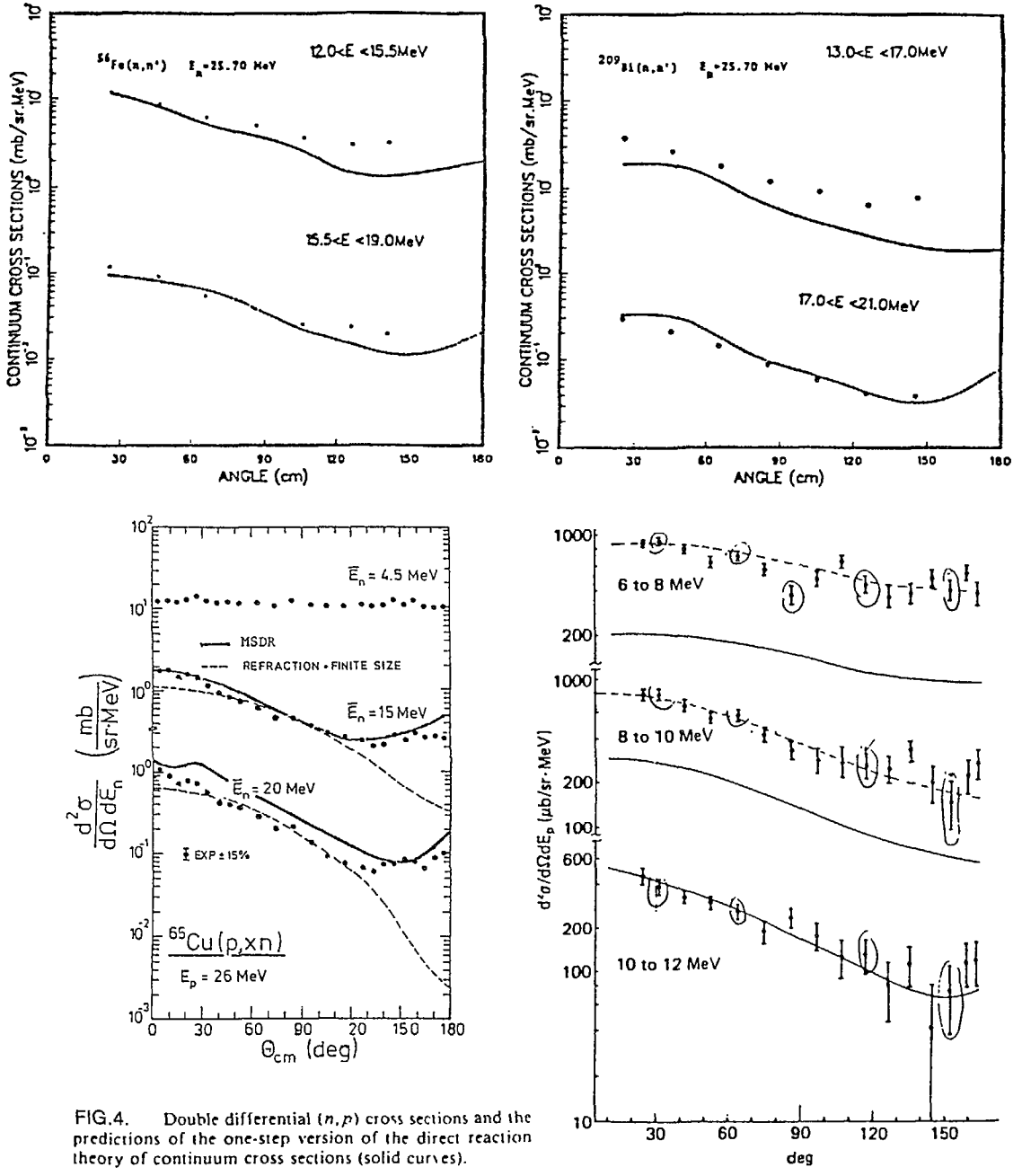

FIG.4. Double differential (n,p) cross sections and the predictions of the one-step version of the direct reaction theory of continuum cross sections (solid curves).

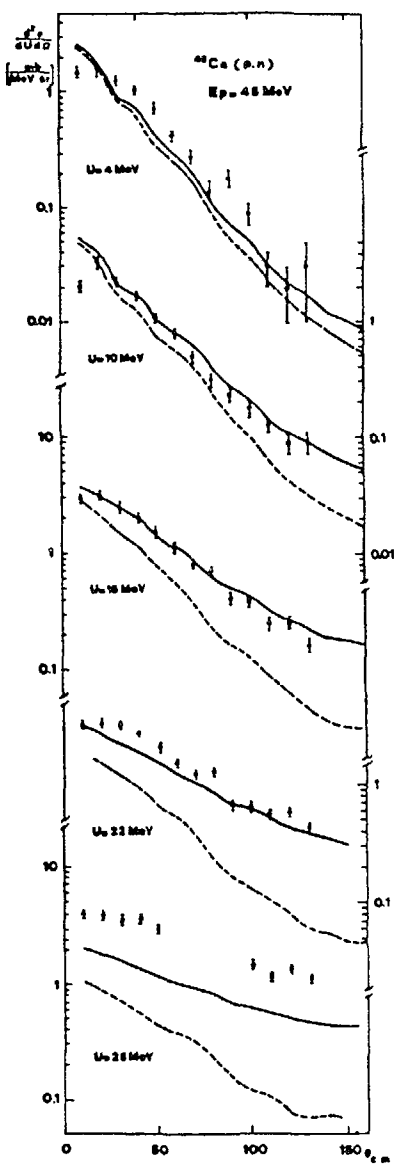

Comparison between calculated and experimental differential cross sections for the $^{48}Ca(p,n)$ reaction at several excitation energies of the residual nucleus. At the highest excitation energy (u = 28 MeV), the experimental cross section exceeds the calculated value due to the presence of multiple particle emission. --- single-step contribution; —— total.

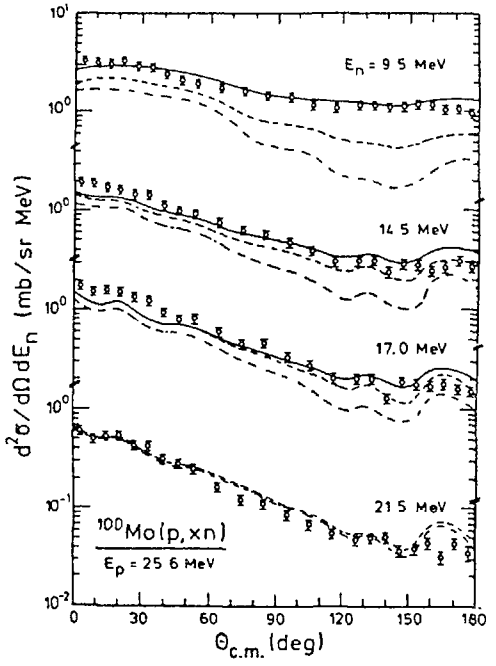

Experimental angular distributions (circles) of neutrons from $^{100}Mo(p,xn)$ for the bins (E_n,E_n+0.5 MeV). Calculations are first step SMDE (dash-dotted line), SMDE of the first three steps (dashed), and the sum SMDE plus SMCE (solid line).

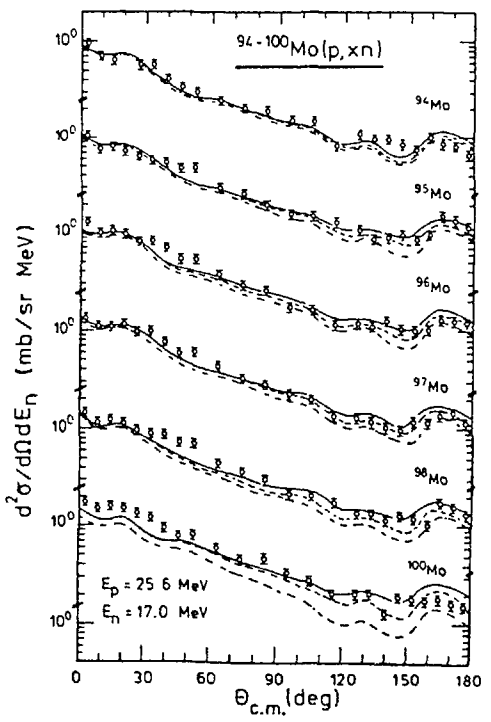

Angular distributions of neutrons from $^{94-100}Mo(p,xn)$ for the bin 17.0—17.5 MeV.

FIG.5.

ions, and from 15.5 to 17 MeV range the average over unlike and like nucleon interactions in the multi-step calculations. The latter extends up to 6-steps providing at 45 MeV 53% of the total cross section for ^{208}Pb, 45% for ^{48}Ca and ^{90}Zr, 28% for ^{120}Sn (at 35 MeV) and 18% for ^{120}Sn and ^{65}Cu (at 25 MeV).

The successful applications of the FKK teory have encouraged the author to use it in interpreting the recently measured (n,n') cross sections on ^{184}W at neutron energies 11.5 and 26 MeV[27]. In this analysis difficulties have been encountered, which might then be traced to the averaging of the elementary DWBA cross sections. It has been stated that these cross sections, corresponding to different ph-configurations do not neccessarily display such a regular pattern like shown in ref.[18]), where only particular ph-pairs have been considered . Moreover the average appeared to fluctuate from one spectral energy bin to another. This was caused by the fact that some of the ph-configurations dominated the average over a definite energy interval. In order to overcome this difficulty the average had to be extended over almost the whole energy range considered, ignoring energy conservation. This is equivalent to assuming a broad (~10 MeV), uniform response function. Then a satisfactory description of the measured angular distributions, both in shape and magnitude has been obtained.

4. Conclusions

Both the FKK and the DWBA theories evaluate the one-step direct emission in the same manner and agree in that up to 30 MeV of incident energy the higher order contributions play little role. At these low energies however consideration of the multi-step compound emission, which even at 45 MeV contributes significantly at high excitations, has to be included in the analysis of experimental data. Above 30 MeV the multi-step direct component becomes important and here the two theories differ in its evaluation. The DWBA MDR theory provides two-step contributions, which add enough cross section for fitting the experimental data up to 62 MeV, whereas the FKK statistical theory indicates that up to six-steps may contribute considerably. Though the overall good description pertaining specially the angular distributions indicates that basically the two approaches are correct there remain magnitude problems related probably to the assumed approximations. For the purpose of nuclear data evaluation specially interesting is the description of the strong forward peaking of experimental double diffirential neutron cross sections at energies as low as 11-14 MeV[27-29].

REFERENCES

1. T. Tamura, T. Udagawa and H. Lenske, Phys. Rev. C26/1982/379
2. H. Feshbach, A. Kerman and S. Koonin, Ann. Phys. 125/1980/429
3. K. McVoy, Proc. 4-th Int. Conf. on Nuclear Reaction Mechanisms, Varenna, Italy, June 10-15, 1985
4. D. Agassi, H.A. Weidenmüller and G. Mantzouranis, Phys. Reports 22C/1975/145
5. T. Udagawa, K.S. Low and T. Tamura, Phys. Rev. C28/1983/1033
6. M.S. Hussein and R. Bonetti, Phys. Lett. 112B/1982/189
7. I. Kumabe, M. Haruta, M. Hyakutake and M. Matoba, Phys. Lett. 140B/1984/273
8. H. Feshbach, Ann. Phys. 159/1985/150
9. B. Carlson and A. Merchant, Contribution to the 1-st IAEA-NDS Research Coordination Meeting on Methods for Calculation of Fast Neutron Nuclear Data, Bologna, Italy, October 7-10, 1986
10. K. Chen, G. Friedlander, G. Harp and J. Miller, Phys. Rev. C4/1971/2234
11. H. Bertini, G. Harp and F. Bertrand, Phys. Rev. C10/1974/2472
12. G. Mantzouranis, H. Weidenmüller and D. Agassi, Z. Phys. A276/1976/145
13. G. Mantzouranis, Phys. Rev. C14/1976/2018
14. A. Bohr and B. R. Mottelson, Nuclear Structure /Benjamin, London, 1975/, Vol. II.
15. G. Traxler, A. Chalupka, R. Fischer, B. Strohmaier, M. Uhl and H. Vonach, Nucl. Sci. Eng. 90/1985/174
16. K. Liu and G.E. Brown, Nucl. Phys. A265/1976/385
17. L. Avaldi, R. Bonetti and L. Colli-Milazzo, Phys. Lett. 94B/1980/463
18. R. Bonetti, M. Camnasio, L. Colli-Milazzo and P.E. Hodgson, Phys. Rev. C24/1981/71
19. Y. Holler, A. Kaminsky, R. Langkau, W. Scobel, M. Trabandt and R. Bonetti, Nucl. Phys. A442/1985/79
20. E. Mordhorst, M. Trabandt, A. Kaminsky, H. Krause, W. Scobel, R. Bonetti and F. Crespi, Phys. Rev. C34/1986/103
21. T. Tamura, Proc. 4-th Int. Symp. on Neutron Induced Reactions, Smolenice, Czechoslovakia, June 1985
22. T. Tamura, T. Udagawa, D.Feng and K. Kan, Phys. Lett. 66B/1977/109
23. S. Tsai and G. Bertsch, Phys. Lett. 73B/1978/247
24. T. Tamura and T. Udagawa, Phys. Lett. 71B/1977/273
25. O. Dragun, A. Ferrero and A. Pacheco, Nucl. Phys. A369/1981/149
26. I. Kumabe, K. Fukuda and M. Matoba, Phys. Lett. 92B/1980/15
27. A. Marcinkowski, R. Finlay and J. Rapaport, unpublished
28. D. Hermsdorf et all., Zentralinstitut für Kernforschung Rossendorf, Report ZfK-277, 1975
29. A. Takahashi et all., Osaka University, OKTAVIAN Report A83-01, 1983
30. H. Feshbach, Proc. of XCIth Int. School in Phys. "Enrico Fermi" 1984, Ed. A. Molinari and R. Ricci (North Holland 1986)

236 MICROSCOPIC COMBINATORIAL APPROACH TO QUASI-PARTICLE STATE DENSITY IN DEFORMED NUCLEI

G. REFFO, M HERMAN
Comitato Nazionale per la Ricerca e per
lo Sviluppo dell'Energia Nucleare
e delle Energie Alternative,
Bologna, Italy

Abstract

A microscopic combinatorial approach is used to investigate the influence of the nuclear deformation on the distributions of quasi-particle states. It is shown that nuclear deformation tends to suppress strong fluctuations observed in similar calculations performed in the space of spherical shell-model s.p.s.. The dependence of the pairing effects on the deformation is analysed. The applicability of the formula by Williams is examined and found to be only valid for strongly deformed medium and heavy nuclei.

1. THE MODEL

Starting from the shell-model spectrum of the single particle states (s.p.s.), the total energy of each configuration is determined through the superconductivity theory. Configuration dependence is introduced into the BCS by the blocking method, as proposed by Wahlborn /1/ and then generalized by Hilman and Grover /2/, to allow for blocking of more than one orbital. Accordingly, for each generated configuration, a set of two BCS equation is solved.

$$\sum_i{}' \; 2 V^2_{i\beta} = \eta \qquad (1)$$

$$\sum_i{}' \; [(\zeta_i - \lambda_\beta)^2 + \Delta^2_\beta]^{-1/2} = 2/G \qquad (2)$$

where

$$V^2_{i\beta} = \frac{1}{2} \left(1 - \frac{\zeta_i - \lambda_\beta}{[(\zeta_i - \lambda_\beta)^2 + \Delta^2_\beta]^{1/2}}\right) \qquad (3)$$

The prime superscript indicates that the summation runs only over unblocked orbitals. Here the ζ_i are shell-model orbital energies, η stands for the number of paired nucleons and λ_β and Δ_β are the Fermi energy and correlation function which are to be determined. The latter two are found by minimization of the sum of the two squared BCS equations. Each configuration enters the BCS equations through the blocking, which removes orbitals occupied by unpaired nucleons from the summations in Eqs.1 and 2. Thus the solution of the BCS equations should be in principle repeated for each configuration. For spherical nuclei advantage is taken of the orbital energy degeneracy. When next considered configuration differs from the preceding one only by the displacement of an exciton within the same subshell,the solution of the BCS equations is not needed.

The total configuration energy according to the BCS model reads:

$$E_\beta = \sum_j \zeta_j + \sum_i{}' \; 2V^2_{i\beta}\zeta_i - \frac{\Delta^2_\beta}{G} \qquad (4)$$

where the first summation includes only blocked orbitals. The excitation energy is calculated in turn as the difference between the total energy of a configuration and the total energy of the ground state.

For some configurations it is not possible to find a real solution for the two BCS equations. In these cases it is assumed that the pairing correlation disappears and the total energy is calculated according to the free gas model.

To generate all possible configurations of excitons one is forced to account also for configurations in which two unpaired particles occupy the same orbital above the Fermi energy. This presents a certain conceptual difficulty since two particles in time reversed states should be treated, like all other pairs, in the frame of the BCS model. This is however unacceptable because the BCS model ascribes to each orbital some probability of being occupied, in general lower than 1, while in our case the orbital is definitely occupied In fact there is no possibility to fix the position of a pair in the BCS model. To treat excitations involving promoted pairs, we therefore extend the application of the blocking method. Accordingly, both particles are taken as noninteracting fermions and the orbital in which they are placed is excluded from the BCS considerations. This procedure is a rather rough approximation and its drawback can be seen if one compares the energy of the configuration with two excitons placed in the same orbital with the energy of configuration in which these two excitons are placed in two different orbitals which however happen to have the same energy.

In order to obtain mixed configurations as well, the state densities for neutrons and protons are convoluted before the level density is calculated. The energy of a mixed configuration is taken to be the simple sum of the energies of the two convoluted configurations, since no interaction between protons and neutrons is assumed. With this approximation, the state density for mixed configurations can be written as

$$\omega_{p,h}(E,M) = \sum_{\substack{M_p M_h \\ M_p+M_h=M}} \int_0^E \omega_p(E_p,M_p)\,\omega_h(E-E_p,M_h)\,dE_p \qquad (5)$$

To reduce edge effects the state densities convoluted in Eq.5 were sorted into 0.1 MeV bins. To reduce fluctuations, the final results were obtained by lumping together states over 0.5 MeV intervals. The spin projection of a mixed configuration is just the sum of the spin projections of the convoluted configurations. Similarly the product of their parities defines the parity of the mixed configuration.

The finite number of orbitals taken into account limits the maximum energy which can be calculated. We take this limit to be the excitation energy of the configuration consisting of only one exciton promoted to the highest orbital. In practice this limit has been increased by 20%.

All configurations with a specified number of particles and holes are generated within the assumed set of the s.p.s. by means of the permutation enumeration algorithm /3/. For each of them a proper coupling of the spin projections is performed to obtain the nuclear states The state density $\omega(E,M)$ is found by counting states with the angular momentum projection M falling in the 0.5 MeV interval centered at the excitation energy E.

Since the deformation of the nuclear potential removes the degeneracy of the s.p.s. belonging to the same spin multiplet we are no more able to obtain the spin distribution of nuclear levels along the lines described in Ref.6. We therefore, consider the M distribution of the state density $\omega(E,M)$ and derive the spin cutoff parameter (E) from its definition

$$\sigma^2(E) = \langle M^2\rangle - \langle M\rangle^2 = \Sigma_i M_i^2/\omega(E) \qquad (6)$$

2. RESULTS AND DISCUSSSION

We have chosen 27Al, 100Mo, and 170Er as examples of light, medium, and heavy nuclei. The calculations were performed in the space of the s.p.s. by Seager and Howard /4/ obtained for different values of the deformation parameter

The calculated state densities, summed over M, are shown in Figs.1, 2, and 3 for the 1-particle 1-hole configurations of neutrons in three nuclei under consideration. The predictions of the Williams' formula /5/ are given for each case to provide the reference between the results for different deformations and to compare this simple description with the microscopic calculations. For this purpose the s.p.s. density g was set to the standard value A/26 (note that we deal with the neutron gas only).

Using the spherical potential very strong fluctuations in the state densities are observed for all nuclei. In the case of 27Al we have in fact well separated groups of states. For 100Mo and 170Er the states are more spread but still, even at the relatively high excitation energies, there are regions where no state exists. Introduction of the small deformation to the nuclear potential (α =0.05) leads to the splitting of the spin multiplets of the s.p.s. which results in a significant smoothing of the state densities. In a nucleus as light as 27Al it is however not enough to bring the calculated state densities into the form which could be reproduced by any closed form expression. This conclusion remains valid also for much higher deformations α =0.1 and α =0.2. The density of the s.p.s. is so low and the irregularities in the energy distribution of the s.p.s. are so strong that even high nuclear deformation is not able to wash out the shell structure effects. In particular, the comparison of the microscopic results with the predictions of the Williams formula shows an evident nonadequacy of the latter in the low energy region (below 10 MeV) where the preequilibrium emission usually dominates. For the heavier nuclei (Figs.2 and 3) even the small deformation α =0.05 results in the qualitative changes in the calculated results. The gaps are partially filled and a remarkable structure of roughly 5 MeV width appears in the spectra. The peak to valley ratio approaches an order of magnitude at low energies and falls down to 4-6 at the end of the energy range, being higher for 100Mo than for 170Er. This structure seems more likely to be detected experimentally than the sharp fluctuations predicted for the spherical nuclei. Increasing the deformation one observes that the valleys in the spectra are gradually filled on the expense of the bumps leading to the step-like curves for α =0.1 and to the relatively smooth ones for α =0.2.

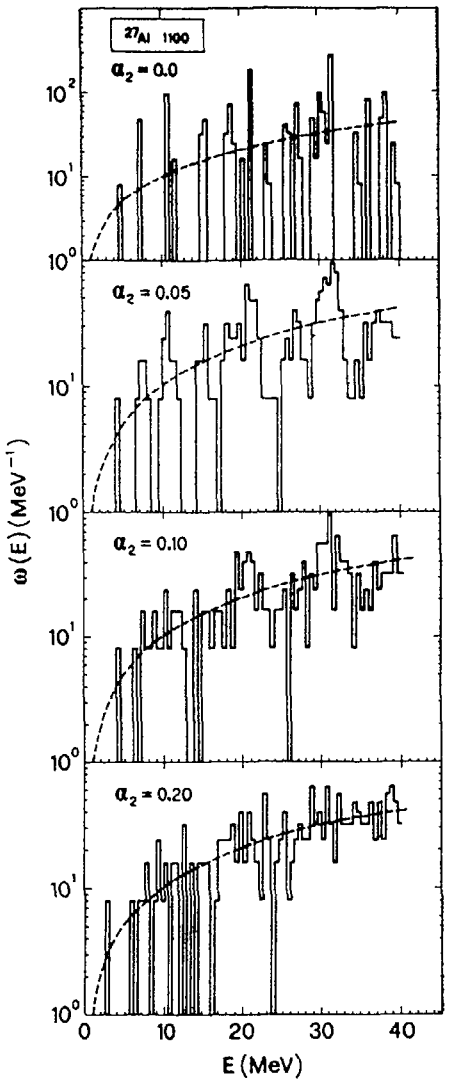

Fig.1

The densities of 1-particle 1-hole neutron states in 27Al calculated in the space of s.p.s. by Seeger-Howard for different values of the deformation parameter (histograms). Solid line represents predictions of the formula by Williams with g=A/26.

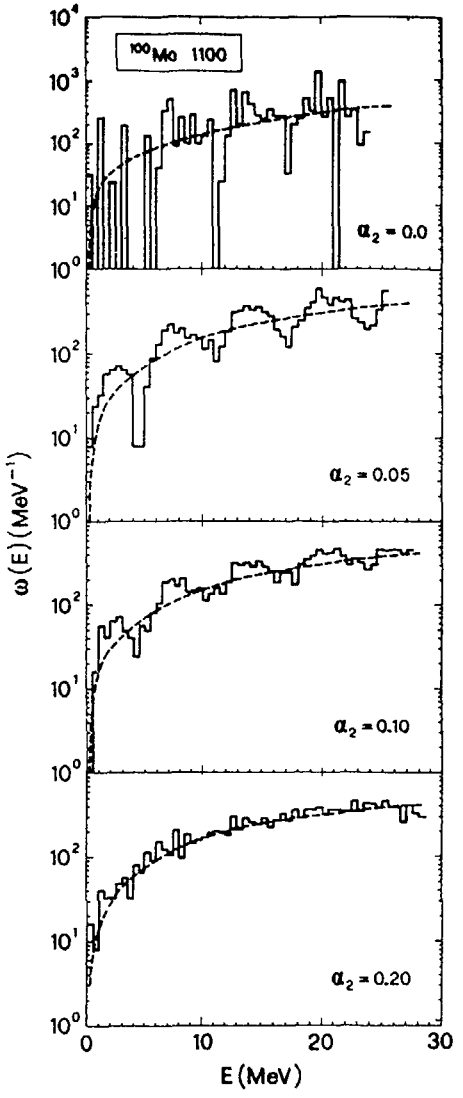

Fig.2

The same as Fig.1 but for 100Mo.

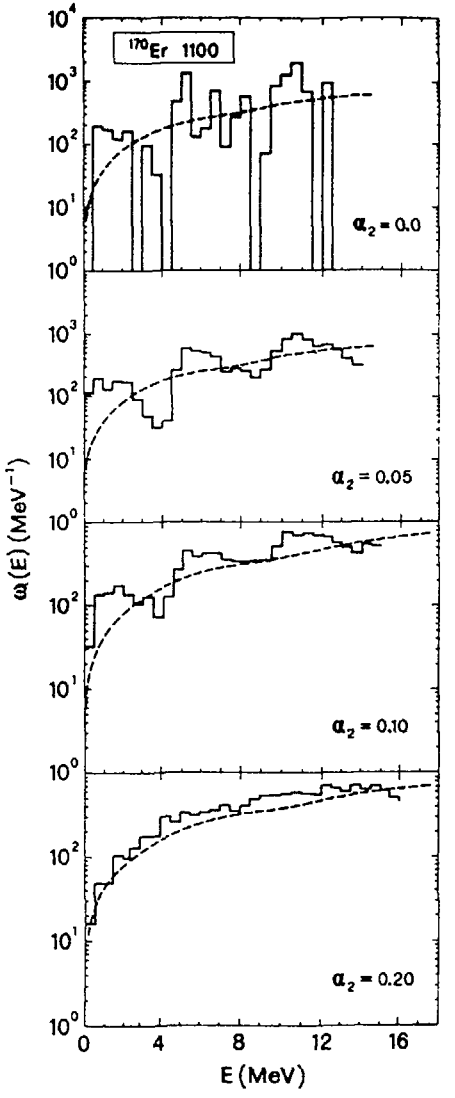

Fig.3

The same as Fig.1 but for 170Er.

It is surprising, how well the Williams' formula describes the general trend of the state densities for two heavier nuclei, in spite of the very low exciton number and of the fact that no attempt have been undertaken to adjust the s.p.s. density g. For the deformations as high as =0.2 the Williams formula may be considered exact, while for the less deformed nuclei the shell structure is expected to show up in a form of the broad structure which is missing in the closed form expression.

Let us now consider the configurations with a higher number of quasiparticles. The results of the microscopic calculations of the state densities, together with the predictions of the Williams formula, are shown in Figs.4 and 5 for the case of four neutron quasiparticles in 27Al and 100Mo. The higher number of excitons results in the damping of the fluctuations, but for $\alpha=0$ the Williams formula is still not applicable. For 100Mo it may be considered reasonable at $\alpha=0.1$. In the case of 27Al already $\alpha=0.05$ deformation makes the spectrum of the states smooth enough to be described by the closed expression above 15 MeV with the accuracy typical for two exciton configurations in heavier nuclei. The deformation, however, does not lower significantly the threshold energy and therefore the Williams formula predicts states in the region where there are none. This has a strong impact on the preequilibrium emission, resulting in the particle spectra which extend to too high energies. In general, the formula by Williams predicts the densities of states properly only for the highly deformed nuclei and only well above the threshold.

About the role of the pairing interaction it was pointed out, in /6/, that for even systems the ground state condensation energy gives a measure of the pairing correction. Therefore, it is helpful to consider first the influence of the nuclear deformation on the ground state condensation energy. The solid lines in Fig.6 show a dependence of the ground state condensation energy as a function of the pairing strength parameter G (multiplied by the mass number A) for different deformations. In the case of 100Mo and 170Er the condensation energy decreases with deformation if the pairing strength is kept fixed. On the contrary, the deformation has nearly no influence on the condensation energy of 27Al, which may be related to the particular structure of the s.p.s. close to the chemical potential. Neutrons in 27Al fill the d5/2 subshell, which results in nearly 5 MeV gap in the s.p.s. above the Fermi level. The deformation of $\alpha=0.2$ reduces this gap to about 3 MeV that is not enough to significantly affect pairing correlations.

The condensation energy taken alone, however, is insufficient to conclude on the effect of the deformation on the pairing interaction. In Ref.6 we have related the differ-

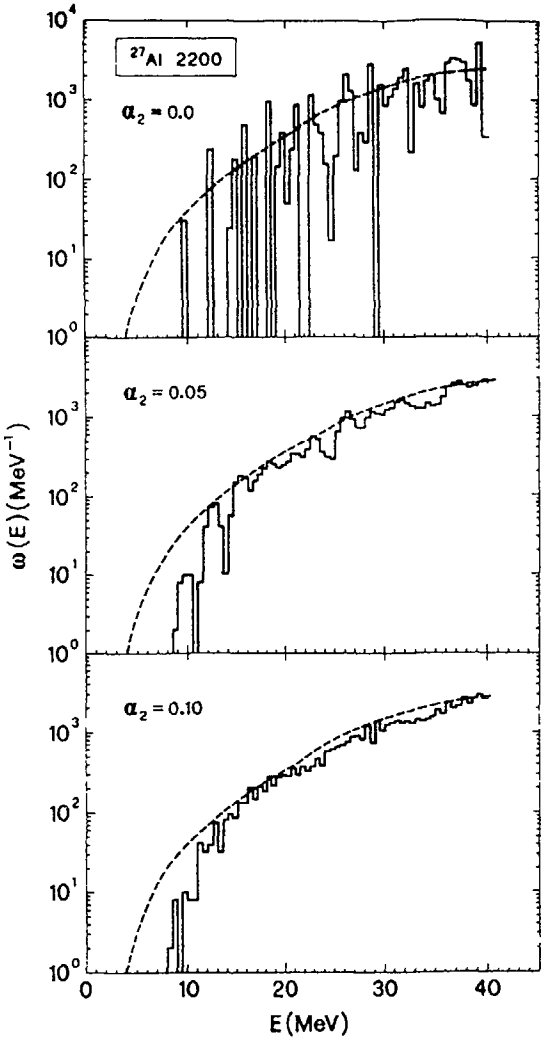

Fig.4

The densities of 2-particle 2-hole neutron states in 27Al calculated in the space of s.p.s. by Seeger-Howard for different values of the deformation parameter (histograms). Solid line represents predictions of the formula by Williams with g=A/26.

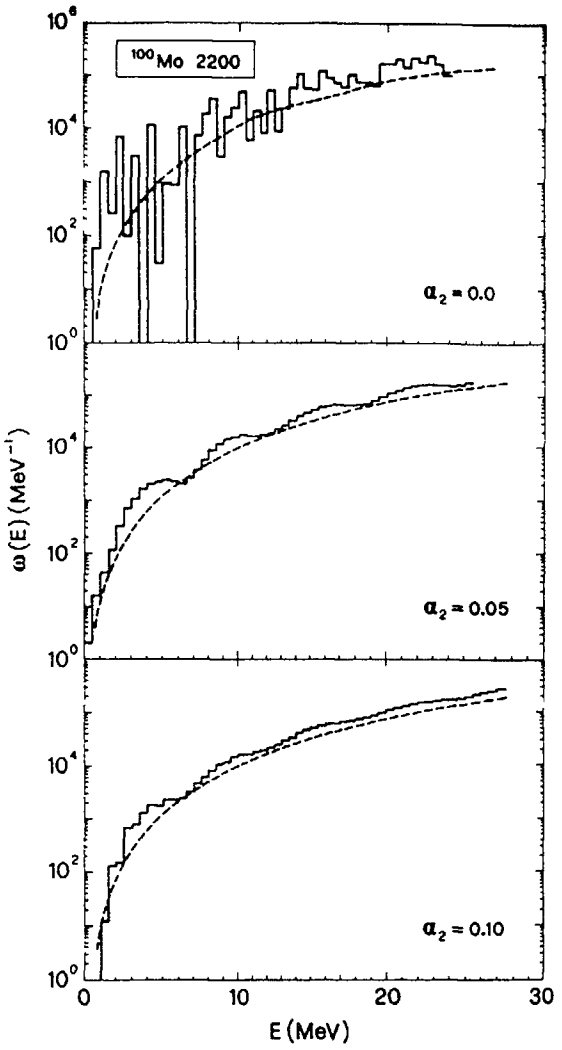

Fig.5

The same as Fig.4 but for 100Mo.

ences in the ground state condensation energies E to the differences of the experimental masses between neighboring nuclei. In this way, the G value is determined as the one which reproduces the so called 'pairing energy' as given by Eq.(1) of the paper by Nemirovsky /7/. The dashed lines in Fig.6 connect (G A,E) pairs which correspond to several arbitrary chosen pairing energies. One observes that, in the case of 100Mo the effect of the deformation on the condensation energy is almost canceled by the necessary adjustment of the pairing strength. For 170Er, on the contrary, the effect of the deformation is found to be very strong and leads to a considerable reduction in the condensation energy.

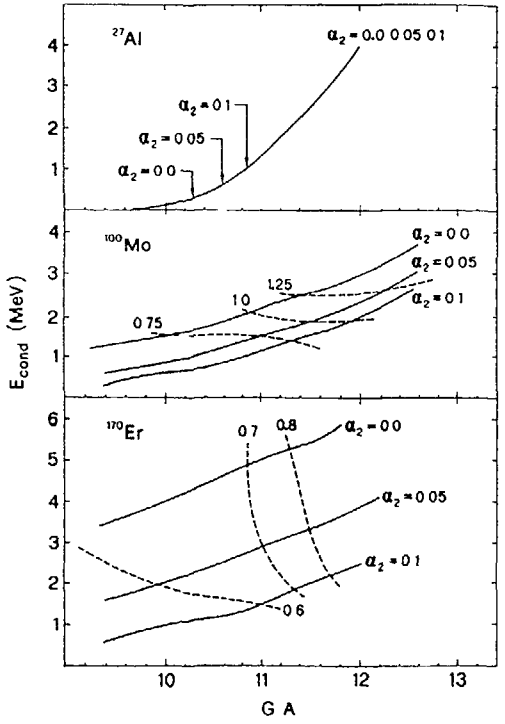

Fig.6

The ground state condensation energy for 27Al, 100Mo and 170Er as a function of the pairing strength parameter G multiplied by mass number A. The curves correspond to several deformation parameters which are indicated in the figure. Dashed lines serve to connect the points corresponding to the indicated pairing energies (see text for an explanation).

To account for the pairing interaction we proposed in Ref.6 to shift the state densities calculated without pairing in a way which assures that the threshold is equal to the one obtained if the pairing interaction is taken into account. Here we review this method in the case of deformed nuclei and in what it regards the structure in the state densities. It turns out that the method does pretty well if the state density is smooth enough, as for example 1-particle 1-hole configurations in 170Er (see Fig.7). In the case of the same configurations in 100Mo pairing interaction rises the first excited state up by 2 MeV, while the characteristic structure in the state density reveals a shift of about 0.5 MeV. Application of the method proposed in Ref.6 leads therefore, to an overestimated displacement (see Fig.7). The structure itself is also slightly affected by the pairing forces.

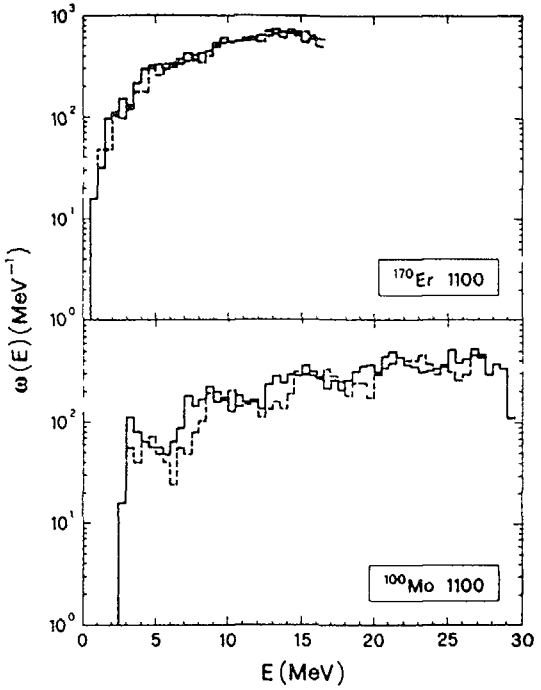

Fig.7

The 1-particle 1-hole neutron state densities for 170Er and 100Mo calculated with the pairing interaction taken into account (solid histogram) compared with the calculation without pairing which are shifted to make the first excited state in both calculations to coincide

Let us now consider the distribution of quasiparticle states according to the projection of an angular momentum M. In Fig.8 we compare M distributions of two exciton states in 100Mo calculated in the space of the spherical and the deformed shell-model s.p.s.. The states are confined to the energy interval 0.5 MeV around 14.25 MeV of excitation energy. Deformation removes the degeneracy of s.p.s. obviously causing fluctuations in the M distribution of

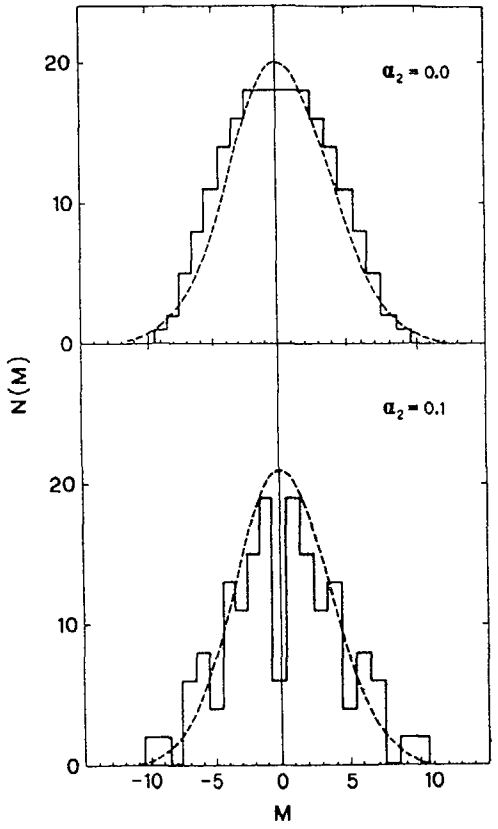

Fig.8

The M distribution of 1-particle 1-hole neutron states in 100Mo for different values of the deformation parameter . States confined to the 0.5 MeV bin centered at 14.25 MeV of excitation energy are taken into account. Solid line represents the Gaussian distribution with the parameter determined from the combinatorial results.

quasiparticle states (see Fig.8). However, if the fluctuations are disregarded a Gaussian may still be considered a good approximation and the spin cutoff factor may be determined for each energy bin from Eq.(6). Analysis of the energy dependence of the spin cutoff factor shows that the deformation has a similar smoothing effect as in the case of state densities but clear fluctuations persist even at high deformations (see Fig.9).

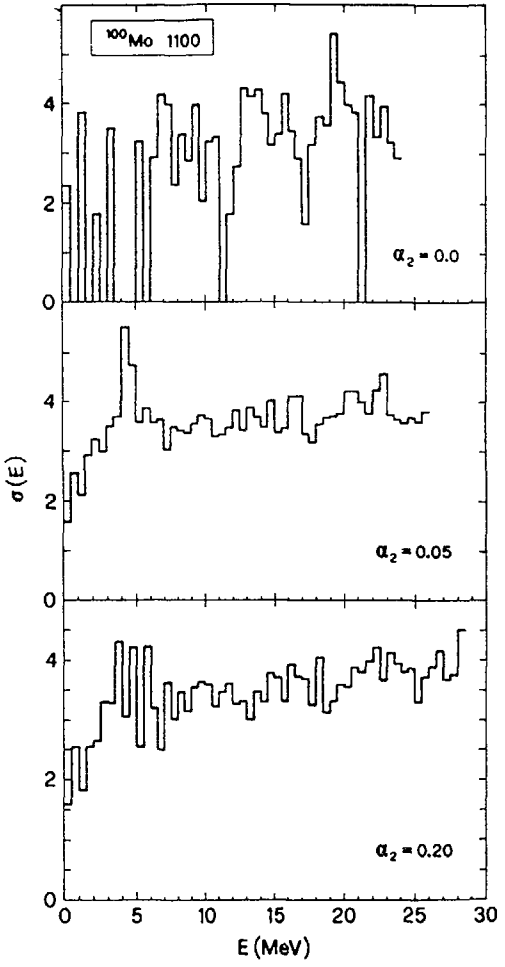

Fig.9

The energy dependence of the spin cutoff parameter for 1-particle 1-hole neutron configurations in 100Mo calculated for several values of the deformation parameter.

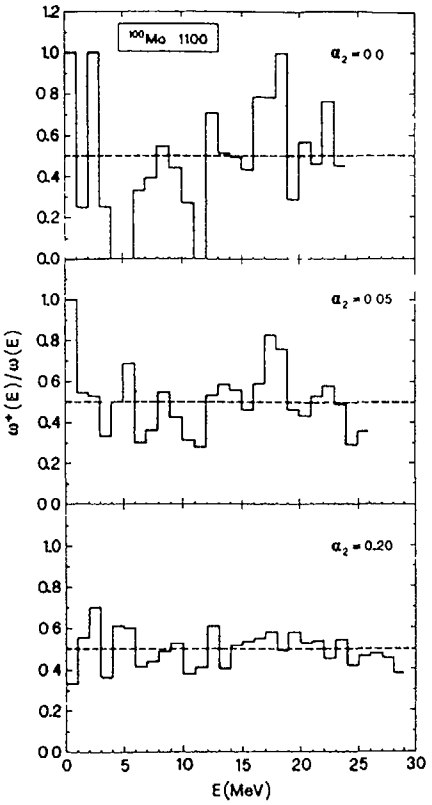

Fig.10

The fraction of the positive parity states among 1-particle 1-hole neutron states in 100Mo calculated for several values of the deformation parameter.

Finally, we show the effect of the deformation on the parity distribution of quasiparticle states. Since deformation does not influence the parity of s.p.s. the ratio of positive to negative parity has to remain the same if all generated quasiparticle configurations are taken into account. Therefore, the deformation may only affect the structure in the energy dependence of the ratio of both parities. In Fig.10 the parity distributions for different values of the deformation parameter are presented for 1-particle 1-hole neutron configurations in 100Mo. For the spherical nucleus one observes strong deviations from the equal parity distribution, which are gradually reduced with the increasing deformation.

3. CONCLUSIONS

The fluctuations and appearance of the thresholds, which exclude states at lower energies, are the two main features which may prohibit describing the distributions of states with fixed number of excitons in terms of the closed form formulae. These effects decrease with more uniform distribution of s.p.s. happening when:

(a) changing to the heavier nuclei
(b) moving out of the closed shells
(c) increasing the deformation.

For obvious reasons the latter two are usually correlated, and therefore, the spherical magic nuclei are the extreme cases for which the shell structure effects are most pronounced.

Our calculation proved that nuclear deformation tends to suppress fluctuations in the state density, in the parity distribution and in the energy dependence of the spin cutoff parameter. However, only for medium and heavy nuclei chracterized by relatively strong deformations ($\alpha > 0.1$), this suppression is enough to make the formula by Williams a good approximation to the state densities. In any case, it is possible only if a proper configuration threshold is cared of. For the light nuclei, even well deformed, the fluctuations and the thresholds cause closed expressions to fail. This remains true also for those heavier nuclei for which deformation is less than 0.1. Increasing the number of excitons relaxes these limits to some extent, but on the other hand, increases usually the threshold energies. The formula by Williams becomes, therefore, applicable but only well above the threshold.

It is difficult to conclude positively on the influence of the deformation as far as the magnitude of the pairing correction is concerned.

The simple correction accounting for the pairing interaction, which was proposed in Ref.6, appears a good approximation as far as the average energy dependence of the state density is concerned. It fails however, if a more detailed structure in the data is of the interest. This is not surprising since, as we have pointed out already in Ref.6, the procedure of shifting the entire distribution by a constant amount, is a kind of manipulation which can not fully describe the real physics which stands behind.

REFERENCES

1. S.Wahlborn, Nucl. Phys. 37,554(1962).
2. M.Hilman and J.R.Grover, Phys. Rev.185,1303(1969).
3. W.H.Payne and F.M.Ives, Amc. Trans. of Math. Soft. 5,2(1979) p.163
4. P.A.Seeger and W.M.Howard, Nucl. Phys. A 238,491(1975).
5. F.C.Williams Jr., Nucl. Phys. A166,231(1971).
6. M.Herman and G.Reffo, Phys. Rev. C36 in press
7. P.E.Nemirowsky, Kurchatov Institute Report IAE-2530 (1975).

PAULI EXCLUSION EFFECT IN MULTIPARTICLE AND HOLE STATE DENSITIES

(Summary)

Jingshang ZHANG
Institute of Atomic Energy,
Beijing, China

A method to calculate the effect of the Pauli exclusion principle in multiparticle and hole state densities is proposed. The model-independent method can be essentially extended to any multi-fermion system. For an application to the exciton model, both the strict expression of state densities and the exact Pauli exclusion correction (PEC) are obtained in the equidistant spacing model. The enhancement of the exact Pauli exclusion correction implies that the Pauli exclusion principle plays a quite important role in state densities.

The m-particle n-hole state density with excitation energy E is defined by

$$\omega(E,m,n)=\sum_{\substack{p_1<\cdots<p_m\\ h1<\cdots<h_n}}\delta\Big(E-\sum_{p=p_1}^{p_m}\varepsilon_p\sum_{h=h_1}^{h_n}\varepsilon_h\Big). \qquad (1)$$

Here ε_p and ε_n are the energies of single particle and hole, recpectively. The delta function in (1) implies that the energy conservation must be satisfied within the combination of ε_p and ε_h. When the m+n fold summation extends over all particle states labelled by p and hole states labelled by h, the restriction $p_1<\cdots<p_m$ and $h_1<\cdots<h_n$ are made to avoid multiple counting in order to satisfy the Pauli exclusion principle.

Eq.(1) can be rewritten in the form

$$\omega(e,m,n)=\sum_{\substack{\mu_1<\cdots<\mu_m\\ \nu_1<\cdots<\nu_n}}\langle\mu_1\cdots\mu_m,\nu_1\ \nu_n|\delta\Big(E-\sum_{\mu=\mu_1}^{\mu_m}H_\mu-\sum_{\nu=\nu_1}^{\nu_n}H_\nu\Big)|\mu_1\cdots\mu_m,\nu_1\ \nu_n\rangle \qquad (2.1)$$

where the product eigenstates have the property

$$H_1|\mu_1\cdots\mu_m,\nu_1\ \nu_n\rangle=\varepsilon_1|\mu_1\ \mu_m,\nu_1\ \nu_n\rangle \qquad (2.2)$$

Carrying out a Laplace transform, one gets

$$Z(\beta;m,n)=\int_0^\infty dE e^{-E\beta}\omega(E;m,n)=Z_p(m)Z(n), \qquad (3)$$

where $$Z_p(m)=\sum_{\mu_1<\cdots<\mu_m}\langle\mu_1\cdots\mu_m|e^{-\beta\sum_\mu H_\mu}|\mu_1\cdots\mu_m\rangle \quad (3.1)$$

and $$Z_h(n)=\sum_{\nu_1<\cdots<\nu_n}\langle\nu_1\cdots\nu_n|e^{-\beta\sum_\nu H_\nu}|\nu_1\cdots\nu_n\rangle \quad (3.2)$$

Since the summation in (3.1) and (3.2) are restricted, we found an approch to reduce the restricted one into independent form and all of the terms can be expressed by complete set of Young patterns, which are denoted by $[N_1,N_2,\ldots N_L]$, where N_i $(i=1,2\ldots L)$ is the square number of i-th line.

$$Z_{p(h)}(N)=N!\ A_N^{(o)}=\sum_{L=1}^{N}\sum_{\alpha=1}^{NL}D(N,L,\alpha)[N_1^\alpha,N_2^\alpha,\ldots N_L^\alpha], \quad (4)$$

where NL is the number of n square L line Young pattern and $D(N,L,\alpha)$ is the coefficient of α-th N pattern L line term.

If we denote by $\nu_i^\alpha(i=1,2\ldots N)$ the number of the line with i squares for the partition $[N_1^\alpha,N_2^\alpha,\ldots N_L^\alpha]$, one has

$$\sum_{i=1}^{N}\nu_i^\alpha=L \quad \text{and} \quad \sum_{i=1}^{N}i\nu_i^\alpha=N.$$

In terms of the permutation group theory, we find out that the value of the coefficient $D(N,L,\alpha)$ in (4) is just the number of the distinct permutation having the cycle structure in the partition $[N_1^\alpha,N_2^\alpha,\ldots N_L^\alpha]$, which reads

$$D(N,L,\alpha)=\frac{N!}{\nu_1^\alpha!(2^{\mu_2^\alpha}\nu_2^\alpha!)(3^{\mu_3^\alpha}\nu_3^\alpha!)\cdots(N^{\mu_N^\alpha}\nu_N^\alpha!)}. \qquad (5)$$

Thus, one can express the N particle (or hole) state density as the following polynomial

$$\omega(E;N)=\frac{g}{N!(N-1)!}\sum_{i=0}^{N}C_{N,i}(gE)^{N-i-1}(-1)^i. \qquad (6)$$

The configyration of each N square L line Young pattern is expressed by $[N_1^\alpha,N_2^\alpha,\ldots N_L^\alpha]$, $\alpha=1,2\ldots NL$. Then the coefficient $C_{N,i}$ in (6) can be obtained by the formula

$$C_{n,i}=\sum_{\alpha=1}^{NL}D(N,L,\alpha)\frac{(N-1)!}{(N-i-1)!\ N_1\cdots N_L} \qquad (7)$$

with $L=N-i$.

For physical reason, the state densities must be positive and increase monotonically with increasing E if there is no restriction on particle-hole energy and the well depth. Thus, a starting point B(N) of gE exists, such that when gE=B(N) then $\omega(E,N)=0$. With the increasing E the ω increases as mentioned above. Conversely, when E decreases from B(N), ω becomes negative, so that gE<B(N) is the unphysical region. The value of B(N) given by the maximum zero point of (6) gives the exact PEC value. The calculated results of B(N) are shown in table 1 for N=2-15.

TABLE 1. VALUES OF PEC FOR PURE PARTICLE AND WHOLE NUMBER N IN THE EQUIDISTANT SPACING MODEL

N	B(N)	$A^k(N)$	N	B(N)	$A^k(N)$
2	0.5	0.5	9	37.26	18.0
3	2.46	1.5	10	46.68	22.5
4	5.66	3.0	11	57.13	27.5
5	9.93	5.0	12	68.59	33.0
6	15.22	7.5	13	81.07	39.0
7	21.52	10.5	14	94.57	45.5
8	28.86	14.0	15	109.09	52.5

B(N): the exact PEC values.

$A^k(N)$: the values of Kalbach's PEC.

The strict particle-hole state density expressed by a polynomial has the form

$$\omega(E;m,n)=g\sum_{i=0}^{m-1}\sum_{j=0}^{n-1}C_{m,i}C_{n,j}\frac{(-1)^{i+j}(gE)^{m+n-i-j-1}}{m!n!(m+n-i-j-1)!}$$

$$=g\sum_{k=0}^{m+n-2}H(m,n,k)\frac{(-1)^{k}(gE)^{m+n-k-1}}{m!n!(m+n-k-1)!} \qquad (8)$$

Without loosing generality, when $m\geq n$ one has

$$H(m,n,k)=\begin{cases}\sum_{j=0}^{k}C_{m,k-j}C_{n,j} & \text{for } k\leq m-1\\ \sum_{j=0}^{n-1}C_{m,k-j}C_{n,j} & \text{for } m-1<k\leq n-1\\ \sum_{j=k-m+1}^{n-1}C_{m,k-j}C_{n,j} & \text{for } n-1<k\end{cases} \qquad (9)$$

The ratios of the exact PEC values and Kalbach's values are shown in table 2, roughly the ratios are closed the factor 2. It is obvious physically that if we arrange N particles in the equidistant spacing model in their ground state, the energy occupied by the first N-1 particles is approximately

$$\sum_{i=1}^{N-1}i/g=N(N-1)/2g. \qquad (10)$$

so that the excitation energy must be larger than the value given by (10) to account for the N-th particle.

TABLE 2. THE RATIOS OF EXACT PEC VALUES AND KALBACH'S VALUES

— — — — $B(m,n)/A^{k}(m,n)$

n \ m	2	3	4	5	6	7
0	1.0	1.638	1.886	1.987	2.029	2.050
1	2.0	2.187	2.215	2.200	2.179	2.164
2	2.366	2.407	2.355	2.294	2.252	2.228
3		2.429	2.375	2.316	2.279	2.257
4			2.339	2.300	2.280	2.261
5				2.283	2.272	2.254
6					2.262	2.244
7						2.227

n \ m	8	9	10	11	12
0	2.062	2.070	2.075	2.077	2.078
1	2.155	2.148	2.140	2.133	2.126
2	2.211	2.194	2.178	2.166	2.156
3	2.235	2.212	2.194	2.181	2.170
4	2.236	2.213	2.199	2.188	2.176
5	2.230	2.212	2.202	2.190	2.174
6	2.223	2.211	2.201	2.186	2.168
7	2.213	2.206	2.196	2.179	2.167
8	2.206	2.200	2.189	2.174	2.167
9		2.194	2.182	2.171	2.166
10			2.172	2.165	2.163
11				2.163	2.160
12					2.155

$A^{k}(m,n)=1/4*m*(m-1)+1/4*n*(n-1)$

246 APPLICATION OF DIFFERENT PRE-EQUILIBRIUM MODELS TO THE DESCRIPTION OF DOUBLE DIFFERENTIAL NEUTRON EMISSION CROSS-SECTIONS — COMPARISONS DISCUSSED FOR THE CASE ^{93}Nb+n

D SEELIGER
Technische Universitat Dresden,
Dresden, German Democratic Republic

Abstract

During the past years a diversity of pre-equilibrium models and computer codes have been developed and used for the theoretical description of DDNECS in the frame of neutron nuclear data evaluations. For the case ^{93}Nb + n different approaches are discussed, briefly. The importance of consideration of direct collective excitations (besides the single-particle pre-equilibrium descriptions) in this case is outlined. A new SMD/SMC-approach presented at this meeting seems promising in this respect. The present paper has to be considered in conjunction with three contributed papers /14,18,19/ where some specific problems are discussed in more detail.

---

1. Introduction

First of all, some remarks concerning the terminology used in the present paper should be explained. Frequently the term 'pre-compound' is used for nuclear reactions which take place before the compound nucleus is reached (sometimes from this reactions additionally the collective direct reactions are excluded!). Here instead of 'pre-compound' the term 'pre-equilibrium' is used, which is more general because it bases on a well defined feature of each statistical system rather than on a specific nuclear reaction model.

In our understanding the term 'pre-equilibrium reactions' designates all those nuclear reactions in which particles occur in the exit channel before the statistical equilibrium of the composite system is reached. This definition is model-independent and, of course, it includes also direct on-step and two-step processes.

Pre-equilibrium and equilibrium reactions practically never occur in a pure manner, but both of them can be more or less pronounced, pending on the type of incident particle and energy, reaction channel, the properties of target nucleus a.s.o.

The model-independent experimental evidence of pre-equilibrium processes is well-known:

i) Evidence of hard components in the spectra of emitted particles, which cannot be expected at a given excitation from fully equilibrated statistical systems;
ii) correlations between the linear momenta of incoming and outgoing particles resulting in a forward peaking of angular distributions;
iii) strong enhancement of the excitation of definite (collective) states in the final nucleus.

Pre-equilibrium reactions meant here are not connected with a definite nuclear reaction model (like the exciton model), they cover a broad range of several decades at the time scale of nuclear processes and can be caused by quite different types of physical interactions (such as single-particle, collective vibrational or collective rotational a.s.o.).

Discussing the application of different pre-equilibrium models one has to take into account, that every nuclear reaction model is based on definite assumptions and approximations, and, therefore, it reflects the reality to a certain extent only. Moreover, quite different models sometimes are able to describe the experimental data with almost the same quality. In this cases different theoretical models cannot exclude each other by comparison with the experiment and the inter-comparison between model s should be carried out at the level of the physical assumptions and foundations inherent in these models. In this cases one has to look also for a widening of the area of application to see the limits of applicability of different approaches. For practical applications the use of simple parametrizations or crude theoretical

estimates is justified, if they can give about the same quality of agreement as the better physically based theories for the crucial experimental data. Both types of theories are necessary and should be developed inparallel. Achievements of the later way of more fundamental developments do not exclude reasonable successes of the former one.

In general, this simple wisdoms are well-known and widely used. However, some of the contrary discussions on pre-equilibrium models in the past could have been changed into more efficient disputes if always this simple rules would have been taken into account.

2. Remarks and precautions concerning the experimental data base

DDNECS at 14 MeV are widely used for comparisons with statistical pre-equilibrium models from the very beginning of the development of the exciton model /1/ up to now /2/. The reasons for this are the following:

(i) The inclusion of DDNECS up to 20 MeV incidence energy into the evaluated nuclear data files was of high practical importance and priority during the last decade.

(ii) Already the first comparisons between experimental neutron emission spectra and relative calculations in the frame of evaporation theory plus exciton model indicated that pre-equilibrium emission is of high importance in this reaction channels /1/.

As an example on Fig. 1 angle integrated neutron emission spectra for five samples of natural elements at 14.6 MeV incidence energy are shown together with a fit of equilibrium (Weißkopf-Ewing) plus pre-equilibrium (Exciton Model) spectra shapes /1/. Besides the great success obtained in this way for the theoretical description of DDNECS, Fig. 1 demonstrates also a few difficulties and problems connected with the application of statistical pre-equilibrium theories to this type of experimental nuclear

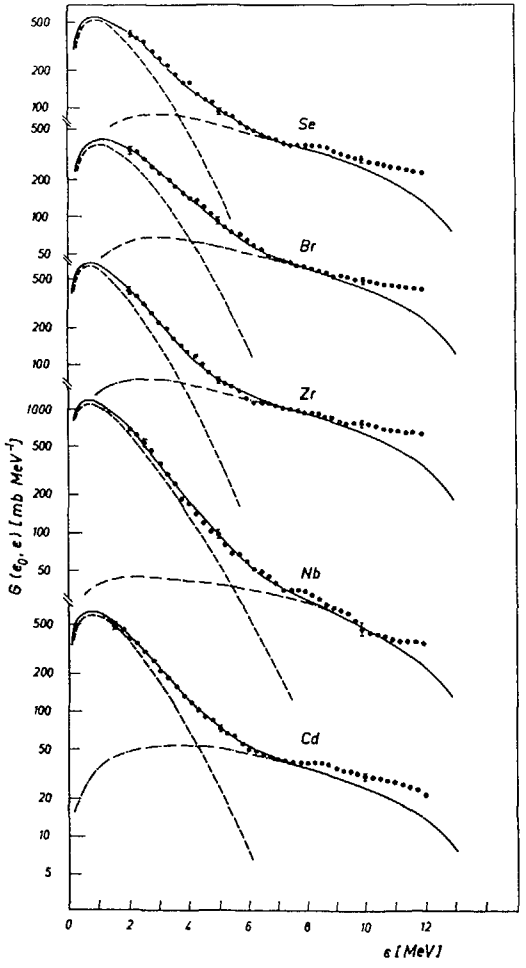

Fig. 1 Angle-integrated neutron emission spectra at 14 MeV for several elements compared with a theoretical curve presenting a sum of evaporation plus pre-equilibrium emission calculated with the exciton model (relative calculations fitted to the experiment) taken from one of the first analyses /1/

data:

(i) The upper end of the emission spectra generally was underestimated by the exciton model. This was not surprising, because already at that time the strong collective enhancement of the excitation of low-lying 2^+ and 3^- states in gg-nuclei in (nn') reactions was a well-known effect /3/.

(ii) In principle, the final nuclei occur in isolated states up to the neutron binding energy, i.e. down to 6 - 7 MeV at the neutron emission energy scale. Within the region of a few MeV above the groundstate the density of real nuclear excitation levels is rather limited. In contrast to this, the application of the exciton model assumes the existence of hypothetic particle-hole states with a high density (good statistics) in this range of final nucleus excitation. The justification for this artificial procedure mainly came from successes in practical applications rather than from theoretical foundations. Therefore, it belongs to empirical findings rather than to theoretical expectations, that for non-magic nuclei and after subtraction of the strong collective excitation of a few final states the neutron emission spectra below the neutron binding energy quite reasonably can be described by statistical pre-equilibrium theories.

(iii) Further difficulties arise from the experimental procedures used for the determination of DDNECS. Measurements carried out for the first time with a broad dynamical range using TOF method in the 70-s were characterized by a comparatively moderate energy resolution of 1...4 ns/m /1,4,5 and others/, resulting in a smoothing of the structures caused by the collective quadrupole and octupole vibrations. Additionally, uncertainties in the nonelastic neutron emission spectra were caused by the difficulties of elastic peak separation procedures. Therefore, today these experiments should be used up to emission energies of 10 - 11 MeV only and combined with higher resolution experiments /6,7/ at the upper end of the energy scale. In this case instead of the smooth upper end of the spectra shown on Fig. 1 above 10...11 MeV more or less pronounced structures occur at energies were collective levels are located (in odd nuclei the collective strength is spread over a few levels due to particle - core coupling - this also results in 'bumps' in the neutron spectra observed).

(iv) It must be stressed, that the energy dependence of single-particle and collective pre-equilibrium interaction probabilities is quite different. Basing on nucleon-nucleon interaction rates the statistical single-particle exciton model below 20 MeV predicts pre-equilibrium cross sections strongly depending on the incident neutron energy /8/, whereas the cross sections of the excitation of collective modes are almost energy independent /9/. At 14 MeV incident energy usually both components remarkably contribute to the spectra. Erroneous conclusions may be drawn, if pre-equilibrium matrix elements are determined from comparisons with 'smoothed' experiments (i.e. without separation of collective modes) leading to inconsistent descriptions of energy dependences as well as pre-equilibrium emission rates in other reaction channels (f.i. in the (np) channel, where collective excitation is negligible).

Summarizing, one can state, that DDNECS at 14 MeV at one hand are very important nuclear data for applications (f.i. for transport calculations) and easily can be parametrized using exciton and evaporation models but at the other hand very carefully have to be considered if physical conclusions concerning different reaction mechanisms or the validity of different pre-equilibrium models are drawn. Generally, the DDNECS are not very sensitive to changes in the models. Experimental data with high resolution for a broad incidence energy range are needed for a sensitive distinction between single-particle and collective pre-equilibrium components.

In the case ^{93}Nb + n DDNECS data are available at seven incidence energies /10 - 12/ between 5 and 26 MeV and an extensive computer code intercomparison at 14 MeV and 26 MeV /2/ was car-

ried out, recently. Therefore, all the further discussions in the present paper are concentrated on this case. As in many previous papers statistical model approaches, which originally were developed for the description of nuclear reactions in the continua of final states, are applied as an average description in the range of discrete levels below the binding energy. The only exception is made for the strongest collective 2^+, 3^- and 4^+ excitations in the even-even $^{92}_{40}Zr$ - core of the $^{93}_{41}Nb$ nucleus.

Recently, an evaluation of angle-integrated neutron emission spectra at 14.1 MeV was carried out /13/. On Fig. 2 the compiled experimental data are shown. In this case data from experiments with moderate resolution above 10 MeV are already omitted - otherwise the discrepancies within the range 10...12MeV would be much higher. The 'bump' between 11 MeV and 12 MeV with more than 40 mb/MeV definitely is caused by the excitation of 3^- and 4^+ states in the ^{92}Zr core. The experimental evaluation /13/ presented on Fig. 3 again shows this effect, which was missing in the ENDF/B-V evaluation. This shape of the high energy end of the spectra should be compared with experimental spectra shown at the figures below, which partially are still basing on experiments with moderate resolution.

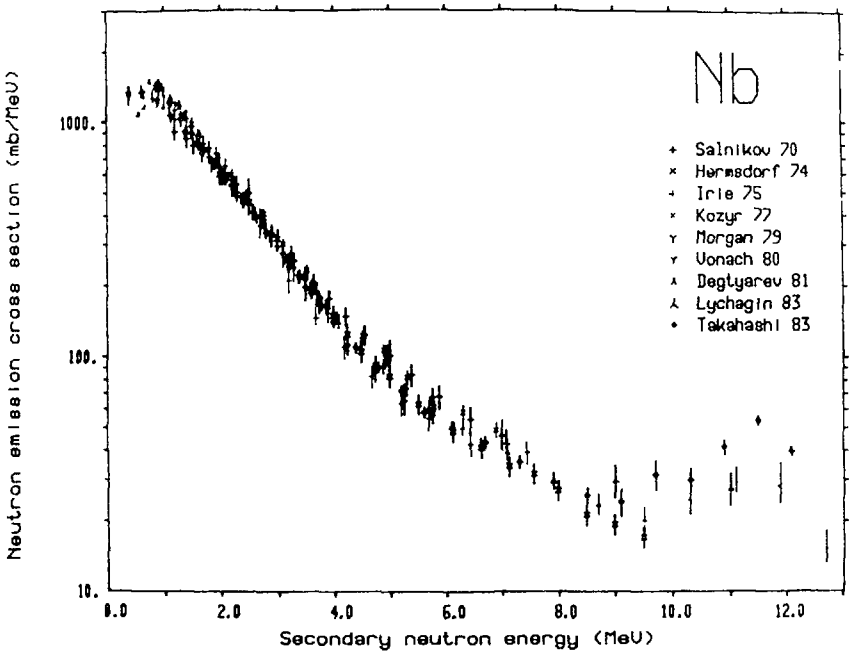

Fig. 2 Compilation of experimental angle-integrated neutron emission spectra for Nb at 14 MeV /13/

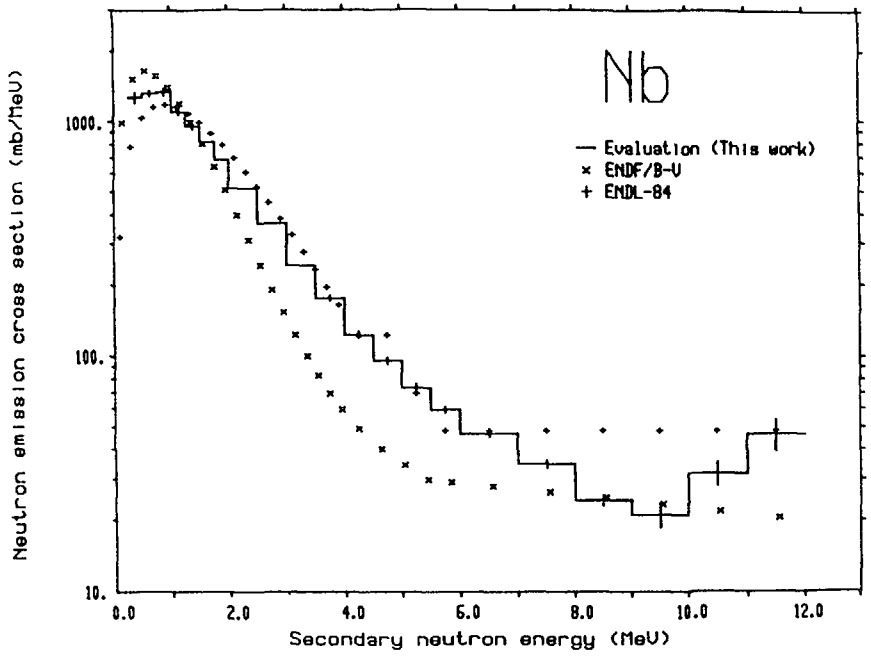

Fig. 3 Evaluation of the angle-integrated neutron emission spectrum for Nb at 14 MeV, basing on experiments shown in Fig. 2, in comparison with ENDF/B-IV and ENDL-84 /13/

3. 'Traditional' pre-equilibrium analyses of neutron emission spectra

In the contributed paper /14/ to this meeting an usual analysis of experimental integrated neutron emission spectra at 14.6 MeV /1/ and at lower energies /10/ using the code STAPRE is presented. In this paper it is shown, that angle-integrated spectra at 14.6 MeV are still reasonably described by the combination of exciton model and Hauser-Feshbach theory except the highest part of the spectrum (though the discrepancies would be higher at the upper end of the spectra, if instead of the experimental data /1/ the evaluation /13/ shown on Fig. 3 would be used!). Below 14 MeV the disagreement between experiment and exciton model predictions becomes stringent - as shown on Fig.4, taken from /14/. By no reasonable variation of exciton model parameters the observed pre-equilibrium spectra at 9.0 MeV and 7.0 MeV (determined as the difference between experiment and HF-calculation) can be explained. The reason for this is the different physical interaction: the lower the incident energy, the higher is the relative contribution of collective excitations of low-lying states to the pre-equilibrium emission.
For neutron emission from ^{93}Nb + n reactions Gruppelaar and Nagel recently carried out an international Nuclear Model and Code Comparison /2/. About 20 different computer codes (or versions) were tested and compared using the experimental neutron and proton emission spectra mainly at 14.6 MeV and 25.7 MeV as a reference.
Concerning the under lying pre-equilibrium physics these codes can be subdivided in three classes:

- Modified Hauser-Feshbach Codes or unified models adopted for pre-equilibrium emission (class "A")
- Exciton model codes basing on the solution of the master equation for both equilibrium and pre-equilibrium emission (class "B")
- Hybrid and geometry-dependent hybrid models (class "C").

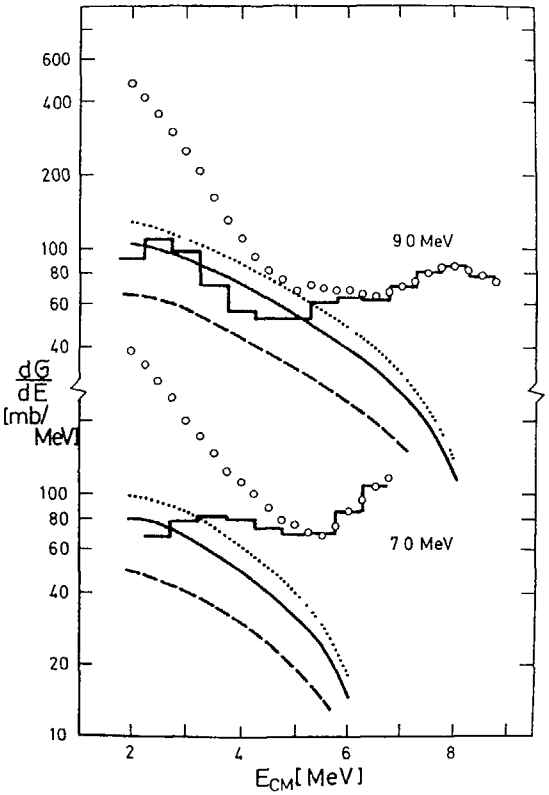

Fig. 4 Angle-integrated neutron emission spectra for Nb at 7.0 MeV and 9.0 MeV /10/ compared with the shape of exciton model curves; full line, dashed and dotted curves - exciton model with reasonable parameter variations; step function - difference between experiment and HF-calculations of the equilibrium emission /14/

At the high-energy end of the spectra (> 10 MeV) the exciton model codes (both classes A and B) give similar shapes, except the endpoint of the spectrum is not the same (see Fig. 5 for an example). This could be caused by different level densities used in the codes, in particular different pairing-energy corrections. But this means also, that the neutron emission spectra are not very sensitive to changes in the models and one has to be very careful in drawing conclusions about the physical validity of small changes introduced in the models.

The geometry-dependent hybrid models predict somewhat different shapes with higher cross sections at high emission energies. This is due to the geometry effect included in the GDH model. However, direct collective excitations are not included in this models, too.

If calculated spectra from all the three classes of models are compared with the evaluation shown on Fig. 3 it becomes evident, that with pre-equilibrium models basing on direct single-particle excitations alone the highest part of emission spectra cannot described reasonably.

The same holds, if pre-equilibrium spectra are calculated in DWBA approximation using 1p1h-wave functions /15/. As an example on Fig. 6 the shell model 1p1h-DWBA calculation is shown again for the niobium emission spectrum at 14.6 MeV in comparison with the 'usual' exciton model analysis /14/. This model also cannot take into account collective effects, but Fig. 6 demonstrates, that practically the direct 1p1h-component and the exciton model component with n = 3 are equivalent concerning the shape of the spectrum (the absolute height of DWBA calculation was adjusted by comparison with experiments).

An alternative direct reaction description can be achieved by introduction of long-ranging QQ-forces into the Hamiltonian to simulate koherence of single-particle excitation, which is typical for collective states /16/.

The results of this type of calculation, again described in more detail in the contributed paper /14/, are shown on Fig. 7. The DWBA calculations in this case show the expected pronounced

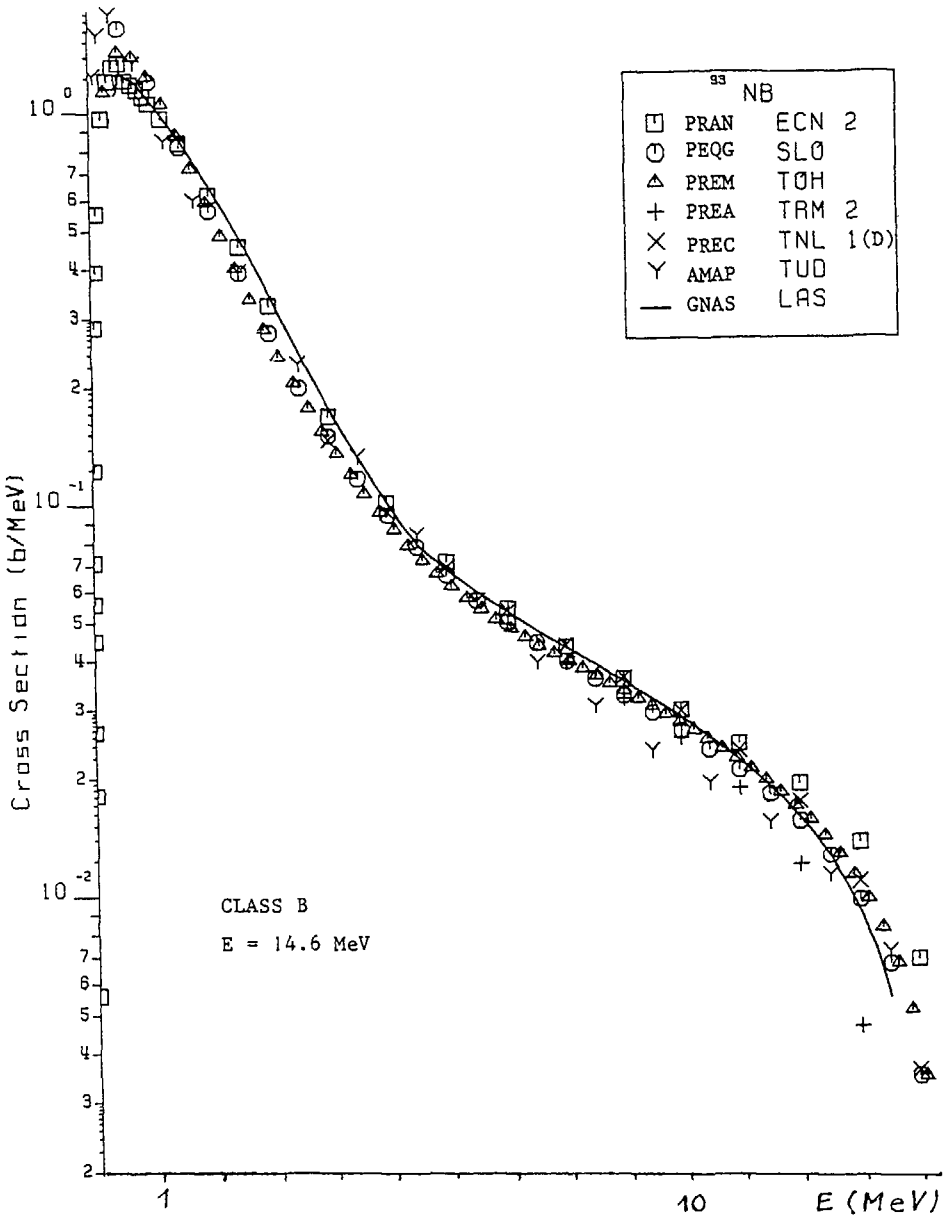

Fig. 5 Intercomparison between different computer code calculations for the angle-integrated neutron emission spectrum at 14.6 MeV for codes of the "class B" /2/

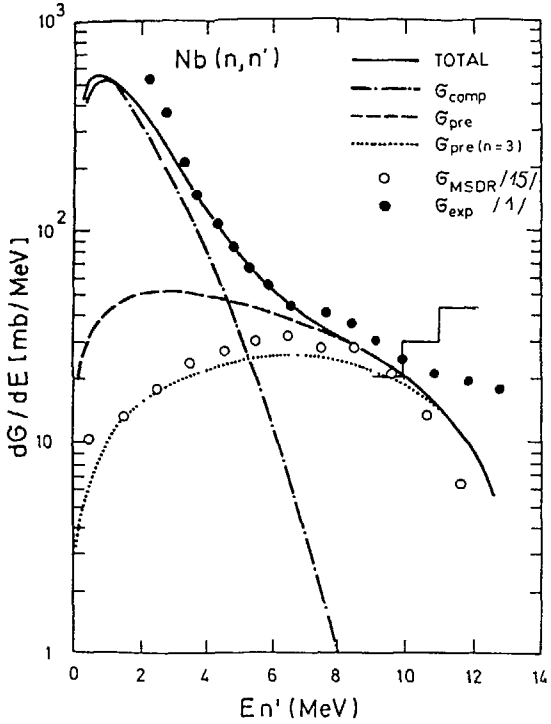

Fig. 6 Experimental neutron emission spectrum at 14.6 MeV /1/ (full points) and evaluated experimental spectrum / / (step function) in comparison with theoretical calculations for primary emission using the exciton model plus HF-theory (different curves) /14/ and DWBA calculations using 1p1h-shell model wave functions /15/

excitation of the collective first 2^+ and 3^- states in the ^{92}Zr core of the ^{93}Nb nucleus. This description now is in agreement with recent experiments (compare with Fig. 3) taking into account the remarks concerning limited energy resolution in the former experiments (see sec. 2).

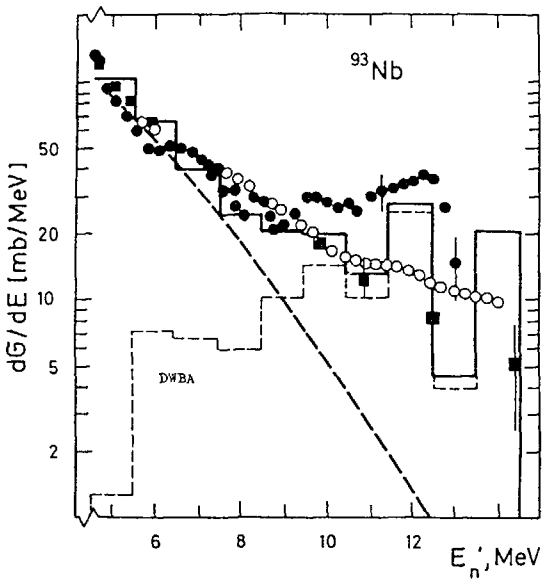

Fig. 7 Experimental neutron emission spectra at 14.6 MeV from Dresden (o), Obninsk (■) and Livermore (●) in comparison with DWBA calculations for phonon excitation of collective states in the ^{92}Zr core (step function) /14,16/

4. SMD and SMC approach applied to niobium data below 30 MeV

In the contributed paper /17/ to this meeting results of calculations of neutron emission spectra in the frame of a new SMD-SMC-model published in /18/ are presented. This model bases on the use of Green's function formalism. Preserving the description of composite states by particle and hole numbers and excitation energy as in the exciton model, open and closed configurations are separately considered by the SMD and SMC calculations. Further beyond single-particle excitations of particle-hole pairs (and their annihilation) there are considered also collective phonon excitations. The corresponding graphes for the first step SMD and SMC interactions are shown on Fig. 8a and 8b, respectively. So far, in the collective excitations only the 2_1^+, 4_1^+

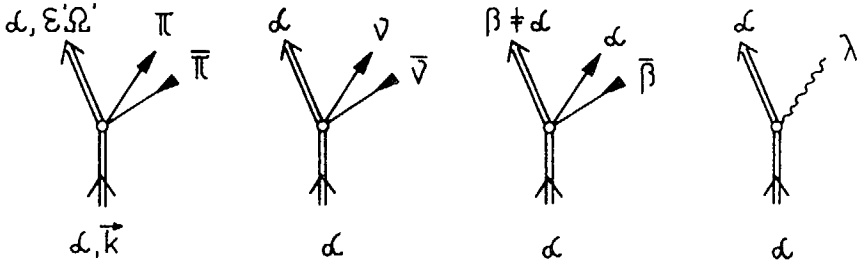

(a) Statistical multistep direct processes including phonon (λ) excitations, creation of particle-hole pairs in the neutron (ν) and proton (π) system and charge exchange reactions ($\beta \neq \alpha$)

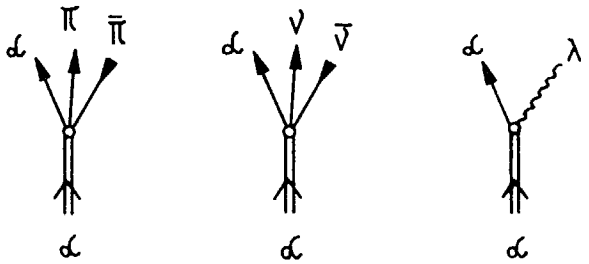

(b) The same for statistical multistep compound interaction

Fig. 8 Modes of first step interaction taken into account in the SMD/SMC-calculation presented in /18/

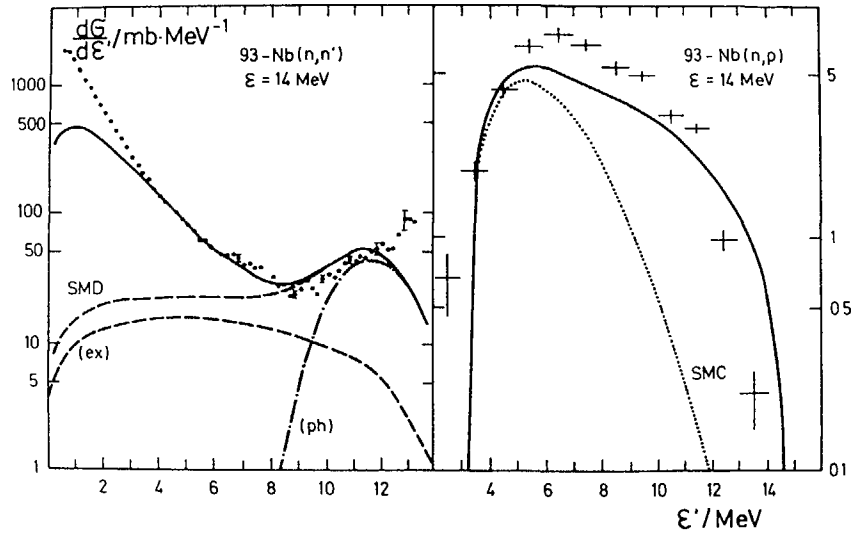

Fig. 9 Primary neutron and proton emission for ^{93}Nb + n at 14 MeV calculated with a new SMD/SMC-approach /17,18/; experimental data from Osaka and Livermore; the curves shown that pre-equilibrium neutron emission is strongly influenced by both particle-hole (ex) and collective (ph) interaction, whereas in the proton emission channel practically no collective excitation occur.

and 3_1^- states in ^{92}Zr core are included. Nevertheless, this new approach allows a reasonable interpretation of the niobium-spectra including the high energy end of them (Fig. 9). Note, that in this approach the pre-equilibrium component in the energy range 2...8 MeV is much lower than predicted in the traditional exciton model (compare pre-equilibrium curves on Figs. 1, and 9). The model presented for the first time allows to combine the time-integrated master equation approach for both pre-equilibrium and equilibrium emission in the frame of a statistical, single-particle description with the phenomenological direct collective interaction in a unique, physically transparent way. In spite of its simplicity, this approach especially will be suitable for nuclear data evaluation purposes.

5. Semi-empirical description of DDNECS for niobium below 30 MeV

In an other contributed paper /19/ to this meeting a method of semi-empirical description of double-differential neutron emission spectra is proposed.

It is shown, that in the case ^{93}Nb + n a simple parametrization of direct collective excitations with a constant (over incident energy) cross section of 200 mb provides a reasonable description of the high energy part of emission spectra in a broad energy range from 5 MeV up to 26 MeV. This method is easily applicable for evaluation of neutron emission spectra. Discrepancies below 14 MeV, shown f.i. on Fig. 4, can be solved in this way, due to the experimentally established fact that pre-equilibrium emission caused by collective direct excitations of vibrational states is almost energy independent (in opposite to this the probability of single-particle direct excitations decreases with decreasing incident energy due to the limitations caused by the Pauli principle).

6. Conclusions

Analyzing secondary neutron emission spectra experimental data selected for comparisons with theory have to be checked carefully. In particular this holds for emission energies below the neutron binding energy, where the ideally occuring line spectra due to the limited energy resolution of spectrometers used are observed as more or less averaged or smoothed neutron spectra. By physical reasons it is necessary to use for comparisons with theoretical models in the high energy range only those experimental spectra, which at least clearly show the structures caused by the strongest vibrational or rotational states. Otherwise, unphysical parametrizations of the statistical single-particle pre-equilibrium models used for comparisons could be the consequence.

Out of the some-what problematic high-energetic part of the spectra, at present there exist several theoretical approaches and computer programmes, which are able to describe experimental neutron emission spectra quite reasonably.

Due to the high contribution of equilibrium emission in the neutron exit channel as well as the problems caused by the mixing of single-particle and collective direct pre-equilibrium processes, it seems very problematic to prove the validity of different pre-equilibrium single-particle models by comparisons with neutron emission spectra at 14 MeV only. In this case the real sensitivity of the check is very low and false conclusions can be drawn easily. It seems much more meaningful to compare theoretical models with experimental data over a broad incidence energy range and for different exit channels, simultaneously. The case ^{93}Nb + n is a very suitable one for this purpose.

A new SMD/SMC-approach presented at this meeting shows, that difficulties discussed over the last years at many conferences concerning the physically consistent description of pre-equilibrium DDNECS might be overcome in a unique, physically transparent way if both single-particle and collective phonon excitations are allowed to occur in the SMD and SMC steps of interactions. In this case the whole neutron emission process including both pre-equilibrium and equilibrium emission caused by single-particle as well as collective interactions, can be predicted in the frame of a single, physically transparent model giving results which are of interest for nuclear data evaluation. No doubt, this approach also presents only a model with certain approximations an limitations, which could be avoided in microscopic approaches at the prize of loosing its simplicity and easy applicability.

REFERENCES

/1/ D. Seeliger et al., 1st Neutron Conf., Kiev, 1971
Proceedings Vol. Im p. 243, Kiev, 1972
D. Hermsdorf et al., J. Nucl. En. 27 (1973) 747;
Kernenergie 19 (1976) 241; ZfK-277(Ü), 1975

/2/ H. Gruppelaar, P. Nagel, NEANDC-204 "U", INDC(NEA)6, 1985

/3/ P.H. Stelson et al., Nucl.Phys. 68 (1965) 97
J. Hohn et al., Nucl.Phys. A134 (1969) 289
B.E. Lechenko et al., Yad.Fiz. 15 (1972) 15

/4/ O.A. Salnikov et al., Yad.Fiz. 122 (1971) 620
/5/ J.L. Kammerdiener, UCRL 51232 (1972)
/6/ A. Takahashi et al., OKTAVIAN-Report A-83-01, 1983, A-87-01, 1987
/7/ T. Elfruth et al., INDC(GDR)-044/GI, 1986, INT(86)-12
/8/ M. Blamm, Nucl.Phys. A213 (1971) 570
/9/ M. Adel-Fawzy et al., Nucl.Phys. A440 (1985) 35
D. Seeliger et al. Nucl.Phys. A460 (1986) 265
/10/ M. Adel-Fawzy et al., EXFOR entry 32001, IAEA
/11/ Simakov et al., Yad.Fiz. 37 (1983) 801
/12/ A. Marcinskowski et al., Nucl.Sci.Eng. 83 (1983) 13
/13/ A. Pavlik, H. Vonach, IRK Vienna, 1987, priv. communication
/14/ S. Mittag et al., contributed paper to this AGM
/15/ T. Tamura et al., Phys.Lett. 66B (1977) 109
I. Kumabe et al., Phys.Lett. 92B (1980) 15
/16/ A.V. Ignatyuk et al., Yad.Konst. 32 (1979) 3
/17/ H. Kalka et al., "Statistical Multistep Direct and Compound Processes below 30 MeV for 93-Niobium" AGM on Nuclear Theory for Applications, Beijing, Oct. 1987, contributed paper
/18/ H. Kalka et al., Zeitschr.f.Phys. A - Atomic Nuclei, 1988, in print
/19/ M. Torjman et al., "A Semi-Empirical Description of Double-Differential Neutron Emission Spectra" AGM on Nuclear Theory for Applications, Beijing, Oct. 1987, contributed paper

MEASUREMENT AND ANALYSIS OF CONTINUOUS SPECTRA FROM INELASTIC NEUTRON SCATTERING ON ^{93}Nb IN THE ENERGY RANGE 7 TO 14 MeV

S. MITTAG, D. SCHMIDT, D. SEELIGER
Technische Universität Dresden,
Dresden, German Democratic Republic

Abstract

Continuous emission spectra from the ^{93}Nb(n,n') reaction were measured at bombarding energies E_o = 7.0, 9.0 and 12.3 MeV. Attention especially was connected with investigation of the high energy spectrum. Including earlier measurement at E_o = 14.6 MeV, a theoretical analysis of angle-integrated spectra as well as angular distributions has been carried out. It could be shown that the single-particle exciton model is not able to explain in the full incident energy range the high-energetic tail of experimental spectra observed, i.e. the pre-equilibrium processes. A further component must be included, which is relevant to collective excitation and which is based on the direct reaction theory.

1. Introduction

Continuous emission spectra from (n,n') reactions have been measured mainly at bombarding energies below 8 MeV and arround 14 MeV /1-7/, reflecting the availability of monoenergetic neutron sources. Using a cyclotron also at E_o = 9 MeV data for some nuclides have been obtained /8/. Recently, an extensive measurement at energies 10 and 12 MeV has

been started at TUNL /9/. But there is still a lack of such data in the energy range between 9 and 14 MeV.

In the present work at bombarding energies E_0 = 7.0, 9.0 and 12.3 MeV emission spectra at different angles from the ^{93}Nb(n,n') reaction have been obtained. Including earlier measurements at E_0 = 14.6 MeV /6/, a description of the experimental data in the full energy range 7.0 ... 14.6 MeV in the framework of existing models is presented. Thus, the aim of this work is to contribute to the discussion carried out at recent Neutron Conferences on the validity and applicability of different theoretical models for the description of continuous neutron spectra.

The low energy spectrum part of the emission spectra varies slightly with bombarding energy and angle only. Here the emission from compound nucleus states dominates and the description within the frame of the complete statistical model is valid. At higher bombarding energies E_0 equilibrium neutron emission from (n,2n), (n,pn) and other many particle reactions has to be taken into account.

In the higher energy region of the emission spectra pre-equilibrium emission is dominant, indicated also by forward-peaking of the angular distributions. (Here and in the following text as "pre-equilibrium processes" all reaction modes are designated, which occur before the statistical equilibrium state of the composite system is reached, independently from the way of theoretical description of these processes.) At E_0 = 14.6 MeV the exciton model is able to describe this pre-equilibrium part quite well. Transition rates and other parameters following from this model have been extracted and the role in mechanism of many particle emission was investigated /10-12/. In sect. 3 the application of the exciton model is extended to lower bombarding energies. An analysis of the angular distributions follows in sect. 4. As result it is evident that the exciton model is not sufficient, especially at excitation energies of the residual nucleus $U \lesssim 3$ MeV.

Further possibilities for the description of continuous pre-equilibrium spectra also arise from recent development of averaged direct reaction models in order to describe angle-integrated continuous spectra as well as angular distributions. In sect. 5 these models are also discussed and compared. It follows the conclusion that direct reaction models are also not able to describe the experimental data at all bombarding energies. A phenomenological superposition of components following from direct and exciton models gives a sufficiently good description of the emission spectra at E_0 = 14.6 MeV. The physical reason for this comes from the specific features of the (n,n') reaction, which shows remarkable contributions from collective enhancement processes, almost independently from incident energy.

Finally, some conclusions are drawn with respect to the applicability of different models for the description of neutron induced reactions.

2. Experimental procedure and results

The experiments had been performed at the 10 MeV tandem accelerator in the ZfK Rossendorf, using a TOF-spectrometer with eight detectors /13/. The detection threshold due to n/γ-discrimination was nearly 1 MeV, further experimental characteristics can be summarized to: flight path about 3 m, over-all time resolution 2.5 ns, distance sample - target 18 cm, size of the cylindrical sample Ø 3.5 x 3.1 cm^2 and sample weight 193.13 g.

As neutron source a deuterium gas target /14/ was employed covering the incident energy range from 6.0 to 12.3 MeV. The source neutrons show an energy spread in order of 160 to 100 keV connected with an intensity near $10^8 s^{-1} sr^{-1}$. Beside the monoenergetic DD-neutrons disturbing neutrons occur due to (d,n) reactions on carbon and oxygen and from the deuteron break-up continuum, which are taken into account. As source strength monitor a small TOF-detector at angle Θ_{LAB} = 20° was used. The detector efficiency curves had been measured experimentally using the well known ^{252}Cf method /15/ which were continued for energies above 6 MeV by Monte Carlo calculations as proposed in ref. /16/. By this method the efficiency error estimated contributes less than 5 % to the total error. The measurements were performed in runs of 1mAs deuteron charge in the target, which were summed later for routing. Simultaneously a ^{12}C sample was measured to get model line parameters for elastic peak separation, the ^{12}C sample was a hollow cylinder with dimensions $diam._{out}$ = 2 cm, $diam._{in}$ = 1 cm, height = 3 cm.

A special problem is the separation of elastic and disturbing neutron lines from continuous spectra. The last could be separated by free fit procedure with sufficient accuracy because of their small magnitude in order of some percents with respect to the inelastic scattering effect. The separation of elastic peaks is investigated in detail concerning model line shape, fit procedure modes and influence of angle-integration and described in detail elsewhere /16/. Fig. 1 illustrates the effect and deviations of different separation modes. It must be stressed here that without a very careful separation of elastic peak from continuous inelastic spectra considerable uncertainties in the high energy part of double

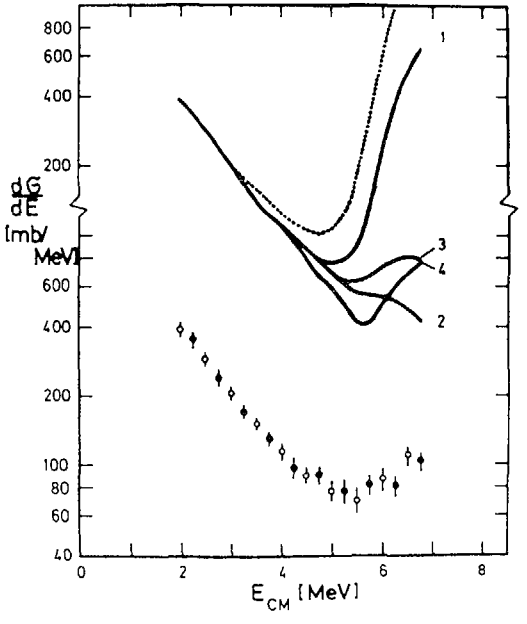

Fig. 1
Different modes of elastic peak separation ($^{93}Nb(n,n')$ reaction, E_o = 7 MeV).
1: without separation, 2 - 4: different modes, see also ref.[16]);
——— integrated from 40° to 160°,
..... 20° to 160°; ϕ this work,
ϕ taken from ref. /48/.

differential cross sections occur, leading to a following unphysical interpretation by comparison with theoretical reaction models.

Experimental results treated in this way are available at the bombarding energies E_o = 7.0, 9.0 and 12.3 MeV. The angle-integrated spectra are shown in fig. 2. Earlier results /6/ obtained at E_o = 14.6 MeV are included into the interpretation in order to have a consistent connection to former analyses. Angular distributions are represented in 1.0 MeV emission energy intervals (see sect. 4), whereby the foreward asymmetry increases with neutron emission energy as well as incident energy E_o as demonstrated in fig. 3. All angle-integration procedures have used a Legendre polynomial fit of third order, the experimental data are numericaly published elsewhere /17/.

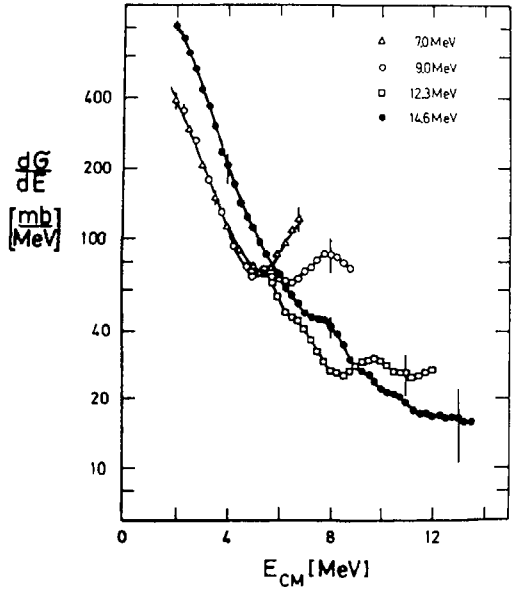

Fig. 2
Angle-integrated spectra from the ^{93}Nb(n,n') reaction; Δ, ○, □ this work, ● taken from ref. /6/.

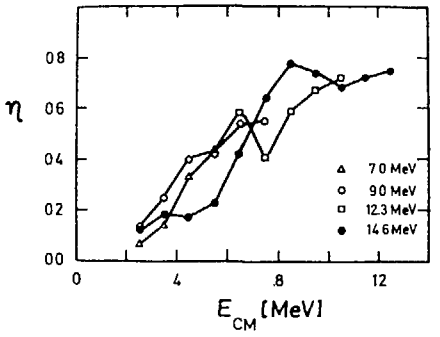

Fig. 3
Asymmetry ratio η versus neutron emission energy (η^{-1} is the ratio of the even Legendre polynomial coefficients sum to the odd one).

3. Analysis of the angle-integrated spectra within the frame of the exciton model

This analysis was performed using the code STAPRE /18/, which contains pre-equilibrium emission (EM), evaporation mechanism from the first compound nucleus (HF) and the evaporation cascade from following compound nuclei (EC):

$$\frac{d\sigma}{dE}(E) = \frac{d\sigma}{dE}(E)^{EM}_{nn'} + \frac{d\sigma}{dE}(E)^{HF}_{nn'} + \frac{d\sigma}{dE}(E)^{EC}_{Mn'}. \qquad (1)$$

The evaporation part is described by a generalized Hauser-Feshbach formalism in the following manner

$$\frac{d\sigma}{dE}(E)^{HF}_{nn'} = \frac{\pi}{k_n^2} \frac{\sum_{l_o s_o} T_{nl_o}(E_o) \sum_{l_1 s_1} T_{n'l_1}(E)}{N(E^*)} \ast$$

$$\ast \; S^{(E_o,E)}_{l_o s_o l_1 s_1} \varrho_{n'}(E, I', \pi') \cdot f \qquad (2)$$

$$\text{with } N(E^*) = \sum_{\nu} \sum_{I'\pi'} \sum_{s\ell} \int_0^{E^* - B_\nu} dE_\nu T_{\nu l}(E_\nu) \varrho_\nu(E^* - B_\nu - E_\nu, I', \pi')$$

$$+ \sum_{I'\pi'} \sum_{\gamma L} \int_0^{E^*} dE_\gamma T_{\gamma_{\gamma L}}(E_\gamma) \varrho_\gamma(E^* - E_\gamma, I', \pi') .$$

The $T_{\nu l}$ and $T_{\gamma xL}$ are the transmission coefficients for particles ν and γ-quanta with multipole type xL, respectively, the factor $S^{(E,E')}_{l_o s_o l_1 s_1}$ is the well known Moldauer's width fluctuation correction. The $T_{\nu l}$ are averaged according to

$$T_{\nu l} = (2l + 1)^{-1} \left[(l + 1) T^{\nu}_{l, l+\frac{1}{2}} + l T^{\nu}_{l, l-\frac{1}{2}} \right] . \qquad (3)$$

The level density for particles ν is estimated to be independent on parity

$$\varrho_\nu(E, I, \pi) = \frac{1}{2} \varrho_\nu(E, I) \qquad (4)$$

and is taken from the back-shifted Fermigas model according to

$$\varrho_\nu(E,I) = w_\nu(E,I) - w_\nu(E,I+1) \qquad \text{with}$$

$$w_\nu(E,I) = \frac{\exp\left[2\sqrt{a(E - \quad - h^2 I^2/2\Theta_{eff})}\right]}{12\sqrt{2\Theta_{eff}/h^2}\,(\sqrt{a}\ t)^3} \qquad (5)$$

$$E - \Delta = at^2 - \frac{3}{2}t + h^2 I^2/2\Theta_{eff}$$

whereby Θ_{eff} is an effective momentum of inertia. The reducing factor f in eq.(2) takes into account that the compound nucleus formation probability is reduced by particle emission from pre-compound states:

$$f = 1 - \sum_{k=o}^{K} b^{(k)}(n) \frac{\lambda^e(n)}{\lambda(n)} \qquad (6)$$

see also eq.(9) and deviates from unity in order of 10 percents or less.

Formula (4) is replaced by

$$\varrho(E, I, \pi) = \sum_i \delta(E - E_i)\, \delta_{II_i}\, \delta_{\pi\pi_i} \qquad (7)$$

if isolated levels with known spin I_i and parity π_i have to be taken into account. In our case this is not essential because of the small compound cross sections at low residual excitation energies ($U \leq 1.5$ MeV).

The optical parameters were taken from ref. /19/, which give a better agreement to the experimental data than the parameter set from ref. /20/. The level density parameters are taken from ref. /21/.

The equilibration process of the composite system is treated in the framework of the exciton model /22-24/. In the code STAPRE the following expressions are used:

$$\frac{d\sigma}{dE}(E_n,)^{EM}_{nn'} = \sigma_n^{abs} \sum_{k=o}^{K} \sum_n b^{(k)}(n) \frac{\lambda^e_{n'}(n, E_{n'},)}{\lambda(n)} \qquad (8)$$

$b^{(k)}(n)$ is the population probability of n-exciton states resulting from k internal transitions given by

$$b^{(k+1)}(n) = b^{(k)}(n+2)\frac{\lambda_-(n+2)}{\lambda(n+2)} + b^{(k)}(n)\frac{\lambda_o(n)}{\lambda(n)} + b^{(k)}(n-2)\frac{\lambda_+(n-2)}{\lambda(n-2)} \qquad (9)$$

$$b^{(o)}(n=p+h) = \delta_{pp_o}\delta_{hh_o}$$

with

$$\lambda_+(n) = 2\pi \langle|M|^2\rangle\, g(gE^* - C_{p+1,\ h+1})^2/\hbar(p+h+1)$$
$$\lambda_-(n) = 2\pi \langle|M|^2\rangle\, gph(p+h-2)/\hbar$$
$$\lambda_o(n) = 2\pi \langle|M|^2\rangle\, g(gE^* - C_{p,h})(p+h-1)/\hbar \qquad (10)$$
$$\lambda(n) = \lambda_+(n) + \lambda_-(n) + \lambda_o(n) + \lambda^e(n)$$
$$\lambda^e(n) = \sum_\nu \int dE_\nu \lambda^e_\nu(n, E_\nu)$$
$$C_{p,h} = \frac{1}{2}(p^2 + h^2) \qquad \text{and} \qquad g = \frac{6}{\pi^2} a .$$

"a" is the same level density parameter as in eq. (5), whereby

$\lambda_\nu^e(n,E_\nu)$ is the emission rate for the particle ν given by

$$\lambda_\nu^e(n,E_\nu) = \frac{2s_\nu+1}{\pi^2\hbar^3}\,\mu_\nu E_\nu\,\sigma_\nu^{inv}(E_\nu)\left(\frac{Z}{A}\right)^{z_\nu}\left(1-\frac{Z}{A}\right)^{p_\nu-z_\nu} \ast \ast \binom{p_\nu}{z_\nu} \frac{w(p-p_\nu,h,E^\ast-B_\nu-E_\nu)}{w(p,h,E^\ast)} \qquad (11)$$

with the density formula according to ref. /25/

$$w(p,h,E) = g(gE - A_{p,h})^{p+h-1}/p!h!(p+h-1)!$$
$$A_{p,h} = \tfrac{1}{4}(p^2+h^2+p-3h) \qquad (12)$$

$E^\ast$ is the excitation energy of the composite system $E^\ast = E_o + B_n$. The matrix element $\langle|M|^2\rangle$ of internal transitions giving the strength of the residual interaction is chosen to be energy-dependent

$$\langle|M^2\rangle = FM\cdot E^{-1}\cdot A^{-3} \quad ; \quad FM = \text{const.} \qquad (13)$$

but it doesn't depend on the exciton number as proposed in ref. /26/. This fact is not essential if the neutron emission from the n=3 state dominates as in the case represented here. The absolute height of the pre-equilibrium emission spectrum depends mainly on the choice of the quantity FM. The value FM = 87 MeV^3 is found to give the best fit to the E_o = 14.6 MeV data. A comparison with values obtained by other authors (for instance ref. /27/) is not simply possible, because according to eqs.(8)-(12) other quantities have also influence on the spectrum normalization: the cross section σ_n^{abs}, $\sigma^{inv}(E)$ depending on optical parameters used, the level density "a" forming the level spacing g and other pecularities formulated concretely in the used code. Usually in other pre-equilibrium calculations, the single-particle density g is taken from the Fermigas model g = A/13 due to the much broader distribution of the first particle and hole states arround the Fermi energy in comparison with their distribution within the equilibrium compound state. Therefore, the comparatively small value of FM used here for the absolute calculations is not really in contradiction with higher values reported in other exciton model calculations.

The comparison of these calculations with the experimental data is shown in fig. 4. It can be seen that for excitation energies of the residual nucleus U $\leq$ 3 MeV the experimental data cannot be described by this formalism. The relative difference between theory and experiment increases with de-

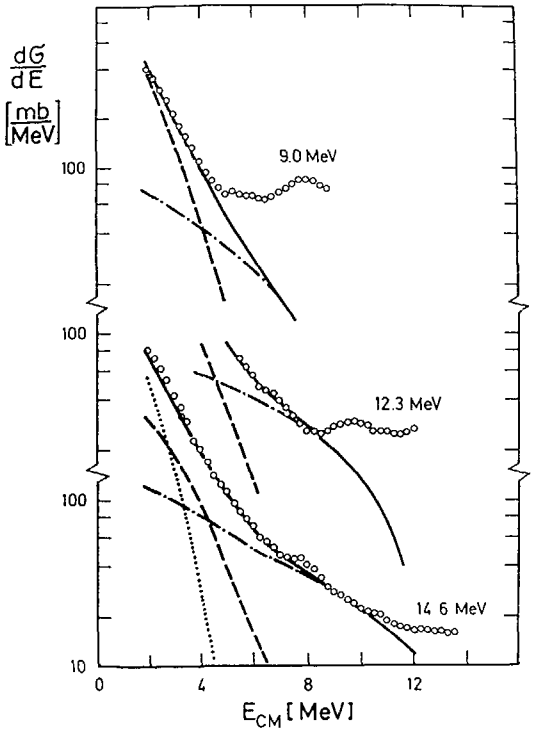

Fig.4 Description of the emission spectra in the frame of the exciton model at different incidence energy
– – – – HF-contribution
– · – · pre-equilibrium part
..... secondary neutrons
——— sum of all contribut.

creasing of the bombarding energy. By a reasonable variation of the $\langle |M|^2 \rangle$ energy dependence this difference cannot remarkably reduced as demonstrated in fig. 5 for the lowest bombarding energies. Here it should be noted that these results are related to the exact elastic peak separation: earlier measured spectra with free peak separation fit we could describe quite well within this model assuming an energy dependence of the matrix element $\langle |M|^2 \rangle \sim (E^*)^{0.8}$. But the reason for this was, that shape as well as absolute magnitude of the inelastic neutron spectra were changed (smoothed and reduced) by the elastic peak separation with free fit procedure. But such result following from insufficient experimental data represents a failure and is not proper for further discussion. Similar aspects are valid also for evaluation of earlier results from ref. /28,29/, where an energy independence of $\langle |M|^2 \rangle$ was derived from inconsistent experimental data.

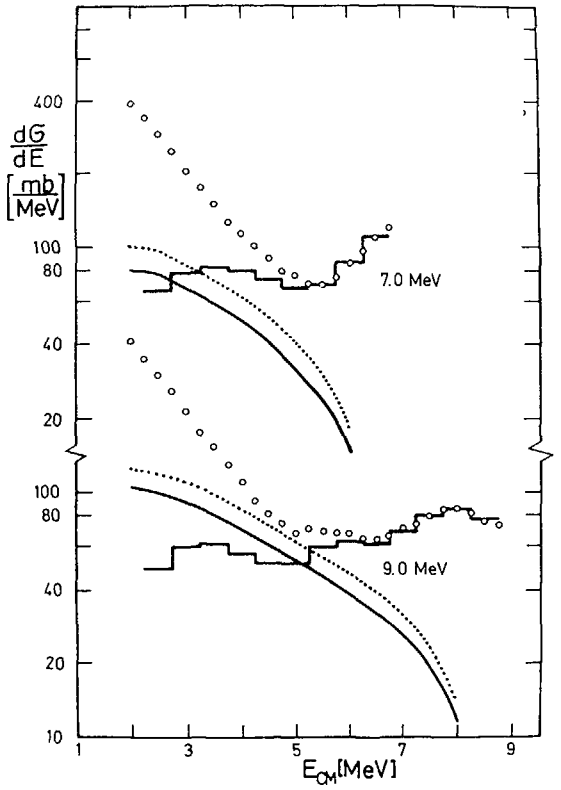

Fig.5 Comparison of the experimental pre-equiliorium spectrum part with the calculated exciton model predictions: step function - experimental spectra with HF- contribution subtracted; dotted and full curves - exciton model predictions within reasonable variation of parameters

4. Description of angular distributions with the generalized exciton model

For description of angular distributions from continuous neutron emission, different models have been developed as overviewed in refs. /30-33/. In the present work the application of the statistical generalized exciton model /34,35/ to bombarding energies lower than 14 MeV is investigated. But we can expect the validity of this model only for such emission energies, where the angle-integrated spectra are described quite well by the exciton model. The calculations base on the following formalism.

Beside the total energy E (sum of bombarding energy E_o, binding one of incident particle B_i and Fermi energy E_F), also

the total linear momentum $\underline{p}$ is taken into consideration, forming the partition function $Z_{p,h}$

$$Z_{p,h}(\beta,\vec{v}_o) = \sum_k \exp\left[-\beta(E_k - \vec{v}_o\vec{p}_k)\right] , \qquad (14)$$

β means the inverse temperature and $\underline{v}_o$ the mean velocity of the exciton gas, the sum is over all particle-hole states contributing to the given energy E and linear momentum $\underline{P}$:

$$E = \sum_i E_i^{(p)} + \sum_i E_i^{(h)} , \quad \vec{P} = \sum_i \vec{p}_i^{(p)} + \sum_i \vec{p}_i^{(h)} . \qquad (15)$$

Usually, the single-particle (single-hole) energies $E^{(p)}$ ($E^{(h)}$) and momenta $\vec{p}^{(p)}$ ($\vec{p}^{(h)}$) are counted as positive (negative) from the center of the Fermi sphere with Fermi energy $E_F = p_F^2/2\,m$. Following standard procedures the level density is than given to

$$\varrho_{p,h}(E,\vec{P}) = \frac{1}{(2i\pi)^4} \int_{-\infty}^{+\infty}\int d\beta d(\beta\vec{v}_o) e^{\beta(E - \vec{v}_o\vec{P})} Z_{p,h}(\beta,\vec{v}_o) \qquad (16)$$

which can be solved by the saddle-point approximation. The linear momentum can be separated into two perpendicular components $\vec{p} = \vec{p}_\parallel + \vec{p}_\perp$ with $\vec{p}_\parallel \vec{v}_o = p\,v_o$, $\vec{p}_\perp \vec{v}_o = 0$. (17)

Before particle emission, these components have the values $p_\parallel^{(o)} = \sqrt{2mE}$, $p_\perp^{(o)} = 0$, but after particle emission under the angle θ with energy E' $p_\parallel = \sqrt{2mE} - \sqrt{2m(E_F + E' + B_f)}\cos\theta$ and $p_\perp = \sqrt{2m(E_F + E' + B_f)}\sin\theta$, giving level densities $\varrho_{p,h}(E,p_\parallel,p_\perp)$.

Following this formalism the code RONEP /34/ is written to calculate relative angular distributions including some simplifications according to

$$\frac{d^2\sigma}{d\Omega dE}(E',\theta) \sim \frac{2\mu}{\pi^2\hbar^3} E'\,\sigma^{inv}(E') \sum_{\substack{n=n_o \\ \Delta n=2}}^{\bar{n}} \frac{\varrho_{p-1,h}(E-E_F-E'-B_f,p_\parallel,p_\perp)}{\varrho_{p,h}(E,p_\parallel^{(o)},p_\perp^{(o)})}$$

$$\bar{n} = \sqrt{2g_o(E-E_F)} . \qquad (18)$$

This code has been refined by introduction of the n-exciton life time τ_n according to

$$\tau_n(E) = \left[\lambda_n^+(E)\right]^{-1} \prod_{n'=n_o}^{\bar{n}} \left[1/(1 + \Gamma_{n'}(E)/\lambda_{n'}^+(E))\right]$$

$$\lambda_n^+(E) = (\pi/\hbar)\,\langle|M|^2\rangle\,\frac{g(gE)^2}{n+1} , \quad \langle|M|^2\rangle = FM'\cdot A^{-3}MeV^2$$

$$g = A/13, \quad \Gamma_n(E) = \frac{2s+1}{\pi^2\hbar^3}\mu_n\beta_n(\pi r_o^2 A^{2/3})\,\frac{(n+1)}{2n}\,\frac{E_o}{g}\,(\frac{E_o}{E})^{n-1} \qquad (19)$$

$$\frac{d^2\sigma}{d\Omega\,dE}(E',\theta)_{nn'} = \sigma_n^{abs} \sum_{\substack{k=k_o \\ \Delta k=2}}^{\bar{k}} \tau_k(E-E_F)\frac{2s_{n'}+1}{\pi^2\hbar^3}\,\mu_{n'}\beta_{n'}E'\sigma^{inv}(E') \cdot$$

$$\cdot \frac{\varrho_{k-1}(E-E_F-E'-B_f,p_\parallel,p_\perp)}{4\pi\cdot\varrho_k(E,p_\parallel^{(o)},p_\perp^{(o)})}$$

in order to obtain normalized angular distributions similar to the STAPRE code formalism.

In comparison to eqs.(8)-(12), the formalism here is restricted to λ^+-transitions which contribute the main part to the emission spectra. Furthermore, the correction due to Pauli's principle is neglected because this effect is in our case in order of some percents. These and other different formulations in the code used here, i.e. the formalism as outlined

above, lead to small deviations in the spectrum shape shown in fig. 6. The normalization had been carried out also to the integral E_o = 14.6 MeV data resulting the constant FM' = 23.9. In order to simulate the $\langle|M|^2\rangle \sim E^{-1}$ dependence, for lower bombarding energies E_o = 12.3 and 9.0 MeV the constants FM' = 26.7 and 32.2. had been chosen, respectively.

The calculations of angular distributions were carried out in 1 MeV bins and compared with the experimental results in figs. 7 and 8. The energy bins drawn correspond to these parts of the spectra where the exciton model (and evaporation part) are able to describe the integral spectra. The evaporation part is assumed in all cases to be isotropic. It can be seen that this model is able to describe all data quite well, although the statistical suppositions are not well fulfilled. An other model for the description of angle-dependent neutron emission from pre-equilibrium states is obtained by introduction of free nucleon-nucleon scattering /31,32,36/.

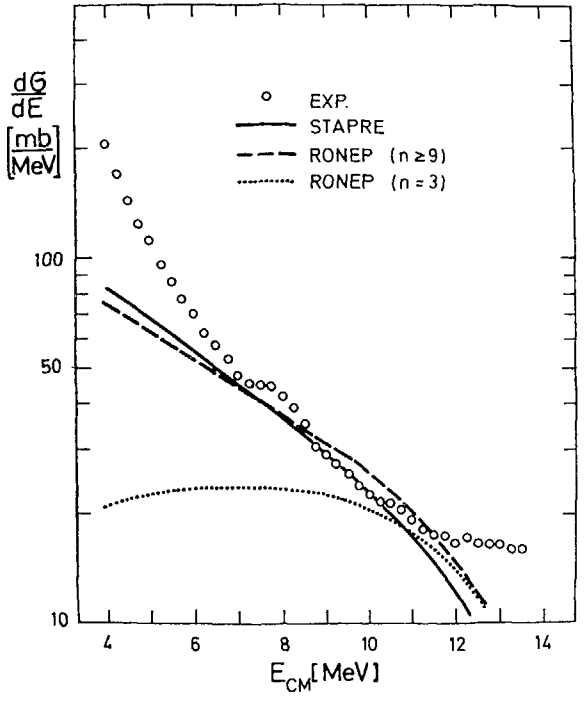

Fig. 6 Comparison of the integral spectra at E_o = 14.6 MeV with calculations from the codes STAPRE and RONEP

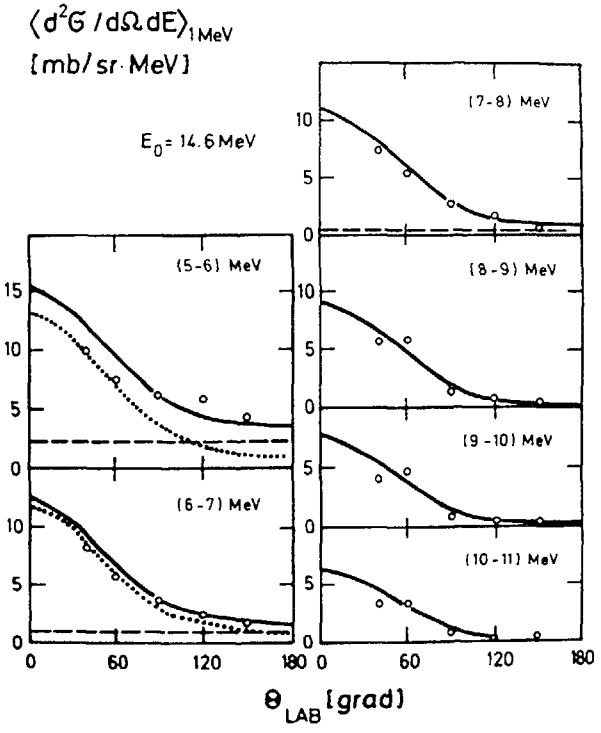

Fig. 7
Angular distributions from the ^{93}Nb(n,n') reaction (o) in comparison with calculations in the frame of the generalized exciton model (- - - isotropically assumed HF-part, ... generalized exciton model, ——— sum).

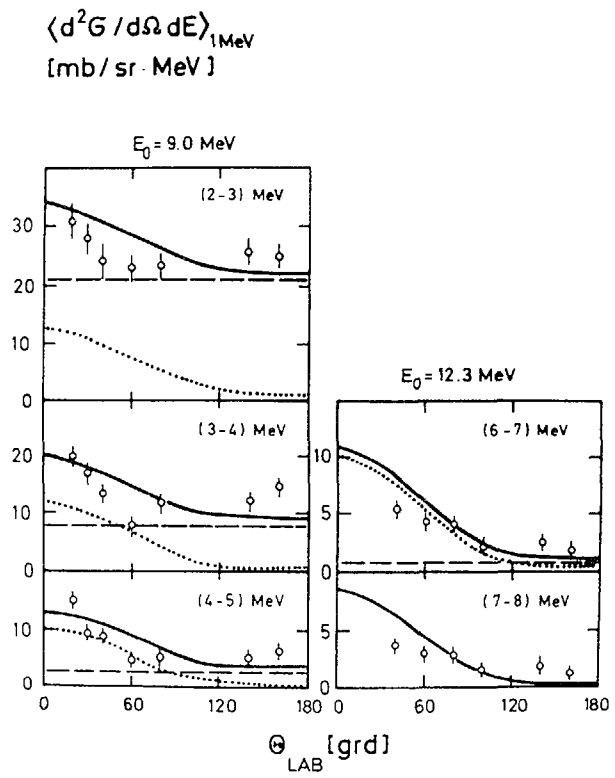

Fig. 8
As fig. 7, but for incident energies E_o = 9.0 and 12.3 MeV, respectively.

This formulation is relevant to the generalized exciton model referred above and gives similar results. This point has been checked by comparison of the foreward-backward angle asymmetry ratio $\sigma(0^o)/\sigma(180^o)$ calculated at E_o = 14.6 MeV which shows almost the same results.

5. Direct reaction models for description of continuous spectra

Direct reaction models take into consideration only excitation of pre-equilibrium states with relatively simple configurations. Such formalism has been widely used to explain angular distributions from low-lying excited states. The simplest approximation is the DWBA containing the transition matrix element for internal excitation of the nucleus:

$$\frac{d\sigma^{DWBA}}{d\Omega} = \left(\frac{\mu}{2\pi\hbar^2}\right)^2 \frac{k_f}{k_i} \sum_{if} \left| \int dV \chi_f^{(-)*} \langle \phi_f | V_{eff} | \phi_i \rangle \chi_i^{(+)} \right|^2 \quad (20)$$

In this notation the $\chi^{(+)}_{i/f}$ describe the particle motion in the input/output channels. The obtained results strongly depend on the type of effective interaction V_{eff} following from the structure model used. For low-lying isolated levels the collective model can be applied in connection with following averaging over the experimental energy resolution, as demonstrated at bombarding energies below E_o = 9 MeV for the ^{113}In(n,n') reaction /37/ and for the ^{93}Nb(n,n') one /38/ also. For ^{93}Nb the weak coupling model should be valid approxemately: in a structure calculation based on single-particle coupling to the ^{92}Zr core (one and two phonon states) nearly 80 % of the wave function is given by weak coupling of the $g_{9/2^+}$ proton /39/. This model could be taken for the excitation energy region up to ~3 MeV, where spectroscopic characteristics as well as the collective nature and deformation parameters are well known for the low-lying excited states, i.e. for bombarding energies below ~8 MeV. Therefore, an application in the full energy range investigated here is not possible.

A further possibility for a structure model is the introduction of the shell model in order to extend the excitation energy range which can be taken into consideration. This pro-

cedure was demonstrated in refs. /40,41/, where pure 1p1h-excitation was classified into spin, parity and excitation energy bins, respectively:

$$\langle \phi_f | V_{eff} | \phi_i \rangle = \langle (j_1^{-1} j_1')_{I\pi} | v | g.s. \rangle \; ; \qquad (21)$$

j_1 represents an occupied orbit within an averaged shell model creating a hole in the orbit j_1'. The transition strength v is adjusted on low-lying 2^+ levels in even-even nuclei. Fig. 9 shows the result for the bombarding energy E_0 = 14 MeV. Shape and magnitude of the integral spectrum are similar to the n=3-component following from the exciton model. This result

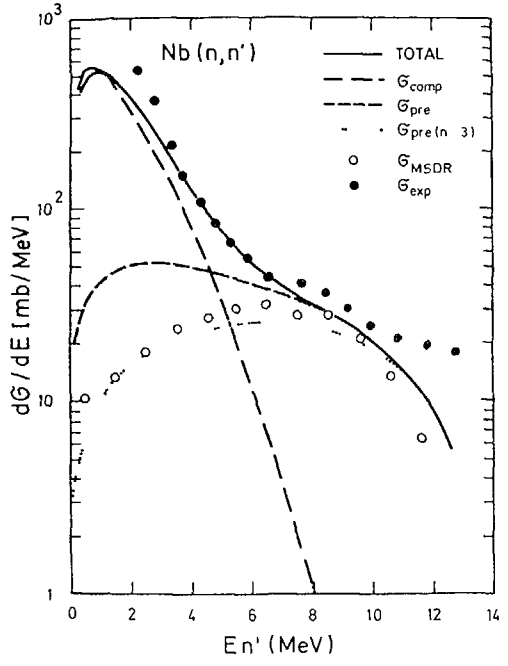

Fig.9 Comparison between experimental emission spectrum at 14.6MeV and theoretical calculations with the direct 1p1h-DWBA theory (open circles) and the usual exciton model (dashed and dotted curves)

demonstrates in a direct way, that the direct reaction model formalism is not in contradiction to the exciton model. But the foreward-backward ratio in the angular distributions calculated is essentially smaller than those following from the generalized exciton model. Nevertheless, this model cannot take into account collective effects and is also not able to overcome the discrepancies shown in sect. 3.

For this purpose we have to choose a structure model which contains beside uncorrelated 1p1h-excitation also collective transition strength. This can be achieved by introduction of long-ranging QQ-forces into the Hamiltonian to simulate the coherence of singel-particle excitation /42,43/. In this way the form factor is replaced by transition density $\varrho_L(r,U)$ depending on multipole order L and excitation energy U:

$$\langle \phi_f | V_{eff} | \phi_i \rangle = \int dV' v_L(r,r') \varrho_L(r',U) \; , \qquad (22)$$

$v_L(r,r')$ denotes the multipole component of the effective interaction between incoming particle and the nucleus. Such procedure has been undertaken to describe multipole giant resonances, i.e. collective effects at high excitation energy /44,45/. Thus, the excitation strength spectrum can be obtained for uncorrelated single-particle excitation as well as collective interaction.

The result of such calculation at E_0 = 14 MeV is shown in fig. 10. A typical property of a spectrum following from this model is a decreasing at higher excitation energy. The evaporation spectrum is drastically enhanced in fig. 10 in order to describe the full spectrum by these two components. But this enhancement is not consistent whith calculations at lower

bombarding energies. As seen in fig. 10, at emission energy $E_{n'}$ = 6 MeV the emission spectrum is explained completely by evaporation mechanism. But in contradiction to this fig. 7 shows for that energy region a typical foreward peaking in the angular distributions. That is in agreement with fig. 4, where the evaporation part at $E_{n'}$ = 6 MeV describes only ~30 % of the experimental spectrum.

That means, in the energy range of emitted neutrons $E_{n'}$ ≈6.. ..12 MeV this direct reaction model cannot describe the emission spectrum sufficiently. That is mainly due to the absence of pre-equilibrium states with more complicated configurations as estimated for instance in the exciton model.

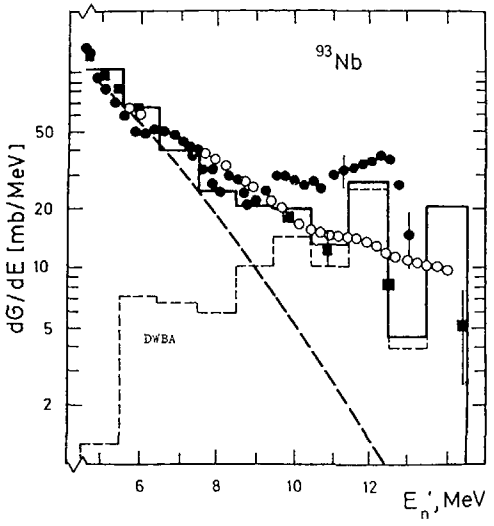

Fig.1o Comparison between experimental neutron emission spectra at 14 MeV and theoretical predictions using DWBA approximation with a microscopic structure model plus enhanced equilibrium emission; ■ -data from Obninsk, o - data from Dresden, • - data from Livermore

Similar conclusions were found in ref. /46/ in the case of the $^{40}Ca(n,n')$ reaction at E_o = 14 MeV using a more simple reaction model containing also collective and singe-particle excitation.

6. Conclusions

At higher bombarding energies the uncorrelated 1p1h-excitation dominates and the exciton model is able to describe the main part of pre-equilibrium emission in continuous neutron spectra. For the (n,n') reaction at lower excitation energies the collective excitation of low-lying states is dominant. That leads to discrepancies between exciton model predictions and experimental spectra at low excitation energy up to U ≈ 3.. ..4 MeV. This spectrum part can be described quite well in the frame of the collective model (DWBA or coupled channels representation) if the spectroscopic characteristics and the deformation nature of the levels are known. In general, that is the case mostly for excitation energies of some MeV.

The semi-microscopic model /42/ cannot give a remarkable refinement at present time because the basis of the single-particle states is limited. Thus, the single-particle excitation at higher excitation energies is underestimated. Furthermore, the spectral distribution of the deformation parameters with higher multipolarity L = 4 depends strongly on the single-particle spectrum included. For realistic calculations a renormalization using experimental informations is necessary. But than the direct use of the collective model has to be preferred.

It is completely clear that at bombarding energies above 10 MeV both components: single-particle excitation following from the exciton model and direct excitation must to be taken into account for description of continuous neutron emission spectra. Such superposition of both components can be carried out as proposed in ref. /47/. However, doing this one must take into account that the semi-microscopic model partially also contains single-particle excitation, making a phenomenological superposition of components from both reaction models questionable. This is the reason why the superposition of components following from the exciton and collective model seems to give a more consistent description in comparison with the procedure mentioned above.

The investigation of this question in detail is of high interest, especially in a wide range of bombarding energy. But trying this, the question of exact determination of the experimental high energy spectrum part is important. Because of the magnitude of the elastic scattering especially at foreward angles this requires measurements with very high experimental energy resolution.

ACKNOWLEDGEMENTS

The authors thank Dr.W.Pilz for help at measurement and data reduction and Dr.D.Hermsdorf for prepa ring of some computer codes and similar problems. Fruitful discussions with Prof.A.V. Ignatyuk, Prof.R. Reif and Dr.P. Mädler are gratefully acknoledged.

REFERENCES

/ 1/ Coles, R.E. and Porter, D., Aldermaston AWRE-089/70 (1970)

/ 2/ Thomson, D.E., Phys. Rev. 129, 1649 (1963)

/ 3/ Lovchikova, G.N., Kotelnikova, G.V., Salnikov, O.A., Simakov, S.P., Trufanov, A.M. and Fetisov, N.I., Yad. Konst. 33, 71 (1979)

/ 4/ Simakov, S.P., Lovchikova, G.N., Salnikov, O.A., Trufanov, A.M., Pilz, W., Förtsch, H., and Streil, T., Yad. Konst. 39, 7 (1980)

/ 5/ Hopkins, J.C. and Drake, D.M., Nucl.Sci.Eng. 36, 275 (1969)

/ 6/ Hermsdorf, D., Meister, A., Sassonoff, S., Seeliger, D., Seidel, K. and Shahin, F., EXFOR 30397

/ 7/ Vonach, H., Chalupka, A., Wenniger, F. and Staffel, G., Brookhaven National Laboratory BNL-NCS-51245, 343 (1980)

/ 8/ Biryukov, N.S., Zhuravlev, B.V., Kornilov, N.V., Plyaskin, V.I., Rudenko, A.P., Salnikov, O.A. and Trykova, N.V., Yad. Fiz. 19, 1190 (1974)

/ 9/ Walter, R.L. and Gould, C.R., Brookhaven National Laboratory BNL-NCS-51245, 259 (1980)

/10/ Meister, A., Seeliger, D. and Seidel, K., Zentralinstitut für Kernforschung Rossendorf ZfK-324, 32 (1976)

/11/ Hermsdorf, D., Sassonoff, S., Seeliger, D. and Seidel, K., Proc.Int.Conf. on Nuclear Physics, Munich, 1973, J.de Boer and H.J.Mang (North Holland Publishing Company) p. 514

/12/ Seidel, K., Seeliger, D. and Meister, A., preprint TU-Inform. 05-09-74, Technische Universität Dresden (1974)

/13/ Eckstein, P., Helfer, H., Kätzmer, D., Kayser, J., Krause, R., Lehmann, D., Meiling, W., Pilz, W., Rumpf, J., Schmidt, D., Seeliger, D., and Streil, T., Nucl.Instr. Methods 169, 533 (1980)

/14/ Mittag, S., Pilz, W., Schmidt, D., Seeliger, D. and Streil, T., Kernenergie 22, 237 (1979)

/15/ Adel-Fawzy, M., Förtsch, H., Mittag, S., Pilz, W., Schmidt, D., Seeliger, D. and Streil, T., Kernenergie 24, 107 (1981)

/16/ Schmidt, D. and Seeliger, D., report INDC(GDR)-18/L, IAEA (1982)

/17/ Adel-Fawzy, M., Förtsch, H., Mittag, S., Schmidt, D., Seeliger, D. and Streil, T., EXFOR 32001

/18/ Uhl, M. and Strohmaier, B., Institut für Radiumstrahlung und Kernforschung Vienna IRK-76/01 (1976)

/19/ Becchetti, F.D. and Greenlees, G.W., Phys.Rev. 182, 1190 (1969)

/20/ Holmqvist, B. and Wiedling, T., Nucl.Phys. A 188, 24 (1972)

/21/ Dilg, W., Schantl, W., Vonach, H. and Uhl, M., Nucl.Phys. A 217, 269 (1973)

/22/ Griffin, J.J., Phys.Lett. 17, 478 (1966)

/23/ Cline, C.K. and Blann, M., Nucl.Phys. A 172, 225 (1971)

/24/ Braga-Marcazzan, G.M., Gadioli-Erba, E., Milazzo-Colli, L. and Sona, P.G., Phys. Rev. C 6, 1398 (1972)

/25/ Williams Jr., F.C., Nucl.Phys. A 166, 231 (1971)

/26/ Kalbach, C., Z.Physik A 287, 319 (1978)

/27/ Holub, E. and Cindro, N., Proc.II.Int.Conf. on Neutron Induced Reactions, Smolenice, 1979, I.Ribansky and E. Betak (VEDA Publishing House of the Slovak Academy of Sciences) p. 133

/28/ Biryukov, N.S., Zhuravlev, B.V., Kornilov, N.V., Plyaskin, V.I., Salnikov, O.A. and Trykova, V.I., Yad.Fiz. 19, 1201 (1974)

/29/ Plyaskin, V.I. and Trykova, V.I., Yad.Konst. 21, 49 (1976)

/30/ Seeliger, D. and Sassonoff, S., ECHAYA 11, 967 (1980)

/31/ Akkermans, J.M. and Gruppelaar, H., Z.Physik A 300, 345 (1981)

/32/ Akkermans, J.M., Z.Physik A 315, 83 (1983)

/33/ Chatterjee, A. and Gupta, S.K., Z.Physik A 313, 93 (1983)

/34/ Mädler, P. and Reif, R., Nucl.Phys. A 337, 445 (1980)

/35/ Mädler, P. and Reif, R., Nucl.Phys. A 373, 27 (1982)

/36/ Akkermans, J.M. and Gruppelaar, H., Stichting Energie-onderzoek Centrum Nederland ECN-60, Petten (1979)

/37/ Lovchikova, G.N., Ignatyuk, A.V., Lunev, V.P., Simakov, S.P. and Trufanov, A.M., Yad.Fiz. 36, 6 (1982)

/38/ Simakov, S.P., Lovchikova, G.N., Lunev, V.P., Salnikov, O.A. and Titarenko, N.N., Yad.Fiz. 37, 801 (1983)

/39/ Van Heerden, I.J., Mc Murray, W.R. and Saayman, R., Z.Physik 260, 9 (1973)

/40/ Tamura, T., Udagawa, T., Feng, D.H. and Kan, K.-K., Phys.Lett. 66 B, 109 (1977)

/41/ Kumabe, I., Fukuda, K. and Matoba, M., Phys.Lett. 92 B, 15 (1980)

/42/ Ignatyuk, A.V., Lunev, V.P. and Pronyaev, V.G., Yad. Konst. 32, 3 (1979)

/43/ Ignatyuk, A.V., Proc.II.Int.Conf. on Neutron Induced Reactions, Smolenice, 1979, I. Ribansky and E. Betak (VEDA Publishing House of the Slovak Academy of Sciences) p. 245

/44/ Bertsch, G.F. and Tsai, S.F., Phys.Reports 18 C, 125 (1975)

/45/ Liu, K.F. and Brown, G.E., Nucl.Phys. A 265, 385 (1976)

/46/ Reif, R., Kernenergie 20, 177 (1977)

/47/ Schmidt, D. and Seeliger, D., Proc. III. Int.Conf. on Neutron Induced Reactions, Smolenice, 1982, P.Oblozinsky (Institute of Physics, EPRC, Slovak Academy of Sciences) p. 115

/48/ Simakov, S.P., FEI Obninsk, private communication

A SEMI-EMPIRICAL DESCRIPTION OF DOUBLE-DIFFERENTIAL NEUTRON EMISSION SPECTRA

M. TORJMAN, H. KALKA, D. HERMSDORF,
D. SEELIGER
Technische Universität Dresden,
Dresden, German Democratic Republic

Abstract

A simple procedure of semi-empirical parametrization of the direct contributions in double-differential neutron emission cross sections is proposed. For the case ^{93}Nb + n in the broad incidence energy range from 5 MeV to 26 MeV this model is proved. In addition to spectra calculations with the exciton model it provides a satisfactory description of the experimental behaviour in the full neutron incidence and emission energy range including angular distributions.

1. Introduction

The knowledge of accurate double-differential neutron emission cross sections in the whole incidence energy range up to 20 MeV is of crucial interest for fusion reactor blanket and shielding calculations /1/. Theoretical predictions are needed, especially, to fill the gap of missing experimental data on double-differential neutron emission cross sections in the incidence energy range between 7 MeV and 14 MeV. One of the few cases, for which experimental double-differential neutron emission cross sections are available in the whole energy range, is ^{93}Nb + n.

Therefore, this case is a very suitable one for testing the applicability of different models and computer programmes along the energy scale /2,3/. In this way, the most suitable theoretical approaches could be selected for the calculation of the main body of missing information on double-differential neutron emission cross sections. The present paper is one attempt in this direction mainly aiming a simple theoretical description of the highest part of emission spectra suitable for data evaluation.

2. Exciton Model Calculations

During the last 20 years the exciton model and its later modifications was widely and succesfully used for calculations of neutron emission spectra /4-7/.
However, this simple statistical multistep reaction model does not describe single-step direct excitations of non-collective and especially of collective modes which are responsible for the highest part of experimental neutron emission spectra. (It is well-known for many years, that the direct collective excitation of low-lying states by inelastic scattering of neutrons occurs with high probability.)

An empirical ansatz for the average description of the direct part (DI) in the double-differential neutron emission cross sections is presented in sec. 3 which has to be added to the emission spectra calculated by the exciton model (EM), where the assumption is made, that the anisotropy of angular distributions is due to the direct excitation only:

$$\frac{d^2\sigma(\varepsilon)}{d\varepsilon' d\Omega} = \frac{1}{4\pi}\left[\frac{d\sigma^{EM}(\varepsilon)}{d\varepsilon'} + \frac{d\sigma^{DI}(\varepsilon)}{d\varepsilon'}\sum_L (2L+1)\, a_L(\varepsilon') P_L(\cos\theta)\right] \qquad (1)$$

The expansion coefficients $a_L(\varepsilon')$ are taken from the Kalbach-Mann systematics /8/.

The emission spectrum of the exciton model

$$\frac{d\sigma^{EM}(\varepsilon)}{d\varepsilon'} = \sigma_{abs}(\varepsilon)\sum_{n=3}^{\bar{n}} \tau_n W_n(\varepsilon') \qquad (2)$$

is calculated without free fitting parameters by means of the code AMAPRE /9/. The life-time τ_n is taken from (up to $t = \infty$) time integrated master equations including in this way also the compound nucleus neutron emission. For the emission rates $W_n(\varepsilon')$ from n-exciton states the well-known formula basing on the detailed balance principle is used. The transition rates λ_n^+ and λ_n^- which occur in the master equation are calculated by the Golden Rule using final state densities of Oblozinsky et al. /10/.

The mean square matrix element is estimated from the imaginary part of the optical model.

Nuclear structure influence (shell and pairing effects) on the exciton state density are taken into account following /11,12/. Further details of our exciton model calculations are reported elsewhere /9,13/.

As yet, calculations with the code AMAPRE do not include the emission of secondary neutrons. However, for investigations of the high-energy part of the spectra this is not necessary. The results of this calculations are shown by dotted lines in Figs. 1 - 3.

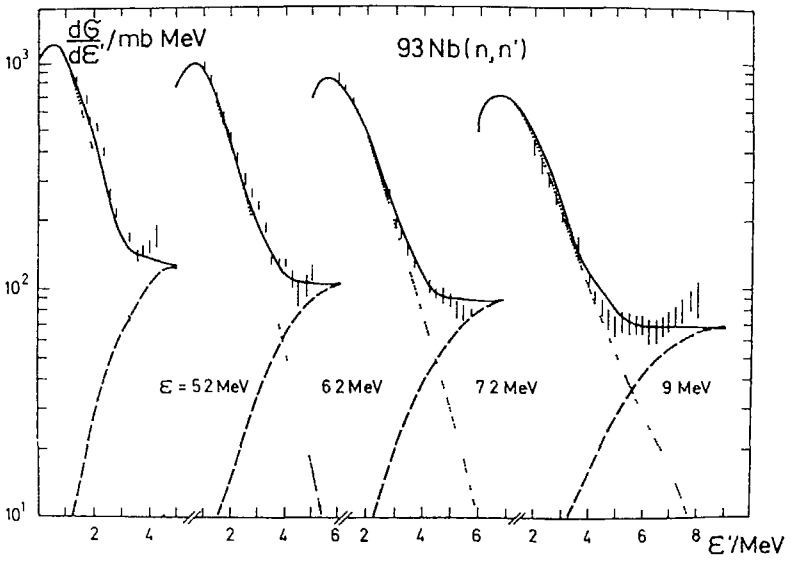

Fig. 1 Experimental integrated emission spectra at ε = 5.2, 6.2, 7.2 and 9.0 MeV /19,20/, dotted line - exciton model calculation; broken line - parametrization of direct contribution proposed in the present paper, full line - sum of both contributions

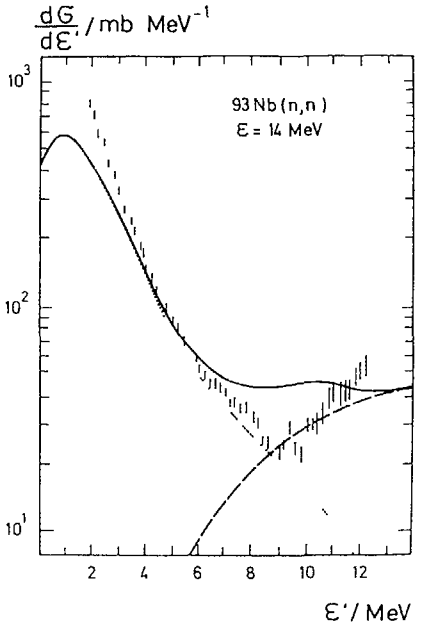

Fig. 2 as fig. 1 for ε = 14 MeV incident energy; experimental data from ref. /21/

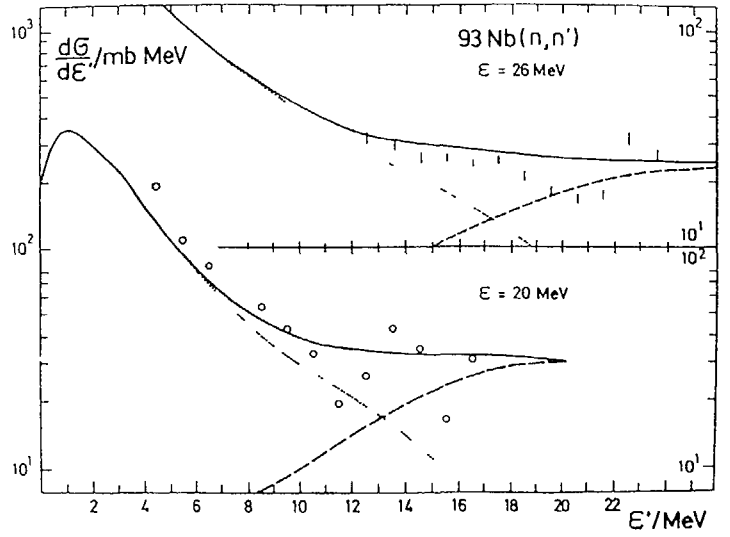

Fig. 3 as fig. 1 for ε = 20 MeV and 25.7 MeV incident energy; experimental data from refs. /23/24/

3. Parametrization of the Direct Contribution

The usual way of calculating direct reaction contributions by DWBA or CC methods is well-known /14/. The task is more involved in the case of statistical multistep direct theory /15,16/. Special nuclear structure informations are needed in both cases for practical calculations which are usually both difficult and time-consuming.
On the other hand it was found from comparison with experiments, that the direct part in the spectra shows a simple systematical behaviour, suitable for crude empirical parametrization /17,18/.
Basing on this observations we propose the following empirical ansatz for the direct contribution to the differential cross section in (1):

$$\frac{d\sigma^{DI}(\varepsilon)}{d\varepsilon'} = \frac{C_1}{\varepsilon}\, g(\varepsilon,\varepsilon') \tag{3}$$

With a normalization constant C_1[mb] and the shape function

$$g(\varepsilon,\varepsilon') \equiv \frac{\frac{d\sigma^{DI}(\varepsilon)}{d\varepsilon'}}{\frac{d\sigma(\varepsilon)}{d\varepsilon'}} = \exp\left\{-\frac{(\varepsilon-\varepsilon')^2}{2D^2}\right\} H(\varepsilon,\varepsilon') \tag{4}$$

which is given by a Gaussian having the width

$$D = \frac{\varepsilon}{C_2} \tag{5}$$

and the Heavyside step function $H(\varepsilon,\varepsilon')$.

In the case of ^{93}Nb we found that using the constants C_1 = 600 mb and C_2 = 3 a reasonable description of the experiments is obtained, as shown at Figs. 1 - 3 by broken lines.
The parametrization of the direct part (3) leads to a constant energy-integrated value, independent of incidence energy,

$$\sigma^{DI}(\varepsilon) = \int d\varepsilon' \frac{d\sigma^{DI}(\varepsilon)}{d\varepsilon'} = \frac{C_1}{C_2}\left(\frac{\pi}{2}\right)^{1/2}. \tag{6}$$

The sum of both contributions (1) shown as full line is in satisfactory agreement with the experimental emission spectra in a very broad incidence energy range, except the lowest part of the spectra, where secondary neutrons from the (n, 2n) reaction occur.
To compare the calculated angular distributions with experimental data we use the Legendre polynomial expansion

$$\frac{d^2\sigma(\varepsilon)}{d\varepsilon' d\Omega} = \frac{1}{4\pi}\frac{d\sigma(\varepsilon)}{d\varepsilon'}\sum_L (2L+1) f_L(\varepsilon,\varepsilon') P_L(\cos\Theta). \tag{7}$$

Comparing (7) with the model ansatz (1) and the definition (4) we get the relation between f_L and the Kalbach-Mann coefficiets a_L as

$$f_L(\varepsilon,\varepsilon') = g(\varepsilon,\varepsilon')\, a_L(\varepsilon') \quad \text{for } L \geq 1 . \tag{8}$$

Formula (8) can be interpreted as the reduction of Kalbach-Mann coefficients due to the dominance of isotropic multistep compound emission at lowest emission energies. (This is understandable, because the $a_L(\varepsilon')$ coefficients had been fixed at high incidence energies, where the direct process is dominant.)
Both coefficients $a_L(\varepsilon')$ and $f_L(\varepsilon,\varepsilon')$ are shown on Figs. 4 - 6 for L = 1,2. It is evident, that the reduced coefficients $f_L(\varepsilon,\varepsilon')$ give a much better description of the experimental angular distributions than the $a_L(\varepsilon')$ coefficients.

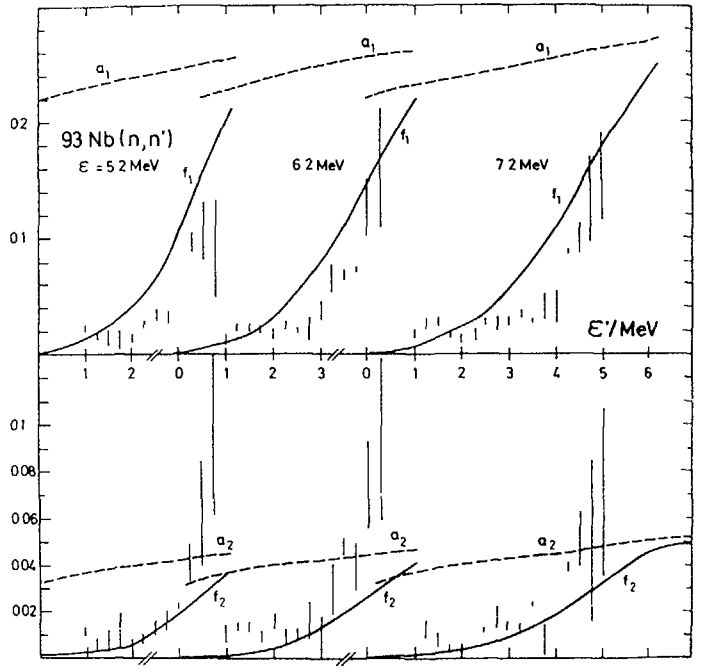

Fig. 4 Legendre coefficients of angular distributions for 5.2, 6.2, 7.2 and 9 MeV /19,20/; broken lines - $a_L(\varepsilon')$, full lines - $f_L(\varepsilon,\varepsilon')$ for L = 1,2

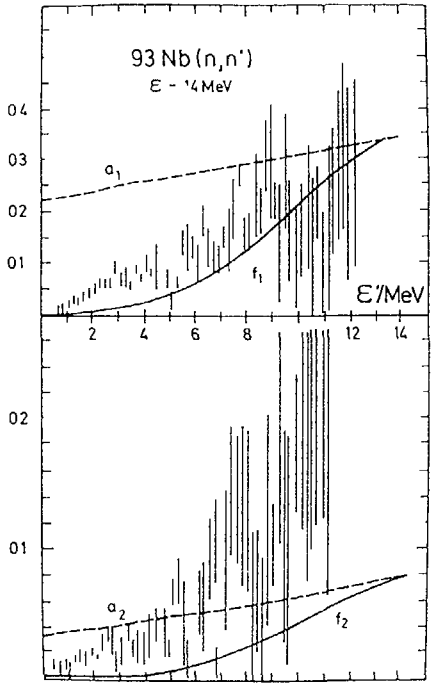

Fig. 5 as fig. 4 for E = 14 MeV; experimental data from /21/

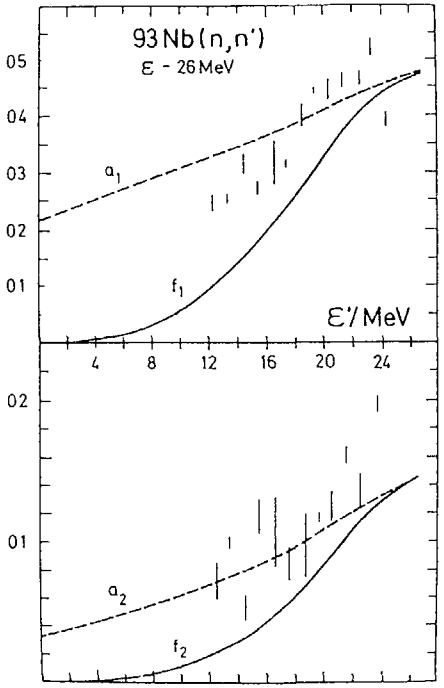

Fig. 6 as fig. 4 for E = 25.7 MeV; experimental data from /23/

4. Conclusions

In the case ^{93}Nb + n the simple parametrization of direct excitations introduced here give a reasonable description of the experimental spectra over broad incident and emission energy ranges, including the highest part of the spectra.
Below 14 MeV the calculations with the exciton model predict neutron emission with only a very small part of pre-equilibrium emission, whereas direct contributions to the spectra in (1) are constant (about 200 mb) and independent of incidence energy.

At higher incident energies the exciton model calculations show a remarkable part of pre-equilibrium emission which is separated on the energy scale from the main range of direct (collective) excitation. At 14 MeV the present analysis overestimates the part of emission spectra, where both the direct (collective) contribution and the pre-equilibrium part of the EM calculation are in the same order of magnitude.
This might be caused by a double-counting of emission processes from n_0 = 3 states in the EM and the direct (two-step) contribution. Further investigations for other nuclei are needed for coming to conclusions about the possibilities of the use of the parametrization proposed for nuclear data evaluations.

REFERENCES

/1/ Proceedings of the IAEA AGM on "Nuclear Data for Fusion Reactor Technology, Gaussig, December 1-5, 1986, IAEA-TECHDOC-Vienna, 1987

/2/ D. Seeliger, Status of experimental and theoretical double--differential neutron emission data in /1/, p.

/3/ D. Seeliger, Measurements of Cross Sections and Spectra for Neutron Emitting Channels by Fast Neutron Spectroscopy, INDC(NDS)-173/GI and INT(85)-3, IAEA, Vienna, Sept. 1985, ed. M.K. Metha, p. 26 - 61

/4/ J.J. Griffin, Phys. Lett. 17 (1966) 478; 24B (1967) 5

/5/ M. Blann, Ann. Rev. Nucl. Sci. 25 (1975) 123

/6/ K. Seidel, D. Seeliger, R. Reif, V.D. Toneev, Particles and Nuclei 7 (1976) 499

/7/ D. Seeliger, K. Seidel, D. Wolfarth, Proc. Neutron Conf., Kiev, 1971, Vol. I p. 243-252, Naukova Dumka, Kiev 1972

/8/ C. Kalbach, F.M. Mann, Phys. Rev. C23 (1981) 112

/9/ H. Kalka, PhD-Thesis, Technical University Dresden, 1986

/10/ P. Oblozinsky, I. Ribansky, E. Betak, Nucl.Phys. A226 (1974) 347

/11/ C.Y. Fu, Nucl. Sci. and Eng. 86 (1984) 344

/12/ W. Dilg et al., Nucl. Phys. A217 (1973) 269

/13/ M. Torjman, H. Kalka, D. Hermsdorf, D. Seeliger, to be publ.

/14/ N. Austen, Direct Nuclear Reaction Theories, N.Y., Interscience-Wiley, 1969

/15/ H. Feshbach, A.K. Kerman, S. Koonin, Ann.Phys. 125 (1986) 429

/16/ T. Tamura, T. Udagawa, H. Lenske, Phys.Rev. C26 (1982) 379

/17/ A.I. Blokhin et al., IZV AN USSR 49 (1985) 962

/18/ M. Torjman, Diploma Work, TU Dresden, 1987

/19/ D. Schmidt et al., EXFOR 32001, 1983

/20/ S.P. Simakov et al., Yad. Fiz. 37 (1983) 801

/21/ A. Takahashi et al., Report OKTAVIAN-A-83-01 (1983), Osaka

/22/ D. Hermsdorf et al., ZfK-277(Ü) 1975

/23/ A. Marcinkovski et al., Nucl. Sci. and Eng. 83 (1983) 13

/24/ G.N. Lovchikova et al., FEI-Report 1603 (1984)

STATISTICAL MULTISTEP DIRECT AND COMPOUND PROCESSES BELOW 30 MeV FOR ^{93}Nb

H. KALKA, D. SEELIGER
Technische Universität Dresden,
Dresden, German Democratic Republic

F.A. ZHIVOPISTSEV
State University Moscow,
Moscow, Union of Soviet Socialist Republics

Abstract

A simple reaction model for statistical multistep direct (SMD) and multistep compound processes (SMC) including quasiparticle and phonon exitations is presented and tested on 93-Nb(n,n') and (n,p) at incidence energies between 5 and 26 MeV.

1. The model

The double-differential emission cross section of this model described in detail elsewhere /1/ is given by

$$\frac{\partial^2\sigma_{\alpha\beta}(\varepsilon)}{\partial\varepsilon'\partial\Omega'} = \frac{1}{4\pi}\left[\frac{d\sigma^{SMC}_{\alpha\beta}(\varepsilon)}{d\varepsilon'} + \frac{d\sigma^{SMD}_{\alpha\beta}(\varepsilon)}{d\varepsilon'}\sum_L (2L+1)\,a_L(\varepsilon')P_L(\cos\theta')\right] \qquad (1)$$

where the incidence nucleon of type $\alpha = \pi$ or ν (proton or neutron) has the kinetic energy ε, and β, ε' refer to the outgoing particle. Here, the SMC-process,

$$\frac{d\sigma^{SMC}_{\alpha\beta}(\varepsilon)}{d\varepsilon'} = \sigma^{SMC}_{\alpha}(\varepsilon)\sum_{n_0=5}^{\bar{n}} \tau_n \Gamma_{n\beta}(\varepsilon') \qquad (2)$$

is calculated beginning at exiton number $n_0 = 5$ up the equilibrium stage $\bar{n} = (2gE)^{1/2}$. $g = A/13$ and $E = \varepsilon + B_\alpha$ are the single particle state density and excitation energy. The mean life time τ_n is taken from the time integrated (up to $t = \infty$) master equation.

The damping and escape widths are given by the Golden Rule,

$$\Gamma_n^{(\Delta n)}\downarrow = 2\pi\,(3/8)\,\overline{V_{bb}^2}\,\rho_n^{(\Delta n)}\,, \qquad \Delta n = -2,+2 \tag{3}$$

$$\Gamma_{n\beta}^{(\Delta n)}(\varepsilon')\uparrow = 2\pi\,\overline{V_{bu}^2}(\varepsilon')\,\rho_{n\beta}^{(\Delta n)}(U)P_\beta(\varepsilon')\,, \qquad \Delta n = -2,0,+2 \tag{4}$$

The factor 3/8 in (3) reduces a two-component to an one component master equation /2/, whereas the penentration factor P_β in (4) is 1 for neutrons and $\sigma_\pi(\varepsilon')/\sigma_\gamma(\varepsilon')$ for protons, and $\sigma_\alpha(\varepsilon')$ are the reaction cross section of particle-type $\alpha = \pi$ or γ. By using (4) there is no reference to the detailed balance principle or inverse cross sections in this model.

The final state densities $\rho_{n\beta}^{(\Delta n)}(U)$ are calculated in two steps: at first, the diagram method /3/ with distinction between protons and neutrons is used, and in the second step the formulas are reduced by a binominal ansatz /2/ to the one-component form. In (3) and (4) the Pauli principle is considered by the usual energy shift. Pairing and shell-effects as well as bound/unbound restrictions are ignored throughout.

With the approximation

$$\overline{V_{bu}^2}(\varepsilon') = \overline{V_{bb}^2}\,\rho(\varepsilon') \tag{5}$$

the bound-unbound matrix element is reduced to a bound-bound one. Here,

$$\rho(\varepsilon') = (2s+1)4\pi V_N m\,(2\pi\hbar)^{-3} m\,(2m\varepsilon')^{1/2} \tag{6}$$

is the state density of a particle in the nuclear volume $V_N = 4\pi r_0^3 A/3$. In this way all $\overline{V_{bb}^2}$ in (2) cancel and the SMC-model becomes free of matrix elements, i.e., the shape of the SMC-emission is independent of matrix elements at all. Its absolute value is only determined by the "normalization constant"

$$\sigma_\alpha^{SMC}(\varepsilon) \equiv \sigma_\alpha(\varepsilon) - \sum_\beta \sigma_{\alpha\beta}^{SMD}(\varepsilon) \tag{7}$$

which is the difference between the reaction cross section and the energy integrated SMD-cross section.

In (2) the SMC-emission (from $n \geq 5$) is assumed to be isotropic. The anisotropy comes only from the single- and two-step processes of SMD, whereby the reduced Legendre coefficients $a_L(\varepsilon')$ are taken from the the Kalbach-Mann systematics /4/.

The basic formulas for the SMD-processes are already given by Feshbach e.a. /3,5/. Assuming an adiabatic behaviour of the target nucleus, i.e., the accessible final state density will be the same after each collision, the single- and two-step processes can be written as

$$\frac{d\sigma_{\alpha\beta}^{(1)}(\varepsilon)}{d\varepsilon'} = \frac{2\pi V_N}{\hbar v_\alpha}\,\frac{1}{2\pi^2}\,W_{\alpha\beta}(\varepsilon,\varepsilon') \tag{8a}$$

$$\frac{d\sigma_{\alpha\beta}^{(2)}(\varepsilon)}{d\varepsilon'} = \frac{2\pi V_N}{\hbar v_\alpha}\,\frac{1}{2\pi^2}\sum_{\gamma=\pi,\nu}\int \frac{\rho(\varepsilon_1)}{4\pi}\,W_{\alpha\gamma}(\varepsilon,\varepsilon_1)W_{\gamma\beta}(\varepsilon_1,\varepsilon')\,d\varepsilon_1\,. \tag{8b}$$

Multiplying (8) by $P_\alpha(\varepsilon)P_\beta(\varepsilon')$ coulomb effects caused by protons in the entrance and/or exit channel are considered.

In contrast to the SMC-processes in the SMD-part we include besides the excitation of non-collective particle-hole states (excitons) also the excitation of low lying collective modes (phonons) /6/. Therefore the transition probability $W_{\alpha\beta}$ is the sum of two contributions,

$$W^{(ex)}_{\alpha\beta}(\varepsilon,\varepsilon') = 2\pi^2\left\{\delta_{\alpha\beta} + (1-\delta_{\alpha\beta})\frac{N\delta_{\beta\nu}+Z\delta_{\beta\pi}}{A}\right\}\overline{V^2}(\varepsilon,\varepsilon')\left(\frac{g}{2}\right)^2(\varepsilon-\varepsilon'+B_\alpha-B_\beta) \qquad (9a)$$

$$W^{(ph)}_{\alpha\beta}(\varepsilon,\varepsilon') = 2\pi^2\delta_{\alpha\beta}\sum_\lambda \mathcal{K}_\lambda\,\overline{V^2}(\varepsilon,\varepsilon')\,\delta(\varepsilon-\varepsilon'-\omega_\lambda) \qquad (9b)$$

with the abbreviation

$$\mathcal{K}_\lambda \equiv \left(\beta_\lambda^2 / \sum_\lambda \beta_\lambda^2\right)\mathcal{K} \qquad (10)$$

In this simple approximation the relation between the exciton and phonon mean square matrix elements is given by an energy-independent constant $\mathcal{K}$. β_λ denotes the deformation parameter of multipolority λ at energy ω_λ.

The unbound-unbound matrix element $\overline{V^2}(\varepsilon,\varepsilon')$ can be approximated /1/ by an unbound-bound one

$$\overline{V^2}(\varepsilon,\varepsilon') \simeq \overline{V^2}(\varepsilon)\,\varrho(\varepsilon') \qquad (11)$$

if $\varrho(\varepsilon')$ is given by (6).

The energy dependence of $\overline{V^2}(\varepsilon)$ can be obtained directly from the (optical model) reaction cross section for neutrons, $\sigma_\nu(\varepsilon)$. The latter is splitted into a (direct) single-step and a multistep contribution,

$$\sigma_\alpha(\varepsilon) = \sum_{\beta=\nu,\pi}\sigma^{(1)}_{\alpha\beta}(\varepsilon) + \sigma^{(M)}_\alpha(\varepsilon) \qquad (12)$$

$\sigma^{(M)}_\alpha$ includes all processes in which the incomming particle prduces a composite system, and which decay by further collisions to more complex states. Ignoring bound/unbound restrictions in the final state densities all multistep processes (without SMC/SMD-distinction) are considered in $\sigma^{(M)}_\alpha$, which is given by

$$\frac{2\pi V_N}{\hbar v_\alpha}\left[\left(\frac{A+Z\delta_{\alpha\nu}+N\delta_{\alpha\pi}}{2A}\right)\left(\frac{g}{2}\right)^2\frac{E^2}{2} + \sum_\lambda \mathcal{K}_\lambda\right]\overline{V^2}(\varepsilon)\left(\frac{g}{2}\right) \qquad (13)$$

2. Results

The following input values are taken for the neutron induced reaction on 93-Nb: B_ν = 7.26 MeV, B_π = 6.57 MeV, r_0 = 1.2 fm. Only three low-lying phonon states are considered (λ^π = 2^+, 3^-, 4^+; ω_λ = 0.93, 2.34, 3.39 MeV; B_λ = 0.13, 0.18, 0.11) which are taken from 92-Zr /7/. All delta functions in (9b) are replaced by Gaussians of width 1 MeV (and 2 MeV for ε = 26 MeV). For $\sigma_\alpha(\varepsilon)$ the reaction cross section of the OM (Wilmore-Hodgson for neutrons; Becchetti-Greenlees for protons) is used in a parametrized form /8/.

The calculated mean squared matrix element can well be approximated by

$$\overline{V^2}(\varepsilon) = \begin{cases} \text{const}/a & \text{for } \varepsilon \leq a \\ \text{const}/\varepsilon & \text{for } \varepsilon > a \end{cases} \qquad (14)$$

and $a \simeq 10$ MeV. This qualitative behaviour is almost independent of introduced in (10), if $\mathcal{K} \simeq 300 \div 1000$. We take $\mathcal{K}$ = 700 for all calculations, which turns out to by a upper bound (see Fig. 2).

The calculated neutron spectra at incidence energies ε = 5.2, 7.2 and 9 MeV are depicted in Fig. 1. There is a good agreement with experimental data. For ε = 14 MeV neutron and proton spectra are shown in Fig. 2. The only discrepancy in the low energy part of the neutron spectrum is due-to the neglection of (n, 2n) in our

calculations at present. Finally the emission spectrum and the first two reduced Legendre coefficients of the double differential cross section, $f_L = \left(\frac{d\sigma^{SMD}}{d\varepsilon'} \Big/ \frac{d\sigma}{d\varepsilon'} \right) a_L(\varepsilon')$ and L=1,2 are plotted in Fig. 3.

At high incidence energies ($\varepsilon \gtrsim$ 20 MeV) the role of two-step processes of mixing type (in the first step a direct, and in the second step a SMC-process) is still in question. Such SMD/SMC-transitions are discussed in /6/ but ignored in the present model, as yet.

In Table 1 all energy-integrated SMD-contributions for different incidence energies are summarized. The single-step process is divided into a pure exciton and phonon part, denoted by (ex), (ph). In the some way the two-step processes are splitted into four parts: (exex), (exph), (phex), (phph). Also the excitation of three-phonon states are calculated, (phphph).

With increasing incidence energy the direct excitation of phonon states decrease, whereas the contribution of non-collective states increases in this model. Furthermore, the contribution of all direct two-step processes at $\varepsilon <$ 10MeV can be neglected.

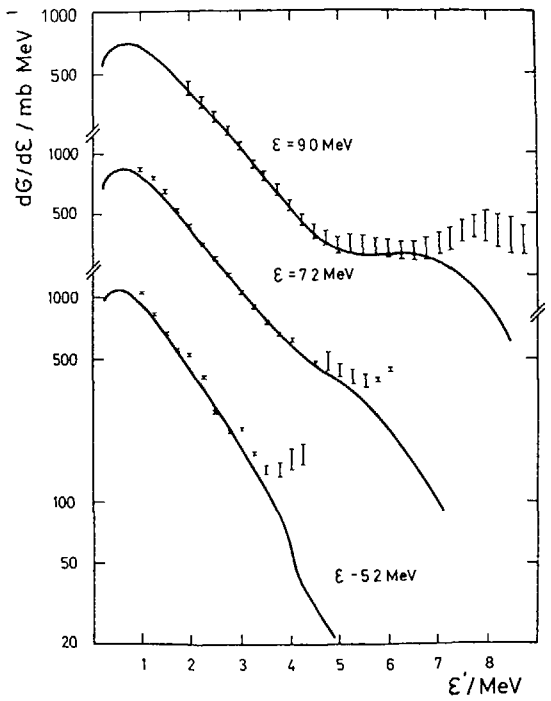

FIG 1

Energy spectra of 93-Nb(n,n') at incidence energies 5.2., 7.2 and 9 MeV.

Experimental data from /7,9/

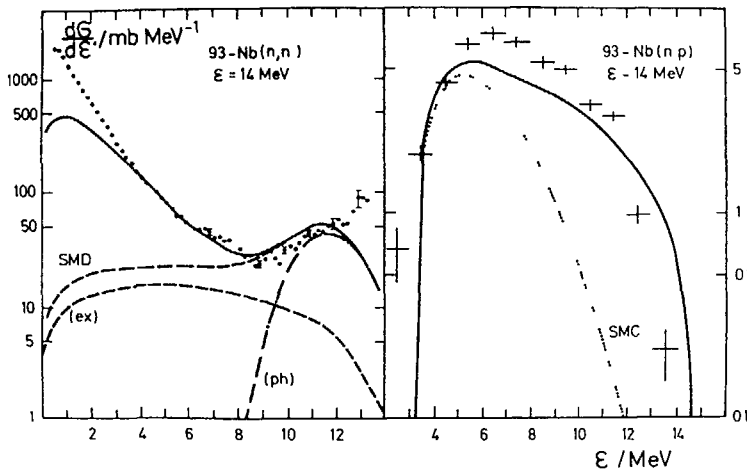

FIG 2

Energy spectra of 93-Nb(n,n') and (n,p) at 14 MeV. The curves labelled with (ex) and (ph) correspond to the direct single-step excitation of exciton and one-phonon states. The multistep direct and compound contributions labelled with SMD and SMC. The full curve is the sum of SMD and SMC. Experimental data from /10,11/.

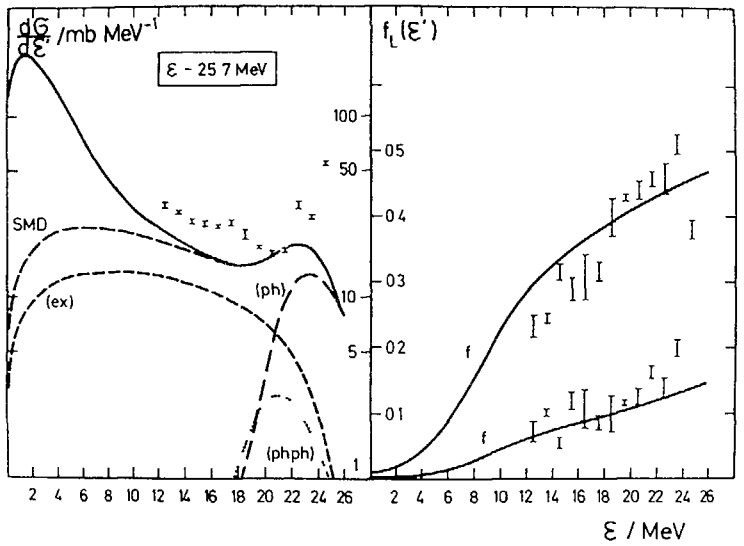

FIG 3

Energy spectrum and the reduced Legendre coefficients f_1 and $_2$ of 93-Nb(n,n') at 25.7 MeV. The curve labelled with (phph) denotes the contribution of the direct two-phonon excitation. For all other indications see Fig. 2. Experimental data from /12/.

TABLE 1.

Mean square unbound-bound matrix element, neutron reaction cross section, the individual SMD-contributions (in mb) for (n,n'), and the calculated total (n,p) cross section at different incidence energies $\mathcal{E}$ for 93 Nb. For abbreviations we refer to the text.

/MeV	5,2	7,2	9,0	14,0	20,0	25,7
$\overline{V^2(\mathcal{E})}\cdot 10^4/MeV^2$	1,94	1,85	1,71	1,31	0,92	0,66
$\sigma_\gamma(\mathcal{E})$ / mb	2036	1960	1905	1781	1651	1535
(ex)	30,1	54,6	79,3	147	211	149
(ph)	169	166	173	140	102	73,6
(exex)	0	0,2	0,9	10,9	32,1	57,5
2(exph)	0,1	2,5	7,6	49,2	81,8	95,1
(phph)	0,4	7,3	13,6	32,8	24,9	16,9
(phphph)	0	0,1	0,7	6,2	6,0	3,8
$\sigma_{\nu\pi}(\mathcal{E})$ /mb	1,5	5,8	11,3	36,7	79,7	120

The present model reproduces the 93-Nb(n,n') and (n,p) experimental spectra and angular distributions satisfactorily over a broad incidence energy range. A particular advantage of this model is its simplicity for practical calculations and its physical consistency. Further work is required to test the model in a broad target mass range.

REFERENCES

/1/ H. Kalka, D. Seeliger, F.A. Zhiropistsev, 1987, submitted to Z. Phys. A

/2/ S.K. Gupta, Z. Phys. A 303 (1981) 329

/3/ H. Feshbach e.a., Ann. Phys. 125 (1980) 429

/4/ C. Kalbach, F.M. Mann, Phys. Rev. C23 (1981) 112

/5/ H. Feshbach, Ann. Phys. 159 (1985) 150

/6/ F.A. Zhiropistsev, V.G. Sukharevsky, Phys. of Elem.Part. and At. Nucl., Dubna, 15 (1984) 1208

/7/ S.P. Simakov e.a., Yad. Fiz. 37 (1983) 801

/8/ A. Chatterjee e.a., Pranama 16 (1981) 391

/9/ M. Adel-Fawzy e.a., EXFOR 32001, IAEA-NDS, 1982

/10/A. Takahashi e.a., OKTAVIAN-Report A 83-01 (1983)

/11/G. Traxler e.a., Nucl. Sci and Eng. 90 (1985) 174

/12/A. Marcinkovski e.a., Nucl. Sci and Eng. 83 (1983) 19

APPLICATION OF NUCLEAR MODELS TO THE CALCULATION OF 20–100 MeV NEUTRON INDUCED REACTION DATA*

E.D. ARTHUR, M. BOZOIAN, D.G. MADLAND,
R.T. PERRY, W.B. WILSON, P.G. YOUNG
Los Alamos National Laboratory,
Los Alamos, New Mexico,
United States of America

Abstract

A variety of theoretical and empirical nuclear models have been applied (and in some cases developed) to the problem of the calculation of neutron reactions in the incident energy range from 20-100 MeV. These models are described with emphasis on their suitability for description of higher energy neutron reaction processes. Results obtained from these models are compared with available proton- and neutron-induced experimental data. Finally neutron data libraries developed via such methods are described.

I. INTRODUCTION

An extensive effort is currently under way at Los Alamos to develop evaluated data libraries for neutron-induced reactions up to incident energies of 100 MeV. Such data libraries, utilized in Monte Carlo or discrete ordinate transport codes, will have useful applications in areas ranging from accelerator design to radiotherapy using high energy neutrons. This data effort differs significantly from previous ones, which were generally based upon use of intranuclear cascade/evaporation (ICE) models. In these instances ICE models, appropriate for very high energies (≥ 1 GeV), have been used at lower energies to produce cross section data for particular problems of interest, or to produce processed data libraries (e.g., the HILO[1] multigroup data set). Use of these ICE models at lower energies leads to conditions where their physical assumptions and calculated results can be suspect.[2,3] In contrast, the current data library development has been based on use of preequilibrium statistical models which have been developed and extensively tested for nucleon-nucleus reactions in the energy range of tens of MeV. These models and their particular application to produce neutron data libraries from 20-100 MeV will be discussed here. Likewise their validation through available proton- and neutron-induced experimental data will also be illustrated. Finally, a description of the data bases currently under development, both for transport and activation applications, will be provided, along with examples of calculated cross sections, particle emission spectra (n,p,d,α), as well as gamma-ray production.

*Work supported by the US Department of Energy and Department of Defense.

II. THEORETICAL AND EMPIRICAL MODELS

Reliable calculations of higher energy neutron reaction data required development, improvement, or utilization of several models which are briefly discussed here. Such efforts centered around extension of optical and reaction theories (preequilibrium and statistical models), utilization of nuclear level densities more appropriate for higher excitation energies, as well as development of systematics needed to describe angular distributions associated with continuum particle emission.

A. Phenomenological Optical Model Development.

In order to determine penetrabilities (transmission coefficients) and inverse cross sections required for preequilibrium-statistical model calculations, as well as to produce overall constraining values for neutron total and nonelastic cross sections, realistic optical model parameters are required appropriate to the incident energy range of interest. While various optical parameter sets, either for specific nuclei or global, are available at lower incident energies (generally < 50 MeV), we felt that no global set was suitable for the description of nucleon-nucleus reactions in the energy range above 50 MeV. To correct this deficiency, we developed a parameter set based upon, as a starting point, the Schwandt et al.[4] set which was determined from proton data (elastic scattering, spin observables) in the range $80 \leq E_p \leq 180$ MeV. This set, which was derived via analyses performed using a relativistic Schrodinger-type equation, consists of a local, energy-dependent, complex Woods-Saxon potential. In order to optimize for our applications, we found it necessary to replace the energy dependence obtained in Ref. 4 for the strength of the imaginary potential (third-order polynomial in incident energy) with a linear energy dependence. In addition, the energy dependencies of the geometrical parameters associated with the imaginary potential were deleted. All other potential parameters (for real and spin-orbit terms) were kept equal to those of Ref 4. Specifically, we divided the incident energy range into two regions, above and below E_i = 140 MeV, for which different forms for the imaginary potential were assumed as shown in Table I.

Figure 1 compares proton reaction cross sections calculated from this modified potential with experimental data for ^{27}Al in the range between 50 and 400 MeV. Also shown by the dotted line are values resulting from use of the original Schwandt values. These deviate significantly from the higher energy experimental data because of the strong dependence on energy of the imaginary

TABLE I

MODIFICATIONS TO SCHWANDT OPTICAL MODEL POTENTIAL TO COVER THE ENERGY RANGE 50 MeV ≤ E_n,E_p ≤ 400 MeV

	Schwandt	Modification
Region I	$a_I = a_0 + a_1E$	$a_0 \rightarrow a_0$ - 0.05 fm
(E_n,E_p ≤ 140 MeV)		
Region II	$W_V = W_0 + W_1E - W_2E^2 + W_3E^3$	$W_V \rightarrow W_0' + W_1'E$
(E_n,E_p > 140 MeV)	$r_I = r_0 - r_1E$	$r_I \rightarrow r_0'$
	$a_I = a_0 + a_1E$	$a_I \rightarrow a_0'$

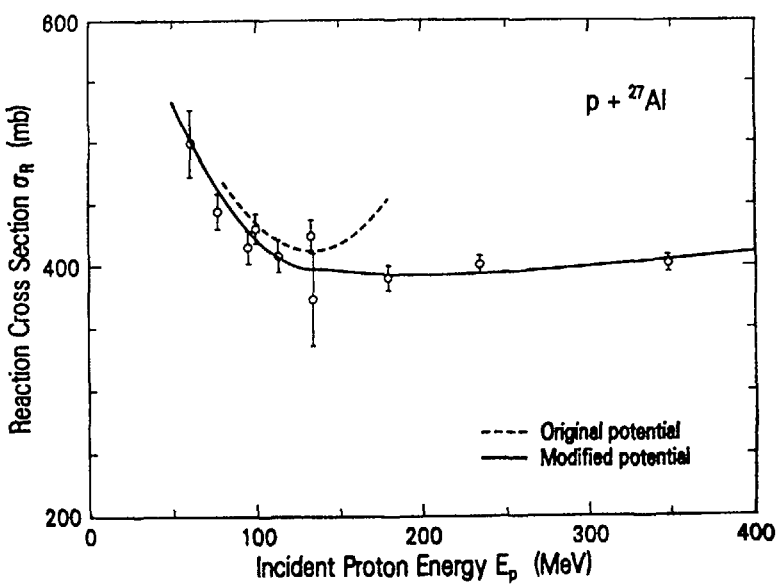

Fig. 1. The fit to available 50-400-MeV proton reaction data for ^{27}Al using the modified optical potential discussed in the text is shown. Also illustrated are results obtained through use of the original potential of Ref 4.

potential. The modifications appearing in Table I produce good agreement with these data and do not seriously degrade fits obtained in Ref 4 to elastic scattering and polarization data. The potential modified in this manner was then transformed for use with incident neutrons by application of the Lane model[5] as well as subtraction of a Coulomb correction term, $0.4Z/A^{1/3}$. Figure 2 compares n + ^{27}Al total cross sections calculated from our potential with experimental data. Also shown by

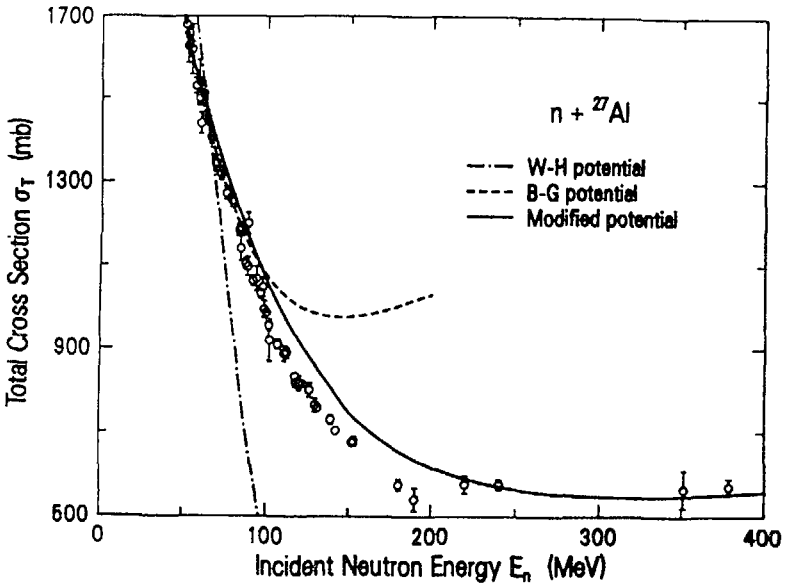

Fig. 2. A comparison of the neutron optical model potential results, determined after isospin and Coulomb corrections, with total cross-section data for ^{27}Al. The dashed and dash-dot curves illustrate results from earlier global potentials[6,7] that are applicable at lower energies.

the dotted and dash-dot curves are results calculated from the global potentials of Becchetti-Greenlees[6] and Wilmore-Hodgson,[7] respectively. Both of these older potentials were obtained for lower energy data and are shown only to illustrate the need for a potential applicable at higher energies.

To summarize, a useful parameterization of a global nucleon-nucleus phenomenological optical model potential has been developed based upon modification of the absorptive part of a parameter set developed for protons. Use of proton reaction and neutron total cross section data to produce parameter constraints were key ingredients. More details concerning this potential can be found in an accompanying contributed paper to this meeting.[8]

B. Preequilibrium Model Extensions.

The preequilibrium model formalism chosen for use in this effort is based upon the one-component exciton model developed by Kalbach[9]. This model utilizes equispaced state densities for each exciton configuration and assumes a purely phenomenological form for the effective mean square matrix elements for residual interactions necessary for transition rate determination. In order to improve the model's usefulness in the calculation of spectra produced in higher energy bombardments, the effects of a diffuse nuclear surface have been introduced via the phenomenological approach developed by Kalbach in Ref 9. Basically the excitation energy available to a hole degree of freedom is limited by the assumption of a shallower depth of the nuclear potential near the nuclear surface. Hole degrees of freedom having excitation energies exceeding the effective well depth are excluded from the normally calculated state densities. Schematically the resulting particle-hole densities are written as

$$\omega(p,h,E,V) = \omega(p,h,E,\infty)\ f(p,h,E,V)\ , \qquad (1)$$

where $\omega(p,h,E,\infty)$ is the infinite well result and the surface correction function f is given by

$$f(p,h,E,V) = \sum_{i=0}^{h} (-1)^i \left[\begin{matrix} h \\ i \end{matrix}\right] \left[\frac{E-iV}{E}\right]^{h-1} \theta(E-iV)\ . \qquad (2)$$

Here E is excitation energy, V is the depth of the nuclear potential relative to the Fermi level, and p,h are the numbers of particle and hole degrees of freedom. The quantity θ is zero for a negative argument and unity for a positive one.

Likewise, similar corrections can be applied to standard transition rates obtained for the case of an infinite well depth. Therefore to include surface effects in the initial projectile-target interaction, Kalbach has assumed

$$V = V_0 = 38 \text{ MeV for } h > 1; \qquad V = V_1 \text{ for } h=1\ .$$

To determine the functional form for the effective well depth V_1 as a function of projectile energy, a series of higher energy emission spectra were fit in Ref. 9 to extract these effective well depth values. These resulting values were parameterized as a function of incident energy via

$$V_1 = 11 + 27\left[1-\exp\left(\frac{E-27}{5}\right)\right]^{-1} \text{(MeV)}\ , \qquad (3)$$

which reduces to an asymptotic value of 11 MeV at high energies and to the standard Fermi energy value of 38 MeV at low energies. The effect of inclusion of this surface effect approximation is illustrated in Fig 3 where a comparison is made with 90 MeV ^{58}Ni(p,xn) spectral data[10]. At the higher energy end of the emission spectrum, this correction increases the calculated value by more than a factor of two, thereby improving significantly the agreement with experimental data.

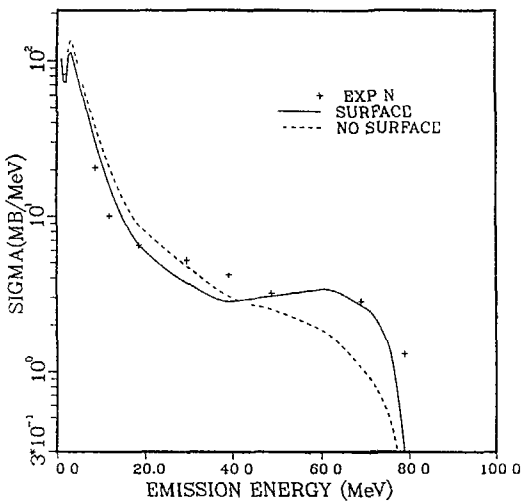

Fig. 3. A comparison of spectra calculated with (solid curve) and without (dashed curve) the surface effects contribution discussed in the text with 90-MeV ^{58}Ni (p,xn) data.[10]

A second effect occurring in higher energy preequilibrium reactions is the possibility that after a preequilibrium particle emission has occurred in the target nucleus, the residual system still contains enough energy to emit other particles in a preequilibrium phase. The extension of the exciton model to include such multistage preequilibrium contributions is described in detail in Ref 11 and 12. Basically for each residual system, one begins with a new initial exciton number m = n - p_i (p_i is the emitted particle number) at an excitation energy $U = E - \varepsilon_b - B_i$ (ε_b,B_i are the emitted particle emission and binding energies). The starting condition is determined by results occurring in the previous preequilibrium cycle so that the initial probability q that the excited nuclear system has an exciton number m at time t is

$$q(m,t=0) = \omega_b(n,\varepsilon_b)\ \tau(n)\ . \qquad (4)$$

Here $\omega_b(n,\varepsilon_b)$ is the emission rate computed for the n^{th} exciton number of the previous preequilibrium iteration. The mean lifetime $\tau(n)$ for the n^{th} exciton configuration is also determined from the previous iteration. In our calculations using the GNASH code system[13] (to be discussed later), we computed such multistage preequilibrium components for $\Delta Z = 0,1$ and $\Delta N = 1,0$ from the Z and N of the target system. Because in such multistage preequilibrium calculations the lower exciton numbers generally produce the largest starting values for ω_b, we restricted our calculations to initial conditions involving the first five exciton configurations occurring in the target system. Starting from these initial exciton numbers, the ensuing sum in the residual system went up to a maximum exciton number of seven.

Figure 4 illustrates the effect of including such multistage preequilibrium emission in calculated neutron emission spectra produced in 90 MeV p + ^{27}Al reactions. The contribution is not large at this energy, but does become important at higher energies, producing almost a factor of two enhancement around E_i= 200 MeV. In addition such contributions can have significant effects on calculated activation product yields.

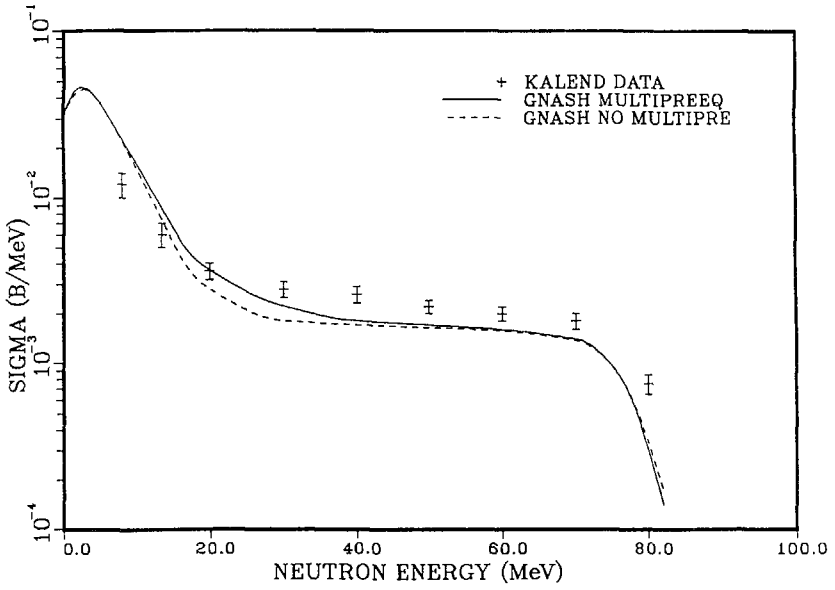

Fig. 4. A comparison with 90-MeV ^{27}Al(p,xn) data[10] to illustrate the effects of multistage preequilibrium contributions on the calculated spectrum.

C. Nuclear Level Densities Appropriate for High Excitation Energies.

The theoretical description of the nuclear level density at high excitation energies presents a major problem in the present statistical or evaporation model calculations. Such difficulties are complicated by the effect of shell closures on the Fermi gas level density parameter and their propagation to higher energies. To address such difficulties in the present higher energy calculations, we implemented the phenomenological level density model developed by Ignatyuk et al.[14]. In this model the Fermi gas parameter a is assumed to be energy dependent in contrast to the assumption made in other models such as that of Gilbert-Cameron[15] or the back-shifted Fermi gas model.[16] Thus a(U) is given by

$$a(U) = a\,[1+f(U)\delta W/U]\ , \qquad (5)$$

where a is the asympotic value occurring at high energies. Shell effects are included in the term δW which is determined via $\delta W = M_{exp}(Z,A) - M_{ld}(Z,A,\alpha)$. In our calculations we determined the experimental masses through use of the 1977 Wapstra mass compilation[17] and calculated M_{ld} through use of standard liquid drop expressions evaluated at a deformation α. The energy dependence of a(U) occurs via the term f(U) which is given by

$$f(U) = 1-\exp(-\gamma U);\ \gamma=0.05\ \text{MeV}\ . \qquad (6)$$

Thus, this model permits shell effects to be included at low excitation energies while at high energies such effects disappear as a(U) reaches the asymptotic value a. . This form is in better agreement with results from microscopic Fermi gas models than the assumption of energy independence for a.

Finally, the asymptotic form of $a(U)\rightarrow a$ was fit as a function of mass using the expression

$$a/A = \eta + \beta A\ . \qquad (7)$$

Our fits to s-wave resonance data produced best fit values for η and β of 0.1375 and $-8.36\text{X}10^{-5}$, respectively.

The effect of the Ignatyuk level density formalism on calculated cross sections is illustrated in the two following figures. Figure 5 compares the ^{208}Pb level density calculated using the Ignatyuk and Gilbert-Cameron forms. At low energies the two results are in rough agreement while at higher energies the effect of the energy dependence of the Ignatyuk form becomes apparent. In Figure 6 total neutron production calculated for n + ^{208}Pb reactions using these two

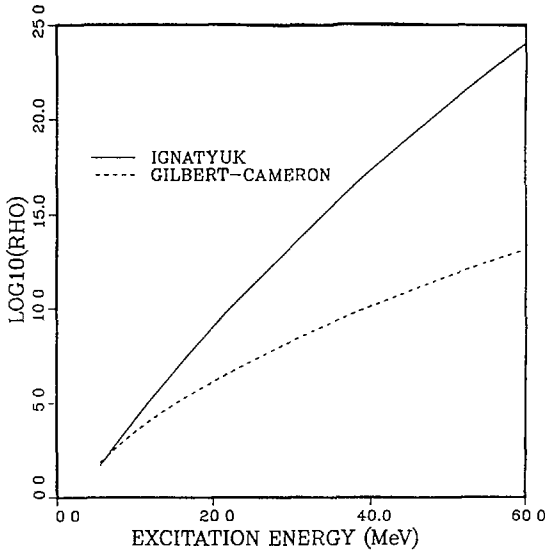

Fig. 5. The level densities calculated for ^{208}Pb using the Ignatyuk (solid curve) and Gilbert-Cameron (dashed curve) models are compared.

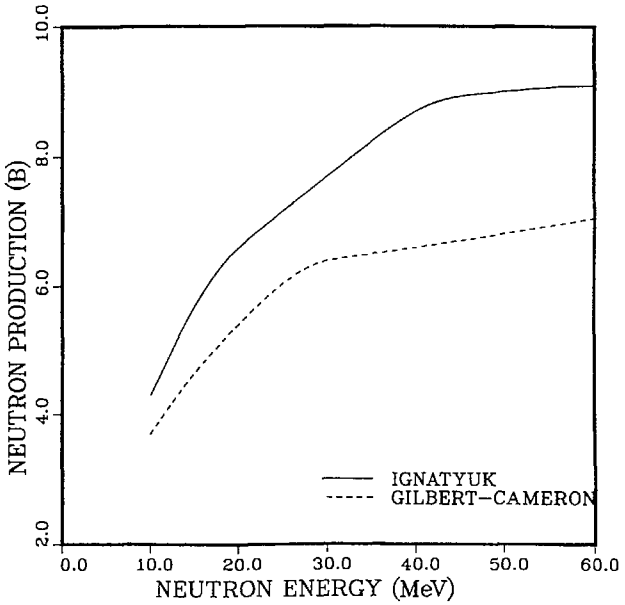

Fig. 6. Total neutron production cross sections for n+^{208}Pb reactions for $10<E_n<50$ MeV are compared with calculations using the Ignatyuk and Gilbert-Cameron models.

level density models is illustrated. The use of the Gilbert-Cameron level density leads to large differences between lead isotopes involved in neutron decay chains and tantalum and mercury isotopes which mainly occur in proton and alpha particle emission reactions . These level densities are enhanced relative to the lead isotopes because of 20-30 percent differences in calculated Fermi gas parameters and lead to increased competition from charged-particle emission in this example. Use of the Ignatyuk model eliminates shell effects at higher incident (and excitation) energies so that charged-particle competition is reduced, thereby increasing neutron production.

D. Approximations to the Hauser-Feshbach Formalism.

In the course of the present higher-energy neutron reaction calculations, alternative computational methods to the standard Hauser-Feshbach model became desirable from the point of view of shortened computing times and in order to increase the number of compound systems addressed in one computation. One obvious method is use of the Weisskopf[18] evaporation theory which is simple and permits rapid computation. Use of such theory also permits detailed treatment of gamma-ray cascades through the formulation outlined by Buttner.[19] However in comparisons of evaporation and Hauser-Feshbach calculations significant shortcomings were identified in gamma-ray production cross sections that were unacceptable because of our need for reasonably accurate gamma-ray data in the neutron libraries. To circumvent this problem, we implemented an approximation to the standard Hauser-Feshbach model based upon a formulation developed by Blann[20] known as the " s-wave approximation" approach. In this model the standard Hauser-Feshbach cross section expression

$$d\sigma/d\varepsilon_b) = \frac{\pi}{k^2}\sum_{I=0}^{\infty}(2I+1)T_I(2s_b+1)\sum_{\ell=0}^{\infty}T_b^{\ell}(\varepsilon)\sum_{J=|I-\ell|}^{I+\ell}\frac{\rho(E,J)}{D}\ , \qquad (8a)$$

is replaced by

$$d\sigma/d\varepsilon_b) = \frac{\pi}{k^2}\sum_{I=0}^{\infty}(2I+1)T_I(2s_b+1)\sum_{\ell=0}^{\infty}(2\ell+1)T_b^{\ell}\frac{\rho(E,I)}{D}\ . \qquad (8b)$$

In these expressions T_I is the transmission coefficient for the I^{th} partial wave of the projectile, $\rho(E,J)$ is the spin dependent level density for the residual nucleus, and D is the total width obtained by integrating over all emission energies and all exit channels. In going from Eq. (8a) to (8b) the assumption has been made that $\rho(E,J)$ can be replaced with $\rho(E,I)$, which means that the spin

distributions in both the compound and residual systems are considered to be the same. Of particular importance is the fact that the spin distribution in the initial compound system is determined by a standard sum over incident channel transmission coefficients available from an optical model calculation. This spin distribution is then projected unchanged throughout the problem.

Figures 7 and 8 compare n+Fe gamma-ray production data obtained via Hauser-Feshbach, evaporation, and s-wave approximation calculations. Figure 7 illustrates that at lower incident energies, simple evaporation model calculations significantly underpredict the Hauser-Feshbach results, while the s-wave approximation produces reasonable agreement. The discrepancy decreases at higher incident energies so that above 50 MeV, total gamma-ray production cross-section results are similar from the three models. Figure 8a illustrates the gamma ray production spectrum calculated at 36 MeV using these models, and confirms the conclusions stated above. Not only is the overall cross section obtained from the evaporation model lower, but the discrete gamma-ray line around 1.2 MeV does not appear. (Note that the 0.846-MeV line does appear in all calculations since (n,n') cross sections for scattering from the first excited state were calculated separately using DWBA methods and then were provided to these calculations.) Figure 8b

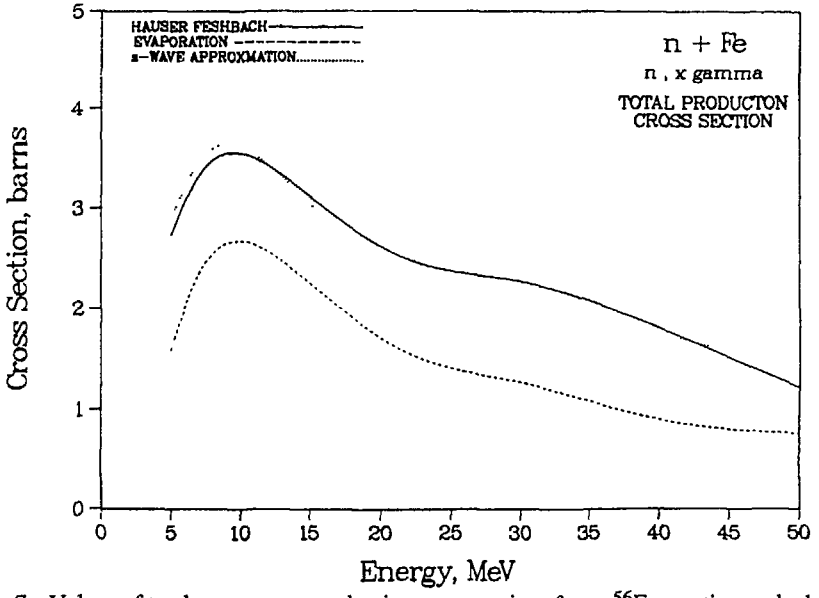

Fig. 7. Values of total gamma-ray production cross sections for n+^{56}Fe reactions calculated using the Hauser-Feshbach, evaporation, and s-wave approximation models are compared.

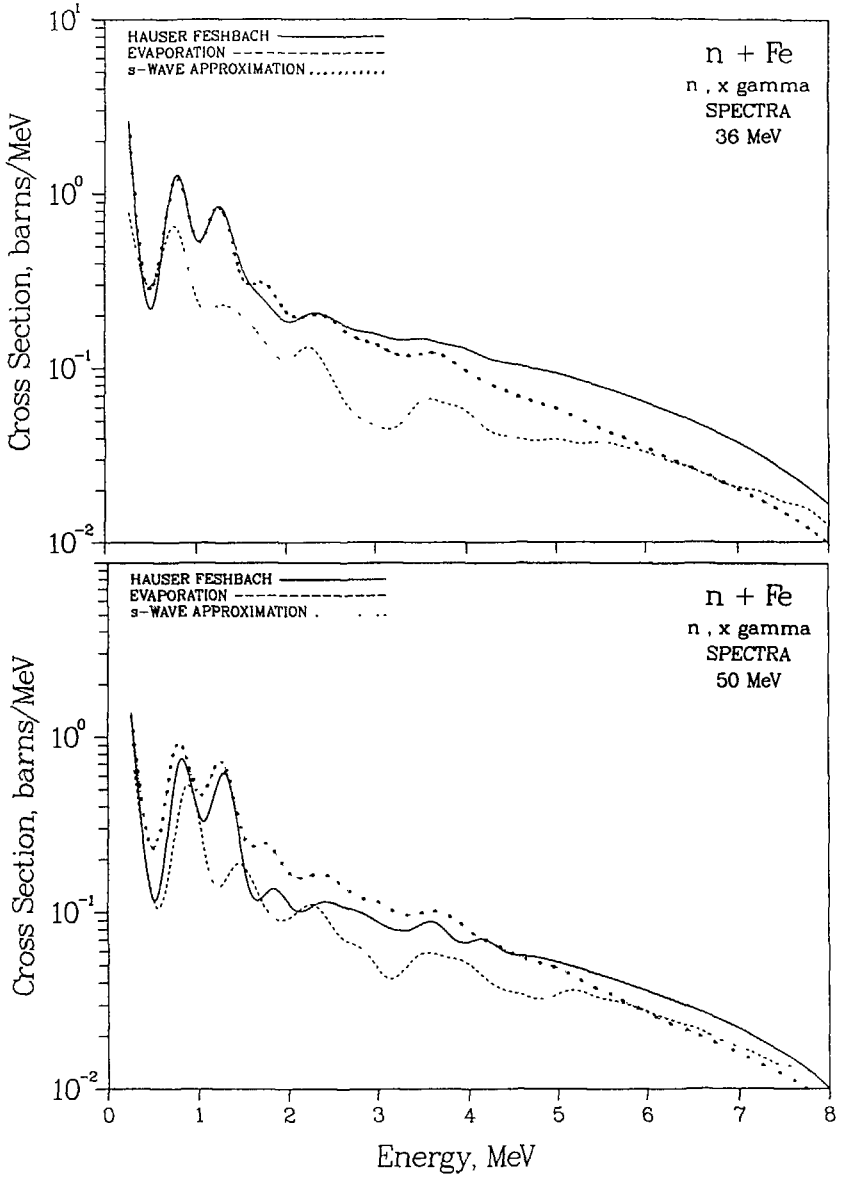

Fig. 8. The gamma-ray production spectra for 36-MeV n+^{56}Fe reactions calculated using the three models discussed in the text are compared in the upper half (Fig. 8a); the same comparison is made at 50 MeV in the lower half (Fig. 8b).

illustrates a similar spectrum at 50 MeV and shows that differences between the different model results are significantly smaller. Again no structure around 1.2 MeV appears in the evaporation calculation.

In summary, these comparisons indicate that use of the s-wave approximation can produce gamma-ray production results comparable to those obtained from Hauser-Feshbach calculations. At higher energies (E > 50-60 MeV) it appears that evaporation models can be used to provide an acceptable level of accuracy for gamma ray production data, although we have used this model mainly in our activation library and for heavier materials in the full transport libraries.

E. Phenomenology of Angular Distributions in the Continuum.

A final effort required in the production of higher energy neutron data libraries was development of a method* to describe angular distributions associated with particle emission to the continuum. Although preequilibrium models have been generalized[21] to allow calculation of angular distributions, deficiencies still exist in such calculated results, particularly for back-angle data.* The approach adopted here was an extension of previous systematics developed by Kalbach and Mann[22] to higher energies through utilization of available data involving a variety of projectile types (n,p,d,α). Attempts to utilize the Legendre polynomial expressions of Ref 22 were not successful so that a new form based on hyperbolic sines and cosines was developed. Using this form one can extract a slope parameter for the angular distribution (plotted as a function of cos θ) which, for the energy range considered here, has a straightforward dependence on exit channel energy and very little,if any, dependence on projectile energy or type. The systematic behavior of the slope parameter is illustrated in Figure 9, where slopes determined from (p,p'),(p,d), and (α,α') data on ^{56}Fe and ^{58}Ni at different energies are shown as a function of exit energy. These systematics were utilized in a functional form for double differential cross sections given by

$$d^2\sigma/d\varepsilon_b d\Omega) = \frac{1}{4\pi}\frac{d\sigma}{d\varepsilon_b}\frac{a}{\sinh(a)}\left[\cosh(a\cos\theta) + f_{MSD}\sinh(a\cos\theta)\right] , \qquad (9)$$

where f_{MSD} represents the fraction of reactions occurring through multistep direct processes (ones involving unbound particle-hole configurations) in preequilibrium calculations. In our implementation we utilized the preequilibrium contribution calculated from the first compound nucleus to determine the MSD fraction. The form chosen for the slope parameter a is based upon a preliminary form developed by Kalbach given by

* The results described here were provided in personal communication by C. Kalbach, Duke University, 1987, and will appear in a future Los Alamos report and journal publication.

$$a = 0.04\varepsilon + 1.8 \times 10^{-6}\varepsilon^3 , \qquad (10)$$

in which $\varepsilon = \varepsilon_b + S_b$, where ε_b is the energy of the emitted particle and S_b is a liquid drop model separation energy with the pairing and shell terms removed. Double differential spectra calculated using this expression will be provided later in the paper.

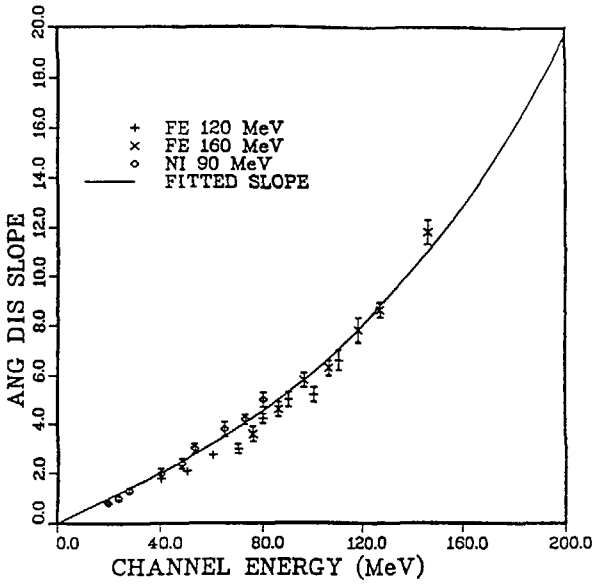

Fig. 9. The systematic behavior of the slope parameter for continuum angular distributions as determined from ^{56}Fe data.

F. Model Implementation into the GNASH Code.

The theoretical and empirical models discussed here were implemented into the GNASH[19] nuclear model code system for use in the calculation of higher energy neutron data. Figure 10 illustrates this system. The current GNASH[13] version allows a choice of the Hauser-Feshbach, evaporation, and s-wave approximation models, and uses identical input files (optical model transmission coefficients, nuclear levels, direct-reaction cross section data, and nuclear masses) and produces output files identical in form for further translation into ENDF-formatted files. For all models one-step preequilibrium corrections are applied, while for the evaporation and s-wave approximation models, multistage contributions are also calculated. For the Hauser-Feshbach statistical model version simplified inputs are available while for the other models an automated

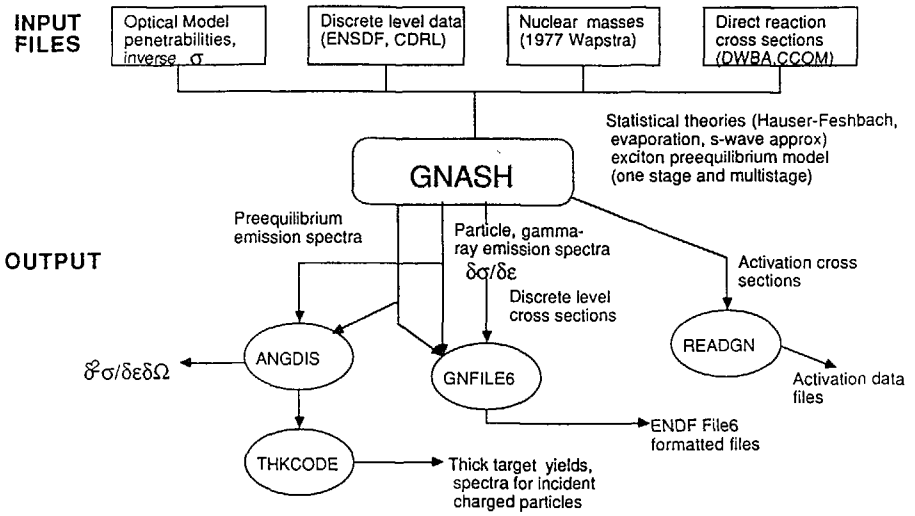

Fig. 10. An illustration of the GNASH nuclear model code system used to produce the results discussed in this paper.

chaining of all possible reaction paths occurs based on ΔZ and ΔN information provided by the user. The number of compound nuclei that can be included in each calculation for current versions of the Hauser-Feshbach, s-wave approximation, and evaporation models are 10, 40, and 70, respectively, with up to 6 emissions occurring from each compound system. In addition to angle-integrated spectra, activation yields, and gamma-ray lines calculated in the main GNASH module, the auxiliary modules ANGDIS, THKCODE, and GNFILE6 allow production of double differential spectral data, thick target yields and spectra for incident charged particles, and ENDF/B File 6 formatted data,[23] respectively. We have also developed additional utility codes for creating standard ENDF/B files, activation data files, and natural element files.

III. VALIDATION OF CALCULATED RESULTS

In order to validate the models, parameters, and calculational results occurring in the energy range from 20-100 MeV, an extensive set of comparisions have been made with existing experimental data. Some of these have appeared as part of the discussions associated with the preceeding sections, while other examples will be provided here. Because of the paucity of neutron-induced experimental data above 20 MeV, many of these comparisons involve use of proton-induced reaction data. For example, an important source of data pertaining to particle emission spectra are found in (p,xp) measurements made by Bertrand and Peelle[24] and (p,xn) and (p,xp) measurements made by Kalend et al.[10] Figure 11 compares 61-MeV ^{56}Fe(p,xp) spectra with our calculations. Although there is some underprediction, the agreement obtained does indicate the suitability of the parameters and model used. The structure appearing in our calculations results from direct-reaction contributions occurring from collective states in ^{56}Fe, as calculated via DWBA methods, and agrees with the experimental results. Figure 12 compares our calculations to angle-integrated (p,xn) data measured for 90 MeV p + ^{58}Ni reactions. Here also the agreement is quite good although comparisons with (p,xp) data measured in the experiment again indicate some underprediction. Figure 13 compares double-differential spectra obtained in this experiment for ^{27}Al(p,xn) reactions at angles of 30 and 60 degrees with our calculations that utilized the angular distribution systematics described in Section II-D. Again the agreement is quite good.

A final source of proton-induced spectra data comes from recent measurements of neutron spectral yields by Kiziah[25] resulting from 50 MeV protons stopping in thick targets. Although more complicated to compare with, such experiments sample neutron production over a

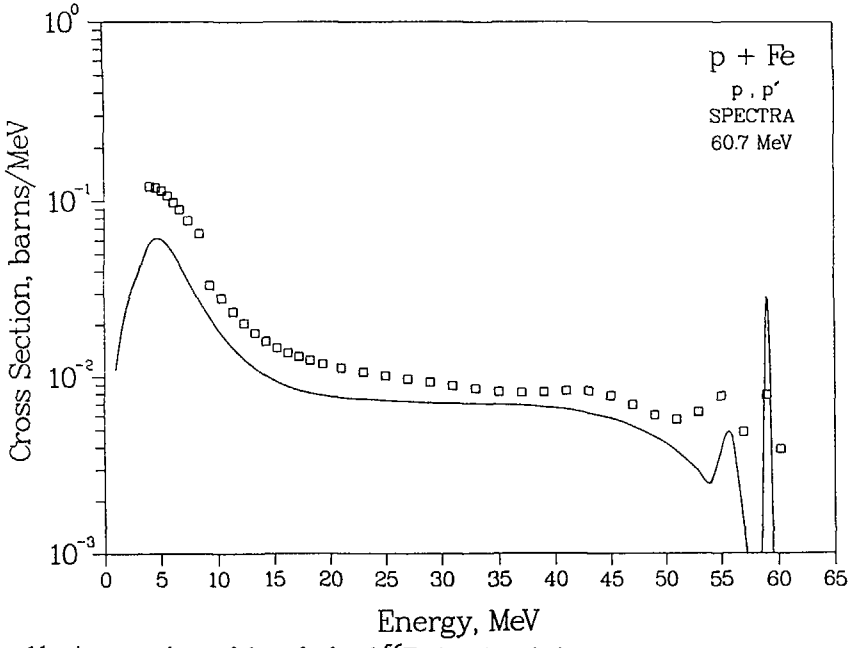

Fig. 11. A comparison of the calculated ^{56}Fe (p,xp) emission spectra for 61-MeV protons with data measured by Bertrand and Peelle.[24]

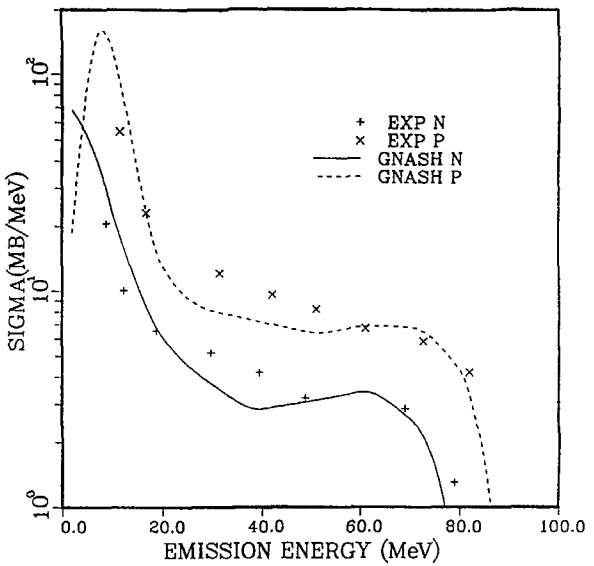

Fig. 12. Angle-integrated proton and neutron production spectra for 90-MeV proton reactions on ^{58}Ni calculated using the methods described in the text are compared with the data of Kalend.[10]

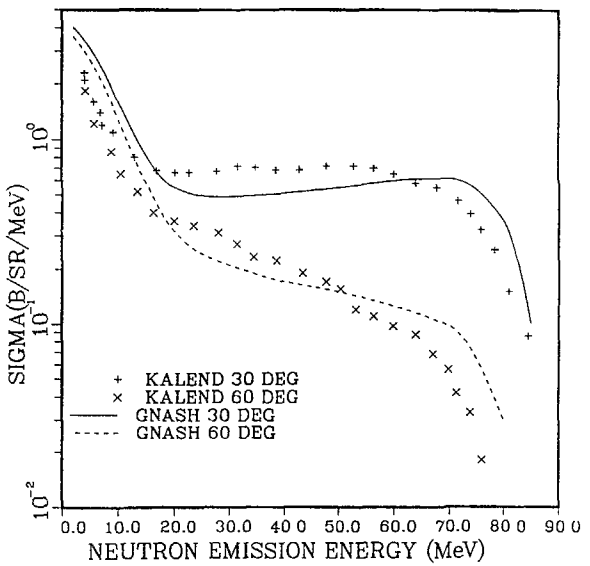

Fig. 13. Double differential neutron emission spectra (30° and 60°) calculated for 90-MeV p+^{27}Al reactions are compared with the Kalend data[10] to illustrate the applicability of the angular distribution systematics developed for the present effort.

distribution of proton energies from 50 MeV and below during the course of the stopping of the proton in the target. Figure 14 compares our calculations with the ^{27}Al(p,xn) data of Kiziah at an angle of 30 degrees. The agreement again is seen to be good. Intranuclear cascade calculations, as discussed in the Introduction, have been the main source of higher energy data in previous applications. These have been shown to overpredict the ^{27}Al(p,xn) experimental results by factors of 3 to 4.

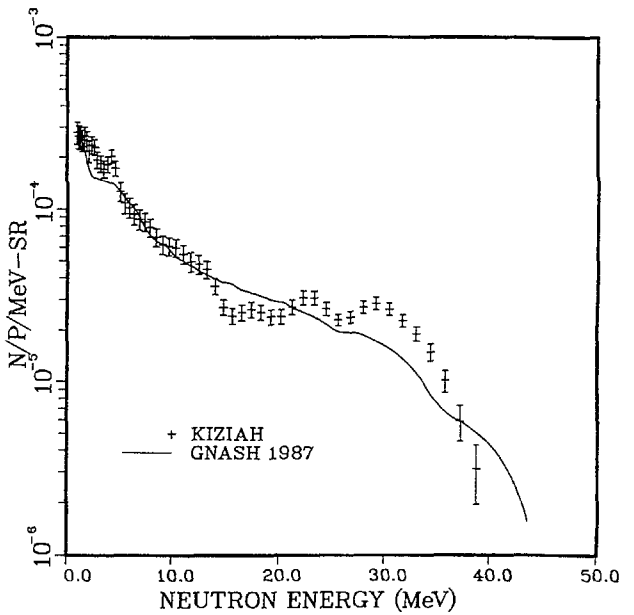

Fig. 14. The thick-target neutron spectral yield at 30° resulting from the stopping of 50-MeV protons in an aluminum target is compared with the data of Kiziah.[25]

As will be discussed in Section IV, production of activation data was also a key motivation for our higher energy neutron reaction calculations. Measurement of higher energy neutron-induced activation data are also very scarce (or nonexistent) so that we again turned to proton activation data for comparison purposes. Figure 15 compares our calculations for production of ^{18}F from p + ^{27}Al reactions with the available data. Once more, the agreement is reasonable, especially when the extent of the energy range is considered along with the complexity of the reaction paths that occur to produce specific residual systems such as ^{18}F.

Although higher energy neutron reaction data are sparse compared with proton-induced results, new information is now becoming available as a result of efforts at Ohio University,

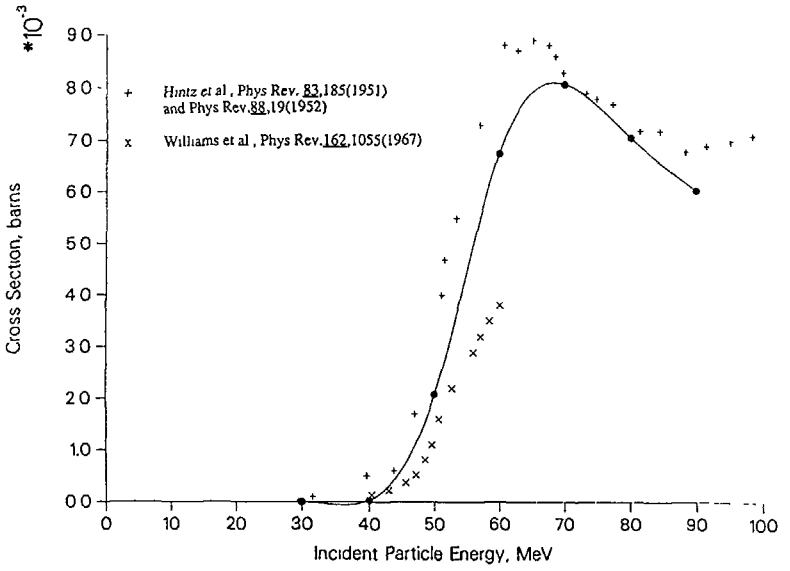

Fig. 15. Calculations of activation cross sections are compared with data for ^{18}F production from p+^{27}Al reactions.

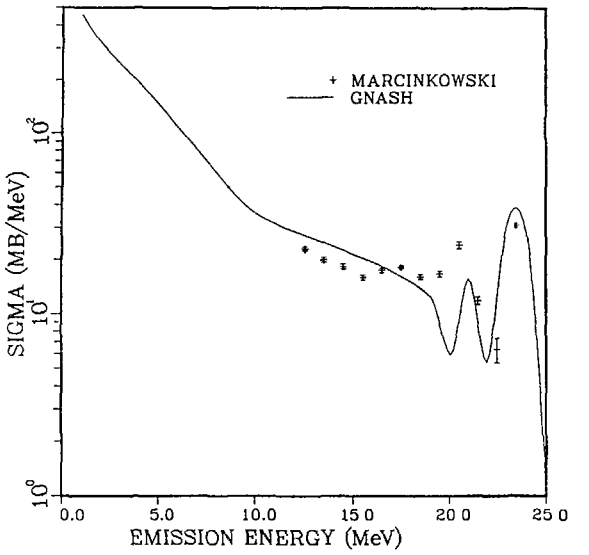

Fig. 16. The calculated angle-integrated neutron emission spectrum for 26-MeV n+^{56}Fe are compared with data measured by Marcinkowski et al.[26]

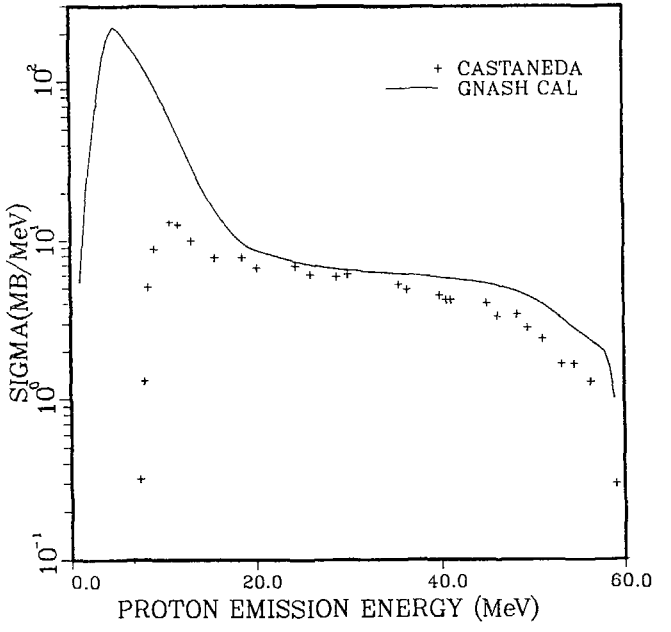

Fig. 17. A comparison of the angle integrated proton emission spectra calculated for 60-MeV n+^{58}Ni reactions is made with the data of Casteneda,[27] which are integrated only up to angles of 70°.

University of California-Davis, and the Los Alamos WNR Facility. Such data are obviously invaluable to the validation process described here, and particle emission data are of particular importance. Figure 16 compares our calculated neutron emission spectra to 26 MeV n+^{56}Fe neutron emission data measured by Marcinkowski et al.[26] that has been integrated over angle. The agreement is reasonable even considering the structure in the measured spectrum which again results from scattering from collective states in ^{56}Fe. Higher energy charged-particle emission data is available as a result of measurements made at the Davis Cyclotron. Figure 17 compares our angle-integrated calculated $^{58}Ni(n,xp)$ spectrum with data measured by Castaneda et al[27] at neutron energies of 60 MeV that have been integrated to angles of 70°. The agreement at higher emission energies, which is dominated by forward angles, is good. Similarly, Figure 18 compares our calculation with an $^{16}O(n,x\alpha)$ alpha spectrum measured at 61 MeV by Romero et al.[28] In both cases the agreement is reasonable and again supports the credibility of the present calculations. In fact, for oxygen this is somewhat surprising as some previous Hauser-Feshbach calculations[28] have failed to agree with these data.

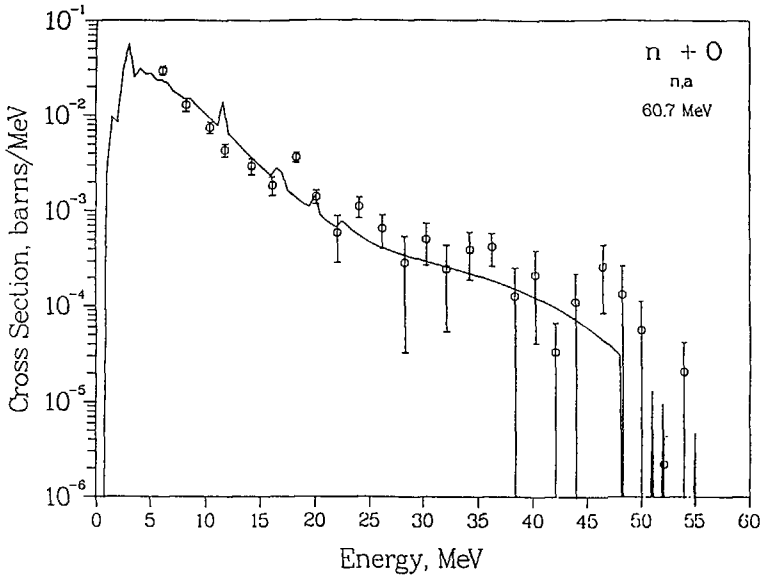

Fig. 18. A similar comparison as Fig. 17 but with the $^{16}O(n,x\alpha)$ data measured by Romero et al.[28] at 61 MeV.

Finally, a new source of information is now available because of high energy (n,xγ) measurements presently under way by Wender et al.[29]. Figure 19 compares our calculated $^{12}C(n,x\gamma)$ spectrum to data measured by Auchampaugh and Wender* at 61 MeV. Even though the calculated results have not been broadened to include resolution effects, there is good agreement with these data. A similar comparison with preliminary 50-MeV Ta(n,xγ) data of Gould and Wender** appears in Fig. 20. In their preliminary analysis these data were fit with the R-parameter form developed by Perkins et al.[30]. Our calculations provide a more extensive analysis and agree with this data, although at lower gamma-ray energies (< 2 MeV), some structure is predicted from the calculated results. Additionally, Figure 21 presents preliminary measured gamma-ray yields from Ta (integrated above $E_\gamma = 2$ MeV) occurring over the incident neutron energy range between 20 and 80 MeV. These experimental data agree with earlier results of Morgan et al.[31] at neutron energies less than 20 MeV. As indicated in the figure, our calculations are in good agreement with these measured gamma ray production data. Because gamma-ray production measurements sample

* This information was provided in 1987 by G. Auchampaugh and S. Wender, Los Alamos National Laboratory.
** This information was provided by C. Gould, Duke University, and S. Wender, Los Alamos, in 1987.

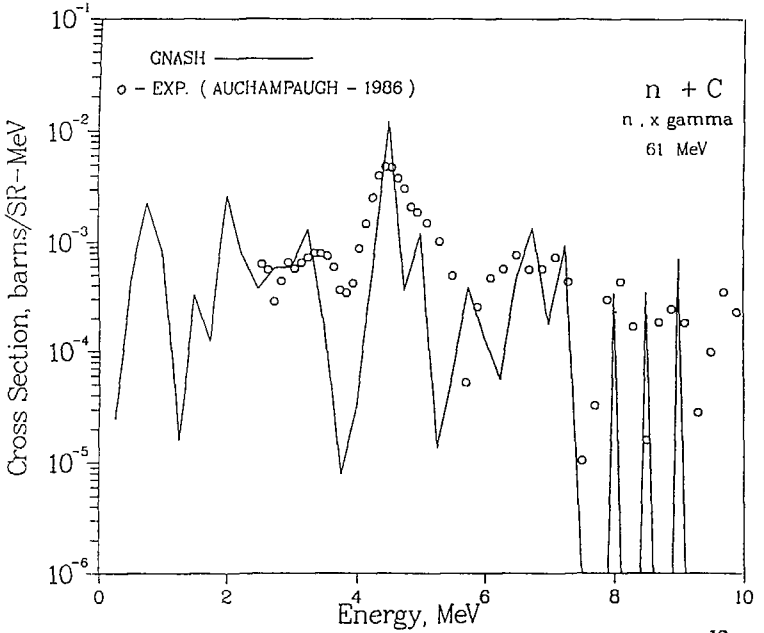

Fig. 19. The calculated gamma-ray production spectrum produced by 61-MeV n+^{12}C reactions are compared with preliminary measurements of Auchampaugh and Wender.

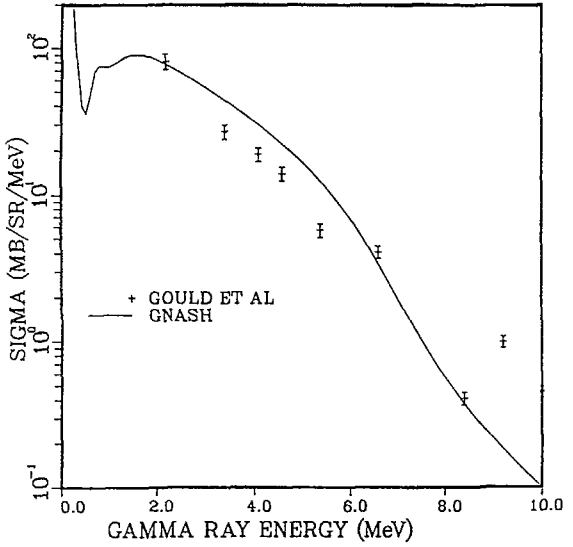

Fig. 20. Calculated gamma-ray production spectra for 50-MeV n+Ta reactions are compared with the preliminary data of Gould and Wender.

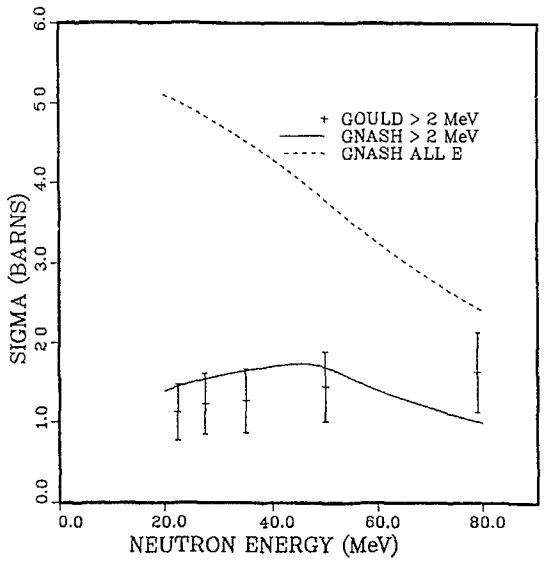

Fig. 21. The calculated gamma-ray production cross section for Ta(n,xγ) reactions with $E_\gamma > 2$ MeV are compared with preliminary results of Gould and Wender in the neutron energy range from 20 to 100 MeV. Also shown by the dashed curve is the total gamma-ray production cross section obtained from the present calculations.

contributions from all reaction paths occurring at a particular incident energy, the comparisons shown here for a heavy nucleus such as tantalum, as well as that shown above for carbon, provide a stringent test of the models used in this energy regime.

IV NEUTRON DATA LIBRARY PRODUCTION

Using the methods described here, ENDF-formatted data libraries describing neutron reactions have been produced that cover the incident energy range from 10^{-11} to either 50 or 100 MeV. Materials for which such libraries have been produced appear in Table II. These libraries include neutron total, elastic,and nonelastic cross sections, angular distributions for elastic scattering as well as production cross sections for neutrons, protons, deuteron,alphas, and gamma rays with their associated energy-angle spectra. Results from the calculations described earlier were translated into the new File 6 representation of ENDF, which permits an accurate representation of coupled energy-angle spectral representations. Use of this representation is essential for higher energy neutron reaction data because of the strong forward peaking occurring at such energies. Although the main emphasis of our effort was the energy range between 20 and 100 MeV, we also required that these results join smoothly with existing ENDF data below 20

TABLE II

HIGHER ENERGY NEUTRON DATA LIBRARIES FOR TRANSPORT CALCULATIONS

Energy Range	Materials
10^{-11} -50 MeV*	^{27}Al, ^{54,56}Fe, ^{58,60,62}Ni, ^{63,65}Cu, ^{182,183,184,186}W, ^{NAT}Fe, ^{NAT}Ni ^{NAT}Cu, ^{NAT}W
10^{-11} -100 MeV	^{1}H, ^{12}C, ^{16}O, ^{27}Al, ^{28}Si, ^{40}Ca, ^{56}Fe

*Also completed for incident protons.

checked against existing experimental data and were found to be comparable or superior to the existing ENDF data.

Figures 22 and 23 provide selected examples of data resulting from this effort. Figure 22 illustrates calculated angle-integrated spectra for neutron, gamma-ray, and charged-particle spectra occurring in 100 MeV n+^{28}Si reactions. Figure 23 illustrates production cross section excitation functions calculated for neutron reactions on copper up to 50 MeV.

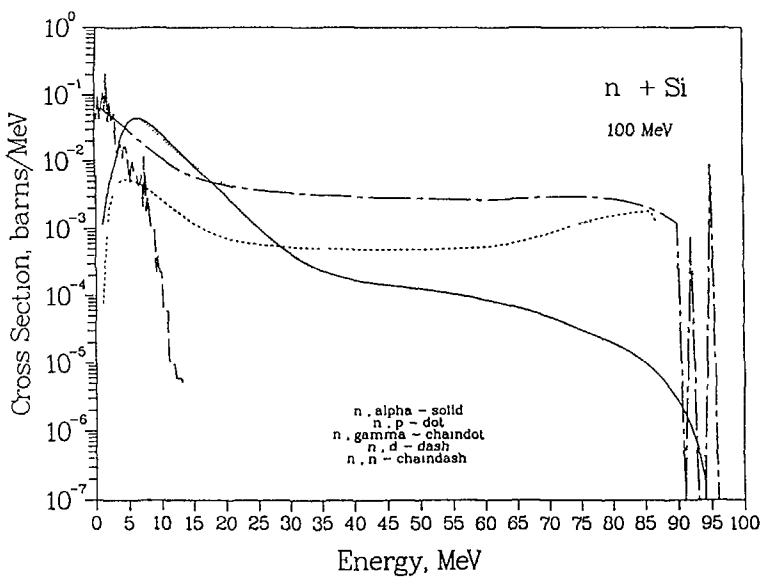

Fig. 22. An illustration of angle-integrated neutron, charged-particle, and gamma-production spectra for 100 MeV n+^{28}Si resulting from the present calculations.

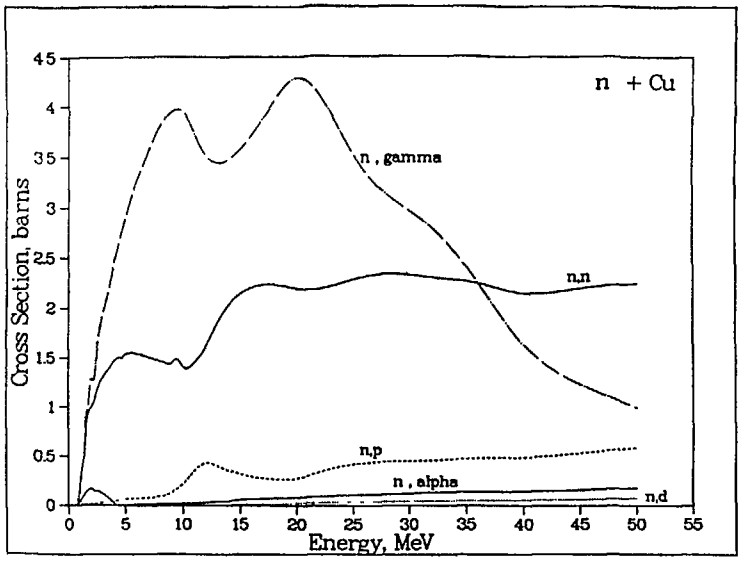

Fig. 23. Calculated excitation functions for neutron, charged-particle, and gamma-ray production occurring in n+Cu reactions up to E_n = 50 MeV.

As noted earlier, a principal motive for the present higher energy calculational effort was production of neutron-induced activation cross sections for use in the activation analysis code REAC2.[32] Presently this code contains an activation cross section data base up to 30 MeV that was generally obtained from ENDF data or from normalized THRESH[33] code results. The present effort will augment this data base by extending it to 100 MeV via the reasonably realistic nuclear model calculations that have been discussed here. Table III provides a list of target isotopes for which calculations have been completed thus far. From these calculations excitation functions for approximately 500 reaction products have been determined including total tritium production values. Figures 24 and 25 provide examples of such activation and tritium production data for ^{56}Fe resulting from our calculations.

TABLE III

LIST OF TARGET NUCLEI FOR WHICH NEUTRON ACTIVATION CALCULATIONS HAVE BEEN CARRIED OUT TO E_n = 100 MeV

Target Nuclide	GNASH Calc.	READGN Calc.
^{1,2}H		
^{10,11}B	C	P
^{12,13}C	C	C
^{14,15}N	C	C
$^{16\text{-}18}$O	C	C
$^{20\text{-}22}$Ne	C	C
$^{24\text{-}26}$Mg	C	C
^{27}Al	C	C
$^{28\text{-}30}$Si	C	C
^{36,38,40}Ar	C	C
$^{39\text{-}41}$K	C	C
$^{40,42\text{-}44,46,48}$Ca	C	C
$^{50,52\text{-}54}$Cr	C	C
^{55}Mn	C	C
$^{54,56\text{-}58}$Fe	C	C
^{59}Co	C	C
$^{58,60\text{-}62,64}$Ni	C	C
^{63,65}Cu	C	C
$^{64,66\text{-}68,70}$Zn	C	C
^{90,91,92,94,96}Zr	C	C
$^{92,94\text{-}98,100}$Mo	C	C
$^{142\text{-}146,148,150}$Nd	C	P
$^{144,147\text{-}150,152,154}$Sm	C	P

C: complete P: in progress

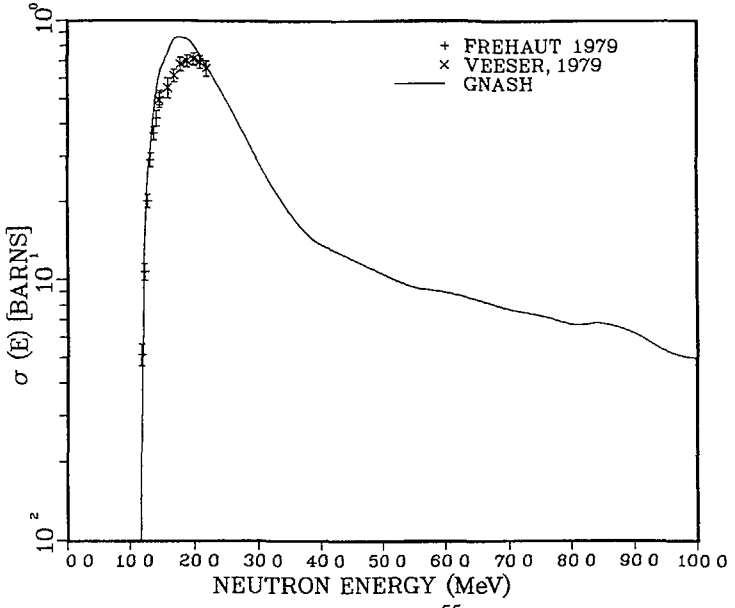

Fig 24 The calculated cross section for production of ^{55}Fe from neutron reactions on ^{56}Fe for neutron energies up to 200 MeV

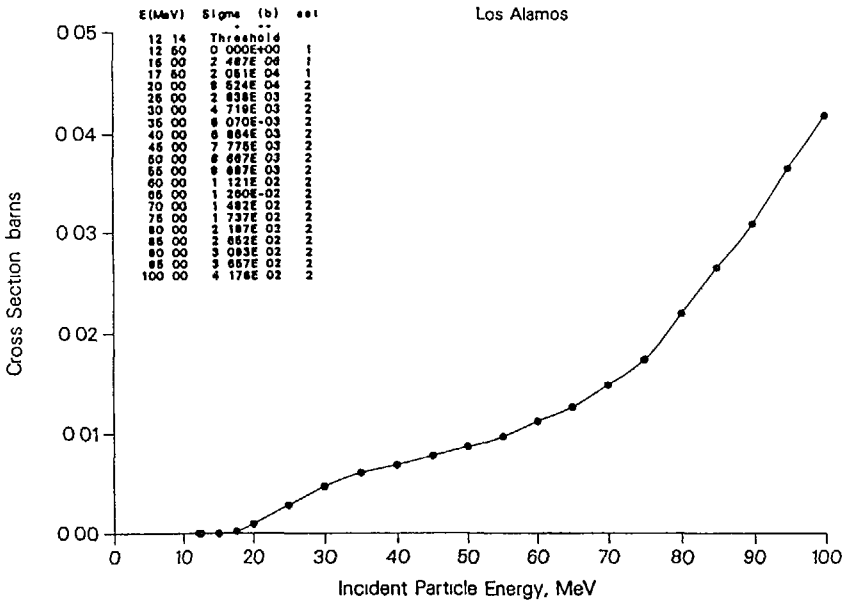

Fig 25 The calculated total tritium production cross section determined for n+^{56}Fe reactions up to 100 MeV

V SUMMARY

An extensive effort has begun to extend neutron transport and activation data libraries from 20 MeV (present ENDF upper limit) to 100 MeV To do so required utilization and development of a variety of models appropriate for reaction calculations in this energy regime Additionally parameter development, such as that used in phenomenological optical models, was also required Results of calculations employing such methods were benchmarked against available proton and neutron reaction data where reasonable agreement (generally ≤ 20-30 percent) was obtained The results from such a development and validation effort have been used to produce an extensive and reliable data base suitable for applications requiring higher energy neutron reaction data

Future efforts will be directed at enlarging the number of nuclides in the neutron library to include other structural and shielding materials as well as several actinides A parallel effort is in progress to develop similar libraries for incident protons, and such a library has already been created for proton energies to 50 MeV The actinide calculations will require development and extension of the fission model presently in the GNASH code to handle higher energy reactions This effort will be complemented by an ongoing program at WNR to measure particle and gamma-ray cross sections and spectra, as well as fission cross sections and ratios for several actinides up to neutron energies of 200 MeV or higher At this stage we await new experimental data that will provide additional evidence for our predictive capability and, hopefully, will lead to further refinements in the physics content of our code system

REFERENCES

1. R. G. Alsmiller, Jr., and J. Barish, Nucl. Sci. Eng. 69, 378 (1979).
2. K. Shin et al., Phys. Rev. C 29, 1307 (1984).
3. K. Kwiakowski et al., Phys. Rev. Lett. 50, 1648 (1983).
4. P. Schwandt et al., Phys. Rev. C 26, 55 (1982).
5. A. M. Lane, Phys. Rev. Lett. 8, 171 (1962); *ibid* Nucl. Phys. 35, 676 (1962).
6. F. D. Becchetti, Jr., and G. W. Greenlees, Phys. Rev. 182, 1190 (1969).
7. D. Wilmore and P. E. Hodgson, Nucl. Phys. 55, 673 (1964).
8. D. G. Madland, "A Preliminary Medium-Energy Nucleon-Nucleus Phenomenological Optical-Model Potential," IAEA Advisory Group Meeting on Nuclear Theory for Fast Neutron Data Evaluation, Beijing, 12-16 October, 1987.
9. C. Kalbach, Phys. Rev. C 32, 1157 (1985).
10. A. M. Kalend et al., Phys. Rev. C 28, 105 (1983).
11. H. Machner, Phys. Reports 127, 309 (1985).
12. H. Gruppelaar and J. M. Akkermans, "The GRAPE Code System for the Calculation of Precompound and Compound Nuclear Reactions- GRYPHON Code Description and Manual," ECN-164 (1985).
13. P. G. Young and E. D. Arthur, "GNASH: A Preequilibrium-Statistical Nuclear Model Code for Calculations of Cross Sections and Emission Spectra," Los Alamos Scientific Laboratory report LA-6947 (1977).
14. A. V. Ignatyuk, G. N. Smirenkin, and A. S. Tishin, Sov. J. Nucl. Phys. 21, 255 (1975).
15. A. Gilbert and A. G. W. Cameron, Can. J. Phys. 43, 1446 (1965).
16. W. Dilg, W. Schantl, and H. Vonach, Nucl. Phys. A 217, 269 (1973).
17. A. H. Wapstra and K. Bos, At. Data and Nucl. Data Tables 19, 175 (1977).
18. V. F. Weisskopf and D. H. Ewing, Phys. Rev. 57, 472 (1940).
19. H. Büttner, A. Lindner, and H. Meldner, Nucl. Phys. 63, 615 (1965).
20. M. Blann and M. Beckerman, Nucleonika 23, 1 (1978).
21. G. Mantzouranis, D. Agassi, and H. A. Weidenmüller, Phys. Lett 57B, 220 (1975).
22. C. Kalbach and F. M. Mann, Phys. Rev. C 23, 112 (1981).
23. R. E. MacFarlane, "ENDF-VI Development" in Applied Nuclear Science Research and Development Progress Report: June 1, 1984-May 31, 1985," Los Alamos National Laboratory report LA-10513-PR (1985); C. Dunford, Brookhaven National Laboratory, personal communication (1987).
24. F. E. Bertrand and R. W. Peelle, Phys. Rev. C 8, 1045 (1973).
25. R. R. Kiziah et al., "Energy and Angular Distribution of Secondary Neutrons from Targets Bombarded by 50-MeV Protons," AFWL-TR-87-63 (Preliminary Version) (1987).
26. A. Marcinkowski et al., Nucl. Phys. A 402, 220 (1983).
27. C. M. Castaneda et al., Phys. Rev. C 28, 1493 (1983).
28. J. L. Romero et al., Rad. Effects 94, 13 (1986).
29. S. A. Wender et al., "Experimental Status of E2 Giant Resonances Seen in Neutron Capture," Workshop on Radiative Capture, Univ. of Uppsala, Aug. 27, 1987 [Los Alamos informal document LA-UR-87-2601 (1987)].
30. S. T. Perkins, R. C. Haight, and R. J. Howerton, Nucl. Sci. Eng. 57, 1 (1975).
31. G. L. Morgan et al., "Gamma-Ray Production Cross Sections of Tantalum and Carbon for Incident Neutron Energies between 0.007 and 20 MeV," Oak Ridge National Laboratory report ORNL-TM-3702 (1972).
32. F. M. Mann, D. E. Lessor, and J. S. Pintler, Rad. Effects 92, 207 (1986).
33. S. Pearlstein, "Neutron Cross Sections and their Uncertainties Obtained from Nuclear Systematics," Proc. of Conf. on Nuclear Cross Sections and Technology, Washington, DC, March 3-7, 1975, Vol. 1, p. 332.

QUASI-FREE SCATTERING APPROACH TO THREE BODY DIRECT PROCESS AND ITS APPLICATION TO NUCLEAR DATA

Benai ZHANG, Weili SUN
Institute of Applied Physics and
Computational Mathematics,
Beijing, China

Abstract

This paper has studied three body break-up process. The wave function of the relative motion of collision particles is chosen to be plane wave. We obtained the angular-energy double differential cross section of each secondary particle, the differential cross section of two- particle correlation, and the integral cross section in the simple computational form.

I. INTRODUCTION

The main task of theoretical treatment for nuclear reaction is to determine the transition matrix of the corresponding collision process. Dr.Jackson proposed quasi-free scattering approach to treating three body break-up in 1971, which has obtained a lot of experimental supports. Then, Dr.Sakamoto suggested in 1975 a further simplization on the wave function of the relative motion between both clusters in target nucleus. Research papers concerned with this subject, experimentally and theoretically, have been occuring in recent years. However all these investigations just bear upon the particle correlation behavior in order to understand better nuclear reaction mechanism. This paper is also based on the approximation by Dr.Jackson and by Dr.Sakamoto, but aims at practical calculation of nuclear data.

II. BASIC ASSUMPTION

We deal with the direct three body process as follows

$$a + B \text{ --- } a' + b_2 + + b_3$$

where, a and a' is the same particle with mass of m_1, and b_2 with m_2, b_3 with m_3, respectively. The differential cross section can be easily written out according to general collision quantum theory with convenient notation

$$d^3\sigma = \frac{(2\pi)^4}{\hbar}\frac{|T_{if}|^2}{V_{rel}}\int(E^{(f)} - E^{(i)})\int(K^{(f)} - K^{(i)})\prod_{j=1}^{3}dK_j \qquad (2.1)$$

the approximation of quasi-free model means that the target B can be treated as one compound made of both clusters b_2 and b_3, the interaction between the incident particle a and target B occurs just between a and b_2, namely, b_3 may be regarded as a spectator. Following Jackson's proposal

$$T_{if} = t_{2a}\langle f|\int(\vec{r}_a - \vec{r}_2)|i\rangle \qquad (2.2)$$

where, t_{2a} is the amplitute of free scattering between a and b_2,

$$|t_{2a}|^2 = \frac{\hbar^4}{(2\pi)^4}\left(\frac{m_1 + m_2}{m_1 m_2}\right)^2\left(\frac{d\sigma}{d\Omega^*}\right)_{2a} \qquad (2.3)$$

$(d\sigma/d\Omega^*)_{2a}$ stands for off-shell scattering differential cross section in mass-center system of the two collision particles, which is assumpted as isotropic

$$\left(\frac{d\sigma}{d\Omega^*}\right)_{2a} \approx \frac{\sigma_{2a}^{(0)}}{4\pi}$$

For more simplificasion, the initial and final states are treated in plane wave approach, and the asymmetrilization is neglected as well. Hence, we obtain

$$d^3\sigma = \frac{\hbar^3}{\sqrt{2E_a}} \frac{(m_1+m_2)^2}{m_1^{3/2}m_2^2} \frac{\sigma_{2a}^{(0)}}{4\pi} |g_{if}|^2 \delta(\sum_{j=1}^{3} E_j - Q - E_a) \delta(\sum_{j=1}^{3} \vec{K}_j - \vec{K}_a) \times \prod_{j=1}^{3} dK_j \qquad (2.5)$$

where

$$g_{if} = (2\pi)^{-3/2} \int_{r_{23}>R} e^{i\vec{K}_3 \cdot \vec{r}_{23}} \Psi(\vec{r}_{23})\, d\vec{r}_{23} \qquad (2.6)$$

R is nuclear radius of the target B, $\vec{r}_{23} = \vec{r}_2 - \vec{r}_3$ denotes the relative coordinate of two cluster particles, b_2 and b_3, Ψ is the following wave function

$$\Psi(r_{23}) = A j_\ell(\alpha r_{23}) Y_{\ell 0}(\hat{r}_{23}) \qquad r_{23} \le R \qquad (2.7a)$$

$$= B i h_\ell(i\beta r_{23}) Y_{\ell 0}(\hat{r}_{23}) \qquad r_{23} \gtrsim R \qquad (2.7b)$$

where, $\hat{r} = \vec{r}/r$, A, B are two normalization constants, α and β is respectively the internal and external momentum wave number of relative motion of cluster particles.

III. MAIN RESULTS

a). Differential Cross Section For Two-Particle-Correlation

For instance, for the correlation of particle a and b_2, we have

$$\frac{d\sigma}{dE_1 d\Omega_1 d\Omega_2} = \frac{(2l+1)|B|^2}{2\pi^2\hbar^3} \frac{K_1 K_2 (m_1+m_2)^2 (d\sigma/d\Omega^*)_{2a} J_\ell(K_3,\beta,R)}{K_a m_2 (1+\frac{m_1}{m_3}(1-\frac{K_a}{K_2}\cos(\vec{\Omega}_1\cdot\vec{\Omega}_a)) + \frac{K_1}{K_2}\cos(\vec{\Omega}_2\cdot\vec{\Omega}_1))} \qquad (3.1)$$

where, E_2 and E_3, therefore, K_2, and K_3, can be easily determined by kinematics as the function of K_1, Ω_1, Ω_2

$$J_\ell(x,\beta,R) = \frac{R^2}{\beta x(x^2+\beta^2)} (\beta J_{\ell+1/2}(xR) K_{\ell+3/2}(\beta R) - x J_{\ell+3/2}(xR) K_{\ell+1/2}(\beta R))^2 \qquad (3.2)$$

where, J_ν, K_ν is the first and second kind of Bessel function respectively.

b). Differential Cross Section Of Each Secondary Particle

Let j=i,2,3 stands for a', b_2, b_3 respectively. The angular energy double differential cross section of each particle has been derived as follows

$$\frac{d\sigma}{dE_j d\mu_j} = t_j \sqrt{E_j} \sqrt{S_j - E'_j} f_j \qquad \mu_j = \vec{\Omega}_j \cdot \vec{\Omega}_a \qquad (3.3)$$

where

$$S_j = \frac{M-m_j}{M}\left(\frac{A}{A+1}E_a + Q\right) \qquad A = \frac{m_B}{m_1} \qquad (3.4)$$

$$E'_j = E_j + (A+1)^{-2}\frac{m_j}{m_1}E_a - 2(m_1 m_j E_a E_j)^{1/2} M^{-1}\mu_j \qquad (3.5)$$

t_j, S_j, E'_j is a constant respectively, related to E_a, E_j, and mass.

(1). When j=1,2

$$f_j = \sum_{\ell'=0}^{\infty} \sum_{\ell''=|\ell-\ell'|}^{\ell'+\ell} A^{(\ell)}_{\ell'\ell''} (M^{(\ell)}_{\ell'\ell''}(j))^2 \qquad (3.6)$$

where

$$A^{(\ell)}_{\ell'\ell''} = (2l'+1)(2l''+1)(C^{\ell 0}_{\ell' 0 \ell'' 0})^2 \qquad (3.7)$$

$$M^{(\ell)}_{\ell'\ell''} = \sqrt{\frac{2}{\pi\beta}} \int_R^\infty x^{1/2} j_{\ell'}(K_j^{(1)}x)\, j_{\ell''}(K_j^{(2)}x) K_{\ell+1/2}(\beta x)\, dx \qquad (3.8)$$

$K_j^{(i)}$ is a constant related to E_a, E_j, and mass, $C^{\ell 0}_{\ell' 0 \ell'' 0}$ is C-G coefficient.

(2). When j=3

$$f_j = (2l+1) J_\ell(K_3,\beta,R) \qquad (3.9)$$

c). The Integral Cross Section

$$\sigma = \iiint d\sigma \qquad (3.10)$$

For convenient calculation, we have expressed σ as a simple integral with a single variable, which is not listed here.

d). How to determine $|B|^2$

According to the continuities of $\Psi(r_{23})$ and its space defferential at R, and the assumption that probability of cluster formation should be D, namely

$$\int |\Psi|^2 r_{23}^2 d\vec{r}_{23} = D \tag{3.11}$$

It can be found out

$$\alpha \frac{j_{\ell-1}(\alpha R)}{j_\ell(\alpha R)} = i\beta \frac{h_{\ell-1}^{(1)}(i\beta R)}{h_\ell^{(1)}(i\beta R)} \tag{3.12}$$

$$\frac{B}{A} = -\frac{\alpha}{\beta} \frac{j_{\ell-1}(\alpha R)}{h_{\ell-1}(i\beta R)} \tag{3.13}$$

and

$$A = \sqrt{2D}\left(-R^3\left(1+\frac{\alpha^2}{\beta^2}\right) j_{\ell-1}(\alpha R)\, j_{\ell+1}(\alpha R)\right)^{-1/2} \tag{3.14}$$

with

$$\beta = \sqrt{2\mu_{23}\varepsilon_b}/\hbar \tag{3.15}$$

where ε_b is the bound energy of the clusters in target nucleus. Hence, α , A, $|B|^2$ may be easily determined when D is given. All these formulas listed above include just some integrals with a single variable at the most. They are very convenient in actual calculation.

IV. APPLICATION

The formulation in Section III holds for any angular momentum of relative motion of cluster particles. Many experiments provides the following information.

Target	Spin and Parity of ground state	Cluster-form	L value
^{6}Li	1	He + D	0
^{7}Li	3/2	He + P	1
^{9}Be	3/2	He + He	0
		n + ^{8}Be	1

Under the bombardment of neutron, proton, deutron and helium particles, these nuclei may cause the direct break-up in the above cluster-forms. In the case listed above, we obtain (assuming D=1)

1). When l=0

$$J_0(x,\beta,R) = \frac{e^{-2\beta R}}{x^2\beta^2}\left(\frac{(\beta(1+\frac{1}{xR})-\frac{1}{R})\sin(xR)+x\cos(xR)}{x^2+R^2}\right)^2 \tag{4.1}$$

In (3.7), Only one term is needed, namely, $A^{(0)}_{\ell'\ell''} = 2l'+1$

From (3.12), (3.13), (3.14), we obtain

$$\beta = -\alpha\,\mathrm{ctg}(\alpha R) \tag{4.2}$$

$$B = -\cos(\alpha R)e^{\beta R} A \tag{4.3}$$

and

$$A = \left(\frac{2\alpha^2\beta}{1+\beta R}\right)^{1/2} \tag{4.4}$$

2). When l=1

$$J_1(x,\beta,R) = \left(\frac{Sin(xR)}{\beta^2x^2R} + \frac{1}{x^2+R^2}\left(\frac{\sin(xR)}{\beta} - \frac{\cos(xR)}{x}\right)\right)^2 \tag{4.5}$$

In eq.(3.7), only two terms are needed, namely (4.6)

$$A^{(1)}_{\ell'\ell'-1} = l' \qquad A^{(1)}_{\ell'\ell'+1} = l'+1 \tag{4.7}$$

From (3.12), (3.13), (3.14), we have

$$\left(\frac{\alpha}{\beta}\right)^2 = \frac{(\alpha R)\,\mathrm{ctg}(\alpha R) - 1}{1+\beta R} \tag{4.8}$$

$$B = -\sin(\alpha R)\, e^{\beta R} A \tag{4.9}$$

and

$$A = (2\alpha^3)^{1/2}\left(\alpha R + \left(-1+(2+\beta R)\left(\frac{\alpha}{\beta}\right)^4 + (1+\beta R)\left(\frac{\alpha}{\beta}\right)^2\right)\frac{\sin^2(\alpha R)}{\alpha R}\right)^{-1/2} \tag{4.10}$$

A preliminary numerical research has been done on the angular energy double differential spectrum of secondary particles, results obtained are quite satisfactory.

REFERENCES

1 D.E.Jackson, Advances in Nucl. Phys. (1971) No.4
2 Y.Sakamoto, Phys, Rev C11 (1975) 668
3 M.Goldberger, Collision theory (1964)

DWBA CALCULATIONS FOR THE (n,p) REACTION CROSS-SECTION

Ziqiang YU
Department of Physics

Yixin ZUO
Department of Mathematics

Nankai University,
Tianjin, China

Abstract

Direct (n,p) cross sections for the Na, Mg, Al and Si target nuclei have been calculated by using DWBA in the zero-range approximation and added to the results obtained by the statistic theory. The n-p effective interaction strength which vary linearly with the incident neutron energy are determined by comparisions with experimental data.

I. INTRODUCTION

The (n,p) cross sections calculated in the framework of the Hauser-Feshbach and pre-equilibrium statistic theory only are found to be generally lower than the experimental data for energies higher than ten Mev. It indicates that the idrect process may contribute significantly to cross section and has to be considered.

The direct process for (n,p) reaction is treated as a knock-out reaction and calculated by conventional DWBA theory. Since the neutron and proton are light particles, the zero-range approximation can be used.

The (n,p) reaction cross sections for targets Na, Mg, Al and Si are calculated in DWBA and added to those obtained from the statistic theory. The combined results are then compared with the experimental data.

II. DWBA METHOD

For A(a,b)B reaction the transition matrix elements in DWBA are [1]

$$T_{\beta\alpha}(\vec{K}_\beta,\vec{K}_\alpha)=J_{\beta\alpha}\int d\vec{r}_\alpha d\vec{r}_\beta d\xi_\beta \chi^{(-)}_\beta(\vec{K}_\beta,\vec{r}_\beta)\psi^*_B(x_B)\psi^*_b(x_b)W_{\alpha\beta}\psi_a(x_a)\psi_A(x_A)\chi^{(+)}_\alpha(\vec{K}_\alpha,\vec{r}_\alpha) \quad (1)$$

The differentail cross section is

$$\frac{d\sigma_{\beta\alpha}}{d\Omega}=\frac{\mu_\alpha\mu_\beta}{(2\pi\hbar^2)^2}\left(\frac{K_\beta}{K_\alpha}\right)\frac{1}{(2I_A+1)(2I_a+1)}\sum_L B_L P_L(\cos\theta_\beta) \quad (2)$$

and the integral cross section is

$$\sigma_{\beta\alpha}=\frac{\mu_\alpha\mu_\beta}{\pi\hbar^4}\left(\frac{K_\beta}{K_\alpha}\right)\frac{B_0}{(2I_A+1)(2I_a+1)} \quad (3)$$

where ψ are the internal states, $J_{\beta\alpha}$ is the Jacobian, $\chi^{(\pm)}$ are the distorted wave functions. In terms of angular momentum transfers, corresponding to the vector relations

$$\begin{aligned}&\vec{I}_a+\vec{L}_\alpha=\vec{J}_a\ ,\quad \vec{I}_b+\vec{L}_\beta=\vec{J}_b\ ,\\ &\vec{I}_B-\vec{I}_A=\vec{J}_{BA}\ ,\quad \vec{I}_b-\vec{I}_a=\vec{J}_{ba}\ ,\quad \vec{J}_{ba}+\vec{J}_{BA}=\vec{l}\end{aligned} \quad (4)$$

We may expand the T matrix elements and obtain coefficents of the legendre as

$$B_L=\hat{L}\sum_{J_{BA}}\sum_{\substack{J_{ba}J'_{ba}l'\\ J_{ba}l}}\sum_{\substack{L_\beta L'_\alpha J'_b J'_a\\ L_\beta L_\alpha J_b J_a}}(-1)^{J_a-J'_a-J_{BA}+I_a+I_b-L_\alpha}\hat{J}_{BA}\hat{J}'_{ba}\hat{J}^2_b\hat{J}'^2_b\hat{J}^2_a\hat{J}'^2_a\hat{l}'\hat{l}^2\hat{L}_\alpha\hat{L}'_\beta\hat{L}_\beta$$
$$\times\begin{Bmatrix}l' & J'_{ba} & J_{BA}\\ L'_\beta & I_b & J'_b\\ L'_\alpha & I_a & J'_a\end{Bmatrix}\begin{Bmatrix}l & J_{ba} & J_{BA}\\ L_\beta & I_b & J_b\\ L_\alpha & I_a & J_a\end{Bmatrix}W(L'_\alpha J'_a L_\alpha J_a;I_a L)W(J'_b L'_\beta J_b L_\beta;I_b L)W(J_a J_b J'_a J'_b;J_{BA}L)$$
$$\times C(L'_\alpha L L_\alpha;000)C(L'_\beta L_\beta L;000)\,\mathcal{X}^{L'_\beta J'_b L'_\alpha J'^*_a}_{l' J'_{ba} J_{BA}}\cdot\mathcal{X}^{L_\beta J_b L_\alpha J_a}_{l J_{ba} J_{BA}} \quad (5)$$

where

$$\mathcal{X}^{L_\beta J_b L_\alpha J_a}_{l J_{ba} J_{BA}}=\frac{4\pi}{K_\beta K_\alpha}\int dr_\alpha r_\alpha\int dr_\beta r_\beta X^{J_b}_{L_\beta}(K_\beta,r_\beta)g^{L_\beta L_\alpha}_{l J_{ba} J_{BA}}(r_\alpha,r_\beta)X^{J_a}_{L_\alpha}(K_\alpha,r_\alpha) \quad (6)$$

III. KNOCK-OUT REACTION

For knock out reaction, the target consists of a "core" and the emitted particle, A=C+b, while the residual nucleus is comprised of the core plus projectile, B=C+a. Therefore the Jacobian is $J_{\beta\alpha}$ and the parentage expansions for the target and residual nucleus are [2]

$$\psi_{I_A M_A}(\vec{r}_{bc},\xi_b,\xi_c)=\sum_{I_c M_c j_b}\psi_{I_c M_c}(\xi_c)\alpha^{AC}_{l_b j_b}\psi_{l_b j_b m_{jb}}(\vec{r}_{bc},\xi_b)$$
$$\times C(I_c j_b I_A;M_c,m_{jb},M_A) \quad (7a)$$

$$\psi_{I_B M_B}(\vec{r}_{ac},\xi_a,\xi_c)=\sum_{I'_c M'_c j_a}\psi_{I'_c M'_c}(\xi_c)\alpha^{BC}_{l_a j_a}\psi_{l_a j_a m_{ja}}(\vec{r}_{ac},\xi_a)$$
$$\times C(I'_c j_a I_B;M'_c m_{ja}M_B) \quad (7b)$$

where α_{lj} is the parentage coefficient. Taking the zerorange approximation we obtain

$$\mathcal{X}^{L_\beta J_b,L_\alpha J_a}_{l J_{ba}J_{BA}}=\frac{\sqrt{\pi}\hbar^2}{\sqrt{M_\alpha M_\beta}}\frac{1}{\sqrt{E_\alpha E_\beta}}\frac{\hat{L}_\alpha\hat{L}_\beta}{\hat{l}}i^{L_\alpha+L_\beta-l}C(L_\beta L_\alpha l;000)\frac{B}{A}$$
$$\times\int dr_\alpha X^{J_b}_{L_\beta}(K_\beta,\tfrac{A}{B}r_\alpha)f^{ZR}_{l J_{ba}J_{BA}}(r_\alpha)X^{J_a}_{L_\alpha}(K_\alpha,r_\alpha) \quad (8)$$

$$f^{ZR}_{l J_{ba}J_{BA}}(r_\alpha)=\sum_{I_c l_a j_a l_b j_b}\lambda^{l-l_a-l_b}(-1)^{I_A-I_c+j_b+2I_a+2I_b}\frac{1}{\sqrt{4\pi}\hat{l}}$$
$$\times\hat{I}_A\hat{I}_B\hat{l}_a\hat{j}_a\hat{l}_b\hat{j}_b\hat{J}_{BA}\hat{J}_{ba}C(l_a l_b l;000)W(j_a I_B j_b I_A;I_c J_{BA})$$
$$\times\begin{Bmatrix}j_a & I_a & l_a\\ j_b & I_b & l_b\\ J_{BA} & J_{ba} & l\end{Bmatrix}\left[-G\left(\frac{A}{C}\right)^3\right]\alpha^{BC}_{l_a j_a}\alpha^{AC}_{l_b j_b}U_{l_a j_a}\left(\frac{A}{C}r_\alpha\right)$$
$$\times U_{l_b j_b}\left(\frac{A}{C}r_\alpha\right) \quad (9)$$

where G is the strength of zero-range interaction. The n-p effective interaction is taken to be a YukaWa type [3]

$$V_{np}=U_0\frac{e^{-\mu r}}{\mu r} \quad (10)$$

with U_0=52 Mev, μ^{-1}=1.15fm. Then

$$G_0=\int d\vec{r}\,V_{np}=4\pi U_0\mu^{-3} \quad (11)$$

It is known that in the higher energy region than ten Mev, the direct process starts to contribute besides the statistic process. The higher energy the direct process becomes

more important. The theoretical cross section would be the weighted sum of both. No attempt has been made to deduce the values of the weight factor theoretically, and they are determinated experimentally. We assume that G^2 varies linearly with the incident energy:

$$G^2 = G_0^2 \alpha [1 + \beta (E_L - E_0)] \qquad (12)$$

where E_L is the incident neutron energy in the laboratory system. The parameters α , β and E_o are adjustable, so that the theoretical cross sections $\sigma_{np}^T(E_L) = \sigma_{np}^S(E_L) + \sigma_{np}^D(E_L)$ are in agreement with the experimental values $\sigma_{np}^{EX}(E_L)$.

IV. CALCULATED RESULTS

The DWBA calcutations are performed for the reaction $^{23}Na(n,p)^{23}Ne$, $^{24}Mg(n,p)^{24}Na$, $^{27}Al(n,p)^{27}Mg$ and $^{28}Si(n,p)^{28}Al$. The residual nuclei are left in from the ground state up to third excited state. The results are written as $\sigma_{np}^D(E_L,k)$ (k =0,1,2,3). The cross sections from direct process are taken approximately to be $\sigma_{np}^D(E_L) = \sum_k \sigma_{np}^D(E_L,k)$. Therefore the theoretical cross sections are $\sigma_{np}^T(E_L) = \sigma_{np}^S(E_L) + \sigma_{np}^D(E_L)$, where $\sigma_{np}^S(E_L)$ are calculated by using the program MUP-II in the framework of the Hauser-Feshbach and pre-equilibrium statistic theory. The results are illustrated in Figs 1-4. The dashed curves are the results from $\sigma_{np}^S(E_L)$ alone. The solid curves demonstrates the total contributions $\sigma_{np}^T(E_L)$. The experimental data are taken from the commondatory values [4]. As mentioned above in order to agree with the experimental data the parameters α , β and E_o are adjustable. In our calculations, for example, α =1, β =0.32, E_o=12Mev for $^{27}Al(n,p)\ ^{27}Mg$ reaction; and α =1.4, β =0 for $^{23}Na(n,p)^{23}Ne$ reaction.

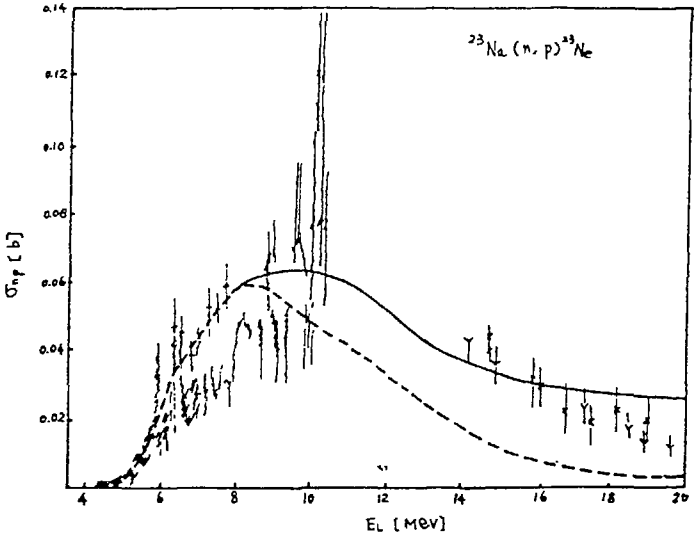

FIG. 1.

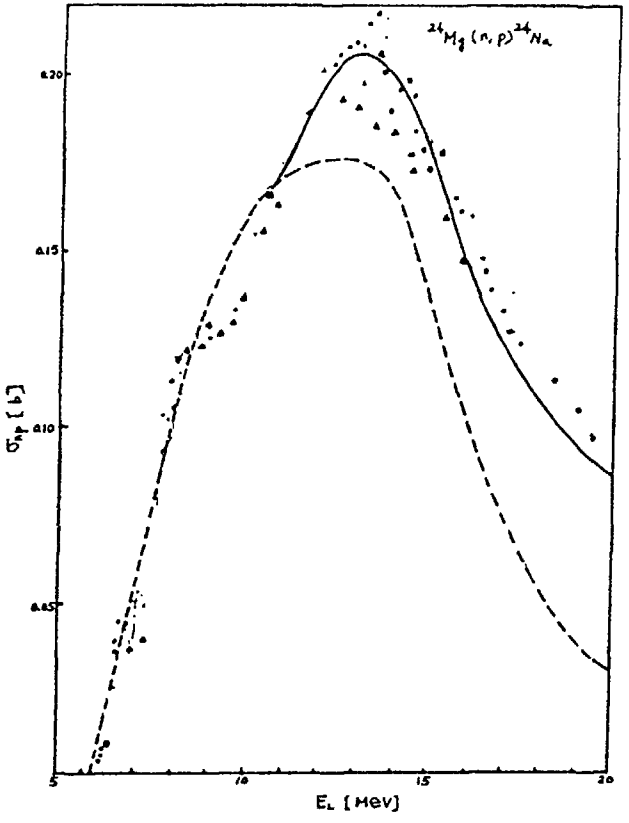

FIG. 2.

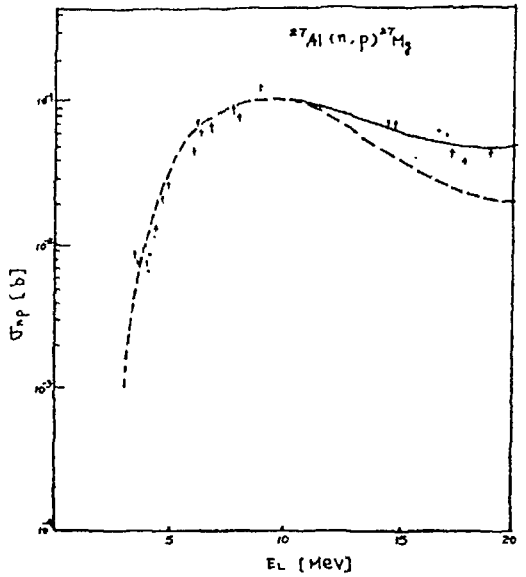

FIG. 3.

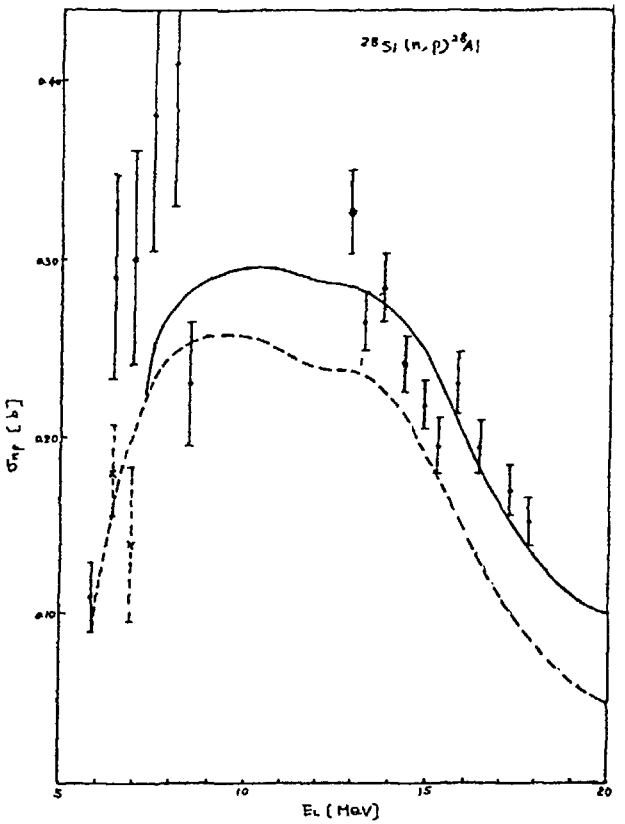

FIG. 4.

REFERENCES

1) G.R.Satchler, Direct Nuclear Reaction (Oxford University Press, New York, 1983).
2) G.R.Satchler, Nucl. Phys. 55, 1 (1964).
3) A.Agodi and G.Schiffrer, Nucl. Phys. 50, 337 (1964).
4) Shi Zhao-min et. al. unpublished.

ISOMERIC CROSS-SECTION

(Session V)

SYSTEMATICS OF ISOMER RATIOS FOR NEUTRON INDUCED ACTIVATION REACTIONS AT 14.5 MeV

H. GRUPPELAAR, J. KOPECKY
Netherlands Energy Research Foundation,
Petten, Netherlands

Abstract

The present status of the knowledge on branching ratios of the isomeric and ground-state cross-sections at 14 to 15 MeV is reviewed. Earlier systematics for the isomer ratios of the (n,n'), (n,p), (n,t), (n,α) and (n,2n) reactions are examined and new systematics for these reactions are presented. A comparison with model calculation is discussed. The (n,2n) isomer ratios show a behaviour different from that of the studied binary reactions.

Introduction

In contrast to many systematics of total (energy-integrated) cross-sections for neutron-induced reactions at 14-15 MeV, those [1,2] predicting the ratio of cross-sections for isomeric and ground states are incomplete and weakly founded. Empirical formulae for total cross-sections give fits to experimental data relating essentially the cross-section only to one parameter, namely the asymmetry N-Z/A. In order to predict isomeric cross-sections certainly more parameters are needed, in particular the spins of ground and metastable states J_m and J_g and parameters related to the distribution and population of competing levels.

Model calculations

In order to base the present treatment on some quantative grounds, compared to previous phenomenological approaches, the pre-equilibrium and statistical Hauser-Feshbach code GNASH [3] has been used to study the dependence of the branching ratio on the isomeric spin by calculating the pertinent cross-sections. The standard input for the ^{93}Nb target, used in a comparative study on different calculation codes [4], has been used with the following simplifications:

1. Only two discrete levels were considered, the ground state and the isomeric state at E_x = 0.1-0.3 MeV, with no decay from isomeric to ground state assumed. The spins of these states were varied.
2. The level continuum started at the matching energy of E_m = 0.5 MeV.
3. The composite formula of Gilbert-Cameron was used for the level-density description (the adopted level-density parameters can be found in ref. [4]).
4. The γ-ray multipolarities higher than the octupole radiation have been neglected.

Such calculations reveal only the general trend as to how the corresponding cross-sections and thus the isomer ratio depends upon the spins J_g and J_m. The level densities for nuclei with mass number close to A=100 are certainly descriptive for many other nuclei (except for the very light ones). However, the strongly varying Q values at other mass regions influence the residual energy involved in decay processes. Further, the spin-probability distribution function P(J) depends sensitively on the spin cut-off parameter and this may lead again to deviations with the data for other masses.

Another aspect typical for each nucleus is the population of low-lying discrete levels, which cannot be satisfactorily described by a continuum. They are usually levels with 1 to 3 MeV excitation energy and their decay to ground and isomeric states can significantly affect the isomer ratio.

The following observations regarding properties of ground and isomeric states have been made from the available experimental information. For the majority of product nuclei the energy of the isomeric state does not exceed $E_x \sim 0.3$ MeV. The isomeric and ground-state spins can be categorized in two groups: high-spin isomers ($J_m > J_g$) with the ground-state spin usually having low values (J_g = 0-2), and low-spin isomers ($J_m < 3$), where J_g values are approximately four units larger than J_m.

The calculations have been carried out for the (n,n'), (n,2n), (n,p) and (n,α) reactions. The spin J_m was varied in steps from 0 tot 15 (or 1/2 to 29/2), while J_g was set to 0 or 1/2 for $J_m > J_g$ and $J_g = J_m + 4$ for $J_g > J_m$. These, or very similar, spin configurations are most frequently found among the experimental data. The results are presented in figs. 1 and 2 in which the isomeric branching ratio $\sigma_m/(\sigma_m + \sigma_g)$ is plotted versus the isomeric spin.

An inspection of these figures shows that for all reactions that were studied similar parabolic dependence has been obtained with largest values of the isomer ratio centered around J_m = 3 to 4. The calculated curves do not differ very much among the considered reactions; only the (n,2n) reaction displays a slower decrease of isomer ratios for $J_m > J_g$ spins.

The reason for this last-mentioned effect is probably that the emission of two successive neutrons leads to a residual nucleus with rather low (average) excitation energy and thus the number of subsequent gamma rays is restricted ($n_\gamma \lesssim 3$). Consequently, the possibility to populate the ground state (with a low spin) from high-spin states is smaller compared to one-step reactions, for which the average excitation energy is much larger.

Another question, common to all reactions, is how the value of the ground-state spin influences the isomer ratio. If J_g starts to increase moderately, up to $J_g = J_m - 4$, the calculation indicates that the population of the ground state (in competition with the population of the isomeric state with $J_m > 6$) becomes less favoured and consequently the isomer ratio increases. This effect can cause a substantial spread in the isomer ratios for large values of J_m, cf. Ref. [7].

The data library covering isomeric and ground state cross-sections for the (n,p) and (n,α) reactions has been taken from the compilation of Forrest [5], while for the (n,t) reaction, data presented by Qaim [2] have been used. These libraries are rather complete and cover all major experimental information to date. The (n,n') isomer ratios have been evaluated from the σ_m(n,n') compiled by Vonach [6] and by applying the assumed constant value of σ_t ~ 400 mb [6] to all nuclei In this study a new library has been compiled for the (n,2n) reaction based on a literature search covering entries up to the end of 1986, see ref [7].

The present calculations have demonstrated, that there is no significant difference between the calculated curves for the considered one-step reactions and thus it seems that one common systematic can be applied to all experimental values. The experimental data points from the above-quoted data libraries are displayed in fig 1, together with the theoretical prediction (solid curves), which has been evaluated as an unweighted mean value of calculated curves from the (n,n'), (n,p) and (n,α) reactions No physical reason has been found not to include the (n,t) data in this comparison as well.

The expected broad parabolic dependence, as predicted by the present model calculations, having a maximum at J_m values between 3 and 5, agrees reasonably with the data. This general tendency, earlier suggested only empirically [1,2], is supported by the present treatment. There is also good agreement with the recently proposed systematics for (n,n') cross-sections of reactions leading to metastable states by Vonach [6]. The available information on the isomeric cross-sections at high values of J_m is rather scanty mainly because they do not appear frequently.

The preferential population of isomeric states with J_m between 3/2 and 3 in the (n,t) reaction, as suggested by Qaim [2], may be an effect of the limited amount of data. Evidently, more experimental information is required in order to clarify this problem.

The isomeric cross-section ratios for the (n,2n) reaction form the most complete set of experimental data [7]. A plot of these values versus the spin J_m is displayed in fig. 2. The tendency of the distribution of data does not differ substantially from the reactions described above, except that for high J_m values larger isomer ratios are found, both experimentally and theoretically.

The slight overestimation of experimental points by the present theoretical predictions may be due to the neglect of the influence of the discrete levels or to variations in the particular nuclear parameters. However, it can be concluded that this study forms a firm base to understand the dependence of the isomer ratio on J_m and certainly enables systematic predictions. The scatter in experimental data gives some indication of the uncertainties involved.

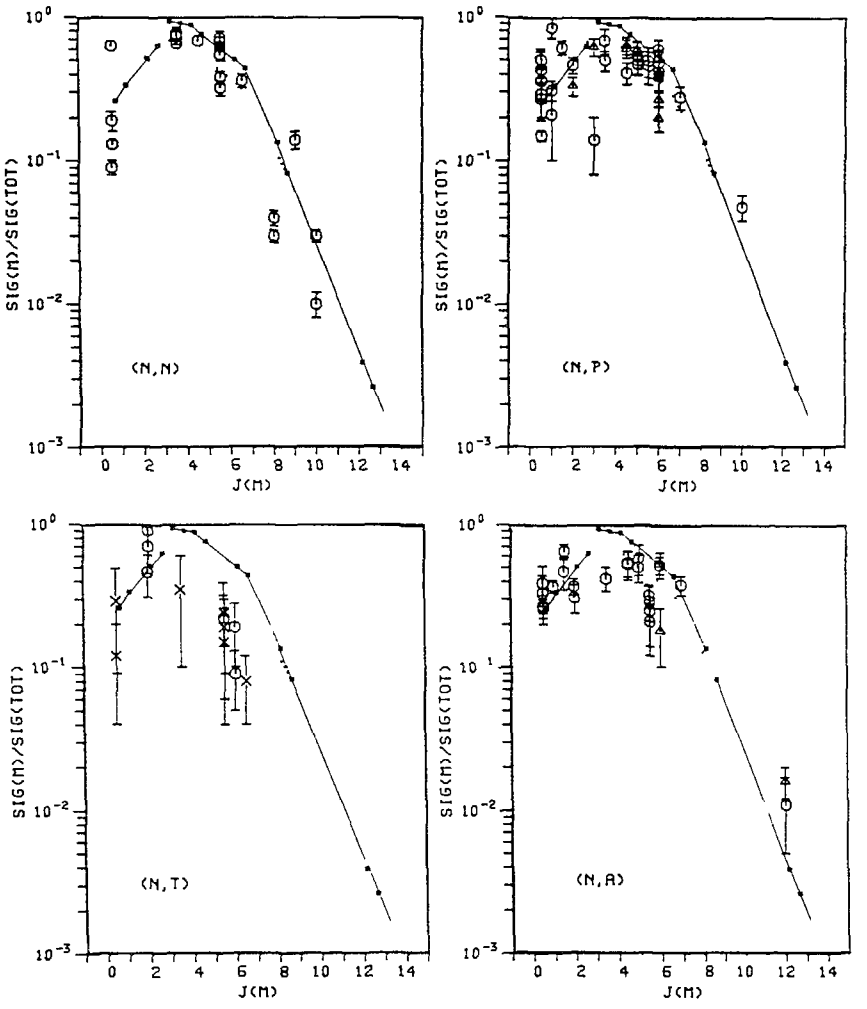

Fig. 1. Experimental isomeric cross-section ratios for the (n,n'), (n,p), (n,t) and (n,α) reactions at about 14.5 MeV plotted as a function of the isomeric spin For the (n,n') reaction the σ_t values have been assumed constant with σ_t ~ 400 mb. The calculated curves (solid curves) are plotted as well The dotted curves represent adjustments to obtain a new systematic. The used symbols have the following meaning:
0 = all cross-sections σ_t and σ_m are from experiment;
X = the σ_t value was estimated from the systematics;
Δ = the value of J_m is uncertain (quoted in brackets in compilations).

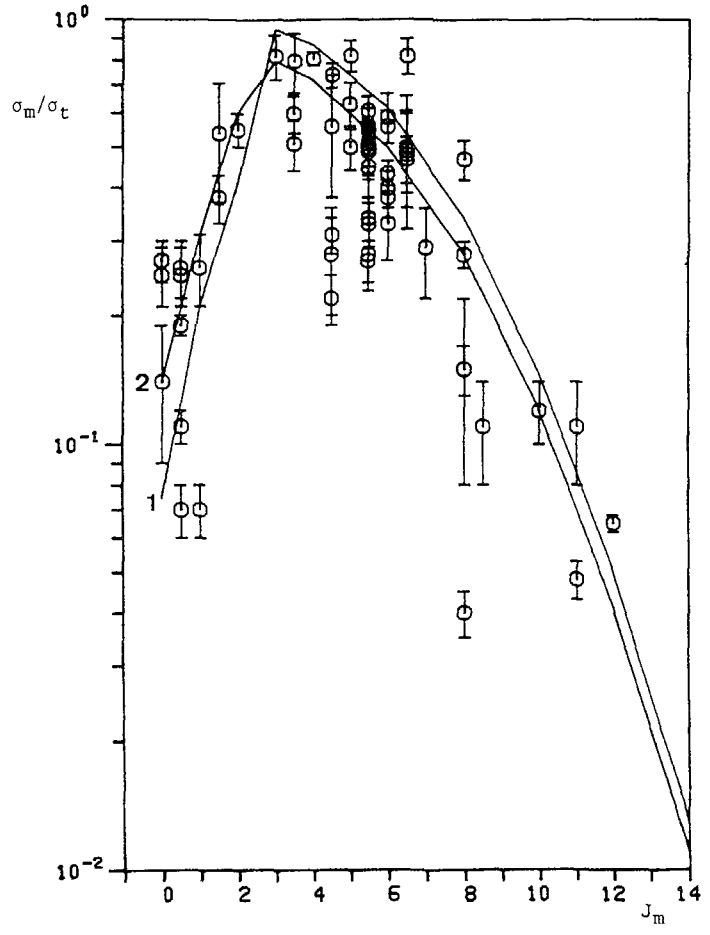

Fig. 2. Experimental isomeric cross-sections for the (n,2n) reaction based on the experimental data library compiled in ref. [7]. The calculated prediction (curve No. 1) is plotted as well as the data adjusted one (curve No. 2).

For practical purposes, e.g. updating of large data files [8], the easiest way to predict isomer ratios seems to be a shift of the calculated curves to obtain optimum agreement with the mean values of data points (dotted lines in fig. 1 and curve No. 2 in fig. 2), using their spread as the uncertainty. For important nuclei in terms of the induced radioactivity in safety studies, especially those with isomers with high spins, the influence of the ground-state spin on the isomer ratio should be taken into account [8].

REFERENCES

[1] Uray, I. et al.: Z. Phys. A287 (1978), 51.
[2] Qaim, S.M.: Nucl. Phys. A438 (1985), 384.
[3] Young, P.G.; Arthur, E.D.: GNASH: A preequilibrium, statistical nuclear-model code for calculation of cross-section and emission spectra, Los Alamos Scientific Lab. Report, LA-6947 (1977).
[4] Gruppelaar, H.; Nagel, P.: Pre-Equilibrium Effects: An International Model and Code Comparison, NEANDC-204"U" (1985).
[5] Forrest, R.A.: IAEA Advisory Group Meeting on Nuclear Data for Fusion Technology, Gaussig (DDR), 1-5 Dec. 1986 and AERE R 12419 (1986).
[6] Vonach, H.K.: IAEA Advisory Group Meeting on Nuclear Data for Fusion Reactor Technology, Gaussig (DDR), 1-5 Dec. 1986.
[7] Kopecky, J; Gruppelaar, H.: Systematics of neutron-induced isomeric cross-section ratios at 14.5 MeV, ECN-200 (1986).
[8] Gruppelaar, H.; Kopecky, J.; Van der Kamp, H.A.J.; Nierop, D.: ECN-report to be published.

INTERCOMPARISON OF NUCLEAR MODEL COMPUTER CODES

(Session VI)

INTERCOMPARISON OF NUCLEAR MODEL COMPUTER CODES

P.E. HODGSON
Nuclear Physics Laboratory,
Oxford University,
Oxford, United Kingdom

Abstract

The present state of the programme of intercomparison of nuclear model computer codes, organised under the auspices of the NEA Data Bank in Paris, is reviewed. The different types of intercomparison are described, and the general principles underlying the intercomparisons are critically discussed.

---

1. Introduction

There are now very many nuclear model computer codes used in many countries to calculate nuclear structure properties and the cross-sections of nuclear reactions. It is evident that if the results of calculations made with these codes are to be of any value, then the codes must be correct. This has two distinct meanings, corresponding to two different types of intercomparison exercise. Firstly, it is necessary to ensure that the code carries out to an acceptable accuracy the calculation for which it is designed. Secondly, the theory used in the code must be able to give results in accord with experiment. This paper is concerned with the methods used to verify that these two criteria are satisfied, and they are referred to as code intercomparisons and theory intercomparisons respectively.

2. Code Intercomparisons

There are several standard theories, for example the optical model and the Hauser-Feshbach theory, that have been embodied in many different codes written by different authors. The mathematical formalisms used are identical, and so with the same input parameters they should give exactly the same results. Such calculations are so lengthy that it is not practicable to carry out even one test case by hand, and so it is by no means trivial to ensure that such a code is correct. The method of verification frequently used is to compare two codes written by different authors quite independently of each other; if the results of several test calculations agree, then it is highly probable that both codes are correct.

Experience shows, however, that not all codes in current use have been checked in this way. Furthermore, codes are frequently altered by users without proper documentation, so that they may give incorrect results in the hands of subsequent users. It is now a frequent experience that when given the same input parameters, different codes give appreciably different results, and this of course may invalidate any calculations made with them.

To tackle this situation, the NEA Data Bank in Paris started several years ago a program of nuclear model code intercomparisons, with the aim of establishing standard results for specified sets of input parameters for a range of codes in current use. It is intended that these standard results should serve as international benchmarks that enable any user to verify that his code is working correctly before he uses it to analyse data.

An intercomparison exercise for a particular type of code begins by establishing several standard sets of input data, and these are sent to users of codes of that type. The users perform the calculations and send the results back for intercomparison. There is always more or less serious disagreement between the results obtained with different codes. These errors or differences are of several types, which will be illustrated by the example of a standard optical model calculation:

1. Errors of coding. Gross errors will have already been detected and removed, leaving rather subtle errors. The codes may give correct results for some ranges of parameters but fail for others, and so may not always appear during the first checks. An example of such an error is the use of a recurrence relation in the unstable direction when calculating the Legendre polynomials.
2. Inadequate choice of internal parameters. For example, an optical model calculation must always have a sufficient number of partial waves, and this number is governed by a cut-off value of the orbital angular momentum. The cut-off criterion may not be sufficiently accurate, so that partial waves are omitted that should be included. Usually the criterion is that the partial wave cut-off is applied after two successive phase-shifts are less than say 10^{-4}. It is necessary to specify two, since any particular phase-shift may accidentally be zero, even though higher partial waves still contribute. Similar internal parameters are those in the formula that specifies the number of integration steps, and those used to fix the matching radius. In a well-written program these should all be chosen well on the safe side, so that there is no chance that they can introduce errors in the calculation.
3. Different choice of external parameters. Various combinations of the fundamental constants occur in the code, in particular when calculating the wave number from the incident energy and the Coulomb parameter. Some codes take the nucleon mass as unity, others as 1.008, and thus can produce appreciable differences in the final results.

One method of identifying and removing the errors and differences that are responsible for the different results is to choose the two codes that give the closest results, and then to check them systematically for errors on the above list, and to alter them so that the various criteria and parameters are identical. Hopefully this will give results of the required degree of concordance. If not, it is necessary to print out intermediate numbers such as phase shifts and compare them systematically until the source of the discrepancy is found.

It is found that even the *same* code run on *different* computers gives slightly different results, and thus sets a natural limit on the accuracy attainable. As an approximate guide, it is reasonable to aim at agreement to four significant figures for total and reaction cross-sections, and three significant figures for differential cross-sections and polarisations. This is of course more than adequate for any analysis of experimental data.

The earliest code intercomparisons carried out at the Data Bank were deficient in several respects:

1. The input parameters were too complicated, leading to different interpretations. The potentials specified should be in the physical region but need not be those that actually fit data. It is better to have simple numbers such as $V = 50$, $W = 10$ etc. It is undesirable to include asymmetry or Coulomb correction terms, since these do not give whole numbers and different users may evaluate them to different numbers of significant figures, so that there are small differences in their input data.
2. Comparisons were made for total cross-sections, but not for differential cross-sections and polarisations, which of course are much more sensitive to differences between the codes.
3. The discrepant results were simply tabulated without any follow-up to identify and correct the discrepancies, which in some cases were very large.
4. The Coulomb-dependent parts of the codes were not adequately tested. This is important even for neutron data evaluation since neutron-induced reactions often produce charged particles.

For these reasons a new series of code intercomparison was planned, the first on the optical model. The intercomparisons were made with proton potentials and, when the two selected codes finally agreed, a further calculation was made with the charge set to zero, giving a benchmark for neutrons also. This intercomparison has been published (Hodgson and Sartori, 1985).

At the present time an intercomparison exercise for Weisskopf-Ewing and Hauser-Feshbach statistical model calculation is in progress, and it is hoped to work also on pre-equilibrium codes in the future.

3. Theory Intercomparisons

When it has been established that the code is correct, in the sense that it gives with sufficient accuracy the results of a calculation with the theory it embodies, the next task is to see how well it accounts for the experimental data, compared with other codes embodying different theories developed to explain the same phenomena. For example the various types of exciton model theories can be compared with chosen sets of experimental data. Such an intercomparison has indeed been made by Gruppelaar and Nagel (1985).

There are several ways of carrying out such intercomparisons. One way is to ask the users to fit a given set of cross-section data at one energy, and ask them to predict the cross-section at a different energy. This was the method adopted by Gruppelaar and Nagel.

It is a familiar experience that many of these theories are able to fit quite well any given set of data, by judicious adjustment of parameters. They are not nearly so good, however, at predicting an unknown cross-section. A much more severe type of intercomparison is therefore to invite the users to predict a cross-section unknown to them, and compare the results with each other and with the experimental results, that were not previously known to the participants. Such an intercomparison exercise is in progress for pre-equilibrium codes and the results are being compared by Vonach.

A list of code intercomparisons, both completed and in progress, is given in the Table.

Table: Computer Code Intercomparisons

Nuclear Theory	Author
Statistical Model	Prince *et al*, 1983
Coupled-Channels	Sartori, 1984
Optical Model	Hodgson and Sartori, 1985
Pre-Equilibrium	Gruppelaar *et al*, 1985
Weisskopf-Ewing and Hauser-Feshbach	Hodgson and Sartori (in progress)
Pre-Equilbrium	Vonach and Nagel (in progress)

ACKNOWLEDGEMENTS

This work has been made possible by the farsighted support of Mr J. Rosen and Dr N. Tubbs of the NEA Data Bank. The intercomparisons in which I have participated have relied on the computer expertise and willing co-operation of my colleague Dr E. Sartori, also of NEA Data Bank.

REFERENCES

H. Gruppelaar and P. Nagel, "International Nuclear Model and Code Comparison on Pre-Equilibrium Effects", NEANDC–204U, INDC(NEA)6, Newsletter of the NEA Data Bank No.32, September 1985.

P.E. Hodgson and E. Sartori, "International Nuclear Model Code Comparison Study of the Spherical Optical Model for Charged Particles", NEANDC–198U INDC(NEA)5, May 1985.

A. Prince, G. Reffo and E. Sartori, "International Nuclear Model Code Intercomparison. Spherical Optical and Statistical Model Study", NEANDC–152A, INDC(NEA)4, October 1983.

E. Sartori, "Report on the International Nuclear Model Code Intercomparison. Coupled Channel Model Study", NEANDA–182A INDC(NEA)3, January 1984.

LIST OF PARTICIPANTS

Austria

H. Vonach — Institut für Radiumforschung und Kernphysik, Boltzmanngasse 3, A-1090 Vienna, Austria

Belgium

A.J. Deruytter — CEC Joint Research Centre, Bureau Central de Mesures Nucleaires, Steenweg Naar Retie, B-2440 Geel, Belgium

China (see separate list)

Federal Republic of Germany

F. Fröhner — Institut für Neutronenphysik und Reaktortechnik, Kernforschungszentrum, Postfach 3640, D-7500 Karlsruhe, FRG

France

C.A. Philis — Service de Physique et Techniques Nucleaires, Centre d'Etudes de Bruyeres-le-Chatel, B.P. No. 12, F-91680 Bruyeres-Le-Chatel, France.

German Democratic Republic

D. Seeliger, H. Märten — Sektion Physik, Technische Universität Dresden, Mommsenstrasse 13, DDR-8027 Dresden, GDR

Italy

E. Menapace, G. Reffo — E.N.E.A. - Centro Ricerche Energia "E. Clementel", Div. Fis. e Calcolo Scientifico, Via Mazzini 2, I-40138 Bologna, Italy

Japan

Y. Kanda — Department of Energy Conversion Engineering, Interdisciplinary Graduate School of Engineering Sciences, Kyushu University, Kasuga Fukuoka 816, Japan

T. Ohsawa — Department of Nuclear Engineering, Kyushu University - 36, Hakozaki, Higasi-ku, Fukuoka, Japan

Netherlands

H. Gruppelaar — Department of Physics, Netherlands Energy Research Foundation (ECN), P.O. Box 1, 3 Westerduinweg, NL-1755 ZG Petten

Poland

A. Marcinkowski — Department P-1, Institute for Nuclear Studies, Ul-Hoza 69, PL-00681 Warsaw, Poland

Sweden

H. Condé — Gustav Werner Institute, Uppsala Institute, P.O. Box 531, S-751 21 Uppsala, Sweden

United Kingdom

P. Hodgson — Dept. of Nuclear Physics, University of Oxford, Nuclear Physics Laboratory, Keble Road, Oxford, OXI 3RH, United Kingdom

U.S.A.

M. Blann — Lawrence Livermore National Laboratory
L-280
P.O. Box 808
Livermore, California 94550
U.S.A.

P.G. Young — Los Alamos National Laboratory
MS, B243
Los Alamos, New mexico 87545
U.S.A.

USSR

B.D. Kuzminov — Fiziko-Energeticheskij Institut
Ploschad Bondarenko
249 020 Obninsk
Kaluga Region
U.S.S.R.

V. Pronyaev — Centr Po Jadernym Dannym
Fiziko-Energeticheskij Institut
Ploschad Bondarenko
249 020 Obninsk
Kaluga Region
U.S.S.R.

IAEA

V.A. Konshin
Wang Da Hai (Scientific Secretary)
J.J. Schmidt

88-05613

List of Chinese Participants

Institute of Atomic Energy, Beijing.

Ma Zhongyu, Shi Xiangjun, Wang Shunuan, Cai Dunjiu, Liu Tingjin, Zhang Jingshang, Zhuo Yizhong, Jiang Chenglie, Zhou Enchen (Local organizer)

Institute of Applied Physics and Computational Mathematics, Beijing.

Du Xiangwan
Zhang Benai

Peking University, Beijing.

Huang Feizeng

Qinghua University, Beijing.

Chen Zhenpeng

Fudan University, Shanghai.

Ho Yukun

Guizhou University, Guizhou.

Lu Haitao

Wuhan University, Wuhan.

Lio Dunhuan

Jilin University, Changchun.

Zhu Yaoyin

Lanzhou Ued